

EXPERIMENTAL STUDIES OF MICROWAVE PROPAGATION THROUGH FIRES FOR
THROUGH-WALL, SEARCH-AND-RESCUE RADAR IN FIREFIGHTING

By

Andrew Kenneth Gerken Temme

A DISSERTATION

Submitted to
Michigan State University
in partial fulfillment of the requirements
for the degree of
Electrical Engineering —Doctor of Philosophy

2015

ABSTRACT

EXPERIMENTAL STUDIES OF MICROWAVE PROPAGATION THROUGH FIRES FOR THROUGH-WALL, SEARCH-AND-RESCUE RADAR IN FIREFIGHTING

By

Andrew K. Temme

Finding people trapped inside of a burning house is extremely difficult, dangerous, and time consuming. Smoke, heat, unfamiliar floor plans, and possible structural collapse all combine to challenge a firefighter's ability to find a person. Thermal imaging cameras, the most advanced technology available to firefighters today, are able to see through smoke but are unable to see through walls and household items. Through-wall radar and vital-sign detection radar offer an imaging modality that may be able to help firefighters find victims from outside of a room or even a house.

Flames can interact with electromagnetic (radar) waves because the flames create a weakly-ionized plasma. Previous work has looked at small flames fueled by pure gases or flames from wildfires. Combustable items in a house are typically petroleum-based products that have different combustion reactions compared to previously studied flames and fire-induced plasmas. Because of this, it is unknown how electromagnetic waves interact with flames found in a house fire.

This dissertation investigates the question of how electromagnetic waves interact with flames in a house fire. This is an open problem, with many variables, that poses a subtle and difficult measurement task. This work focuses on creating experimental techniques to explore this problem. From an electromagnetic metrology perspective, the physical phenomena of interest are difficult to measure due to ill-defined physical boundaries, characteristic lengths of varying magnitude, inhomogeneity, and varying time scales. The experimental methods studied here primarily focus on transmission measurements through flames a few feet in height. Additionally, this work presents a proof-of-concept two-wire transmission line for bench-scale, material-characterization of solids, liquids, gases, and flames.

Results from this work provide a metrological foundation for future studies in this area. An experimental setup that can withstand direct exposure to flames was developed and preliminary measurements recorded. Data taken during the development of this setup showed a time-dependance that corresponded to transmissions through the flame and the solid fuel being consumed. Calibration procedures were used to verify measurements of standard materials; the calibration procedure should be refined for larger flame measurements. Transmitters were placed inside of a burning house and signal propagation was measured, which required the design of fire-proof enclosures for the transmitters. Measured results demonstrated that transmissions may not be affected when sent from a firefighter inside of a house with fire conditions suitable for an offensive, interior attack. It is unknown if severe conditions, such as a flashover, would affect transmissions. Plasmas were observed in interferometric measurements of live-fire experiments performed in the laboratory.

This work has explored an open problem in electromagnetics with live-saving applications to the fire service. Results from this work warrant additional study in this area to improve techniques, with the goal of putting search-and-rescue radars into the hands of firefighters.

Copyright by
ANDREW KENNETH GERKEN TEMME
2015

This work is dedicated to those who lost their life due to the earthquake on January 12, 2010 in
Port-au-Prince, Haiti.

ACKNOWLEDGMENTS

I know that finishing my dissertation and receiving a PhD was not fully my own doing. Many people and organizations have helped me along the way. I have made every effort to acknowledge those who have helped me during this process. Please accept my sincere apology if I have somehow missed you. If I have, please let me know. I live to help others and truly appreciate when others help me. Thank you to everyone who has helped me in this endeavour.

First and foremost, I thank and praise God for the talents, intelligence, and heart that He has given me. I pray that my work will be helpful to others. He has given me this amazing opportunity and blessed me throughout.

People

Dr. Rothwell has been my advisor—either academic and/or research—since freshman year at MSU. Thank you for all the advice over the years. You have guided me down a winding path and helped me to explore numerous areas of engineering. Your love of teaching and writing inspire me to strive for the highest quality in all that I do. Thank you for bringing me into the Electromagnetic Research Group.

My dissertation committee has been encouraging as well as excited by my work throughout. I would like to thank Drs. **Edward Rothwell**, **Prem Chahal**, **John Verboncoeur**, and **Indrek Wichman** for their support and guidance. I have enjoyed working with you.

Thank you to **Dr. Raoul Ouedraogo** for mentoring me when I first entered the Electromagnetics Group. His guidance and excitement have inspired me and shown just how much one can accomplish while loving life. Special thanks to **Dr. Alejandro Diaz** for working with and funding me while I worked on metamaterial research with Raoul.

Dr. Xiabo Tan brought me into his lab as a freshman and sophomore. He turned me loose on my own projects while mentoring me. Thank you for this introduction to research and setting me down this path. **Drew Kim** was influential in connecting me with Dr. Tan as well as involving me in college K–12 outreach activities. Thank you Drew.

I would also like to thank all of my **teachers** over the years. So many of you encouraged me to explore new topics and push my self beyond the regular assignment, striving to learn more. Thank you for starting me down this path.

My family has been a source of encouragement and guidance. At some of the lowest points, you have provided reasons for continuing and advice. Seeing what you have accomplished is inspiration. My parents, **Kenneth and Miriam Temme**, have always gone out of their way to make sure that my siblings and I had the best possible education and experiences. Thank you for all the time you have spent driving us around to different schools and programs. You have given so much for us. Thank you **Karsten** for always being there as an older brother with advice from having gone down many of the same roads. I've always looked up to you. **Marliese** has helped so much along the way. Your experience outside of engineering has given me perspectives that the our other siblings could not. Thank you for always offering me a place to stay and food when I leave campus to get a break. Good luck with the rest of your program. **Jacob** has been a great brother and friend through out all of my life. You've taught me so much and answered so many annoying questions—you have been especially helpful with my combustion questions. Thanks for spending all the time playing games with me.

Throughout my time as a graduate student and even before, **Hanna** has always been there from discussing new ideas, to smiling and nodding, to consoling me when I've fallen apart, to making me work at times when I haven't wanted to. I am not sure how I would have finished without you. I know I probably would have taken a little bit longer or maybe not have even finished. You pushed me and made me stick to it. I thank you for everything. Throughout it we have gone from just dating to being married. Those are significant life experiences even outside of graduate school. The travel and time apart has been hard. Thank you for putting up with all of it and helping me to finish. Now its your turn to graduate.

I would like to thank **Kathryn Bonnen** for her support and amazing cooking abilities throughout my graduate and undergraduate career. Thank you for always being there for Hanna and I, and we hope we can do the same for you.

In addition to Dr. Rothwell, I would like to thank **Dr. Shanker Balasubramaniam** for hiring me that first summer. He has supported me throughout and always looked out for me, even squirreling away some funds to help near the end of my program.

Roxanne Peacock has been a great help throughout my research in placing orders and assisting in me obtaining necessary equipment. More than once she has gone out of her way to assist when I came in at the last moment. Roxanne has also been one who is easy to talk to about life in school and out. I have enjoyed our many conversations.

Gregg Mulder and **Brian Wright** of the Electrical and Computer Engineering (ECE) Shop have been crucial to me completing my PhD. They continually offer their knowledge, equipment, and guidance. I cannot express enough how thankful I am for all the times you have bent over backwards to help me. Gregg has been an amazing ham radio elmer—keep it up!

Korede Oladimeji and **Dr. Junyan Tang** have been indispensable in lab work. These two have answered questions, retrieved data, and done so many other tasks to assist when I was on or off campus. They have helped make it possible for me to spend time in Minnesota.

Many other people have also donated their knowledge, skill, and time to assist me. My other labmates including **Jonathan Frasc**, **Jennifer Byford** and **Dr. Benjamin Crowgey**. The ECE department secretaries including **Meagan Kroll**, **Laurie Rashid**, **Pauline Vandyke**, **Michelle Stewart**, and **Jennier Woods** have always been helpful and resolved so many issues for me.

Katy Luchini Colbry has been immensely helpful since my freshman year. Thank you for all the help, advice, and food you have provided to me and the other students. You contribute so much to MSU and the College.

Rafmag Cabrera and **Dr. Nelson Sepúlveda** offered their assistance in placing wire bonds onto my balun circuit boards.

So much of this work has depended on inspiration. This was provided again and again by my involvement with the **Bath Township (MI) Fire Department** (BTFD). Call after call reminded me of why I am an engineer trying to solve problems to help others. The department and especially **Chief Arthur Hosford** took a chance by hiring some kid from Wyoming and a student at MSU to

be on the department. I hope the township has found their investment in me and my training to be worthwhile. I have learned so much while on calls that has impacted my research. The experience gained from being a BTFD firefighter will guide my work for years to come. All of the firefighters on the department have been supportive of my work. A special thanks to **Kevin Douglas** who has picked up me numerous times from the airport as well as being a good friend and partner on too many calls when it was just us.

Dave Snider and **Haslett True Value** have been a tremendous help throughout. Dave is knowledgeable and helpful to all the students who come in. Best of luck with the store. Dave has also been a great leader on the fire department and supported my work there and this work.

I wish to thank **Rick Taylor** for helping me barrow needed parts and equipment from the MSU physical plant. Additionally, thank you for your mentoring on the fire department. I will always remember the true care and concern you express for every patient. May God bless your ministry.

Dana and Mary Scherer have been kind enough to have allow me to stay with them when I returned to East Lansing during the last year and a half of my program. They have been very easy going and wonderful hosts. Thanks for providing me a bed, a roof, and great company.

I wish to thank those at **NIST** and **Underwriters Laboratories** who have taken time to discuss my research and even given me tours, especially **Bob Backstrom** and **Daniel Madrzykowski**.

Thank you to **Dr. Ross** for his assistance and advice along the way and on personal side projects. He has also allowed the Electromagnetics Research Group to use his WaveCalc program. This has been useful over and over.

Gregory Charvat has been a great sounding board, especially as I was beginning my research. I appreciate his invitation to work with him along with **Hisham Bedri** and **Dr. Ramesh Raskar** of the MIT Media Lab on new radar imaging techniques. This project has been exciting and promising, as well as providing a peak into the another institution.

Funding

Attending and completing graduate school is a costly endeavor. I wish to acknowledge those who have contributed financially.

I was supported on a **National Science Foundation (NSF) Graduate Research Fellowship (GRFP)** for much of my time in graduate school. I was selected in the spring of 2010 as a fellow. I postponed my first year and used other funding from Michigan State University and the Electrical and Computer Engineering Department. My second through fourth years of graduate school were directly covered by the GRFP. I remained a fellow for my final time in graduate school in order to continue interactions with NSF. As requested by NSF, the following is a formal acknowledgement of their support:

This material is based upon work supported by the National Science Foundation Graduate Research Fellowship under Grant No. 0802267. Any opinion, findings, and conclusions or recommendations expressed in this material are those of the author and do not necessarily reflect the views of the National Science Foundation.

Part of my work has been supported by the **IEEE Antennas and Propagation Society** through a Doctoral Research Award from the November 2012 funding cycle. Please look in upcoming issues of the Antennas and Propagation Society Magazine for a write up about my work and my future plans.

I was supported in the summer of 2014 by a **Department of Electrical and Computer Engineering Graduate Excellence Fellowship** as well as a research assistance position from **Dr. Edward Rothwell**.

I received a Dissertation Completion Fellowship from the **MSU Graduate School**. Thank you for supporting me and allowing me to finish. The Graduate School has also awarded me travel funds for attending the 2014 IEEE International Symposium on Antennas and Propagation and USNC-URSI Radio Science Meeting held jointly July 6–11, 2014, at the Memphis Cook Convention Center in Memphis, Tennessee. Travel was also supported by the **Dean's Office**

of the College of Engineering. Other travel has been supported from the **Dr. Dennis Nyquist Fellowship.**

Materials and Equipment

A large amount of my research has been conducted due to the kindness of others as my budget for equipment and materials was limited.

The **Lansing Fire Department (LFD)** has been very helpful with my experiments including allowing the use of their training facility. LFD has been supportive of this work since they were approached in the late summer of 2012. Special thanks goes to **Chief of Training Dan Oberst, Fire Marshal Brad Drury,** and **Captain Marshaun Blake** of the Fire Marshal's Office (ranks at the time of the experiments).

I would like to thank **The Club at Chandler Crossings** for donating furniture which I used in fire experiments. The **Merdian Township Fire Department** has been gracious enough to lend me their burn pan on multiple occasions allowing me to conduct measurements. The **MSU Physical Plant** donated sheet metal for construction of a radar corner reflector. **DeLau Fire Services** allowed me to take measurements of their burn pan at the Fire Safety Week Open House on October 10, 2012 at Lansing Fire Station 8.

The **MSU Engineering Machine Shop** has been helpful throughout. They have helped with manufacturing of numerous devices, always willing to answer my questions and offer advice.

The **MSU Engineering Division of Engineering Computing Services (DECS)** has been extraordinary. After talking with students at other universities, I am amazed by the support that we receive from DECS. Rarely have I ever received a negative answer from DECS and I have had many out-there requests.

Many of my experiments have relied on equipment on loan from the manufacturer. I have used a Field Fox analyzer from **Agilent** as well as a handheld ZVH from **Rohde and Schwarz.** Some of this has been supplied through **ElectroRent.**

The **MSU Surplus Store** has been helpful throughout my research. It has also lead to me purchasing various, non-essential items. When possible, the Surplus Store allowed me to pickup

samples and other materials needed for experiments at little or no cost. This was extremely important because of the limited funding for experiments.

Elvit Potter from MSU Environmental Health and Safety (EHS) assisted in a live burn experiment early on in this work. He was kind enough to take time out of his day to setup and run the Bullex Fire Extinguisher Trainer. Tang was assisting me that day and received a brief fire extinguisher training from Elvit after my experiment.

Joan Fetty from Unifrax generously donated Fiberfrax Duraboard to assist in my research. This donation was crucial and I am very grateful. Thank you.

Software

I have used numerous pieces of software along the way. My interest in programming and laboratory techniques has led me to create many new and different programs for data collection and analysis.

Throughout my work, the **MSU High Performance Computing Center** (HPCC) has been an important resource. **Dr. Dirk Colbry** and **Dr. Benjamin Ong** have been invaluable in making the HPCC useful to me and other electromagnetic students.

I wish to thank **Alex Arsenovic** for his work on Scikit-RF¹, an open source RF engineering package written in Python.

This dissertation was typeset using a class derived from **Alexandra Diem's** dissertation style² which she adapted from **Matthias Liebisch** of DBIS-Lehrstuhl at Friedrich Schiller University in Jena, Germany.

¹<http://www.scikit-rf.org/>

²https://bitbucket.org/akdiem/dissertation_template and
<http://akdiem.wordpress.com/other/latex-template-for-dissertations/>

PREFACE

Any corrections, updates, or new editions will be posted online and will be listed in the errata on the following pages.

Due to university deadlines for degree completion, it was not possible to include all ancillary information in this version which has been submitted to the university. At least one additional version, to be released in 2016, is planned.

As website addresses can change over time, a definitive URL cannot be given here. I will attempt to maintain a link to the most up-to-date version of this dissertation at any or all of my following pages:

- ORCID: orcid.org/0000-0001-9259-4579
- Google Scholar: scholar.google.com/citations?user=eK4xvf8AAAAJ
- LinkedIn: linkedin.com/in/atemme
- Github: github.com/temmeand
- Bitbucket: bitbucket.com/temmeand
- Michigan State University Gitlab: gitlab.msu.edu/temmeand

If these site are inactive, please perform an internet search for my name and the title of this dissertation. The reader may also try contacting the Electromagnetic Research Group and/or the Graduate School at Michigan State University to request an up-to-date version if it is not available elsewhere.

At the time of writing, valid email addresses for me are `temmeand@msu.edu` and `temmeand@gmail.com`.

ERRATA

December 2015

- Git hash: gradSchool:fbff463
- Initial publication

TABLE OF CONTENTS

| | |
|---|-------------|
| LIST OF TABLES | xx |
| LIST OF FIGURES | xxii |
| Part I Motivation, Objective, and Background | 1 |
| Chapter 1 Motivation and Objective of this Work | 2 |
| 1.1 Motivation | 2 |
| 1.2 Objective | 4 |
| Chapter 2 Basic Theory of Fields and Plasmas | 5 |
| 2.1 Electromagnetic Fields and Waves | 6 |
| 2.2 Plasmas | 14 |
| 2.2.1 Characteristic Length | 15 |
| 2.2.2 Debye Sphere | 16 |
| 2.2.3 Charge Neutrality | 16 |
| 2.2.4 Collision Dampening | 16 |
| 2.3 Plasma Model for Electromagnetic Fields | 17 |
| Chapter 3 Literature Review | 20 |
| 3.1 Early Work | 20 |
| 3.2 Wildland Fire Papers | 22 |
| 3.3 Losses in Wildland Fires Investigated by Boan | 22 |
| 3.3.1 Loss Mechanisms | 23 |
| 3.3.2 FDTD Simulations | 24 |
| 3.4 Experimental Measurements Conducted by Mphale | 28 |
| 3.5 Conclusion | 31 |
| Part II Large-scale Fire Experiments | 32 |
| Chapter 4 Radio Wave Transmission Through Furniture Cushion Flames | 33 |
| 4.1 Experimental Methods | 34 |
| 4.2 General Measurement Procedure | 41 |
| 4.3 Safety Precautions | 41 |
| 4.4 Go/No-Go Criteria | 42 |
| 4.5 Results | 42 |
| 4.6 Discussion | 51 |
| 4.7 Experiment Design Observations and Suggestions | 53 |
| 4.8 Conclusion | 61 |

| | | |
|------------------|---|------------|
| Chapter 5 | Experiments Using a Propane Burn Pan | 62 |
| 5.1 | Experiment at EHS | 64 |
| 5.1.1 | Experimental Setup | 64 |
| 5.1.2 | Experimental Procedure and Data Processing | 68 |
| 5.1.3 | Results and Discussion | 69 |
| 5.2 | Experiment at BTFD | 75 |
| 5.2.1 | Duraboard Insulation and Burn Chamber Design | 75 |
| 5.2.2 | Experimental Setup | 78 |
| 5.2.3 | Experimental Procedure and Data Processing | 78 |
| 5.2.4 | Results and Discussion | 79 |
| 5.3 | Conclusion | 82 |
| Chapter 6 | Interferometry | 83 |
| 6.1 | Microwave Interferometer Theory | 84 |
| 6.2 | Experimental Setup | 88 |
| 6.3 | Results | 99 |
| 6.3.1 | ECE Hood Experiment Results | 99 |
| 6.3.2 | Calorimeter Experiment Results | 102 |
| 6.3.3 | Shutter Experiment Results | 106 |
| 6.3.4 | Mesh Experiment Results | 111 |
| 6.4 | Discussion | 115 |
| 6.5 | Conclusion | 116 |
| Chapter 7 | Transmissions from Inside of a House Fire | 117 |
| 7.1 | Transmitters | 118 |
| 7.1.1 | Insulation | 119 |
| 7.1.2 | 144 MHz CW Transmitter | 121 |
| 7.1.3 | 440 MHz CW Transmitter | 123 |
| 7.1.4 | 900 MHz XBee Transmitter | 123 |
| 7.1.5 | 2.4 GHz and 5 GHz Wi-Fi Transmitter | 125 |
| 7.1.6 | Transmitter Placement | 128 |
| 7.2 | Receivers | 132 |
| 7.3 | Video Recordings | 135 |
| 7.4 | Results and Discussion | 137 |
| 7.5 | Conclusion | 148 |
| Part III | Bench-Scale Diagnostics using a Two-Wire Transmission Line | 149 |
| Chapter 8 | Transmission Line Characteristics | 153 |
| 8.1 | Electric Potential | 156 |
| 8.1.1 | Potential of Single Line Charge | 157 |
| 8.1.2 | Potential of Two Line Charges | 158 |
| 8.1.3 | Equipotential Surfaces | 159 |
| 8.1.4 | Application to Two-Wire Transmission Line | 166 |

| | | |
|-------------------|--|------------|
| 8.1.5 | Visualization of the Potential | 170 |
| 8.2 | Electric and Magnetic Fields | 171 |
| 8.3 | Radiation Resistance | 177 |
| 8.3.1 | Closely Spaced Wires | 179 |
| 8.3.2 | Discussion and Recommendations | 180 |
| 8.4 | Distributed Circuit Model | 181 |
| 8.4.1 | Capacitance | 184 |
| 8.4.2 | Conductance | 185 |
| 8.4.3 | Inductance | 187 |
| 8.4.4 | Resistance | 188 |
| 8.4.5 | Summary of Parameters | 191 |
| Chapter 9 | Three Short Calibration Method | 193 |
| 9.1 | Introduction | 193 |
| 9.2 | Calibration Theory | 194 |
| 9.2.1 | One-Port Calibration | 195 |
| 9.2.2 | Two-Port Calibration | 199 |
| Chapter 10 | Double-Y Balun | 204 |
| 10.1 | Introduction | 204 |
| 10.2 | Design Overview | 207 |
| 10.3 | CPS and CPW Design Equations | 211 |
| 10.3.1 | Coplanar Strip | 211 |
| 10.3.2 | Coplanar Waveguide | 212 |
| 10.4 | Design Software Tools | 213 |
| 10.5 | Balun Holder | 215 |
| 10.6 | High-Temperature Modifications | 223 |
| 10.6.1 | Design Modifications | 223 |
| 10.6.2 | Heat Transfer Analysis | 225 |
| 10.7 | Affects of Air Bridges | 227 |
| 10.7.1 | Full Two-wire transmission line System | 228 |
| 10.7.2 | Back-to-Back Balun | 238 |
| 10.7.3 | Summary | 247 |
| 10.8 | Final Balun Design | 247 |
| Chapter 11 | Bench-Scale Experiment Results | 254 |
| 11.1 | Solid Material Measurement | 254 |
| 11.1.1 | Calibration | 256 |
| 11.1.2 | POM Measurement | 259 |
| 11.2 | Liquid Calibration | 262 |
| Chapter 12 | Conclusion and Future Work | 276 |

| | |
|---|----------------|
| Part IV Future Work and Conclusions | 278 |
| Chapter 13 Future Work | 279 |
| 13.1 Next Iteration | 279 |
| 13.2 Outstanding Challenges and Questions | 280 |
| 13.3 Future Directions | 280 |
| Chapter 14 Conclusion | 282 |
| 14.1 Fire Experiments | 282 |
| 14.2 Two-Wire Transmission Line | 283 |
| 14.3 Summary | 284 |
| APPENDICES | 285 |
| Appendix A Network Parameters | 286 |
| Appendix B Cable and Connector Information | 291 |
| Appendix C Further details on Sample Trough | 296 |
| Appendix D Weather Records | 299 |
| Appendix E Site Safety Plan | 301 |
| Appendix F Selected Pages from Laboratory Notebook 00010 | 303 |
| Appendix G Selected Pages from Laboratory Notebook 00011 | 316 |
| Appendix H VNA Data Collection Code | 333 |
| Appendix I Wavecalc Macros | 342 |
| Appendix J Arch Range | 345 |
| Appendix K IPython notebook: Single-Layer | 349 |
| Appendix L IPython notebook: Bullex-at-ORCBS-2013-08-08 | 359 |
| Appendix M IPython notebook: Bullex-at-BTFD-2013-12-06 | 371 |
| Appendix N IPython notebook: analysis-of-2015-02-15 | 382 |
| Appendix O IPython notebook: AR8200-data-fit | 397 |
| Appendix P IPython notebook: CPW-CPS-Impedance | 400 |
| Appendix Q IPython notebook: WireTemperature | 443 |

| | |
|---|------------|
| Appendix R IPython notebook: T-lineCalibration-diss | 451 |
| Appendix S IPython notebook: T-lineCalibration-With-Water-diss | 486 |
| BIBLIOGRAPHY | 508 |

LIST OF TABLES

| | |
|--|-----|
| Table 3.1: Summary of n_e and v_{eff} results published by Mphale. | 30 |
| Table 4.1: Experiment configuration for each sample. | 40 |
| Table 5.1: Measurements in EHS replicate sets and zero-fill time. | 68 |
| Table 6.1: Minimum thickness to meet the slab approximation criterion for select frequencies. | 85 |
| Table 6.2: Theoretical phase differences for various parameters. | 86 |
| Table 6.3: Summary of interferometric experiments. | 88 |
| Table 7.1: Lookup table for LM values to dBm. | 134 |
| Table 8.1: Summary of equations for the calculation of the circuit parameters of a two-wire transmission line. | 192 |
| Table 9.1: Summary of equations to calculate the S-parameters of a transition of a 1-port calibration. | 200 |
| Table 9.2: Summary of equations to calculate the S-parameters of transitions for a 2-port calibration. | 202 |
| Table 9.3: Relations between S-parameters and T-parameters. Reprint of Table A .1 | 203 |
| Table 11.1: Foam insert labels and thicknesses. | 256 |
| Table A .1: Relations between S-parameters and T-parameters [3, p. 541] and [123]. | 289 |
| Table B .1: Cable numbering scheme, lengths, connector type, gender, and label. . . | 292 |
| Table B .2: Results from gaging the assorted connectors in the lab. | 293 |
| Table B .3: Results of gaging the cables provided with the Satimo system. | 294 |

| | |
|---|-----|
| Table B .4: Results of gaging the 85052D calibration kit. | 295 |
| Table D .1: Observed temperature and humidity at the site of the experiment. | 300 |
| Table D .2: Weather observations from NOAA/NWS at Capitol City Airport in Lansing for May 30, 2013. | 300 |

LIST OF FIGURES

| | | |
|--------------|--|----|
| Figure 2.1: | Generic dispersion (ω - β) diagram. | 14 |
| Figure 2.2: | Dispersion (ω - β) diagram for a collisionless plasma. | 18 |
| Figure 2.3: | Dispersion (ω - β) diagram for a plasma with collisions. | 19 |
| Figure 4.1: | Material sample burning during an experiment. | 33 |
| Figure 4.2: | Diagram of experimental layout when the antennas were (a) 25.5 ft and (b) 9.5 ft away from the shelf. | 35 |
| Figure 4.3: | Schematic of experimental setup, (a) side view (b) top view. | 35 |
| Figure 4.4: | Photograph of the experimental setup showing the laser level, antennas, burning sample, wire shelf, sand, cable mats, wind indicator, video tripod, and instrumentation table. | 36 |
| Figure 4.5: | Metal holder used for metal plates, Plexiglas samples, and other planar samples. | 38 |
| Figure 4.6: | Material samples for the experiment. | 39 |
| Figure 4.7: | A purple sample with ignition sample removed and displayed. | 39 |
| Figure 4.8: | Ignition sample in aluminum foil tray. | 40 |
| Figure 4.9: | Example experimental setup in a laboratory setting. | 43 |
| Figure 4.10: | Plexiglas control measurements (S_{21}) compared to theoretical values for a lossless material with permittivity of 2.5. Each material is 1 in thick. | 44 |
| Figure 4.11: | Processed data from burn 1. The two curves at the front are for the Plexiglas standard. | 45 |
| Figure 4.12: | Processed data from burn 2. The two curves at the front are for the Plexiglas standard. | 46 |
| Figure 4.13: | Processed data from burn 3. The two curves at the front are for the Plexiglas standard. | 47 |

| | |
|--|----|
| Figure 4.14: Processed data from burn 4. The two curves at the front are for the Plexiglas standard. | 48 |
| Figure 4.15: Processed data from burn 5. The two curves at the front are for the Plexiglas standard. | 49 |
| Figure 4.16: Video stills from burn 4. The time stamps show the synchronized time for each camera. | 50 |
| Figure 4.17: Cardboard used to ignite cushions for samples b5 and b6. | 53 |
| Figure 5.1: Example fire extinguisher training using the Bullex Intelligent Training System. | 63 |
| Figure 5.2: Experimental setup at MSU EHS showing the Bullex system and wire shelf. | 65 |
| Figure 5.3: Ignited system during experiments at MSU EHS. | 66 |
| Figure 5.4: Schematic of the EHS experimental layout. | 67 |
| Figure 5.5: Dimensions of the burner. | 67 |
| Figure 5.6: Average measured transmission through a one inch thick Plexiglas sample. | 71 |
| Figure 5.7: Unwrapped phase of the average measured transmission through a one inch thick Plexiglas sample. | 72 |
| Figure 5.8: Average measured transmission through an ignited Bullex system. . . | 73 |
| Figure 5.9: Unwrapped phase of the average measured transmission through an ignited Bullex system. | 74 |
| Figure 5.10: Label for the donated Unifrax Fiberfrax Duraboard LD. | 76 |
| Figure 5.11: Photos from a burn using a Bullex system in a burn chamber. | 77 |
| Figure 5.12: Average measured transmission through a burn chamber with the Bullex system ignited. | 80 |
| Figure 5.13: Unwrapped phase of the average measured transmission through a burn chamber with the Bullex system ignited. | 81 |

| | | |
|--------------|---|-----|
| Figure 6.1: | Normalized phase difference versus frequency for a constant electron density. | 85 |
| Figure 6.2: | Minimum thickness to meet the slab approximation criterion versus frequency with reference lines for 1, 6, 9.5, and 20 GHz. | 86 |
| Figure 6.3: | Minimum thickness to meet the slab approximation criterion versus frequency with reference lines for 1, 6, 9.5, and 20 GHz. | 87 |
| Figure 6.4: | Schematic drawing of interferometer dimensions. | 88 |
| Figure 6.5: | Experimental setup in the ECE hood for interferometer measurements. | 90 |
| Figure 6.6: | Experimental setup in the cone calorimeter for interferometer measurements. | 91 |
| Figure 6.7: | Configuration of the metal shutter. | 92 |
| Figure 6.8: | Configuration of the metal shutter as seen from the side. | 93 |
| Figure 6.9: | Photo of a flame being drawn into the side of the shutter. | 94 |
| Figure 6.10: | Experimental setup for the mesh interferometer measurements. | 95 |
| Figure 6.11: | Transmission measurements in the mesh experimental setup in various configurations with no fire demonstrating the frequency limits of the mesh for shielding, panel 1 | 96 |
| Figure 6.12: | Transmission measurements in the mesh experimental setup in various configurations with no fire demonstrating the frequency limits of the mesh for shielding, panel 2 | 97 |
| Figure 6.13: | Transmission measurements in the mesh experimental setup in various configurations with no fire demonstrating the frequency limits of the mesh for shielding, panel 3 | 98 |
| Figure 6.14: | Phase difference in 3D from burning methanol for the ECE hood experiment. | 99 |
| Figure 6.15: | Phase difference from burning methanol for the ECE hood experiment. | 100 |
| Figure 6.16: | Phase difference in 3D from burning sodium chloride solution for the ECE hood experiment. | 100 |

| | |
|---|-----|
| Figure 6.17: Phase difference from burning sodium chloride solution for the ECE hood experiment. | 101 |
| Figure 6.18: Phase difference in 3D from burning methanol in the cone calorimeter experiment. | 102 |
| Figure 6.19: Phase difference from burning methanol in the cone calorimeter experiment. | 103 |
| Figure 6.20: Phase difference from burning sodium chloride solution in the cone calorimeter experiment. | 103 |
| Figure 6.21: Phase difference from burning salt in the cone calorimeter experiment. | 104 |
| Figure 6.22: Phase difference 3D from burning Plexiglas in the cone calorimeter experiment. | 104 |
| Figure 6.23: Phase difference from burning Plexiglas in the cone calorimeter experiment. | 105 |
| Figure 6.24: Phase difference 3D from burning methanol in the shutter experiment. | 106 |
| Figure 6.25: Phase difference from burning methanol in the shutter experiment. . | 107 |
| Figure 6.26: Phase difference 3D from burning a second sample of methanol in the shutter experiment. | 107 |
| Figure 6.27: Phase difference from burning a second sample of methanol in the shutter experiment. | 108 |
| Figure 6.28: Phase difference 3D from burning sodium chloride solution in the shutter experiment. | 108 |
| Figure 6.29: Phase difference from burning sodium chloride solution in the shutter experiment. | 109 |
| Figure 6.30: Phase difference 3D from burning Plexiglas in the shutter experiment. | 109 |
| Figure 6.31: Phase difference from burning Plexiglas in the shutter experiment. . . | 110 |
| Figure 6.32: Phase difference 3D from burning methanol in the mesh experiment. | 111 |
| Figure 6.33: Phase difference from burning methanol in the mesh experiment. . . | 112 |

| | |
|---|-----|
| Figure 6.34: Phase difference 3D from burning sodium chloride solution in the mesh experiment. | 112 |
| Figure 6.35: Phase difference from burning sodium chloride solution in the mesh experiment. | 113 |
| Figure 6.36: Summary panel of interferometric measurements, each with own color scale. | 113 |
| Figure 6.37: Summary panel of interferometric measurements normalized to the same color scale. | 114 |
| Figure 7.1: Plan view of the first story of the burn house. | 120 |
| Figure 7.2: Transmitter for 144 MHz. | 122 |
| Figure 7.3: Transmitter for 440 MHz. | 124 |
| Figure 7.4: 900 MHz transmitter setup. | 125 |
| Figure 7.5: Transmitters for Wi-Fi and 900 MHz XBee. | 127 |
| Figure 7.6: Placement of the 144 MHz transmitter. | 129 |
| Figure 7.7: Placement of the 440 MHz transmitter. | 130 |
| Figure 7.8: Placement of the 900 MHz XBee and Wi-Fi transmitters. | 131 |
| Figure 7.9: Receivers as positioned for measurements. | 132 |
| Figure 7.10: Photo showing the receiver location relative to the house including vehicles in between the two. | 133 |
| Figure 7.11: Best fit curve for the AR8200. | 135 |
| Figure 7.12: Receiving 900 MHz XBee module. | 136 |
| Figure 7.13: Measurement laptops and Wi-Fi receiver adapter (arrow). | 137 |
| Figure 7.14: Post-fire conditions for the 144 MHz transmitter. | 139 |
| Figure 7.15: Post-fire conditions in the 440 MHz transmitter room. | 140 |
| Figure 7.16: Post-fire conditions for the XBee and Wi-Fi transmitter. | 141 |

| | |
|--|-----|
| Figure 7.17: Post-fire condition of the 144 MHz transmitter room. | 142 |
| Figure 7.18: Post-fire condition of the ceilings in the 144 MHz and 440 MHz transmitter rooms. | 143 |
| Figure 7.19: Post-fire conditions in the living room. | 144 |
| Figure 7.20: Measured signal strengths before, during, and after the house burn. . . | 146 |
| Figure 7.21: Measured signal strengths near the time of the fire. | 147 |
| Figure 7.22: Temperature versus time from the XBee modules. | 147 |
| Figure 7.23: Example of a two-wire transmission line with an attached short circuit (right) and balun (left) manufactured for this work. | 151 |
| Figure 7.24: General notation used for a two-wire transmission line. | 152 |
| Figure 8.1: A single line charge. | 157 |
| Figure 8.2: Geometry of two line charges. | 158 |
| Figure 8.3: Examples of equipotential surfaces surrounding two line charges. . . . | 163 |
| Figure 8.4: The geometry of a two-wire transmission line. | 167 |
| Figure 8.5: Electric potential of a two-wire transmission line system. | 172 |
| Figure 8.6: Electric potential of a two-wire transmission line system. | 172 |
| Figure 8.7: Electric and magnetic fields of a two-wire transmission line. | 175 |
| Figure 8.8: Magnitude of electric field. | 175 |
| Figure 8.9: Magnitude of E_x | 176 |
| Figure 8.10: Magnitude of E_y | 176 |
| Figure 8.11: Radiation resistance for a two-wire transmission with line open, short, or purely reactive (resonant line); matched (non-resonant line); and $Z_0/2$ loads. | 180 |
| Figure 8.12: Circuit model for a differential length of transmission line. | 181 |

| | | |
|---------------|---|-----|
| Figure 9.1: | Block diagrams and signal flow graphs for (a) a one-port network and (b) a two-port network. | 194 |
| Figure 9.2: | Block diagram showing the transition that is to be removed and the one-port network that is to be measured. | 195 |
| Figure 9.3: | Illustration of calibration measurements showing the three different distances for a one-port calibration. | 198 |
| Figure 9.4: | Block diagram showing the transitions that are to be removed and the two-port network that is to be measured. | 200 |
| Figure 9.5: | Illustration of calibration measurements showing the six different distances for a two-port calibration. | 200 |
| Figure 10.1: | Illustration of the layout of transmission structures in a double-y balun. | 207 |
| Figure 10.2: | Schematic of CPW and CPS lines with common dimensions. | 208 |
| Figure 10.3: | A CPW to CPS double-y balun. | 208 |
| Figure 10.4: | Sample output from the IPython design notebook used to assist in conveying the optimized design.. . . . | 214 |
| Figure 10.5: | Assembly drawing for the balun support structure. | 217 |
| Figure 10.6: | Drawing for the main Plexiglas support structure. | 218 |
| Figure 10.7: | Drawing for manufacturing a shorting plate. | 219 |
| Figure 10.8: | Drawing showing critical dimensions for samples. | 220 |
| Figure 10.9: | Drawings for plastic pieces that clamp the cable when it first enters the holder. | 221 |
| Figure 10.10: | Drawing for the pieces that clamp the circuit board. | 222 |
| Figure 10.11: | An example of the metal rods lifting the traces off of the balun. | 225 |
| Figure 10.12: | Temperature at the tip of a 20 AWG, copper/tungsten wire versus the distance from the flame to the tip. | 226 |
| Figure 10.13: | Positioning of the air bridges (black lines) at the center of the balun. | 227 |

| | |
|---|-----|
| Figure 10.14: Experimental setup similar to that used for measuring the effective- ness of air bridges. | 228 |
| Figure 10.15: Measurement setup to test the air bridges. | 230 |
| Figure 10.16: Zoomed-in view of the right balun from Figure 10.15. | 231 |
| Figure 10.17: Two-wire transmission line system S-parameters with no air bridges installed. | 232 |
| Figure 10.18: Two-wire transmission line system S-parameters with air bridges in- stalled only at the “Y”s. | 233 |
| Figure 10.19: Two-wire transmission line system S-parameters with all air bridges installed. | 234 |
| Figure 10.20: Reflection measurement (S_{11}) of a two-wire transmission line system with various air bridges installed. | 235 |
| Figure 10.21: Transmission measurement (S_{21}) of a two-wire transmission line sys- tem with various air bridges installed. | 236 |
| Figure 10.22: Power balance for a two-wire transmission line system with various air bridges installed. | 237 |
| Figure 10.23: Back-to-back balun with all air bridges installed. | 239 |
| Figure 10.24: Back-to-back balun S-parameters with no air bridges installed. | 240 |
| Figure 10.25: Back-to-back balun S-parameters with air bridges installed only at the “Y”s. | 241 |
| Figure 10.26: Back-to-back balun S-parameters with all air bridges installed. | 242 |
| Figure 10.27: Reflection measurement (S_{11}) of a back-to-back balun with various air bridges installed. | 243 |
| Figure 10.28: Transmission measurement (S_{21}) of a back-to-back balun with vari- ous air bridges installed. | 244 |
| Figure 10.29: Power balance for a back-to-back balun with various air bridges in- stalled. | 245 |
| Figure 10.30: Power balance of all air bridges install for the transmission line system and the back-to-back balun. | 246 |

| | |
|---|-----|
| Figure 10.31: Manufactured double-y baluns. | 248 |
| Figure 10.32: Double-Y dimensional drawing, page 1. | 250 |
| Figure 10.33: Double-Y dimensional drawing, page 2. | 251 |
| Figure 10.34: Double-Y dimensional drawing, page 3. | 252 |
| Figure 10.35: CPW and CPS dimensions for the final double-y balun design. | 253 |
| Figure 11.1: Two-wire transmission line experimental setups. | 255 |
| Figure 11.2: Foam spacers used in calibration measurements. | 256 |
| Figure 11.3: Short circuit built for the two-wire transmission line. | 257 |
| Figure 11.4: One-port S-parameters of a short circuit located in four different positions along a two-wire transmission line. | 258 |
| Figure 11.5: One-port S-parameters of a short circuit located 13.6 mm from the Plexiglas holder by the foam I spacer. | 260 |
| Figure 11.6: Measurements of a POM sample layered between two foam spacers on a line terminated by a short circuit. | 261 |
| Figure 11.7: Balun with copper rods and copper short. | 262 |
| Figure 11.8: Liquid measurement experimental setup. | 263 |
| Figure 11.9: Calibrated one-port S-parameters for a transmission line with a short circuit in distilled water. | 265 |
| Figure 11.10: Liquid measurement container, page 1. | 268 |
| Figure 11.11: Liquid measurement container, page 2. | 269 |
| Figure 11.12: Liquid measurement container, page 3. | 270 |
| Figure 11.13: Liquid measurement container, page 4. | 271 |
| Figure 11.14: Liquid measurement container, page 5. | 272 |
| Figure 11.15: Liquid measurement container, page 6. | 273 |

| | |
|--|-----|
| Figure 11.16: Liquid measurement container, page 7. | 274 |
| Figure 11.17: Liquid measurement container, page 8. | 275 |
| Figure A .1: S-parameter block diagram and signal flow graph for a two-port network. | 287 |
| Figure C .1: Metal trough used to hold samples. | 297 |
| Figure C .2: Side view of the metal trough. | 297 |
| Figure C .3: Center view of the trough showing alignment cue. | 297 |
| Figure C .4: Top-down view of the trough showing alignment marks. | 298 |
| Figure F .1: Laboratory Notebook 00011:7 | 304 |
| Figure F .2: Laboratory Notebook 00011:14 | 305 |
| Figure F .3: Laboratory Notebook 00011:15 | 306 |
| Figure F .4: Laboratory Notebook 00011:16 | 307 |
| Figure F .5: Laboratory Notebook 00011:111 | 308 |
| Figure F .6: Laboratory Notebook 00011:112 | 309 |
| Figure F .7: Laboratory Notebook 00011:114 | 310 |
| Figure F .8: Laboratory Notebook 00011:126 | 311 |
| Figure F .9: Laboratory Notebook 00011:127 | 312 |
| Figure F .10: Laboratory Notebook 00011:128 | 313 |
| Figure F .11: Laboratory Notebook 00011:129 | 314 |
| Figure F .12: Laboratory Notebook 00011:130 | 315 |
| Figure G .1: Laboratory Notebook 00011:3 | 317 |
| Figure G .2: Laboratory Notebook 00011:4 | 318 |

| | |
|--|-----|
| Figure G .3: Laboratory Notebook 00011:5 | 319 |
| Figure G .4: Laboratory Notebook 00011:7 | 320 |
| Figure G .5: Laboratory Notebook 00011:8 | 321 |
| Figure G .6: Laboratory Notebook 00011:9 | 322 |
| Figure G .7: Laboratory Notebook 00011:10 | 323 |
| Figure G .8: Laboratory Notebook 00011:11 | 324 |
| Figure G .9: Laboratory Notebook 00011:12 | 325 |
| Figure G .10: Laboratory Notebook 00011:13 | 326 |
| Figure G .11: Laboratory Notebook 00011:14 | 327 |
| Figure G .12: Laboratory Notebook 00011:30 | 328 |
| Figure G .13: Laboratory Notebook 00011:31 | 329 |
| Figure G .14: Laboratory Notebook 00011:32 | 330 |
| Figure G .15: Laboratory Notebook 00011:78 | 331 |
| Figure G .16: Laboratory Notebook 00011:79 | 332 |
| Figure J .1: Arch range rail showing the degree markings. | 346 |
| Figure J .2: Dimensional drawing of the ruler used to mark angular distance along the rail of the arch range. | 347 |
| Figure J .3: Ruler used to mark angular distance the rail of the arch range. | 348 |
| Figure P .1: notebook figure | 415 |
| Figure P .2: notebook figure | 416 |
| Figure P .3: notebook figure | 426 |
| Figure P .4: notebook figure | 427 |

| | | |
|---------------|---------------------------|-----|
| Figure P .5: | notebook figure | 429 |
| Figure P .6: | notebook figure | 430 |
| Figure P .7: | notebook figure | 435 |
| Figure P .8: | notebook figure | 438 |
| Figure Q .1: | notebook figure | 446 |
| Figure Q .2: | notebook figure | 448 |
| Figure Q .3: | notebook figure | 450 |
| Figure R .1: | notebook figure | 458 |
| Figure R .2: | notebook figure | 460 |
| Figure R .3: | notebook figure | 461 |
| Figure R .4: | notebook figure | 462 |
| Figure R .5: | notebook figure | 465 |
| Figure R .6: | notebook figure | 466 |
| Figure R .7: | notebook figure | 469 |
| Figure R .8: | notebook figure | 470 |
| Figure R .9: | notebook figure | 474 |
| Figure R .10: | notebook figure | 476 |
| Figure R .11: | notebook figure | 477 |
| Figure R .12: | notebook figure | 479 |
| Figure R .13: | notebook figure | 480 |
| Figure R .14: | notebook figure | 481 |
| Figure R .15: | notebook figure | 482 |

| | |
|---|-----|
| Figure R .16: notebook figure | 483 |
| Figure R .17: notebook figure | 484 |
| Figure R .18: notebook figure | 485 |
| Figure S .1: notebook figure | 494 |
| Figure S .2: notebook figure | 495 |
| Figure S .3: notebook figure | 496 |
| Figure S .4: notebook figure | 497 |
| Figure S .5: notebook figure | 498 |
| Figure S .6: notebook figure | 499 |
| Figure S .7: notebook figure | 501 |
| Figure S .8: notebook figure | 502 |
| Figure S .9: notebook figure | 504 |
| Figure S .10: notebook figure | 505 |

Part I

Motivation, Objective, and Background

Chapter 1

Motivation and Objective of this Work

1.1 Motivation

When fighting a house fire, the primary goal of firefighters is to save lives; in addition, firefighters are concerned with protecting property and the environment [1]. Knowing whether there is someone inside of a burning house dictates how these goals are reached. Currently there are no tools to tell firefighters if someone is still inside of a burning house. Instead, firefighters rely on bystanders for information about occupants and use clues such as children's toys outside, cars in the driveway, and the time of day to determine the likelihood of someone being inside. None of this information, however, tells a firefighter where a victim is actually located. Radar offers a possible solution to this problem, allowing for faster rescues and fewer fire fatalities. Providing firefighters with more definitive knowledge of the victims' whereabouts inside of a fire will enable firefighters to better assess risks, plan actions, and protect the lives of both occupants and firefighters.

Searching a fire structure for a trapped victim is a tedious, time-consuming, and dangerous process. Smoke causes limited visibility; high temperatures make some areas inaccessible; and firefighters must watch for structural failures. Firefighters may be able to stand and look

through a room if there is no smoke, heat, or fire. More often, though, they must crawl under heavy smoke and search the house using only their senses of touch and hearing. Searches are done in an ordered manner that emphasizes covering all areas in a thorough but time consuming process. Although firefighters are trained to work with speed and efficiency, the current methods for finding and rescuing victims of house fires are slow and inefficient.

Thermal imaging cameras (commonly called thermal imagers or TICs) are the most advanced pieces of technology available today for firefighters to conduct search-and-rescue operations for trapped victims. These handheld devices use infrared (IR) emissions to display a thermal image on a small screen. Smoke does not typically obscure this image; however, many common household items, such as floors, windows, mirrors, or furniture, do obscure or create false thermal images.

The ideal search-and-rescue equipment would allow a firefighter to access critical information about a burning building, such as the building layout, structural health/stability, status of utilities (electricity, gas, water), fire location and spread, air movement, and victim locations. For fire commanders, the equipment would be able to track firefighters as they move within the building. After the main fire is out, firefighters perform “overhaul” to identify where small fires and hot spots remain in the structure; the ideal equipment would allow firefighters to complete this overhaul process without having to tear apart walls, ceilings, and floors.

Radar offers an imaging modality that may provide firefighters with their ideal solution. In the last decade, military applications have driven research priorities for through-wall radar. Doppler shifts and movement detection are two techniques used by through-wall radar to locate people behind an obstacle. This type of radar could help firefighters locate victims in structures, but flames can generate a plasma that can be problematic for current radar technologies.

While it is known that radio waves interact with plasmas differently than other media [2], there has been limited research on understanding fire-induced plasmas and even less work to understand how radar interacts with fire-induced plasmas. The overarching goal of the work

described here is to improve the understanding of how fire-induced plasmas and radar interact, with the longer-term goal of improving imaging techniques for firefighters.

In addition to improving search-and-rescue operations, there are other potential applications and uses of through-wall radar for firefighting such as:

- locating fires of different sizes (ranging from individual hot spots to fully involved rooms),
- detecting hazards caused by a fire such as backdraft, which is a dangerous explosion, or flashover, when an entire room instantly ignites, and
- detecting flow paths of air that affect fire behavior.

Far-reaching uses that would require significant research and development include fire extinguishment and assisting in on-scene tracking of responders

It is easy to see that through-wall radar offers significant potential benefits to fire victims and to firefighters conducting a search-and-rescue operation for trapped victims, yet there are many years of research and development ahead in order to bring radar technologies to the fire ground.

1.2 Objective

The broader goal of this research is to assist firefighters in minimizing the time that it takes to find a trapped victim, thus improving fire victims' chances of survival. In a narrower scope, the objective of this work is to investigate the interaction between electromagnetic waves and fire-induced plasmas using basic laboratory equipment and existing radar systems. This is not intended to be a development of a radar system.

Chapter 2

Basic Theory of Fields and Plasmas

In order to understand the interaction between electromagnetic fields and fire-induced plasmas, this chapter lays out the basics of electromagnetic fields, waves, and plasmas. This general, mathematical discussion is the foundation for the experimental design and result analysis later in this dissertation.

Assumption

The focus of this chapter will be unmagnetized plasmas in the form of a homogeneous slab that is infinite in two dimensions and transverse electromagnetic (TEM) waves.

For these types of plasmas and waves, the interaction between fields and plasmas depends on frequency and parameters of the plasma. This means that below some frequency, essentially no radar waves will propagate through the fire-induced plasma. At a high enough frequency, the fire will have no effect on the radar waves. The questions investigated herein are what are the particular frequency ranges of interest and to what extent are the radar waves affected?

2.1 Electromagnetic Fields and Waves

Electric and magnetic fields together constitute electromagnetic fields. They may be independent of one another; however, they are coupled to one another if they change in time. This is shown by Maxwell's equations which are the governing equations for electromagnetic fields.

Maxwell's equations in differential form are [3, §3.6]

$$\begin{aligned}\nabla \cdot \vec{D} &= \rho \\ \nabla \cdot \vec{B} &= 0 \\ \nabla \times \vec{E} &= -\frac{\partial \vec{B}}{\partial t} \\ \nabla \times \vec{H} &= \vec{J} + \frac{\partial \vec{D}}{\partial t}\end{aligned}\tag{2.1}$$

where \vec{D} is the electric flux density, ρ is the electric charge density, \vec{B} is the magnetic flux density, \vec{E} is the electric field, \vec{H} is the magnetic field, \vec{J} is the electric current density, t is time, and ∂ is the partial differential.

An important case is when the electric and magnetic fields vary sinusoidally in time. In this case, the fields may be expressed in terms of the complex exponential $e^{j\omega t}$ where $j = \sqrt{-1}$ represents a complex number, which is often expressed as i in other disciplines; and $\omega = 2\pi f$ is the angular frequency and f the frequency in Hertz. Multiplying a quantity, called a phasor, by $e^{j\omega t}$ and taking the real part gives the time-varying form of the quantity. Appendix 4 of [3] covers phasors in more detail.

Assumption

The time convention $e^{+j\omega t}$ is used throughout this work.

Maxwell's equations may be expressed using phasors as [3, §3.8]

$$\begin{aligned}
\nabla \cdot \vec{D} &= \rho \\
\nabla \cdot \vec{B} &= 0 \\
\nabla \times \vec{E} &= -j\omega \vec{B} \\
\nabla \times \vec{H} &= \vec{J} + j\omega \vec{D}.
\end{aligned} \tag{2.2}$$

While the fields are denoted in the same way in both of the above forms, those in Equation (2.1) are for instantaneous values while the fields in Equation (2.2) represent phasors. The time and positional dependence of the fields above and elsewhere are implicit, as is common in the literature.

To study the interactions between fields and plasmas, the plasma is expressed as regular matter, referred to as a medium in electromagnetics, and a special model for the permittivity, ϵ , of the plasma is used. Interactions between fields and linear, isotropic media require the following constitutive relations [3, §3.6]:

$$\vec{J} = \sigma \vec{E} \tag{2.3}$$

$$\vec{D} = \epsilon \vec{E} \tag{2.4}$$

$$\vec{B} = \mu \vec{H} \tag{2.5}$$

where σ is the conductivity, ϵ is the permittivity, and μ is the permeability of the material. Regular dielectrics have a relative permittivity greater than one; however, plasmas can have a relative

permittivity less than one as will be shown later. It is common to express permittivity and permeability as relative values, denoted by the subscript r ,

$$\epsilon = \epsilon_0 \epsilon_r \quad (2.6)$$

$$\mu = \mu_0 \mu_r \quad (2.7)$$

where ϵ_0 and μ_0 represent the permittivity and permeability of free space, respectively. The speed of light in free space is defined as

$$c_0 = 299,792,458 \text{ m/s} \approx 3 \times 10^8 \text{ m/s} \quad (2.8)$$

$$= \frac{1}{\sqrt{\mu_0 \epsilon_0}} \quad (2.9)$$

and will be used later to simplify equations. The permeability of free space is defined as

$$\mu_0 = 4\pi \times 10^{-7} \text{ H/m}. \quad (2.10)$$

This gives the value of the permittivity of free space as

$$\epsilon_0 = \frac{1}{\mu_0 c_0^2} = 8.854187817620389 \times 10^{-12} \text{ F/m} \quad (2.11)$$

For a given material, the permittivity may be expressed as

$$\epsilon = \epsilon' - j\epsilon''. \quad (2.12)$$

The imaginary portion, ϵ'' , captures losses in the material. These losses are commonly expressed through either the conductivity, σ , or the loss tangent, $\tan\delta$, depending on whether

the material is considered a conductor or a dielectric, respectively. These three parameters are related by

$$\epsilon'' = \sigma / \omega = \epsilon_0 \epsilon_r \tan \delta. \quad (2.13)$$

Permittivity may also be expressed as

$$\epsilon = \epsilon \left(1 - j \frac{\sigma}{\omega \epsilon} \right). \quad (2.14)$$

Other models exist to represent the permittivity of a material, such as the model presented later in this chapter for a plasma.

Another useful constant is the intrinsic impedance of a medium,

$$\eta = \sqrt{\frac{\mu}{\epsilon}} \quad (2.15)$$

In the case of free space [3, p. 276],

$$\eta_0 = \sqrt{\frac{\mu_0}{\epsilon_0}} = 367.73 \approx 120\pi\Omega. \quad (2.16)$$

The intrinsic impedance represents the ratio of the electric field to the magnetic field. Given the electric field, the magnetic field may be calculated using

$$\vec{H} = \frac{\hat{k} \times \vec{E}}{\eta}. \quad (2.17)$$

The quantity k is the complex wave number. It is used here to represent the direction of propagation for a wave. Further discussion appears with Equation (2.25).

Energy is transferred from point to point by electromagnetic waves. These waves consist of coupled electric and magnetic fields that vary in space and time, and are solutions to the

wave equation. In Sections 3.8–3.11 of their book [3], Ramo, Whinnery, and Van Duzer provide a derivation from Maxwell's equations to the wave equation,

$$\nabla^2 \vec{E} = \mu\epsilon \frac{\partial^2 \vec{E}}{\partial t^2}. \quad (2.18)$$

The above three-dimensional wave equation reduces to the one-dimensional case,

$$\frac{\partial^2 E_x}{\partial z^2} = \mu\epsilon \frac{\partial^2 E_x}{\partial t^2}, \quad (2.19)$$

in rectangular coordinates that is known as the one-dimensional Helmholtz equation. The E-field in Equation (2.19) is directed in the x direction as denoted by the subscript. The forms are similar for y and z directed electric fields. In phasor notation, the wave equation is

$$\frac{\partial^2 E_x}{\partial z^2} = -\omega^2 \mu\epsilon E_x. \quad (2.20)$$

One possible representation of the solution is the plane-wave solution [3, §3.10],

$$E_x = c_1 e^{-jkz} + c_2 e^{+jkz}, \quad (2.21)$$

where c_1 and c_2 are real constants. The time-varying form of Equation (2.21) is

$$E_x(z, t) = \text{Re} \left\{ E_x e^{j\omega t} \right\} \quad (2.22)$$

$$= \text{Re} \left\{ c_1 e^{-jkz} e^{j\omega t} + c_2 e^{+jkz} e^{j\omega t} \right\} \quad (2.23)$$

$$= c_1 \cos(\omega t - kz) + c_2 \cos(\omega t + kz). \quad (2.24)$$

Here k is the complex wave number defined as

$$k = \beta - j\alpha. \quad (2.25)$$

The parameters β and α can be frequency dependent, thereby making k frequency dependent. The wave number is also medium dependent and is calculated using any of the following relations:

$$k = \omega \sqrt[\pm]{\mu\epsilon} \quad (2.26)$$

$$= \omega \sqrt{\mu_0\epsilon_0} \sqrt[\pm]{\mu_r\epsilon_r} \quad (2.27)$$

$$= \frac{\omega}{c_0} \sqrt[\pm]{\mu_r\epsilon_r}. \quad (2.28)$$

The \pm on the square root function has been used to remind the reader to select the appropriate sign for the physics of the problem since plasmas behave differently than more common media and may require special cases. In this work β and α should both be positive. The physical meaning of α and β is seen when $k = \beta - j\alpha$ is substituted into Equation (2.24).

$$E_x(z, t) = \text{Re} \left\{ c_1 e^{-j(\beta-j\alpha)z} e^{j\omega t} + c_2 e^{+j(\beta-j\alpha)z} e^{j\omega t} \right\} \quad (2.29)$$

$$= \text{Re} \left\{ c_1 e^{-\alpha z} e^{-j\beta z} e^{j\omega t} + c_2 e^{+\alpha z} e^{+j\beta z} e^{j\omega t} \right\} \quad (2.30)$$

$$= c_1 e^{-\alpha z} \cos(\omega t - \beta z) + c_2 e^{+\alpha z} \cos(\omega t + \beta z). \quad (2.31)$$

It is common to reference some constant point on a sinusoid when looking at the behavior of the argument, for example the maximum or the zero crossing. As time t increases, the position z of the reference point must also increase. The c_1 sinusoid is therefore a wave traveling in the positive z direction and the c_2 sinusoid is traveling in the negative z direction. The phase of the wave is kept constant by β , hence β is named the phase constant. The parameter α is only

in the exponential terms of Equation (2.31) and hence determines how quickly the sinusoid attenuates (decays) or grows, hence the name attenuation constant. As the c_1 wave propagates in the positive z direction, it decays. The c_2 wave also decays as it propagates even though the exponential looks to be growing. Since the wave is propagating in the negative z direction, z decreases and the exponential term decays.

In the wave, the argument of the cosine should be constant. In order for this to occur, the positional term βz must be proportional to the time term ωt . The ratio ω/β determines this relationship. Since $\omega = 2\pi f$ has units of radians per seconds and β has units of radians per meter, the ratio has units of meters per second. It is therefore a velocity and is known as the phase velocity of the wave,

$$v_{ph} = \frac{\omega}{\beta} = \frac{1}{\sqrt{\mu\epsilon}} = \frac{c_0}{\sqrt{\mu_r\epsilon_r}}. \quad (2.32)$$

The phase velocity may also be expressed as $v_p = f\lambda$ where λ is the wavelength. The wavelength is the distance between two successive points with the same phase, e. g. the peak of the first wave to the peak of the second wave. Rearranging this expression as well as making substitutions provides various forms for the calculation of the wavelength [4, p. 51],

$$\lambda = \frac{v_p}{f} = \frac{2\pi}{\beta}. \quad (2.33)$$

Because β can be frequency dependent, the phase velocity can vary with frequency. This means that waves of different frequencies will travel at different rates. If the waves together carry information, such as the envelope in an AM radio broadcast, then this information may be distorted, an effect called dispersion, by the differences in phase velocity. A medium that

causes dispersion is said to be dispersive. The information itself travels at a rate that is different than the phase velocity and known as the group velocity,

$$v_g = \frac{d\omega}{d\beta} \quad (2.34)$$

$$= \frac{v_p}{1 - (\omega/v_p)(dv_p/d\omega)}. \quad (2.35)$$

The idea that the group velocity represents the “velocity of energy travel” is appropriate for this dissertation but is not always true; see Ramo *et al.* [3, pp. 260–264] and their references of [5, pp. 330–340] and [6]. If v_g is constant, then no dispersion occurs. This is akin to saying that the phase velocity is equal for all frequencies. Normal dispersion occurs if $v_g < v_{ph}$. If $v_g > v_{ph}$, then the dispersion is known as anomalous dispersion [7, p. 269]. A backward propagating wave occurs if $v_g < 0$. The group velocity is always less than or equal to the speed of light, while v_{ph} is greater than or equal to the speed of light in a vacuum, c_0 . The phase velocity is able to be greater than the speed of light without violating the theory of relativity because no physical quantity (mass or energy) is moving at this speed [3, p. 303].

A common way to conceptualize the frequency dependence of a media is to create a dispersion diagram, which is also known as an ω - β diagram. While frequency is usually the independent variable in figures and is placed on the horizontal axis, a dispersion diagram conventionally makes frequency the dependent variable and plots ω along the vertical axis versus α or β . Figure 2.1 shows a generic ω - β plot. First, the dotted, blue line is the dispersion relation for free space, i. e. $\omega = c_0\beta_0$, and is known as the light line. The slope of the light line is constant, therefore there is no dispersion in free space. The solid, red line is the frequency response of β . Shown are reference lines for group and phase velocities. We see that the group velocity is the slope of β and that the phase velocity is the slope of the line going from the origin to β . Because the slope of β in Figure 2.1 is not constant, the generic medium represented is dispersive. Finally the dashed, green line is the frequency response of α . When β goes to zero, the group

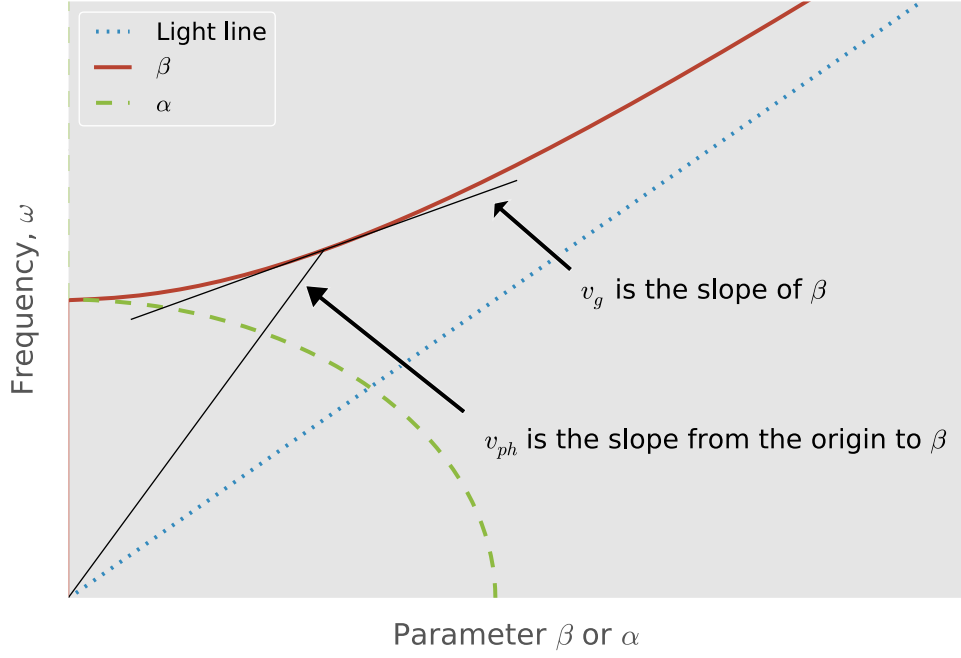


Figure 2.1: Generic dispersion (ω - β) diagram.

velocity becomes zero which means no information is carried by a wave in the medium and the phase velocity is infinity. This frequency is known as the cut-off frequency because propagation is cut off at frequencies below it. At this point it is easy to see these velocities if we examine the behavior of the reference velocity lines at this point. The group velocity line would be horizontal and the phase velocity line would be vertical giving the aforementioned velocity values.

2.2 Plasmas

Plasmas are generally known as the fourth state of matter; in simple terms, plasmas are hot, ionized gases. More precisely, plasmas are “macroscopically neutral substances containing many interacting free electrons and ionized atoms or molecules, which exhibit collective [effects] due

to long-range Coulomb forces... [They possess] enough kinetic energy to overcome, by collisions, the binding energy of the outermost orbital electrons" [2, pp. 1–2].

The following four criteria must be satisfied for matter to be in a plasma state [2, chap. 1]:

1. the overall size must be large compared to the characteristic length,
2. the electron density inside a Debye sphere (described below) must be large,
3. it must be macroscopically charge neutral, and
4. electron oscillations should not be overly damped by collisions.

Assumption

To discuss these criteria for a plasma, values will be used that represent a flame from a plant-based fuel, such as grasses or pine needles. These values were selected from the literature review in Chapter 3 and are discussed further there. The electron density is $n_e = 1 \times 10^{16} \text{ m}^{-3}$, the collision frequency is $\nu_{\text{eff}} = 1 \times 10^{10}$ collisions per second, and the temperature is around 866 K (1000°F).

2.2.1 Characteristic Length

The Debye Length, λ_D , is the characteristic length for a plasma given by

$$\lambda_D = \sqrt{\frac{\epsilon_0 k_B T}{n_e e^2}} \quad (2.36)$$

where $k_B = 1.3806488 \times 10^{-23} \text{ J/K}$ is the Boltzmann constant, T is the temperature in Kelvin, n_e is the electron density, and $e = 1.6021766208 \times 10^{-19} \text{ C}$ is the elementary charge. The Debye length describes the distance over which the electric field from one charged particle affects other charged particles. Given the above values for a flame, the Debye length is approximately 0.02 mm. Almost all flames are large compared to this length, especially those found in a house fire.

2.2.2 Debye Sphere

A Debye sphere is the sphere surrounding a particle that has a radius of λ_D . To shield the charged particle at the center of the sphere from the effects of electrostatic fields outside of the sphere, there must be a large number of charged particles inside the sphere. Effectively, a particle only interacts with those particles that are contained inside its own Debye sphere. This shielding of the center particle is known as collective shielding or Debye shielding, and is an important characteristic of all plasmas. The expression

$$n_e \lambda_D^2 \gg 1 \quad (2.37)$$

should be true in order for collective shielding to be effective in a Debye sphere. The left hand side is roughly 80 for the selected flame values, thereby satisfying this criterion.

2.2.3 Charge Neutrality

As a consequence of the collective shielding observed in a Debye sphere, the plasma on the whole should be charge neutral.

2.2.4 Collision Dampening

In order for a plasma to not lose energy and become a neutral gas, the collision frequency, ν_{eff} , must be less than the plasma frequency,¹ ω_{pe} , i. e. $\nu_{\text{eff}} < \omega_{\text{pe}}$, [2, p. 10]. The plasma frequency,

$$\omega_{\text{pe}} = \sqrt{\frac{n_e e^2}{m_e \epsilon_0}} \quad (2.38)$$

¹In an open system with an energy input, i. e. non-adiabatic, the collision frequency may be greater than the plasma frequency if the net energy gain rate is greater than the collisional losses.

where m_e is the mass of an electron, is the angular frequency at which electrons oscillate inside the plasma in order to remain neutrally charged on average after having been displaced by small disturbing forces. The collision frequency is the rate at which free electrons collide with and transfer energy to heavier, relatively-stationary particles.

For the generic flame-plasma parameters, $\nu_{pe} = \omega_{pe}/2\pi \approx 9 \times 10^9$. Earlier ν_{eff} was selected to be 1×10^{10} . We see that these two values are comparable. Because of this, flame-plasmas are sometimes classified as weakly-ionized plasmas.

2.3 Plasma Model for Electromagnetic Fields

Assumption

As stated earlier, the focus here is on unmagnetized plasmas.

Of interest for this dissertation is how electromagnetic waves interact with plasmas. Maxwell's equations and the constitutive equations presented in Section 2.1 govern how the fields will interact with the plasma if it is modeled as a dielectric. An acceptable model for the permittivity of an unmagnetized plasma is [2, p. 412], [7, p. 216],

$$\epsilon_r = \frac{\epsilon}{\epsilon_0} = \left[1 - \frac{\omega_{pe}^2}{\omega^2 + \nu_{\text{eff}}^2} \right] - j \frac{\omega_{pe}^2 \nu_{\text{eff}}}{\omega (\omega^2 + \nu_{\text{eff}}^2)}. \quad (2.39)$$

Using this as the permittivity of the plasma, we are able to treat the plasma as a regular medium and carry out traditional analysis such as propagation studies, material characterization, or transmission line problems. A consequence of the condition that the plasma is unmagnetized is that the plasma is isotropic, meaning that the transmission through the plasma will be the same regardless of the direction of travel through the plasma.

First, we notice that ϵ_r is a complex value dependent not only upon plasma parameters, but also frequency. As frequency increases, the real part approaches one and the imaginary part approaches zero. Thus at sufficiently high frequencies, determined by the plasma properties,

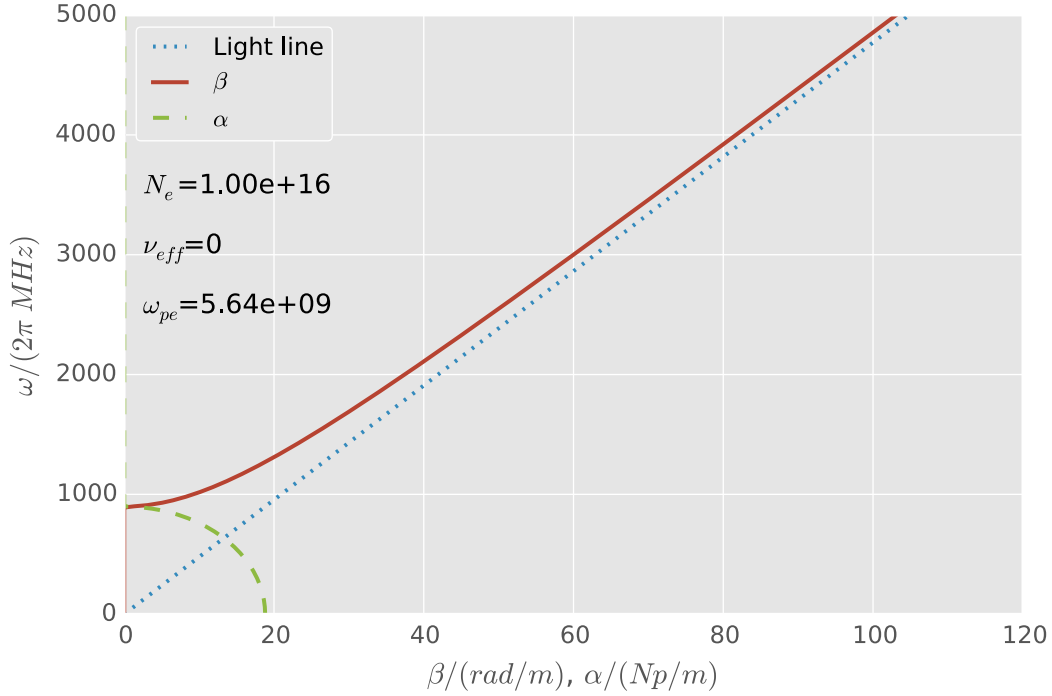


Figure 2.2: Dispersion (ω - β) diagram for a collisionless plasma.

the plasma appears to be free space. This is reasonable given that at extremely high frequencies, the particles cannot oscillate quickly enough to keep up with the changing fields [2, p. 407]. At lower frequencies, the real portion will be less than one, even negative. A typical dielectric has a real part greater than one. The imaginary part of the model will always be negative signifying that the plasma is lossy. In a collisionless plasma the imaginary part is equal to zero and the plasma is lossless since $\nu_{\text{eff}} = 0$.

In Figure 2.2 we see the cut-off and free-space behavior discussed above. At the lowest frequencies, absorption is highest. It decreases to zero at the plasma frequency, at which point the phase constant begins to increase. At higher frequencies, the phase constant approaches the light line meaning that the plasma has less of an effect on the electromagnetic fields.

Figure 2.3 shows the case for a plasma with collisions. We see that both α and β are zero at zero frequency. At low frequencies, both begin to grow. Again at the higher frequencies,

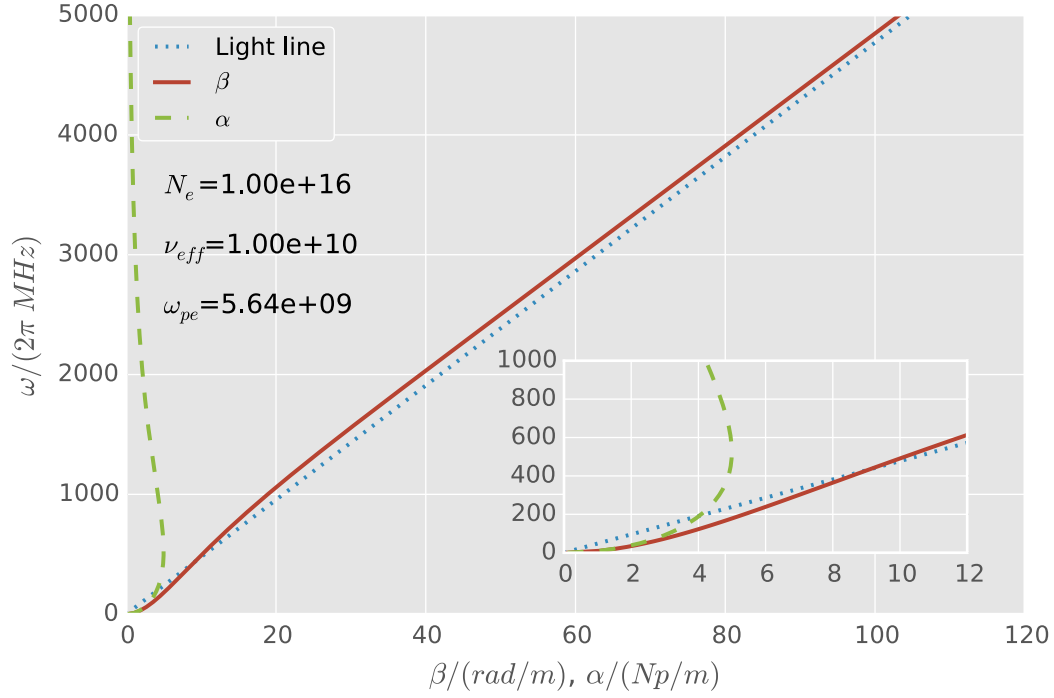


Figure 2.3: Dispersion (ω - β) diagram for a plasma with collisions.

the plasma approaches free-space behavior (losses tend towards zero and the phase constant approaches that of free space, β_0). Unlike the collisionless case, there is no abrupt cut-off behavior. The attenuation is very large, however, and it is reasonable for there to be some region where the wave is “cut off” because the attenuation is relatively large.

It was assumed in the above discussion that the plasma was semi-infinite, homogeneous slab. If the plasma is not homogeneous and there exist density gradients, the properties of the plasma will change spatial. In this case, dispersion and gradual reflection will occur.

Chapter 3

Literature Review

The following literature review shows that flames can affect electromagnetic waves at a laboratory scale and for certain fuels. It also reviews work on electromagnetic waves interacting with plant-fueled fires of various sizes. Through this review, no prior work was found studying how electromagnetic waves and flames from common household items interact. Understanding this background information is important in order to find people trapped by a house fire using radar. Below is a review of the current literature on the interaction between electromagnetic waves and flames.

3.1 Early Work

Research into electromagnetic propagation through flames began in the 1940s by Sugden at the University of Cambridge [8]. In this paper, a 10 GHz wave was attenuated by 0.6 dB/cm by the flame produced at the end of a rifle barrel when the rifle was fired.

Following this initial paper, a series of four papers were authored by Sugden and his students in the early 1950s [9–12]. Work began by studying the attenuation of a coal-gas/air flame between 3 GHz and 37.5 GHz [9]. The flame was 1.45 cm wide and was artificially seeded with

This chapter began as a class project for BE 820 during the Fall 2012 semester.

alkali-metal salts. The flame temperature was roughly 2200 K. Through attenuation measurements, it was found that the flame had an electron number density of $n_e = 2.0 \times 10^{17} \text{ m}^{-3}$ and a collision frequency of $\nu_{\text{eff}} = 8.8 \times 10^{10} \text{ s}^{-1}$. Later work by Sugden found the electron number density to be $n_e = 0.8 - 1.5 \times 10^{17} \text{ m}^{-3}$ for a hydrogen-air flame seeded with alkali salts [11]. Flame temperatures in this case were between 1900 K and 2000 K. It is important that the flames were seeded with alkali-metal salts. This group of elements has relatively low ionization energies, which allows for the electrons to be easily removed and ensures that a plasma would form in the flame. Additionally, we know that the ionization is the result of the flame temperature and not the combustion reaction since the alkali metals are not responsible for combustion in these types of flames.

In 1954 Adler studied clean, unseeded flames from pure jet fuel. Flame temperatures were around 1920 K. Using propagation theory, it was found that the electron number density was $n_e = 1.9 \times 10^{12} \text{ m}^{-3}$ and that the collision frequency was $\nu_{\text{eff}} = 6.5 \times 10^8 \text{ s}^{-1}$ [13]. This shows that unseeded flames create a weaker plasma than seeded flames (as expected). The importance of this result is that it is not necessarily the fuel that dictates that plasma parameters but other constitutive materials that may be brought into the combustion region through some mass transport mechanism.

Also in 1954, Shuler studied unseeded hydrogen-oxygen and acetylene-oxygen flames for various fuel-air ratios [14]. He found that the electron number density varied between $2.3 - 6.3 \times 10^8 \text{ cm}^{-3}$ for hydrogen-oxygen flames, $1.42 - 1.66 \times 10^{10} \text{ cm}^{-3}$ for lean acetylene-oxygen flames, and $0.644 - 3.47 \times 10^{10} \text{ cm}^{-3}$ for rich acetylene-oxygen flames. In the acetylene-oxygen flames, the highest electron number density occurred when the flame was the hottest at 3285 K. This last result is expected because the charged particles would have higher average kinetic speeds and energies leading to more ionized particles.

There is little published literature on this topic from the late 1950's to the 2000's. Other work that is somewhat related (refraction, plasmas, atmospheric propagation) went on; however, no one seemed to pick up Sugden's work, which is not highly cited.

3.2 Wildland Fire Papers

The most recent research relating to electromagnetic wave propagation through flames has come from Dr. Johnathan Boan at the University of Adelaide [15–19] and Drs. Mphale and Heron at James Cook University in Australia [20–33]. The work at James Cook University was done in collaboration with the University of Botswana. Collectively these works investigated how electromagnetic waves propagate through fires fueled by organic matter specifically related to Australian wildland fires. These papers are discussed in the following sections.

3.3 Losses in Wildland Fires Investigated by Boan

Jonathan Boan, a student of Associate Professor Chris Coleman, submitted his PhD thesis titled *Radio Propagation in Fire Environments* in 2009 to the University of Adelaide, Australia [19]. During his time as a student, Boan had a Workshop on the Applications of Radio Science best student paper [16], two IEEE Antennas and Propagation Society (AP-S) Symposium papers [15, 18], and an IEEE Antennas and Wireless Propagation Letter [17] according to his personal bibliography listed at the front of his thesis [19]. All of these papers focused on propagation through fire and include both simulations and experiments. Boan's work investigated the loss mechanisms associated with a wildland fire flame front. He breaks down wave propagation into refraction, scattering, and plasma effects as described next.

3.3.1 Loss Mechanisms

Refraction is the physical phenomena that changes the direction of travel of a wave when it pass from one medium to a second medium that has a different index of refraction, $n = \sqrt{\mu_r \epsilon_r}$ for real values of μ_r and ϵ_r [3, p. 278]. Refraction is numerically calculated using Snell's law that describes the relationship between the incident angle, θ_1 , in medium 1 with the real index of refraction n_1 and the refracted angle, θ_2 , in medium 2 with the real index of refraction n_2 and is given by [34]

$$\frac{\sin \theta_1}{\sin \theta_2} = \frac{n_2}{n_1}. \quad (3.1)$$

For gases this may also be expressed in terms of temperature, pressure, and the concentrations of constitutive substances of the gas. All of these have large gradients around a fire resulting in varying indices of refraction as one moves towards the center of the flame. Moving inward, subrefractive conditions can occur that lead to waves being bent upwards and away from a receiving antenna in-line with the transmitting antenna [16]. Subrefraction causes waves to bend away from the ground instead of being bent down towards it, or being ducted through the atmosphere. Both subrefraction and ducting are nonstandard means of propagation [35]. Subrefraction occurs when the index of refraction increases with height rather than decreases, which occurs under normal atmospheric conditions.

Scattering occurs when a wave is deflected in one or multiple directions different than the original. During a fire, waves are primarily scattered through two mechanisms [16]. The first is scattering from smoke particulates and small particles entrained in the fire plume. The second is scattering due to changes in the index of refraction. Not all energy carried in a wave is transferred through an interface between media when it is refracted; some of the energy is reflected from the interface. Air turbulence is also included in this second cause of scattering. Swirling and mixing air around the fire will result in additional scattering [36–43]. Boan does not include

scattering in any of his analyses, instead noting this as an area of future work [19]. He also overlooks the scattering from entrained particles, writing that “the changes in the refractive index are known to be small and therefore strong scattering is not expected [16].”

During combustion, charged particles are created through chemical ionization as part of the chemical reaction of combustion and through thermal ionization [19, 20, 44]. According to Boan, thermal ionization is the primary cause of charged particles in a fire [19]. The primary species ionized during combustion of plant based fires is thought to be alkali-metals and graphitic carbon [25]. This thermal ionization may be due to the relatively low ionization energies of alkali metals [45].

3.3.2 FDTD Simulations

Boan began his work by studying finite-difference, time-domain [46] (FDTD) simulations of electromagnetic propagation through flames. Boan had identified refraction, scattering, and combustion-induced plasma as the three primary loss mechanisms at the beginning of [16]. In order to simplify the work at this stage of his research, Boan did not consider scattering from the flame or smoke particles in [15] or [16].

FDTD simulations typically require a great deal of memory and time to solve large (in terms of wavelength) simulation domains. Numerical dispersion is common when the simulated time scale is relatively long. Wildland fires are physically large events, spanning from tens of feet to tens of miles. Flame height can range from inches to over fifty feet. These physically large, and even larger in terms of wavelengths, dimensions make simulation of wildland fires difficult.

Boan has used the work of Akleman and Sevgi related to tropospheric propagation to manage the large domain [47]. Akleman and Sevgi present a 2-D, FDTD technique that may be used for propagation problems over long distances. This technique uses a broad-band pulse that is traced over the length of the simulation domain by a spatial window so that the entire simulation domain does not need to be held in memory for the duration of the simulation.

Since combustion creates a weakly-ionized gas, Boan combines the above FDTD technique with the work of Nickisch and Franke [48] to add a cold plasma model to [47]. Boan further enhances his FDTD simulations by adding work from Young [49] to properly simulate the expected dispersion caused by the flame being a lossy medium. This is done by “evaluating the polarization current of the medium [15]” by altering the standard forms of Maxwell’s equations to

$$\epsilon \frac{\partial \vec{E}}{\partial t} = \nabla \times \vec{H} - \sigma \vec{E} - \vec{J}_p \quad (3.2)$$

$$\mu \frac{\partial \vec{H}}{\partial t} = -\nabla \times \vec{E} \quad (3.3)$$

to include a term for the polarization current,

$$\frac{\partial \vec{J}_p}{\partial t} = -\nu_{\text{eff}} \vec{J}_p + \epsilon_0 \omega_p^2 \vec{E}. \quad (3.4)$$

In [15] and [16], Boan considers TE_z polarization and models the ground as a perfect electrical conductor. Boan’s code uses the FDTD approach of Lan [50] with a higher order algorithm from Zygidis [51] and artificial anisotropy [15] to handle dispersion.

Boan also notes that the settling time of the simulation medium must be taken into account. He states that the polarization current will have short settling times because “the collision frequency [ν_{eff}] under atmospheric pressures is normally very high $\sim 10^{11} \text{ sec}^{-1}$ [15]” according to data published by Itikawa [52].

The effects of refraction and how it is implemented in these simulations is discussed in [16, 19] and is originally presented in [34] and [53]. For a gas, the Lorentz-Lorenz relation is [34]

$$\alpha = \frac{3}{4\pi n_{\text{mol}}} \frac{\epsilon - 1}{\epsilon + 2} = \frac{3}{4\pi n_{\text{mol}}} \frac{n^2 - 1}{n^2 + 2} \quad (3.5)$$

where α is the electric polarizability of the gas, n_{mol} is the number density of the molecules in the gas, and n is the refractive index for the gas. Values for the electric polarizability may be found in reference text such as the *CRC Handbook* [45]. This can be written as

$$L_1 = \frac{n^2 - 1}{n^2 + 2} = \frac{4\pi n_{\text{mol}}}{3} \alpha = \frac{4\pi}{3} \frac{\rho N_A}{M} \alpha \quad (3.6)$$

where L_1 denotes the Lorentz-Lorenz coefficient, ρ is the density of the gas, N_A is Avagadro's number, and M is the molecular weight of the gas¹. For a homogenous gas mixture in a known, reference state (denoted by the superscript \circ) the Lorentz-Lorenz coefficient is given as [53]

$$L^\circ = \sum_i \frac{(n_i^\circ)^2 - 1}{(n_i^\circ)^2 + 2} = \sum_i \rho_i^\circ \left(\frac{4\pi N_A \alpha_i}{3M_i} \right) \quad (3.7)$$

where the sum is over the values for each gas in the mixture. Ciddor [53] then gives the Lorentz-Lorenz coefficient for a mixture at an unknown state

$$L = \sum_i \frac{\rho_i}{\rho_i^\circ} \frac{(n_i^\circ)^2 - 1}{(n_i^\circ)^2 + 2}. \quad (3.8)$$

The index of refraction for the gas mixture in this unknown state is therefore

$$n = \sqrt{(1 + 2L)/(1 - L)}. \quad (3.9)$$

The ideal gas law may be used to express the Lorentz-Lorenz coefficient as a function of variables besides pressure. Boan uses Equation (3.8) and Equation (3.9) to calculate the index of refraction in simulations for air composed of nitrogen, oxygen, and carbon dioxide [16].

¹In [19] Equation (3.6) instead has the term α^{-1} . This is believed to be a mistake probably made during typesetting as dimensional analysis and [34] reach the expression given here.

A simple numerical simulation is carried out in [15] that uses a 2D Gaussian temperature distribution

$$T = 300 + 1050 \exp \left(- \left(\frac{x - 100}{20} \right)^2 - \left(\frac{y}{15} \right)^2 \right) \quad (3.10)$$

where T is the temperature in Kelvin while x and y are position variables in meters. Boan uses alkali-metal concentrations of 0.57% for potassium, 0.58% for calcium, and 0.43% for magnesium for simulations. He references [20] for a description on how these values are used to calculate electron density in the flame. This calculation is further developed in later work by Mphale and discussed in Section 3.4.

Results from this Gaussian temperature distribution show that at the maximum temperature, which would be the center of the flame, attenuation is temperature dependent near the ground. Above the temperature distribution little attenuation is observed. As one moves further away from the maximum temperature, signal strength begins to recover. A simulation was conducted with no plasma effects which Boan uses to suggest that refraction alone has only minor effects on the wave when propagating through the temperature distribution. Given a spatially longer temperature distribution, and hence a longer propagation path, Boan suggests that refraction effects would be more influential.

A more complex simulation was carried out in [16]. Here data from an actual fire in Jarrahdale, Western Australia, published in [54], was used to create a Fire Dynamics Simulator [55] (FDS) simulation. Trees were 8 m in height. Boan used a pilot fire for ignition of the entire simulation and included a $3 \text{ m} \cdot \text{s}^{-1}$ wind.

Results concerning the effect of refraction caused by the fire suggest that refraction has only a small effect on propagation; Boan posits that the wave is pushed upwards by refraction. The signal strength does appear to widen or rise as it propagates; however, this could simply be due

to the wave expanding or it could be caused by the antenna pattern. It could also be caused by numerical dispersion that has not been properly corrected.

Effects of fire-induced plasmas seem more definitive, but how Boan separated the effects is not described in the text. Assuming that plasma and refractive effects may be separated, we can conclude that a fire-induced plasma affects signal propagation. In the published figures for a radio frequency of 150 MHz, plasma effects are greatest in what appear to be the highest temperature regions of the fire. Below 1200 K there appears to be little reduction in signal strength. As temperature increases, signal strength decreases. Assuming that Boan's simulation has been coded to only add plasma effects (and ones that are dependent on flame temperature), it is plausible that electromagnetic waves are effected by fires, albeit only in the hottest regions of the flame. This is expected if the plasma is primarily generated by thermal ionization as suggested by Boan. Molecules would only be ionized in the hottest regions of the flame because this is the only area in which significant energy exists.

One of Boan's contribution is the integration of FDS data into the FDTD simulations so that a more realistic temperature profile from a fire may be simulated. It does not appear that these simulations include scattering or dielectric effects of the fuel.

3.4 Experimental Measurements Conducted by Mphale

A large body of work on the topic of electromagnetic wave propagation through fire has been produced by Dr. Kgakgamatso Mphale and his advisor Dr. Mal Heron. Mphale was a PhD student at James Cook University, Australia, and also associated with the University of Botswana. He was supported by the Staff Development Office of the University of Botswana and by Emergency Management Australia (EMA) under project number 60/2001. One of Mphale's earliest works was the project report for EMA [20].

Mphale carried out numerous studies using an experimental burner. The hexagonal wood frame was lined with 20.3 cm (8 in) thick Fiberfrax insulation to create a 50 cm (19.69 in) diameter, circular burn chamber. Cutouts for X-band horn antennas (8.0–12.0 GHz) were placed on opposite sides to facilitate transmission and reflection RF measurements. On the other four sides, two 25 mm (1 in) holes were drilled to allow air flow into the burner [21, 24, 25, 29–32].

Fuels for these burns were ground litter that had fallen from *Eucalyptus platyphylla* (poplar gum or eucalyptus) and *Pinus Caribea* (pine) trees along with *Panicum maximum* (Guinea grass). Samples were dried in the laboratory for at least ten days. These fuels were selected because of their prevalence in Australia. Some samples were washed, dried and prepared for inductively coupled plasma-atomic emission analysis to determine the alkali and alkaline content [30]. Each fuel was burned individually in the constructed burner and arranged so that flames would fully cover the bottom surface of the burner. As was noted in [17, 19], waves propagating above a fire suffer relatively little degradation—instead propagation needs to be through the flame to observe an interaction. The burner was constructed and fuel was loaded so that for the majority of the time that fuel was burning, waves propagated through the flame [30].

Results from Mphale’s experiments are presented as signal losses, electron densities, and collision frequencies. Intermediate data is not reported. This is primarily due to observation that the absorption of a plasma is related to n_e and ν_{eff} , hence those are the important factors to report [56]. A summary of results from Mphale’s experiments and three simulations are presented in Table 3.1. The bottom row summarizes the ranges seen in all experimental data only, i. e. the summary row does not include simulations).

The first two results are from simulations where the fuel had 0.5% and 3.0% potassium, respectively, to represent generic, plant-based fuel. The objective of [27] was to demonstrate a variance in plasma characteristics based on potassium content, which is important in wildland fires because trace alkali metals in plants are the primary contributor to plasmas for this fuel

Table 3.1: Summary of n_e and ν_{eff} results published by Mphale.

| n_e/m^{-3} | $\nu_{\text{eff}}/\text{s}^{-1}$ | Fuel | Ref. |
|--------------------------------|----------------------------------|---------------------------|----------|
| 6.3×10^{15} | - | 0.5% Potassium Simulation | [27] |
| 1.5×10^{16} | - | 3.0% Potassium Simulation | [27] |
| $0.51 - 1.35 \times 10^{16}$ | $3.43 - 5.97 \times 10^{10}$ | Pine | [24, 25] |
| $0.76 - 3.21 \times 10^{16}$ | $1.11 - 2.44 \times 10^{10}$ | Pine | [30] |
| 2.63×10^{16} | - | Guinea Grass | [29] |
| $0.32 - 1.18 \times 10^{16}$ | $2.80 - 3.95 \times 10^{10}$ | Guinea Grass | [30] |
| 5.061×10^{15} | 1.0×10^{11} | Prescribed Grassfire | [33] |
| 2.26×10^{16} | 5.84×10^{10} | Eucalyptus | [21] |
| 2.19×10^{16} | 6.18×10^{10} | Eucalyptus | [21] |
| 3.40×10^{16} | - | Eucalyptus Simulation | [26] |
| 1.46×10^{16} | - | Eucalyptus | [29] |
| $0.77 - 1.47 \times 10^{16}$ | $1.47 - 3.52 \times 10^{10}$ | Eucalyptus | [30] |
| $0.5061 - 3.40 \times 10^{16}$ | $1.11 - 6.18 \times 10^{10}$ | - | - |

type. The tabulated results show that as potassium content increases, electron number-density increases as well.

The prescribed grassfire in [33] was a plot of land on the James Cook University campus that had a perimeter of 393 m and a RF propagation path of roughly 44 m. Ray tracing was used in [26] to calculate path losses. All other results listed in the table are from experiments carried out in the hexagonal burn chamber.

Table 3.1 shows that the expected electron number for a wildland fire is on the order of 10^{16} m^{-3} and that the collision frequency is on the order of 10^{10} s^{-1} .

Mphale has developed a theoretical background and an experimental setup that allows for an accurate analysis of electromagnetic propagation through flames. He allows for variability in data and thoughtfully analyzes the results.

3.5 Conclusion

Initial work in the 1950's demonstrated that fire-induced plasmas can have an effect on propagating electromagnetic waves. Recent work has shown that plant-based fuels burned during a fire can produce weakly ionized plasmas. These plasmas have somewhat localized effects, primarily in the most intense combustion zones. Recent research has focused on the effect that large wildland fires may have on handheld radio communications. Of interest to this review is the effect that fire-induced plasmas could have on search-and-rescue radar during a house fire. Certainly a fully engulfed compartment fire will reach sufficient temperatures to create a plasma to some extent. Further research is needed in order to determine how compartment fire behavior and common household fuels create fire-induced plasmas and affect wave propagation. This literature review has found no research that addresses these issues to date.

Part II

Large-scale Fire Experiments

Chapter 4

Radio Wave Transmission Through Furniture Cushion Flames



Figure 4.1: Material sample burning during an experiment.

This research began with an experiment designed to evaluate ideas about how to measure and study the interaction between electromagnetic waves and fire-induced plasmas. To do this, an outdoor measurement range was set up at the City of Lansing (MI) Fire Department's (LFD) training site that consisted of two antennas with a burning sample in between them. This produced a flame that directly interfered with the transmission path. Sofa cushions were used for samples as they could be readily obtained while being similar to one another for replication purposes. The goal was to evaluate the experimental setup, experimental techniques, and the analytical techniques which would be used in later work.

4.1 Experimental Methods

The setup and design of this experiment was based on experience with other transmission measurements in a laboratory setting, fire fighting experience, and rough estimates. Equipment constraints dictated some of the setup while cautionary steps to protect the equipment dictated other aspects. The main experimental setup consisted of two tripod-mounted antennas, a wire shelf on which samples were burned, and a measurement unit. Ancillary equipment included a laser level and video cameras. A diagram of the layout is shown in Figure 4.2, a schematic of the measurement setup is shown in Figure 4.3, and a photo of the experiment is shown in Figure 4.4

Samples were placed on a wire shelf in the middle of an asphalt-covered area. A wire shelf was used because it could withstand direct contact with flames, was acquired for a low cost, could be easily cleaned, and had an adjustable height. While it was expected that the metal shelf would itself affect the transmissions, we planned to remove the effects through post-processing of the data.

Two antennas were placed approximately 9.5 ft or 25.5 ft from the shelf, depending on the dataset in a roughly north-south line. There were no specific reasons for these distances other than trying to limit the fire danger to the antennas and that the asphalt was in decent condi-

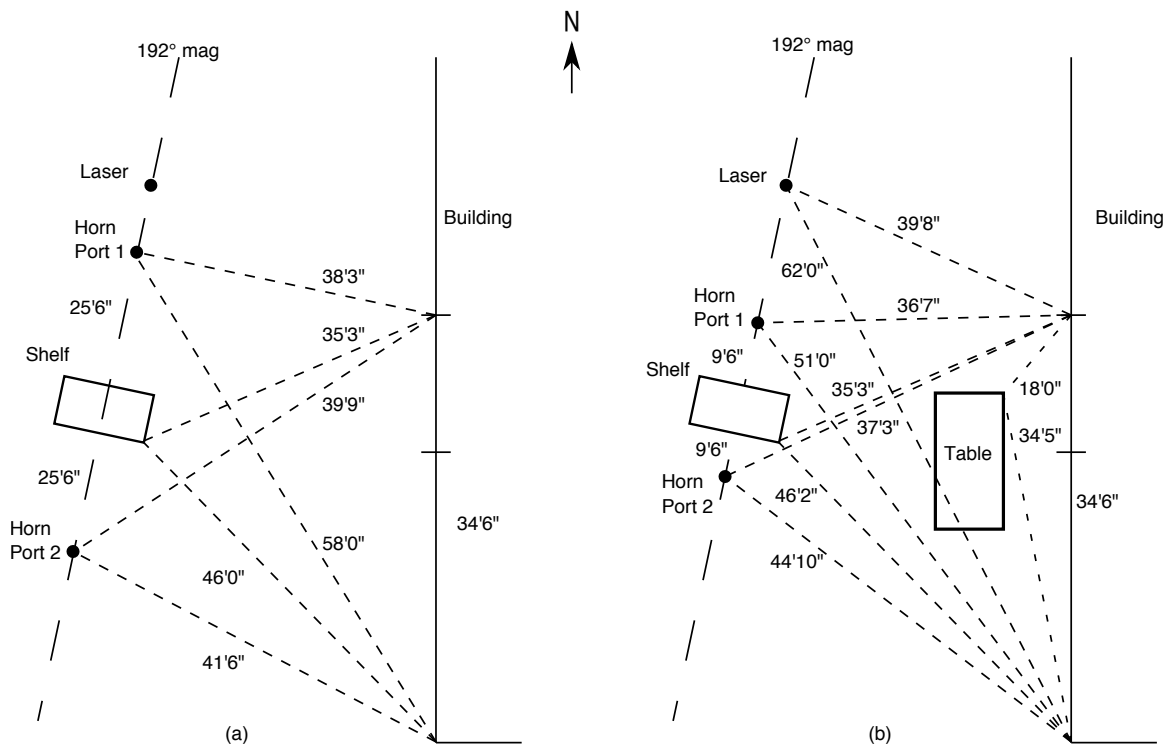


Figure 4.2: Diagram of experimental layout when the antennas were (a) 25.5 ft and (b) 9.5 ft away from the shelf.

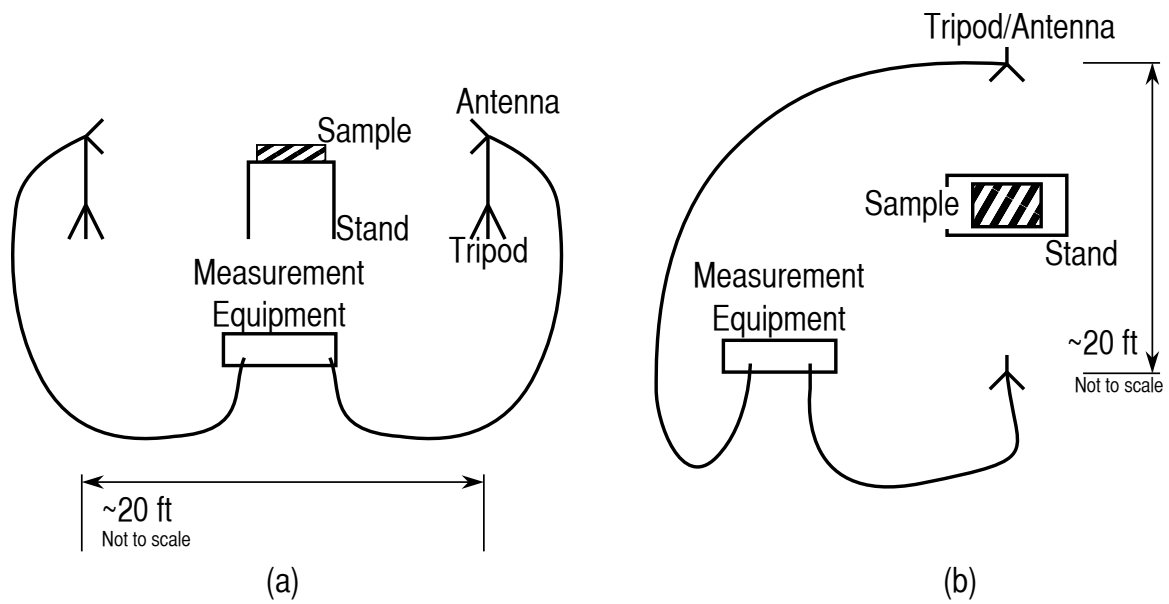


Figure 4.3: Schematic of experimental setup, (a) side view (b) top view.

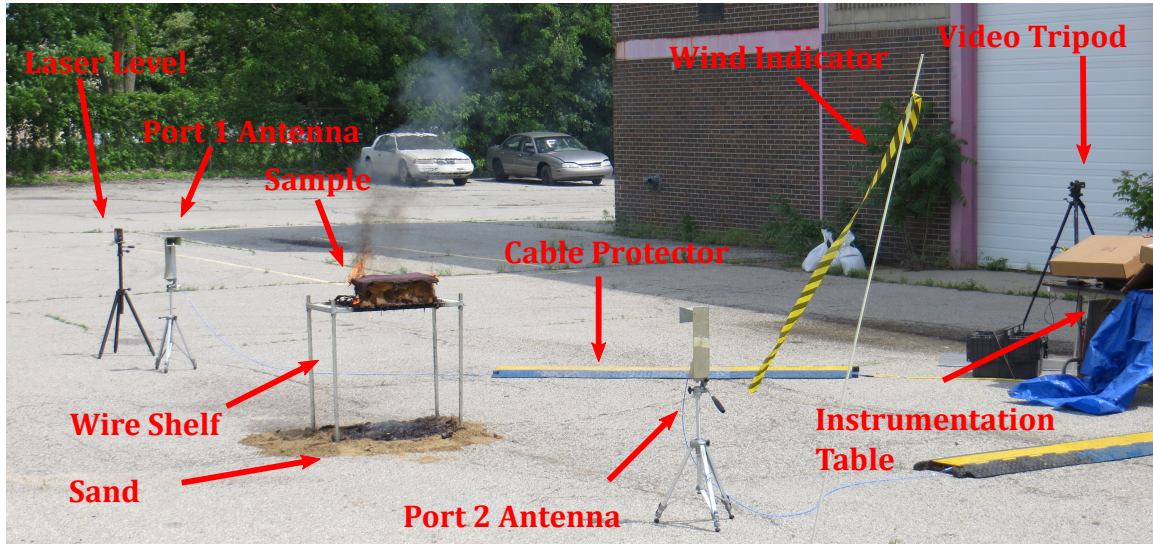


Figure 4.4: Photograph of the experimental setup showing the laser level, antennas, burning sample, wire shelf, sand, cable mats, wind indicator, video tripod, and instrumentation table.

tion at those spots. The antennas were American Electronic Laboratories H-1498 broadband horn antennas covering the frequency range of 2 GHz to 18 GHz. The antennas and shelf were squared to one another along the measurement line using a laser level, which emitted vertical and horizontal lines. Sand was spread underneath the shelf in order to capture slag from the burned samples and to protect the asphalt.

A measurement unit (HP8753D Vector Network Analyzer (VNA) connected to a laptop using a USB-GPIB) was located east of the shelf on a folding table designated as the instrumentation table. Cables were run from each antenna to the measurement unit underneath cable protectors/mats¹. A tarp was set up so that the instruments could be easily covered in the event of rain. Cardboard was used to cover the VNA and the laptop from the sun to allow for easier reading of the displays and to help keep instrument temperatures more constant. Transmission properties (S_{21}) were recorded during the experiment as quickly as the VNA could acquire data using the Python code found in Appendix H. A full-two port calibration using an Agilent 85052D

¹Extending from port 1 of the VNA to the northern antenna were cables numbered 013, 039, and 038 with appropriate adapters. Extending from port 2 of the VNA to the southern antenna were cables numbered 040, 037, and 046 with appropriate adapters. Information about individual cables can be found in Appendix B.

3.5 mm economy mechanical calibration kit was performed at the end of the cables so that the measurement reference planes were the ports of the antennas.

Data was further calibrated through post-processing which used measurements of an essentially empty measurement range and of a metal plate, placed normal to the direction of propagation in the same location where samples would be. Post-processing correction used the following general formula:

$$S_{21}^{corr} = \frac{S_{21}^{meas} - S_{21}^{plate}}{S_{21}^{empty} - S_{21}^{plate}} \quad (4.1)$$

where *corr* is the corrected dataset, *meas* is the dataset to be corrected, *plate* is the dataset for a plate calibration standard, and *empty* is the dataset for a transmission path with no sample [57, 58]. The objects that were in the *empty* range measurement were those that would be there when the sample was burned, e.g. the wire shelf. A Plexiglas sample, 2 ft by 2 ft by 1 in thick, was measured as an experimental control before each sample was burned. This sample has been measured in the lab multiple times over the years by other students and also before this experiment. This data was processed in the same way as other data and was used to check the performance of the measurement system by comparing it to laboratory measurements and published data.

In order to keep the metal plate and the Plexiglas samples vertical, they were placed into a metal trough as shown in Figure 4.5. Wood shims were used to hold the metal or Plexiglas in place and ensure that the plate was vertical. The *empty* measurement used for Plexiglas samples contained the metal trough which was not in the *empty* for the samples. By including the trough in the Plexiglas *empty* measurements, we could account for its effects in the appropriate measurements. The burning samples were not affected since that paired *empty* did not include the trough. Additional details about the trough are in Appendix C .

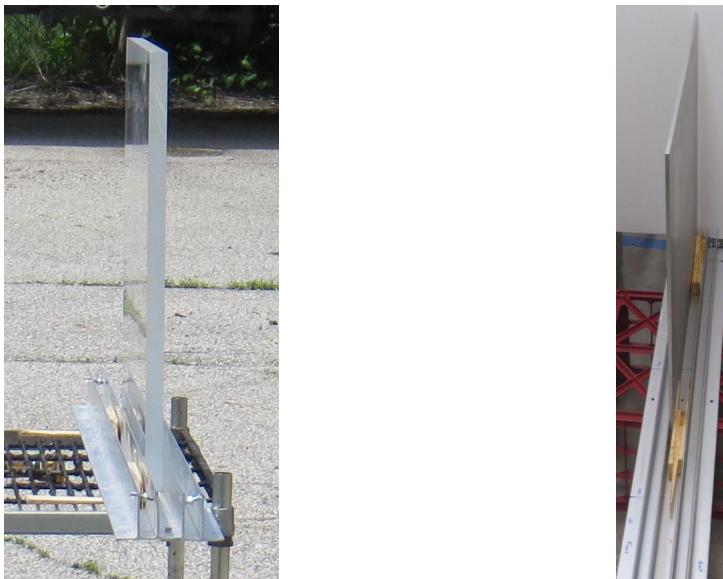


Figure 4.5: Metal holder used for metal plates, Plexiglas samples, and other planar samples.

Weather observations were made because the ambient temperature can have an effect on equipment stability, likewise, wind can effect the fire behavior. A combination digital thermometer and hygrometer was placed on the instrumentation table. Observed weather and official NOAA/NWS observations from the Lansing airport are recorded in Appendix D .1. Black and yellow striped surveying tape was attached to a fiberglass pole and placed SSW of the measurement line as a wind indicator. This wind indicator is visible in some video and photographs.

Video cameras were placed on tripods just north of the instrumentation table and to the SSE of the measurement line. Videos were manually started and stopped before and after each sample.

Samples for this experiment were furniture cushions obtained from the MSU Surplus Store as individual cushions at no cost. No information about the cushion material or flame retardants was available. There were two different styles of cushion as seen in Figure 4.6; five were of a smaller size with purple and blue upholstery, which will be referred to as purple samples, and two were of a larger size with orange upholstery, which will be referred to as orange samples.



Figure 4.6: Material samples for the experiment.

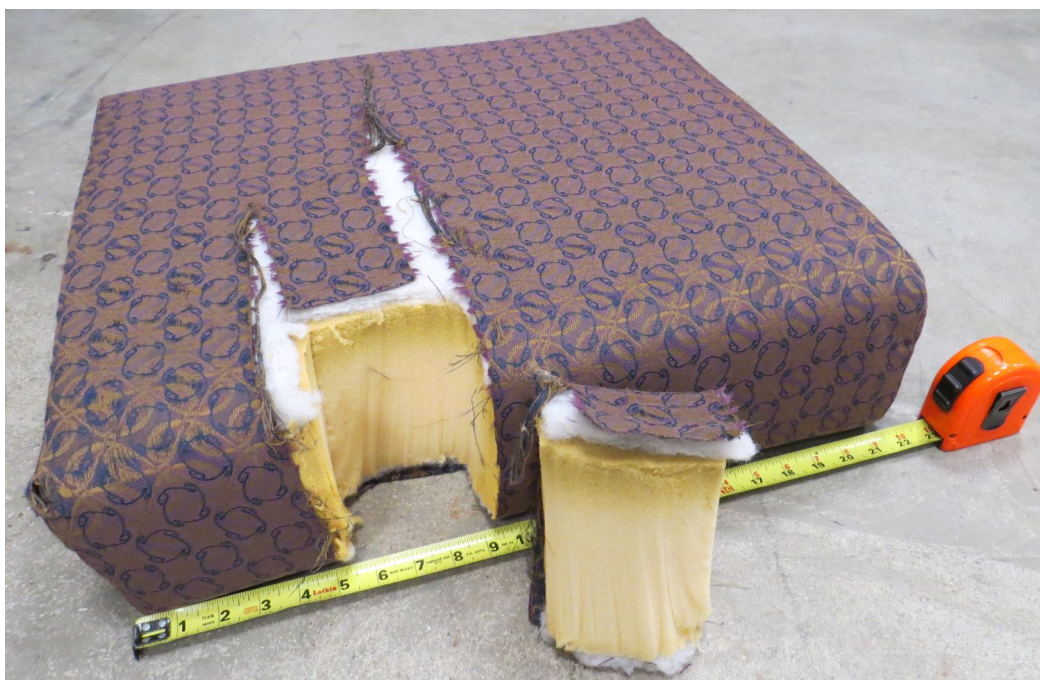


Figure 4.7: A purple sample with ignition sample removed and displayed.

A BernzOmatic TS3000 propane torch was used to ignite samples. Prior to the experiment day a piece was cut out of a purple sample, Figure 4.7, placed in an aluminum foil tray, and ignited using the torch, Figure 4.8. The small sample ignited relatively easily once the torch burned through the upholstery and the foam had direct flame contact. A sustained flame was observed until the solid foam was combusted or melted at which point a pool fire remained. It appeared that the samples had some sort of flame retardant but that ignition for the experiment would not be problematic. Ignition on the day of the experiment turned out to be more difficult than expected, as discussed later.



Figure 4.8: Ignition sample in aluminum foil tray.

Table 4.1: Experiment configuration for each sample.

| Burn | Sample | Antenna Dist Ft | Start GHz | Stop GHz | Num Pts | IFBW Hz | Avg Fact | Power dBm |
|------|--------|--------------------|--------------|-------------|---------|------------|----------|--------------|
| B1 | Purple | 25.5 | 2 | 6 | 1601 | 3000 | 4 | 10 |
| B2 | Purple | 25.5 | 2 | 6 | 1601 | 3000 | 4 | 10 |
| B3 | Orange | 9.5 | 2 | 6 | 1601 | 3000 | 4 | 10 |
| B4 | Orange | 9.5 | 2 | 6 | 1601 | 3000 | 4 | 10 |
| B5 | Purple | 9.5 | 2 | 6 | 1601 | 3000 | 4 | 10 |
| B6 | Purple | 9.5 | 2 | 6 | 26 | 3000 | 4 | 10 |

A total of six samples were measured. The seventh sample was kept for future small-scale tests and as a reference². This sample was the one used in the ignition investigation. The configuration for each sample is shown in Table 4.1.

²It turns out the primary use for this remaining sample has been as a shock absorber for the VNA during transportation. The VNA is placed on top of the cushion when transported to further dampen road vibrations that may damage the VNA.

4.2 General Measurement Procedure

The general experiment procedure was as follows:

1. Measure with only metal sample tray on wire shelf
2. Measure a metal plate
3. Measure a known Plexiglas sample
4. Measure only the wire shelf
5. Measure the sample
6. Ignite sample
7. Measure throughout the burn
8. (Self) Extinguish
9. Remove sample
10. Repeat 1–7 for remaining samples
11. Repeat 1–2 after all samples burned

4.3 Safety Precautions

The following safety precautions were observed:

- A safety briefing upon MSU's arrival in the morning and before the first burn
- Everyone was made aware of the RF cables and told not step on, drive over, impact, nor load any cable

- Appropriate personal protective equipment (PPE) was worn when needed
- A site safety plan was prepared for this experiment. This can be found in Appendix E .1.

A handline was stretched and charged from the fire hydrant in the southwest corner of the LFD facility. Additionally a fire extinguisher was at the instrumentation table ready for use.

LFD personnel were present in the morning to assist with setting up the facility and to give the go-ahead for the experiment.

4.4 Go/No-Go Criteria

The following criteria were used to determine if the experiment could begin or was to be interrupted:

- Unsafe wind conditions (No go)
- Imminent rain (No go)
- Final approval of LFD personnel (Go)

4.5 Results

Data from the experiment were post-processed by time gating and normalizing using Equation (4.1). A rectangular window was used to time gate the data to 40 ns for burns 1 and 2, and to 17 ns for the other burns using the program WaveCalc provided by Dr. Ross of John Ross and Associates. The length of time for the window was selected to block out any received signals after the direct signal was received. Figure 4.9 shows a calibration plate being measured in the lab to illustrate the experimental setup. Plates and empty measurements were taken before burns 1, 2, 3, and 6. Burns 4 and 5 were processed using the calibration measurements from burn 3.



Figure 4.9: Example experimental setup in a laboratory setting.

Data for sample B6 were not analyzed because this dataset was taken at twenty-six frequency points instead of 1601 points. The number of points was reduced to try to decrease the time between datasets; however, this resulted in lowering the time resolution (required for gating) to an unusable level.

A one-inch thick sample of Plexiglas was used as a control material. Plexiglas has a permittivity of about $\epsilon_r = 2.5$ [59]. Data taken just before burning samples 1, 2, and 3 were analyzed and compared to the theoretical results for Plexiglas using the IPython notebook in Appendix K. Figure 4.10 shows the results for sample 3.

Figure 4.11 through Figure 4.15 show the data for each of the first five experiments. The front axis is frequency in GHz, the right axis is the data sample number and represents increasing time, and the vertical axis is phase in degrees. The front two curves in each figure are the results for the known Plexiglas sample. This provides a control measurement for comparison.

Figure 4.16 shows video stills from burn 4. Video was taken of all experiments. The two cameras were synchronized after the experiments.

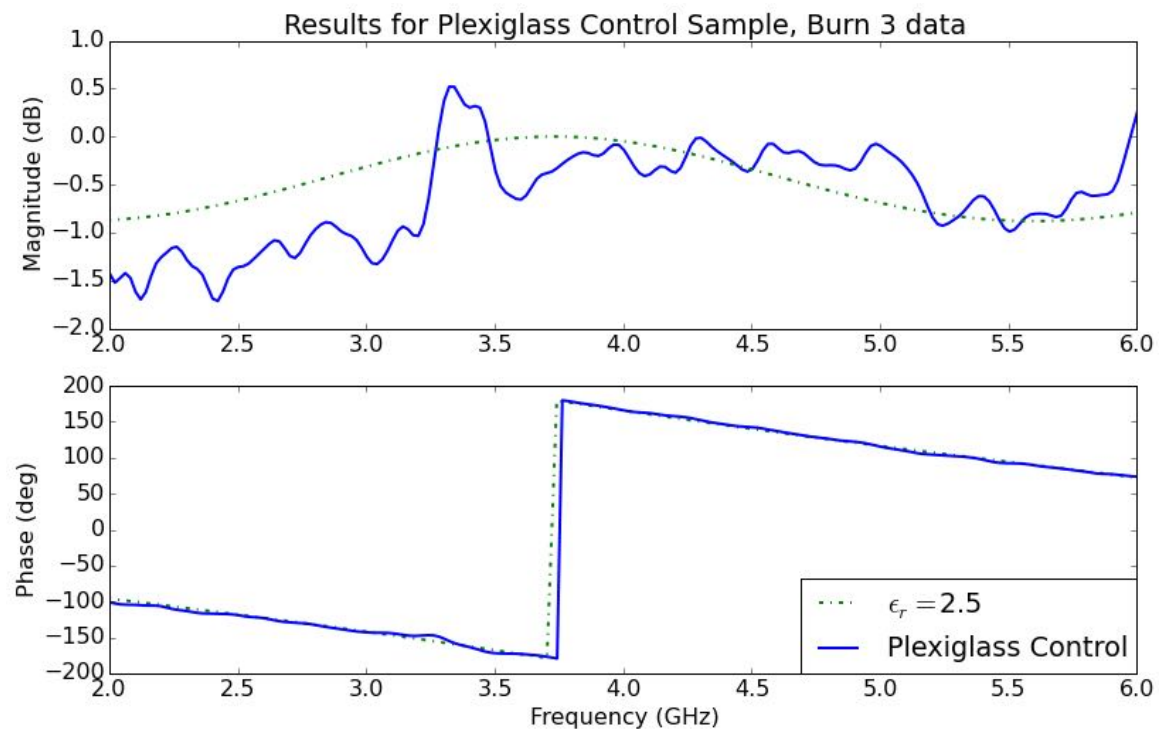


Figure 4.10: Plexiglas control measurements (S_{21}) compared to theoretical values for a lossless material with permittivity of 2.5. Each material is 1 in thick.

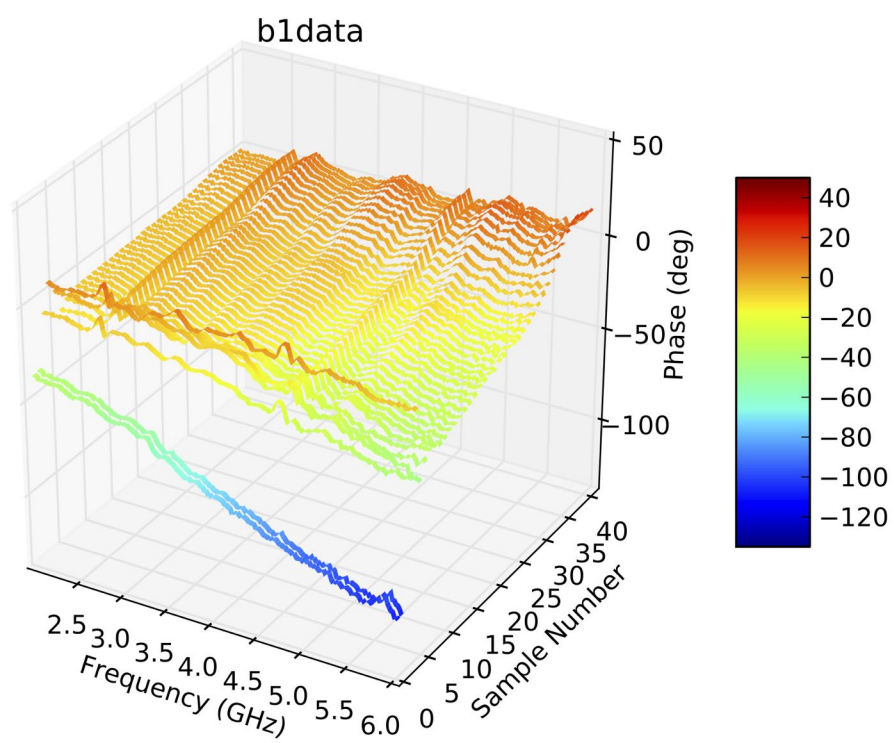


Figure 4.11: Processed data from burn 1. The two curves at the front are for the Plexiglas standard.

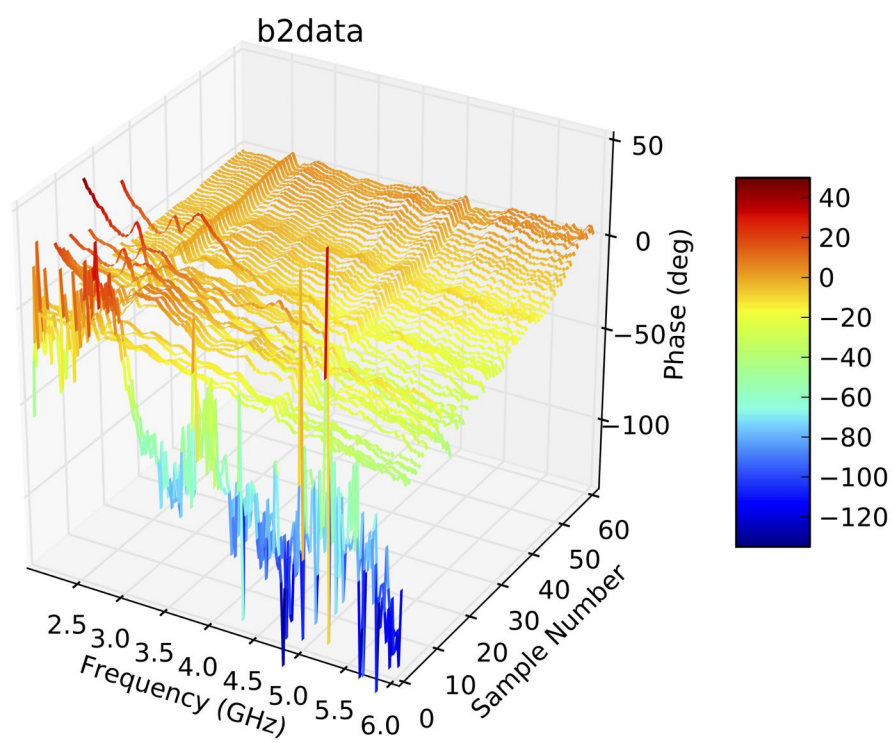


Figure 4.12: Processed data from burn 2. The two curves at the front are for the Plexiglas standard.

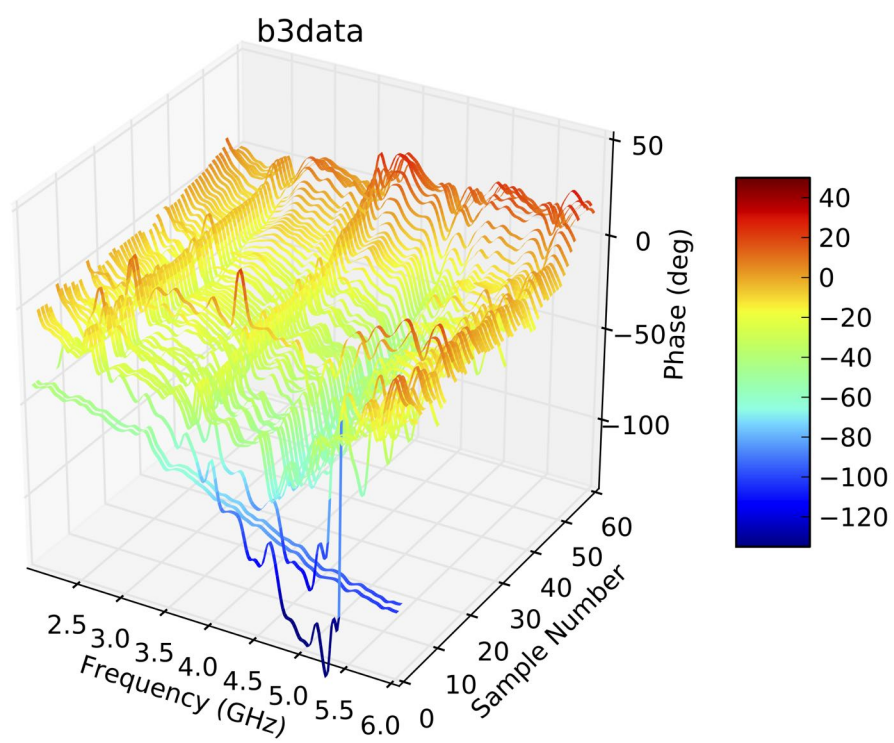


Figure 4.13: Processed data from burn 3. The two curves at the front are for the Plexiglas standard.

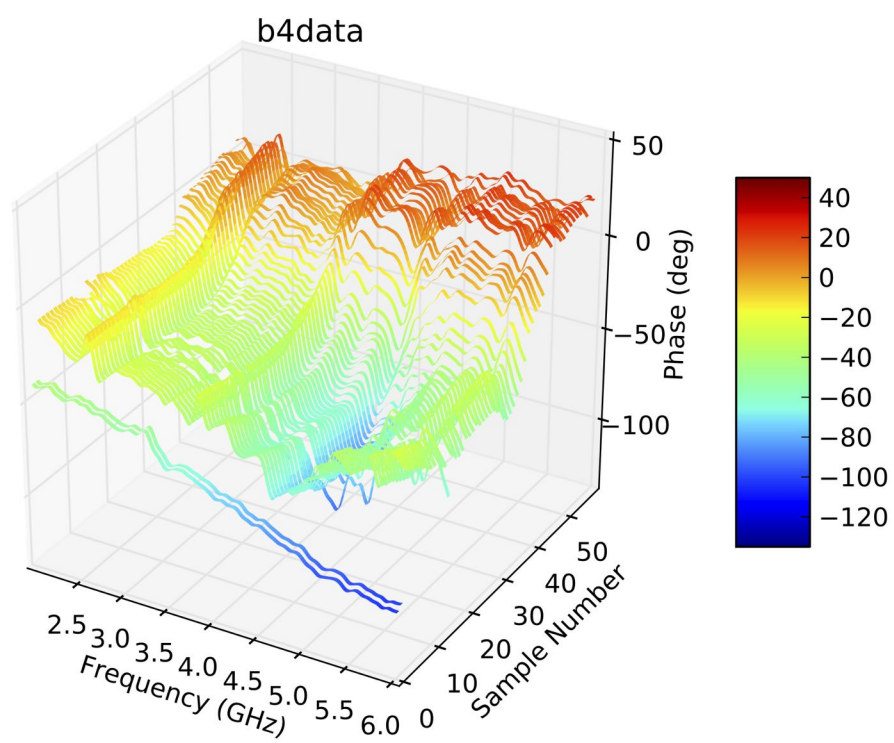


Figure 4.14: Processed data from burn 4. The two curves at the front are for the Plexiglas standard.

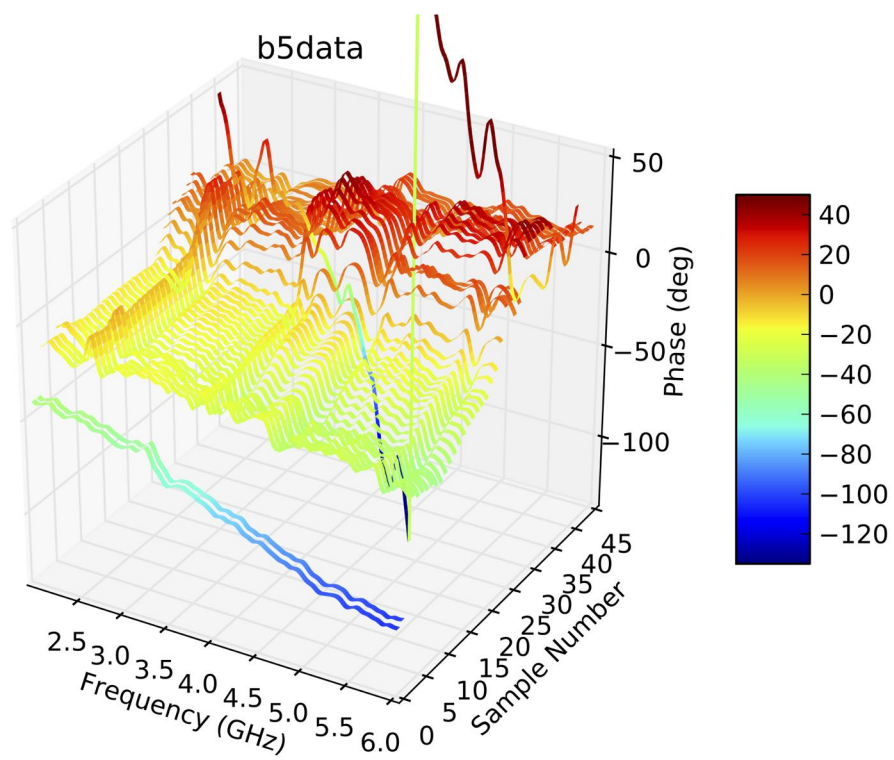


Figure 4.15: Processed data from burn 5. The two curves at the front are for the Plexiglas standard.



Figure 4.16: Video stills from burn 4. The time stamps show the synchronized time for each camera.

4.6 Discussion

The results above were very promising. The most impressive aspect of the above results is that a time dependent trend is observed. Such a trend suggests that the measurement procedure works in an outdoor range without means of focusing the antenna beams. It demonstrates that some physical phenomenon is being measured, most likely the cushion material getting smaller combined with very slight effects of the actual flame.

The observed trend is a non-linear increase in phase as time progresses. This change increases as frequency increases. The phase approaches zero as time goes on which is when the fire self-extinguishes. It is believed that the phase approaches zero because the measurement system is essentially being returned to an empty state as there is no cushion left on the shelf. At this time, though, it is difficult to say how much of the time-dependent trend is caused by the cushion changing and how much is caused by the fire.

When the experiment was designed, we did not expect the cushion material to interact with the transmissions very much because the cushion is mostly foam. Foams can be transparent at radio frequencies and is often used to fabricate support structures in laboratory experiments. There are, however, many types of foam and not all fall into this transparent category.

In a real-world use case, measuring furniture or building materials that are burning should not be a problem. The time scale of this mass reduction is significantly larger than the time scale of human motion that would be detected by a radar system. In the case of this experiment, I measured over a very long time scale hence why this measurement of the cushion is observable.

These observations meant that future experiments were needed so that the effect of the fire could be measured more accurately. A screen enclosure could be used to prevent the electromagnetic waves from interacting with the fuel. A screen would allow air, gases, and flames to enter and exit while electromagnetically isolating the cushion.

During the experiment it was noticed that the cushions were difficult to light and it was hard to create a sustained flame. This was in contrast to the ignition test that was done before the experiment. It is believed that lighting the cushions was difficult because of the slight wind and the flame retardants in the cushion. It has been demonstrated that modern furniture primarily constructed with foam burns faster and hotter, even with flame retardants, than legacy furniture that is made using solid wood and cotton batting [60, 61]. The peak temperature is about the same for both types of furniture; however, the time to reach this peak is less and the heat release rate is higher for modern furniture. This is due to foam being made of energy-rich hydrocarbons which leads to higher temperature flames when compared to cotton or other natural batting material. Heat builds during a compartment fire which helps to overcome the flame retardants present in most furniture. There was no enclosure in which to build heat during this experiment. This made it more difficult to create a sustained flame. The effect of wind on flame movement, and to some extent heat escaping from the flame, was the primary reason why future experiments used some manner of fire-resistive enclosure.

The first sample, B1, was ignited on the windward side. Sample B2 was ignited on the three non-windward sides. Sample B3 was ignited from underneath in one corner and the bottom center. Sample B4 was placed on top of a sheet of cardboard. The cardboard and cushion were ignited from underneath at the center. Samples B5 and B6 had cardboard pieces arranged as shown in Figure 4.17. These were lit from the bottom center.

It was found that ignition from underneath allowed the heat to build in small pockets leading to a sustained flame which eventually broke through the top of the cushion. Once through the top, the cushion quickly became fully involved. Placing cardboard underneath provided a material that was easily lit, reducing the time required for ignition.



Figure 4.17: Cardboard used to ignite cushions for samples b5 and b6.

4.7 Experiment Design Observations and Suggestions

The discussion section above identifies some outcomes and challenges, as well as remaining questions. This section identifies touches on these previous items and adds additional outcomes and challenges that experimental work needs to address.

First, let us consider the main finding above: a burning cushion effects the propagation of EM waves as it burns. This result was observed multiple times. The propagation was initially different than propagation through unobstructed space and then would gradually return to near the unobstructed state. This time dependence is important and has two possible explanations. One is that the fire is effecting the wave propagation. The second is that the cushion itself is effecting the wave propagation. Both of these may be occurring at the same time. The validity of either explanation is what needs to be investigated and the two need to be made

experimentally independent. This is the main conclusion and challenge which is further investigated in the following chapters.

The experiment also helped to identify other methodological and procedural challenges. These are listed below.

- Equipment

- Power

Power is required at the experiment site. The primary concern is power for the measurement equipment. Additional equipment to consider when assessing power needs includes cameras (affected by standing by, temperature, etc.), laptops, and ignition systems. Electronic ignition systems may require a large power input which must be considered in the experimental design. Battery backups or uninterruptible power supplies should be used, especially for network analyzers or other critical test equipment.

If a generator is used, it should be tested with measurement equipment prior to use. Portable generators may not produce the clean power needed by laboratory quality equipment.

- Time required to set up equipment and experiment

From a logistical perspective, setup time is important. Combustion experiments are difficult to perform inside a laboratory. This means transportation and setup of equipment must now be incorporated into the plans. Additional personnel are required.

- Equipment warm-up time

The experiment schedule should allow enough time for instrumentation to warm up and stabilize.

- Calibration of equipment

Calibration of the equipment is challenging for multiple reasons. First, it is time consuming. If problems arise or the calibration is found to be inaccurate, it will need to be re-performed. When others are waiting to help and expect a set schedule, this can be problematic.

Due to these experiments being performed outside, environmental factors will change and can effect this calibration. This may include spurious emissions, uncontrolled transmitters, and weather/temperature.

Calibration also effects the duration of a frequency sweep. It can slow down the actual dwell time at each individual frequency. More importantly, it slows down the overall time between successive sweeps for two reasons. First, all four S-parameters need to be measured (in most cases) in order to compensate for all errors. Secondly, calculations must be performed to compensate for the errors and to produce or save calibrated data.

- Ignition of sample

Ignition of a sample is not always straight forward. Test ignitions should be performed prior to an actual experiment. One should consider using a pilot flame, small amounts of accelerants, or tinder/kindling. It may be necessary to provide an extra wind break around the ignition source. A remotely-operated ignition is preferred, but often unrealistic due to cost or complexity.

- Sample acquisition time

Acquisition time is dependent on many things including averaging factor, calibration, number of points, and intermediate frequency bandwidth (IFBW). A duplicate experiment should be set up (in the laboratory if possible) prior to the experiment in order to determine the acquisition time and other timing issues.

- Dynamic flame

Fire is a dynamic phenomenon. The motion of a flame is fluid to the eye, meaning that one can consider it to be a fast motion compared to the speed of the equipment used to take electromagnetic wave measurements. This means that it can be challenging to measure the flame in one state for an entire frequency sweep. Further, the flame will not be consistent between samples or sweeps.

- Synchronization of still images, video, and annotations to sample using either sample number or time stamp

This is a significant challenge faced when processing the data. It is very important to know what was occurring at the time of (and during) a particular sample. Recording of the experiments using written notes, digital photography, and videos is essential in identifying what is changing between or during a measured data point. When multiple cameras are in use, synchronization of the cameras is challenging but essential.

- Cable and connector integrity, protection, and related site safety

Test cables are expensive and relatively fragile compared to cables with which most people are familiar such as extension cords. They are also susceptible to damage from the environment. Care needs to be taken to protect the cables when outside of the laboratory including during transportation.

The same is true for connectors. Dropping, throwing, and other physical abuse will damage RF connectors. Anything to which they may be connected could be damaged as well. Dirt and other foreign bodies may get into or on the connector and ruin other connectors when attached. Again, connectors should be carefully handled and protected outside of the laboratory (and in the laboratory for that matter).

While probably not a major problem, noise from power cables may be transferred to measurement cables. Keep this in mind when setting up cables and try to have them cross at right angles.

Test cables as well as other cables create a site safety hazard. It is relatively easy to re-route power cables. Test cables are harder because any added length increases attenuation. Cables should be clearly marked and protected. Regular cable mats with built in trays or PVC pipes can be used to cover, protect, and route test cables and regular cables.

- Water danger to equipment

Test equipment is just as susceptible to water damage as other electronics (unless you are lucky enough to have a FieldFox network analyzer, in which case, I would love to use it). The main difference between the two is that test equipment is significantly more expensive to fix. Be careful!

- Durability

Equipment and experimental setups are moved a great deal when experiments are done outside of the laboratory. Durability as well as proper handling need to be included from the initial experiment design stage. The experimental setup must be durable to ensure that successive experiments have the same environment. It is also important to ensure that the measurement occurs in the same environment as the calibration.

- Infrastructure protection

The infrastructure of the experimental environment, e. g. asphalt, extension cords, buildings, and water supply, need to be protected from the heat, flame, and smoke of experiments. Sand and/or sheetrock can be used for ground protection. Duraboard from Fiberfrax or other fire-rated insulation can be used to protect buildings and

other large objects. Trip protection such as mats may protect cables. PVC pipes may be used also to cover and protect cables.

- Ambient heat danger to equipment

Test equipment, and to some extent regular electronics, have environmental temperature limits. Proper cooling (or heating) may be required.

- Fire danger to equipment

The flame being measured obviously poses a fire danger to all nearby objects. Test equipment is particularly of concern mainly due to its cost. Ensure all objects are fire resistive or properly insulated.

- Fire suppression

During live-fire experiments, it is critical that the fire can be put out if need be. If possible, there should be two independent suppression methods. A fire extinguisher and a charged hose line were normally used for the experiments in this dissertation.

- Environment

- Weather

Weather must be watched and considered. Neither fire nor electronic equipment do well in rain. Wind can have various effects on fire and create very animated flames. Burning may not be permitted if there are red flag warnings due to dry conditions. Transportation and setup also require decent weather. Fluctuating temperatures affect equipment calibrations and measurements.

- Air flow (ventilation) causes moving flame

For measurement purposes, it would be ideal if the flame did not move. Air flow caused by the flame, as well as by outside sources like wind, will cause the flame to move and dance. This makes measuring the flame properties difficult.

- Movement in the area of the experiment

Movement within the field of view of the antennas will cause measurement errors. It can be difficult to convey this to those who are not experienced with electromagnetic experiments. A quiet zone needs to be established around the flame and antennas.

Water from fire hoses will interfere with electromagnetic wave propagation. Other suppression methods such as fire extinguishers or sand for smothering along with the people involved, will alter propagation as well.

- Systematic

- Unable to distinguish between measurements of the sample and of the flame

A major systematic challenge is separating the fuel from the flame so that only the flame is measured. This item is discussed above.

- Repeatability of fuel or flame size

It is difficult to repeat the behavior of a flame. Numerous outside factors effect this behavior including ventilation.

- Flame size compared to antenna field of view; flame size vs wavelength

It is difficult to create flames large enough compared to the antenna field of view. The flame must be large enough to impact direct transmission of waves while limiting other modes of propagation such as diffraction.

- Distance from flame

Flames and antennas should be in close proximity to ensure observation of the effects on direct propagation. This must be balanced with thermal risks to equipment.

- Validity of plane wave or plasma slab approximations

When size of and distance to the flame are considered, one should also consider the shape of the wavefront relative to the shape of the flame. Ideally, one would be able to assume a plane wave incident on a slab of plasma.

- Flame duration

Equipment requires a set amount of time to make a measurement. Flames need to have enough fuel and behave in the same manner for a long enough period of time so as to allow for the desired number of measurements to be taken.

- Flame vs. soot/smoke

It is known from weather and other radar research that smoke and soot are detectable [36–43]. The aim of this research is not to measure these byproducts but to measure the flame itself. The effects should be separated, hopefully through careful experimental design so that the smoke is not even measured. Future research should study both flames and smoke.

- Noise due to no, or limited, calibration information

Non-laboratory setups may not lend themselves to system calibration. In some instances, a partial calibration may be performed. Calibration attempts are also hindered by the overall environment changing during an experiment so that the initial state is different than the final state or the state at any time during the fire.

- Mass transport

The sample is being consumed and the measured material is being removed from the measurement space through mass transport mechanisms including combustion and rising air.

4.8 Conclusion

This experiment was designed to analyze how a fire affects radio waves transmitted through it. The results did not provide any insights into how radar might be used in an actual house fire but suggested that future experiments should be completed. This experiment showed that the experimental setup and procedure are usable but require improvement. This experiment also showed that there exists some temporal effect on transmission properties. Observed time-dependent changes could be due to the fire or the elimination of the cushion; at this time the two physical processes cannot be separated. Experiments conducted later in this dissertation attempted to isolate these two processes as described in the subsequent chapters. In addition, later experiments utilize some sort of compartment in order to increase the heat around the cushions and eliminate wind.

Chapter 5

Experiments Using a Propane Burn Pan

One observation from the experiment in Chapter 4 at the LFD training center was that it was difficult to know if the measurements were of the flame or of the cushion. A propane-fueled fire extinguisher training system was used to try to isolate the fuel source from the fire. One downside to this approach is that propane is a relatively clean burning fuel, which is undesirable because the impurities and trace molecules in the fuel source are thought to be the particles primarily responsible for creating a fire-induced plasma.

The propane system was used for experiments at MSU's Environmental, Health, and Safety (EHS) office and at the Bath Township (MI) Fire Department (BTFD) station. At the EHS office, the unit was open to the surroundings but at the BTFD station it was enclosed by a fireproof chamber. Notes from the EHS burn were recorded in a laboratory notebook and are provided in Appendix F for reference. Unfortunately, there were no notes recorded for the BTFD experiment.

Thank you...

Elvet A. Potter from MSU EHS and Dr. Junyan Tang assisted with the experiment at the EHS office. Lansing (MI) Fire Department loaned the Bullex system used for the BTFD experiment with which Korede Oladimeji assisted.



Figure 5.1: Example fire extinguisher training using the Bullex Intelligent Training System.

5.1 Experiment at EHS

5.1.1 Experimental Setup

Two experiments were carried out to measure the propagation through a flame produced by a Bullex Intelligent Training System. This system is a propane fueled burner used for fire extinguisher training as demonstrated in Figure 5.1. Propane fuel is split into two pipes that each form an almost-closed square. These pipes are visible in Figure 5.2. Water is added to the tray beneath the pipes to act as a heat sink and keep the unit from overheating. An overflow drain in the right and left sidewall keep the water from flooding the propane piping (left cutout visible in Fig. 5.2). Power is supplied from a 12 VDC, vehicle cigarette lighter style plug. The fire is started using a remote controller that also configures various settings such as the difficulty of the training. The propane supply hose, power supply, and control cable are seen disconnected on the left in Figure 5.2. Once the unit is remotely ignited by an instructor, a student uses a refillable water extinguisher to simulate putting out the fire by spraying four sensors on the front of the unit (visible in Fig. 5.3)¹. If the student does not extinguish the fire in thirty seconds, the system will turn off to prevent itself from overheating.

The overall experimental layout can be seen in Figure 5.3a and is sketched in Figure 5.4. The antennas were spaced 13 feet and 1 inch apart and aligned along the crack in the concrete. The tray for holding the metal calibration plate and Plexiglas sample was 44 inches from the upper right antenna in Figure 5.3a. This antenna was connected to port 1 of an HP 8753D VNA by cables numbered 003 and 039, and the other antenna was connected via cables numbered 040 and 037 to port 2 (see Appendix B). From the port 1 antenna to the nearest edge of the burner was 56.5 inches. The dimensions of the burner are given in Figure 5.5. The average dimension is provided because it represents the approximate size of the flame since the flame

¹The sensors are on the front of the unit because the spray from a fire extinguisher should be aimed in front of the fire and moved into the base of the fire using a side-to-side sweeping motion. Untrained users will normally spray the flames above the base of the fire which does little to extinguish a fire.



Figure 5.2: Experimental setup at MSU EHS showing the Bullex system and wire shelf.

is larger than the piping but does not completely fill the burn pan area. A laptop connected to the HP 8753D VNA, calibrated to the ports of the antennas using an 3.5 mm calibration kit, was used to measure 1601, S_{21} data points between 2 GHz and 6 GHz.



(a) View along the path of propagation of the EHS setup with the system lit.



(b) Front view of the EHS setup with the system lit.

Figure 5.3: Ignited system during experiments at MSU EHS.

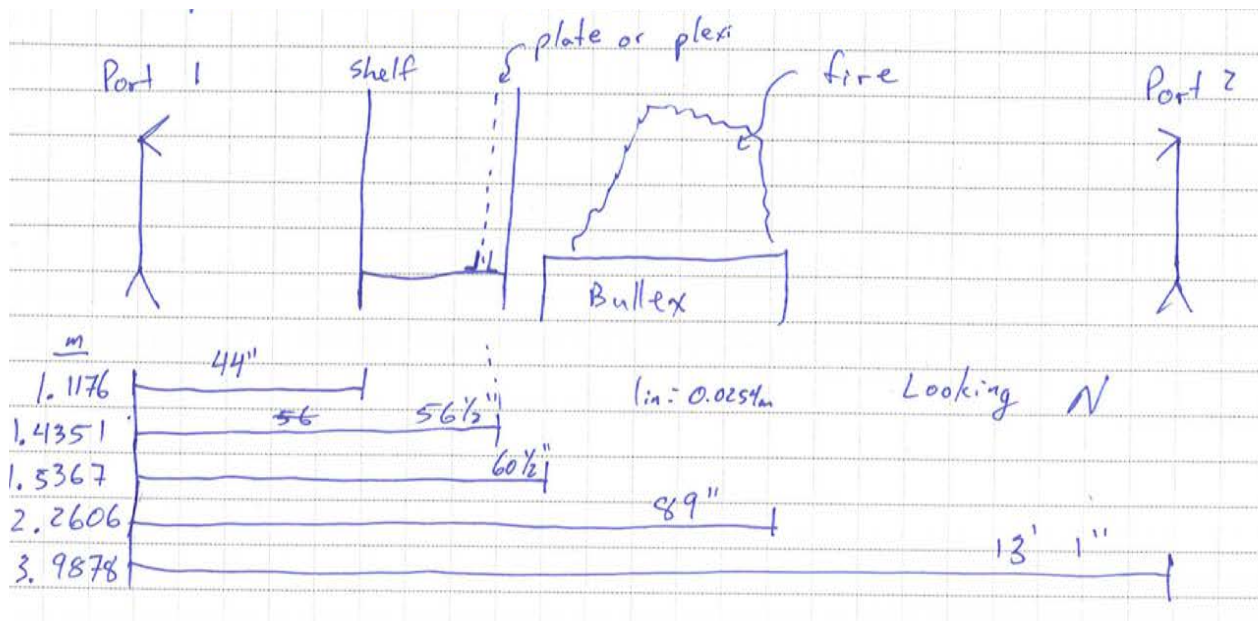


Figure 5.4: Schematic of the EHS experimental layout. This sketch is from page 14, which may be found in its entirety in Figure F.2 of Appendix F, of Laboratory Notebook 00010

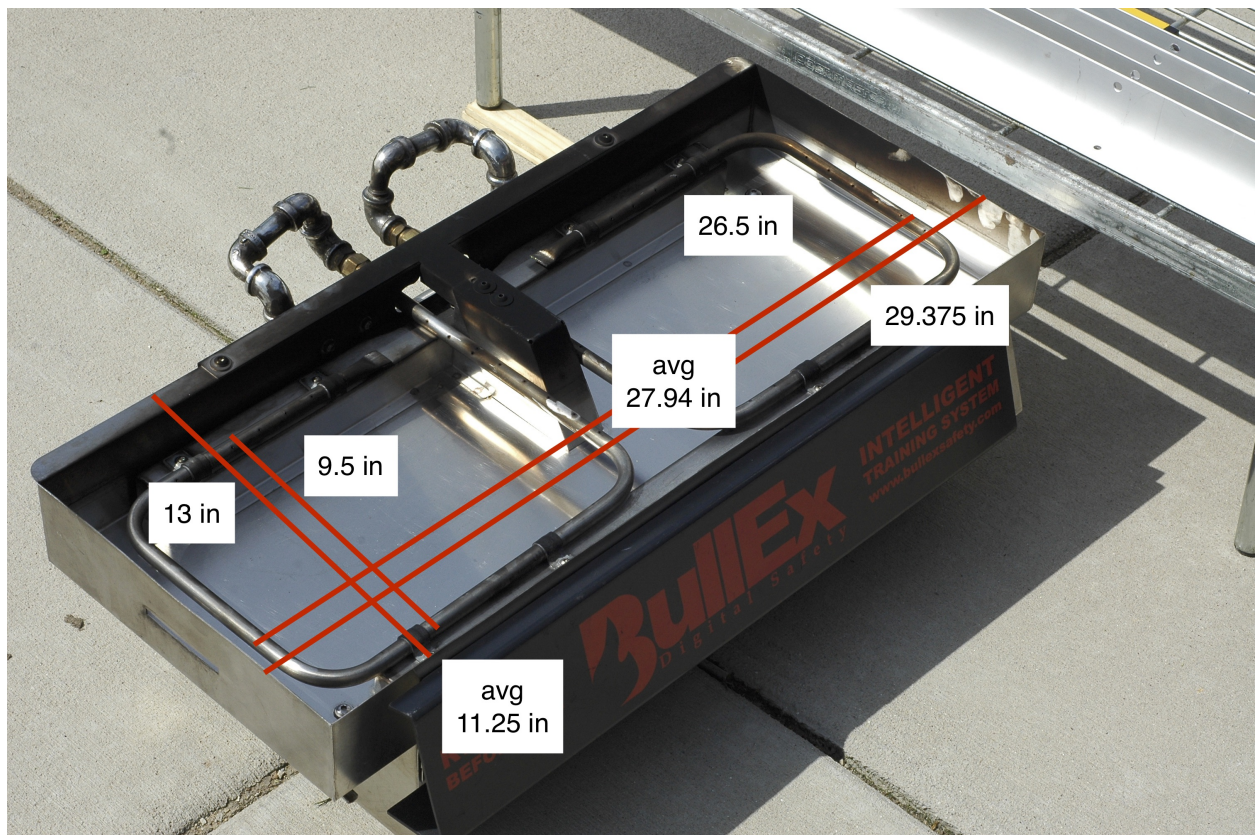


Figure 5.5: Dimensions of the burner.

Table 5.1: Measurements in EHS replicate sets and zero-fill time.

| Set 1 | Set 2 | Set 3 | Pts set to zero |
|--------|--------|--------|-----------------|
| empty | empty | empty | |
| plate | plate | plate | |
| Plexi. | Plexi. | Plexi. | 2–390 ns |
| burn 1 | burn 1 | burn 1 | 5–390 ns |
| burn 2 | burn 2 | burn 2 | 5–390 ns |
| burn 3 | burn 3 | burn 3 | 5–390 ns |
| | | burn 4 | 5–390 ns |

5.1.2 Experimental Procedure and Data Processing

Three replicate sets of data were measured with each replicate set consisting of measurements used for calibration—an “empty”, metal plate, and Plexiglas—and either three or four measurements with the burner lit as listed in Table 5.1. The empty measurement consisted of the shelf, metal tray, and burner. The metal plate and Plexiglas measurements were of 2 feet by 2 feet by either 1/4 inch thick metal plate or 1 inch thick piece of Plexiglas, respectively. The tray and shelf were left in place for the lit burner measurements (see Fig. 5.3b). One data set took approximately 18 seconds to be measured and saved for the VNA configuration used. As noted earlier, the burner will only run for thirty seconds before it shuts itself down; therefore, only one data set could be taken every time the burner was lit.

After the experiment, data was calibrated and time gated to remove noise and to shift the measurement plane using an IPython notebook (App. L) and Wavecalc [62]. Data was first calibrated using the formula

$$S_{21}^{corr} = \frac{S_{21}^{meas} - S_{21}^{plate}}{S_{21}^{empty} - S_{21}^{plate}} e^{-jk_0 d_x} \quad (5.1)$$

where *corr* is the corrected data, *meas* is the sample measurement, *plate* and *empty* correspond to the respective measurements, k_0 is the free space wavenumber, and d_x is the thickness of the sample—for Plexiglas, d_x is 1 inch and for the burner d_x is 27.94 inches. Next, the

data was time gated using Wavecalc [62] by applying a cosine taper (exponent $k = 2$, fraction of bandwidth $r = 10$) weighting function to the frequency domain data, performing an IFFT (exact, 4096 data points), setting the time points listed in Table 5.1 to zero (zero filling), performing an FFT (exact, 8192 data points), and truncating the data to the frequency range 2.5 GHz–5.5 GHz. The final frequency range is smaller than the original because the cosine taper weighting makes the edges of the signal taper to zero. From the documentation for Wavecalc, the cosing taper weighting is calculated from:

$$w_{CT}(n\Delta) = \begin{cases} 1 & \text{for } r(N-1) \leq n \leq (1-r)(N-1) \\ \sin^k\left(\pi \frac{rn}{2(N-1)}\right) & \text{otherwise} \end{cases} \quad (5.2)$$

where N is the number of points, Δ is the sampling interval, k is an exponent with a value greater than one, and r is the fraction of the width to which the tapered portion of the weighting function is applied. This Wavecalc processing was automated using the macro template in Listing I .1 and Listing I .2 in Appendix I . Gated data was important back into the IPython notebook where it was averaged and plotted against a theoretical curve.

5.1.3 Results and Discussion

The average transmission of all three Plexiglas measurements is plotted in Figure 5.6 along with theoretical curves for a slab of Plexiglas ($\epsilon_r = 2.5$) surrounded by free space and the theoretical curve for free space. An area that may concern some since this is not an active system is the peak over 0 dB found around 3 GHz in the measured magnitude. This is most likely caused by the low-loss nature of Plexiglas. It is reasonable for experimental data like this to be slightly greater than 0 dB for a low-loss material being measured in an unrefined system with probable diffraction and the wide beam widths of the unfocused antennas. The phase shows good agreement with the theoretical Plexiglas curve. A best fit line, having $r = -0.997$, of the mean Plexiglas phase

is plotted along with the unwrapped phases in Figure 5.7. The theoretical and best fit lines are almost on top of one another. Considering that the permittivity of Plexiglas varies in the literature between $\epsilon_r = 2.4$ and $\epsilon_r = 2.8$ [59,63], this close of a measured value is very acceptable.

The transmissions through the lit burner exhibit behavior similar to the Plexiglas measurements. The magnitude oscillates around 0 dB, probably because of low-losses as in the Plexiglas case. No cut-off behaviour is observed in this measured magnitude which suggests that, if there is a fire-induced plasma, either the plasma frequency is significantly lower than the measured frequencies or the system does not accurately measure the plasma because the plasma region occupies a relatively small volume of the measured space.

The phase in Figure 5.8 is slightly shifted from the free space theoretical curve and Figure 5.9 shows the unwrapped phases. The mean phases from all three burns are essentially the same and just barely differ from the free space curve. Slight changes in the permittivity could have caused this as well differences in the distance traveled. Wind during the experiment caused the flames to be very dynamic which makes determining the actual size of the flames virtually impossible since there are no cleanly defined boundaries or dimensions.

These results suggest that the effects of any plasma created by the fire are minimal over this frequency band for this setup. One reason for this may be the relatively small size of the flame. The direct path between the antennas goes through the very top of the flame, or even over the flame if the wind is deflecting the flame resulting in little energy is interacting with the flame, especially the higher-energy portions in the combustion zone near the fuel source that are most likely to create a plasma. Additionally, the flame presents a small cross-section compared to its depth which limits the total amount of energy that propagates through the flame. The burner was oriented this way so that the propagating wave would travel through any plasma for the maximum possible distance. A theoretical analysis of the orientation for this unfocused system remains to be completed. Finally, there may be few plasma effects observed because of the fuel used in this experiment. Propane is a clean burning fuel and no additional

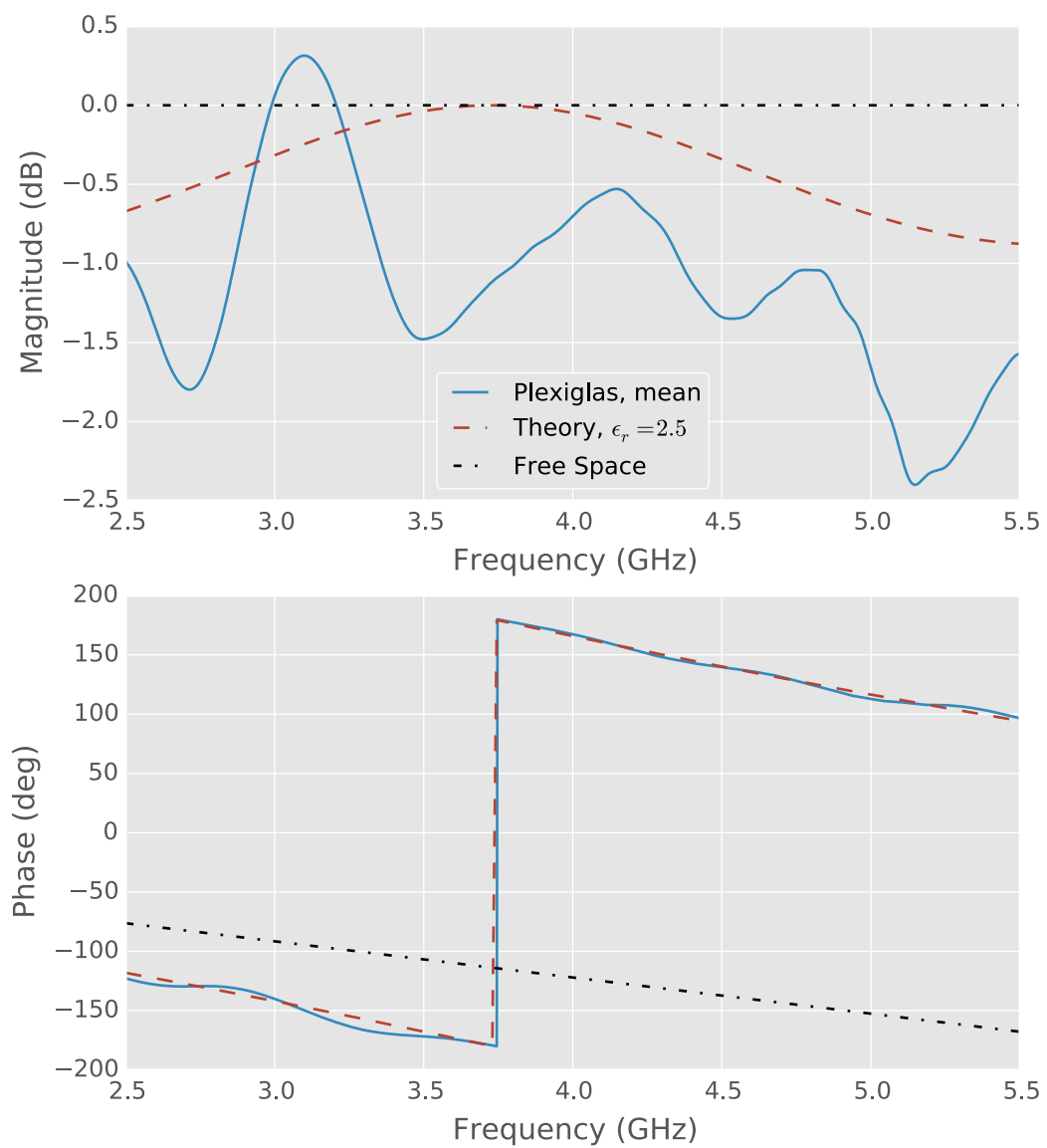


Figure 5.6: Average measured transmission through a one inch thick Plexiglas sample.

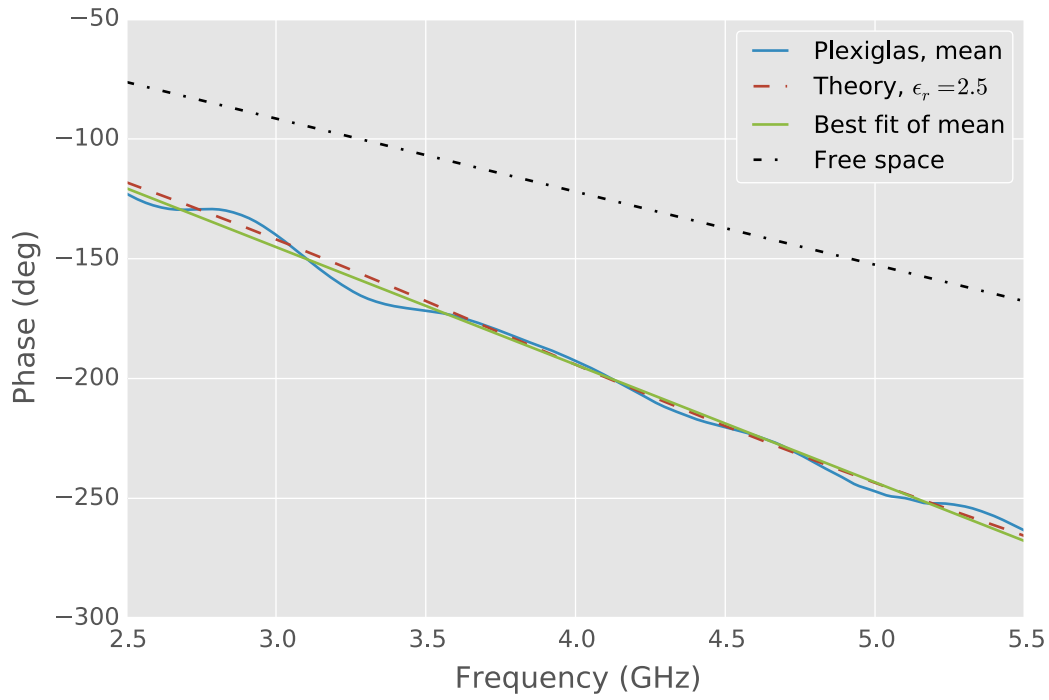


Figure 5.7: Unwrapped phase of the average measured transmission through a one inch thick Plexiglas sample.

compounds were mixed into the flame. In the previous work examined in Chapter 3, the flames with observed plasmas either had salt added to them or were fueled by complex sources that had small concentrations of easily ionized particles.

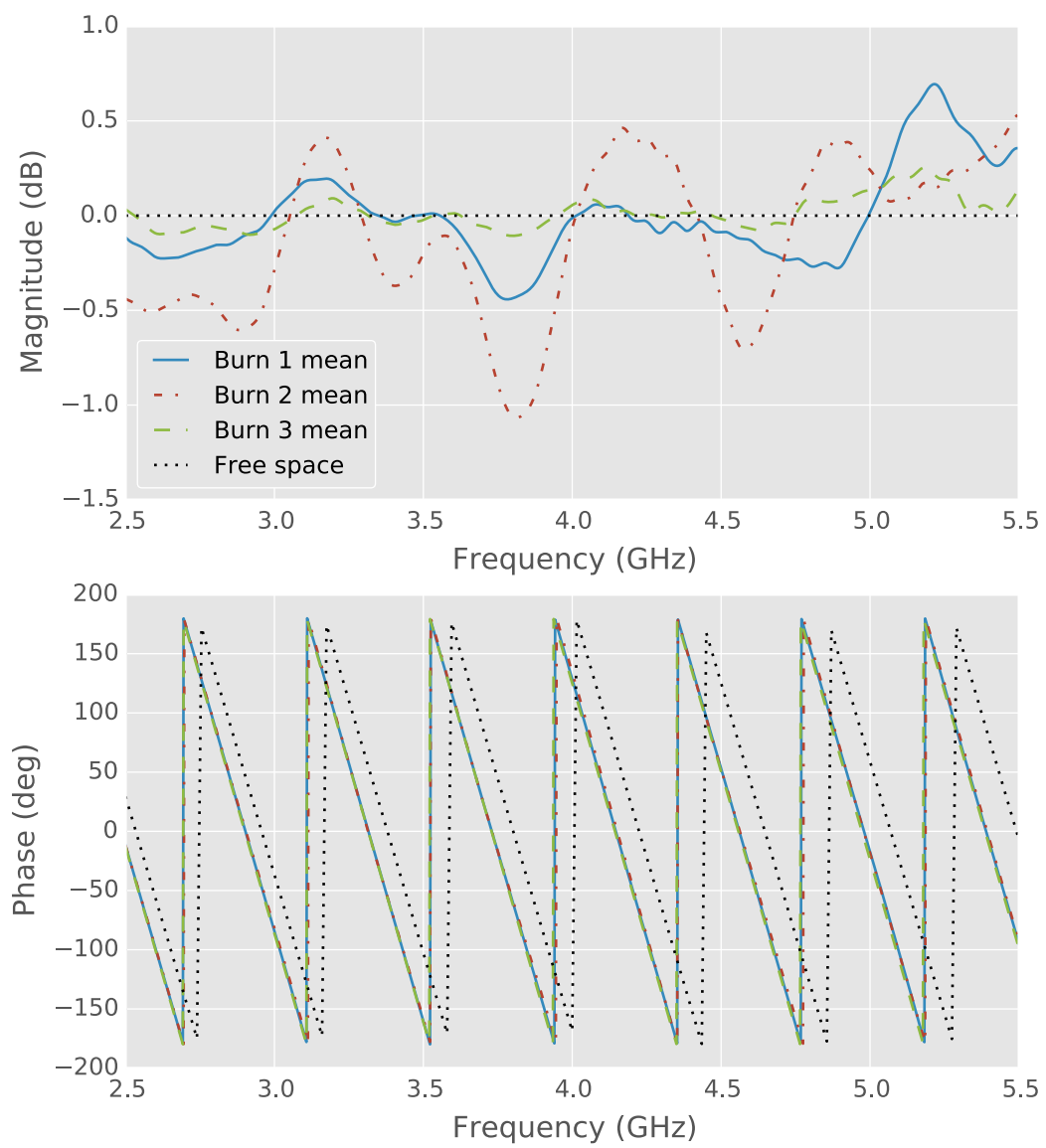


Figure 5.8: Average measured transmission through an ignited Bullex system.

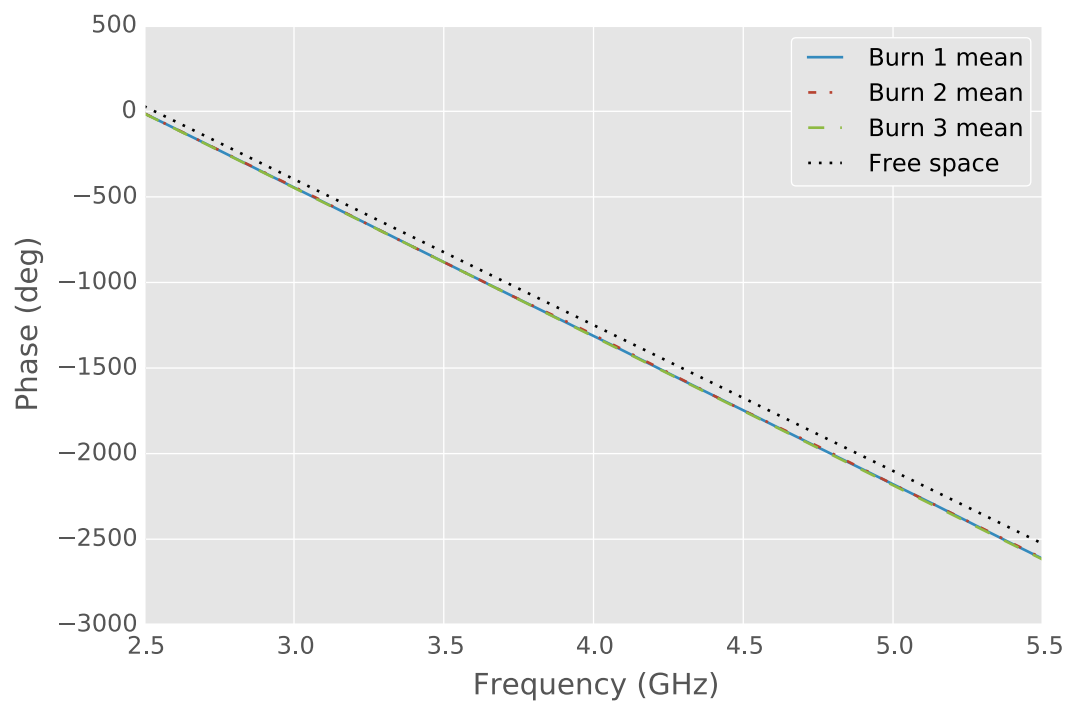


Figure 5.9: Unwrapped phase of the average measured transmission through an ignited Bullex system.

5.2 Experiment at BTFD

This experiment was designed to address issues observed in the EHS experiment by trying to protect the burner from the wind with a chamber, rotating the burner to increase the cross-sectional area presented to a propagating wave, and decreasing the distance between antennas. The chamber, built using Duraboard fire insulation, also protects measurement equipment, such as the antennas, from the fire.

5.2.1 Duraboard Insulation and Burn Chamber Design

Thank you...

Unifrax generously donated the Duraboard insulation for this research.

Fiberfrax Duraboard LD insulation is manufactured by Unifrax and is a rigid ceramic fiber board with thermal stability up to 3000°C and can withstand direct flame contact. The donated boards were 4 feet by 2 feet and 1 inch thick. Additional product information is available from the label in Figure 5.10. While the board is rigid, it has little abrasion resistance as a hole could quickly and easily be rubbed through the board. The board is easily cut with a utility knife or drilled with regular bits; in fact, a bolt can be pushed through the board although this would cause pieces to come off from the backside. When cutting, it was important to cut through the entire thickness of the board to ensure a clean finish unlike sheet rock that may be scored and snapped. Not cutting through the entire board results in pieces flaking off and jagged edges being left. When working with Duraboard, a particle mask, eye protection, gloves, and a lab coat should be worn; the MSDS sheet for Duraboard is available from Unifrax.

The chamber consisted of 4 feet by 4 feet walls that were connected to one another and raised off of the ground; no roof/ceiling was used. Squares of steel perforated sheet joined the Duraboard panels using four bolts. Solid 90° angle steel stock was used at the bottom corners. In addition to through bolt holes, the stock had tapped holes for attaching perforated



Figure 5.10: Label for the donated Unifrax Fiberfrax Duraboard LD.

90° angle stock as legs, which allowed the ground clearance of the chamber to be adjusted. All bolt holes were pre-drilled using a hand drill and then a 1 inch piece of copper tubing was inserted through the hole. The tubing protected the Duraboard from abrasion caused by the threads of the bolts. On the bolts, flat washers were used against the Duraboard and a split lock washer was used between the nut and flat washer. The inside of the burn chamber is seen in Figure 5.11a along with two of the perforated squares.

This design evolved as it was used. Assembly of the chamber was difficult for only one person and risked snapping the insulation if improperly lifted or supported. This was especially true when installing the bolts since the insulation was not completely secured and could easily sway; however, once fully assembled, the chamber was sturdy. The legs were difficult to attach and ended up not being used for experiments. Instead, the chamber was either placed on blocks or placed directly on the ground. The original design aimed to reduce the amount of metal used since this could interfere with measurements. A mechanically improved design would use a metal frame on to which the insulation is attached and a calibration procedure would be used to account for any effects of the metal frame.



(a) Burn chamber prior to ignition.



(b) Photo taken during a burn.

Figure 5.11: Photos from a burn using a Bullex system in a burn chamber.

5.2.2 Experimental Setup

The burn chamber described in the previous section was placed around the Bullex burner as seen in Figure 5.11a. The trough for holding the calibration plate is seen in front of the burner. The trough is aligned to a parking stripe on the asphalt which served to align the rest of the setup. One horn antenna is seen on the right of the photo—the other antenna is behind the wall on the upper left. Relative to the transmission path between the two antennas, the burner was rotated by ninety degrees compared to the EHS experiment. This was done so that the flame would present a larger cross section instead of appearing deeper. The antennas are only about four feet apart compared to 13 feet at the EHS experiment. The gap in the wall seen on the left was required to ignite the burner using a propane torch since the built-in starter was not functioning. Data was again captured using the HP 8753D VNA and laptop.

5.2.3 Experimental Procedure and Data Processing

Measurements were less extensive in this experiment than the EHS experiment because of factors which affected the time available to take measurements including assembling the burn chamber, troubleshooting the igniter, responding to emergency calls, and the early sunset in December. First, two empty measurements were taken, followed by a plate measurement, and then five burns were measured (Fig. 5.11b). Because of the limited burn time of the burner and the long data acquisition time of the VNA, only one measurement for the first two burns and two measurements for the last three burns were captured. It was possible to capture two measurements for the latter experiments because the timing between the ignition sequence and data acquisition was refined. No Plexiglas measurements were taken. Data was processed using the steps given in Section 5.1.2 with points between 3 ns and 380 ns set equal to zero (zero filled) using the macro in Listing I.3. Appendix M is the IPython notebook for this experiment.

5.2.4 Results and Discussion

The mean transmission for all measurements is shown in Figure 5.12 along with the theoretical transmission through free space. The results are similar to those for the EHS burn. The magnitude varies around 0 dB over the measured frequency range meaning that there is essentially no loss. The average measured phase is offset from the theoretical phase although the slopes are nearly the same as seen in Figure 5.13 meaning that no plasma effects were measured. Possible reasons for these results are similar to those of the EHS experiment including propagation through the top or above the flame and the fuel source. Flame movement was greatly reduced by the chamber, and while still present, it should not play as significant a role as in the previous experiment.

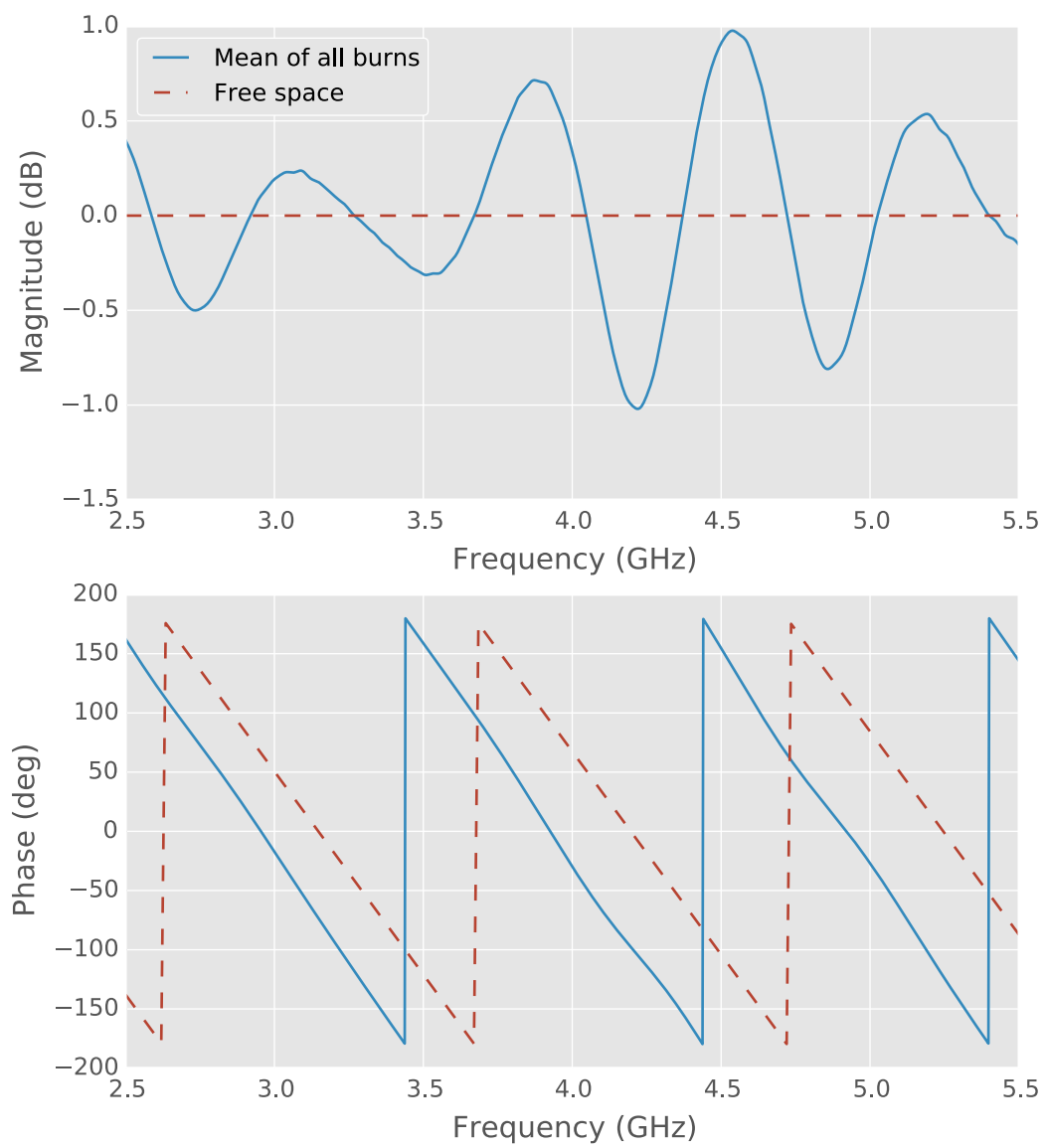


Figure 5.12: Average measured transmission through a burn chamber with the Bullex system ignited.

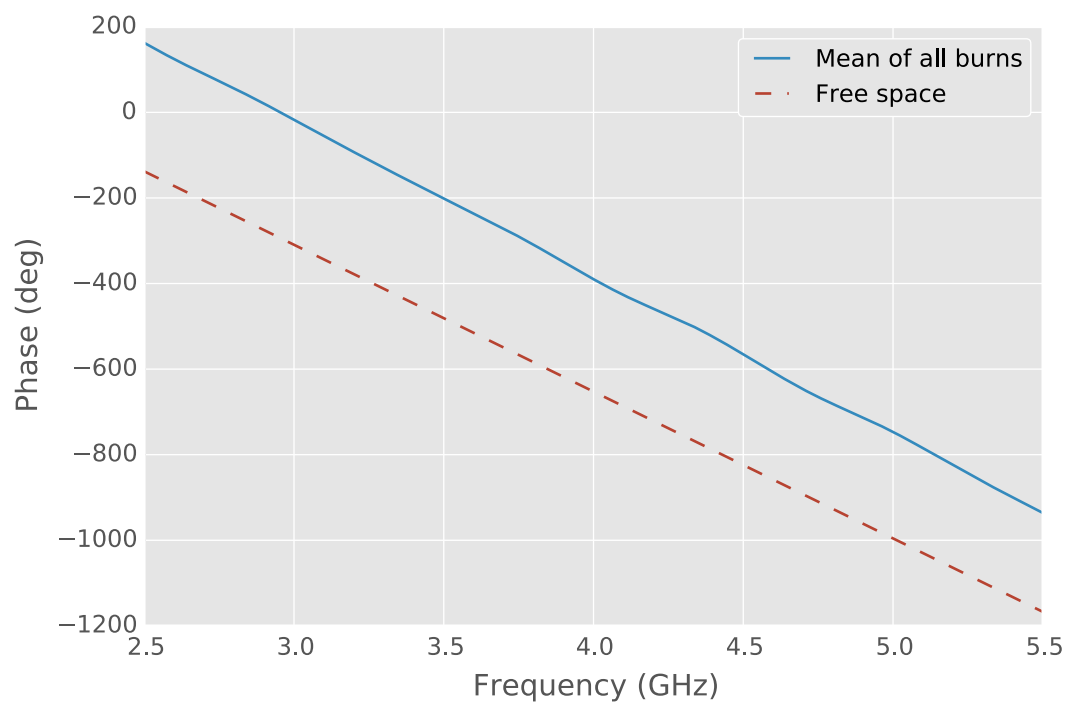


Figure 5.13: Unwrapped phase of the average measured transmission through a burn chamber with the Bullex system ignited.

5.3 Conclusion

The experiments in this chapter used a propane burner to remove the fuel source from the measurement domain, leaving only the flame to be measured. A chamber was constructed to reduce the effects of wind on the flame. The results in this chapter suggest that the transmitted waves primarily traveled through air and with little, if any, interaction with a plasma. While the experimental setup was improved between experiments, further improvements could be made. This includes bringing the base of the flame and the direct transmission path closer to one another, increasing the temporal duration of the burn so more data can be captured, and using a fuel source that is more likely to create a plasma. Further, beamwidth compared to flame size should be investigated.

Chapter 6

Interferometry

A microwave interferometer setup was used to investigate the interaction between electromagnetic waves and flames at a laboratory scale, and explored as a method to characterize fire-induced plasmas from various fuel sources. Samples of methanol (CH_3OH), methanol and saturated sodium chloride (NaCl) solution, and Plexiglas were burnt between two horn antennas. A measurement was taken before ignition to use as a reference and the phase difference was determined in the post-processing stage.

Thank you...

Most of these experiments were carried out using the calorimeter in Dr. Wichman's laboratory or in the fume hood of the Electrical and Computer Engineering (ECE) Shop.

6.1 Microwave Interferometer Theory

Tudisco et al. discuss criteria for and limits of microwave interferometry in [64] where they describe an interferometer at 75 GHz to measure a plasma thruster for space flights. The phase shift in radians is given by

$$\Delta\phi = \angle S_{21}^{sample} - \angle S_{21}^{ref} \quad (6.1)$$

$$= \frac{2\pi}{\lambda_0} \int_0^D \left(1 - \sqrt{1 - \omega_p^2/\omega_0^2}\right) dl \quad (6.2)$$

where ω_p is the plasma frequency, $\omega_0 = 2\pi f_0$ is the microwave frequency, λ_0 is the free-space wavelength of the microwave, and D is the plasma thickness. For low density plasmas ($\omega_0 \gg \omega_p$), the above becomes

$$\Delta\phi = \frac{e^2}{4\pi c_0^2 \epsilon_0 m_e} \lambda_0 \int_0^D n_e dl \quad (6.3)$$

$$= 2.82 \times 10^{-15} \lambda_0 D n_e \quad (6.4)$$

where e and m_e are the charge and mass of an electron, c_0 is the speed of light in free-space, ϵ_0 is the permittivity of free-space, and n_e is the average electron density of the plasma in m^{-3} .

The phase difference as a function of relative permittivity for a dielectric is shown in Figure 6.1. A positive phase difference corresponds to a relative permittivity less than one while a negative phase difference corresponds to a relative permittivity greater than one.

To limit the effects of diffraction and to allow the application of a slab approximation, the ratio of the plasma diameter to the wavelength (D/λ_0) should be large. Heald and Wharton show in [65] that the slab approximation may be used when $D/\lambda_0 > 3$ for cylindrically dense plasmas of constant density measured using optimized, coupled horns. This line is plotted in Figure 6.2 with reference lines for 1, 6, 9.5 and 20 GHz, where 6 GHz and 20 GHz correspond to

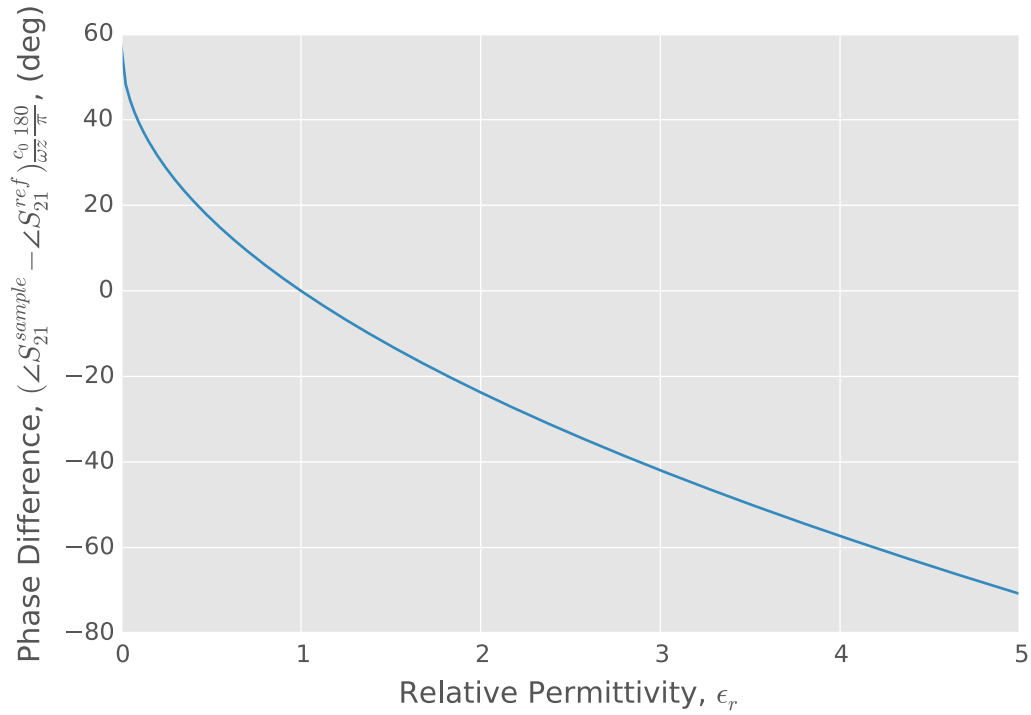


Figure 6.1: Normalized phase difference versus frequency for a constant electron density.

Table 6.1: Minimum thickness to meet the slab approximation criterion for select frequencies.

| Freq (GHz) | D (mm) | D (in) |
|------------|--------|--------|
| 1.000 | 899.38 | 35.41 |
| 6.000 | 149.90 | 5.90 |
| 9.500 | 94.67 | 3.73 |
| 20.000 | 44.97 | 1.77 |

the maximum frequencies of an HP 8753 VNA and an HP 8720 VNA, respectively, and 9.5 GHz corresponds to an upper frequency limit for the mesh experiment in Section 6.2. These minimum distances are also tabulated in Table 6.1.

From the literature review in Chapter 3, the electron density is expected to be in the range of $0.5\text{--}3.4 \times 10^{16} \text{ m}^{-3}$ and the collision frequency to be in the range of $1\text{--}6 \times 10^{10}$ collisions per second. Table 6.2 gives the expected phase difference across the minimum slab thickness for this electron density range at the reference frequencies as calculated by Equation 6.4. It is difficult

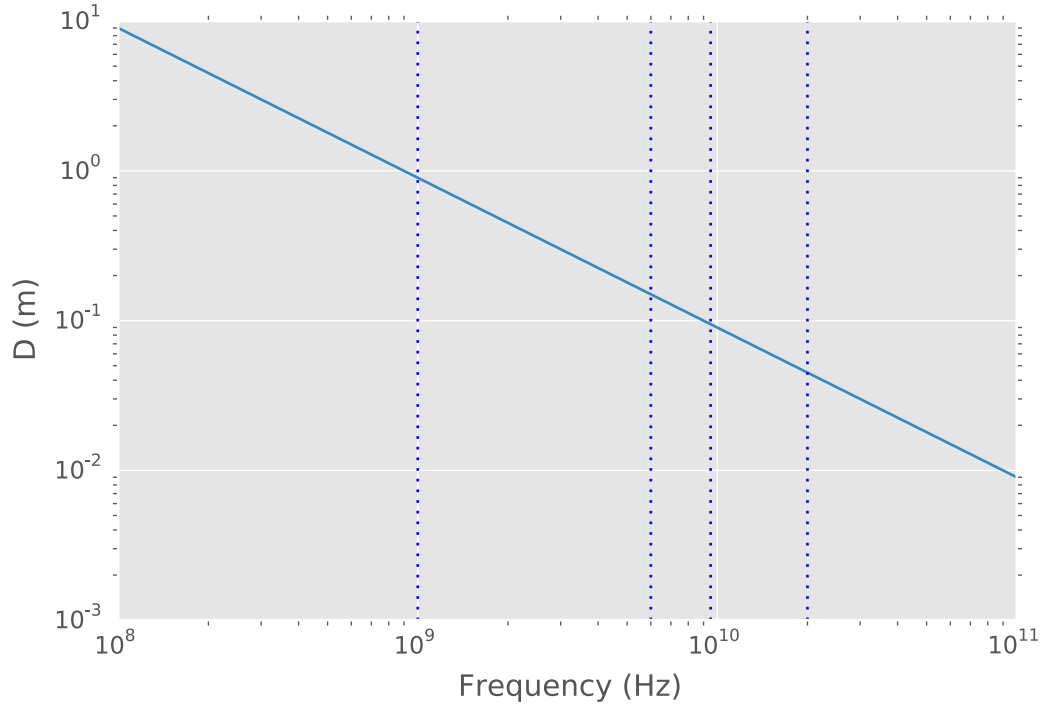


Figure 6.2: Minimum thickness to meet the slab approximation criterion versus frequency with reference lines for 1, 6, 9.5, and 20 GHz.

Table 6.2: Theoretical phase differences for various parameters.

| Freq (GHz) | D (mm) | n_e (m^{-3}) | $\Delta\phi$ (deg) |
|------------|----------|---------------------------|--------------------|
| 1 | 900 | 5×10^{15} | 217.974 |
| 1 | 900 | 3.4×10^{16} | 1482.22 |
| 6 | 150 | 5×10^{15} | 6.05484 |
| 6 | 150 | 3.4×10^{16} | 41.1729 |
| 9.5 | 95 | 5×10^{15} | 2.42193 |
| 9.5 | 95 | 3.4×10^{16} | 16.4692 |
| 20 | 45 | 5×10^{15} | 0.544935 |
| 20 | 45 | 3.4×10^{16} | 3.70556 |

to measure a large phase difference that is over 360° such as at 1 GHz; likewise, it is difficult to measure the small phase differences at 20 GHz due to instrument accuracy.

To visualize system limitations and criteria, electron density versus frequency has been plotted in Figure 6.3 for five phase differences. To assist with applying this information to practical

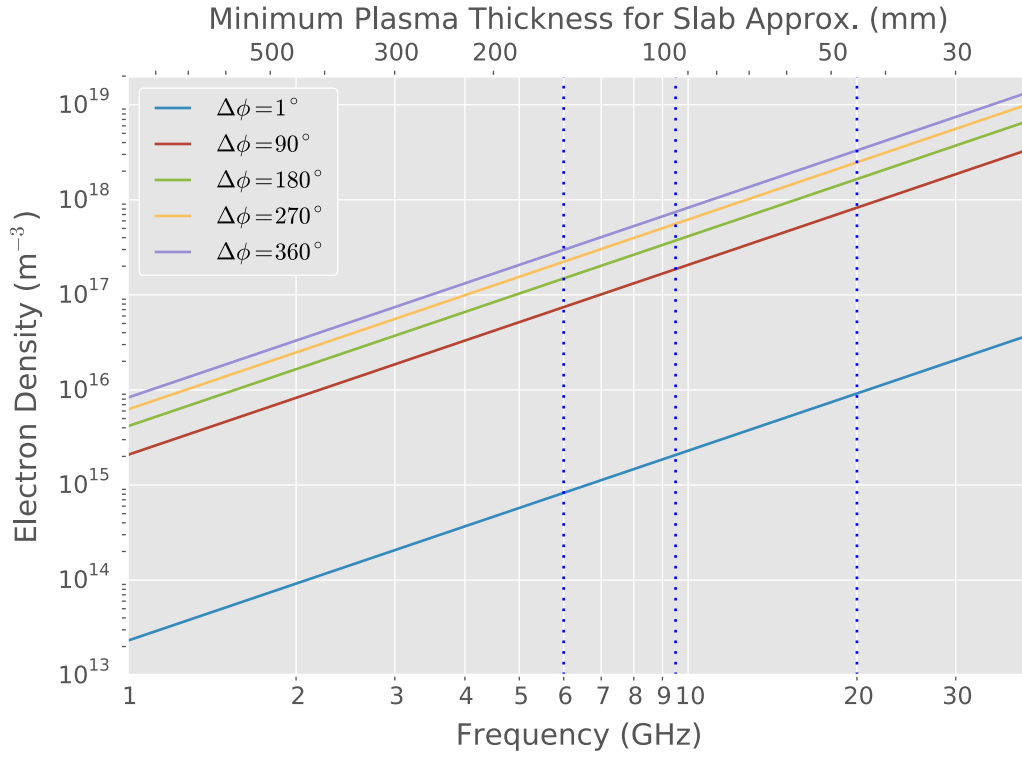


Figure 6.3: Minimum thickness to meet the slab approximation criterion versus frequency with reference lines for 1, 6, 9.5, and 20 GHz.

systems, vertical lines at the frequencies of interest are plotted and the upper horizontal axis is labeled with the minimum plasma thickness for the slab approximation to be valid. The lowest line corresponds to a phase difference of one degree and represents the minimum, practically measurable electron density at a given frequency. As electron density increases, each curve corresponds to a progressively larger phase difference. The upper limit of a system is determined by its ability to measure phase differences over 360° without ambiguity. Difficulties with phase ambiguity may lead to problems interpreting measured data.

Table 6.3: Summary of interferometric experiments.

| Name | VNA | Freq. (GHz) | x (in) [†] | y (in) [‡] | Description |
|--------------|---------|-------------|-----------------------|-----------------------|------------------------------------|
| ECE Hood | HP 8753 | 2–6 | 10.74 | 4.5 | Initial experiments in hood |
| Calorimeter | HP 8753 | 2–6 | 26 | 4 | Basic setup in calorimeter |
| Shutter | HP 8753 | 2–6 | 26 | 4 | Shutter setup at lower frequencies |
| Mesh covered | HP 8720 | 2–18 | 18 | 4.5 | Mesh cover over dish |

[†]Front of horn to front of horn

[‡]Distance between bottom of dish to mid-line of antennas, see Fig. 6.4

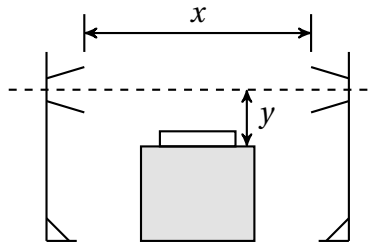


Figure 6.4: Schematic drawing of interferometer dimensions.

6.2 Experimental Setup

A microwave interferometer was setup in four different configurations as listed in Table 6.3. The experimental setup was designed around existing and low-cost solutions as this work was investigatory in nature and a large capital outlay could not be supported. In general, two horn antennas were placed roughly two feet (Fig. 6.4) apart with a 150 mm diameter glass petri dish placed mid-way between the horns on either a cinder block or a piece of Duraboard insulation. In one experimental configuration, pieces of sheet metal were placed around the petri dish to create a shutter so that the only direct coupling between the antennas was through the flame. Three different fuels were burned independently: 1) methanol, 2) methanol with saturated sodium chloride, or 3) Plexiglas samples. A reference measurement was taken before the sample was ignited. While the sample was burning, measurements were acquired as quickly as possible using either an HP 8753D or an HP 8720, which were calibrated to the antenna test ports.

ECE Hood This was the first interferometric setup. The petri dish was placed on top of a cinder block in the ECE fume hood as shown in Figure 6.5.

Calorimeter An interferometric setup was placed around the cone calorimeter (mfg. Fire Testing Technology) in Dr. Wichman's laboratory as shown in Figure 6.6 by placing the petri dish on a piece of Duraboard insulation which replaced the original calorimeter burner.

Shutter Four pieces of sheet metal were placed around the petri dish (Figs. 6.7 and 6.8) to create a shutter. Besides affecting the electromagnetic transmissions, the behavior of the flame was also affected (Fig. 6.9). The pieces of sheet metal were 12.25 inches tall by 7.5 inches wide and were separated by 4 inches at the base with an opening of 5 inches for the flame.

Mesh The petri dish was placed between wire mesh and a piece of sheet metal (Fig. 6.10) that was then placed on top of a cinder block. The goal of the mesh is to electrically shield the fuel from the electromagnetic waves while allowing the flame through. A rule of thumb for mesh electrical shields is that the openings should be less than a tenth of a wavelength at the highest frequency. The mesh that was used had 0.125 inch openings which corresponds to a tenth of a wavelength at 9.5 GHz. Data was captured up to 18 GHz in this experiment; however, only results over a smaller band are used because of the limits of the mesh. Figures 6.11 through 6.12 show the transmission magnitude up to 17 GHz (truncated from 18 GHz due to cosine tapering) for the setup in various configurations without any fire to demonstrate the shielding effectiveness of the mesh versus frequency. As frequency increases, the responses vary more showing that the mesh becomes less effective.

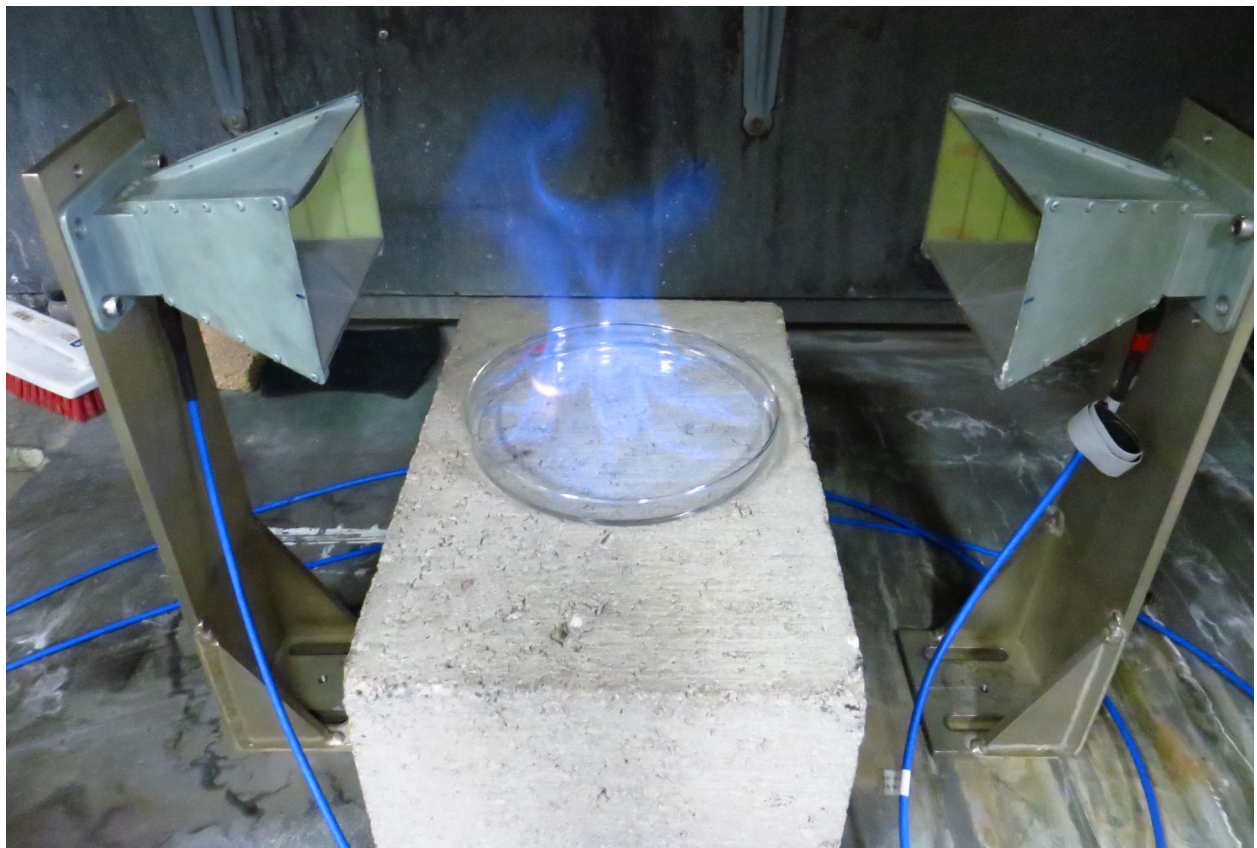


Figure 6.5: Experimental setup in the ECE hood for interferometer measurements.

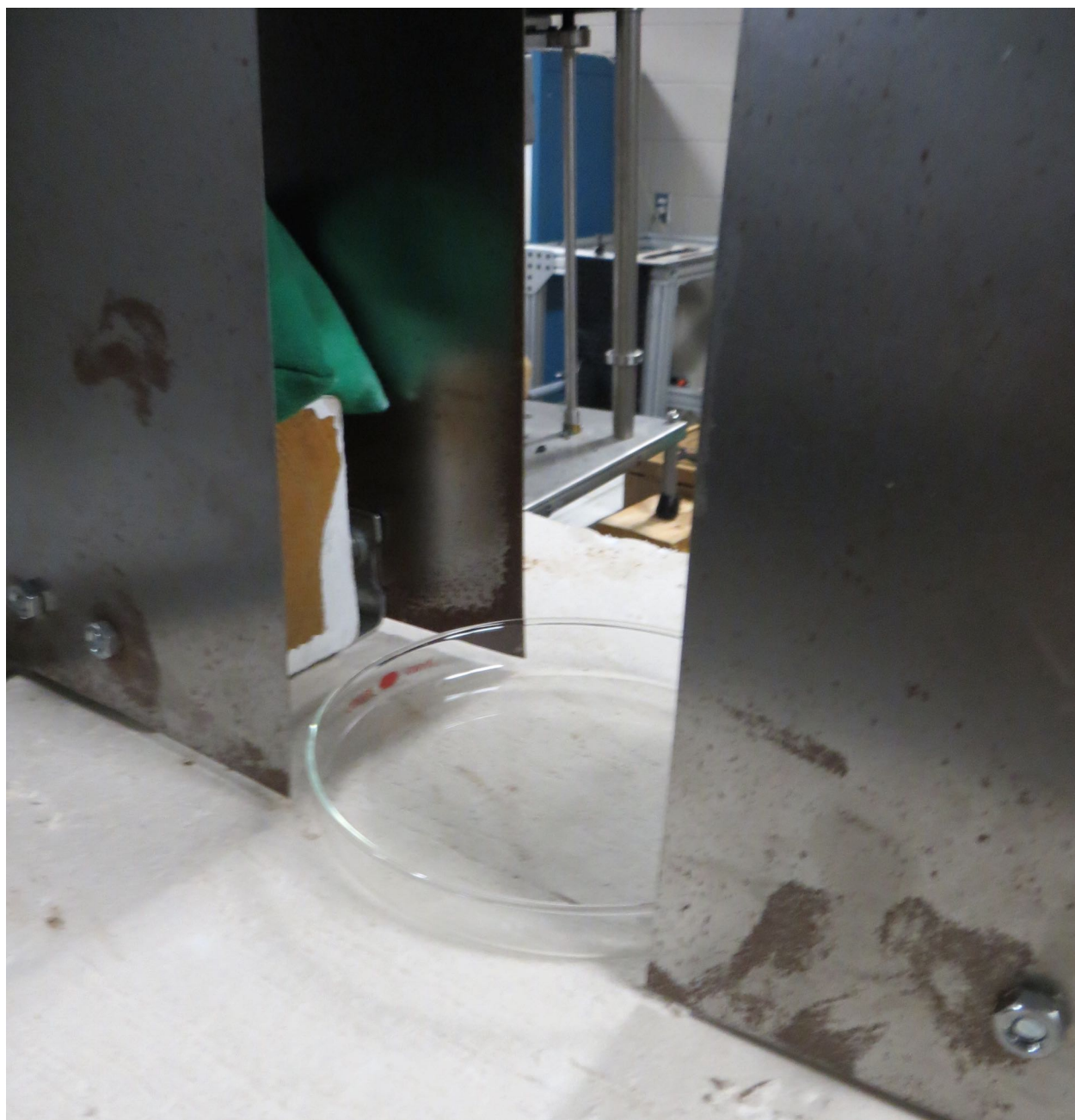


Figure 6.6: Experimental setup in the cone calorimeter for interferometer measurements.



Figure 6.7: Configuration of the metal shutter.



Figure 6.8: Configuration of the metal shutter as seen from the side.



Figure 6.9: Photo of a flame being drawn into the side of the shutter.

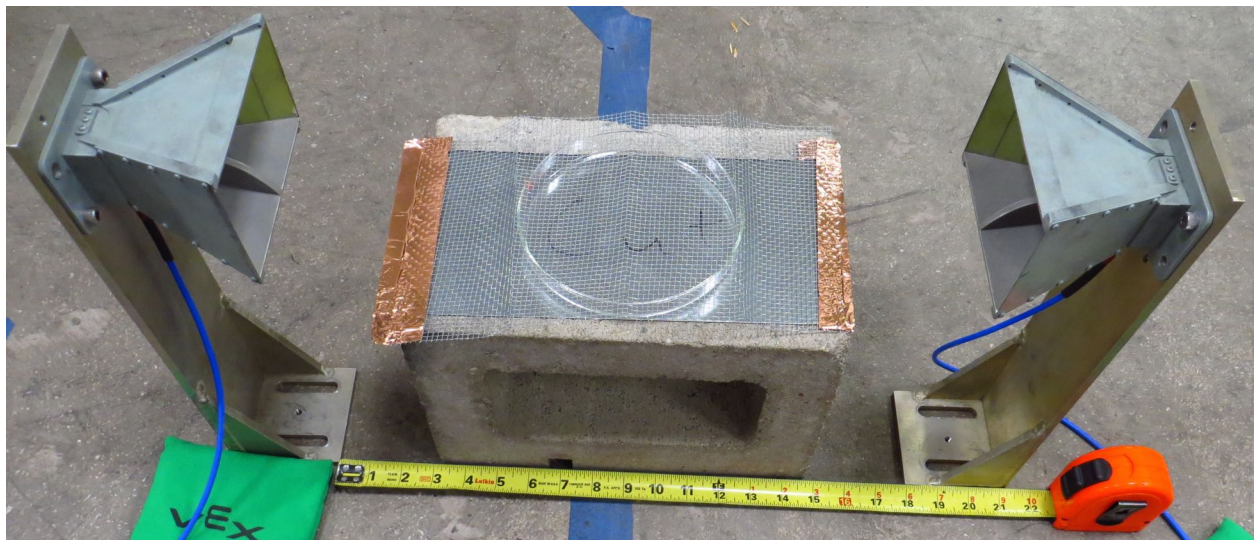


Figure 6.10: Experimental setup for the mesh interferometer measurements.

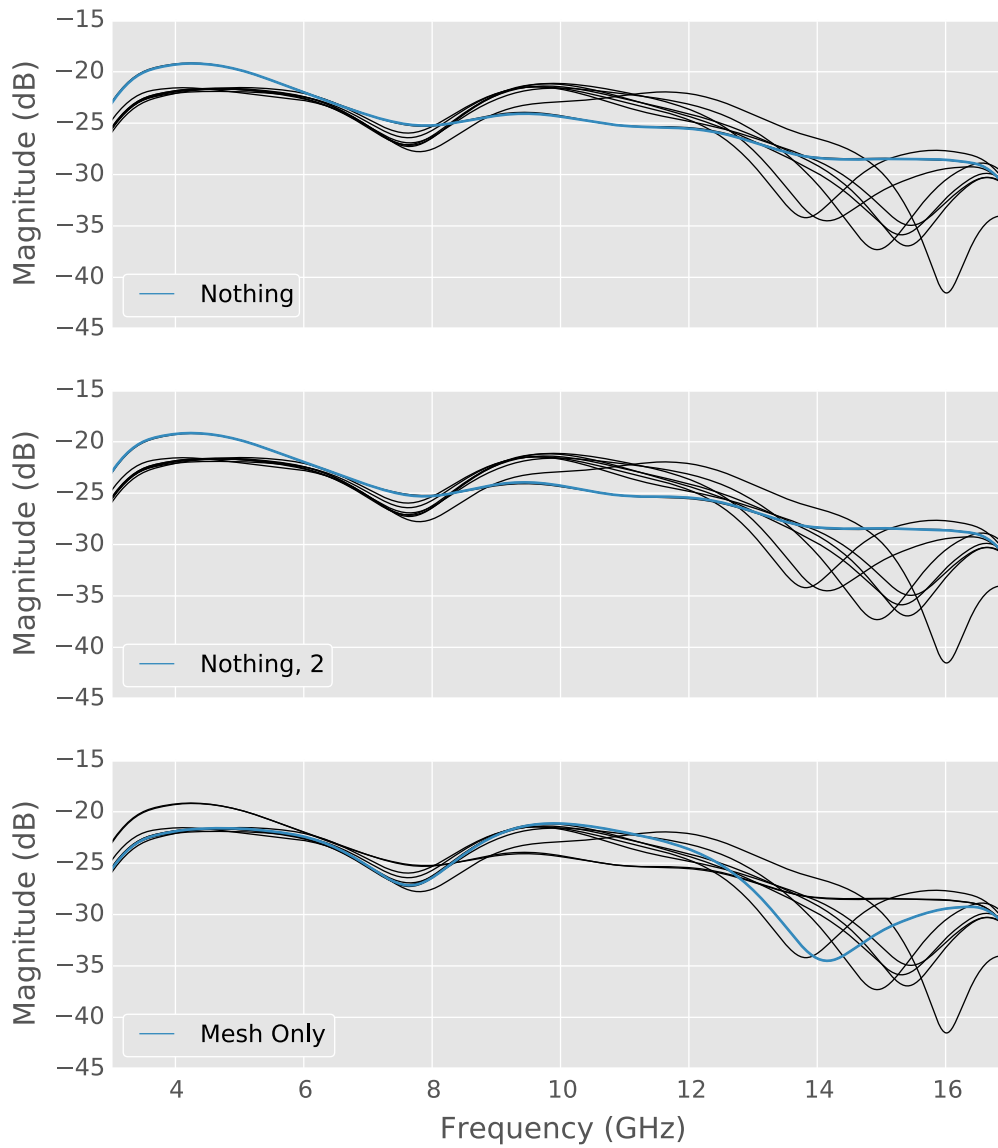


Figure 6.11: Transmission measurements in the mesh experimental setup in various configurations with no fire demonstrating the frequency limits of the mesh for shielding, panel 1

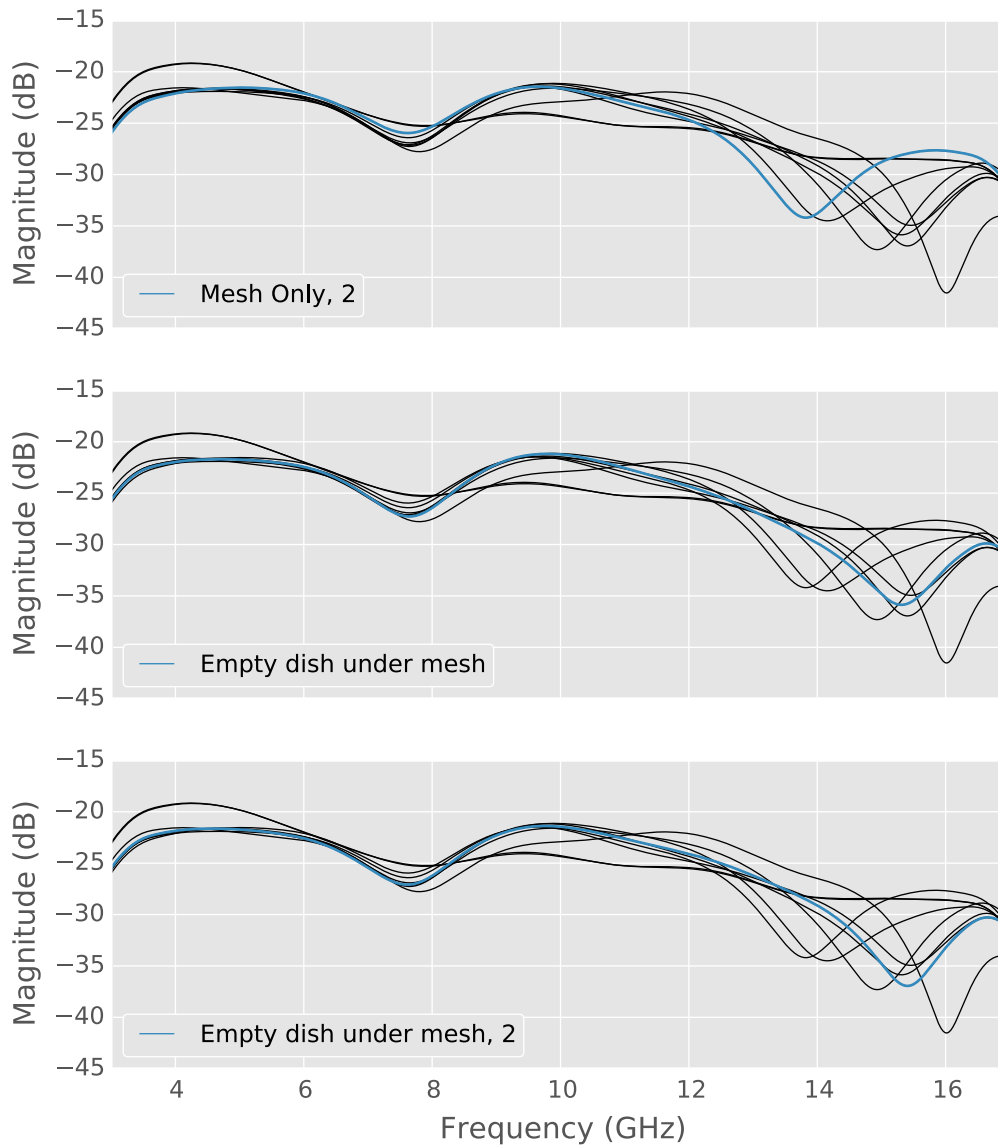


Figure 6.12: Transmission measurements in the mesh experimental setup in various configurations with no fire demonstrating the frequency limits of the mesh for shielding, panel 2

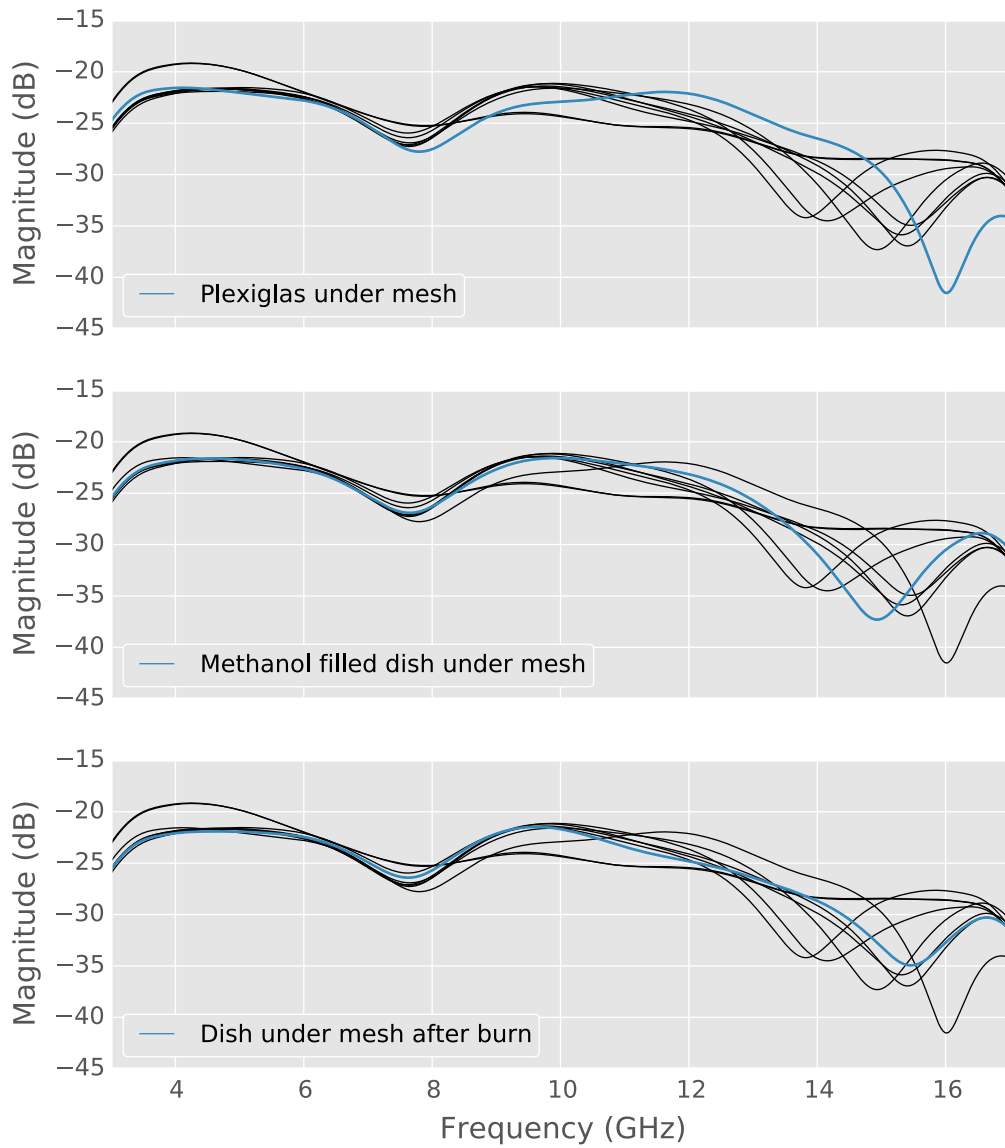


Figure 6.13: Transmission measurements in the mesh experimental setup in various configurations with no fire demonstrating the frequency limits of the mesh for shielding, panel 3

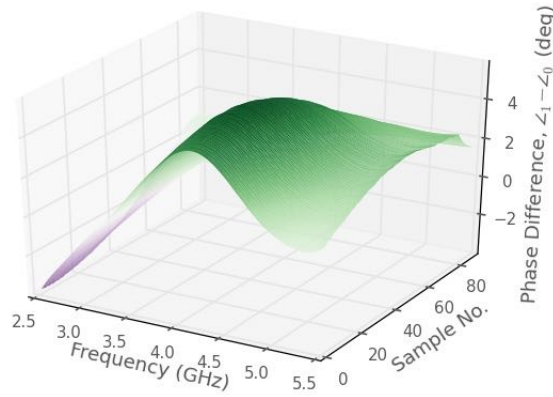


Figure 6.14: Phase difference in 3D from burning methanol for the ECE hood experiment.

6.3 Results

Data from the experiments are presented in the following sections. Data were processed using IPython notebooks similar to the one in Appendix N . The data was time gated as in Section 5.1.2 using Wavecalc macros generated by the IPython notebooks. Most results are truncated to the range of 2.5 GHz to 5.5 GHz due to the cosine weighting applied during processing. In the results presented below, time is indicated by increasing sample number. A final summary panel is presented at the end of the chapter in Figure 6.37.

6.3.1 ECE Hood Experiment Results

Results from the initial interferometric experiment are shown in Figure 6.14 through 6.17. For both the methanol and the sodium chloride burn, the phase is negative below and positive above about 3 GHz at the beginning of the burn. As time progresses and the flame diminishes, the phase difference approaches zero. The greatest electron density is around 2.5×10^{17} and 3.2×10^{17} for methanol and sodium chloride, respectively, both of which occur near 6 GHz.

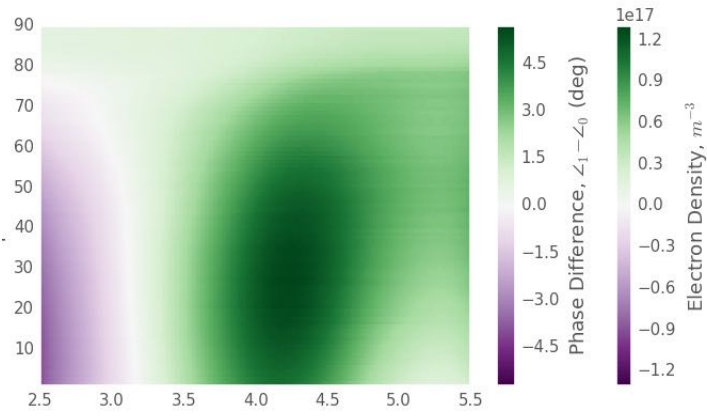


Figure 6.15: Phase difference from burning methanol for the ECE hood experiment.

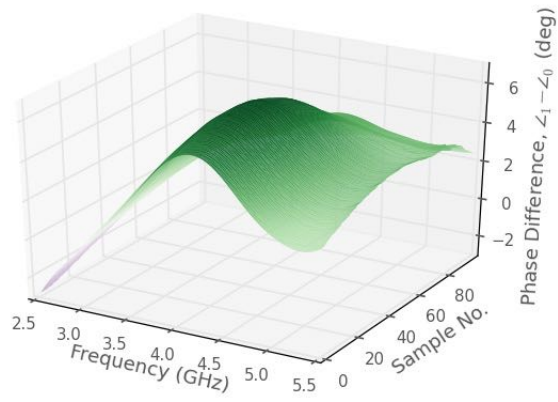


Figure 6.16: Phase difference in 3D from burning sodium chloride solution for the ECE hood experiment.

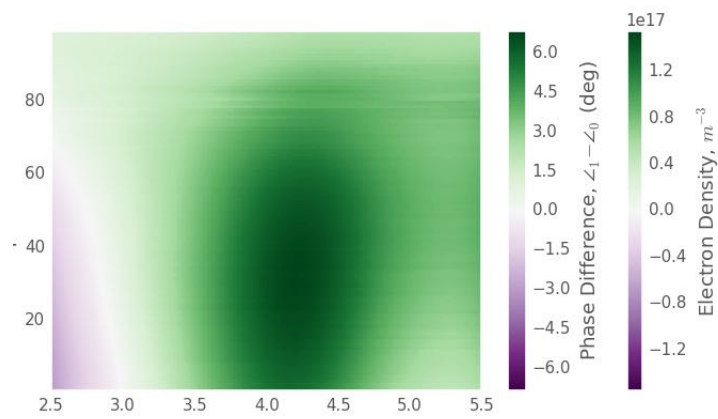


Figure 6.17: Phase difference from burning sodium chloride solution for the ECE hood experiment.

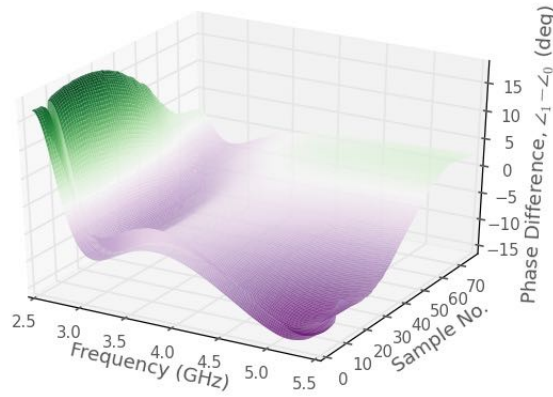


Figure 6.18: Phase difference in 3D from burning methanol in the cone calorimeter experiment.

6.3.2 Calorimeter Experiment Results

Figures 6.18 through 6.23 show the measured phase difference and calculated electron densities for measurements made in the cone calorimeter with no shutter installed. The phase difference is positive at frequencies below about 2.75 GHz and becomes more negative as frequency increases, which is opposite the behavior seen in the ECE hood experiments. As the fuel is consumed, the phase difference approaches zero. This time dependent behavior, however, is not observed in the Plexiglas burn for which the flame size and behavior varied the most due to the surface area changing. In contrast, pool fires, like the methanol or sodium chloride ones, have essentially a constant surface area over which to burn and should have relatively constant results until the end. The greatest calculated electron densities per cubic meter were around 7×10^{17} , 8×10^{17} , and 1.3×10^{18} for methanol, sodium chloride, and Plexiglas fires, respectively.

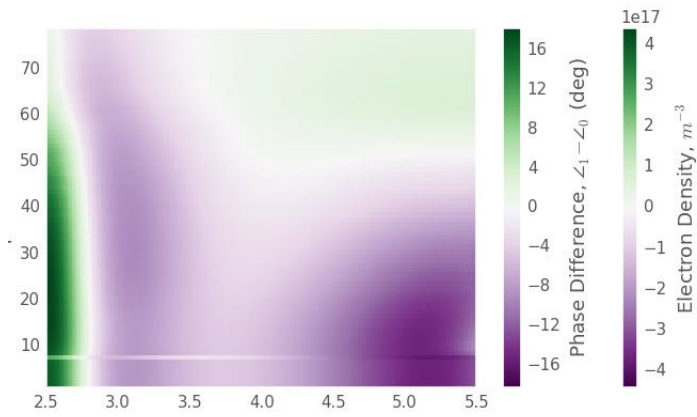


Figure 6.19: Phase difference from burning methanol in the cone calorimeter experiment.

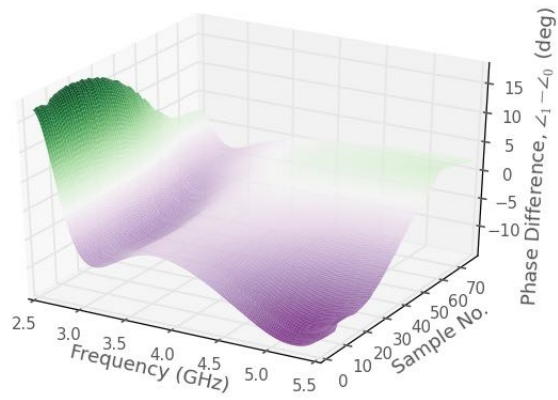


Figure 6.20: Phase difference from burning sodium chloride solution in the cone calorimeter experiment.

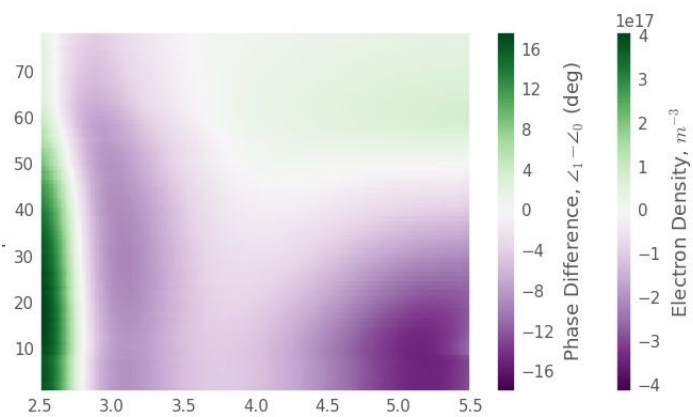


Figure 6.21: Phase difference from burning salt in the cone calorimeter experiment.

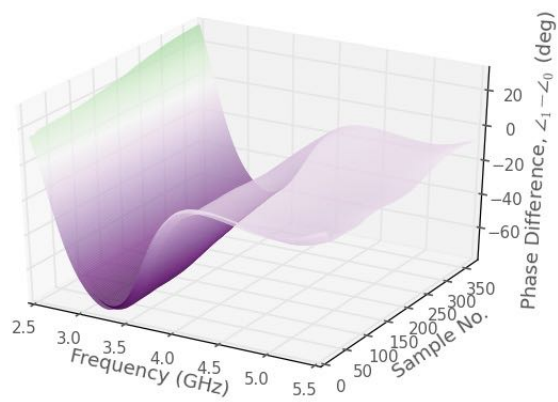


Figure 6.22: Phase difference 3D from burning Plexiglas in the cone calorimeter experiment.

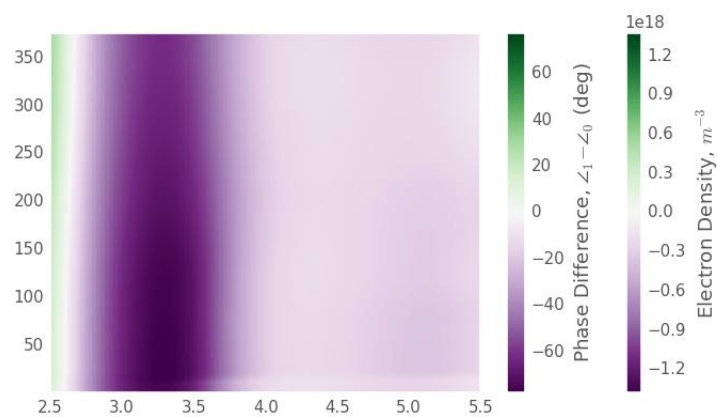


Figure 6.23: Phase difference from burning Plexiglas in the cone calorimeter experiment.

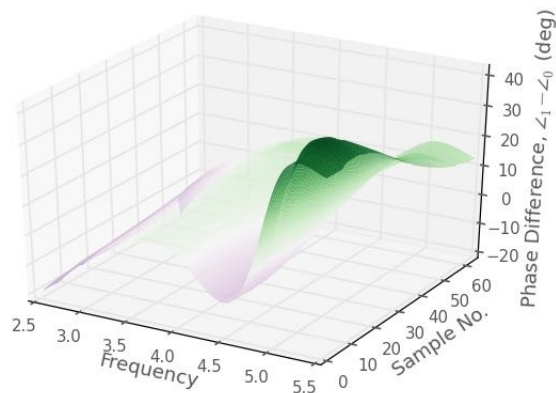


Figure 6.24: Phase difference 3D from burning methanol in the shutter experiment.

6.3.3 Shutter Experiment Results

Figures 6.24 through 6.31 show the measured phase difference and calculated electron densities when a shutter was installed around the flame. For this experiment, a methanol fire was measured two different times. The phase difference is near zero until between 4.5 GHz and 5 GHz in these fires, at which point the phase difference increases. As was seen in the earlier experiments, the phase difference approaches zero as the flame extinguishes. The greatest electron density per cubic meter for methanol (1st and 2nd burns), sodium chloride, and Plexiglas were approximately 1×10^{18} , 1×10^{18} , 8×10^{17} , and 5×10^{17} , respectively. Sample number 7 was not plotted because it was over 30° different than all other samples.

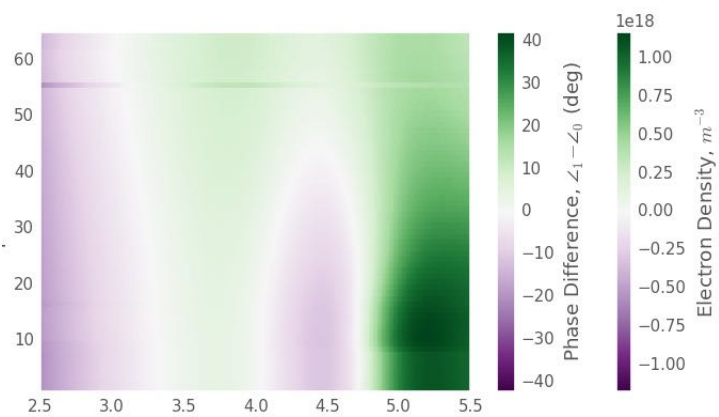


Figure 6.25: Phase difference from burning methanol in the shutter experiment.

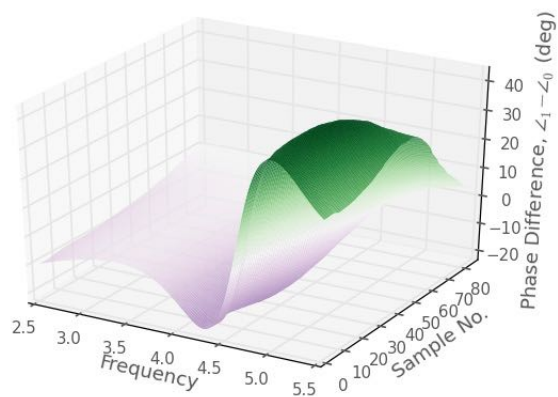


Figure 6.26: Phase difference 3D from burning a second sample of methanol in the shutter experiment.

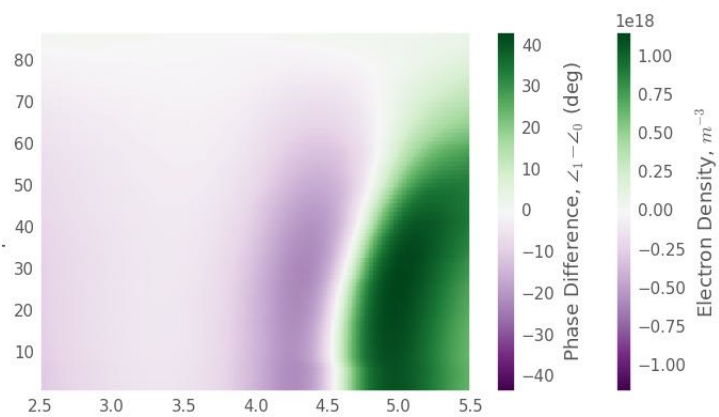


Figure 6.27: Phase difference from burning a second sample of methanol in the shutter experiment.

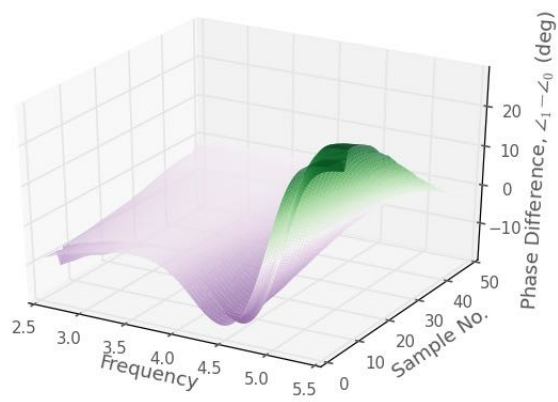


Figure 6.28: Phase difference 3D from burning sodium chloride solution in the shutter experiment.

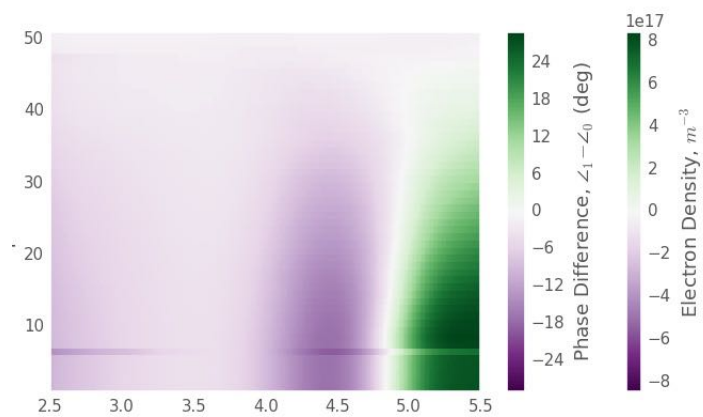


Figure 6.29: Phase difference from burning sodium chloride solution in the shutter experiment.

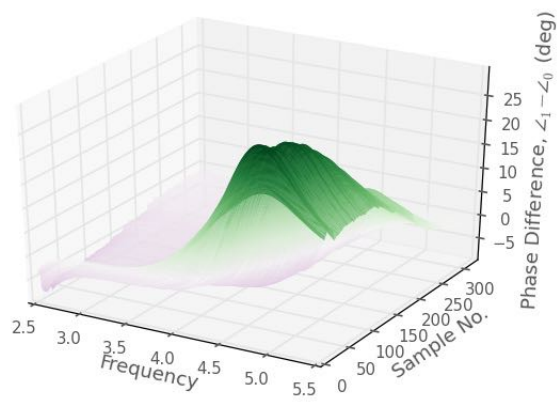


Figure 6.30: Phase difference 3D from burning Plexiglas in the shutter experiment.

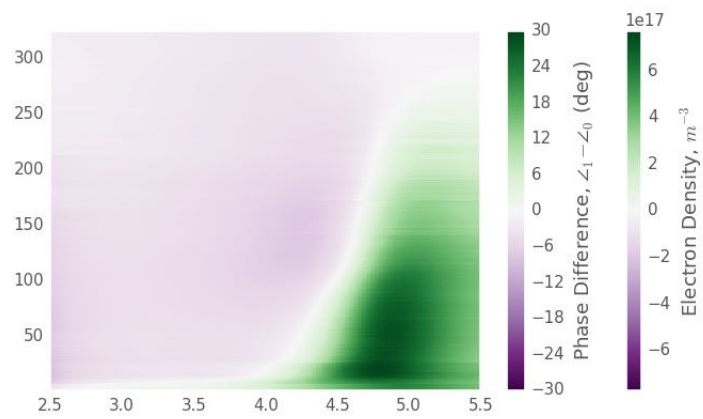


Figure 6.31: Phase difference from burning Plexiglas in the shutter experiment.

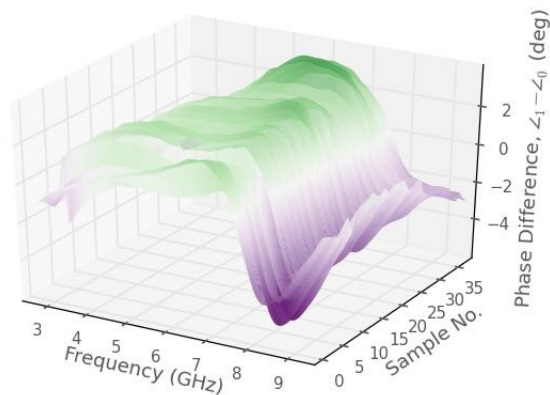


Figure 6.32: Phase difference 3D from burning methanol in the mesh experiment.

6.3.4 Mesh Experiment Results

Results for the experiments in which the petri dish was covered by wire mesh are shown in Figure 6.32 through 6.35. The phase difference peaks around 6 GHz and is negative at either end of the measured frequency band. A time dependence is not observed as in the previous experiments. Peak electron densities were calculated as approximately 2.4×10^{17} for both methanol and sodium chloride. Sample 23 from the methanol burn and samples 9, 10, and 38 from the salt burn were not plotted as they grossly deviated from the other samples.

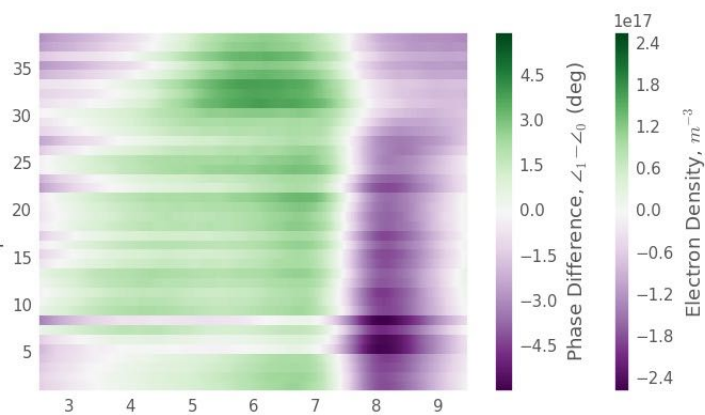


Figure 6.33: Phase difference from burning methanol in the mesh experiment.

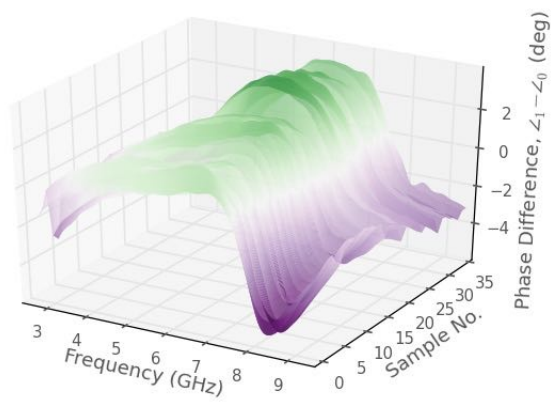


Figure 6.34: Phase difference 3D from burning sodium chloride solution in the mesh experiment.

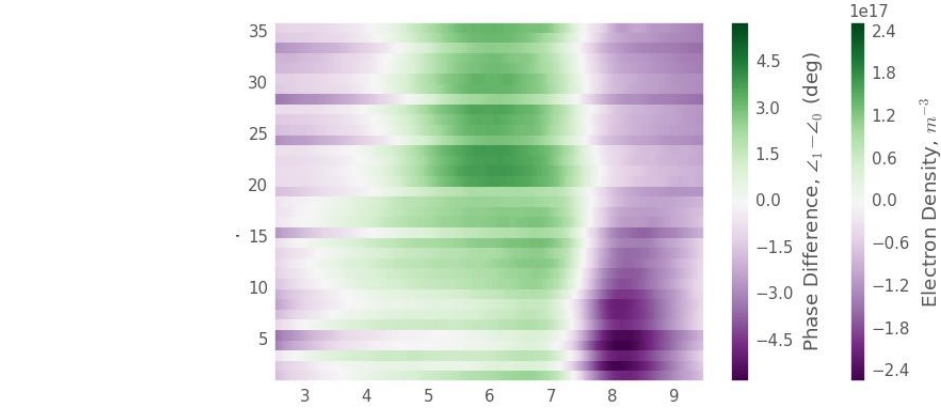


Figure 6.35: Phase difference from burning sodium chloride solution in the mesh experiment.

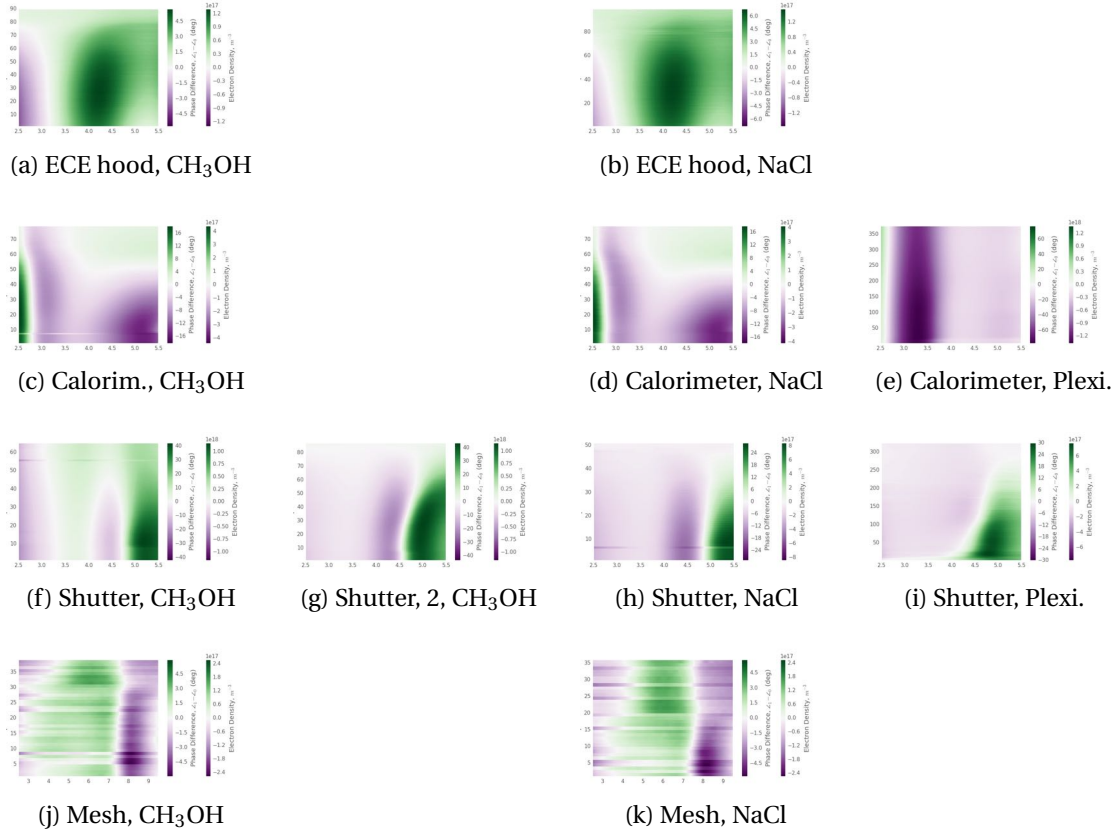


Figure 6.36: Summary panel of interferometric measurements, each with own color scale.

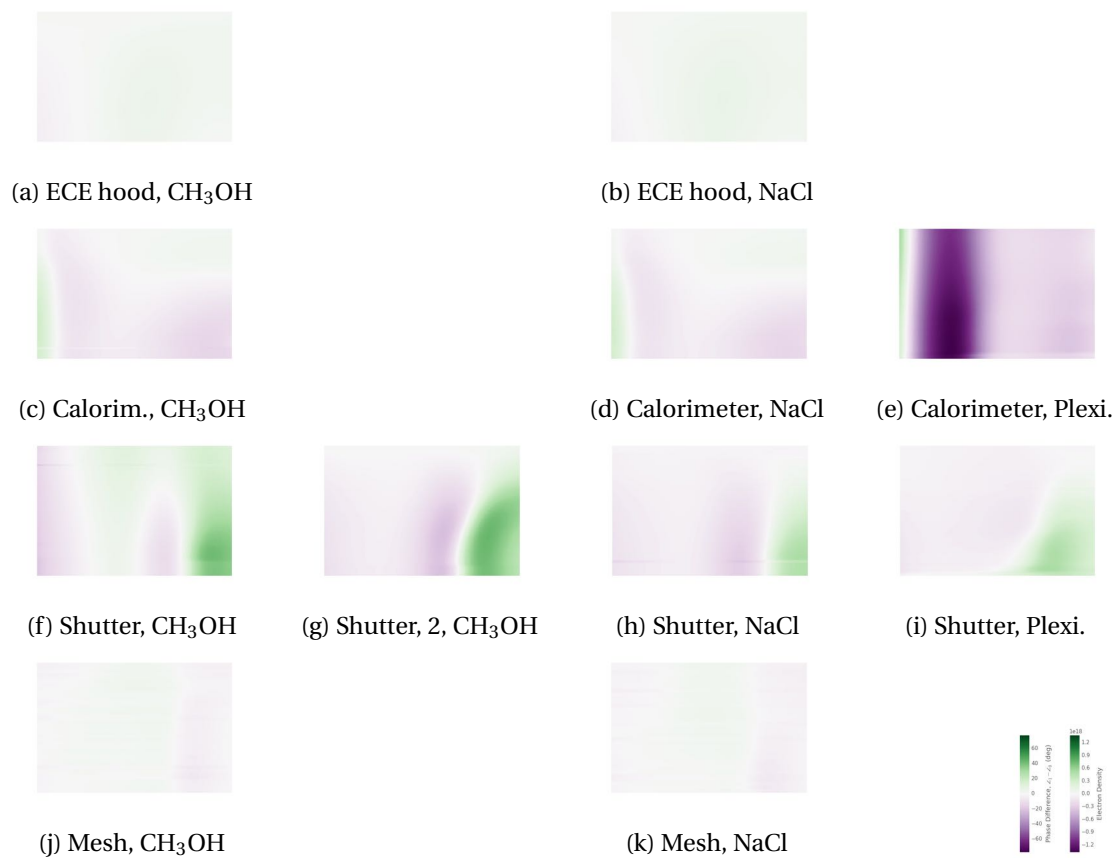


Figure 6.37: Summary panel of interferometric measurements normalized to the same color scale.

6.4 Discussion

The results presented in the previous section provide an initial study on how interferometry may be used to characterize fire-induced plasmas. The first item to note is that the results from the ECE hood and the calorimeter experiments are similar but with a sign difference. The setup of these two experiments were the most similar of all the interferometry setups; therefore, closer agreement is expected. An exact cause for this sign difference is not known; however, phase ambiguity from unwrapping the phase is a likely source of error. Future work should look to develop a robust algorithm for these types of measurements.

The peak electron density measured is one to two orders of magnitude larger than the observed values in wildland fires. Across all samples in interferometer burns, the electron density varied with frequency. The slab approximation used to derive this electron density need a minimum plasma thickness in order to be valid. Measurements were taken across as wide a frequency band as possible—even though the slab approximation may be invalid for portions of the band—since the objective was to investigate the technique and evaluate performance of interferometry. Further theory could be developed, especially in combination with computational simulations in the future to extend the usable frequency range. This may also give insight into the observed variability. Phase ambiguity is another concern here as in the last item and should be further investigated when additional theory is developed.

Many of results show a time dependence by returning to a nearly zero phase difference at the end of the measurement. Due to the relatively long time required to measure one sample (usually between 10 seconds and 30 seconds), it is thought that this time dependence may be partially due to the fuel consumption. This led to the mesh experiment being conducted, for which the only time variance observed should be the transition at ignition and extinguishment. This expected time variance is not observed in the mesh experiments; instead, the response was time invariant. This counter-physical result requires further investigation to explain.

The most promising results are those from the setup which used a shutter. At lower frequencies where the slab approximations are not valid, there is little phase difference. A relatively large, positive phase difference occurs at higher frequencies for which the slab approximation is acceptable. This suggests that there is a fire-induced plasma. The electron density across one sample has less variation compared to measurements from other experimental setups suggesting that the shutter helps to eliminate other propagation paths, thereby improving measurement accuracy.

Overall, these experiments provide useful initial, exploratory results that can help future experiments be developed. Setups making use of wire mesh for shielding as well as shutters should be further investigated. It would be worthwhile to combine the two into one setup. A square fuel dish may be used with a single wall on either side of it.

6.5 Conclusion

This chapter has investigated using interferometric techniques to characterize fire-induced plasmas in the laboratory. Experiments were conducted using various setups and multiple fuels to evaluate this technique. Preliminary results suggest that plasmas may be formed, and that these plasmas may be measured using interferometry. Future work should look to reduce phase ambiguities, increase frequency—initially to X-band (8–12 GHz)—and improve the shutter and mesh/shielding setup.

Chapter 7

Transmissions from Inside of a House Fire

While other experiments have located both the transmitting and receiving antennas outside of the fire, an experiment was conducted with the transmitters placed inside of a burning house. Placing transmitters inside of a fire means that the transmitted signal must propagate through the fire. Negative effects from diffraction, focusing, and other problems associated with transmission measurements in a range setup (as in previous chapters) are mitigated.

This house was burned as part of the Michigan State Police Department's Fire Investigation Class at the end of October 2014. The state police welcomed this work and looked to accommodate it where they could. Since the main objective of this burn was not this research, this experiment worked around the constraints and needs of the investigation class. Insulated transmitters were placed in three separate locations to transmit five frequencies. Signal strength was measured before, during, and after the house burned. For this fire investigation class, fire fighters and law enforcement personnel from around the state learned how to investigate fires, how arson fires are set, about fire growth and behavior, and other related topics. To conclude the class, instructors started multiple fires inside of a house. Fire fighters from area fire departments, using this as a training exercise, entered the house and extinguished the fire. First, fires were set on the first floor and extinguished, then fires were set on the second floor and extin-

guished. The next morning, the students investigated this fire. Once their investigation was completed, another fire was set and the house burnt down.

Further, this experiment simulates how a house fire could effect the transmissions from firefighters inside of a house to those outside of the house. Of the firefighter line of duty deaths that occur when the firefighter is inside of a burning structure, many involve a flashover or other heavy fire conditions. Radio communication failures between incident commanders or officers and the firefighter are common in these cases. While many reasons for these failures exist, one possibility is that the fire blocks or at least degrades transmissions. This, combined with the degradation already caused by the structure, could render communications useless. Such a scenario is made more likely due to modern trunked and/or digital systems which do not work well in very low signal environments¹. This hypothesis is only supported by what both Boan and Mphale say is anecdotal evidence found in [66] and [67]. These two works could not be obtained at the time of writing for review. These two references reportedly say that the radio transmissions between wildland firefighters that were transmitted through a wildfire front (where the largest, most intense flames are) were cut-off sometimes. Additionally, a review of line of duty death reports has not been conducted to determine how likely this scenario is or if there are other obvious causes for radio failures. Much of this theory is based upon personal firefighting and electromagnetic engineering experience.

7.1 Transmitters

It was impractical to place a wideband transmitter and antenna in the house due to the high risk of damaging the instrument. Instead, five frequencies that are commonly used for commu-

¹A common tactic taught to firefighters who are in trouble and cannot make successful communication with anyone is to switch their radio to a simplex, analog channel that does not go through any trunking system, but instead transmits directly to other radios. The reasoning is that the low-level signal may be received by those nearby whereas it could not be received by the trunked/digital system controller located at a tower site some distance away.

nications and for which low-cost transmitters are available were selected. Different transmission modes were used at different frequencies based on transmitter availability. The frequency bands and modes were:

- 144 MHz band transmitting a continuous signal
- 440 MHz band transmitting a continuous signal
- 900 MHz band ZigBee transmitter
- 2.4 GHz IEEE 802.11 g/n (Wi-Fi)
- 5 GHz IEEE 802.11 g/n (Wi-Fi)

The fire ignition points on the first floor and the transmitter locations are shown in Figure 7.1. As noted in the figure, the receivers were approximately 150 ft away from the house. The location was selected based on activities and personnel position for the class. No transmitters were placed on the second floor, therefore, the layout for the second floor is not provided.

7.1.1 Insulation

Transmitters were placed inside of plastic enclosures that had fiberglass batt insulation either inside of or around the box. The plastic enclosures were meant to keep the electronics safe from minor water damage and impacts; therefore, they were selected based upon availability, crush resistance, and water resistance. The plastic enclosures and fiberglass insulation were then placed inside of a box made from Duraboard insulation (see Section 5.2.1). The fiberglass insulation is used to insulate the electronics from any heat that may be transferred through the Duraboard box, which is meant to protect from direct flame exposure. To make the boxes, Duraboard was cut to pieces and joined using twist ties of steel picture-hanging wire that was pushed through adjoining pieces.

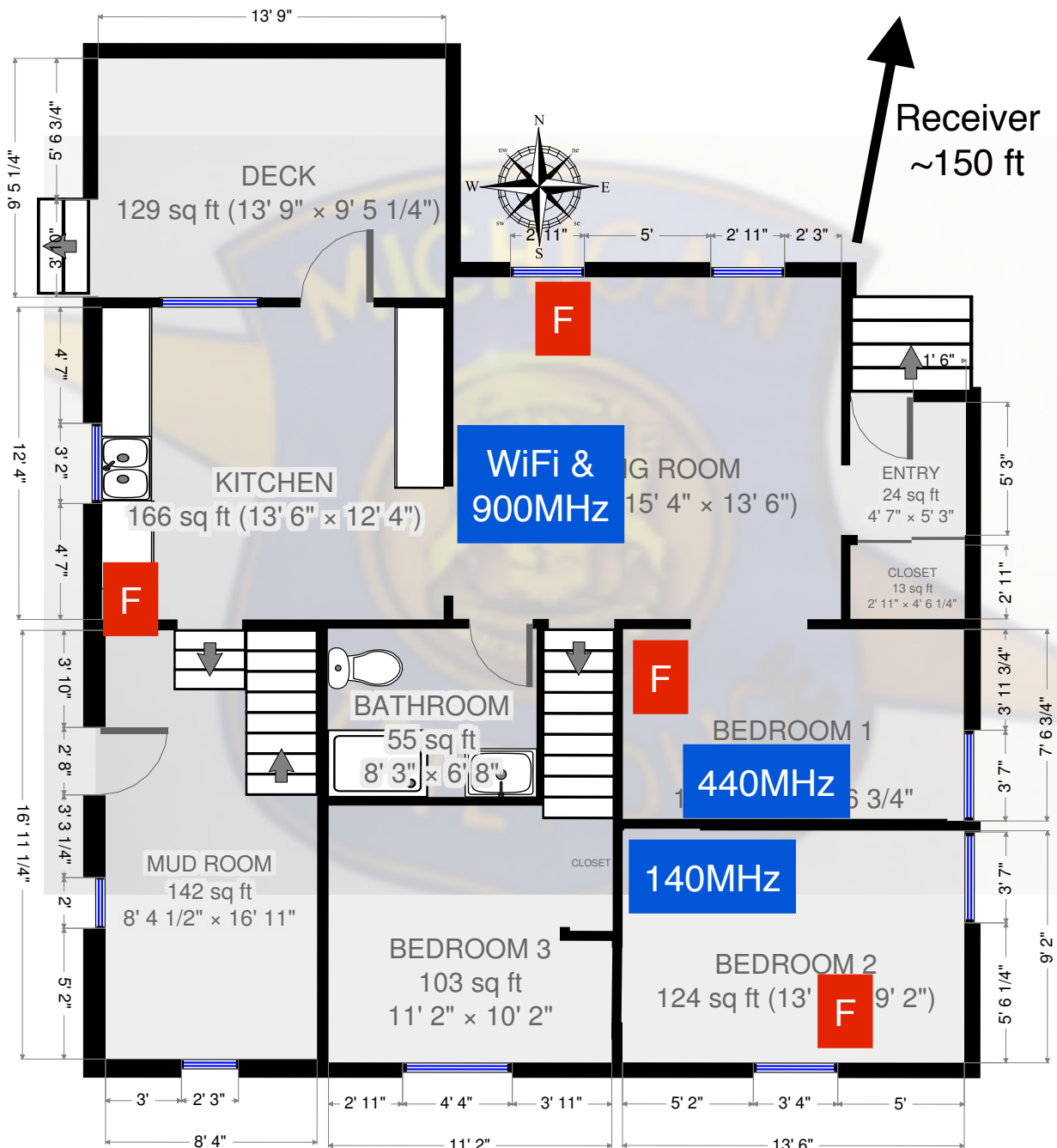


Figure 7.1: Plan view of the first story of the burn house. Blue text boxes indicate transmitter locations and red text boxes indicate ignition points. Original diagram courtesy of Michigan State Police.

The effects of the insulation and plastic enclosures on the transmissions is not a major concern. The transmission properties should not change during the fire, although they may change when water, used to extinguish the fire, is absorbed into the insulation. Since extinguishment is not the time period of interest, this is acceptable. The main concern for the enclosures is that a significantly strong signal is received. This eliminates using metal enclosures (although these could be used if the transmitting antenna was outside of the enclosure with the transmitter, batteries, etc. inside).

7.1.2 144 MHz CW Transmitter

A Micro-Fox 15 transmitter (Fig. 7.2a) from Byonics, LLC [68] was used for the 144 MHz transmitter. This is a small transmitter designed to transmit a continuous tone so that amateur (ham) radio operators can try to locate the transmitter. This activity is known as fox hunting. The transmitter has an output power of 10–15 mW. The Micro-Fox was configured to transmit at 146.565 MHz. This is an amateur radio frequency, so the transmitter was programmed with the author's amateur call sign of "KE7ESD". The Micro-Fox is a small circuit board with a microcontroller, RF chip, and SMA connector. It runs off of a single 9 V battery and has a toggle switch. The transmitter is programmed through a 2.5 mm TRS (headphone) jack. The circuit board and 9 V battery are slid into a plastic tube that has a cross section just large enough for the battery. One end cap of the tube has cut-outs for the SMA connector and toggle switch.

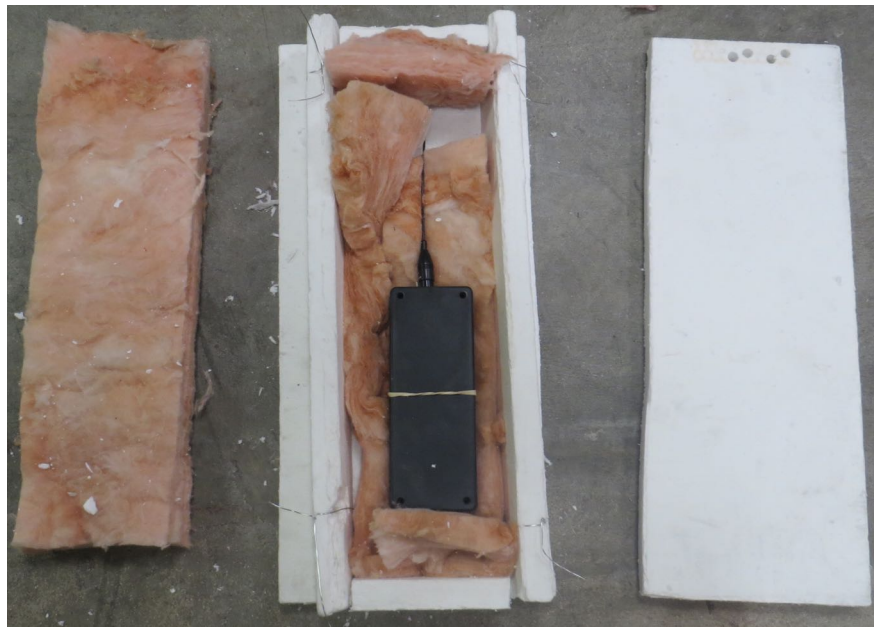
A project box was found that fit the Micro-Fox and then a small hole was cut in the side for the antenna and toggle switch (Fig. 7.2a). A rubber band around the project box allowed it to be easily opened and closed. The project box was placed inside of a Duraboard box, which was large enough for the project box and antenna, and surrounded by fiberglass insulation (Fig. 7.2c). The lid of the Duraboard box was held on using pieces of an aluminum street sign so that it could be easily opened to turn the transmitter on and off. Figure 7.2b shows the closed Duraboard box after the fire.



(a) Transmitter for 144 MHz in plastic project box.



(b) Closed 144 MHz transmitter box after the fire.



(c) Plastic project box for 144 MHz transmitter placed in insulation. *To the left is a piece of fiberglass insulation to be placed on top of the transmitter. The Duraboard piece of insulation on the right is then used to close the box.*

Figure 7.2: Transmitter for 144 MHz.

7.1.3 440 MHz CW Transmitter

A Radio Shack HTX-204 VHF/UHF Dual Band Transceiver (Fig. 7.3a, left) served as the 440 MHz transmitter. It was tuned to 442.125 MHz and controlled by an Arduino Uno-R3 (Fig. 7.3a, top right). The Arduino keyed the radio to transmit the author's call sign and then kept the radio keyed up. The call sign was transmitted every ten minutes as required by FCC regulations. Low (0.35 W), medium (2.5 W), and high (5 W) transmit powers could be selected on the radio. Which power level was used was not recorded at the experiment; however, the medium 2.5 W power level was most likely selected due to battery constraints. The HTX was powered by a lead acid battery (Fig. 7.3a, bottom right) through a regulator since the original battery for the radio was dead.

Like the 144 MHz transmitter, the HTX was placed inside of a project box which was then placed inside of a Duraboard box and surrounded by fiberglass insulation, see Figure 7.3c. The Duraboard box (Fig. 7.3b) was secured closed by twisting the steel wires instead of using pieces of a street sign. All of the photographs in Figure 7.3 were taken after the burn.

7.1.4 900 MHz XBee Transmitter

A Digi XBee-PRO XSC S3B 900 MHz with a wire antenna (Digi Part No. XBP9B-XCWT-001) was used as the ZigBee transmitter. It can transmit up to 250 mW. A SparkFun XBee shield connected the XBee to an Arduino Uno. The Uno controlled the XBee as well as sampling environmental data. The SparkFun Tutorial "Internet Datalogging With Arduino and XBee WiFi" [69] describes how to sample carbon monoxide, methane, ambient light, and temperature². The circuit was built with these sensors; however, only temperature was measured during the experiment. Temperature readings from the XBee's built-in sensor were also recorded. The light sensor was broken during testing. Gas readings could not be taken because the current draw

²Part numbers are not provided since the parts were ordered through the tutorial. It is expected that this tutorial will either be archived or updated to reflect SparkFun inventory.



(a) Open project box showing the 440 MHz transmitter, battery, and Arduino microcontroller.



(b) Closed 440 MHz transmitter box.



(c) Open 440 MHz transmitter box showing plastic project box and fiberglass insulation (pink).

Figure 7.3: Transmitter for 440 MHz.

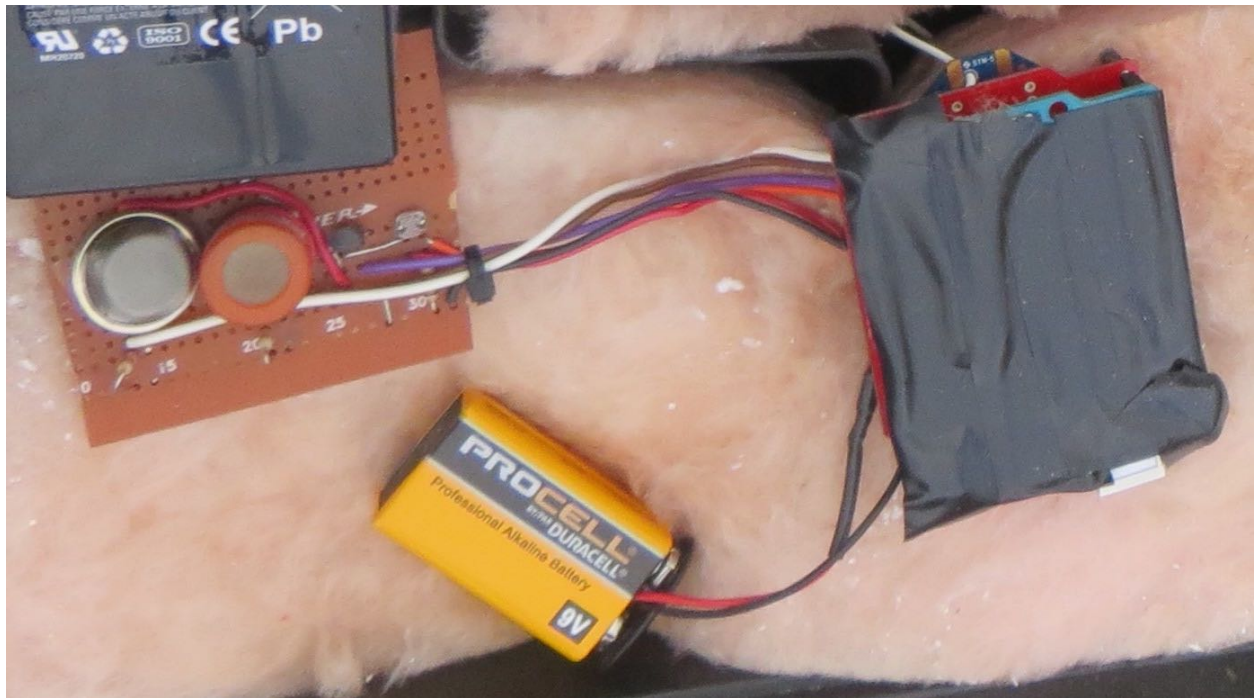


Figure 7.4: 900 MHz transmitter setup. The XBee module and wire antenna are barely visible in the top right because they are covered by the Arduino shield (red) and the Arduino Uno (blue board with electrical tape). The system is powered by a 9 V battery (center). From the left, the methane, carbon monoxide, temperature, and light sensors are visible on another circuit board.

for each sensor was too high and would have drained the battery too quickly. The XBee module was housed in the same container as the Wi-Fi router described in the next section.

7.1.5 2.4 GHz and 5 GHz Wi-Fi Transmitter

To transmit at 2.4 GHz and 5 GHz, a Netgear WNDR3400 router (Fig. 7.5a) was setup to broadcast two SSID's. Channels 6 and 153 were used for the 2.4 GHz and 5 GHz networks, respectively. A lead-acid battery provided power to the router through a regulator.

Thank you...

Dr. John Ross donated the router for this experiment.

The router, battery, and regulator were placed inside of an old electric power tool case. Also placed inside of this tool case were the 900 MHz XBee module and accessories. Fiberglass insulation lined the inside of the tool case to hold all parts in place in addition to providing thermal

insulation (Fig. 7.5a). This is different from the 144 MHz and 440 MHz transmitters that had the fiberglass insulation outside of the project box. The tool case was placed inside of a Duraboard box (Fig. 7.5b). The Duraboard box is shown closed after the fire in Figure 7.5c.



(a) Open tool case showing fiberglass insulation (pink), Wi-Fi router (2.4 GHz and 5 GHz), battery (center-bottom), and 900 MHz XBee and sensors (right).



(b) Open transmitter box showing the tool case enclosing the transmitters.



(c) Closed transmitter box for Wi-Fi and 900 MHz XBee.

Figure 7.5: Transmitters for Wi-Fi and 900 MHz XBee.

7.1.6 Transmitter Placement

The transmitters were placed into the house and turned on shortly before the time of ignition. The location of each Duraboard box is indicated in Figure 7.1. These locations were selected so that at least one fire would be between the transmitter and the receiver. In the figures below, a solid, white or black arrow points to a Duraboard box or where the box is if obscured. A broken, red arrow indicates an ignition point.

The 140 MHz transmitter was placed in the south-east room (Bedroom 2 in Fig. 7.1) of the house against the north wall of the room. It was placed with the antenna vertical under a small desk as shown in Figure 7.6a. An ignition point was on the south wall of this room under the window (Fig. 7.6b). An open doorway to the 440 MHz transmitter room is in the north-east corner of the room (immediately to the right of the photographer in Fig. 7.6b).

On the opposite side of the wall from the 144 MHz transmitter and slightly to the east was the 440 MHz transmitter (Bedroom 1 in Fig. 7.1). As seen in Figure 7.7a, the transmitter is against the wall between a dresser and a chair. The black arrow on the right of Figure 7.7a indicates the approximate location of the 144 MHz transmitter. In the north west corner of this room is an additional ignition point (broken red arrow in Fig. 7.7b). Directly north from the 440 MHz transmitter is a wide opening to the living room.

The tool case with Wi-Fi router and XBee was placed under a table in the living room (Fig. 7.8) next to the door to the kitchen (see Fig. 7.1). An ignition point is north of the transmitters under the window.



(a) 144 MHz transmitter in place under the desk.



(b) The room containing the 144 MHz transmitter. *The view is looking SW. The transmitter is located under the desk in the upper right of the photo. An ignition point is seen under the window on the left. The 440 MHz transmitter is located on the other side of the right wall.*

Figure 7.6: Placement of the 144 MHz transmitter.



(a) Placement of the 440 MHz transmitter. The black arrow on the right indicates the approximate location of the 144 MHz transmitter on the opposite side of the wall.



(b) The room containing the 440 MHz transmitter. The view is looking SW. The transmitter is located behind the dresser. The 144 MHz transmitter is on the opposite side of the wall. An ignition point is seen in the upper right corner of the photo. The door to the room containing the 144 MHz transmitter is immediately to the left of the photographer and the door to the living room is on the right side of the photo.

Figure 7.7: Placement of the 440 MHz transmitter.



Figure 7.8: Placement of the 900 MHz XBee and Wi-Fi transmitters. *The Duraboard box is in the table. At the top of the photo is an ignition point. The kitchen is immediately left of the photographer.*



Figure 7.9: Receivers as positioned for measurements. *The receivers were powered by the generator (right) and controlled by the laptops (right arrow). The XBee receiver is elevated on the spare tire (left arrow) and the 144/440 MHz receiver is next to the laptops (middle arrow).*

7.2 Receivers

The receivers were placed approximately 150 ft north of the house as indicated in Figure 7.1. All receivers were placed in the back of a jeep with the tail gate open (Fig. 7.9). Other vehicles were between the receivers and the house (Fig. 7.10). During the burn, people were moving around this area. None of the vehicles between the receivers and there house were moved during measurements. Vehicles did travel along the north-south road to the east of the receivers.

The receivers were powered by a portable generator and two laptops were used for sampling (Fig. 7.9). One laptop was used for the 144 MHz and 440 MHz receiver and the other was for the 900 MHz XBee and Wi-Fi. An AR8200 Wide Range Receiver from AOR was used to measure the signal strength of the 144 MHz and 440 MHz transmissions. The receiver was placed into a dual



Figure 7.10: Photo showing the receiver location relative to the house including vehicles in between the two.

frequency mode and monitored both frequencies at the same time. The LM command for the AR8200 was used to log the signal strength meter readings of the unit. The time was logged for each value. A table is provided in [70] that relates the value returned by the LM command for the AR8200 Series-2 with a black cabinet to dBm values. This table is repeated in Table 7.1. The original table includes values below -115 dBm which return a 0 value and values above -20 dBm which return a value of 139. The data in the table except for the -20 dBm point were fit to a 6th-order polynomial curve using the IPython notebook in Appendix O . The resulting curve is

$$\begin{aligned}
 y(x) = & (3.24612295 \times 10^{-10})x^6 + (-5.49175302 \times 10^{-8})x^5 + (1.17145927 \times 10^{-6})x^4 \\
 & + (2.61296036 \times 10^{-4})x^3 + (-0.0167315124)x^2 + (0.636706423)x - 114.993119
 \end{aligned} \quad (7.1)$$

Table 7.1: Lookup table for LM values to dBm.

| LM | dBm |
|-----|------|
| 0 | -115 |
| 10 | -110 |
| 27 | -105 |
| 42 | -100 |
| 55 | -95 |
| 68 | -90 |
| 86 | -80 |
| 97 | -70 |
| 103 | -60 |
| 106 | -50 |
| 109 | -40 |
| 112 | -30 |
| 139 | -20 |

which is shown in Figure 7.11 This equation was used to map the recorded LM values to dBm values. The -20 dBm value was not included in the curve fitting because a well-fit line could not be found that included this point, and because no values greater than 107 were recorded at the burn.

The 900 MHz XBee receiver was a ZigBee module identical to the transmitter. A SparkFun XBee Explorer USB board (SparkFun Part No. WRL-11812) was used to interface the computer to the XBee. Note that the particular XBee modules used do not function correctly if the RSSI pin has anything connected to it. A solder jumper must be removed on the USB interface board in order for this module to work. The XBee and the USB board are shown in Figure 7.12. The laptop logged the computer time, the up-time of the Arduino, the temperature from the on-board sensor of the transmitting XBee, the temperature from the off-board temperature sensor, the temperature from the on-board temperature sensor of the receiving XBee, and the received signal strength (RSSI). Values were recorded for the light, CO, and methane sensors; however, these sensors were not operational during the experiment as noted earlier. There are times when the receiving XBee returned an error or non-standard response to the computer. These

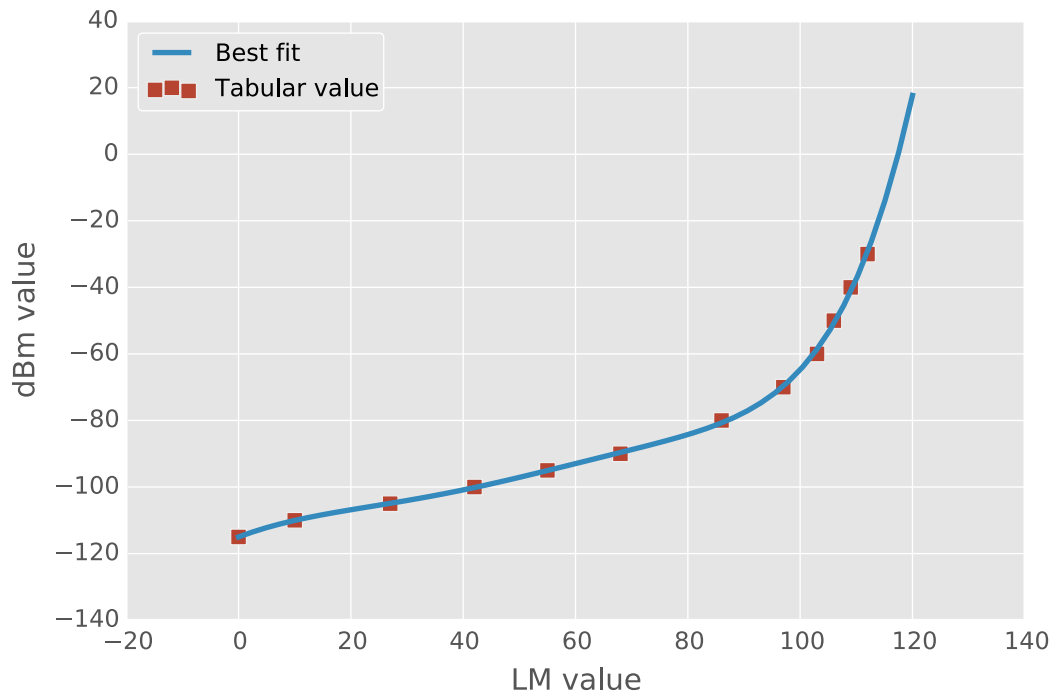


Figure 7.11: Best fit curve for the AR8200.

values were logged and are included in the data files. These errors do not effect other data points.

The program NetSurveyor from Nuts About Nets [71] was used to record the Wi-Fi beacon signal strengths for both channels. A certified refurbished Linksys Wireless Mini USB Adapter AC 580 Dual Band (AE6000) was purchased through Amazon (ASIN: B00LV87XD2) to allow the laptop to monitor the 5 GHz channel. Figure 7.13 shows the measurement laptops, and the Wi-Fi adapter is indicated by the white arrow at the center of the image.

7.3 Video Recordings

Videos were recorded to show fire conditions and to help with the interpretation of data. Video was only recorded for the first floor fires since transmitters were only located on that level. One



Figure 7.12: Receiving 900 MHz XBee module.

camera was placed east of the house, looking into the windows of the rooms for the 144/440 transmitters. Also in the field of view was one of the entrances used by firefighters. This camera is considered the main camera since it was used to piece together a timeline, matching data timestamps to events. The time on the computer recording the 900 MHz XBee and Wi-Fi signal strengths was selected as the standard, or reference, time. The other laptop was one second ahead of this time, meaning that time stamps for the 144 MHz and 440 MHz data should be shifted back by one second. The clock on the main video camera was 57 seconds ahead of the reference time. Digital photos were approximately 11.5 minutes behind the reference time. Another camera was placed to the northwest of the house; however, the camera died before the fire was ignited. A replacement camera was started approximately 14 seconds after ignition.

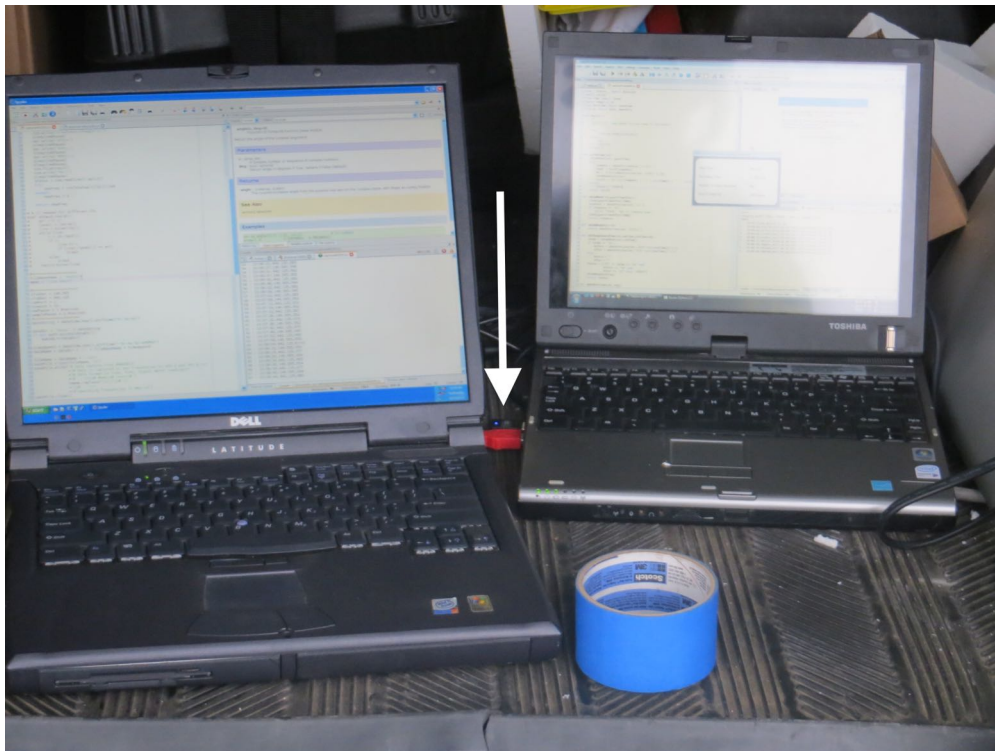


Figure 7.13: Measurement laptops and Wi-Fi receiver adapter (arrow).

7.4 Results and Discussion

Members of the Michigan State Police Bomb Squad ignited the fires remotely using “squib” detonators. All four ignition points were set off at the same time. A similar procedure was used to ignite the second floor fires after the first floor was extinguished.

Data recordings were started after the transmitters were turned on, but before the ignition time. Recording of XBee data was started last at 2.5 minutes prior to ignition. Data was recorded until the transmitters were recovered from the house (after the second floor was extinguished and breathing apparatus not required) and turned off.

The fire was allowed to burn for approximately 3.5 minutes. At this point, fire crews entered the house and began to extinguish the fires, starting in the living room and then moving to the 144/440 rooms. Another crew entered the kitchen on the west side of the house to extinguish the fire there.

Figures 7.14 through 7.19 show post-fire conditions for the rooms and transmitters. The first thing to note is that the fire was much more intense in the living room with the XBee and Wi-Fi transmitters (Fig. 7.16). The furniture is charred with most of the cushioning burned away (Fig. 7.19). This is different than the other two rooms that show little fire damage (Figs 7.14 and 7.15). Smoke damage is noticeable on the walls in these rooms (Fig. 7.18). The furniture immediately next to each of these ignition points is hardly burned or damaged (Fig. 7.15 and 7.17). In these pictures, some of the ceiling has been pulled down during overhaul to search for hidden fire. From these observations, we can conclude that there were significant flames in the living room with the XBee and Wi-Fi transmitters, while the rooms with the 144 MHz and 440 MHz transmitters were mostly smoke filled with very few flames. This observation is supported by the video recordings as well. No flames are visible in the windows from the 144/440 rooms on the video except for the initial flash from the ignition.



(a) The 144 MHz transmitter and room after the fire. *The right arrow indicates the position of the 440 MHz transmitter on the other side of the wall.*



(b) A close-up view of the 144 MHz transmitter after the fire.

Figure 7.14: Post-fire conditions for the 144 MHz transmitter.



Figure 7.15: Post-fire conditions in the 440 MHz transmitter room. *Note that the sofa and other furniture sustained little fire damaging demonstrating that the fire conditions were not sever in this area.*



(a) Post-fire condition of the living room with XBee and Wi-Fi transmitters.



(b) XBee and Wi-Fi Duraboard box post-fire. *The box is in at least one inch of standing water since the bottom layer of Duraboard is not visible. Also note the charring on the table.*

Figure 7.16: Post-fire conditions for the XBee and Wi-Fi transmitter.



Figure 7.17: Post-fire condition of the 144 MHz transmitter room. *Note that the chair and table in particular have sustained very little damage.*



Figure 7.18: Post-fire condition of the ceilings in the 144 MHz and 440 MHz transmitter rooms. *The 2x4 studs were exposed during overhaul and did not suffer smoke or fire damage. Compare the conditions of the studs to the drywall still attached to it in the bottom of the photo.*



Figure 7.19: Post-fire conditions in the living room. *The fire was much more severe in this room compared to the 144/440 rooms. Almost all of the cushioning on the furniture has been burned and the wood is charred. The whitish pieces on top of furniture are ceiling that were pulled down during overhaul.*

The measured signal strengths are plotted in Figure 7.20 for the entire duration and in Figure 7.21 for a shorter time period containing the fire. The duration of fire is outlined in a vertical box. The data is very noisy and difficult to analyze. In general, however, no significant signal degradation occurs during the fire. Post-fire signal strength tends to be lower than pre-fire strengths. This is most likely due to water and other debris being inadvertently placed near the transmitters. The sharp decrease in signal strength for the 440 MHz transmitter immediately after fire crews entered the house suggests that debris and water effected this transmitter drastically. This transmitter would have been the first transmitter to be hit by fire crews entering the house. The graph shows that all of the signal levels increased once the transmitters were removed from the house, and was reduced when they were turned off. This shows that the measurement system was operating correctly.

The graph shows that the 5 GHz Wi-Fi channel was not detected until after the transmitters were retrieved from the house. It also shows 17 minutes after fire crews entered the house, the 2.4 GHz Wi-Fi signal was lost. The Duraboard box for the Wi-Fi transmitters absorbed a large amount of water which could have acted to shield the 2.4 GHz signal. It is reasonable that it took 17 minutes for enough water to be absorbed because of the time required for overhaul after a fire and for the Duraboard to absorb enough water to impact the signal.

The temperature inside of the tool case, which contained the XBee and the Wi-Fi router, and the temperature at the receivers are plotted in Figure 7.22. The temperature sensor on the XBee is hotter than the discrete, off-board sensor in the tool case. This could either be from a calibration/reference error, or it could be due to the exhaust from the router. The XBee module was right next to the router while the off-board sensor was near the battery (see Fig. 7.5a). These measurements show that the tool case heated up because of the electronics and not because of the fire. Future experiments will need to ensure that the transmitters do not overheat themselves. The Duraboard and fiberglass insulation provided sufficient protection for the in-

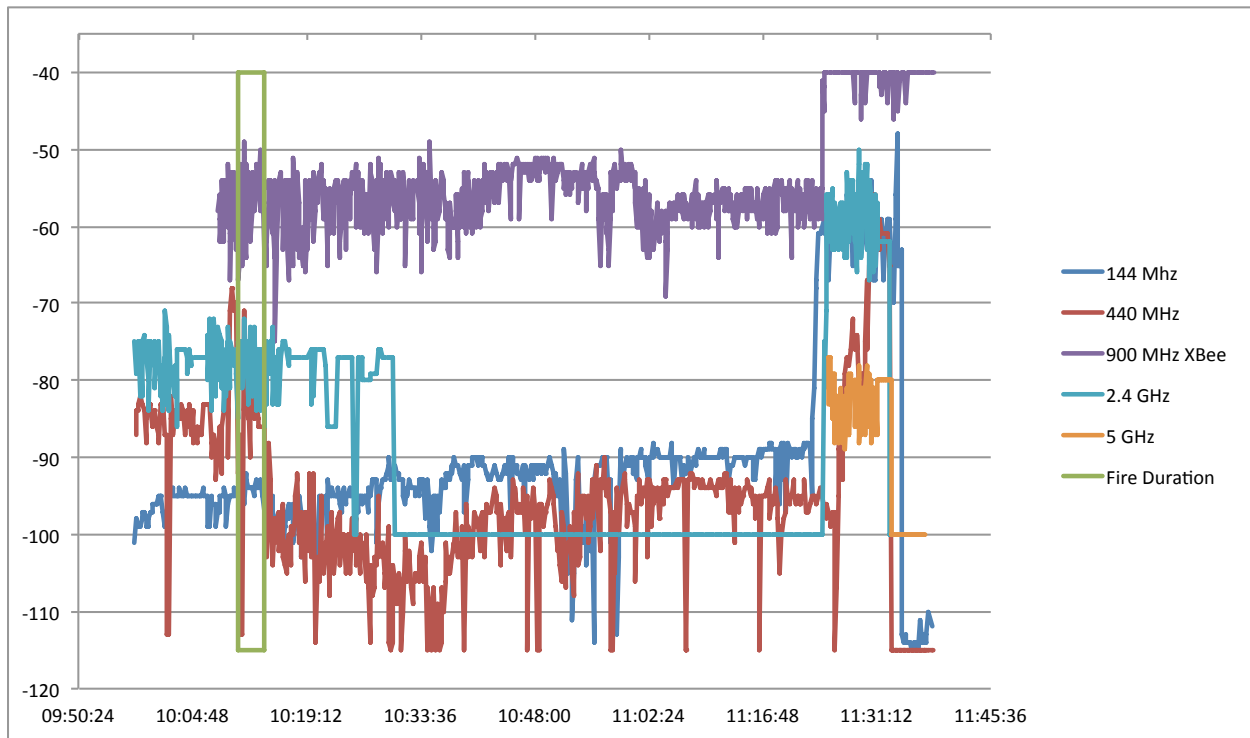


Figure 7.20: Measured signal strengths before, during, and after the house burn.

struments. The temperature at the receiving XBee shows that the outside temperature was fairly constant throughout the burn and data acquisition time.



Figure 7.21: Measured signal strengths near the time of the fire.

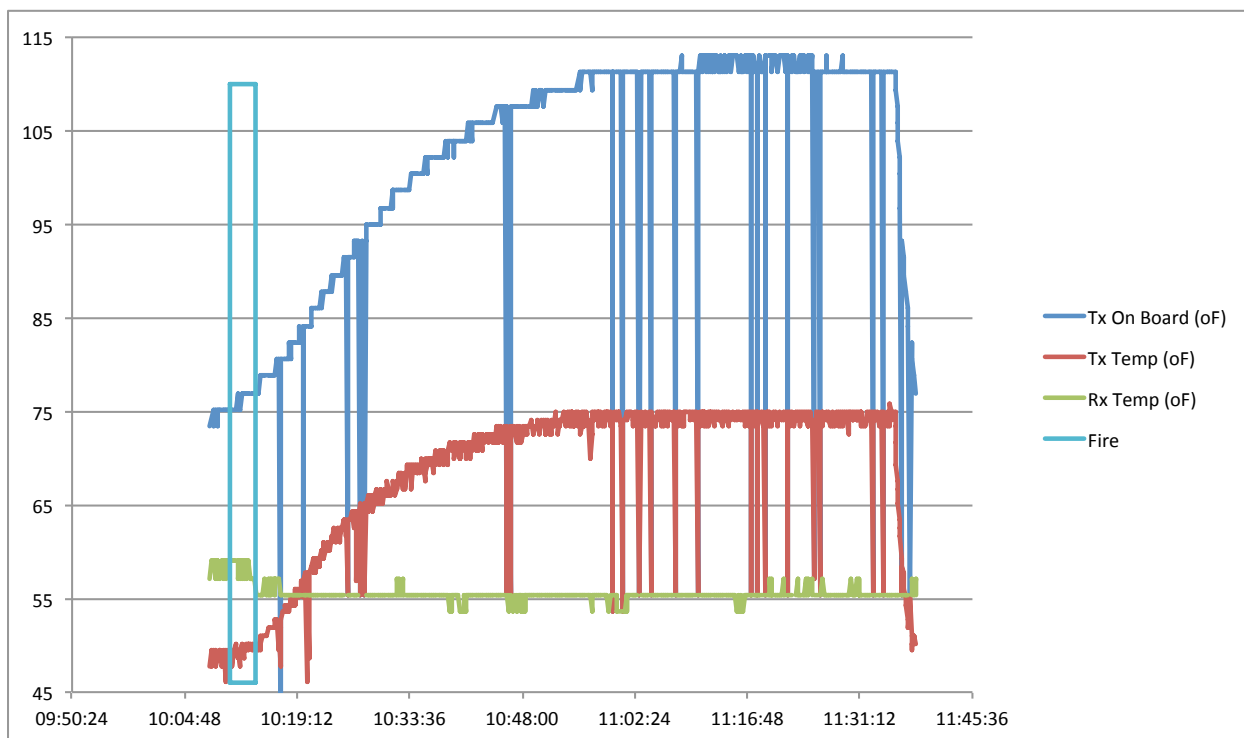


Figure 7.22: Temperature versus time from the XBee modules. *Each module has a temperature sensor on board. A discrete, off-board temperature sensor was also placed inside the tool case with the XBee and Wi-Fi router.*

The measured signal strengths do little to show the effects of fire on radio transmissions. Numerous experimental factors led to these low-quality, and hence inconclusive, results. The receivers should have been placed much closer to the transmitters. This would have increased the absolute strength as well as limiting negative effects from people and other environmental factors. An area should be set up into which no one is allowed to go during the experiment. Additionally, numerous samples should be taken immediately prior to ignition to establish a base line. Finally, fire growth should have been allowed to progress much further than it did in order to allow for sufficient interaction between the waves and flames. These things were unable to be done in this experiment because of the needs and timeline of the fire investigation class.

7.5 Conclusion

This experiment enabled data to be collected during a structure fire on a scale larger than any other experiment in this dissertation. The Michigan State Police and the class instructors accommodated the experiment well, which is greatly appreciated. For an experimentalist, this burned provides useful knowledge on the design, construction, and placement of fire-proof containers for transmitters. The temperature profile obtained showed that heat from the instruments themselves is the primary concern inside of these boxes. The receivers should be closer to the transmitters and the effect of outside objects, such as people, should be mitigated. Finally, fire growth should be allowed to progress to later stages. Balancing objectives of other agencies and experiments is difficult and should be examined further for future joint work. The results of this experiment demonstrate that there is little effect on firefighter communications for fires of limited growth. Sever fire conditions were prevented in this experiment; therefore, it is possible that communications could be affected in larger fires. Study of such fire conditions is an item for future work.

Part III

Bench-Scale Diagnostics using a Two-Wire Transmission Line

Bench-Scale Diagnostics using a Two-Wire Transmission Line

The system and experiments presented earlier rely on antennas to transmit and receive signals that interact with a flame. We must consider the pattern in which the waves are emitted or received by the antennas and how this pattern intersects with the flame. Overall, the system utilizes a large volume of space. The various fire sizes and large fuel sources required for these previous systems force experiments to be conducted outside with extra safety precautions. This is not conducive to scientific research.

The objective of this part of this dissertation is to describe a method for bench-scale, low-cost, controllable flame characterization measurements. Overall we are able to operate in a much more controlled environment that offers repeatable conditions. In addition, bench-scale experiments are lower cost than full-scale outdoor experiments.

After brain storming various bench-scale measurement setups, we decided to use a two-wire transmission line to measure flame characteristics. Figure 7.23 shows an example two-wire transmission line with an attached short circuit (right) and a balun (left). A flame to be measured would be placed on the right side of this figure between the two wires. It would fully fill the space between the wires and would come around the outsides as well. If one-port measurements were to be made, the flame would be between the balun and the short (seen on the right of Figure 7.23); for two-port measurements the flame could be at any point along the two-wire line. This transmission structure is open to the environment which allows the flame to interact with the localized and relatively concentrated fields. Different sized transmission lines offer the possibility of varying the volume of space and flame interrogated offering some spatial resolution. Analysis of such a measurement system can be accomplished using transmission line equations. Such equations are easy to implement analytically and computationally.

Furthermore, a two-wire transmission system offers opportunities in other areas of material characterization. The open nature of this transmission line enables the material or environ-

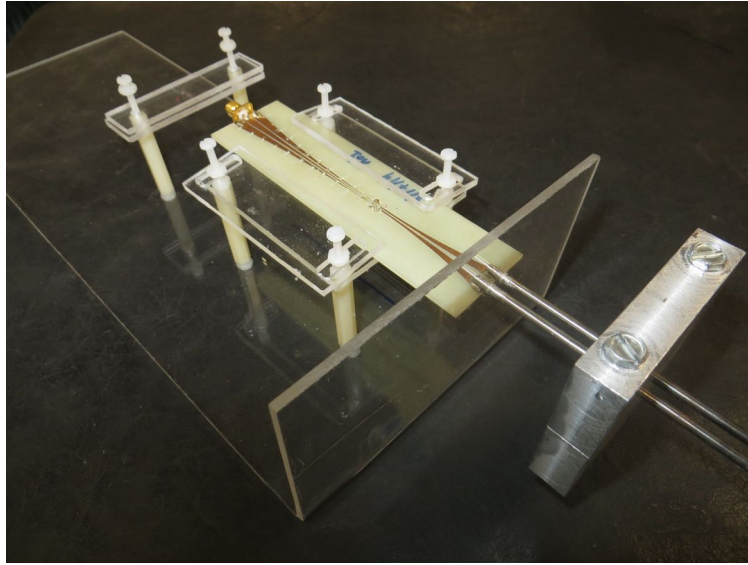


Figure 7.23: Example of a two-wire transmission line with an attached short circuit (right) and balun (left) manufactured for this work.

ment to completely surround and encompass the conductors. Suitable measurement media include liquids, gases, and soft solids. This measurement system can easily be added to pipes or vats. *In situ* measurements of the contained substance could then be made. This *in situ* measurement is very advantageous as many electromagnetic material characterization techniques require samples to be taken and measured *ex situ*. Such measurements are typically costly and destructive. Both one- or two-port measurements can be made which offers additional information for problems with multiple unknowns. Additionally, a two-wire transmission system is relatively low cost compared to coaxial or waveguide systems.

A two-wire transmission line system has some limitations as do other characterization methods. Since the system is open, it is unshielded and susceptible to noise. Field containment relies upon having balanced currents³ on the conductors. Performance can suffer if the conductors are too far apart or common mode currents exist. Since a two-wire transmission line is a balanced system, a balun (balanced-unbalanced) is required to connect to an unbalanced

³Balanced current means that current on one conductor is equal in amplitude and opposite in direction compared to the current on the other conductor. This is known as differential mode current. Currents flowing in the same direction on both conductors is known as common mode current

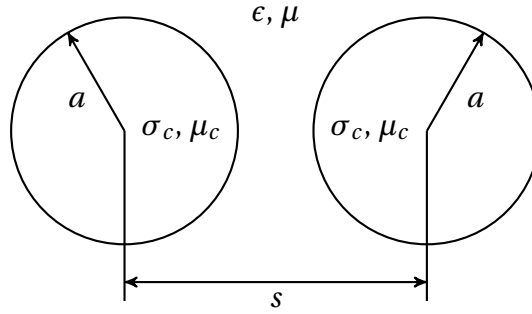


Figure 7.24: General notation used for a two-wire transmission line.

system like a coaxial cable. A balun is required in most implementations since most measurement equipment utilizes coaxial connectors, e. g. type-N, SMA, or 3.5 mm.

An input impedance of $50 \, \Omega$ is the most common impedance seen on measurement equipment. Achieving this low of an impedance for a two-wire transmission line is difficult and results in high sensitivity to errors in the transmission line dimensions. An impedance transformer is therefore required in most applications. This is normally incorporated with the balun.

The work in this part of the dissertation covers the theoretical analysis of a two-wire transmission line, design of a balun, manufacturing of an experimental setup, calibration theory, and some material characterizations. At the time of writing, this system had not been tried with a flame due to poor calibration and performance issues. Challenges with this system include the balun design, wideband performance, and trade-offs between heat thresholds and conductivity.

Figure 7.24 shows the geometry and notation used for a two-wire transmission line in the following chapters. The parameter s is the center-to-center distance of the wires with a radius of a , conductivity of μ_c , and a permeability of μ_c . In most cases, μ_c will be μ_0 . If the wires are ferrous, this may not be true. The surrounding media has a permittivity of ϵ and a permeability of μ .

Chapter 8

Transmission Line Characteristics

A two-wire transmission line is a transmission structure made up of two parallel, non-concentric conductors. The diameter of the conductors may be different.

Assumption

In this work, the conductors are defined to be of circular cross-section with equal diameter.

Figure 7.23 shows an example of a two-wire transmission line. Being an open system means no part of the transmission line encloses any other part. This allows for the surrounding medium to change, moving through and around the transmission line structure. This differs from both waveguides and coaxial cables; in these two structures the internal dielectric is enclosed by some part of the transmission line. In order for the medium of the transmission line to change, these closed structures must physically be opened in some manner, have the medium changed, and then be closed again.

In an open structure, fluids (liquids or gases) may move around the system and change with time. Such a structure also allows for solids to easily be placed around the system and changed. In the case of a two-wire transmission line, a solid may be clamped around the conductors or the transmission line inserted into a solid.

Assumption

At this time all work has been carried out under the assumption that the surrounding media completely encompass and touch both conductors. This assumption means that no gaps exist between the conductors and the media.

Creating such a situation in practice is difficult due to manufacturing tolerances. For fluids the flow speed must be low enough that the fluid is able to completely encircle the conductors. Additionally the conductors should not induce turbulence in the fluid.

Given that the two-wire transmission line is an open system, materials can readily be probed or sampled. Potential applications could be found in areas such as shipping, material storage, geology, health care, and manufacturing. One can envision adding or placing a two-wire transmission line into storage vats, pipes, gels, soil samples, meat, vegetables, soft solids, fume hoods, smoke stacks, furnaces, combustion chambers, and fire alarm system. A two-wire transmission line could easily be retrofitted to existing pipes, vats, other holding containers, or transportation vessels. The transmission line could be setup as either a one-port or a two-port device. This allows for mounting and sensing options to meet customer needs.

While current experiments have been carried out using vector network analyzers (VNA), other simpler, cheaper, and lower bandwidth devices could be used. This allows budgets, equipment, and desired measured parameters to be matched.

Analytically, the measured response of the two-wire transmission line system is dependent upon the permittivity, ϵ , and permeability, μ , of the media surrounding the transmission line.

Assumption

This body of work assumes that the permeability is unchanged, i. e. $\mu = \mu_0$ or $\mu_r = 1$.

From a materials stand point, materials are not typically defined or designed by their relative permittivity or permeability. Instead other material parameters define these values. For example in radar absorbing material, the mixing fraction of ferrous particles helps to define ϵ_r and μ_r . In plasmas it is the electron density, n_e , and the collision frequency, ν_{eff} ; In liquids it can

be the temperature and conductivity. In all cases ϵ_r and μ_r are dependent variables often only considered for RF design purposes. Correlating measurements of ϵ_r and μ_r to other parameters is important for the aforementioned sensing applications. Proper model selection and fitting must be carried out in order for the sensors to be useful to non-RF engineers and technicians.

We begin this chapter by finding the electric potential (voltage) of the two-wire transmission line. Using this, we are able to find the electric and magnetic fields. By knowing the field structure, we are able to predict some behaviors of the two-wire transmission line as well as gain design insights for the material measurement system. To better understand losses in this system, we also examine the radiation resistance of the transmission line. We finish by creating a distributed circuit model of the two-wire transmission line that is based upon material characteristics in order to predict system behavior and in the future assist in characterizing the material.

Many texts were used to develop this chapter. Perhaps the most straight-forward text for finding the electric potential is by Cheng [72]. Section 4-4.2 covers finding the electric potential and the capacitance-per-unit-length for a two-wire transmission line. Chapter 9, and Section 9-3 in particular, cover the distributed circuit model. This text is highly recommended as the starting point for anyone beginning to work in this area. Plonsey and Collin [73, pp. 63–72, 361–370] is a second text that is highly recommended. Next, the text by Bewley [74, pp. 43–46] has another take on the electric potential and expresses certain equations in forms not used elsewhere. We would be remiss not to mention the text by Ramo, Whinnery, and Van Duzer [3] as it was an excellent resources used to piece together all the other parts. Finally, King [75, pp. 13–19, 23–31, 487–492] provides a very in-depth discussion of transmission lines in his text. This has nice discussions on radiation resistance specific to two-wire transmission line that is not found in other texts. The notation and mathematical derivations can be difficult to follow.

The mathematical derivations in this chapter are very verbose with few steps omitted. This is for the benefit of all readers since not all have the same mathematical ability. While one step

is evident and trivial to one reader, another reader may find the step to be a roadblock. The aforementioned texts all leave out derivations that are not obvious or require significant work and insights. The goal here is to assist all readers so that none spend minutes, hours, or days stuck in the math.

8.1 Electric Potential

The electric potential for a two-wire transmission line is used for finding the field structure of the transmission line and for developing the circuit model. We first find the electric potential of one and two line charges, then extend this to the case of a two-wire transmission line.

Assumption

We assume that the potential is equal everywhere on a conductor (although not necessarily equal to the potential on another conductor).

Electric potential is the work done by an electric field to move a charge from one point to another and has units of volts. It is a conservative field meaning that only the beginning and final points are important but not the path taken between the two points. The potential is also relative meaning that some point must be made a reference and the potential for all other points are relative to this reference point [3, pp. 17–22]. The term electric potential is usually used when describing the field while the term voltage is usually used to describe the potential in a circuit. Other potential fields exist such as the vector magnetic potential; however, when used by itself, the term potential usually refers to the electric potential.

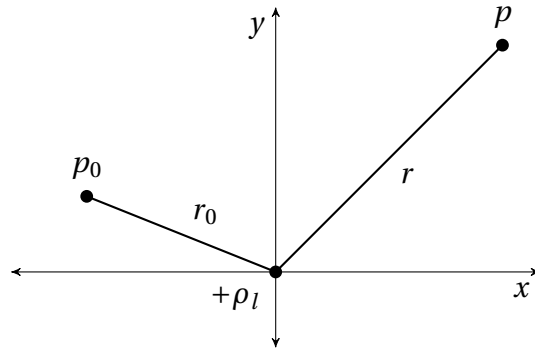


Figure 8.1: A single line charge. Shown are the reference point p_0 at radius r_0 , and an observation point p at radius r .

8.1.1 Potential of Single Line Charge

The electric potential, V , at the point p with respect to the reference point p_0 for a single, infinitely-long line charge with density ρ_l , as shown in Figure 8.1, is given by

$$V_s(r) = - \int_{p_0}^p \vec{E} \cdot d\vec{l} \quad (8.1)$$

where the subscript s denotes single line charge. The point p_0 has a radius of r_0 and the point p has a radius of r .

The electric field is found using Gauss's law,

$$\oint \vec{E} \cdot d\vec{S} = \frac{Q_{enc}}{\epsilon} \quad (8.2)$$

where ϵ is the permittivity of the medium surrounding the transmission line, Q_{enc} is the amount of charge enclosed by the volume of integration, and $\vec{E} = \hat{r}E_r$ for this problem. Integrating the electric field over a cylinder gives

$$\int_0^L \int_0^{2\pi} E_r r d\phi dz = E_r L r 2\pi = \frac{\rho_l L}{\epsilon} \quad (8.3)$$

$$\Rightarrow E_r = \frac{\rho_l}{2\pi r \epsilon} \quad (8.4)$$

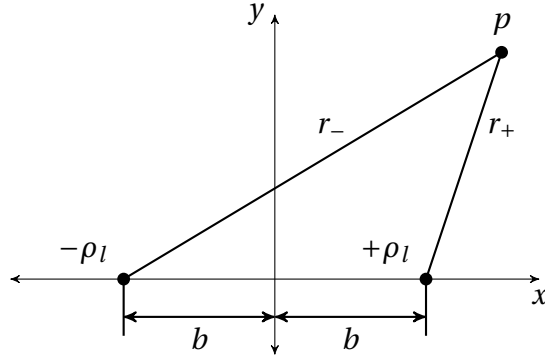


Figure 8.2: Geometry of two line charges.

This is substituted into Equation (8.1) and the order of integration reversed to remove the negative sign. Because the electric potential is a conservative field and the electric field has only a radial component, we are only concerned with the change in radius. The limits of integration are therefore r to r_0 . The electric potential for a single line charge is then

$$V_s(r) = \int_r^{r_0} \frac{\rho_l}{2\pi r \epsilon} dr$$

$$V_s(r) = \frac{\rho_l}{2\pi \epsilon} \ln\left(\frac{r_0}{r}\right)$$

(8.5)

The reference point p_0 is not specified at this time; it may not be placed at infinity or the potential would be infinity at all other points [72, p. 163]. We will see that it is in fact canceled in later equations.

8.1.2 Potential of Two Line Charges

The total potential from two line charges is found through the sum of the potentials of each line charge, which is known as the principle of superposition. The two line charges, with density of $\pm\rho_l$, are placed at $(\pm b, 0)$, respectively, as shown in Figure 8.2. The lengths r_- and r_+ are

$$r_- = \sqrt{(x+b)^2 + y^2} \quad \text{and} \quad r_+ = \sqrt{(x-b)^2 + y^2} \quad (8.6)$$

where x and y are the coordinate of p . The combined potential at p is the sum of Equation 8.5 evaluated once for r_+ and once for r_- .

$$V_d(p) = V_s(r_+) + V_s(r_-) = \frac{+\rho_l}{2\pi\epsilon} \ln\left(\frac{r_0}{r_-}\right) + \frac{-\rho_l}{2\pi\epsilon} \ln\left(\frac{r_0}{r_-}\right) \quad (8.7)$$

where the subscript d denotes double line charge. The common terms may be factored out and the logarithms combined to reach the final expression:

$$V_d(p) = \frac{\rho_l}{2\pi\epsilon} \left[\ln\left(\frac{r_0}{r_+}\right) - \ln\left(\frac{r_0}{r_-}\right) \right] \quad (8.8)$$

$$= \frac{\rho_l}{2\pi\epsilon} \left[\ln\left(\frac{r_0 r_-}{r_+ r_0}\right) \right] \quad (8.9)$$

$$\boxed{V_d(p) = \frac{\rho_l}{2\pi\epsilon} \ln\left(\frac{r_-}{r_+}\right)} \quad (8.10)$$

Equation 8.10 is the electric potential of two line charges.

8.1.3 Equipotential Surfaces

We see here that the potential is constant whenever r_-/r_+ is a constant. The surfaces over which the potential is constant are called equipotential surfaces. “Since the potential is single-valued, surfaces for different values of potential do not intersect” [3, pp. 20–21]. We will show that the equipotential lines of Equation 8.10 are circles by re-writing it in the standard form of a circle.

First, we write r_+ and r_- in Cartesian coordinates:

$$V_d = \frac{\rho_l}{2\pi\epsilon} \ln\left(\sqrt{\frac{(x+b)^2 + y^2}{(x-b)^2 + y^2}}\right) \quad (8.11)$$

where we have dropped the functional notation for V_d . The logarithm is removed by solving for it and raising an exponential to each side,

$$V_d \frac{2\pi\epsilon}{\rho_l} = \ln \left(\sqrt{\frac{(x+b)^2 + y^2}{(x-b)^2 + y^2}} \right) \quad (8.12)$$

$$\Rightarrow \exp \left(\frac{2\pi\epsilon V_d}{\rho_l} \right) = \sqrt{\frac{(x+b)^2 + y^2}{(x-b)^2 + y^2}} \quad (8.13)$$

Squaring each side gives

$$\exp \left(\frac{2\pi\epsilon V_d}{\rho_l} \right)^2 = \frac{(x+b)^2 + y^2}{(x-b)^2 + y^2} \quad (8.14)$$

$$\Rightarrow \exp \left(\frac{4\pi\epsilon V_d}{\rho_l} \right) = \frac{(x+b)^2 + y^2}{(x-b)^2 + y^2} \quad (8.15)$$

For simplicity, let

$$g = \exp \left(\frac{4\pi\epsilon V_d}{\rho_l} \right). \quad (8.16)$$

We then have

$$g = \frac{(x+b)^2 + y^2}{(x-b)^2 + y^2}. \quad (8.17)$$

Multiplying each side by the denominator gives

$$g \left((x-b)^2 + y^2 \right) = (x+b)^2 + y^2. \quad (8.18)$$

The $(x \pm b)^2$ terms are expanded and the right side moved to the left side,

$$g \left(x^2 - 2bx + b^2 + y^2 \right) - (x^2 + 2bx + b^2) - y^2 = 0, \quad (8.19)$$

so that it may be written in the form $x^2 a_1 + x a_2 + a_3 = 0$,

$$x^2(g-1) - x2b(g+1) + b^2(g-1) + y^2(g-1) = 0. \quad (8.20)$$

We now multiply by negative one,

$$x^2(1-g) + 2bx(1+g) + b^2(1-g) + y^2(1-g) = 0, \quad (8.21)$$

and divide by the x^2 coefficient $(1-g)$,

$$x^2 + 2bx \frac{(1+g)}{(1-g)} + b^2 + y^2 = 0. \quad (8.22)$$

Next, the b^2 term is moved to the right side and the expression

$$b^2 \left(\frac{(1+g)}{(1-g)} \right)^2 \quad (8.23)$$

is added to both sides,

$$x^2 + 2bx \frac{(1+g)}{(1-g)} + y^2 + b^2 \left(\frac{(1+g)}{(1-g)} \right)^2 = -b^2 + b^2 \left(\frac{(1+g)}{(1-g)} \right)^2. \quad (8.24)$$

We see on the left hand side that the x and b terms come from $(x + bc)^2$. Factoring these terms on the left hand side, and factoring the b^2 term on the right hand side gives

$$\left(x + b \left(\frac{1+g}{1-g} \right) \right)^2 + y^2 = \left(\left(\frac{1+g}{1-g} \right)^2 - 1 \right) b^2. \quad (8.25)$$

This is the standard form for a circle.

We can simplify this equation further if the full of expression for g is returned to it,

$$\left(x + b \left(\frac{1 + e^{\frac{4\pi\epsilon V_d}{\rho_l}}}{1 - e^{\frac{4\pi\epsilon V_d}{\rho_l}}} \right) \right)^2 + y^2 = \left(\left(\frac{1 + e^{\frac{4\pi\epsilon V_d}{\rho_l}}}{1 - e^{\frac{4\pi\epsilon V_d}{\rho_l}}} \right)^2 - 1 \right) b^2. \quad (8.26)$$

Using the definition for the hyperbolic cotangent,

$$\coth(z) = \frac{e^{2z} + 1}{e^{2z} - 1}, \quad (8.27)$$

we can make the following simplification to the left hand side:

$$\frac{1 + e^{\frac{4\pi\epsilon V_d}{\rho_l}}}{1 - e^{\frac{4\pi\epsilon V_d}{\rho_l}}} = -\frac{e^{\frac{4\pi\epsilon V_d}{\rho_l}} + 1}{e^{\frac{4\pi\epsilon V_d}{\rho_l}} - 1} = -\coth\left(\frac{2\pi\epsilon V_d}{\rho_l}\right), \quad (8.28)$$

This same simplification and the identity $\cosh^2(x) = \coth^2(x) - 1$ can be used on the right hand side to give

$$\left(\frac{1 + e^{\frac{4\pi\epsilon V_d}{\rho_l}}}{1 - e^{\frac{4\pi\epsilon V_d}{\rho_l}}} \right)^2 - 1 = \coth^2\left(-\frac{2\pi\epsilon V_d}{\rho_l}\right) - 1 \quad (8.29)$$

$$= \cosh^2\left(-\frac{2\pi\epsilon V_d}{\rho_l}\right). \quad (8.30)$$

The $\cosh(x)$ function is by definition $1/\sinh(x)$. Equation (8.30) is therefore

$$\left(\frac{1 + e^{\frac{4\pi\epsilon V_d}{\rho_l}}}{1 - e^{\frac{4\pi\epsilon V_d}{\rho_l}}} \right)^2 - 1 = \frac{1}{\sinh^2(-2\pi\epsilon V_d/\rho_l)} \quad (8.31)$$

$$= \frac{1}{\sinh^2(2\pi\epsilon V_d/\rho_l)} \quad (8.32)$$

where the last equality holds because of the identity $\sinh(-x) = -\sinh(x)$.

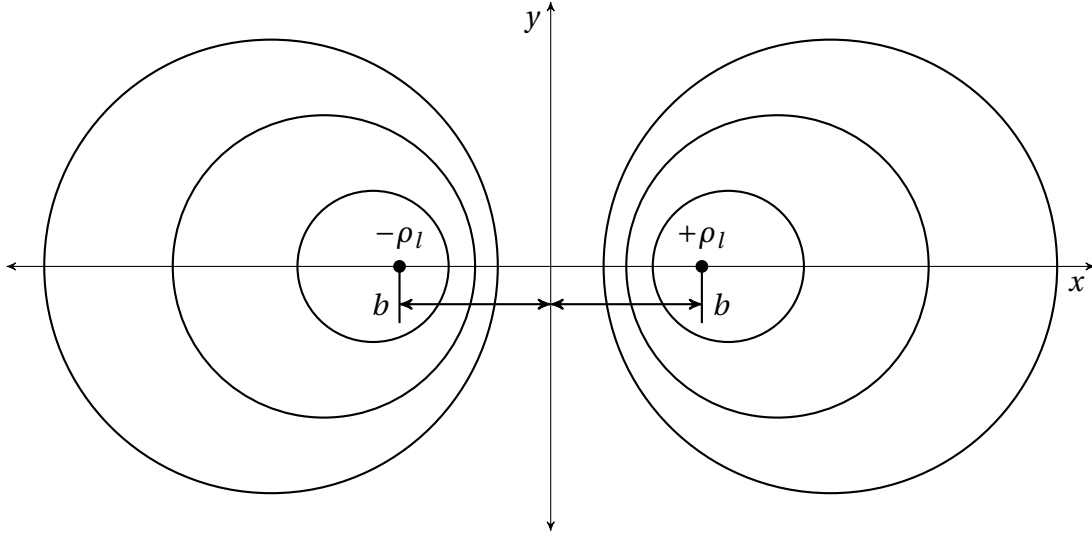


Figure 8.3: Examples of equipotential surfaces surrounding two line charges.

After substituting these simplifications into the equation for a circle given in Equation (8.26), we have

$$\left[x - b \coth \left(\frac{2\pi\epsilon V_d}{\rho_l} \right) \right]^2 + y^2 = \frac{b^2}{\sinh^2(2\pi\epsilon V_d / \rho_l)} \quad (8.33)$$

This describes a family of circles that represent equipotential lines that surround the line charges. The circles are located along the x-axis ($y = 0$) at

$$s_c = b \coth \left(\frac{2\pi\epsilon V_d}{\rho_l} \right) \quad (8.34)$$

and have a radii of

$$a = \left| \frac{b}{\sinh(2\pi\epsilon V_d / \rho_l)} \right| \quad (8.35)$$

An example of these equipotential surfaces is shown in Figure 8.3. Equipotential circles for negative potentials are located in the left half plane, $x < 0$, and those for positive potentials are located in the right half plane, $x > 0$. The y-axis corresponds to a potential of $V_d = 0$.

Two important equations may be derived from the radius and center location. First we square the radius,

$$a^2 = \left(\frac{b}{\sinh(2\pi\epsilon V_d / \rho_l)} \right)^2 \quad (8.36)$$

$$= \frac{b^2}{\sinh^2(2\pi\epsilon V_d / \rho_l)}, \quad (8.37)$$

which may also be written as

$$a^2 = b^2 \operatorname{csch}^2(2\pi\epsilon V_d / \rho_l). \quad (8.38)$$

The identity

$$\operatorname{csch}^2 = \coth^2 - 1 \quad (8.39)$$

is used to write the radius squared as

$$a^2 = b^2 (\coth^2(2\pi\epsilon V_d / \rho_l) - 1). \quad (8.40)$$

Equation (8.34) is now squared,

$$s_c^2 = b^2 \coth^2 \left(\frac{2\pi\epsilon V_d}{\rho_l} \right), \quad (8.41)$$

and solved for \coth^2 ,

$$\coth^2 \left(\frac{2\pi\epsilon V_d}{\rho_l} \right) = s_c^2 / b^2. \quad (8.42)$$

This can now be substituted into Equation (8.40) to get

$$a^2 = b^2(s_c^2/b^2 - 1) \quad (8.43)$$

$$\boxed{a^2 = s_c^2 - b^2} \quad (8.44)$$

This is the first of the two relations that we looked to derive. Equation (8.44) is used to find b when the center and radius of the equipotential surface is known. It is also used to derive the potential for given equipotential surface which we do next.

Equation (8.37), solved for b^2 , is substituted into Equation (8.44),

$$a^2 = s_c^2 - a^2 \sinh^2(2\pi\epsilon V_w/\rho_l). \quad (8.45)$$

The subscript for V has been switched to w to denote wire. The reason for this will explained after the derivation. We now collect the a^2 terms,

$$a^2(1 + \sinh^2(2\pi\epsilon V_w/\rho_l)) = s_c^2, \quad (8.46)$$

and apply the identity $\cosh^2(x) = 1 + \sinh^2(x)$,

$$a^2 \cosh^2(2\pi\epsilon V_w/\rho_l) = s_c^2. \quad (8.47)$$

Solving for $\cosh(x)$ gives

$$\cosh^2(2\pi\epsilon V_w/\rho_l) = \frac{s_c^2}{a^2} \quad (8.48)$$

$$\cosh(2\pi\epsilon V_w/\rho_l) = \frac{s_c}{a}. \quad (8.49)$$

We now apply $\cosh^{-1}(x)$ to both sides,

$$\frac{2\pi\epsilon V_w}{\rho_l} = \cosh^{-1}\left(\frac{s_c}{a}\right), \quad (8.50)$$

and solve for V_w to get

$$\boxed{V_w = \frac{\rho_l}{2\pi\epsilon} \cosh^{-1}\left(\frac{s_c}{a}\right)} \quad (8.51)$$

Equation (8.51) is the potential for the equipotential circle of radius a centered at s_c for a line charge of density ρ_l . We note that this is not expressly a function of where the line charge is placed; instead, that position is implicit in the center and radius of the equipotential surface. This is important because we now have an equation that can be applied to the two-wire transmission line problem since we assumed that the wires have a circular cross section and that the potential is equal everywhere on a wire. Equation (8.51) is therefore the potential of a wire, hence the subscript w .

8.1.4 Application to Two-Wire Transmission Line

We now wish to apply the above equations to the two-wire transmission line system. While the actual system used in this work has conductors of equal radii, we begin with two wires of unequal radii whose geometry is shown in Figure 8.4.

To find the centers of the wires, s_- and s_+ , we start with Equation (8.44) for each wire,

$$b^2 = s_-^2 - a_-^2 \quad (8.52)$$

$$b^2 = s_+^2 - a_+^2. \quad (8.53)$$

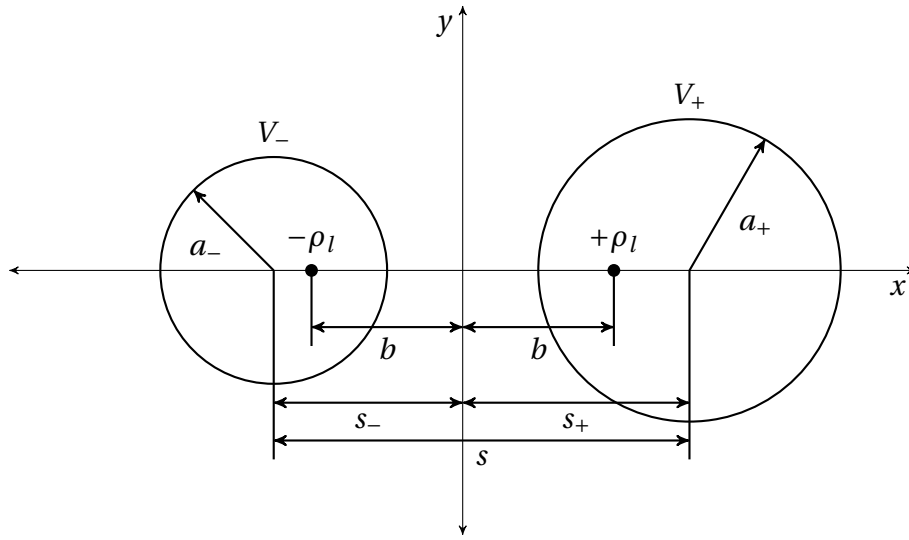


Figure 8.4: The geometry of a two-wire transmission line.

The parameter b is the same in both equations so we may write

$$s_+^2 - a_+^2 = s_-^2 - a_-^2 \quad (8.54)$$

$$\Rightarrow s_+^2 - s_-^2 = a_+^2 - a_-^2. \quad (8.55)$$

The total distance between centers is the sum of the two distances,

$$s = s_+ + s_-. \quad (8.56)$$

Equations (8.55) and (8.56) are solved for s_- and s_+ . From Equation (8.56),

$$s_- = s - s_+ \quad (8.57)$$

which is substituted into Equation (8.55),

$$s_+^2 - (s - s_+)^2 = a_+^2 - a_-^2. \quad (8.58)$$

Completing the square and collecting like terms gives

$$s_+^2 - (s^2 - 2s_+s + s_+^2) = a_+^2 - a_-^2 \quad (8.59)$$

$$2s_+s = s^2 + a_+^2 - a_-^2. \quad (8.60)$$

Dividing each side by $2s$ gives the center location for the potential charged wire,

$$s_+ = \frac{s^2 + a_+^2 - a_-^2}{2s} \quad (8.61)$$

This is now substituted back into Equation (8.57)

$$s_- = s - \frac{s^2 + a_+^2 - a_-^2}{2s}. \quad (8.62)$$

The s term on the right hand side is multiplied by $2s/2s$ and like terms collected to give

$$s_- = \frac{2s^2 - s^2 - a_+^2 + a_-^2}{2s} \quad (8.63)$$

$$s_- = \frac{s^2 - a_+^2 + a_-^2}{2s} \quad (8.64)$$

which is the center of the negatively potential wire.

Caution

Since the wires cannot overlap and should not touch, $s_- + s_+ > a_- + a_+$

The potential on each wire is given by Equation (8.51):

$$V_- = \frac{-\rho_l}{2\pi\epsilon} \cosh^{-1} \left(\frac{s_-}{a_-} \right) \quad (8.65)$$

$$V_+ = \frac{+\rho_l}{2\pi\epsilon} \cosh^{-1} \left(\frac{s_+}{a_+} \right). \quad (8.66)$$

The potential difference (voltage) between the two wires of unequal radius is $V = V_+ - V_-$, which simplifies to:

$$V = \frac{+\rho_l}{2\pi\epsilon} \cosh^{-1}\left(\frac{s_+}{a_+}\right) - \frac{-\rho_l}{2\pi\epsilon} \cosh^{-1}\left(\frac{s_-}{a_-}\right) \quad (8.67)$$

$$= \frac{\rho_l}{2\pi\epsilon} \left[\cosh^{-1}\left(\frac{s_+}{a_+}\right) - \cosh^{-1}\left(\frac{s_-}{a_-}\right) \right] \quad (8.68)$$

In this work, however, the wires have equal radii, $a = a_+ = a_-$. The centers are therefore located at

$$s_- = \frac{s^2 - a^2 + a^2}{2s} = \frac{s}{2} \quad (8.69)$$

$$s_+ = \frac{s^2 + a^2 - a^2}{2s} = \frac{s}{2}. \quad (8.70)$$

Since $s_- = s_+$ the centers are the same distance from the y-axis. Equation (8.68) can be simplified as well. Substituting $s/2$ for s_- and s_+ , and a for a_- and a_+ gives

$$V_\Delta = \frac{\rho_l}{2\pi\epsilon} \left[\cosh^{-1}\left(\frac{s}{2a}\right) - \cosh^{-1}\left(\frac{s}{2a}\right) \right] \quad (8.71)$$

$$\boxed{V_\Delta = \frac{\rho_l}{\pi\epsilon} \cosh^{-1}\left(\frac{s}{2a}\right)} \quad (8.72)$$

Equation (8.72) is the potential difference between the wires with equal radii in a two-wire transmission line. Because the voltage is usually specified, this equation may be used to find the equivalent line charge. This is needed in order to find the potential anywhere around the wires using Equation (8.11) which is repeated here for convenience with a new subscript to denote two-wire transmission line,

$$V_{2w} = \frac{\rho_l}{2\pi\epsilon} \ln \left(\sqrt{\frac{(x+b)^2 + y^2}{(x-b)^2 + y^2}} \right). \quad (8.73)$$

We may substitute in expressions for ρ_l and b from Equations (8.72) and (8.44), respectively. From Equation (8.70) $s_c = s/2$, and b is therefore

$$b = \sqrt{(s/2)^2 - a^2}. \quad (8.74)$$

The potential field for a two-wire transmission line is

$$V_{2w} = \frac{\pi\epsilon V_\Delta}{2\pi\epsilon \cosh^{-1}(s/2a)} \ln \left(\sqrt{\frac{\left(x + \sqrt{(s/2)^2 - a^2}\right)^2 + y^2}{\left(x - \sqrt{(s/2)^2 - a^2}\right)^2 + y^2}} \right) \quad (8.75)$$

$$V_{2w} = \frac{V_\Delta}{2 \cosh^{-1}(s/2a)} \ln \left(\sqrt{\frac{\left(x + \sqrt{(s/2)^2 - a^2}\right)^2 + y^2}{\left(x - \sqrt{(s/2)^2 - a^2}\right)^2 + y^2}} \right) \quad (8.76)$$

It is interesting that there are no material properties in this expression as would be expected. In fact, the material properties determine the relationship between the radius of, spacing between, and voltage difference of the wires. We also notice that the potential is zero midway between the conductors at $x = 0$ since the argument of the logarithm is equal to one. In the right half plane, the argument of the logarithm will be greater than one, so the potential is positive. In the left half plane, the argument will be between zero and one, which gives a negative potential when V_Δ is positive.

8.1.5 Visualization of the Potential

To visualize the potential, we will use the equivalent potential from two line charges as given by Equation (8.10).

Assumption

For the visualizations of the potential, electric field, and magnetic field the following problem parameters are used:

- center-to-center spacing of $s = 4$ m
- wire radius of $a = 1$ m
- relative permittivity of material $\epsilon_r = 6$
- the zero-voltage reference point is at the midpoint between the conductors
- voltage difference of 1 V

Figure 8.5 shows a two dimensional view and Figure 8.6 a three dimensional view of the potential of the two-wire transmission line system. The equipotential circles around each conductor are clearly visible because of the contour plot coloring. We see that the magnitude is symmetrical around each conductor but opposite in polarity as expected.

8.2 Electric and Magnetic Fields

For a TEM wave, the electric field, \vec{E} , is given by

$$\vec{E} = -\nabla_t \Phi \quad (8.77)$$

where

$$\nabla_t = \frac{\hat{x}\partial}{\partial x} + \frac{\hat{y}\partial}{\partial y} \quad (8.78)$$

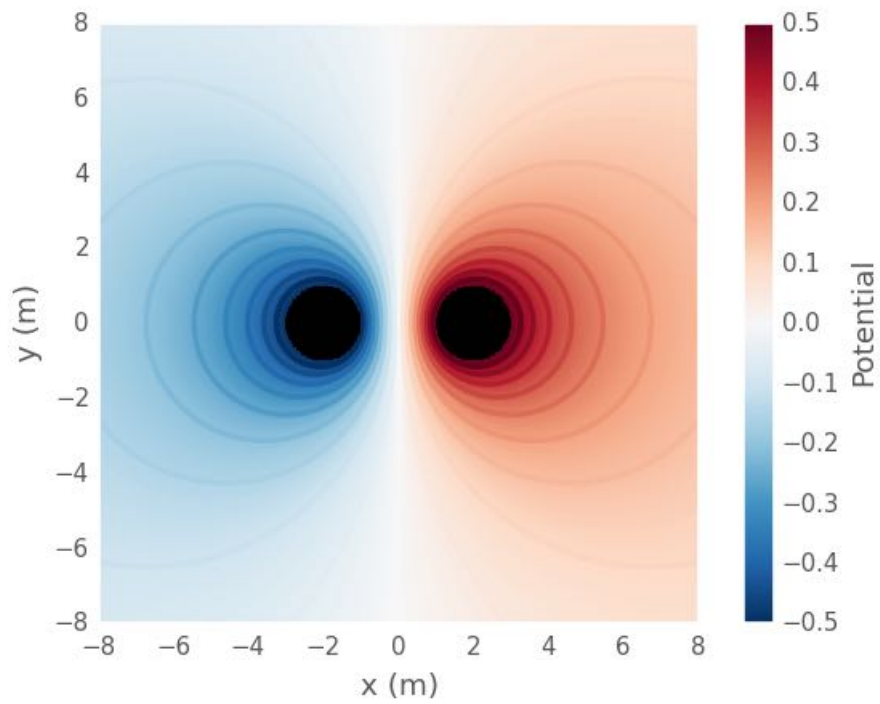


Figure 8.5: Electric potential of a two-wire transmission line system.

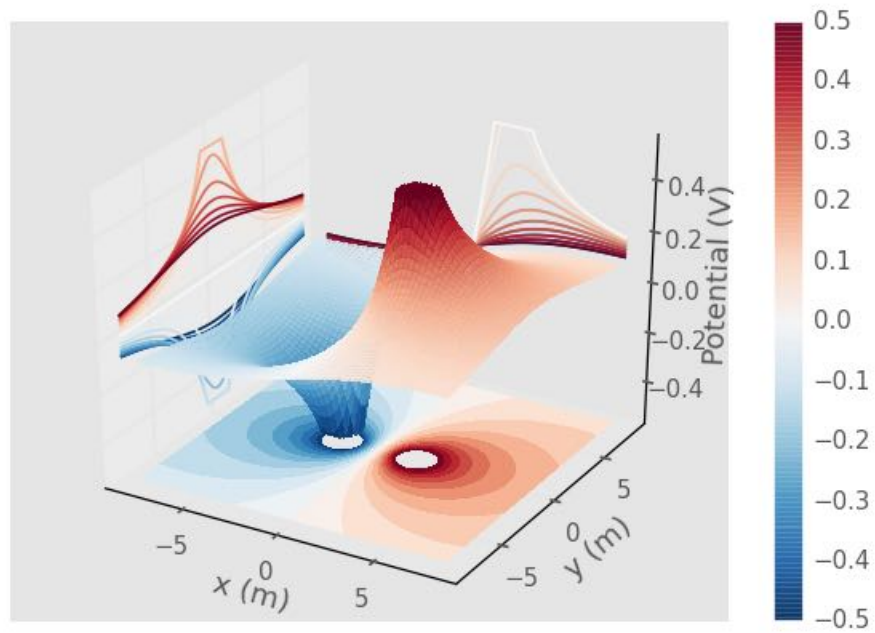


Figure 8.6: Electric potential of a two-wire transmission line system.

is the gradient in the transverse directions. The x component of the electric field is therefore

$$E_x = \frac{-\partial\Phi}{\partial x} \quad (8.79)$$

and the y component of the electric field is

$$E_y = \frac{-\partial\Phi}{\partial y}. \quad (8.80)$$

Computation of the derivative gives

$$E_x = \frac{-\rho_l}{\pi\epsilon} \frac{2b(b^2 - x^2 + y^2)}{[(x-b)^2 + y^2][(x+b)^2 + y^2]} \quad (8.81)$$

and

$$E_y = \frac{+\rho_l}{\pi\epsilon} \frac{4bxy}{[(x-b)^2 + y^2][(x+b)^2 + y^2]} \quad (8.82)$$

The denominator may be expressed using Equation (8.6) to give

$$E_x = \frac{-\rho_l}{\pi\epsilon} \frac{2b(b^2 - x^2 + y^2)}{r_-^2 r_+^2} \quad (8.83)$$

and

$$E_y = \frac{+\rho_l}{\pi\epsilon} \frac{4bxy}{r_-^2 r_+^2}. \quad (8.84)$$

The magnetic field is calculated from the electric field using Equation (2.17),

$$\vec{H} = \frac{\hat{k} \times \vec{E}}{\eta} \quad (8.85)$$

$$= \frac{\hat{z} \times (\hat{x}E_x + \hat{y}E_y)}{\eta} \quad (8.86)$$

$$= \hat{x} \frac{-E_y}{\eta} - \hat{y} \frac{-E_x}{\eta} \quad (8.87)$$

$$= \hat{x} \frac{-E_y}{\eta} + \hat{y} \frac{E_x}{\eta}. \quad (8.88)$$

The magnetic field is therefore

$$H_x = \frac{-E_y}{\eta} = \frac{-\rho_l 4bxy}{\eta\pi\epsilon r_-^2 r_+^2} \quad (8.89)$$

$$H_y = \frac{E_x}{\eta} = \frac{-\rho_l 2b(b^2 - x^2 + y^2)}{\eta\pi\epsilon r_-^2 r_+^2}. \quad (8.90)$$

The electric and magnetic fields are plotted in Figure 8.7. We see that the electric field lines go between conductors while the magnetic field lines circulate around each transmission line in opposite directions. The electric field is strongest between the conductors (Figure 8.8).

As a quick check of the electric field derivation, let us look at the electric boundary conditions. The tangential E-fields should be zero on the conductor. The E_z component is always tangential to the system so it should be zero everywhere. Through the above derivations, we see that this is true. Along the horizontal axis through each conductor, E_x is normal and E_y is tangential, therefore $E_x \neq 0$ and $E_y = 0$. We see in Figure 8.9 that E_x is strongest and that $E_y = 0$ along the x direction from Figure 8.10. Along the vertical axis through each conductor, E_x is tangential and E_y is normal, therefore $E_x = 0$ and $E_y \neq 0$. This is again demonstrated in Figure 8.9 and 8.10.

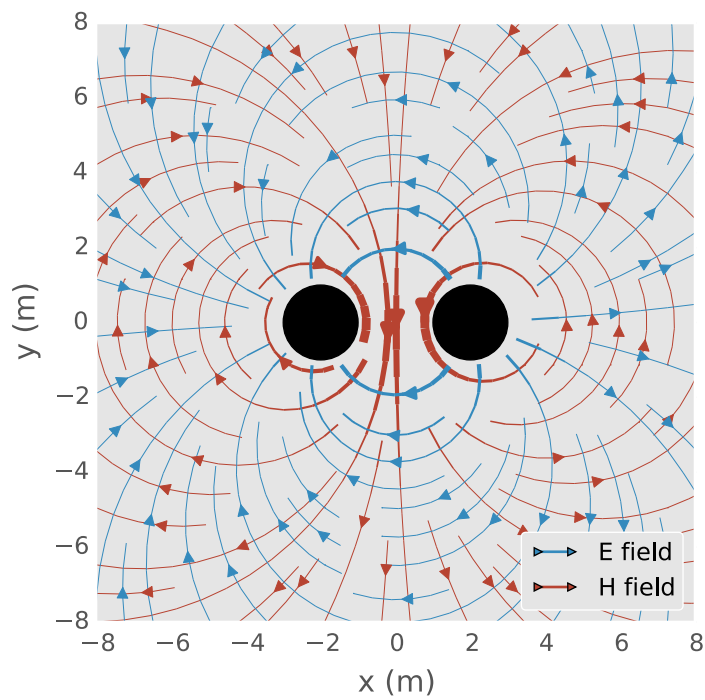


Figure 8.7: Electric and magnetic fields of a two-wire transmission line.

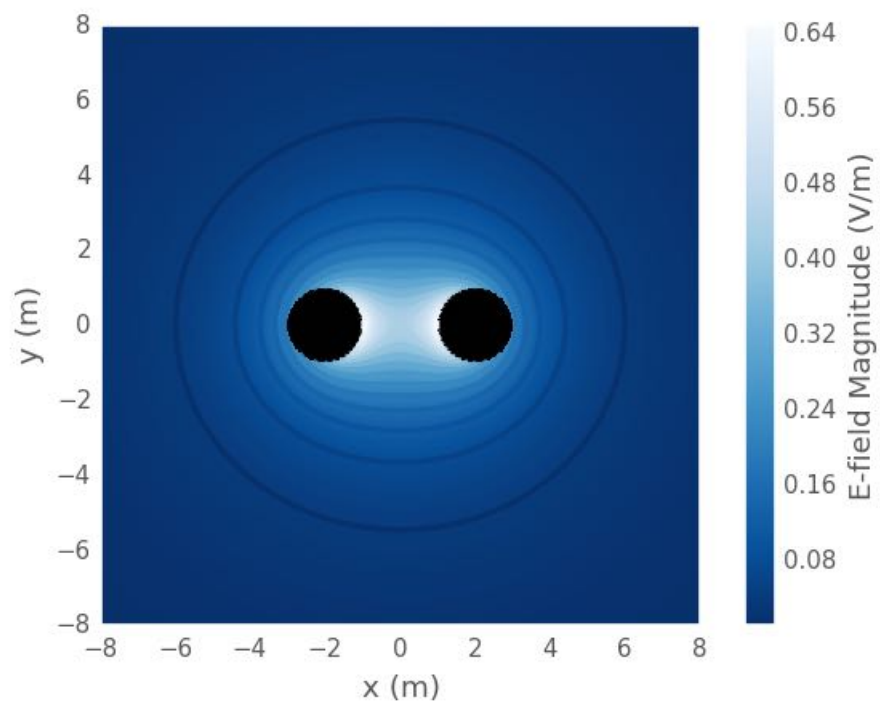


Figure 8.8: Magnitude of electric field.

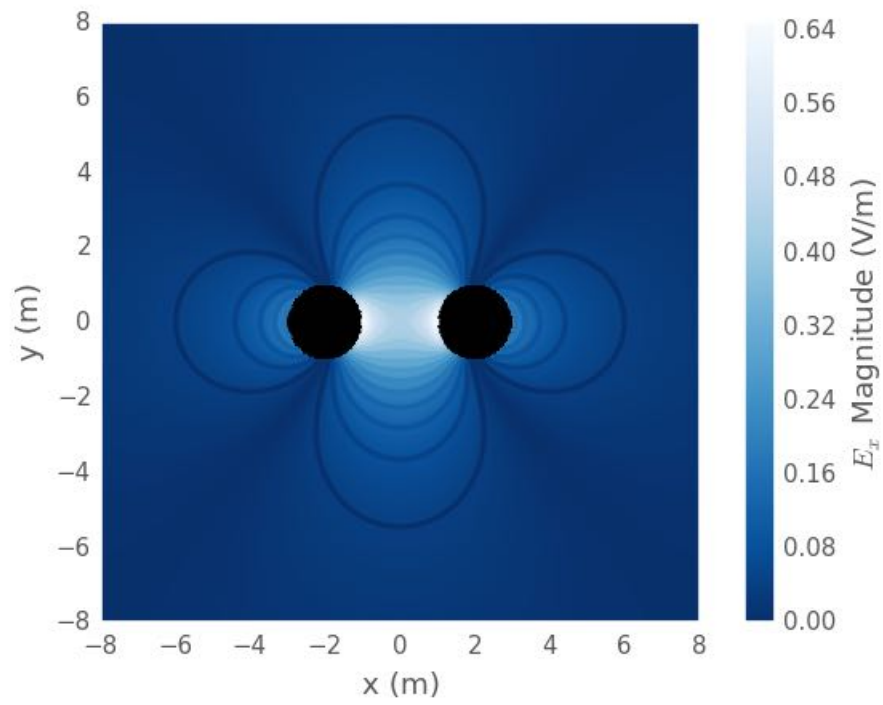


Figure 8.9: Magnitude of E_x .

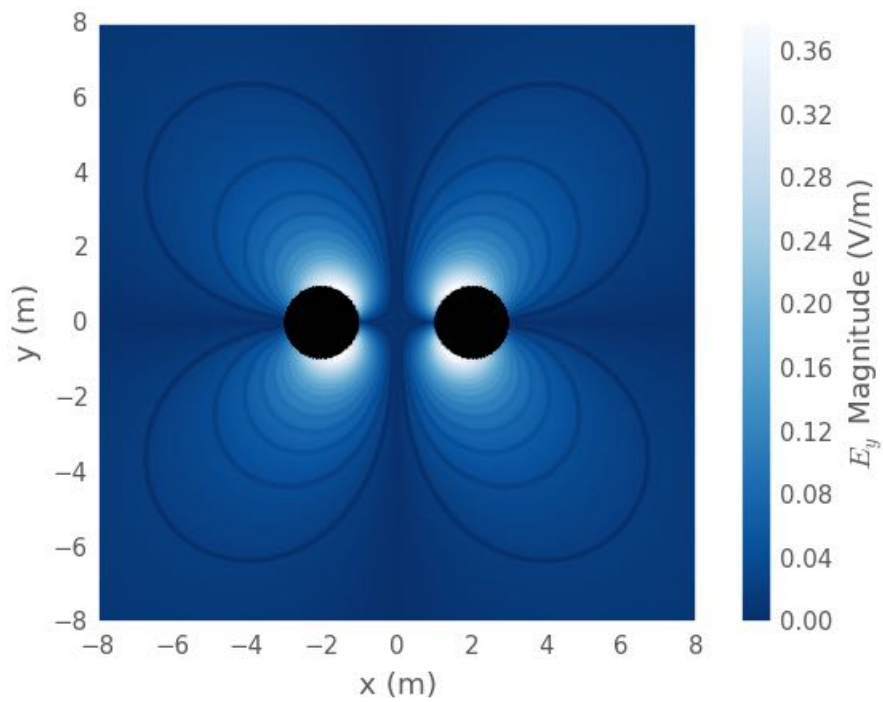


Figure 8.10: Magnitude of E_y .

8.3 Radiation Resistance

A two-wire transmission line relies on the two wires to be sufficiently close so that the currents produce fields that destructively interfere in the far zone and little power is radiated. Because we cannot place the transmission lines at the same point, there exists some amount of separation that results in radiation from the transmission line. In the derivation of the potential, higher-order terms which describe the radiation are not included. This will impact the circuit model presented in the next section. A simple way to include radiation effects is to treat it as a resistance. This work uses King's discussion from [75, pp. 487–492], which is referenced and summarized here.

Assumption

The following assumptions are made:

- the terminal impedances Z_g and Z_L are lumped and small in size compared to a wavelength, meaning that the currents through these impedances are constant in amplitude
- the transmission line is balanced—i.e. the currents are equal but oppositely directed
- the wire radius is significantly smaller than the separation distance: $a^2 \ll s^2$
- the separation distance is small compared to a wavelength in the media: $s \ll \lambda_1$
- the transmission line has little loss: $\alpha^2 / \beta_1^2 \ll 1$

The radiation resistance for a two-wire transmission line is given by [75, p. 488]

$$R^{rad} = \frac{2P}{I_0^2} = \frac{\eta_1}{4\pi} \beta_1^2 s^2 \frac{\cosh(\alpha l + 2\rho_L)}{|\cosh(\gamma l + \theta'_L)|^2} \left(\cosh(\alpha l) - \frac{\sin(2\beta_1 l)}{2\beta_1 l} \right) \quad (8.91)$$

where P is the radiated power; I_0 is the current; η_1 , $\beta_1 = (2\pi)/\lambda_1$, and α are the impedance, phase constant, and attenuation constant, respectively, of the media, denoted by the sub-

script 1, surrounding the transmission line, respectively; s is the center-to-center distance of the two wires; l is the length of the line; and

$$\theta'_L = \rho_L + j\Phi'_L = \tanh^{-1} \left(\frac{Z_L}{Z_0} \right) \quad (8.92)$$

is the alternative complex terminal function made up of the attenuation function ρ_L and alternative phase function Φ' , Z_L is the load impedance, and Z_0 is the characteristic impedance of the transmission line.

Radiation resistance is defined for the entire transmission line system and is dependent upon the terminal impedances. It is a lumped value and not a per-unit-length value like those in the next section. Contributions from R^{rad} can be included in other system-wide calculations by adding it to appropriate impedances.

Special forms of Equation (8.91) may be found for matched, shorted, opened, and purely reactive loads. For a matched—also called a non-resonant—line, $\rho_L = \infty$ which leads to

$$R_{match}^{rad} = \frac{\eta_1}{2\pi} \beta_1^2 s^2 \left(1 - \frac{\sin(2\beta_1 l)}{2\beta_1 l} \right). \quad (8.93)$$

Assumption

This simplification is appropriate if $\rho_L > 3$ and the line is low loss, i. e. αl is small. The first condition means that the line is essentially matched. For $Z_0 = 50\Omega$, this means that $49.75 < Z_L < 50.25$ for $\rho_L > 3$.

If the transmission line is long or a multiple of a wavelength, $2\beta_1 l = n\pi$, then

$$R_{match}^{rad} = \frac{\eta_1}{2\pi} \beta_1^2 s^2 = 60\beta_1^2 s^2. \quad (8.94)$$

When the load is an open, short, or is purely reactive, R^{rad} becomes infinite because I_0 in the denominator of Equation (8.91) is zero for $\beta_1 l + \Phi'_L = (2n + 1)\pi/2$. For such loads, the maximum current, I_m , is chosen as a reference. The radiation resistance is then

$$R_{res}^{rad} = \frac{2P}{I_m^2} = \frac{\eta_1}{4\pi} \beta_1^2 s^2 \left(1 - \frac{\sin(2\beta_1 l)}{2\beta_1 l} \right). \quad (8.95)$$

Assumption

Equation (8.95) holds if $(\alpha l + 2\rho_L) < 0.1$. This means that the line has little loss and that the load is close to an open or short circuit.

This is known as the resonant case because the reflection coefficient approaches ± 1 which sets up a pure standing wave on the line. For a long line or a multiple of a wavelength we have

$$R_{res}^{rad} = \frac{\eta_1}{4\pi} \beta_1^2 s^2 = 30\beta_1^2 s^2. \quad (8.96)$$

The above equations are plotted in Figure 8.11. A curve for $Z_L = Z_0/2$ is also plotted to demonstrate the behavior of the radiation resistance for cases besides the resonant and non-resonant cases.

We see that compared to the matched case, the resonant line has half the radiation resistance. This means that a line with a short or open load will radiate less power than one with a matched load given identical currents.

8.3.1 Closely Spaced Wires

If the wires are closely spaced compared to a wavelength, $a^2 \simeq s^2$, an effective spacing parameter,

$$s_e = \frac{b}{2} \left[1 + \sqrt{1 - \left(\frac{2a}{s} \right)^2} \right], \quad (8.97)$$

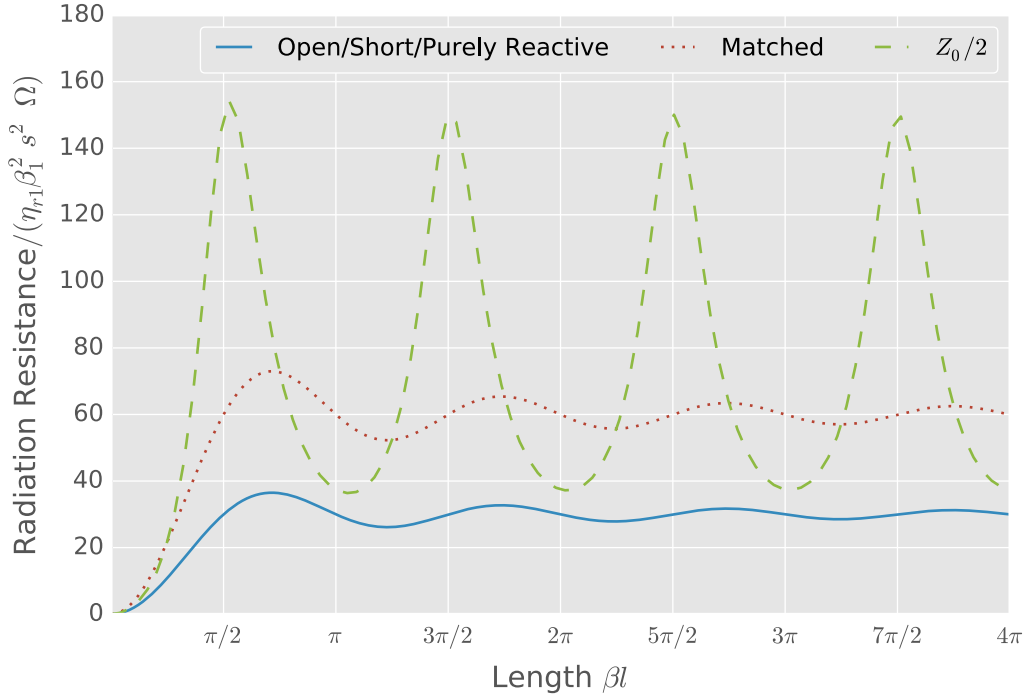


Figure 8.11: Radiation resistance for a two-wire transmission with line open, short, or purely reactive (resonant line); matched (non-resonant line); and $Z_0/2$ loads.

should be used in the above equations in place of s .

8.3.2 Discussion and Recommendations

In his discussion, King points out that the losses due to radiation are not necessarily negligible compared to ohmic losses. He even points to cases where it may be significantly higher. This is easily understood since a two-wire transmission line can be used as an antenna. In such a case, one would like R^{rad} to be as large as possible.

If the transmission line is not balanced, radiation will also be produced. This is the main reason for the use of a balun as discussed elsewhere in this dissertation. King continues by further discussing experimental results related to radiation resistance.

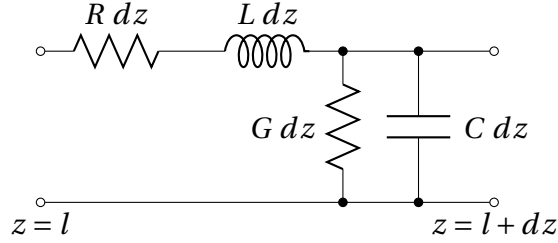


Figure 8.12: Circuit model for a differential length of transmission line.

Radiation resistance should not be ignored in the design of the material measurement system. First, a one-port line with a short instead of a two-port system should be considered the preferred measurement setup if other factors (spacing, etc) lead to higher radiation losses. The two-port system would have matched loads (optimally) which would result in higher radiative losses than the one-port system. Another consideration is the length of the line. We see from Figure 8.11 that radiation resistance oscillates with length. This can be a design challenge or be used as an advantage. The largest challenge might actually be in creating a wideband system that has low loss. The best starting point may be a long, one-port transmission line with closely-spaced wires.

8.4 Distributed Circuit Model

The derivation presented below is based upon numerous references. The reader is directed to [3, 72–75] for more information. I have also presented some of this information at conferences [76, 77].

A transmission line may be modeled as a circuit of lumped elements for a differential length as shown in Figure 8.12. When modeled as a circuit, a transmission line consists of a series resistance, R ; a series inductance, L , that includes both self and external inductance; a shunt conductance, G ; and a shunt capacitance, C , all being per-unit-length values. The differential length circuit then has circuit values of $R dz$, $L dz$, $G dz$, and $C dz$ [3, pp. 214–215, 246–247].

The characteristic impedance of the transmission line is given by [3, pp. 246–247]

$$Z_0 = \sqrt{\frac{R + j\omega L}{G + j\omega C}}. \quad (8.98)$$

Note that this is the characteristic impedance of the transmission line itself and does not account for any loads placed on the line. A load impedance Z_L is transformed by a transmission line and may appear as a different impedance at the other end of the line. The transformed impedance is given by

$$Z_{in} = Z_0 \left[\frac{Z_L + Z_0 \tanh(\gamma l)}{Z_0 + Z_L \tanh(\gamma l)} \right] \quad (8.99)$$

and is dependent upon length l [3, pp. 247]. The term γ is the propagation constant,

$$\gamma = \alpha + j\beta = \sqrt{(R + j\omega L)(G + j\omega C)}, \quad (8.100)$$

as defined for the distributed circuit model [3, pp. 246–247]. The complex wave number, k , which was presented in Chapter 2, for a TEM wave is related to the propagation constant by [3, p. 399] [78]

$$k = -j\gamma = \beta - j\alpha. \quad (8.101)$$

The voltage waves for a single frequency on the transmission line are given by

$$V = V^+ e^{-\gamma z} + V^- e^{\gamma z} \quad (8.102)$$

and the current by

$$I = \frac{1}{Z_0} [V^+ e^{-\gamma z} - V^- e^{\gamma z}] \quad (8.103)$$

where $V^+ \exp(-\gamma z)$ and $V^- \exp(\gamma z)$ represent waves traveling in the positive and negative z direction, respectively [3, p. 246]. Multi-frequency signals are expressed as a sum of individual frequency waves.

Assumption

As noted earlier, the equations are written as cosine-based phasors with the $e^{+j\omega t}$ time factor suppressed.

The parameters R , L , C , and G must be determined so that the characteristic impedance and the propagation constant may be calculated for the two-wire transmission line. The equations derived in this section have $\cosh^{-1}(x)$ terms. It is common to find similar equations in textbooks that use $\ln(x)$. If $s^2 \gg a^2$, that is the center-to-center distance is much larger than the wire diameter, then $\cosh^{-1}(s/a)$ may be simplified to $\ln(s/a)$ and the common form is derived. The inverse hyperbolic cosine function is kept in this work as it is the most-general form and can be used for all s^2/a^2 ratios.

Assumption

The assumptions listed below are made about the two-wire transmission line configuration in the following derivations.

- The wire radius is small compared to a wavelength, $a \ll \lambda_1$.
- The spacing is small compared to a wavelength, $s \ll \lambda_1$.
- The wires do not touch, $s > 2a$.

The wavelength has a subscript 1 to emphasize that this is the wavelength in the media surrounding the transmission line and not the free space wavelength. The wires are considered to be closely spaced if $s^2 \gg a^2$ does not hold.

8.4.1 Capacitance

The per-unit-length capacitance is given by

$$C = Q/|V_\Delta| \quad (8.104)$$

where Q is the charge on one conductor per unit length. From Section 8.1, the line charge ρ_L is equivalent to the charge on the conductor; therefore, $Q = \rho_L$. The denominator V_Δ is the voltage potential between the two conductors which is given by Equation (8.72). Substituting these into the above definition gives

$$C = \frac{\rho_L}{\rho_L/(\pi\epsilon) \cosh^{-1}\left(\frac{s}{2a}\right)} \quad (8.105)$$

which simplifies to

$$C = \frac{\pi\epsilon}{\cosh^{-1}\left(\frac{s}{2a}\right)} \quad (8.106)$$

8.4.2 Conductance

The per-unit-length conductance, G , for a two-wire transmission line is derived using Ohm's Law and the definition for capacitance. Ohm's Law is

$$\frac{1}{G} = R = \frac{V}{I} = \frac{-\int_L \vec{E} \cdot d\vec{l}}{\oint_S \vec{J} \cdot d\vec{S}}. \quad (8.107)$$

The current J is related to the electric field through the constitutive relation $J = \sigma \vec{E}$ (Eqn. (2.3)) where σ is the conductivity of the media surrounding the conductors. Ohm's law can then be written as

$$\frac{1}{G} = \frac{-\int_L \vec{E} \cdot d\vec{l}}{\oint_S \sigma \vec{E} \cdot d\vec{S}}. \quad (8.108)$$

Capacitance is defined as

$$C = \frac{Q}{V} = \frac{\oint_S \vec{D} \cdot d\vec{S}}{-\int_L \vec{E} \cdot d\vec{l}} \quad (8.109)$$

$$= \frac{\oint_S \epsilon \vec{E} \cdot d\vec{S}}{-\int_L \vec{E} \cdot d\vec{l}}. \quad (8.110)$$

$$(8.111)$$

where the constitutive relation $D = \epsilon \vec{E}$ (Eqn. (2.4)) has been used in the numerator. Dividing capacitance by conductance gives

$$\frac{C}{G} = \frac{\oint_S \epsilon \vec{E} \cdot d\vec{S} - \int_L \vec{E} \cdot d\vec{l}}{-\int_L \vec{E} \cdot d\vec{l} \oint_S \sigma \vec{E} \cdot d\vec{S}} = \frac{\epsilon}{\sigma} \quad (8.112)$$

or

$$G = \frac{C\sigma}{\epsilon}. \quad (8.113)$$

The conductance of a two-wire transmission line per unit length is then

$$G = \frac{\pi\sigma}{\cosh^{-1}\left(\frac{s}{2a}\right)} \quad (8.114)$$

when Equation (8.106) is substituted for C . Making use of Equation (2.13) allows the conductance to be expressed as any of the following:

$$\boxed{\begin{aligned} G &= \frac{\pi\sigma}{\cosh^{-1}\left(\frac{s}{2a}\right)} \\ G &= \frac{\pi\omega\epsilon''}{\cosh^{-1}\left(\frac{s}{2a}\right)} \\ G &= \frac{\pi\omega\epsilon_0\epsilon_r \tan \delta}{\cosh^{-1}\left(\frac{s}{2a}\right)}. \end{aligned}} \quad (8.115)$$

8.4.3 Inductance

To find the per-unit-length inductance, L , for a two-wire transmission line, we begin by assuming that the conductivity of the conductors is significantly large such that $R \approx 0$. This allows us to express the propagation constant (Eqn. (8.100)) of the transmission line as

$$\gamma^2 = j\omega L(G + j\omega C). \quad (8.116)$$

This can be expanded to

$$\gamma^2 = j\omega LG + j^2\omega^2 LC \quad (8.117)$$

$$= j\omega LG - \omega^2 LC. \quad (8.118)$$

Factoring $-\omega^2 LC$ gives

$$\gamma^2 = -\omega^2 LC \left(1 - j \frac{G}{\omega C} \right) \quad (8.119)$$

$$= -\omega^2 LC \left(1 + \frac{G}{j\omega C} \right) \quad (8.120)$$

The complex propagation constant for a TEM wave in a dielectric medium is

$$\gamma_{TEM}^2 = (jk)^2 = -k^2. \quad (8.121)$$

The wave number may be written as

$$-k^2 = -\omega^2 \mu \epsilon \left(1 + \frac{\sigma}{j\omega \epsilon} \right) \quad (8.122)$$

from Equation (2.14). Since the dominant mode of a two-wire transmission line is the TEM mode [72, pp. 444–445], these two propagation constants may be compared,

$$-\omega^2 LC \left(1 + \frac{G}{j\omega C} \right) = -\omega^2 \mu\epsilon \left(1 + \frac{\sigma}{j\omega\epsilon} \right). \quad (8.123)$$

giving

$$LC = \mu\epsilon \quad (8.124)$$

where μ is the permeability of the material surrounding the conductors. One may now solve for L , making use of Equation (8.106), to find the per-unit-length inductance

$$L = \frac{\mu}{\pi} \cosh^{-1} \left(\frac{s}{2a} \right). \quad (8.125)$$

This same expression can be found using either the method of images or conformal mapping as discussed in Example 4.6b of [3].

8.4.4 Resistance

The resistance per unit length, R , is derived by finding the electric field, E_{z0} , and the surface current, J_{sz} , which define the surface impedance

$$Z_s = \frac{E_{z0}}{J_{sz}} = R + j\omega L_i, \quad (8.126)$$

where L_i is the internal inductance of the wire.

Assumption

The conductors are assumed to be good conductors as defined by the following criteria [3, pp. 149-150]:

1. $\vec{J} = \sigma_c \vec{E}$, i. e. conductors satisfy Ohm's law,
2. $\omega\epsilon \ll \sigma_c$ so that $\nabla \times \vec{H} = \sigma_c \vec{E}$, and
3. $\rho = 0$, i. e. the net charge density is zero because of the first condition.

Here σ_c is the conductivity of the conductor.

Assumption

We begin by assuming that the current is uniformly distributed on the wires as occurs when the center-to-center distance is significantly larger than the wire radius, $s^2 \gg a^2$. When the wires are close and this condition does not hold, current density increases closest to and decreases away from the other conductor. A modification in the form of an effective radius is provided after the initial derivation to account for this non-uniform density.

We will find the surface impedance first for a unit width of a conductor and then apply this to the wires in our problem. The current density in the conductor is given by [3, p. 151]

$$J_z(x) = J_0 e^{-x/\delta} e^{-jx/\delta} \quad (8.127)$$

where x is the depth into the conductor and δ is the skin depth of the conductor,

$$\delta = \frac{1}{\sqrt{\pi f \mu_c \sigma_c}} \quad (8.128)$$

with μ_c being the permeability of the conductor. We integrate the current density from the surface to an infinite depth to find the total current flowing past a unit width.

$$J_{sz} = \int_0^{\infty} J_0 e^{-x/\delta} e^{-jx/\delta} dx \quad (8.129)$$

$$= \frac{J_0 \delta}{1+j} \quad (8.130)$$

At the surface, the electric field is related to surface current density by [3, p. 154]

$$E_{z0} = \frac{J_0}{\sigma_c}. \quad (8.131)$$

Substituting into Equation (8.126) gives

$$Z_s = \frac{J_0 / \sigma_c}{J_0 \delta / (1+j)} \quad (8.132)$$

$$= \frac{1+j}{\sigma_c \delta} \quad (8.133)$$

For the case of a wire, the circumference, $2\pi a$, is used as the width. The impedance for one wire is therefore

$$Z_1^i = \frac{Z_s}{2\pi a} \quad (8.134)$$

$$= \frac{1+j}{2\pi a \sigma_c \delta}. \quad (8.135)$$

The skin depth can be expanded using Equation (8.128), giving the impedance as

$$Z_1^i = \frac{1+j}{2\pi a} \sqrt{\frac{\omega \mu_c}{2\sigma_c}} \quad (8.136)$$

For two wires, the impedance is $2Z_1^i$ or

$$Z^i = \frac{1+j}{\pi a} \sqrt{\frac{\omega\mu_c}{2\sigma_c}} \quad (8.137)$$

As noted in the assumption at the beginning of this subsection, Equation (8.137) is for uniform current density. If the wires are close (the condition $s^2 \gg a^2$ does not hold), an effective wire radius

$$a_e = a\sqrt{1 - (2a/s)^2} \quad (8.138)$$

should be used in place of the normal radius a as given by King [75, p. 30] and derived by Carson [79]. The effective impedance is therefore

$$Z_e^i = \frac{1+j}{\pi a} \sqrt{\frac{\omega\mu_c}{2\sigma_c(1 - (2a/s)^2)}}. \quad (8.139)$$

The resistance per unit length is the real part of Z^i (Eqn. (8.126)) [75, p. 18],

$$R = \frac{1}{\pi a} \sqrt{\frac{\omega\mu_c}{2\sigma_c}}. \quad (8.140)$$

for $s^2 \gg a^2$ and

$$R = \frac{1}{\pi a} \sqrt{\frac{\omega\mu_c}{2\sigma_c(1 - (2a/s)^2)}}. \quad (8.141)$$

for closely spaced wires.

8.4.5 Summary of Parameters

Table 8.1 summarizes the per-unit-length circuit parameters of a two-wire transmission line.

| | |
|--|-----------------------------|
| $R = \frac{1}{\pi a} \sqrt{\frac{\omega \mu_c}{2\sigma_c}}, \quad \text{use } a_e = a\sqrt{1 - (2a/s)^2} \quad \text{for } a \text{ if closely spaced}$ | (8.140 and 8.141, repeated) |
| $L = \frac{\mu}{\pi} \cosh^{-1}\left(\frac{s}{2a}\right)$ | (8.125, repeated) |
| $G = \frac{\pi\sigma}{\cosh^{-1}\left(\frac{s}{2a}\right)} = \frac{\pi\omega\epsilon''}{\cosh^{-1}\left(\frac{s}{2a}\right)} = \frac{\pi\omega\epsilon_0\epsilon_r \tan\delta}{\cosh^{-1}\left(\frac{s}{2a}\right)}$ | (8.115 repeated) |
| $C = \frac{\pi\epsilon}{\cosh^{-1}\left(\frac{s}{2a}\right)}$ | (8.106, repeated) |

Table 8.1: Summary of equations for the calculation of the circuit parameters of a two-wire transmission line.

Chapter 9

Three Short Calibration Method

9.1 Introduction

This chapter presents a calibration method that places the measurement reference plane at a point along the two-wire transmission line after a balun (discussed in later chapters) transitions from the coaxial cable used by test equipment to the two-wire transmission line. This allows for the device under test (DUT) to be more accurately measured and the effects of the balun removed from the measurements. This calibration procedure has been used in the past for stripline measurements [80].

A vector network analyzer (VNA) with coaxial test cables is typically calibrated to the connector at the end of the cable using a set of known, coaxial loads (e.g. short, open, matched load). Measurements made using this traditional calibration method would include the effects of any transitions from the coaxial cable to a two-wire transmission line and then any effects of the two-wire transmission line until the DUT.

Presented here is a one-port calibration method that is then extended to a two-port calibration method, which may be used for almost any transmission structure. It relies on the measurement of a short circuit (actually any load with a known reflection coefficient can be used)

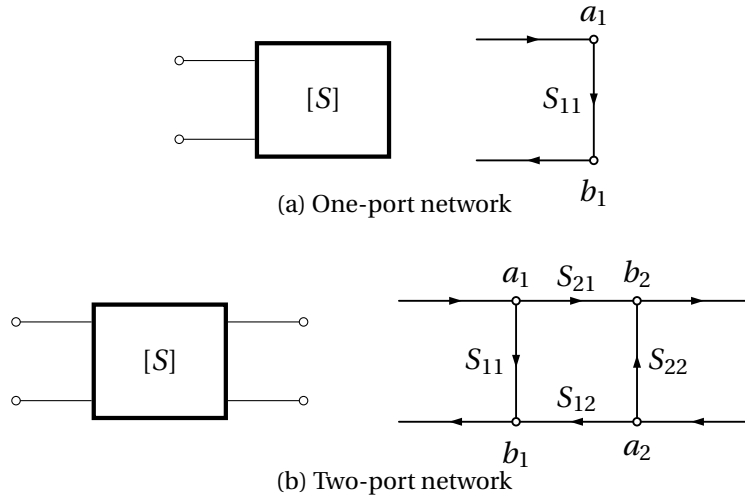


Figure 9.1: Block diagrams and signal flow graphs for (a) a one-port network and (b) a two-port network.

placed at three different positions with respect to a reference point along the transmission path. The transmission structure leading up to the reference point is removed from measurements based on these calibration measurements.

Caution

In the interest of taking the most accurate measurements possible, a traditional coaxial calibration is still expected at the coaxial connector of the balun because the following procedure does not provide the full error correction model that compensates for all errors in the measurement equipment.

9.2 Calibration Theory

A one-port network is illustrated in Figure 9.1a as a block diagram and as a signal flow graph. The input/output relationship of a one-port network is given by

$$[b_1] = [S_{11}][a_1]. \quad (9.1)$$

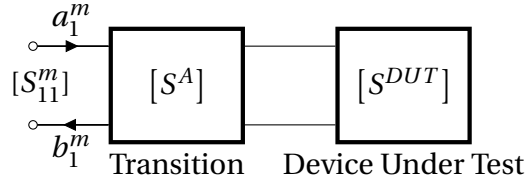


Figure 9.2: Block diagram showing the transition that is to be removed and the one-port network that is to be measured.

Figure 9.1b shows the block diagram and the signal flow graph of a two-port network. The input/output relationship of a two-port network is given by

$$\begin{bmatrix} b_1 \\ b_2 \end{bmatrix} = \begin{bmatrix} S_{11} & S_{12} \\ S_{21} & S_{22} \end{bmatrix} \begin{bmatrix} a_1 \\ a_2 \end{bmatrix}. \quad (9.2)$$

Assumption

The following assumptions are made in the derivations below and when the calibration is applied:

- the DUT is a passive, reciprocal network;
- the system is isotropic;

9.2.1 One-Port Calibration

The following calibration procedure recovers the one-port S-parameters of the DUT, S^{DUT} , by finding some of the S-parameters of the two-port transition, S^A . A block diagram of the measurement setup is shown in Figure 9.2.

The conventional definition for the reflection coefficient is

$$\Gamma = \frac{b}{a}. \quad (9.3)$$

In the one-port case

$$a_1^{\text{DUT}} = b_2^{\text{A}}, \quad (9.4)$$

$$b_1^{\text{DUT}} = a_2^{\text{A}}, \quad (9.5)$$

therefore,

$$\Gamma^{\text{DUT}} = \frac{b_1^{\text{DUT}}}{a_1^{\text{DUT}}} = \frac{a_2^{\text{A}}}{b_2^{\text{A}}}. \quad (9.6)$$

Equation (9.2) for the transition portion of a cascaded network, as shown in Figure 9.2, can now be expressed as

$$\begin{bmatrix} b_1^{\text{A}} \\ a_2^{\text{A}}/\Gamma^{\text{DUT}} \end{bmatrix} = \begin{bmatrix} S_{11}^{\text{A}} & S_{12}^{\text{A}} \\ S_{21}^{\text{A}} & S_{22}^{\text{A}} \end{bmatrix} \begin{bmatrix} a_1^{\text{A}} \\ a_2^{\text{A}} \end{bmatrix} \quad (9.7)$$

Solving the second row gives

$$a_2 = \frac{S_{21}^{\text{A}} a_1}{1/\Gamma^{\text{DUT}} - S_{22}^{\text{A}}}, \quad (9.8)$$

which in turn gives

$$b_1 = a_1 \left(S_{11}^{\text{A}} + \frac{S_{12}^{\text{A}} S_{21}^{\text{A}}}{1/\Gamma^{\text{DUT}} - S_{22}^{\text{A}}} \right) \quad (9.9)$$

when substituted back into the first row.

When the cascaded network (consisting of the transition, transmission line, and calibration standard), is measured, only S_{11}^m can be measured. In this case $a_1^m = a_1^{\text{A}}$ and $b_1^m = b_1^{\text{A}}$, therefore

$$S_{11}^m = S_{11}^{\text{A}} + \frac{S_{12}^{\text{A}} S_{21}^{\text{A}}}{1/\Gamma^{\text{DUT}} - S_{22}^{\text{A}}} \quad (9.10)$$

and

$$\frac{1}{\Gamma^{\text{DUT}}} = S_{22}^A + \frac{S_{12}^A S_{21}^A}{S_{11}^m - S_{11}^A}. \quad (9.11)$$

There are three unknowns (S_{11}^A , S_{22}^A , and $S_{12}^A S_{21}^A$) in the above equation. These values may be found mathematically by using three different values of Γ^{DUT} . Experimentally this is done by measuring three standards with unique, known values of Γ^{DUT} . Let the subscripts 1, 2, and 3 denote values associated with the three different standards. These standards may be any device with a known and repeatable reflection coefficient. One possible set of standards is a short circuit located at three different locations in the transmission system, resulting in

$$\begin{aligned} \Gamma_1 &= -1e^{-j2\beta d_1} \\ \Gamma_2 &= -1e^{-j2\beta d_2} \\ \Gamma_3 &= -1e^{-j2\beta d_3} \end{aligned} \quad (9.12)$$

where d_i is the distance from the new reference plane to the short circuit. Figure 9.3 illustrates a calibration setup for the three distances as used in the calibration of a two-wire transmission line for this dissertation. The set of reflection coefficients in Equation (9.12) is for the case of an ideal short circuit. The accuracy of this calibration scheme relies on how well the short circuit standard (or any standard) can be represented mathematically.

Caution

At the time of writing, an acceptable range of d had not been established. Based upon other calibration and de-embedding techniques, one expects that d should probably be in the range of $0 - \lambda_{\min}/4$ where λ_{\min} is the shortest wavelength in the frequency range of interest.

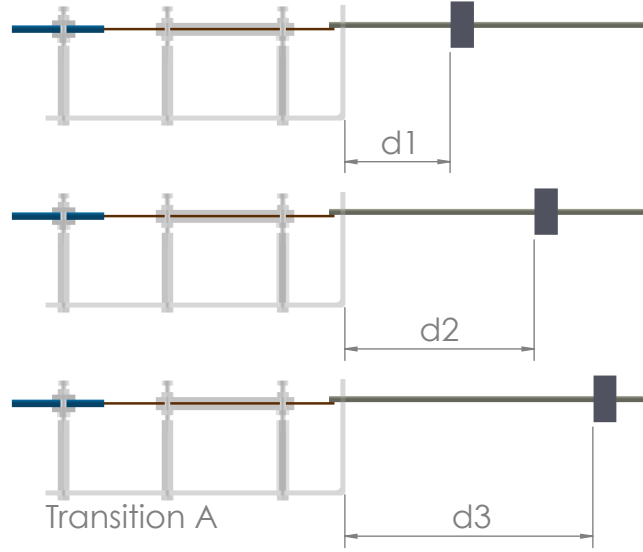


Figure 9.3: Illustration of calibration measurements showing the three different distances for a one-port calibration.

Subtracting the three versions of Equation (9.10) where $m = 1, 2$, or 3 , one gets

$$\begin{aligned}
 S_{11}^1 - S_{11}^2 &= S_{12}^A S_{21}^A \left[\frac{1}{1/\Gamma_1 - S_{22}^A} - \frac{1}{1/\Gamma_2 - S_{22}^A} \right] \\
 &= S_{12}^A S_{21}^A \left[\frac{1/\Gamma_2 - 1/\Gamma_1}{(1/\Gamma_1 - S_{22}^A)(1/\Gamma_2 - S_{22}^A)} \right]
 \end{aligned} \tag{9.13}$$

and

$$\begin{aligned}
 S_{11}^1 - S_{11}^3 &= S_{12}^A S_{21}^A \left[\frac{1}{1/\Gamma_1 - S_{22}^A} - \frac{1}{1/\Gamma_3 - S_{22}^A} \right] \\
 &= S_{12}^A S_{21}^A \left[\frac{1/\Gamma_3 - 1/\Gamma_1}{(1/\Gamma_1 - S_{22}^A)(1/\Gamma_3 - S_{22}^A)} \right].
 \end{aligned} \tag{9.14}$$

Dividing Equation (9.13) by Equation (9.14) gives

$$\frac{S_{11}^1 - S_{11}^2}{S_{11}^1 - S_{11}^3} = \left(\frac{1/\Gamma_2 - 1/\Gamma_1}{1/\Gamma_3 - 1/\Gamma_1} \right) \left(\frac{1/\Gamma_3 - S_{22}^A}{1/\Gamma_2 - S_{22}^A} \right). \tag{9.15}$$

After rearranging we can define the constant

$$K = \left(\frac{1/\Gamma_3 - 1/\Gamma_1}{1/\Gamma_2 - 1/\Gamma_1} \right) \left(\frac{S_{11}^1 - S_{11}^2}{S_{11}^1 - S_{11}^3} \right) = \frac{1/\Gamma_3 - S_{22}^A}{1/\Gamma_2 - S_{22}^A}. \quad (9.16)$$

S_{22} for the transition is given by

$$S_{22}^A = \frac{1/\Gamma_3 - K(1/\Gamma_2)}{1 - K}. \quad (9.17)$$

Once S_{22}^A is computed it may be used in Equation (9.13) to find $S_{12}^A S_{21}^A$,

$$S_{12}^A S_{21}^A = \frac{S_{11}^1 - S_{11}^2}{1/\Gamma_2 - 1/\Gamma_1} \left(\frac{1}{\Gamma_1} - S_{22}^A \right) \left(\frac{1}{\Gamma_2} - S_{22}^A \right). \quad (9.18)$$

Returning now to Equation (9.10), S_{11}^A is found using

$$S_{11}^A = S_{11}^1 - \frac{S_{12}^A S_{21}^A}{1/\Gamma_1 - S_{22}^A}. \quad (9.19)$$

The reflection coefficient of a sample may now be found using Equation (9.11).

Note

The S-parameters S_{12}^A and S_{21}^A are not found individually since only the product of these two S-parameters appear in Equation 9.11.

Table 9.1 provides a summary of the equations used in the one-port calibration procedure.

9.2.2 Two-Port Calibration

The following calibration procedure is used when the DUT is a two-port device as shown in Figure 9.4. Six measurements are needed to perform this calibration. In the case of a two-wire transmission line, one may be able to position the short only three times and measure both S_{11} and S_{22} . This saves the technician from having to move the calibration standard six times. The

$$\Gamma_i = -1e^{-j2\beta d_i} \quad (9.12, \text{repeated})$$

$$K = \left(\frac{1/\Gamma_3 - 1/\Gamma_1}{1/\Gamma_2 - 1/\Gamma_1} \right) \left(\frac{S_{11}^1 - S_{11}^2}{S_{11}^1 - S_{11}^3} \right) = \frac{1/\Gamma_3 - S_{22}^A}{1/\Gamma_2 - S_{22}^A} \quad (9.16, \text{repeated})$$

$$S_{22}^A = \frac{1/\Gamma_3 - K(1/\Gamma_2)}{1 - K} \quad (9.17, \text{repeated})$$

$$S_{12}^A S_{21}^A = \frac{S_{11}^1 - S_{11}^2}{1/\Gamma_2 - 1/\Gamma_1} \left(\frac{1}{\Gamma_1} - S_{22}^A \right) \left(\frac{1}{\Gamma_2} - S_{22}^A \right) \quad (9.18, \text{repeated})$$

$$S_{11}^A = S_{11}^1 - \frac{S_{12}^A S_{21}^A}{1/\Gamma_1 - S_{22}^A} \quad (9.19, \text{repeated})$$

$$\frac{1}{\Gamma^{\text{DUT}}} = S_{22}^A + \frac{S_{12}^A S_{21}^A}{S_{11}^m - S_{11}^A} \quad (9.11, \text{repeated})$$

Table 9.1: Summary of equations to calculate the S-parameters of a transition of a 1-port calibration.

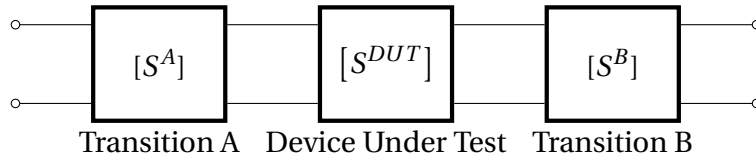


Figure 9.4: Block diagram showing the transitions that are to be removed and the two-port network that is to be measured.

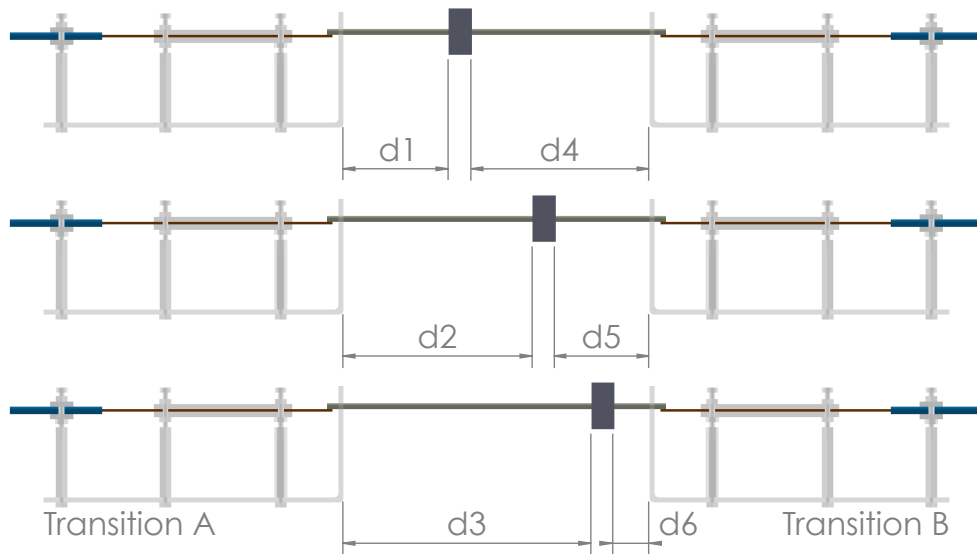


Figure 9.5: Illustration of calibration measurements showing the six different distances for a two-port calibration.

distance from each port to the standard must be known so that the location of the reference plane for each port may be defined. A schematic of this calibration procedure and distances is shown in Figure 9.5.

To determine the S-parameters of Transition A, the procedure and equations given in the previous section may be used (see Table 9.1). Transition B is essentially the same as Transition A except with indices for ports 1 and 2 interchanged. The equations in Table 9.1 may be used if 1 and 2 are switched in all of the equations. Table 9.2 provides a summary of the equations needed to determine the S-parameters of both transitions.

Once the S-parameters of the two transitions are known, the S-parameters of the DUT can be recovered by computing

$$[T^D] = [T^A]^{-1} [T^C] [T^B]^{-1} \quad (9.26)$$

where $[T]$ are the T-parameters, see Appendix A .3. The matrix $[T^C]$ represents the T-parameters for the entire cascaded system as measured at the VNA test ports. Relations for converting between S-parameters and T-parameters are given in Table A .1 and reprinted here as Table 9.3.

Transition A

$$\Gamma_i^A = -1e^{-j2\beta d_i^A} \quad (9.12, \text{ repeated})$$

$$K = \left(\frac{1/\Gamma_3 - 1/\Gamma_1}{1/\Gamma_2 - 1/\Gamma_1} \right) \left(\frac{S_{11}^1 - S_{11}^2}{S_{11}^1 - S_{11}^3} \right) = \frac{1/\Gamma_3 - S_{22}^A}{1/\Gamma_2 - S_{22}^A} \quad (9.16, \text{ repeated})$$

$$S_{22}^A = \frac{1/\Gamma_3 - K(1/\Gamma_2)}{1 - K} \quad (9.17, \text{ repeated})$$

$$S_{12}^A S_{21}^A = \frac{S_{11}^1 - S_{11}^2}{1/\Gamma_2 - 1/\Gamma_1} \left(\frac{1}{\Gamma_1} - S_{22}^A \right) \left(\frac{1}{\Gamma_2} - S_{22}^A \right) \quad (9.18, \text{ repeated})$$

$$S_{11}^A = S_{11}^1 - \frac{S_{12}^A S_{21}^A}{1/\Gamma_1 - S_{22}^A} \quad (9.19, \text{ repeated})$$

$$\frac{1}{\Gamma^{\text{DUT}}} = S_{22}^A + \frac{S_{12}^A S_{21}^A}{S_{11}^m - S_{11}^A} \quad (9.11, \text{ repeated})$$

Transition B

$$\Gamma_i^B = -1e^{-j2\beta d_i^B} \quad (9.20)$$

$$K = \left(\frac{1/\Gamma_6 - 1/\Gamma_4}{1/\Gamma_5 - 1/\Gamma_4} \right) \left(\frac{S_{22}^1 - S_{22}^2}{S_{22}^1 - S_{22}^3} \right) = \frac{1/\Gamma_6 - S_{11}^B}{1/\Gamma_5 - S_{11}^B} \quad (9.21)$$

$$S_{11}^B = \frac{1/\Gamma_6 - K(1/\Gamma_5)}{1 - K} \quad (9.22)$$

$$S_{12}^B S_{21}^B = \frac{S_{22}^1 - S_{22}^2}{1/\Gamma_5 - 1/\Gamma_4} \left(\frac{1}{\Gamma_4} - S_{11}^B \right) \left(\frac{1}{\Gamma_5} - S_{11}^B \right) \quad (9.23)$$

$$S_{22}^B = S_{22}^1 - \frac{S_{12}^B S_{21}^B}{1/\Gamma_4 - S_{11}^B} \quad (9.24)$$

$$\frac{1}{\Gamma^m} = S_{11}^B + \frac{S_{12}^B S_{21}^B}{S_{22}^m - S_{22}^B} \quad (9.25)$$

Table 9.2: Summary of equations to calculate the S-parameters of transitions for a 2-port calibration.

$$\begin{aligned}
T_{11} &= \frac{S_{12}S_{21} - S_{11}S_{22}}{S_{21}} \\
T_{12} &= \frac{S_{11}}{S_{21}} \\
T_{21} &= \frac{-S_{22}}{S_{21}} \\
T_{22} &= \frac{1}{S_{21}}
\end{aligned}
\tag{9.27}$$

$$\begin{aligned}
S_{11} &= \frac{T_{12}}{T_{22}} \\
S_{12} &= \frac{T_{11}T_{22} - T_{12}T_{21}}{T_{22}} \\
S_{21} &= \frac{1}{T_{22}} \\
S_{22} &= \frac{-T_{21}}{T_{22}}
\end{aligned}
\tag{9.28}$$

Table 9.3: Relations between S-parameters and T-parameters. Reprint of Table A .1

Chapter 10

Double-Y Balun

10.1 Introduction

This goal of this work is to use a two-wire transmission line for material characterization. In order to do this, the two-wire transmission line must be connected to test equipment that has coaxial connectors. A device called a balun, for balanced-unbalanced, is used for this connection. Since we would like to perform material characterization over a large frequency span, a wideband balun is desired. This chapter describes a wideband balun called a double-y balun.

A balun provides a balanced feed from an unbalanced structure to a balanced structure. A balanced feed has only differential-mode currents, meaning that currents are equal in magnitude but opposite in direction. This is in contrast to common-mode currents that are equal in magnitude and direction. In a balanced structure, each conductor has the same impedance with respect to ground. This is not the case in unbalanced structure where the impedances are different. One of the conductors is often used as ground in an unbalanced structure. Sometimes the term balanced structure is used to mean that only differential-mode currents are present while the term unbalanced structure is used to describe a structure with both differential- and common-mode currents. A balanced structure as defined above is able to carry both common-

and differential-mode currents [81, pp. 1–4], [82, p. 460]. The most common example of a balanced transmission line is a twisted pair cable like those found in telephone cords or ethernet cables. Many antennas, such as dipoles and spirals, are balanced structures. The most common unbalanced transmission line is a coaxial transmission line used for cable TV and internet service.

The function of a balun is to suppress the common-mode currents while passing the differential-mode current between balanced and unbalanced transmission structures¹. Transitioning from an unbalanced to a balanced transmission line without a balun can cause common-mode currents; therefore, a balun not only suppresses but also does not create common-mode currents [82, p. 460]. Common-mode currents are unwanted because they cause significantly more radiation when compared to the same amount of differential-mode current [82, p. 506]. In a transmission system, this leads to loss and interference. In an antenna system, the radiation caused by the common-mode current can interfere with the desired radiated fields from the differential-mode, thereby altering the radiation pattern of the antenna.

To understand why common-mode currents are responsible for a larger total electric field, consider the currents on a two-wire transmission line. The total electric field is the sum of the electric field from each individual current. In the case of differential-mode currents, the electric fields are directed in opposite directions since the currents are oppositely directed. When added, the fields will mostly cancel—they do not cancel fully since the currents are not located in the same spot but are slightly offset. For common-mode currents, the electric fields are directed in the same direction and therefore produce a stronger field instead of canceling [82, pp. 346–349, §8.1].

¹A common argument for the use of coaxial transmission lines is that they do not radiate compared to an open system because the fields are contained within the outer conductor. This is true for coax with no common-mode currents. The differential-mode currents are on the inner conductor and the inside of the outer conductor. If no balun is used when connecting to a coax, even-mode currents can flow on the *outside* of the outer conductor. These are the fields that usually radiate from a coax and cause interference [82, p.460].

A secondary function of a balun is to match impedances on either side of the balun since the impedances of each transmission line are usually not equal. The combination of reducing even-mode currents and impedance matching helps to ensure that the maximum possible power may be delivered to a load. Baluns may be either narrowband or wideband. Examples of narrowband baluns are choke baluns and bazooka baluns. Wideband baluns include the Marchand and double-y baluns.

A balun used for this work should be wideband since we wish to characterize a material over a large frequency span. Interest in wideband devices, including baluns, has grown since the FCC opened the radio spectrum for ultra-wideband (UWB) emissions in 2002. UWB devices typically operate in the frequency range of 3.1 GHz–10.6 GHz, with other ranges set forth for specific radar and imaging systems. An UWB transmitter has a 10 dB fractional bandwidth of at least 0.20 or a bandwidth of at least 500 MHz [83, 84]. Researchers have looked to develop devices that cover this bandwidth and have continued to increase the operational bandwidth of baluns. Kim et al. reported a balun operating from 0.5 GHz to 110 GHz on a GaAs substrate [85].

While not achieving such a large bandwidth, double-y baluns can provide bandwidths that surpass the normal UWB frequency range [86]. A double-y balun is a planar structure consisting of two different types of transmission structures, e. g. a coplanar strip and a coplanar waveguide. Figure 10.1 illustrates the layout of the transmission structures in a double-y balun. The two structures are laid out end-to-end, along a common center line, on the same layer of a circuit board. Each line is forked into a shorted and an opened stub where the lines meet. This fork creates a “Y” shape and the abutment of the lines means these two “Y”s overlap. The overlap allows for coupling from one transmission structure to the other. Double-Y baluns typically provide wider bandwidths than Marchand baluns because the transmission line stubs used in a double-y are closer to ideal elements at higher frequencies with fewer parasitics [87]. The lower frequency limit of a double-y balun is determined by the length of the transition from the input to the “Y”s at the middle of the balun while the upper frequency limit is determined by

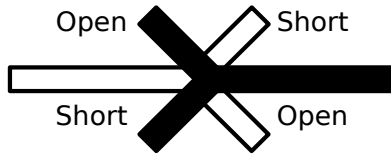


Figure 10.1: Illustration of the layout of transmission structures in a double-y balun.

how small the “Y”s of the balun can be made. A rule of thumb is to make the transition about a quarter of a wavelength at the lowest frequency and to make the stubs less than a quarter of a wavelength at the highest frequency.

Double-Y baluns have been investigated by various people including Trifunović and Jokanović who first published their work in 1991 [88]. Their work has looked at the creation of the baluns using different transmission structures including microstrip lines, coplanar waveguides, and slotlines as well as resonances of the structures, operational bandwidths, and bridging methods [86, 89–92]. Venkatesan has more recently studied the double-y balun design. His particular work closely examined a balun using unbalanced coplanar waveguides and balanced coplanar strips, both of which have impedance matching tapers [81, 93, 94]. In his dissertation [81], Venkatesan has a very good, modern discussion of baluns and the double-y balun in particular. Appendix G in this work contains excerpts from the author’s laboratory notebook covering the initial research and work on the balun design.

10.2 Design Overview

The double-y balun design can be used with various transmission line structures. Manufacturing capabilities and limitations dictated selection of the transmission structures for this dissertation. In-house milling by the Electrical and Computer Engineering (ECE) shop was selected as the manufacturing method due to better availability and turn around time compared to etching. A one-sided balun was desired because alignment errors between layers could occur when milling a double-sided board. To fit this requirement, a coplanar strip (CPS) and a finite-width

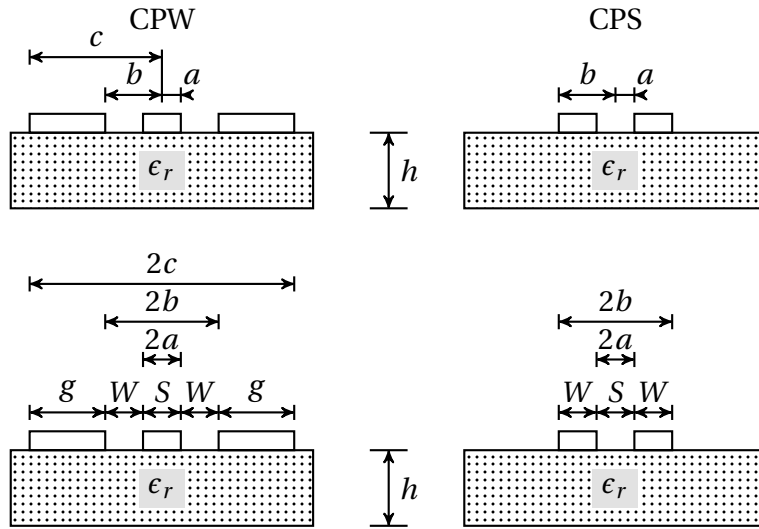


Figure 10.2: Schematic of CPW and CPS lines with common dimensions.

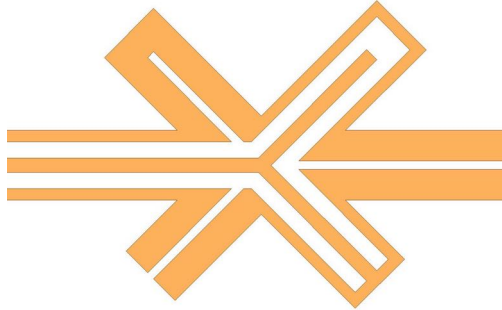


Figure 10.3: A CPW to CPS double-y balun.

ground-plane coplanar waveguide (CPW) were selected. A CPS is a balanced line to which a two-wire transmission line can be connected and the CPW is an unbalanced transmission line to which a SMA connector can be connected. Figure 10.2 is a diagram showing examples of CPW and CPS lines annotated with common notations for dimensions; Figure 10.3 shows a CPW-to-CPS double-y balun.

Caution

In order for the CPW to behave as desired, the two ground plane (traces) must be kept at the same potential. This is accomplished using air bridges which are essentially jumper wires that bridge the center conductor and connect the two ground planes. This ensures that the currents on each ground plane are matched and a proper change from unbalanced to balanced can occur. The use and discussion of air bridges is not covered in many of the references and instead they are usually mentioned in passing. Section 10.7 discusses air bridges more.

Note

The ground plane on either side of the center conductor is comparable in width to the center conductor. A true CPW has ground planes that are significantly larger than the center conductor. The CPW implemented here is called a finite-width-ground-plane coplanar waveguide; however, it is referred to as a CPW for brevity.

Thank you...

The balun was made on a single-sided, FR-4 board material as this was readily fabricated by ECE shop.

The ECE Shop usually mills circuit boards out of 60 mil-thick, FR-4 board with 1 oz/sq. ft copper (corresponds to a thickness of $34.1 \mu\text{m}$ (1.34 mil)) on both sides. FR-4 has a specified relative permittivity of $\epsilon_r = 4.4$ and a loss tangent of $\tan \delta = 0.02$; however, these values can vary from batch to batch and manufacturer to manufacturer. The minimum width of a trace for the ECE Shop milling process is 0.20 mm–0.25 mm (8 mil–10 mil) and the minimum width of a gap is 0.3 mm (12 mil). The shop notes that traces near this minimum width are easily lifted off the substrate, especially with the application of heat. Care should be exercised when soldering such traces. Alignment of the top and bottom traces is estimated to be around 10 mil due to the flipping of the board. Vias can be drilled by the shop, but they are not plated. Because of top-to-bottom mis-alignment and unplated vias, a single-sided balun design was sought for this work

and the double-y was a good match for this. The need for wire bonds was discovered after the balun design had been selected and some design work had been done.

If the balun is manufactured through a board house that can perform vias work, it may be worth while to investigate other types of balun, such as a microstrip-to-slotline or microstrip-to-CPW balun, that can improve bandwidth and/or lower losses. The *Encyclopedia of RF and Microwave Engineering* [87] offers summaries of different types. The work presented in [95–97] is worth reviewing as well.

The balun for this dissertation was designed to meet the following criteria:

- wideband
- easily fabricated,
- low cost, and
- durable.

This work required a balun with as large a bandwidth as possible and a low cutoff frequency. A cutoff frequency in the hundreds of megaHertz was desirable because the expected plasma frequency of the fire-induced plasma was between 500 MHz and 1 GHz. The upper frequency was determined to be at least 6 GHz in order to be able to use the full bandwidth of the HP 8753D network analyzer.

The following steps were needed to synthesize a design:

- Determine coplanar stripline (CPS) and coplanar waveguide (CPW) design equations.
- Program and verify CPS and CPW design equations.
- Program an optimization routine to match impedances of CPSs and CPWs given certain constraints.

10.3 CPS and CPW Design Equations

To design the CPS and CPW transmission structures used on the balun, the impedance was needed. The CPW needed to match a $50\ \Omega$ coaxial cable connector. The CPS needed to match the impedance of the two-wire transmission line. The impedance of the two-wire transmission line is calculated using the equations presented in Section 8.4. Both structures had to be transitioned to the same impedance at the center of the balun. The following equations were used to calculate the impedances and create the balun design. The equations presented here are from *Microstrip Lines and Slotlines*. There are three editions of this book at the time of writing. K. C. Gupta was an author of the 1979 [98] and 1996 [99] editions but not the third in 2013 [100]. Some equation numbers have changed between all three versions. Equations below are taken from the 2nd edition [99]. The basic dimensions used for calculations are denoted in the schematic in Figure 10.2.

10.3.1 Coplanar Strip

The impedance of a symmetric CPS with finite dielectric thickness is [99, (7.75)]

$$Z_{o,cps} = \frac{120\pi}{\sqrt{\epsilon_{re}^{cps}}} \frac{K(k_1)}{K'(k_1)}. \quad (10.1)$$

Here ϵ_{re}^{cps} is the effective relative-permittivity of a CPS with $h/b > 1$ given by [99, (7.17)]

$$\epsilon_{re}^{cps} = 1 + \frac{\epsilon_r - 1}{2} \frac{K(k_2)}{K'(k_2)} \frac{K'(k_1)}{K(k_1)}, \quad (10.2)$$

where k_1 is given by [99, (7.7)]

$$k_1 = \frac{a}{b} = \frac{S}{S + 2W} \quad (10.3)$$

(note that $a \neq S$ but $2a = S$, likewise $2b = S + 2W$), and k_2 is given by [99, (7.16)]

$$k_2 = \frac{\sinh(\pi a/2h)}{\sinh(\pi b/2h)}. \quad (10.4)$$

The parameter S is the gap between the strips, and W is the width of the strip (Figure 10.2). The functions $K(k)$ and $K'(k)$ are the complete elliptic integrals of the first kind and its complement, respectively,

$$K'(k) = K\left(\sqrt{1 - k^2}\right) = K(k'). \quad (10.5)$$

10.3.2 Coplanar Waveguide

The impedance of a CPW with a finite-width ground-plane is [99, (7.29)]

$$Z_{o,cpw} = \frac{30\pi}{\sqrt{\epsilon_{re}^{cpw}}} \frac{K'(k_3)}{K(k_3)}. \quad (10.6)$$

Here ϵ_{re}^{cpw} is the relative permittivity for a CPW given by [99, (7.28)]

$$\epsilon_{re}^{cpw} = 1 + \frac{\epsilon_r - 1}{2} \frac{K(k_4)}{K'(k_4)} \frac{K'(k_3)}{K(k_3)}, \quad (10.7)$$

where k_3 is given by [99, (7.23)]

$$k_3 = \frac{a}{b} \sqrt{\frac{1 - b^2/c^2}{1 - a^2/c^2}} \quad (10.8)$$

(note that $a \neq S$ but $2a = S$, likewise $2b = S + 2W$, and $2c = S + 2W + 2g$), and k_4 is given by [99, (7.27)]

$$k_4 = \frac{\sinh(\pi a/2h)}{\sinh(\pi b/2h)} \sqrt{\frac{1 - \sinh^2(\pi b/2h)/\sinh^2(\pi c/2h)}{1 - \sinh^2(\pi a/2h)/\sinh^2(\pi c/2h)}}. \quad (10.9)$$

The parameter S is the width of the center conductor, W is the width of the gap, g is the width of the ground strip (see Figure 10.2), and K and K' are the complete elliptic integrals of the first kind and its complement, respectively,

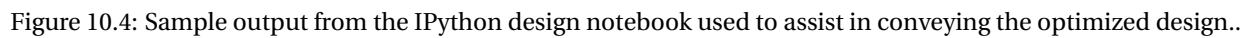
$$K'(k) = K\left(\sqrt{1 - k^2}\right) = K(k'). \quad (10.10)$$

10.4 Design Software Tools

An IPython notebook was used to design the double-y balun. It is reproduced in Appendix P². To aid in reading the output design, the notebook can display the design in a format similar to Figure 10.4 which uses the common notation defined in Figure 10.2.

As indicated in the notebook, the primary references used included the first and second editions of *Microstrip Lines and Slotlines* [98, 99], Jaikrishna Venkatesan's PhD dissertation [81], and *Coplanar Waveguide Circuits, Components, and Systems* [101]. Other important resources include the *Encyclopedia of RF and Microwave Engineering* [87] and the online calculators provided at http://www1.sphere.ne.jp/i-lab/ilab/index_e.htm [102]. Other material used in developing the balun may be found in [85, 86, 89, 91–93, 103–116].

² The notebook was run using SciPy 0.11.0 and NumPy 1.6.1. This is because certain minimization routines are not included in earlier versions of SciPy. There were problems in getting the notebook to run using later versions of SciPy and NumPy, so the intermediate (in terms of age) versions were used. There will probably be significantly newer versions by the time this script gets used again.



10.5 Balun Holder

During testing of the first balun designs, it was common for the copper traces to lift off of the board. This was caused by mechanical stress from the following items:

- Improper installation of SMA connectors

The SMA connectors used in the initial board designs had tabs that extended above and below the board. They are intended to provide mechanical support to the board as well as enhance coupling of the signal to the board. The tabs on the top of the connector were removed for the initial prototype because the boards were thicker than the space between the tabs. For later prototypes, properly sized connectors were purchased.

- Unsoldering of connectors

SMA connectors were limited in quantity when the first prototypes were fabricated. The connectors were unsoldered and moved from board to board. The heat of soldering and the torque inadvertently applied would sometimes cause the traces to lift off of the board.

- Cable stresses

Cables attached to the board mechanically stress the board, connectors, and traces to which the connectors are soldered. A SMA connector that properly fits the board should compensate for stresses normally observed in the laboratory without causing copper traces to lift off the board. Since initial prototypes used modified connectors, these cable stresses impacted the prototype traces.

- Two-wire transmission line

The two-wire transmission line that was attached to the circuit board was made of metal rods. These were often unsupported which caused stress on the traces and damaged some.

A holder was created to relieve these stresses. The final design also keeps the cables in place during calibration and elevates the circuit board away from other materials which could interfere with the fields, i. e. a metal bench top.

Furthermore, the holder helped with the spacing of the two-wire transmission line to ensure the impedance matched the design impedance. A jig was used to properly space the rods when soldering them to the board. Because of the lengths of the rods, however, the rods may flex and the spacing can change away from the board after the rods are soldered and the jig removed. The holder ensures the proper spacing near the board for a better transition.

Figures 10.5 through 10.10 are dimensional drawings of the holder. Figure 7.23 shows pictures of the holder. The holder was designed to allow for changes in position and size. Various lengths, widths, and thicknesses of circuit board are accommodated by the adjustable clamp. The elevation of the circuit board can be changed to allow for the two-wire transmission line to be properly aligned. A cable clamp adjust to keep the cables of various diameters in-line with the board as well as keeping the cable in the same place for calibrations. A piece of Plexiglas was bent to create the base and the side of the holder. Holes for the standoffs and two-wire transmission line were drilled both before and after bending. If the manufacturer can control the precise location and radius of the bend, then the holes for the two-wire transmission line can be properly located and drilled before bending. This makes drilling significantly easier. When the holder was used, mechanical stresses were reduced and measurements were easier to perform compared to experiments that did not use the holder.

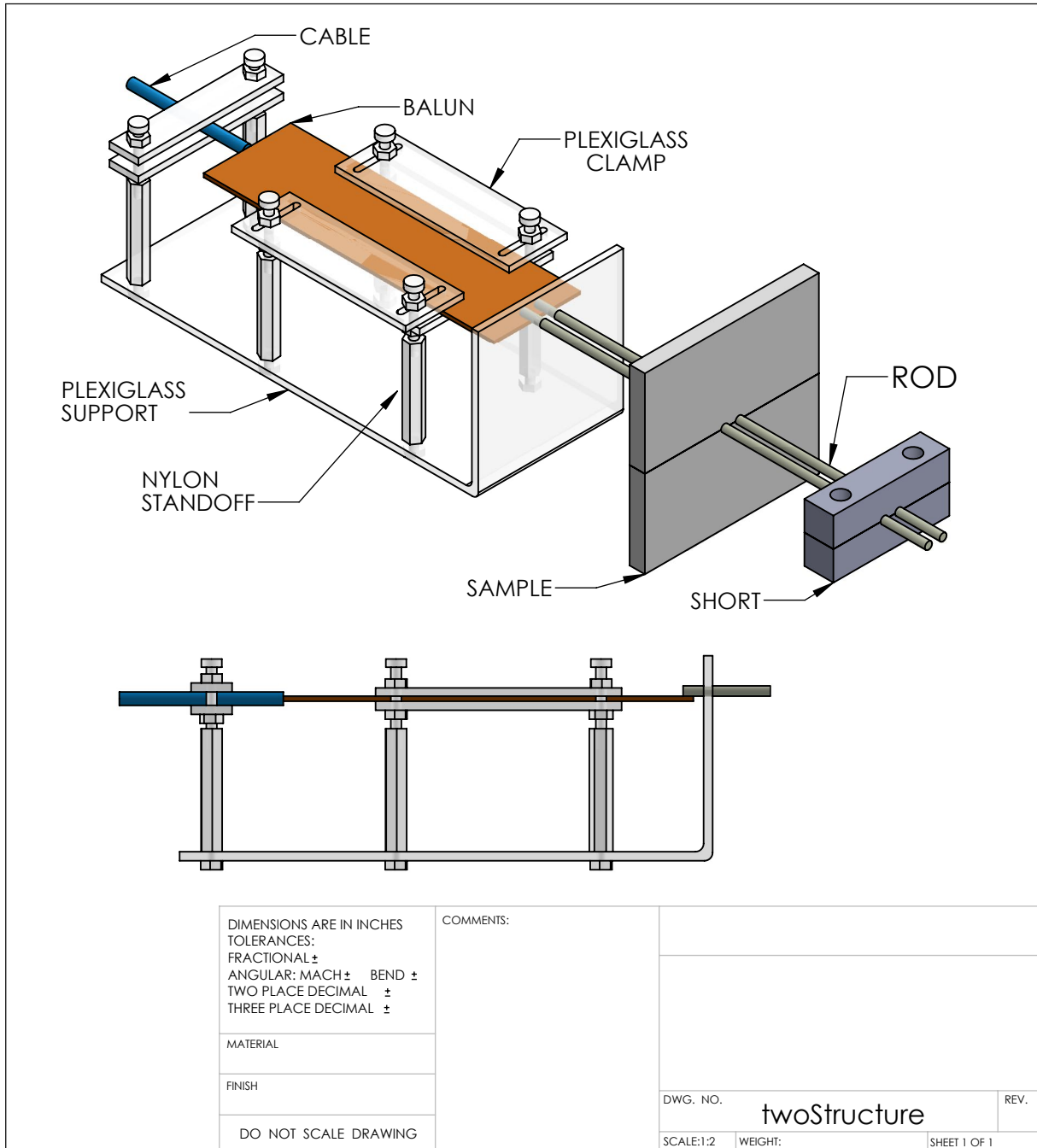


Figure 10.5: Assembly drawing for the balun support structure.

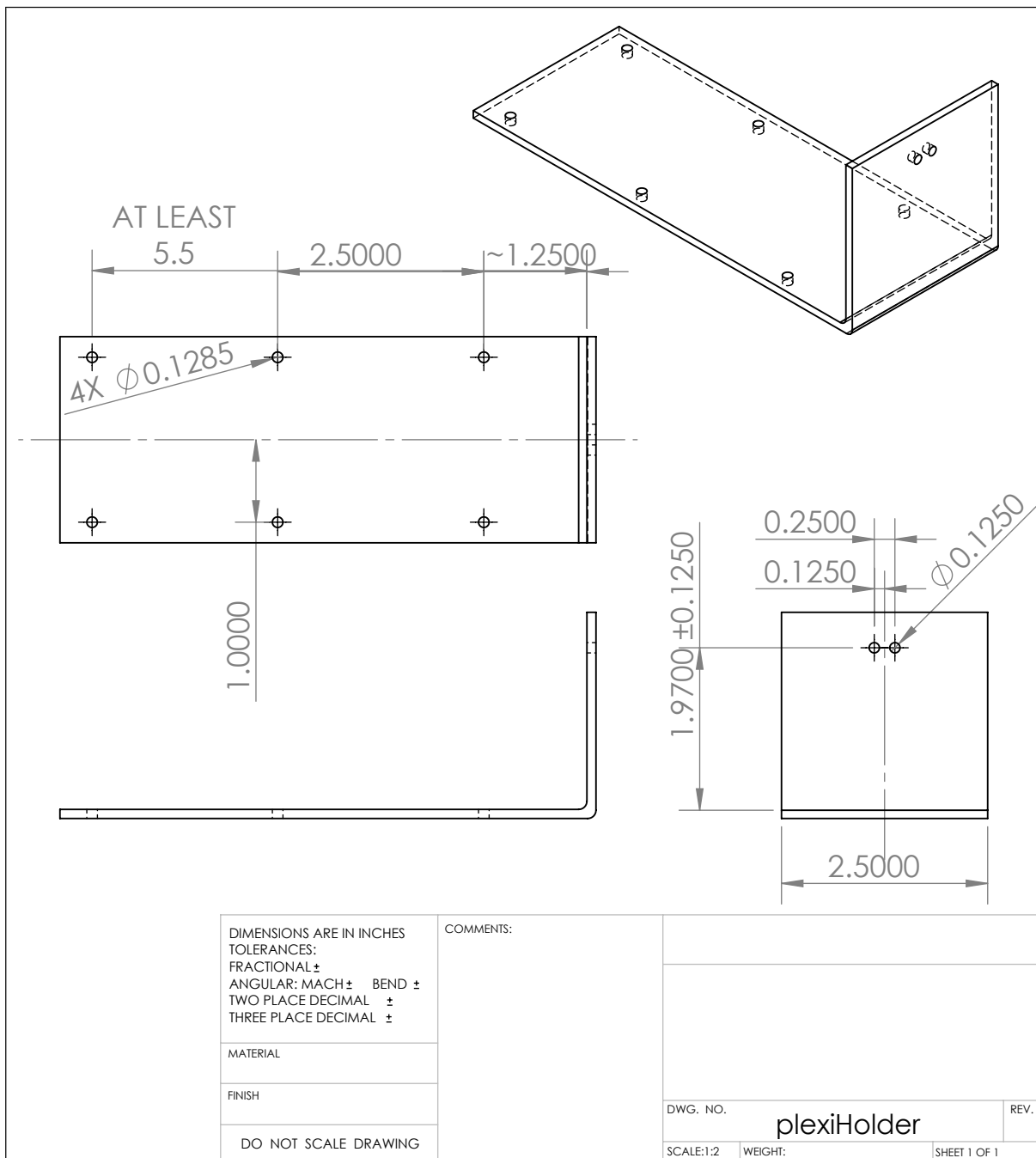


Figure 10.6: Drawing for the main Plexiglas support structure.

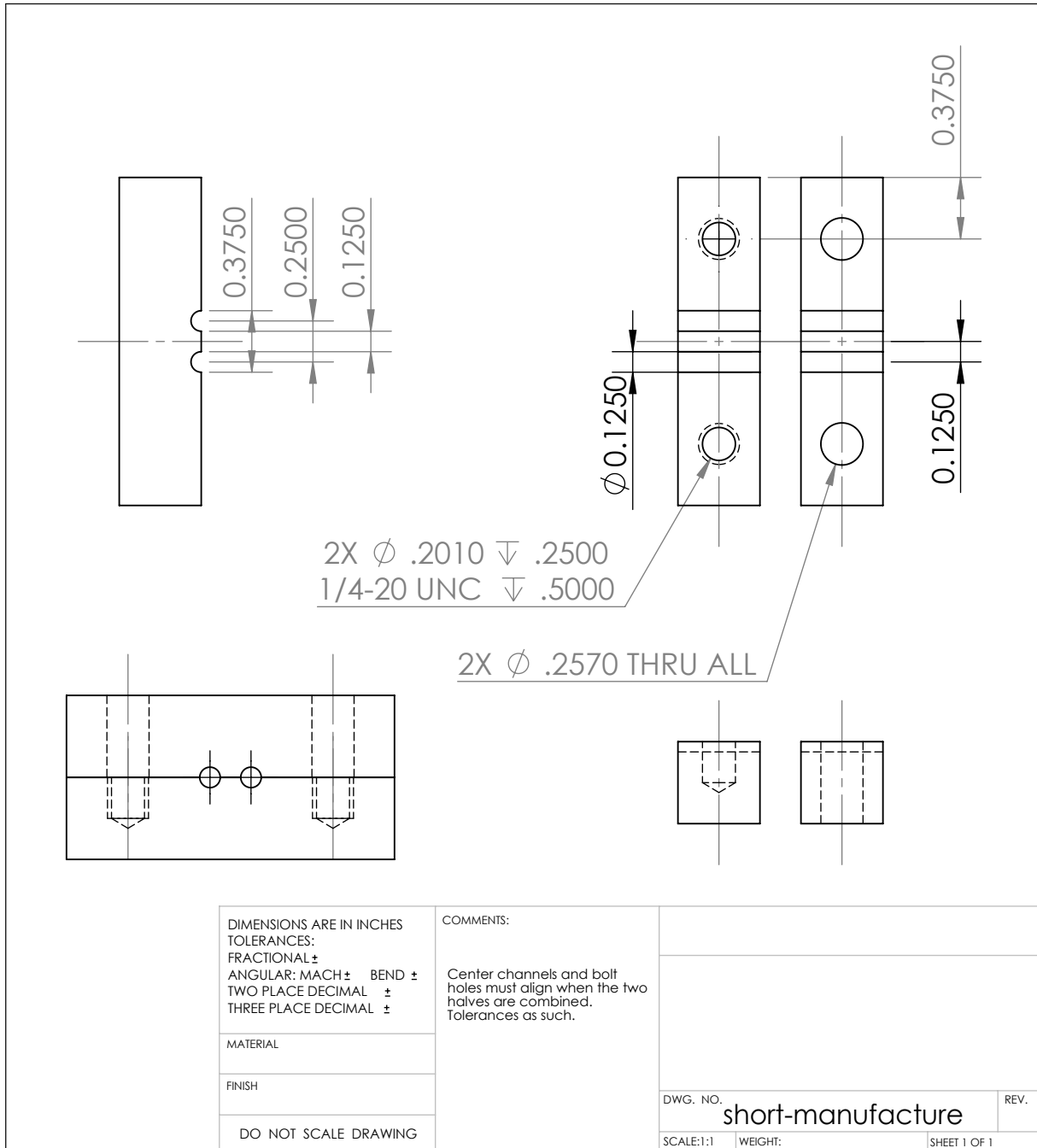


Figure 10.7: Drawing for manufacturing a shorting plate.

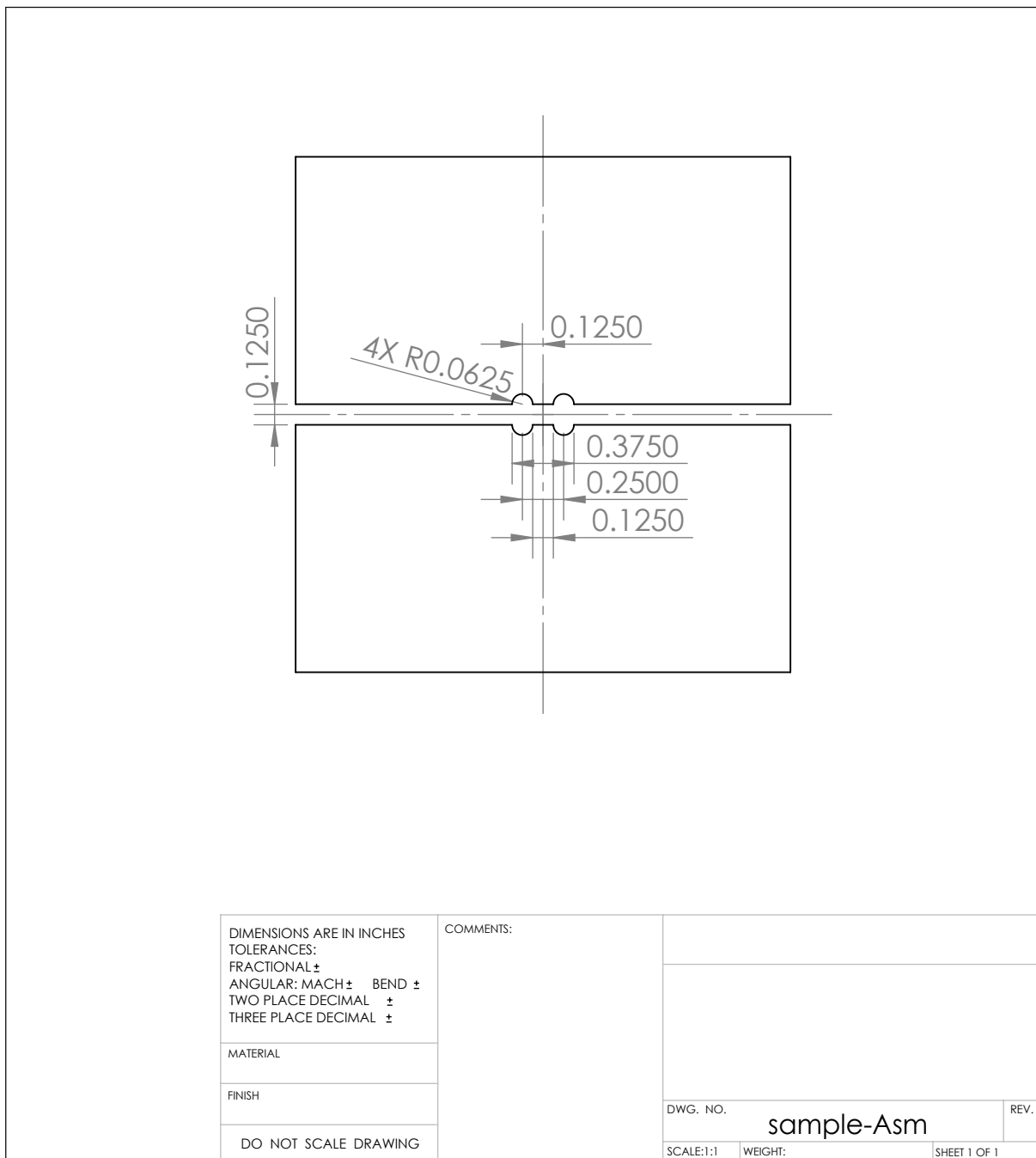


Figure 10.8: Drawing showing critical dimensions for samples.

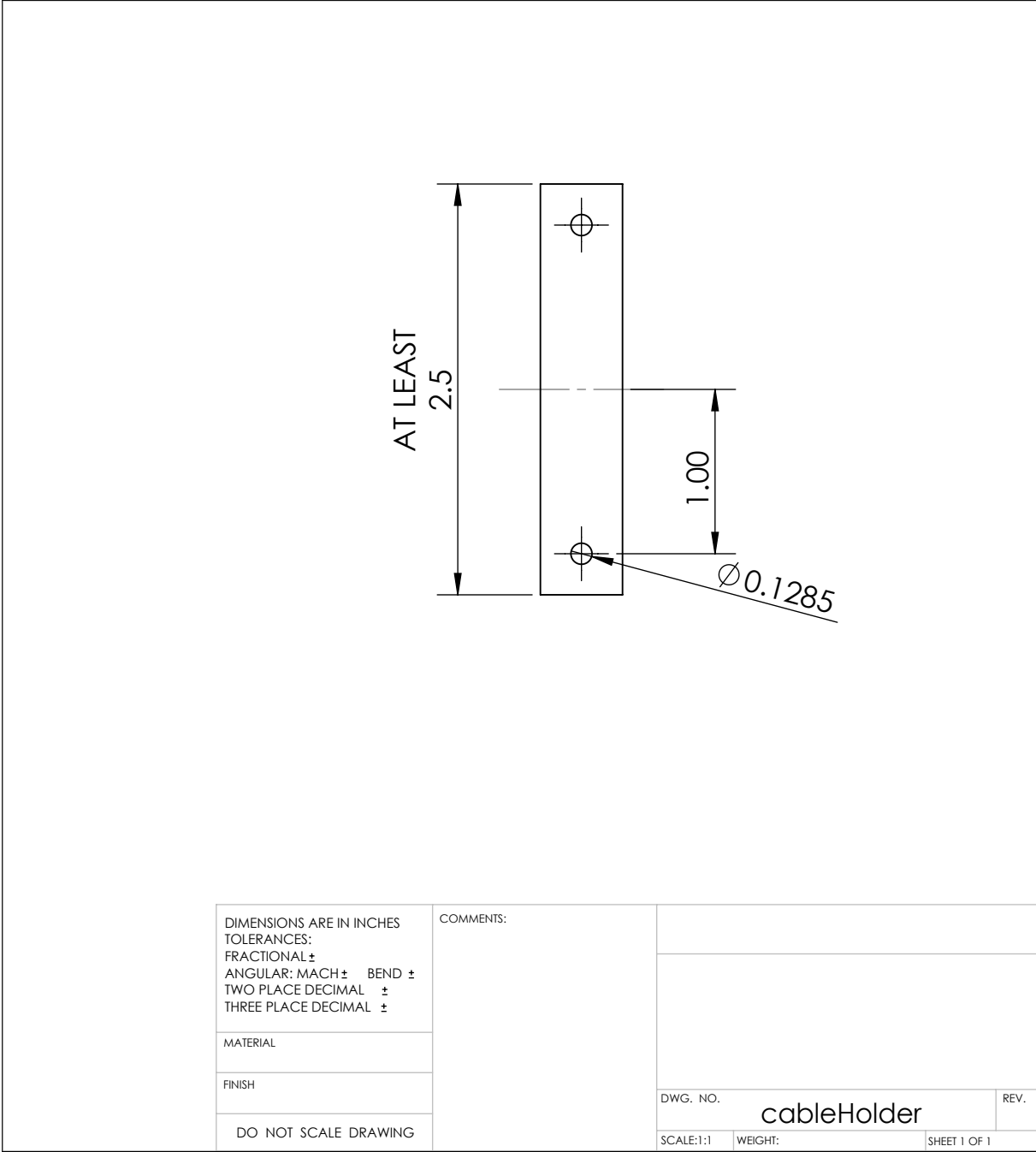


Figure 10.9: Drawings for plastic pieces that clamp the cable when it first enters the holder.

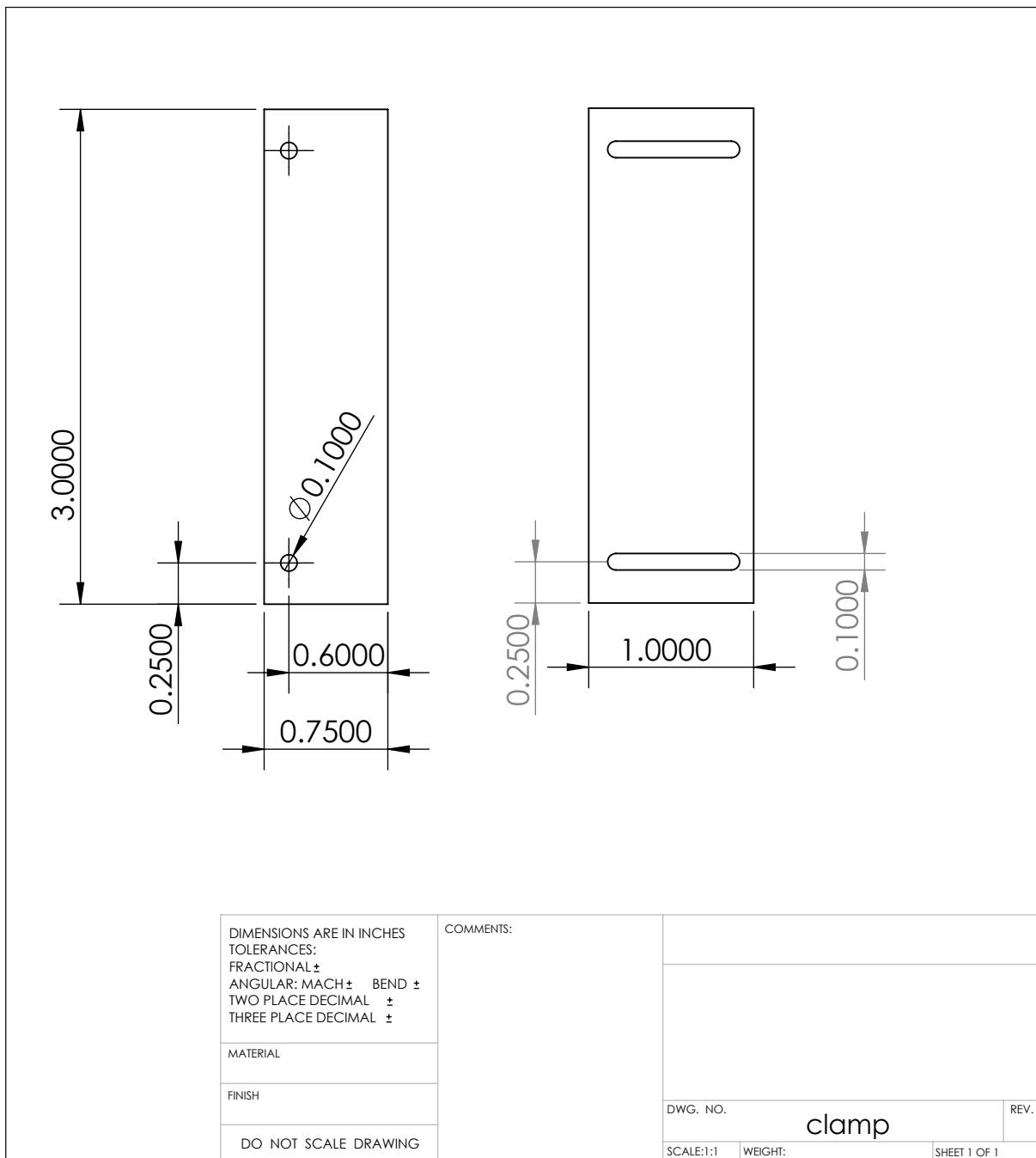


Figure 10.10: Drawing for the pieces that clamp the circuit board.

10.6 High-Temperature Modifications

10.6.1 Design Modifications

The original motivation for the balun and two-wire transmission line were for bench-top flame experiments. The two-wire transmission line would be placed above a fuel source so that the burning flame would burn between and around the two wires, allowing for material measurements to be made. The materials and design of the above prototype needed to be modified to withstand the high temperatures of a flame.

A piece of 1/4 in thick Garolite was purchased from McMaster-Carr (No. 8557K232 Flame-Retardant Garolite (G-10/FR4), 1/4" Thick, 2" Width, 2' Length). Garolite, also called FR-4, was selected because it is rigid, non-metallic, easily machined, and can withstand the expected temperatures.

Thank you...

Roxanne Peacock took care of this order and all of the other orders for this dissertation!

Prototype baluns and initial experiments were carried out using copper or steel rods while tungsten was selected for fire experiments. A short literature search found that plating the tungsten with copper is the easiest way to solder to a tungsten rod [117–119]. Chackett *et al.* provide the most complete instructions [117].

First the tungsten rod should be cleaned. Chackett *et al.* suggest placing the tungsten into a sodium hydroxide solution ("5% caustic soda solution [117]") and applying a voltage of 12 V and current of 1 A for a few minutes. The tungsten serves as the anode and the cathode should be nickel. This is then further electrolytically washed in nitric acid for a few minutes with the polarization switched occasionally. After cleaning, copper is electro-deposited for about 10 minutes from copper sulfate using 2 V and 10–20 mA/cm². Chackett *et al.* suggest a copper sulfate concentrate of 10 g CuSO₄ per 100 ml solution. The times and currents used are not necessarily optimal as noted by Chackett et al. .

Thank you...

Brian Wright assisted me in plating the ends of 1/8 in diameter by 12 in long tungsten welding rods obtained from Diamond Ground Products (part number PT-1/8-12). A Caswell copper electroplating kit was used that the shop already had.

The standard tungsten welding rod from Diamond Ground Products is 7 in long and has the ends marked with green paint. The 1/8 in diameter rod has a tolerance of ± 0.003 in while tighter tolerances may be special ordered. A company representative in April 2014 said it was not uncommon for them to have 12 in and longer length stock available, possibly up to 48 in. Standard quality electrodes come from Chinese manufactures while Diamond Ground Products' premium electrodes are from a German supplier. The green paint is used to indicate the type of electrode. Diamond Ground Products is able supply electrodes with or without the paint; the rods used for this work were un-painted.

After plating, Chackett et al. suggest testing the copper by rubbing it with one's finger. In our case, the copper remained on the tungsten rod when rubbed; however, the copper came off when scratched with a fingernail or other sharp object. After being soldered to the circuit board, the copper was more firmly affixed to the solder and copper trace than to the tungsten rod. Because of the mechanical advantage given by the long rod, the plating would be removed if the rod was pivoted away from the board. This would be a common issue in a laboratory setup because the sample causes a downward force at the end of the two wires which would lift them away from the board—an example of this is seen in Figure 10.11 for a balun with copper rods. The plating would hold the rod, however, when the rod was rotated about its center axis. Soldering was easily accomplished and behaved like soldering copper to copper as would be expected. A possible way to improve the adhesion would be to solder (actually just tin) the tungsten with copper and then solder the copper to the circuit board. Petrunin and Grzhimalkii used a soldering temperature of 1120°C [119] to solder tungsten using copper. Plating was used here because of resource availability.

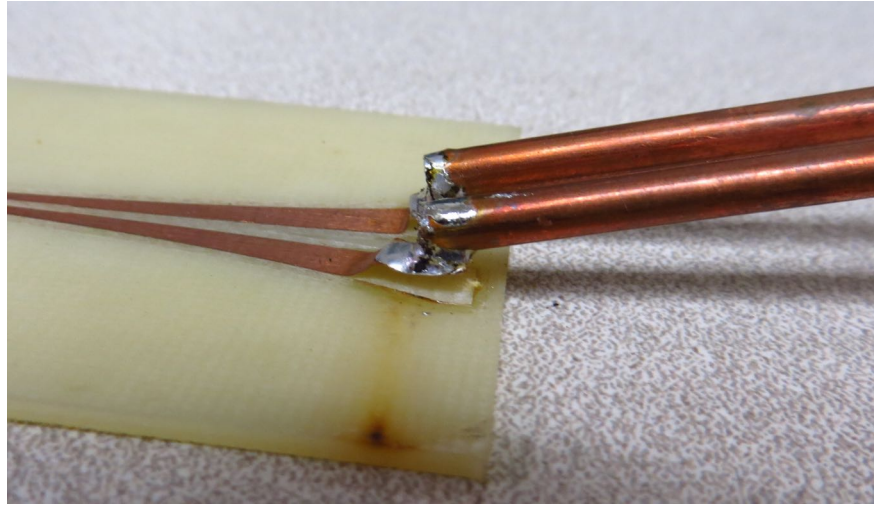


Figure 10.11: An example of the metal rods lifting the traces off of the balun.

10.6.2 Heat Transfer Analysis

There was also concern that the solder between the wires and the balun could melt if heat from the flame traveled down the wire. We can treat the wire as a fin designed to dissipate heat to the surrounding environment in order to find the temperature at the solder junction. A good, introductory reference to fin design is Section 4.5 of *A Heat Transfer Textbook* by Lienhard and Lienhard [120] which is available for free online as part of the MIT Open Courseware Intermediate Heat and Mass Transfer class [121]. Appendix Q is an IPython notebook used to perform the calculations. The temperature of the wire at the tip was estimated to give a maximum temperature that the solder junction could reach. There are various assumptions and limits to this estimate; however, these all push the result to the high side.

I assumed that the wire was 2000°C at the point of the flame that was placed halfway down the length of wire, and that the temperature of the surrounding room was 25°C . The first calculations were done for wires instead of rods because the initial two-wire transmission line design was to use wires. A 45% copper and 55% tungsten, 20 AWG wire with a thermal conductivity of $2.4 \text{ W}/(\text{cm } ^{\circ}\text{C})$ was used. A heat transfer coefficient for air of $20 \text{ W}/(\text{m}^2 \text{ } ^{\circ}\text{C})$ was used. The

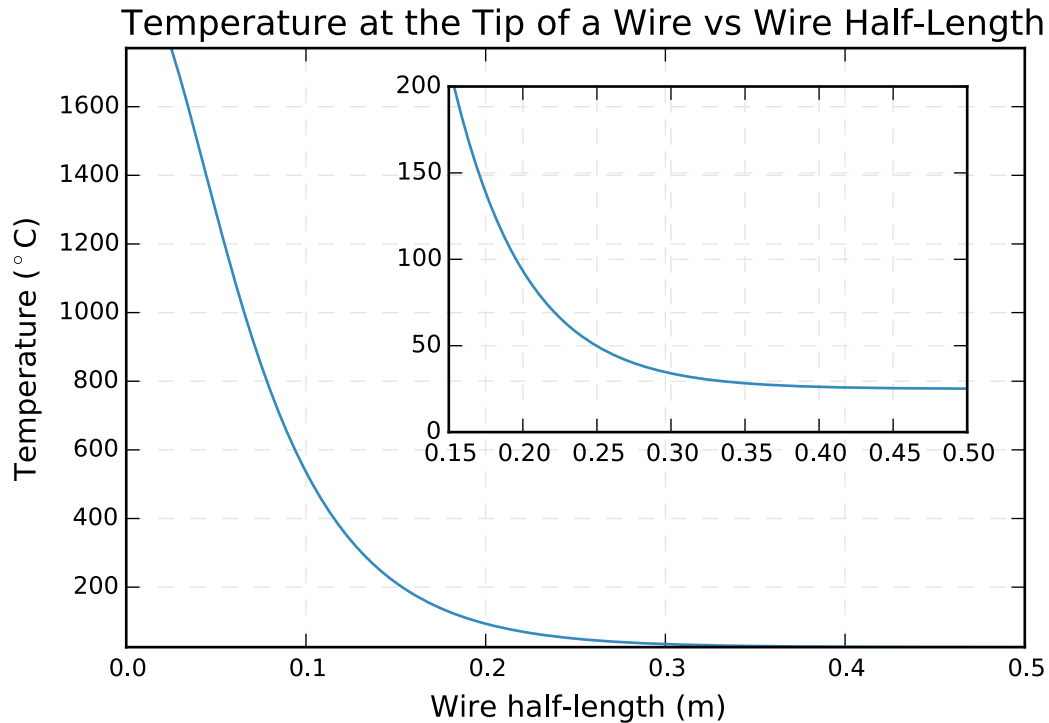


Figure 10.12: Temperature at the tip of a 20 AWG, copper/tungsten wire versus the distance from the flame to the tip.

temperature at the tip for this long, thin wire was found to be almost 25°C. Figure 10.12 shows the tip temperature versus wire half-length (distance from flame to tip).

We can see that for this gauge wire, the solder junction would reach an acceptable level very quickly. Solder usually melts somewhere below, but around, 200°C. We see that the tip temperature reaches this point for a 0.3 m wire and reaches 100°C for a length of about 0.4 m. If a shorter length transmission system is desired, a solder with a higher melting point could be used.

The implemented calculations rely on approximations that can be made for $mL \geq 5$. This condition does not hold for the tungsten welding rods obtained. The calculations should be re-written to use the exact form of the equations instead of approximations and then the problem re-analyzed for the correct sized rods.

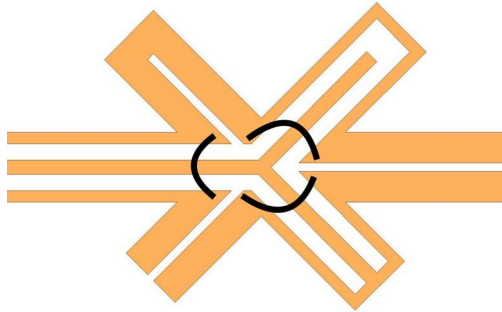


Figure 10.13: Positioning of the air bridges (black lines) at the center of the balun.

10.7 Affects of Air Bridges

As noted earlier, air bridges are important to ensure the correct electrical-current behavior on the balun. This greatly affects the performance of the balun with regards to suppressing common-mode currents and reducing radiation.

These air bridges can be small jumper wires, wire bonds, ribbon bonds, or more significant metal connections. It is especially important to use air bridges where the two lines come together at the center of the balun. The jumpers should be as close to the gap as possible since this is where the fields are concentrated. Figure 10.13 shows the positioning of the air bridges at the center of the balun.

Air bridges were implemented using two different methods. The first was to drill thru-holes as close to the outside edge of the ground planes as possible. While the jumpers should be close to the center edge of the ground plane, the holes were drilled on the outside so as not to damage the traces. A 30 AWG wire was passed through the holes and across the back side of the board. The wire was soldered to the ground plane with the solder normally wicking across the entire width of the ground plane.

The preferred air-bridge method is to use wire bonds. Notes from this procedure including instrument settings and model number appear on pages 78 and 79 of the author's laboratory notebook number 00011 in Appendix G .

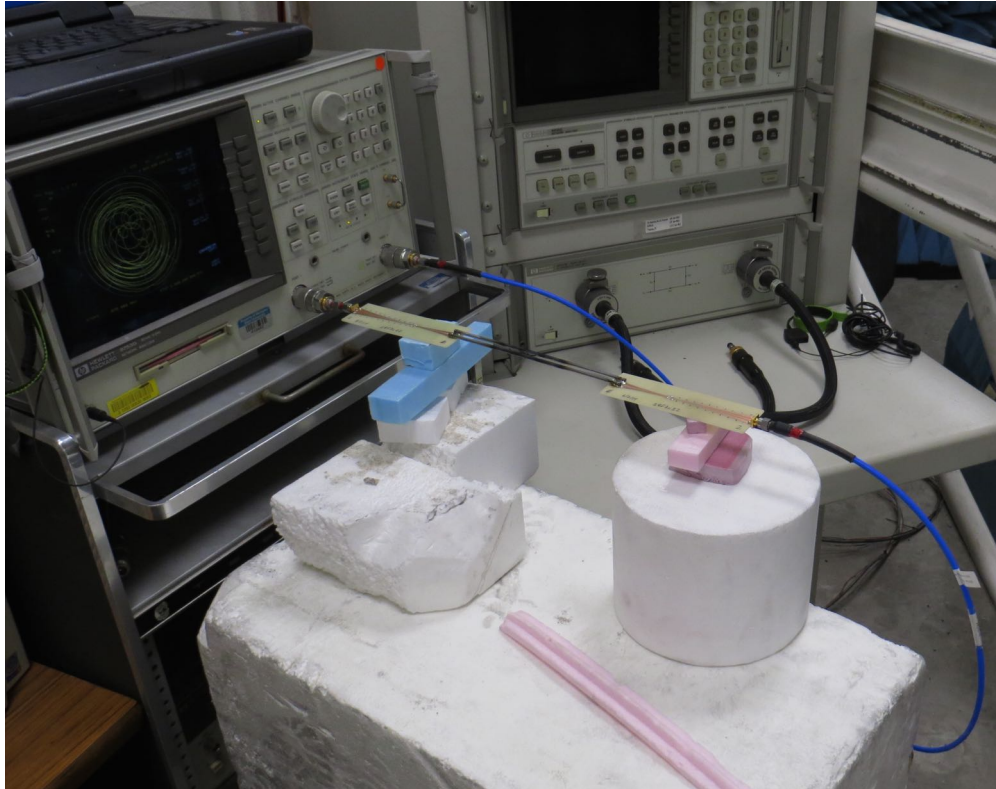


Figure 10.14: Experimental setup similar to that used for measuring the effectiveness of air bridges. *The laptop controlling the measurement is partially visible at the top-left. Below the laptop is the HP 8753D VNA that is performing the measurements. One balun is directly attached to port 1 of the VNA while port 2 is connected via a short cable to the other balun. The balun system is supported by foam blocks. For the measurements presented in this section, only the balun on the right (port 2) was supported.*

Thank you...

Rafmag Cabrera and Dr. Nelson Sepúlveda assisted me in placing these wire bonds.

10.7.1 Full Two-wire transmission line System

To evaluate the performance and demonstrate the necessity of the air bridges, measurements were taken before, during, and after the air bridges were placed on the balun for many of the boards. These measurements could not be done for the baluns with wire bonds because the network analyzer and wire bonding machine were in different buildings. An example measurement setup is shown in Figure 10.14. The measurements of one system that consisted of

two baluns connected by a steel, two-wire transmission line are presented in this section. Figure 10.15 shows the balun as it was being measured. The system measurements are shown in Figures 10.17 through 10.22. The SMA connectors were soldered on to the boards first and the two-wire transmission line connected between the baluns. The full two-port S-parameters of the system were then measured (Figure 10.15a and Figure 10.17). Next, the air bridges near the center “Y”s were install and the system re-measured (Figure 10.18). The remaining air bridges were then added along the length of the CPW’s (Figure 10.15b, Figure 10.15c, Figure10.19). No specific information about the air bridge spacing was found in the previously referenced literature so the air bridges were placed approximately 250 mil apart for a total of ten air bridges along the taper. Finally the power balance of the system is shown in Figure 10.22 when no air bridges, only “Y”s, and all bridges were installed.



(a) Measuring with no air bridges.

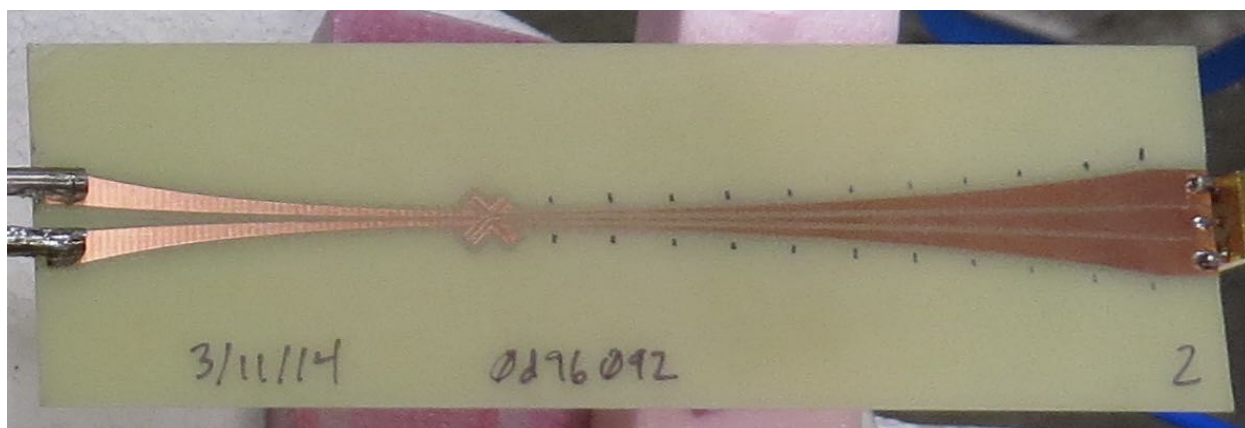


(b) Measuring with all air bridges places.

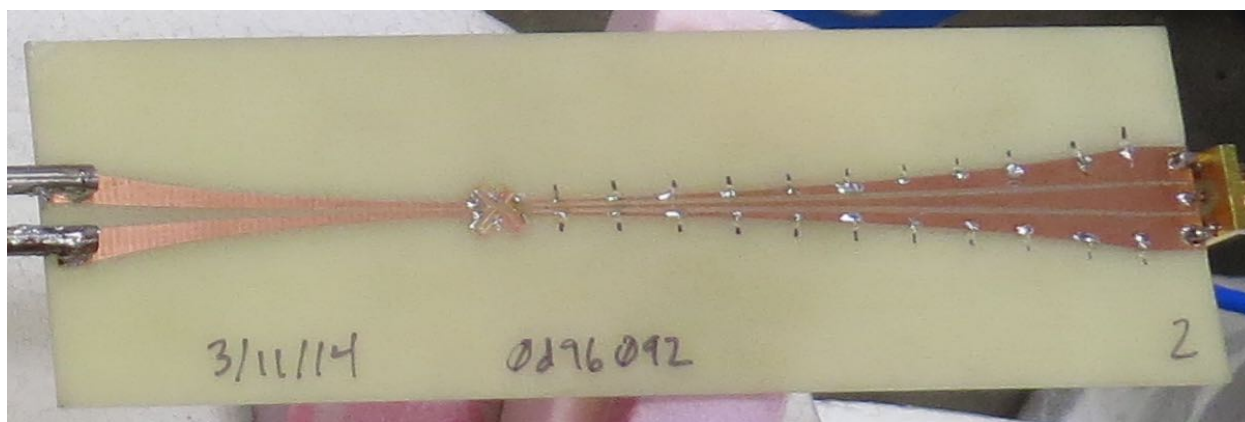


(c) View of the air bridges from the bottom of the balun.

Figure 10.15: Measurement setup to test the air bridges.



(a) Balun with no air bridges.



(b) Balun with all air bridges installed.



(c) Bottom view of all air bridges installed

Figure 10.16: Zoomed-in view of the right balun from Figure 10.15.

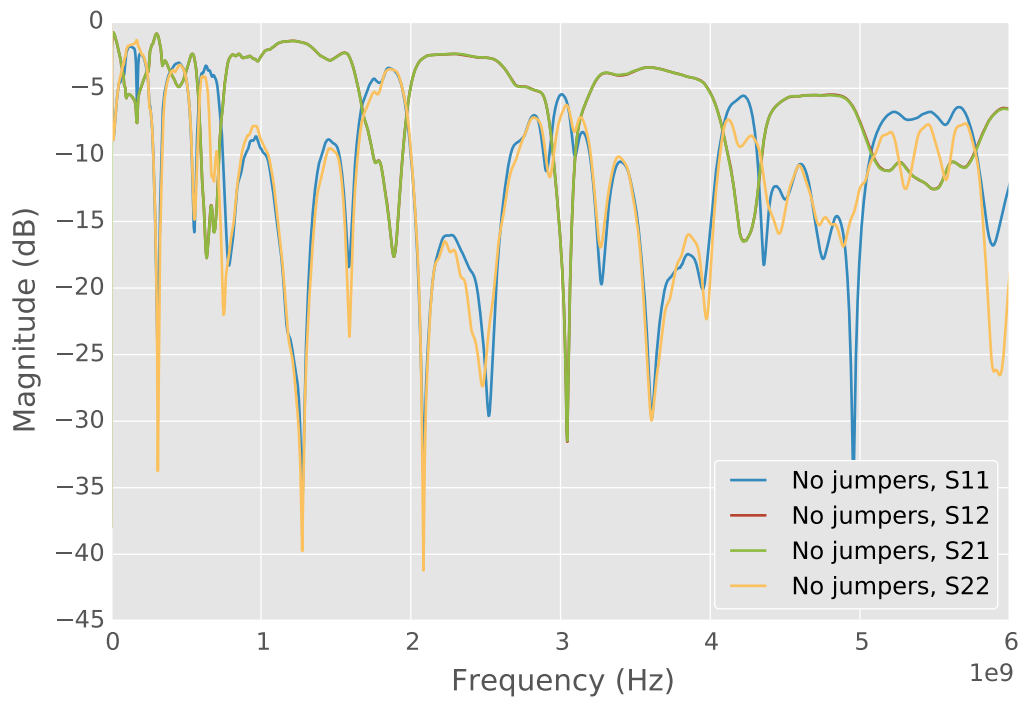


Figure 10.17: Two-wire transmission line system S-parameters with no air bridges installed. *No curve for S_{12} (red) is visible because S_{21} (green) covers it.*

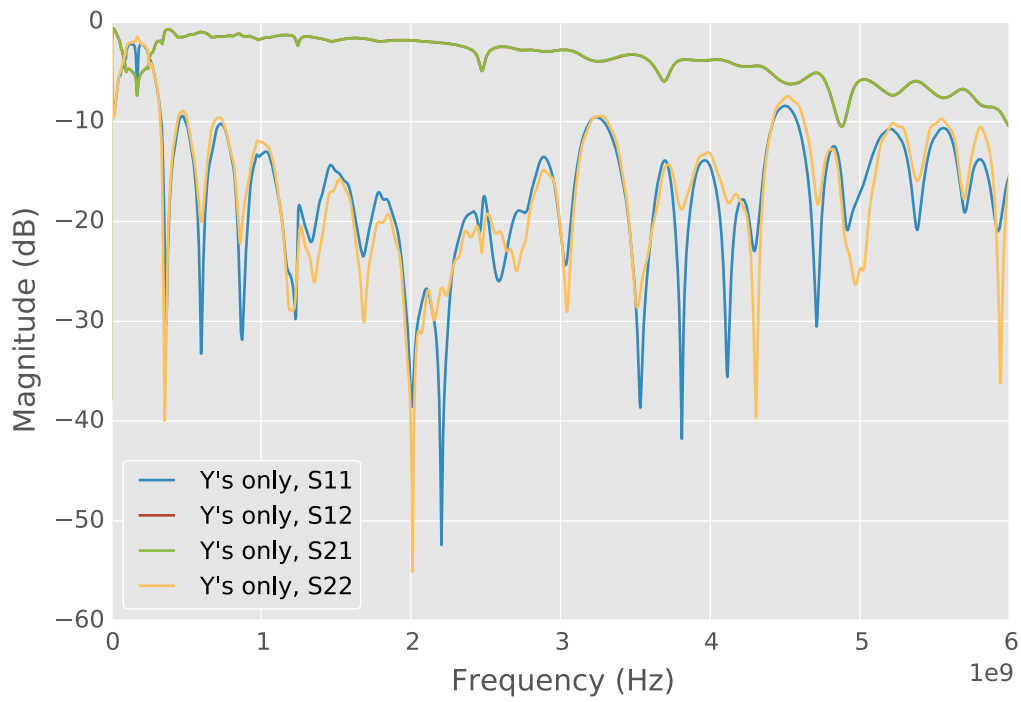


Figure 10.18: Two-wire transmission line system S-parameters with air bridges installed only at the “Y”s. *No curve for S_{12} (red) is visible because S_{21} (green) covers it.*

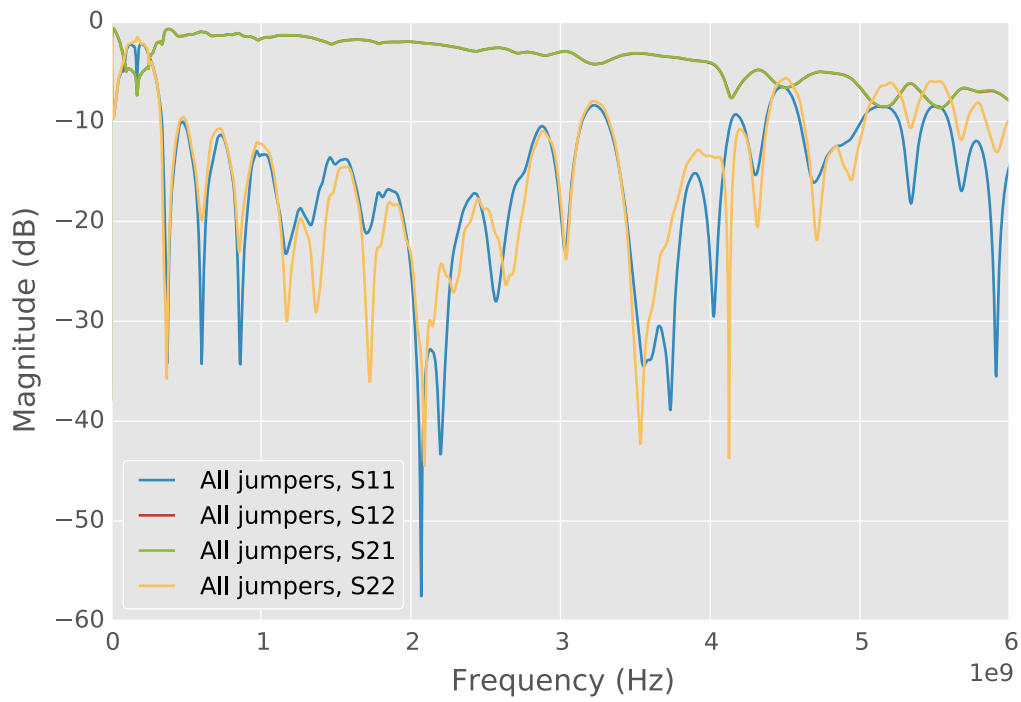


Figure 10.19: Two-wire transmission line system S-parameters with all air bridges installed. *No curve for S_{12} (red) is visible because S_{21} (green) covers it.*

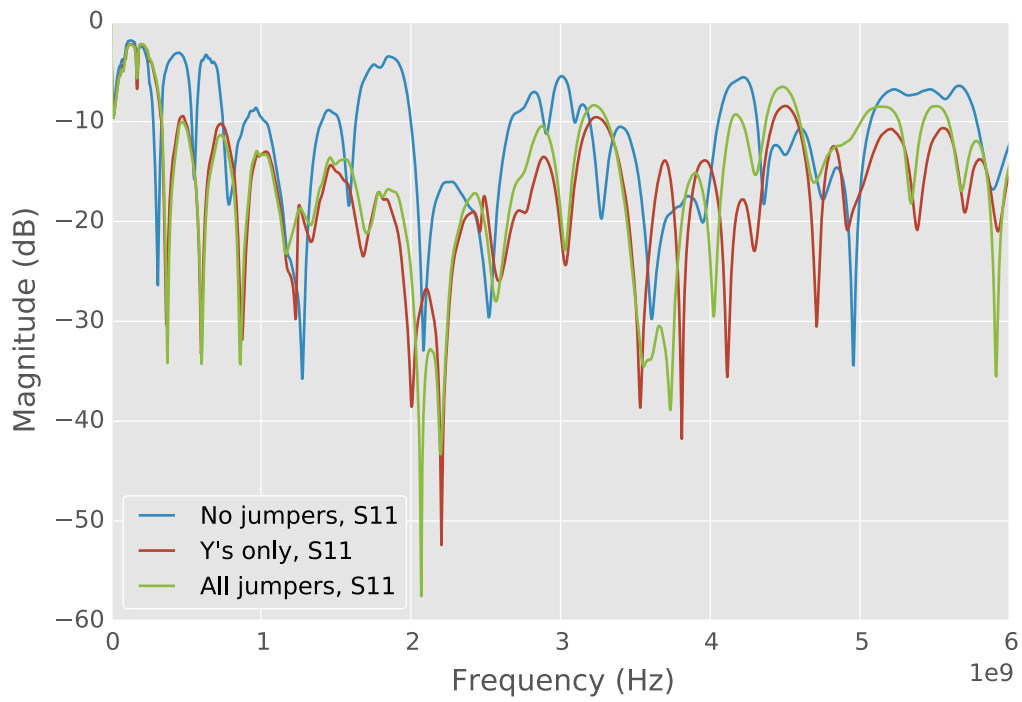


Figure 10.20: Reflection measurement (S_{11}) of a two-wire transmission line system with various air bridges installed.

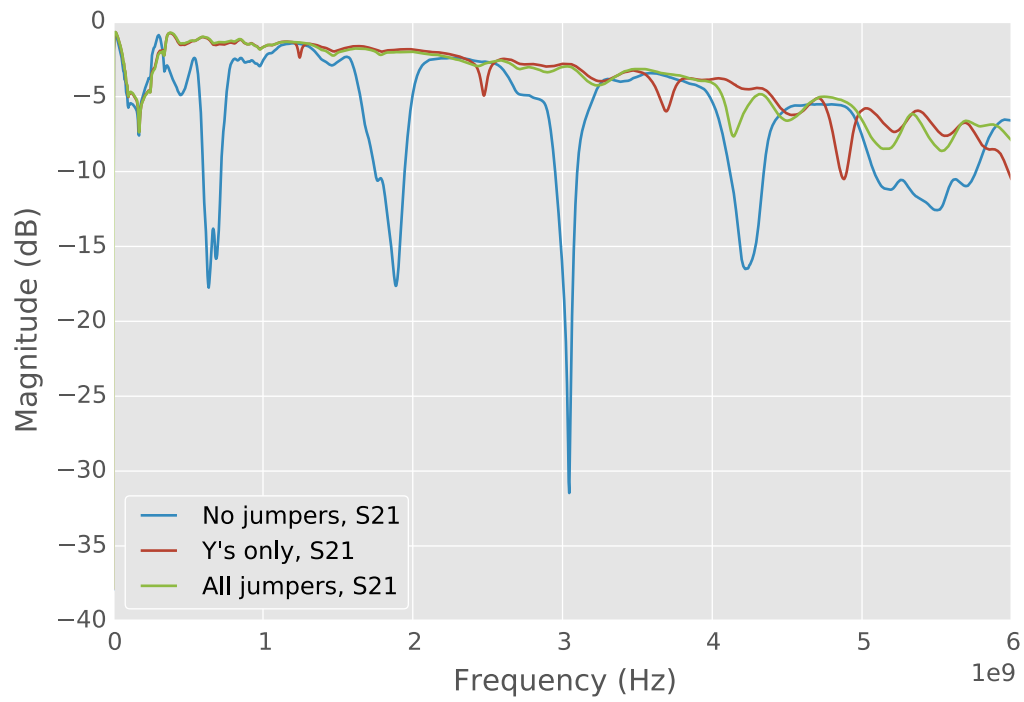


Figure 10.21: Transmission measurement (S_{21}) of a two-wire transmission line system with various air bridges installed.

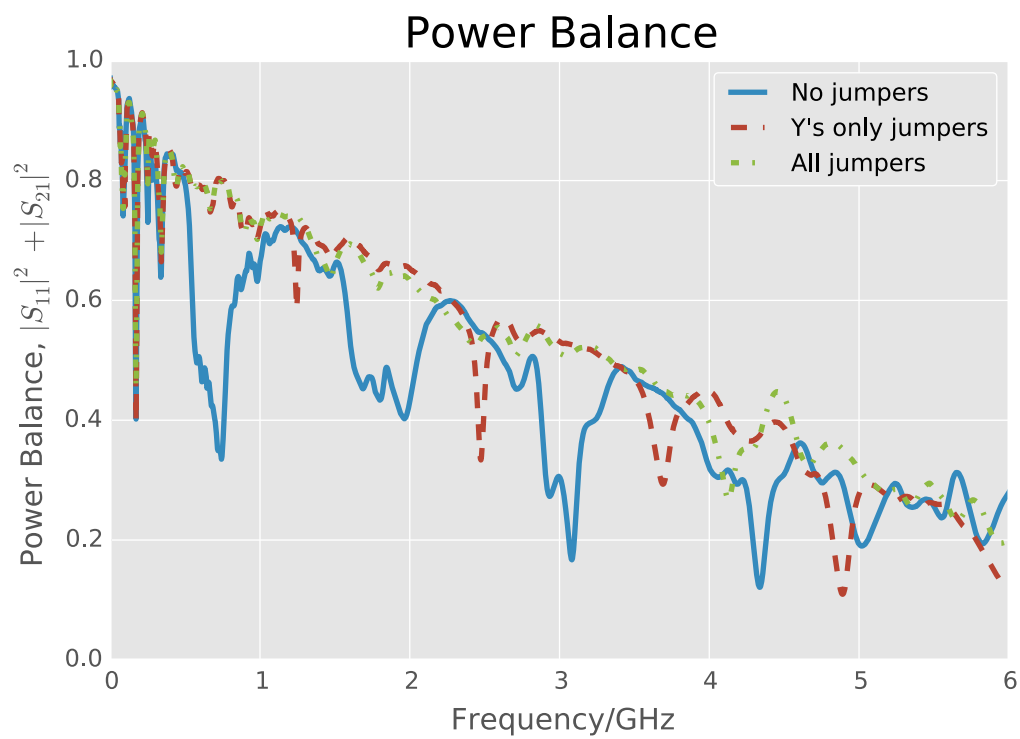


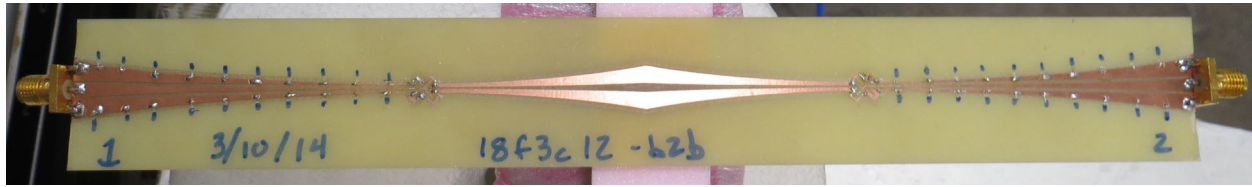
Figure 10.22: Power balance for a two-wire transmission line system with various air bridges installed. *Power losses increase as the power balance decreases towards zero.*

We see that system performance is improved when air bridges are installed, even if only at the “Y”s. First, consider Figure 10.22. A power balance equal to one means that all power sent out of the VNA is returned to it through either port. As the power balance decreases towards zero, more and more power is lost somewhere in the system. For the current system design, power loss is most likely due to radiation. Ohmic losses are likely present because of the two-wire transmission line being made of steel in these measurements; however, the overall behavior of the power balance suggests radiation as the main loss factor. For example, we see areas that are very lossy, e. g. around 3 GHz, where the power loss decrease as air bridges are installed. This suggests that the air bridges are altering the currents and helping to reduce common mode currents and thereby radiation. We note from Figure 10.22 that the first installed air bridges create new or shift existing areas of high loss. These areas, however, are more narrow-banded than when no air bridges were installed. Once all of the air bridges are installed, these areas of loss are smoothed out. We see a fairly linear power loss now that increases (downward slope) with frequency. This suggests that the two-wire transmission line itself is radiating combined with some amount of ohmic losses.

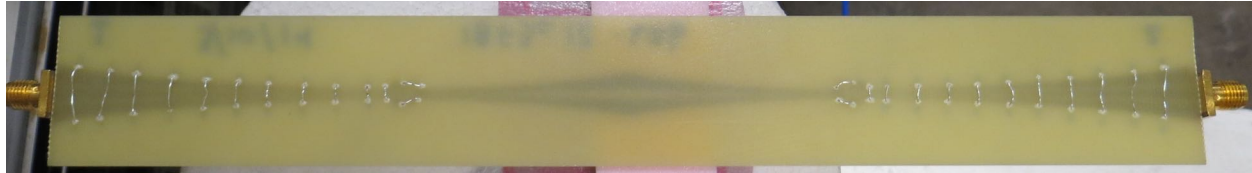
The same analysis can be made using either Figure 10.20 or 10.21. In the case of S_{11} , less power is reflected back to port 1 as the air bridges are installed. This means that more power is transferred into the balun system. The change in S_{21} shows that more power makes it through the balun system as air bridges are installed.

10.7.2 Back-to-Back Balun

In addition to the two-wire transmission line system measured in the previous section, two baluns were manufactured back-to-back as one unit with the CPS traces connected as shown in Figure 10.23. This removes the two-wire transmission line from the system and only measures the balun performance. As in the last section, the balun was measured before any air bridges were installed, when only the “Y”s were installed, and after all air bridges were installed. Air



(a) Front side of the back-to-back balun.



(b) Back side of the back-to-back balun.

Figure 10.23: Back-to-back balun with all air bridges installed.

bridges were installed using the same procedure as the last section. Figures 10.24 through 10.29 show the results of these measurements. We again see that the air bridges improve system performance.

Figure 10.30 shows the power balance for the full two-wire transmission line system measured in the last section and the back-to-back balun of this section. Across almost the entire frequency band the back-to-back balun has less loss than the two-wire transmission line system. This suggests that the actual transmission lines contribute some losses, presumably through radiation and ohmic losses. Only one measurement of each device was taken, therefore, additional measurements would help to determine more accurately how the losses of the devices compare.

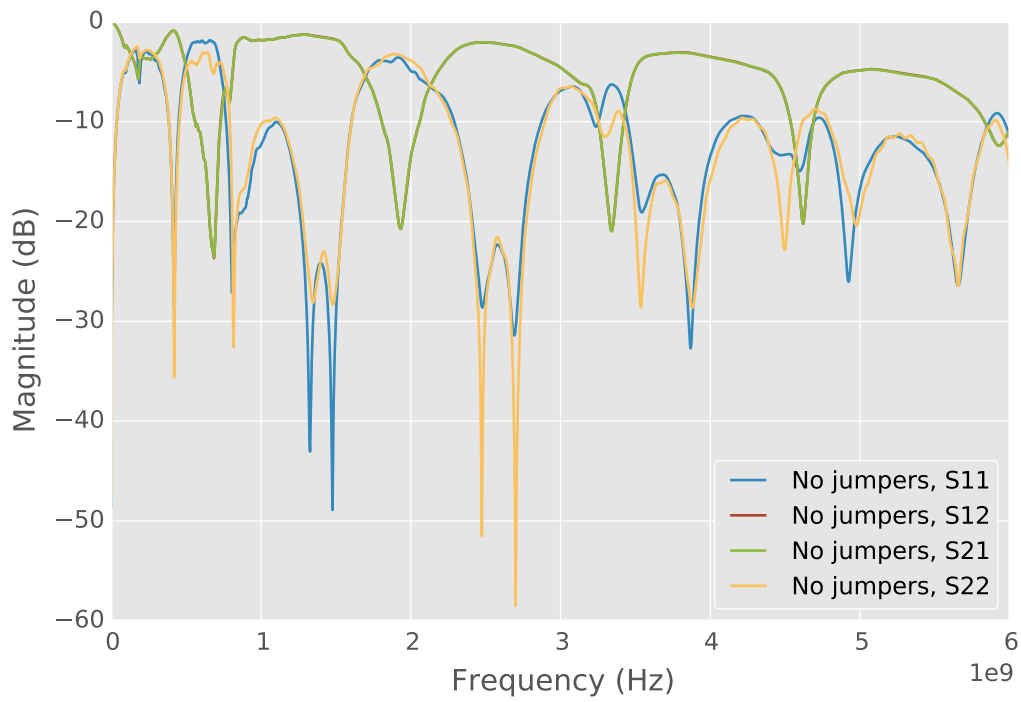


Figure 10.24: Back-to-back balun S-parameters with no air bridges installed. *No curve for S_{12} (red) is visible because S_{21} (green) covers it.*

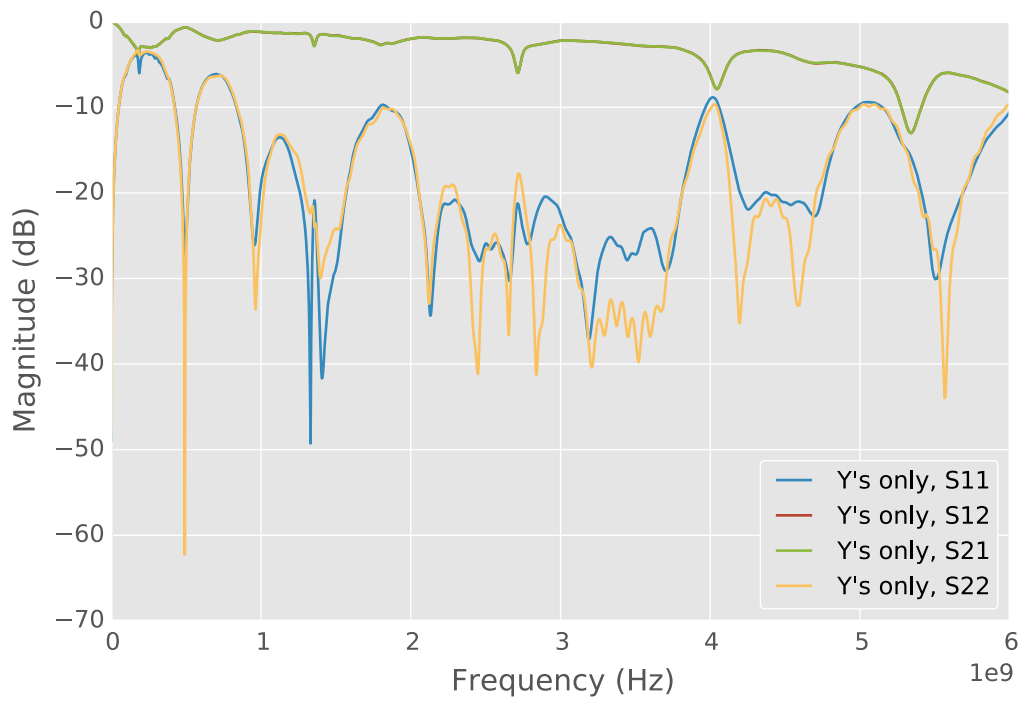


Figure 10.25: Back-to-back balun S-parameters with air bridges installed only at the “Y”s. No curve for S_{12} (red) is visible because S_{21} (green) covers it.

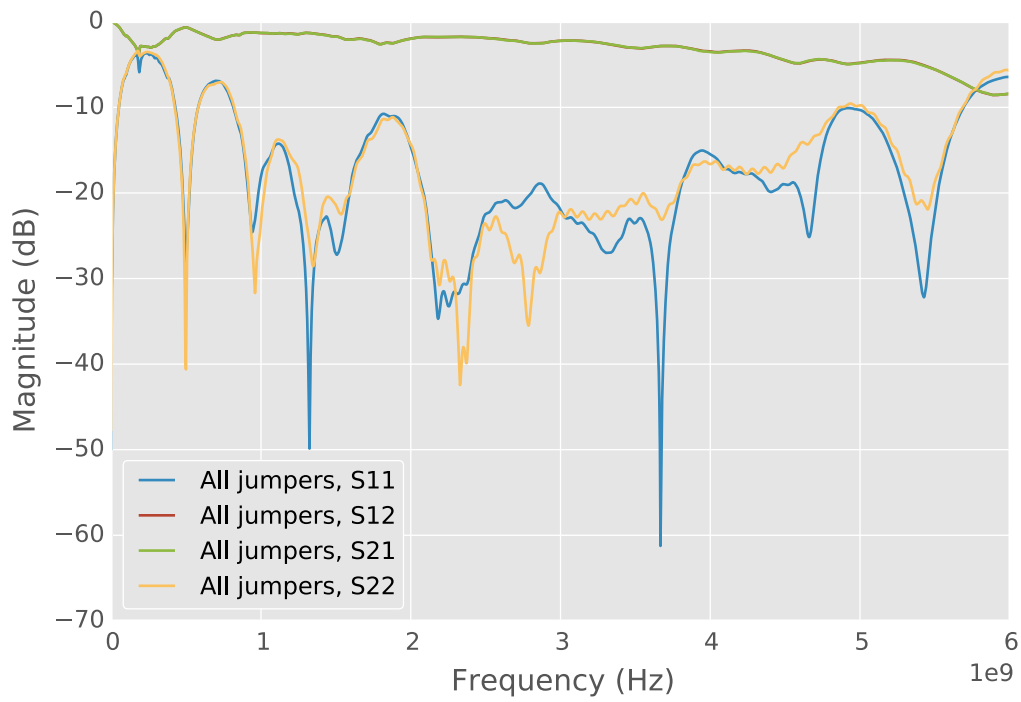


Figure 10.26: Back-to-back balun S-parameters with all air bridges installed. *No curve for S_{12} (red) is visible because S_{21} (green) covers it.*

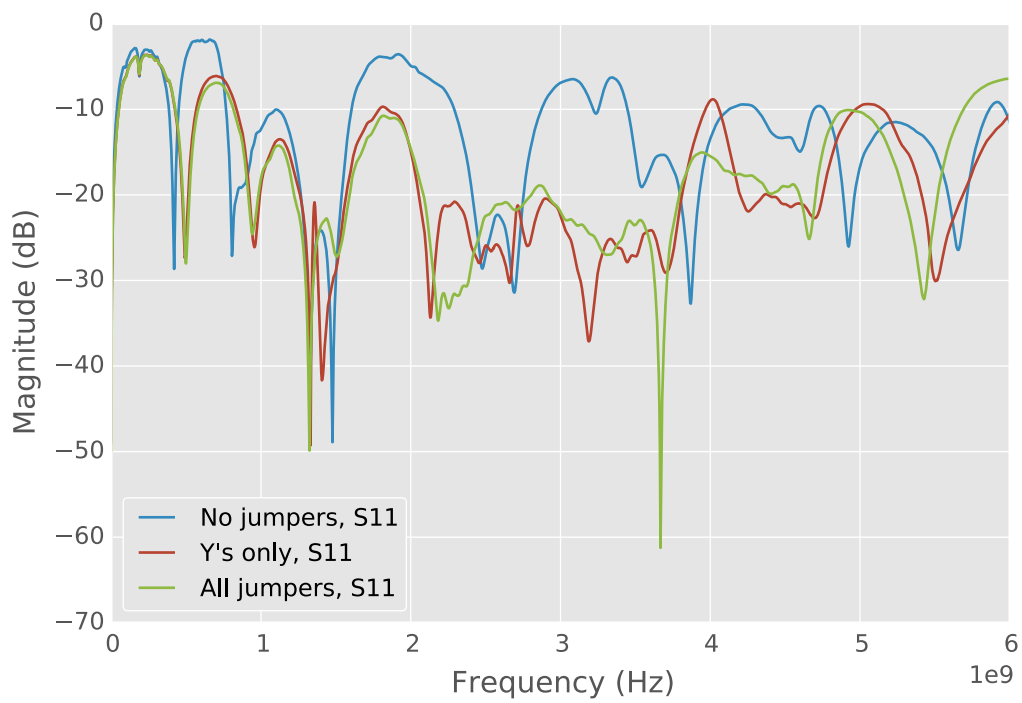


Figure 10.27: Reflection measurement (S_{11}) of a back-to-back balun with various air bridges installed.

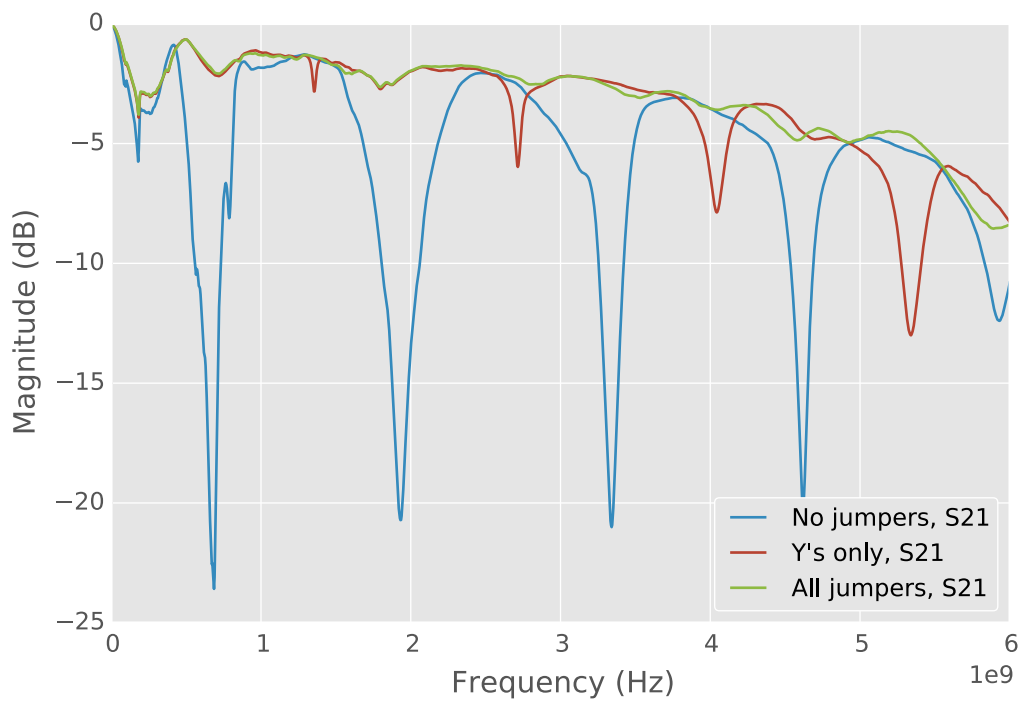


Figure 10.28: Transmission measurement (S_{21}) of a back-to-back balun with various air bridges installed.

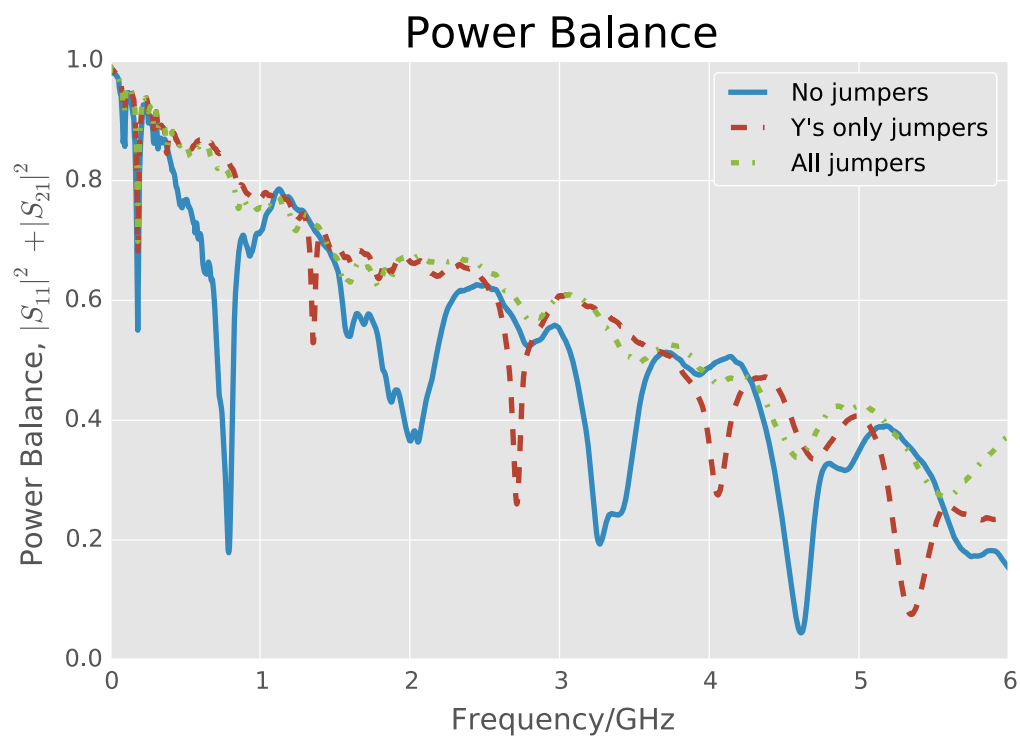


Figure 10.29: Power balance for a back-to-back balun with various air bridges installed. *Power losses increase as the power balance decreases towards zero.*

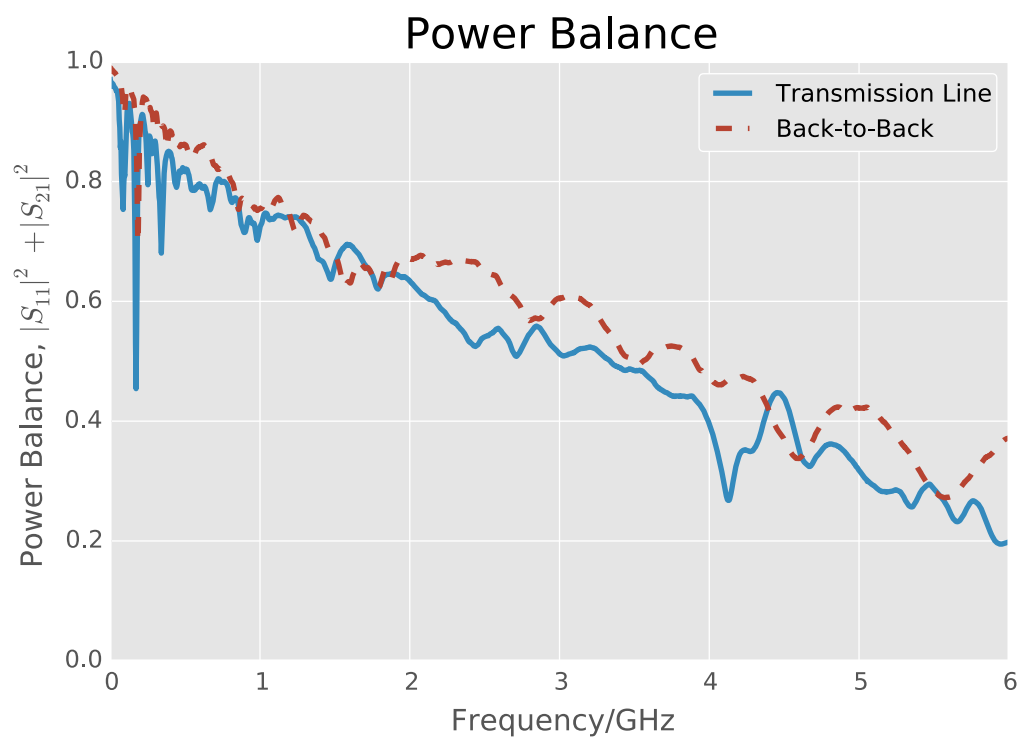


Figure 10.30: Power balance of all air bridges install for the transmission line system and the back-to-back balun.

10.7.3 Summary

In summary, the measurements show that even adding air bridges at the “Y”s improve the system from something that is essentially unusable due to an unpredictable response to a reasonable performing system. By installing all of the air bridges, the system response is improved even more.

10.8 Final Balun Design

During the design process, the balun design was iterated through three designs. All three designs are shown in Figure 10.31. We see that some of the traces are lifted off the boards. Also seen on most of the boards are reference marks for the solder joints of the air bridges. On these boards, the air bridges are jumper wires soldered on the back side of the board as noted earlier in the chapter.

The final double-y balun design has the following characteristics and dimensions which are also illustrated in Figures 10.32—10.35:

- The SMA connector attaches to a CPW that has a 154.11 mil center conductor, a 12 mil gap, and 125 mil ground traces. This CPW is 250 mil long from the edge of the board to the start of the taper.
- Over a length of 2500 mil, the CPW tapers down to a center conductor of 10.31 mil in width, a gap of 17.09 mil, and 10 mil ground traces. The taper is on all edges of the traces and uses the following equation:

$$x(y) = x_0 \left(\frac{x_f}{x_0} \right)^{y/len} \quad (10.11)$$



Figure 10.31: Manufactured double-y baluns.

where y is the linear distance along the center-line of the taper (not the taper curve itself), x is the distance away from a baseline, x_0 is the starting distance from the baseline, x_f is the final distance from the baseline, and len is the total linear length of the taper.

- From the end of the taper to the center of the “Y” is 300 mil. The CPW splits into two, 105 mil long stubs. The stubs are flared 45° away from the center line of the CPW.
- The CPS flares at the same point into stubs at the same angle and of the same length as the CPW. The center gap has a width of 15.23 mil and traces have widths of 24.63 mil.
- A 300 mil CPS goes from the center of the “Y” to the beginning of the taper.
- The CPS taper follows Equation (10.11) over a length of 1500 mil.
- The final gap of the taper is 125 mil with 149.724 mil wide traces.
- There is a 75 mil straight section to which the two-wire transmission line is soldered.

The file versioning system Git was used to track the development of this design. This design is referred to as 0d96092 because this was the hash of the design file in Git.

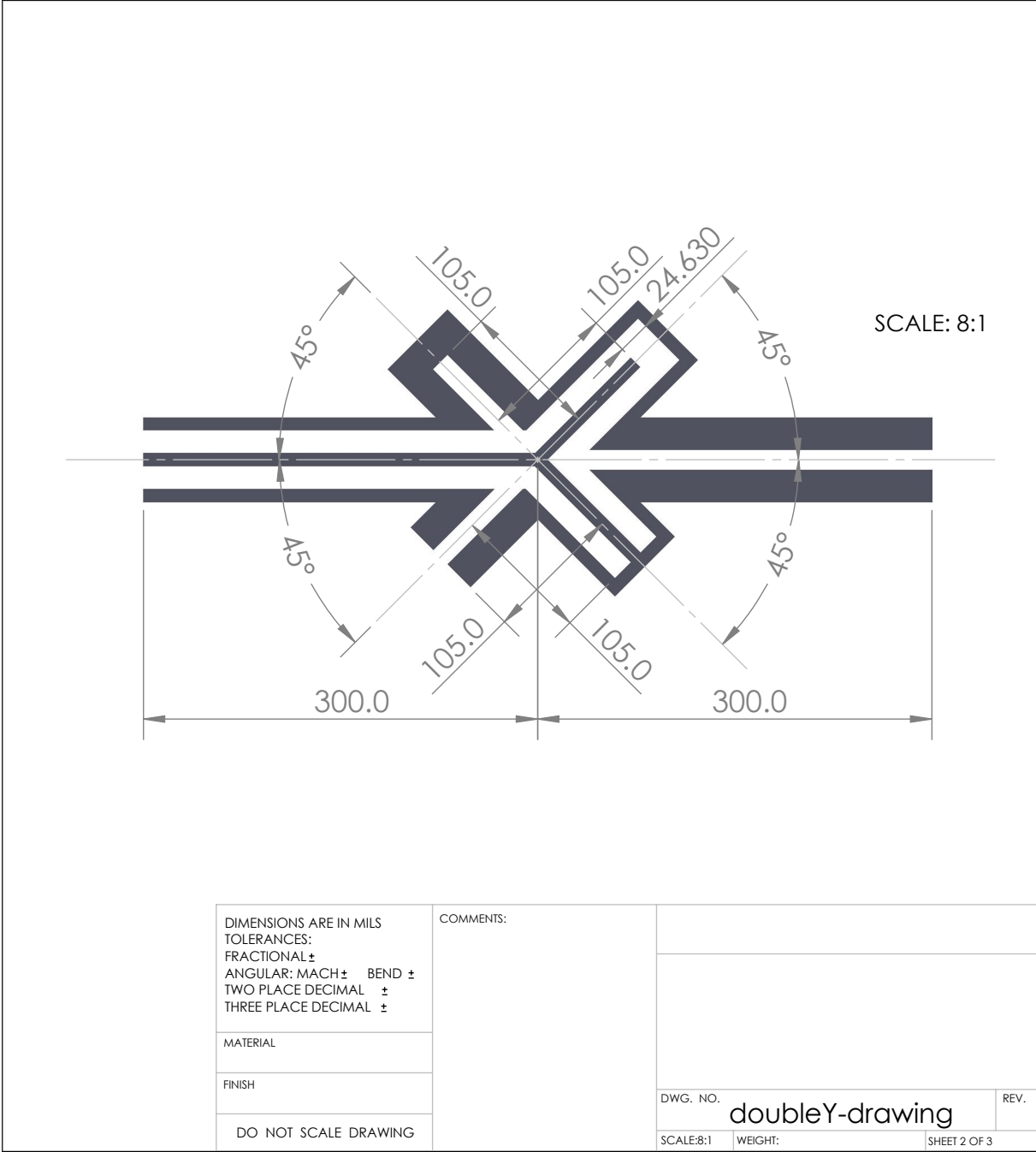


Figure 10.33: Double-Y dimensional drawing, page 2.

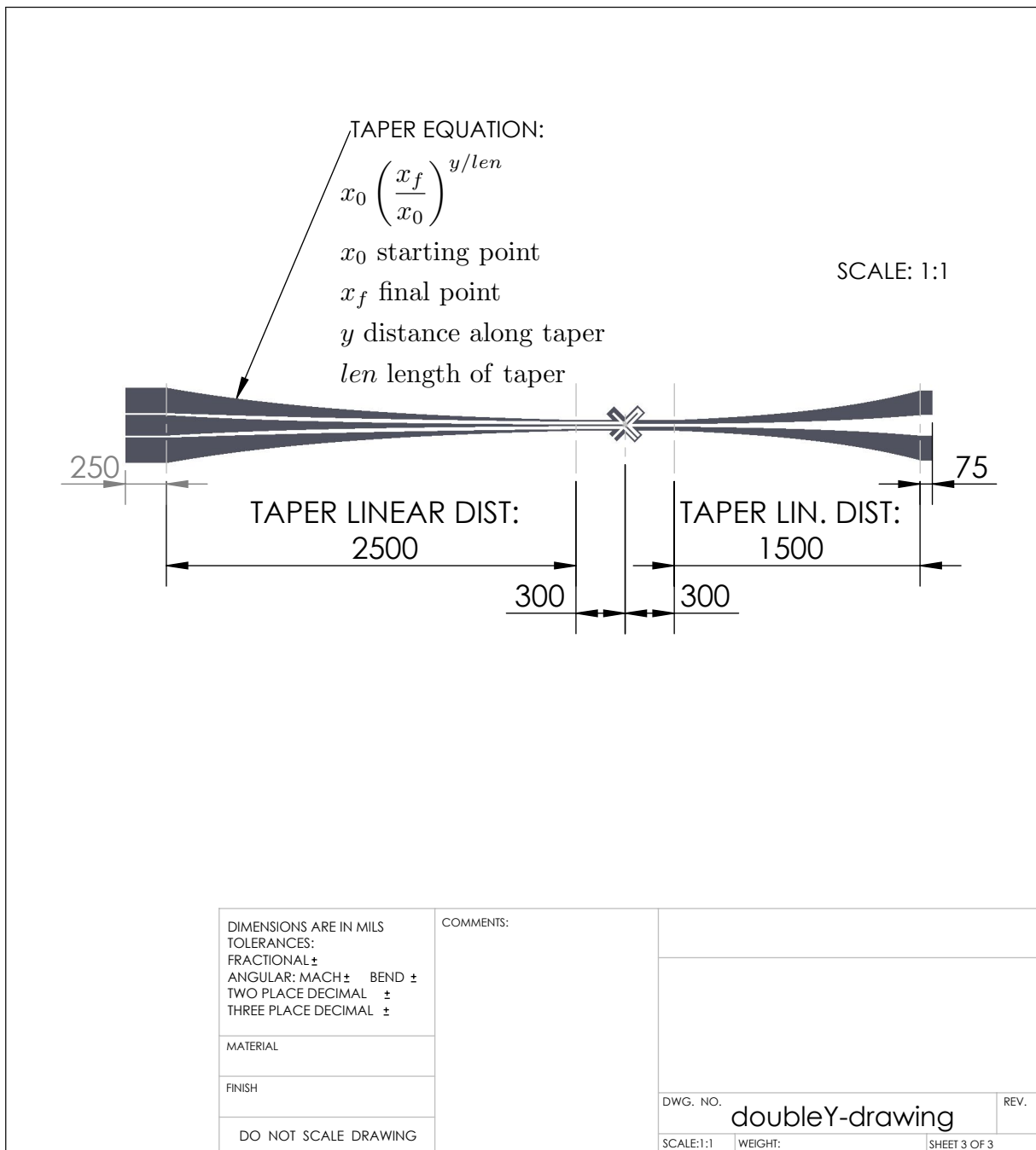


Figure 10.34: Double-Y dimensional drawing, page 3.

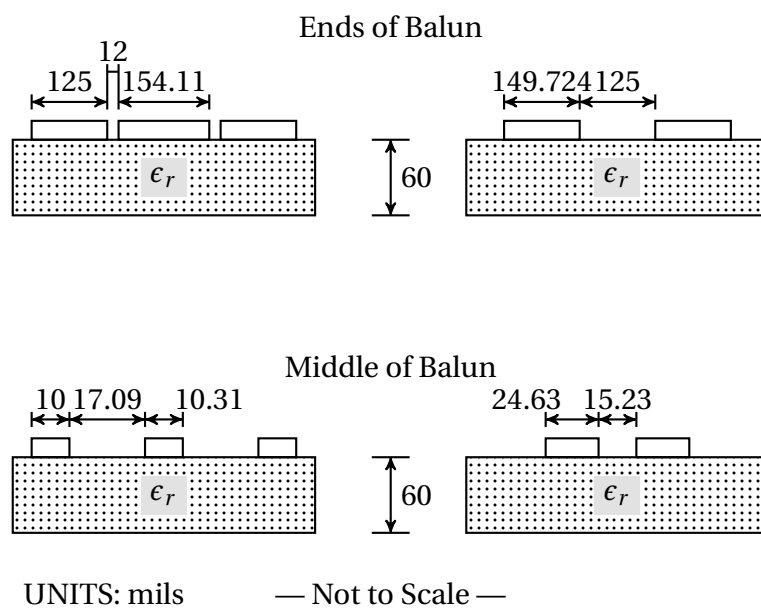


Figure 10.35: CPW and CPS dimensions for the final double-y balun design.

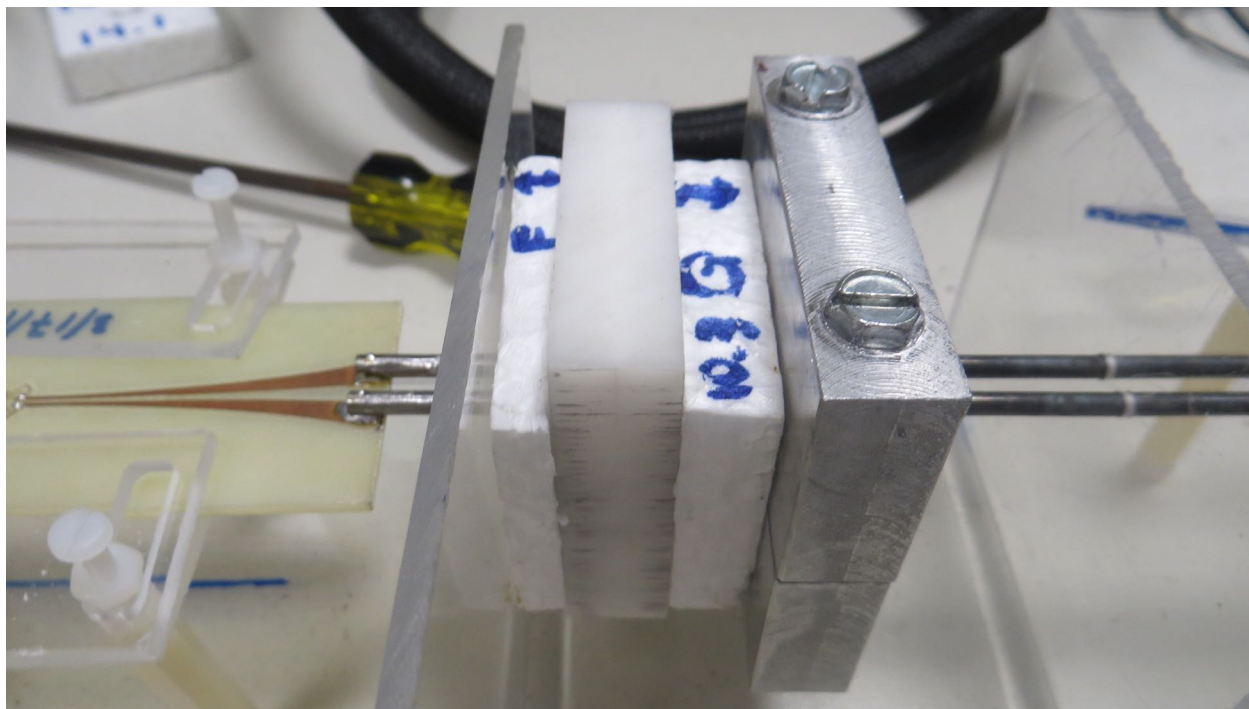
Chapter 11

Bench-Scale Experiment Results

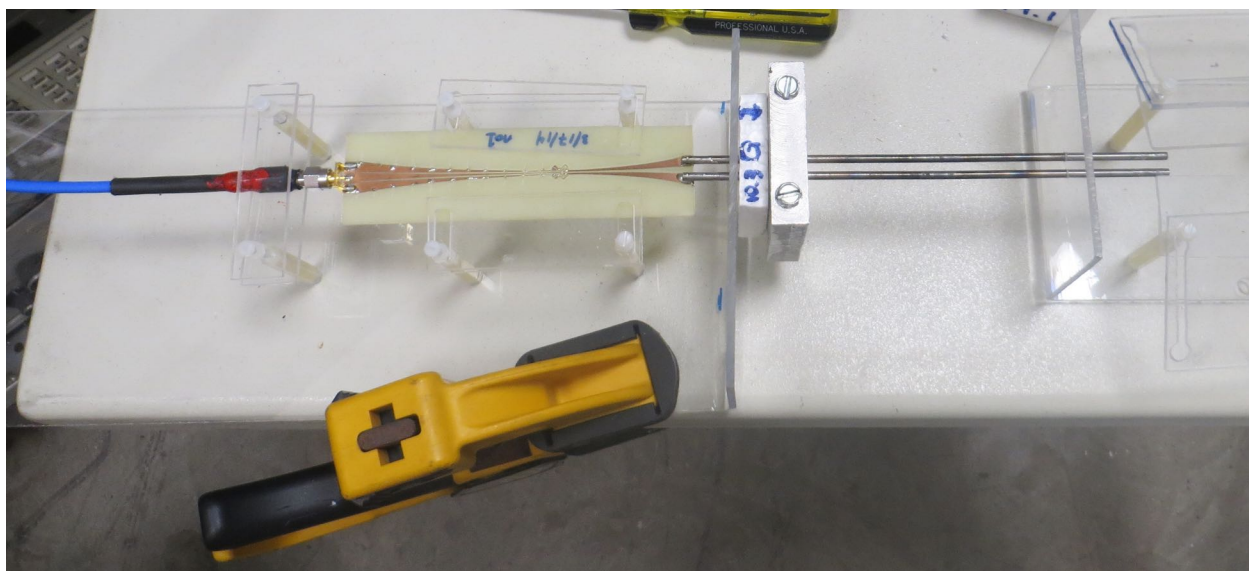
Two experiments are presented in this chapter to demonstrate how a two-wire transmission line may be used for material characterization and how the calibration process from Chapter 9 is used. First, a sample of polyoxymethylene (POM, manufactured by DuPont under the name Delrin) was measured along with a short circuit in four different positions. Second, the two-wire transmission line was placed vertically into a beaker. As distilled water was added, measurements were taken. These experiments serve to demonstrate solid and liquid material measurements.

11.1 Solid Material Measurement

For this experiment, a 12.9 mm thick piece of POM was placed onto the two-wire transmission line with foam on either side of the sample. One piece of foam was compressed between the Plexiglas holder and the POM sample while the other foam piece was compressed between the short circuit and the sample. The balun used was the same as in Section 10.7 with steel rods. This experimental setup is shown in Figure 11.1a. The photos in this section are from an earlier experiment than the data because no photos were taken at the same time as the data.



(a) Material measurement of a POM sample.



(b) Three short calibration setup. *An example setup showing the short circuit placed on a two-wire transmission line with a piece of foam used as a spacer.*

Figure 11.1: Two-wire transmission line experimental setups.

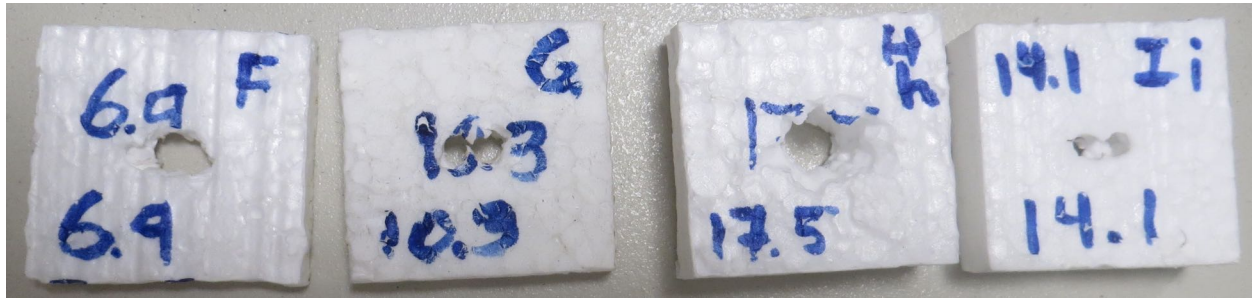


Figure 11.2: Foam spacers used in calibration measurements. *The numbers written on the spacers are the thicknesses in millimeters of the foam when not compressed. The distance used in calculations was measured after the foam was installed and compressed.*

Table 11.1: Foam insert labels and thicknesses. *The table is arranged by thickness and not alphabetically. It just happened that I was thinner than H and the table order is not an error.*

| Label | Thickness/mm |
|-------|--------------|
| F | 5.9 |
| G | 9.7 |
| I | 13.6 |
| H | 17.7 |

11.1.1 Calibration

Before the POM sample could be measured, the two-wire transmission line system needed to be calibrated. The calibration procedure requires that three measurements be made of a load with a known reflection coefficient. An ideal short circuit has a reflection coefficient with magnitude equal to one and a phase shift proportional to the electrical length of the transmission line. For this experiment, a short circuit was measured in four different positions so that three measurements could be used to calibrate the fourth measurement in order to check performance. Pieces of foam (Figure 11.2) were used as spacers between the Plexiglas balun holder and the short circuit (Figure 11.3) as shown in Figure 11.1b. Foam was chosen because it has a relative permittivity close to one so it approximates air in electromagnetic experiments. Table 11.1 shows the labels for the pieces of foam and the thickness of each piece when it was compressed in the experimental setup. The one-port S-parameters of the short circuit in the four different positions are shown in Figure 11.4.

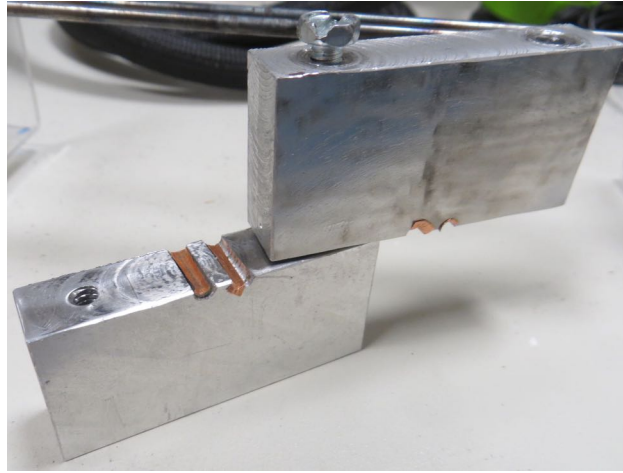


Figure 11.3: Short circuit built for the two-wire transmission line. *Copper tape has been added in an attempt to remove air gaps between the two-wire transmission line and the short circuit block.*

As the foam thickness increases, the short circuit is moved further down the line. This increases the distance that a wave travels along the transmission line and the relative phase change of the wave increases. Numerically the slope of the phase becomes more negative as distance increases. We observe this trend in Figure 11.4 which means that the measurements are reasonable.

To test the calibration, three of the four measurements were used to calibrate the fourth measurement. Foam spacers F, G, and H were used as standards and the sample data was for the foam spacer I. The original sample data set, the corrected data, and a theoretical curve are shown in Figure 11.5. We see that the original sample is much longer electrically because the phase wraps numerous times while the calibrated data does not wrap. Also noted is that there is less loss in the original data than in the theoretical or corrected data. The corrected data is significantly improved compared to the original; however, it does not completely match the theoretical curve. We posit two main reasons for this. First, the theoretical model of the two-wire transmission line is not necessarily complete at this time so there may be effects not currently computed. Not all losses are accounted for since the calibrated data is less than the theoretical data. Perhaps dimensions vary enough throughout the manufactured setup compared to

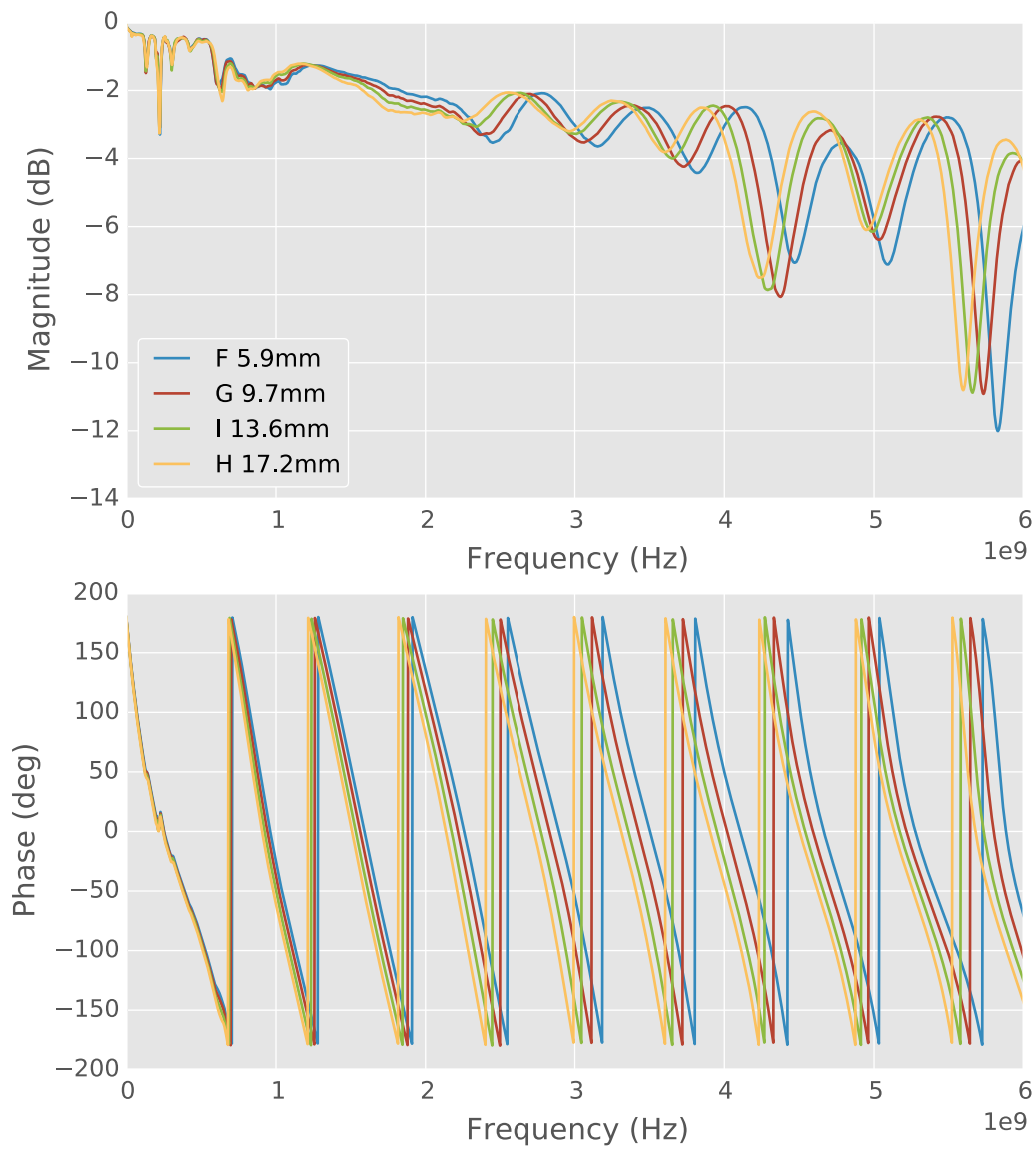


Figure 11.4: One-port S-parameters of a short circuit located in four different positions along a two-wire transmission line.

the model, or maybe the theoretical value used for the calibration standard does not capture all losses. Secondly, non-ideal effects are present as shown by the ripples in the corrected data, e. g. below 1 GHz and above 4 GHz). There could be multiple causes for these effects such as air gaps around the short circuit or uneven wires in the two-wire transmission line.

11.1.2 POM Measurement

Once the calibration measurements were checked, the 12.9 mm thick POM sample was placed onto the transmission line with foam spacer F (6.0 mm) on the balun side of it and foam spacer G (9.8 mm) on the short circuit side of it. The measurement was calibrated using the same measurements as in the previous section. Figure 11.6 shows the original and calibrated measurement as well as the theoretical response for an air-line, i. e. a two-wire transmission line of the same length (28.7 mm) with neither foam nor material sample.

We see that below 1 GHz the magnitude has spikes above 0 dB which does not make physical sense. This is similar to calibrated short circuit measurement although in that case the spikes did not surpass 0 dB. Since the original measurement stays below 0 dB, the error is probably in the calibration measurements and caused by non-ideal effects such as air gaps. Withstanding this error, we notice that the phase has been corrected to an electrically-shorter transmission line. Because the slope is more negative than the air-line case, we know that some portion of the transmission line is surrounded by a medium with $\epsilon_r > 1$.

In summary, we see that the two-wire transmission line system can be calibrated and responds to material samples being placed in-line. The calibration procedure requires additional work at this time in order to improve accuracy and reduce unwanted effects, such as air gaps, that can cause troublesome artifacts in the processed data.

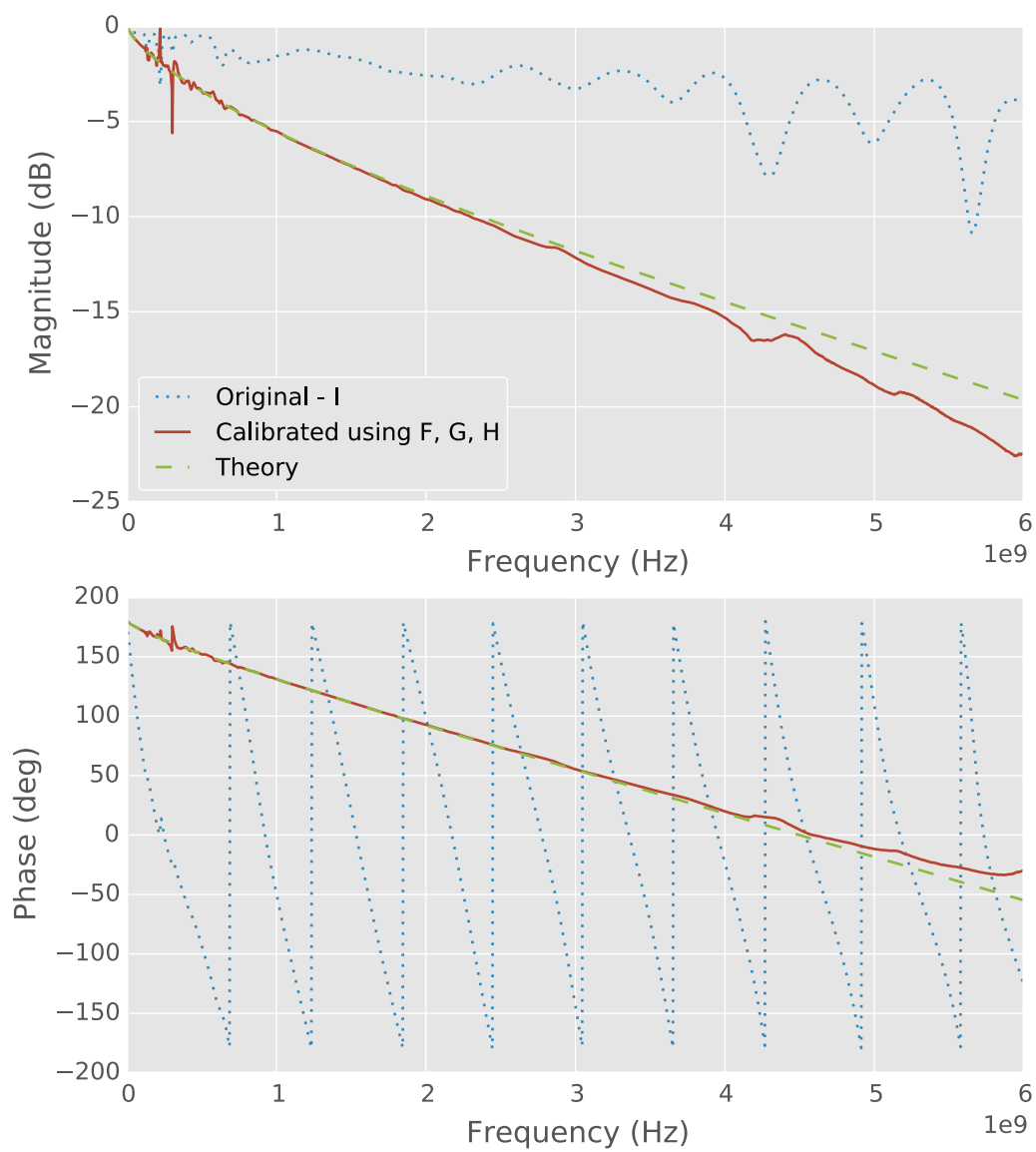


Figure 11.5: One-port S-parameters of a short circuit located 13.6 mm from the Plexiglas holder by the foam I spacer.

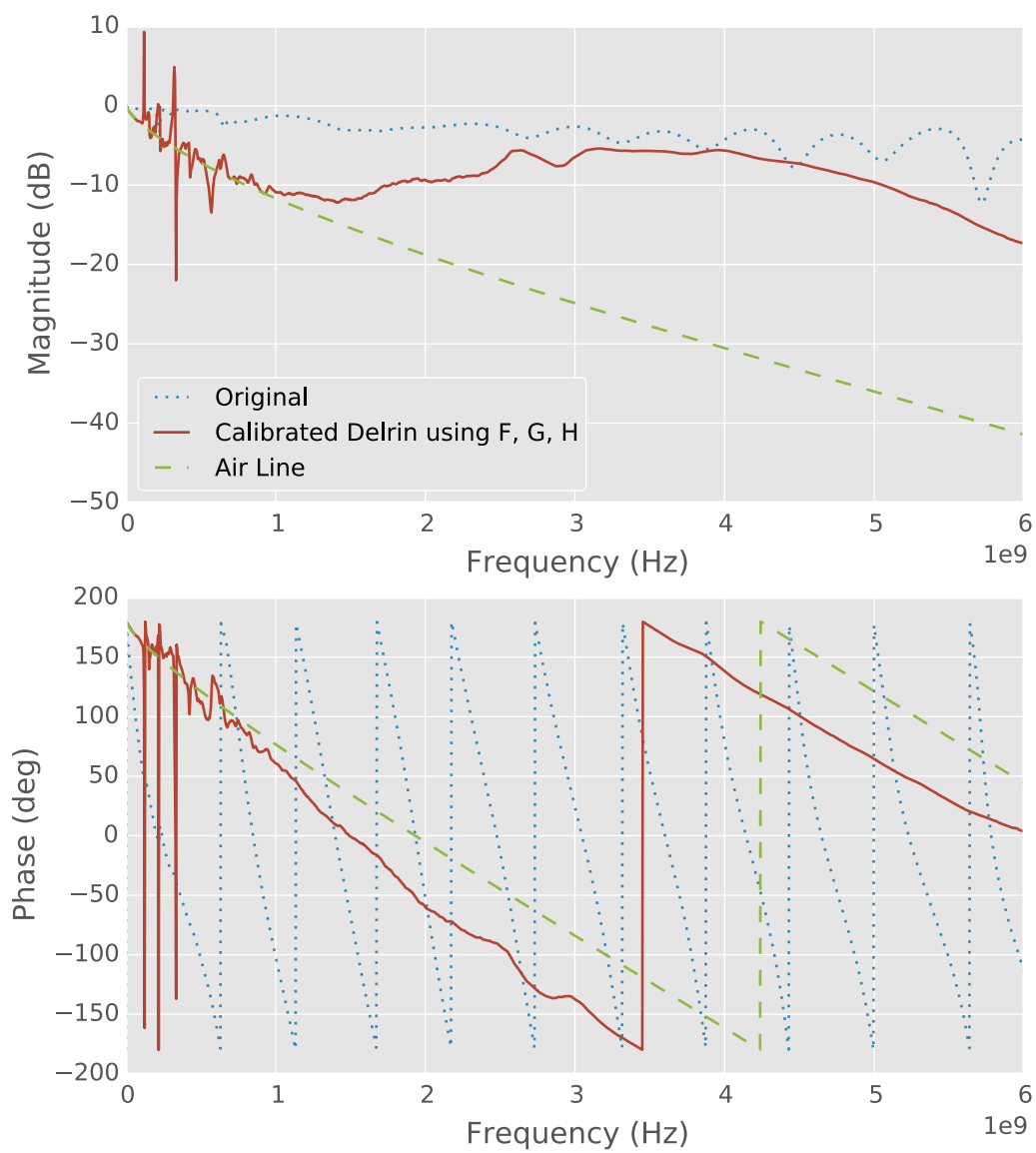


Figure 11.6: Measurements of a POM sample layered between two foam spacers on a line terminated by a short circuit.

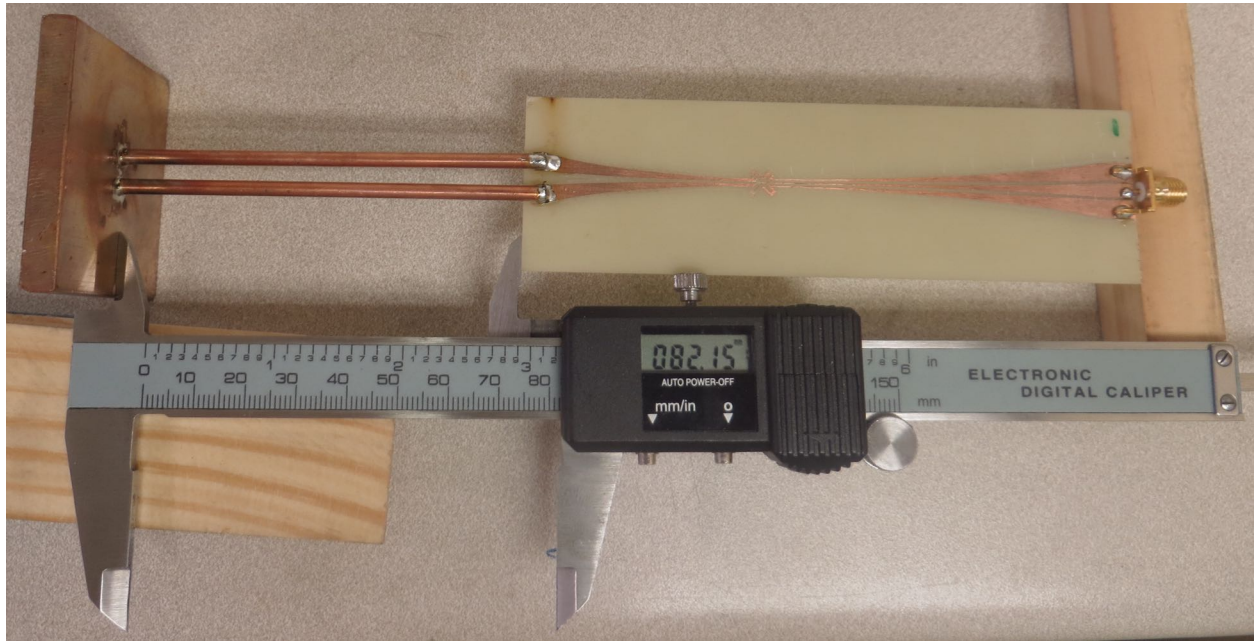


Figure 11.7: Balun with copper rods and copper short.

11.2 Liquid Calibration

For this experiment, a two-wire transmission line was calibrated using distilled water. Copper rods were attached to a balun of design 0d96092 presented in Section 10.8 with wire-bond air bridges. A copper plate was soldered onto the other end of the copper rods. The assembled system is shown in Figure 11.7.

A groove for the balun was cut about half-way through two, one inch by one inch, square plastic tubes. These tubes were set on top of a 1000 mL Pyrex beaker and the two-wire transmission line system suspended down, into the beaker as shown in Figure 11.8. Also shown in this figure is a vertical caliper. A slot was cut in the upper surface of one of the plastic tubes for the full beam of the caliper and a smaller slot was cut in the bottom surface for the depth bar of the caliper. This allowed the caliper to rest on the bottom of the tube and the depth bar to extend down into the beaker. Hot glue was used to secure the caliper in a vertical position. The plastic tubes are secured to the beaker and the beaker secured to the table using painters tape. Next to the beaker is an antenna stand, secured to the table again with tape, that serves as a

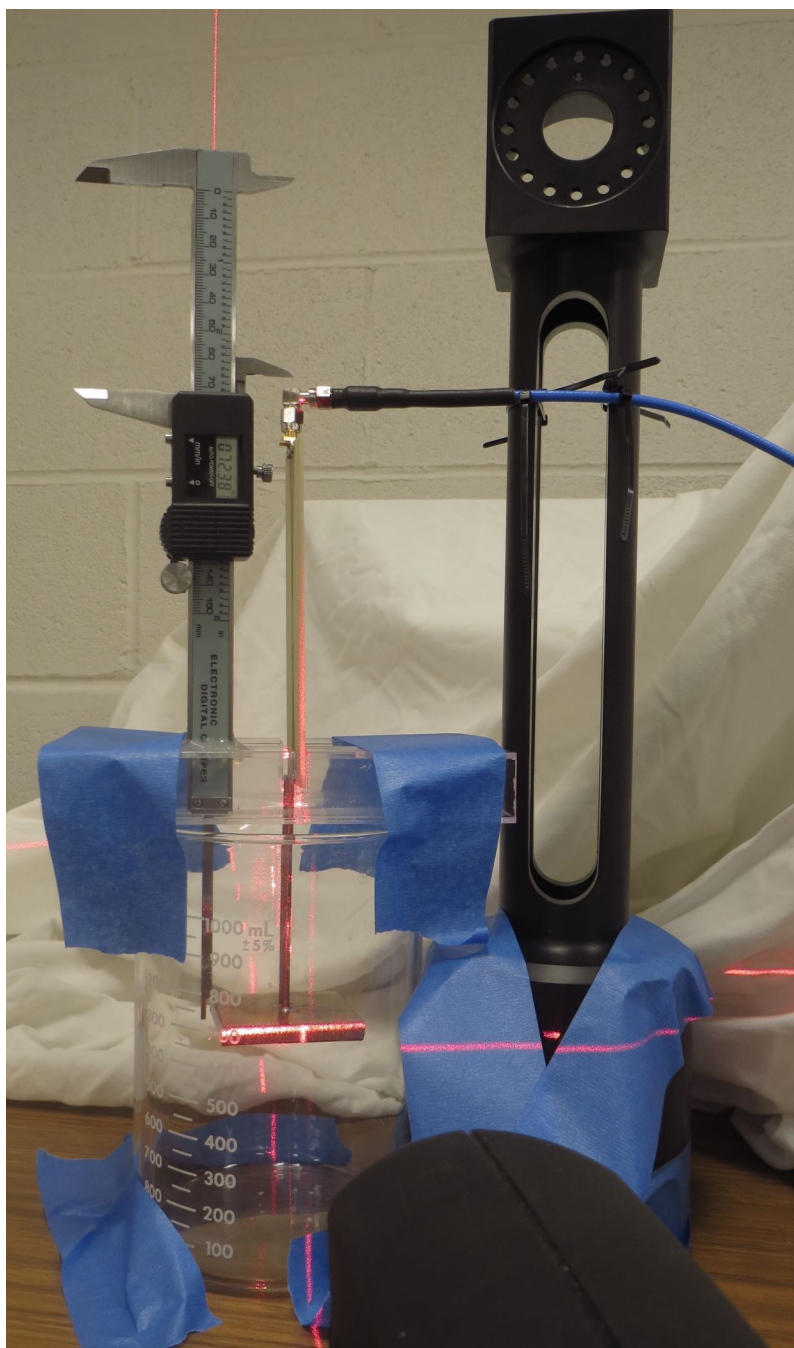


Figure 11.8: Liquid measurement experimental setup.

cable stand. A SMA cable¹ with a right-angle adapter is secured to the stand using zip ties. An HP 8510 VNA is calibrated to the right-angle adapter using a standard 3.5 mm cal kit. The force of the cable on the balun is used to position the balun vertically as checked by a laser level.

Distilled water was purchased in a gallon jug from MSU Stores. The distilled water was added to the beaker, the depth measured, and a measurement taken. There was not a consistent amount of water added each time since the calibration procedure can use any distance. The depth was measured by lowering the depth bar down until the surface tension of the water was broken and water wicked onto the depth bar. The surface tension was broken by a small drop of water that remained on the end of the depth bar when it was raised up.

The system is calibrated using the procedure in Chapter 9; however, the procedure is slightly different than for the previous experiment. Earlier, the short circuit was moved along the length of the line in order to create three different reflection coefficients and the two-wire transmission line was only surrounded by air. In this experiment, the short circuit does not move but the medium surrounding the two-wire transmission line changes. Each calibration measurement has a different length of air and water. This creates different reflection coefficients because the electrical length changes even though the physical length does not.

The theoretical reflection coefficients are calculated based upon the two-wire transmission line going through air and then water. To calculate the transmission line circuit parameters for the water section, the relative permittivity of the distilled water is calculated using the Debye Equation [45, p. 6-14], [7],

$$\epsilon = \epsilon' - j\epsilon'' \quad (11.1)$$

$$\epsilon' = \epsilon_{\infty} + \frac{\epsilon_s - \epsilon_{\infty}}{1 + \omega^2 \tau^2} \quad (11.2)$$

$$\epsilon'' = -\frac{(\epsilon_s - \epsilon_{\infty})\omega\tau}{1 + \omega^2 \tau^2}. \quad (11.3)$$

¹Cable number 2013-05-17-009

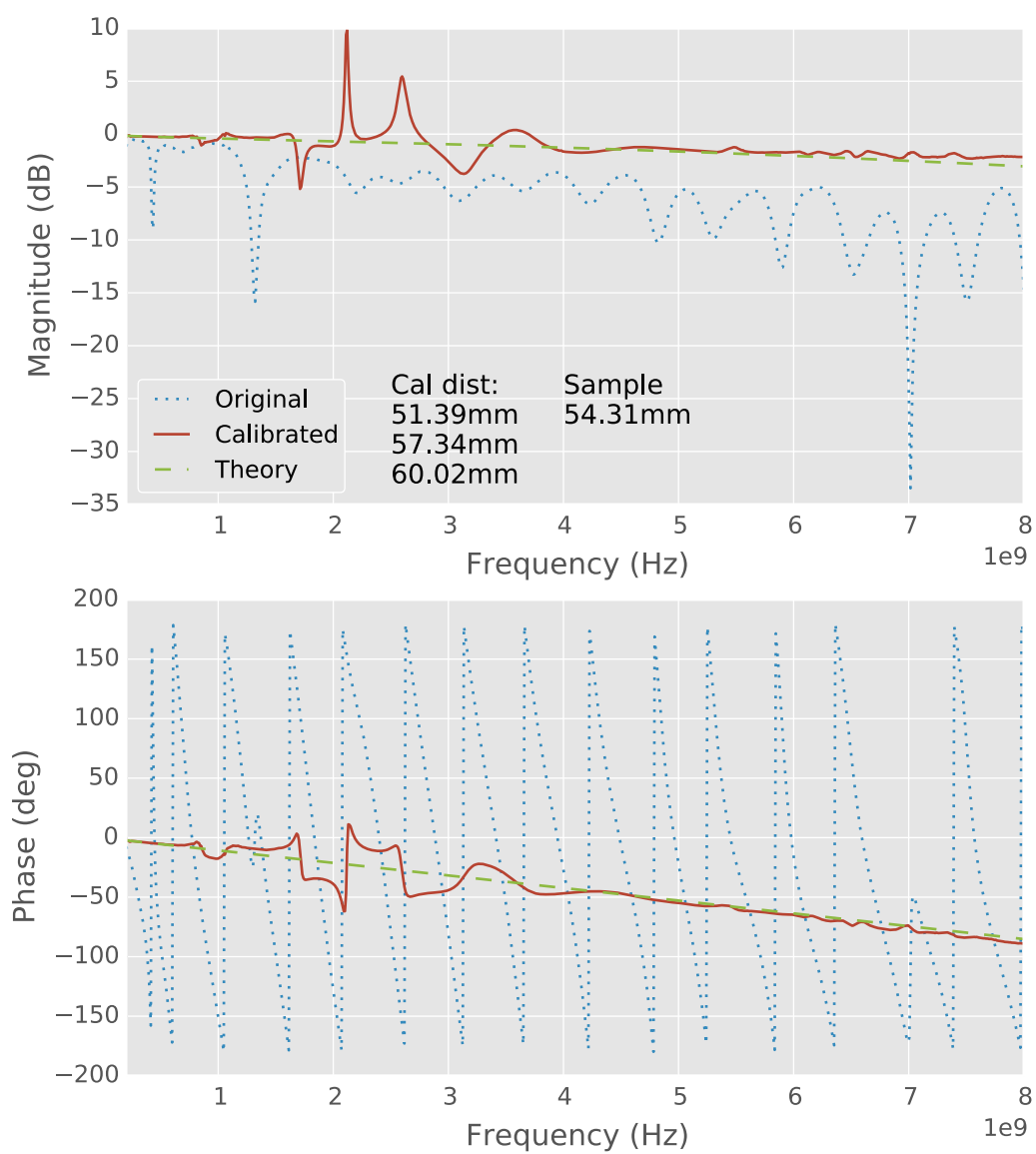


Figure 11.9: Calibrated one-port S-parameters for a transmission line with a short circuit in distilled water.

The Debye Equation is used to model dielectrics based on the following parameters:

- static permittivity, ϵ_s ;
- high frequency limit, ϵ_∞ ; and
- relaxation time, τ .

For distilled water at 25°C, $\epsilon_s = 78.408$, $\epsilon_\infty = 5.2$ and $\tau = 8.27$ ps [45, pp. 6-1 & 6-14].

Figure 11.9 shows one measurement (54.31 mm) that has been calibrated using three other measurements (51.39 mm, 57.34 mm, and 60.02 mm). We see behavior similar to the previous experiment such as a reduction in the electrical length of the system and regions with obviously erroneous data—in this case around 1.5 GHz to 3 GHz. Of particular concern is between 2 GHz and 3 GHz where the calibrated magnitude raises above 0 dB. Overall, however, we see that the raw data has been corrected towards the theoretical data and represents a significant improvement.

Unlike the previous experiment, there are no expected air gaps as the water completely surrounds the two-wire transmission line. One possible source of error is the distilled water. It is unknown how the water used actually matches the parameters used in the Debye Equation. The literature simply lists the parameters as being for water but does not state whether it is distilled water, deionized water, or how it is filtered. This may cause some errors, however, it does not explain oscillations. A possible cause of the largest errors in the region between 2 GHz and 3 GHz is the natural resonance frequency of water.

In this experiment, a simple beaker was used as the container. A longer-term solution would be a specific purpose container. Figures 11.10 through 11.17 are drawings for a container that submerges the balun vertically in a liquid. There is a small hole through which the liquid is added. A wedge is used to securely hold the balun while allowing for new designs. The drawings are the first design iteration of the container. It has not been manufactured and is presented here solely as a concept.

In summary, we again see that the two-wire transmission line system can be calibrated and we see that it can be used to measure a liquid sample. The calibration procedure requires additional work at this time in order to improve accuracy such as determining acceptable frequency ranges for calibration liquids.

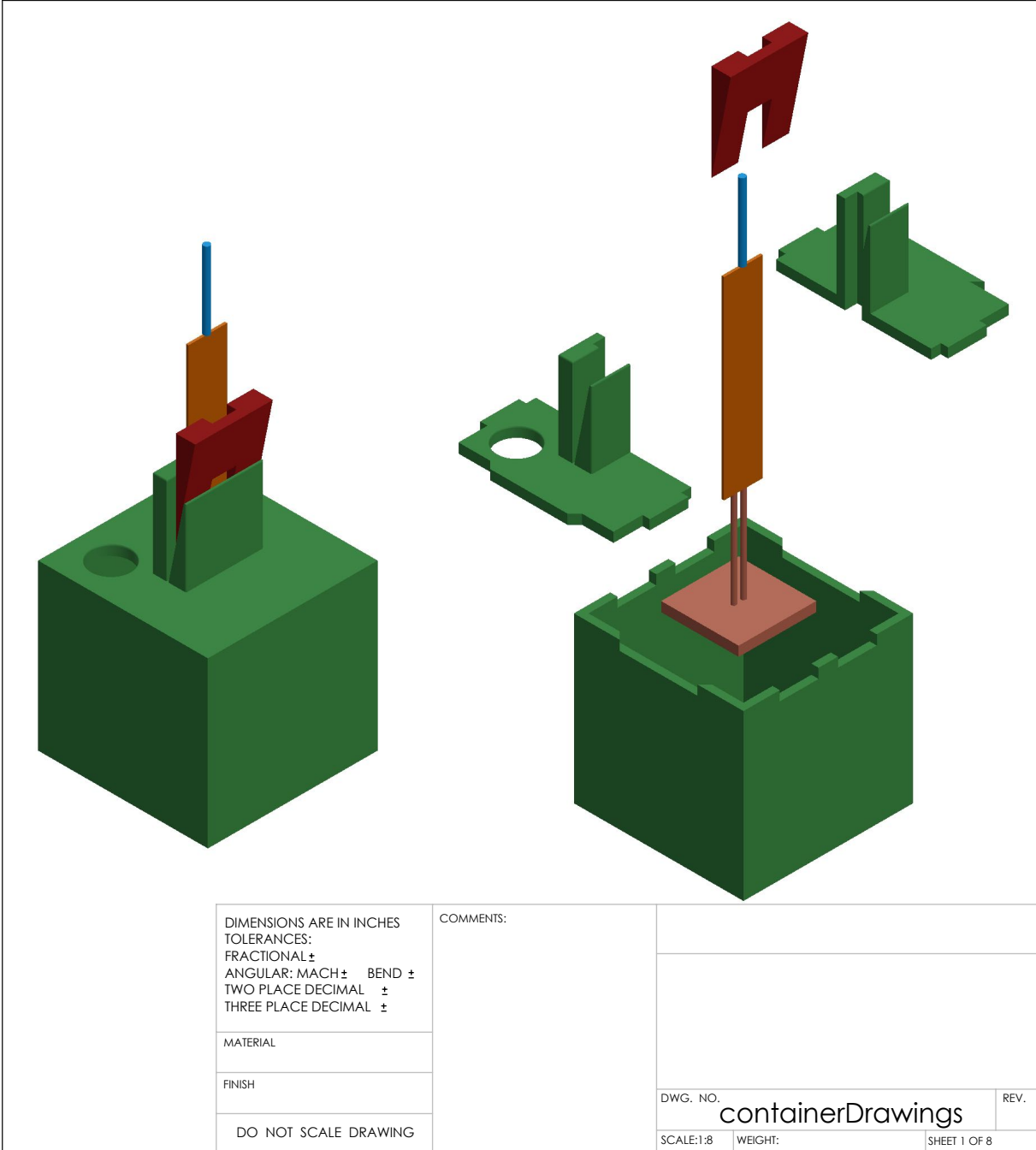
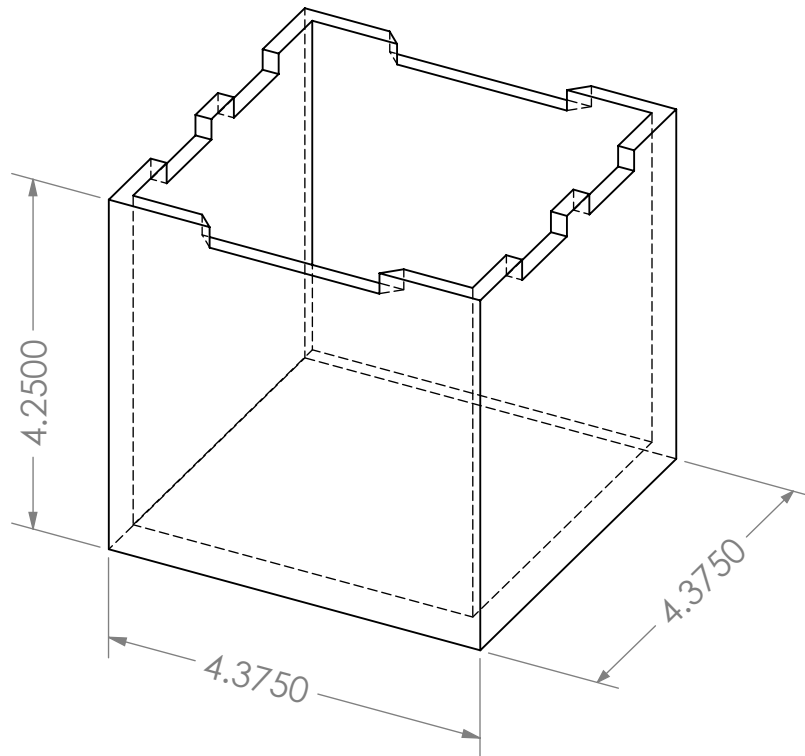


Figure 11.10: Liquid measurement container, page 1.



| | | | |
|---|-----------|-------------------|----------------------|
| DIMENSIONS ARE IN INCHES TOLERANCES: FRACTIONAL \pm ANGULAR: MACH \pm BEND \pm TWO PLACE DECIMAL \pm THREE PLACE DECIMAL \pm | COMMENTS: | | |
| | | | |
| | | | |
| | | | |
| MATERIAL | | | |
| FINISH | | | |
| DO NOT SCALE DRAWING | | | |
| | | DWG. NO. | REV. |
| | | containerDrawings | |
| | | SCALE:1:8 | WEIGHT: SHEET 2 OF 8 |

Figure 11.11: Liquid measurement container, page 2.

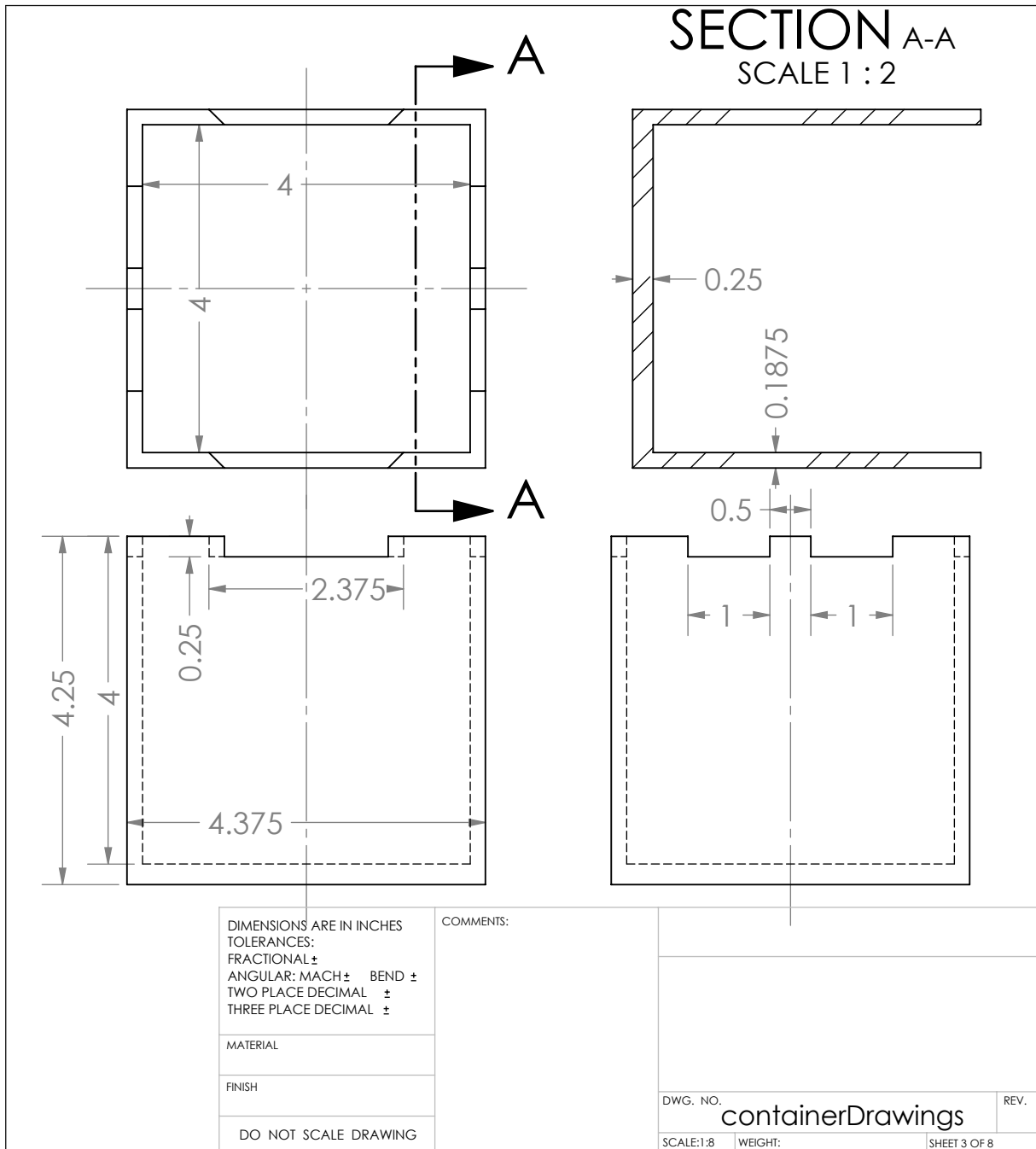


Figure 11.12: Liquid measurement container, page 3.

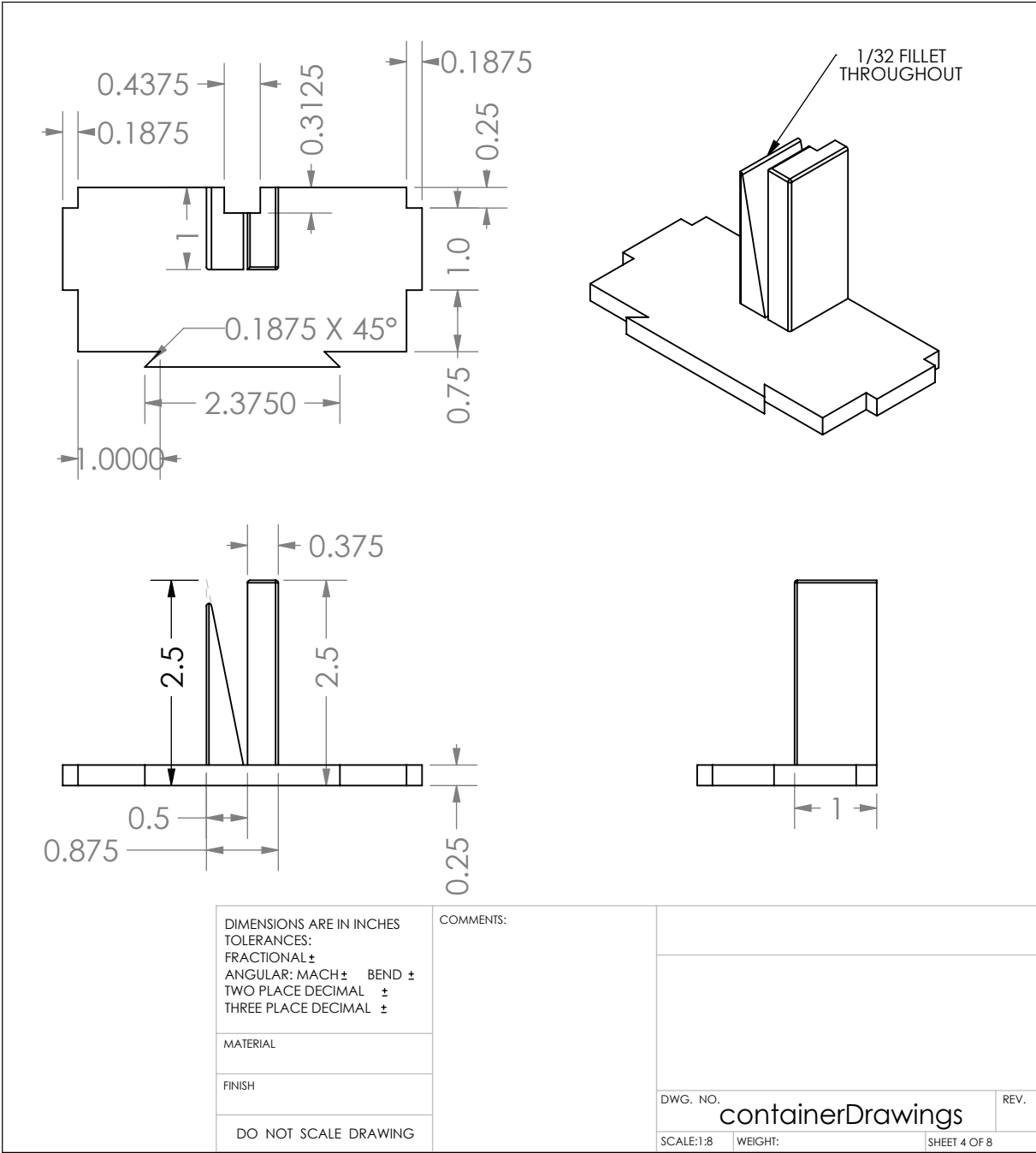


Figure 11.13: Liquid measurement container, page 4.

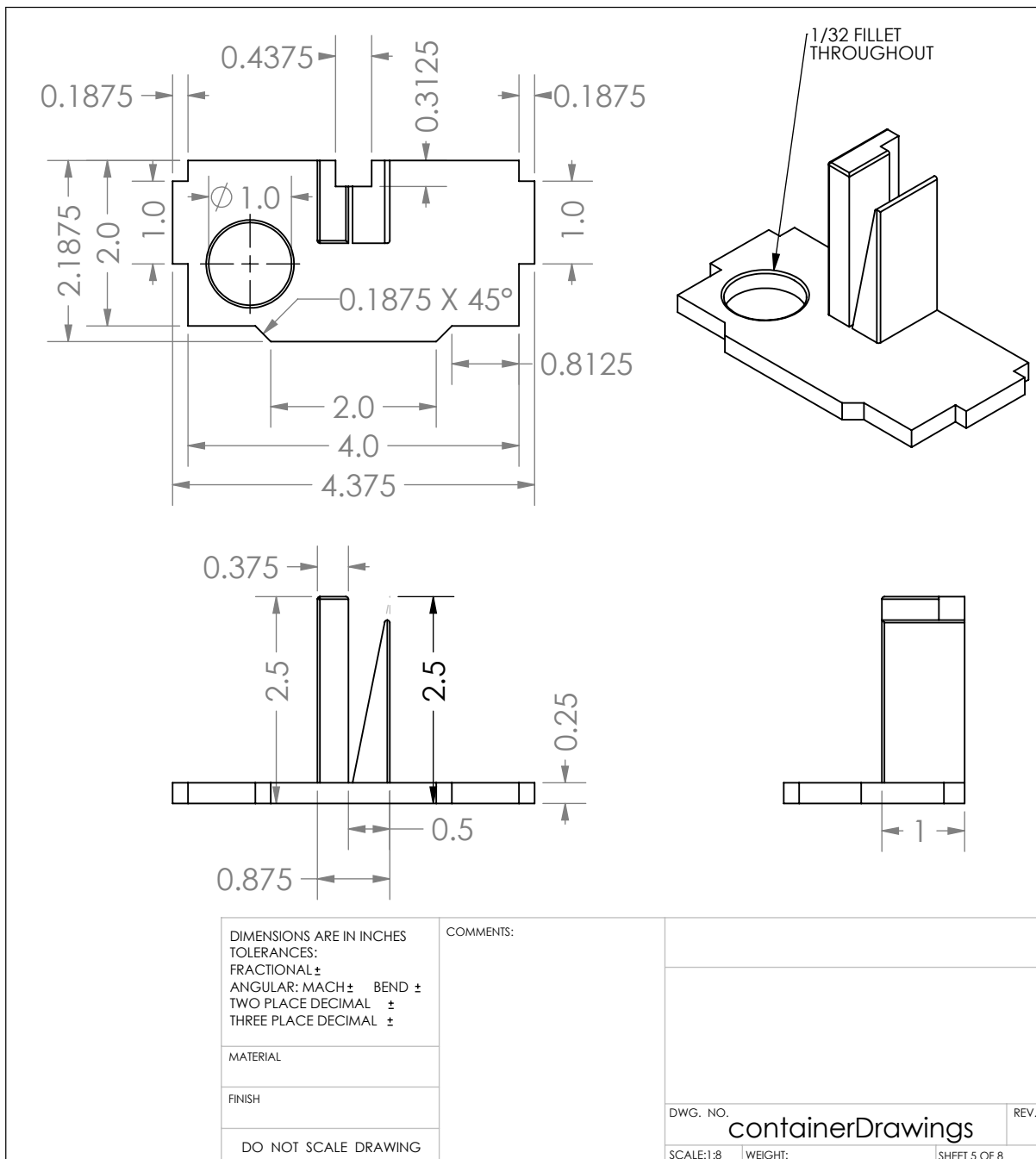


Figure 11.14: Liquid measurement container, page 5.

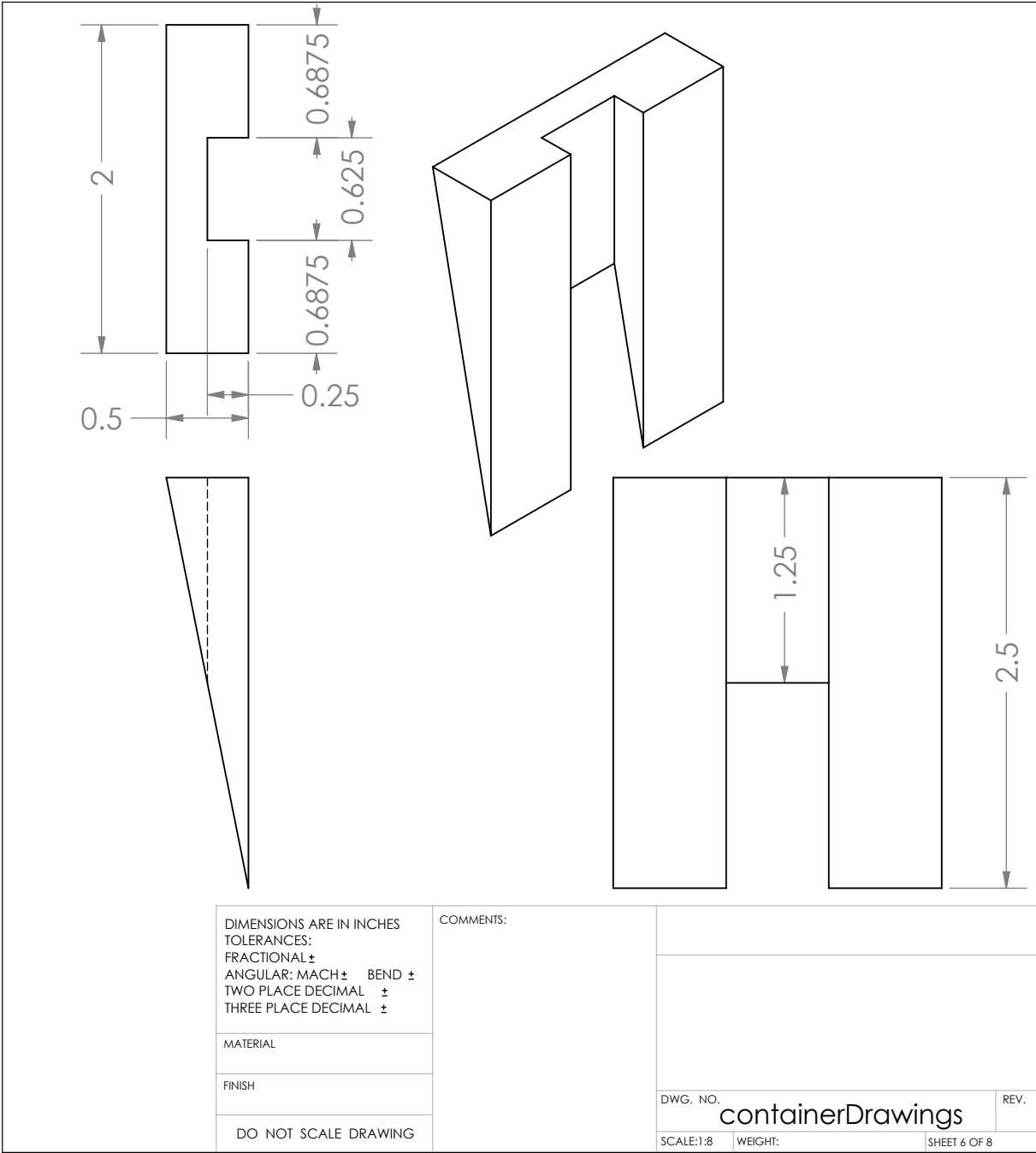


Figure 11.15: Liquid measurement container, page 6.

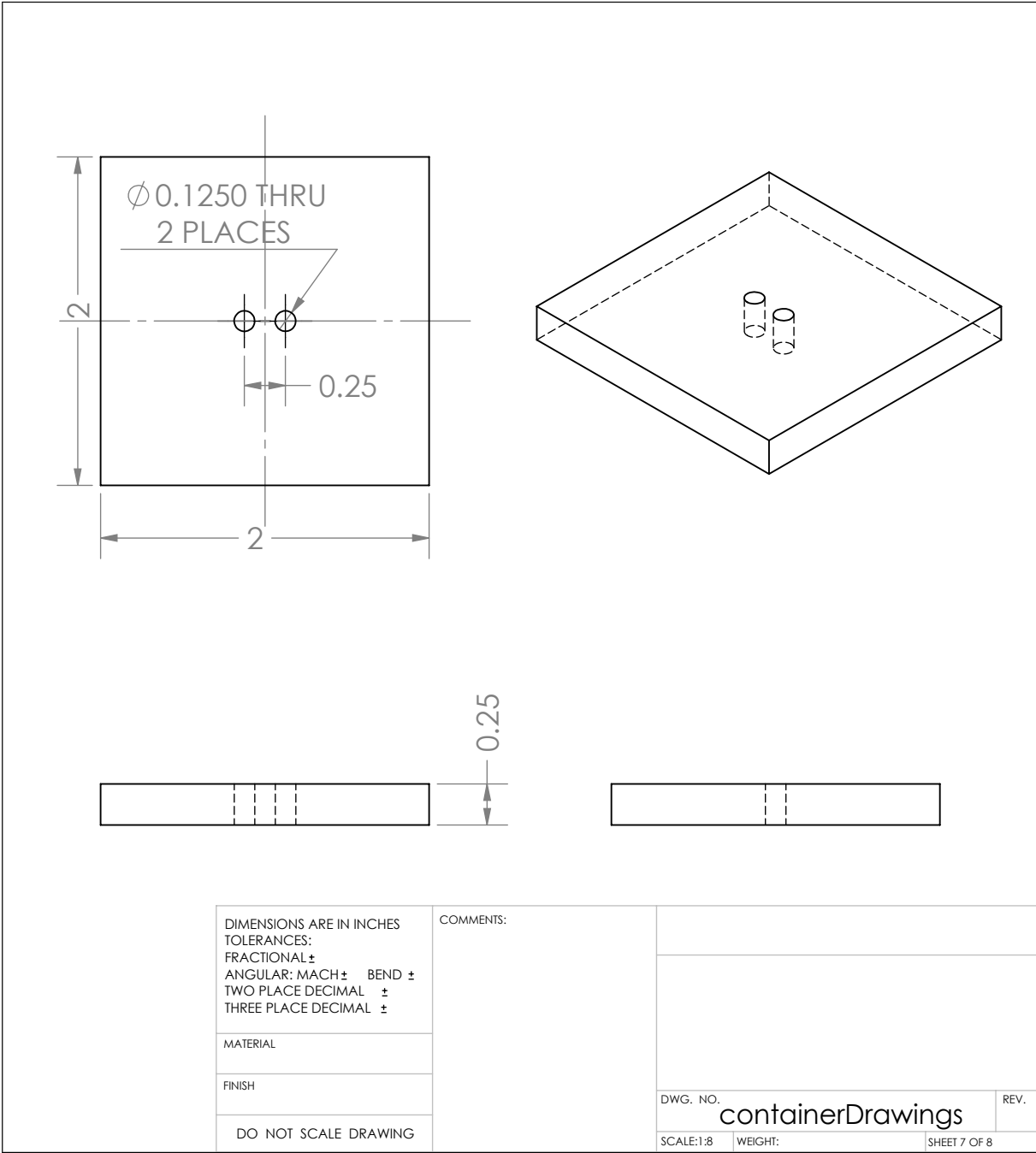


Figure 11.16: Liquid measurement container, page 7.

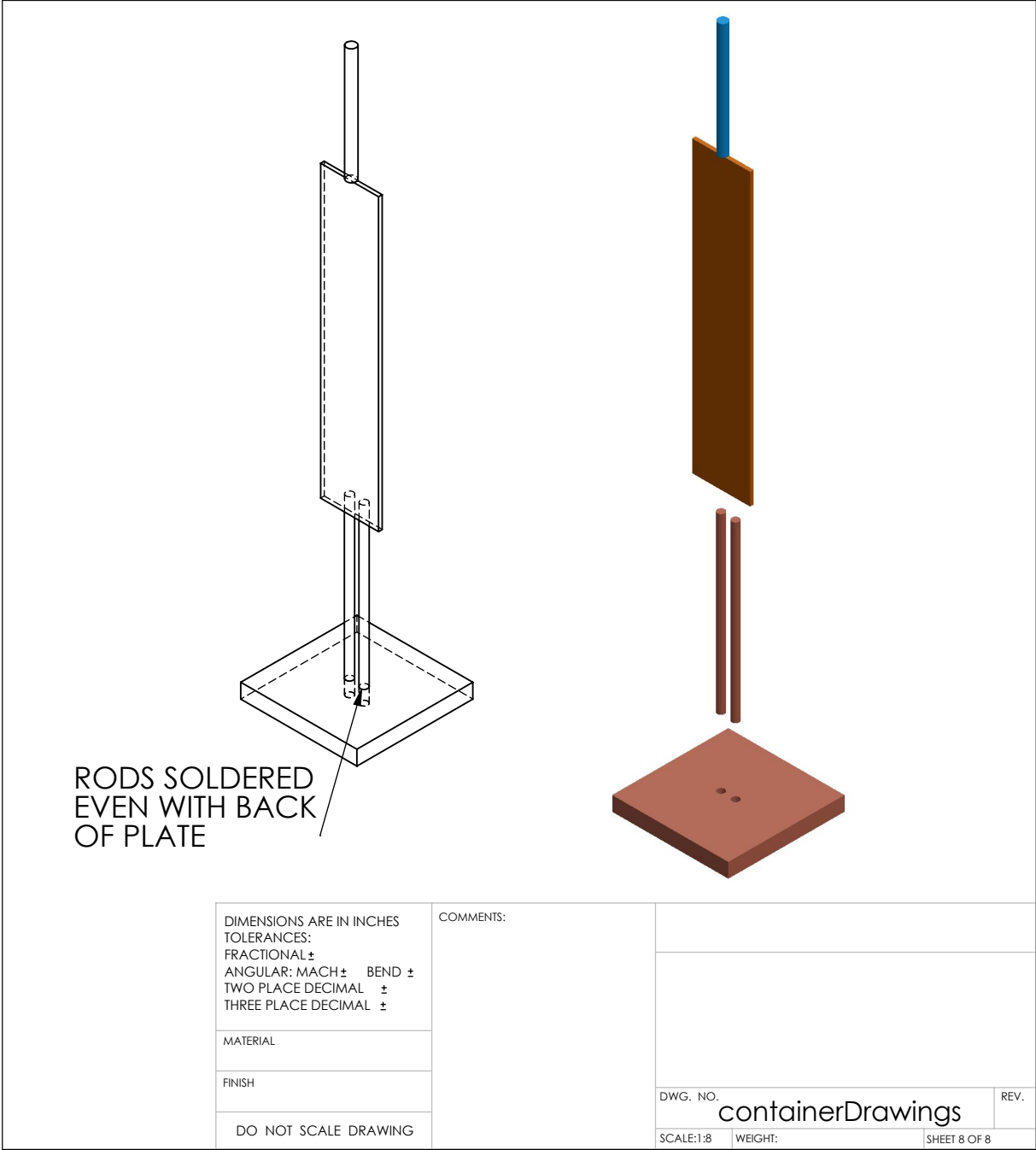


Figure 11.17: Liquid measurement container, page 8.

Chapter 12

Conclusion and Future Work

Part III has focused on a two-wire transmission line material measurement system designed for bench-top experiments. The theory of the system was first developed then a design developed and presented. Finally experimental results were presented to demonstrate the feasibility and current capabilities of the system. The presented system enables bench-scale experiments for measuring the properties of flames.

To begin Part III, the electric potential and fields were derived for a two-wire transmission line. Next, a distributed circuit model was derived and the parameters summarized in Table 8.1 followed by a discussion on how to calibrate a two-wire transmission line and remove the effects of a balun. A double-y balun design was then presented as a way to connect the measurement system to test equipment. Details about designing the balun and ancillary equipment such as a stand and a short circuit were also provided. Because the goal of the system is to measure flames, high-temperature modifications to the design were discussed. Finally, measurements of solid and liquid materials were presented to demonstrate the capabilities of the two-wire transmission line system.

The two-wire transmission line system was demonstrated to be a reasonable material measurement system for solid and liquid materials. Actual measurements of flames were not able

to be conducted. Before these are conducted, there are a few items that should be addressed as illustrated by the initial experiments. First the precision and accuracy of the calibration technique should be improved. This can be done by improving the manufacturing accuracy of the short circuit or other calibration standard. Improved manufacturing will help to eliminate air gaps, lower tolerances, and result in an improvement of the overall system performance. The theoretical reflection coefficient used in the calibration calculations needs to be refined to better match the standard used. This should decrease some of the problems in accuracy of the current calibrations. Second a revision to the balun design should be considered. The goals of this new balun should be lower losses and to not require air bridges. A trade-off for a narrower bandwidth balun should be considered. Finally work presented in [77] based on theory found in [75] should be continued in order to determine the minimum needed size of a material sample and the short circuit for calibration.

Additional work that should be investigated later includes using water for the calibration standard. One should verify the Debye model or establish a modified model for the water used. Resonances of the water should be further investigated including how these affect the calibration process. Additional work is to investigate limits on the electrical length of the system.

In short, Part III has provided a proof-of-concept for a material measurement system that could be used to measure solids, liquids, or gases that merits further investigation.

Part IV

Future Work and Conclusions

Chapter 13

Future Work

13.1 Next Iteration

Results from this dissertation are promising and continued research is merited. For live-fire experiments outside of the lab, work should look to refine transmission measurement techniques. Initially this should involve a further study of antennas, reflectors, and lenses relative to fire size. Setups should look to utilize gas burners and wind protection in order to create large, repeatable flames. Options to create pre-mixed flames and to seed the fuel with trace amounts of other materials, such as alkali salts, should be investigated. Measurement equipment that reduces the time required for to measure one sample should be selected.

The next set of interferometric measurements of flames should refine the mesh and shutter designs. Consideration should be given to measuring at X-band and using some sort of lens for focusing.

A new balun for the two-wire transmission line experimental setup should be created and the calibration method should then be verified further.

13.2 Outstanding Challenges and Questions

Several important questions based on this research remain unanswered. Future work should aim to answer these.

- This research has focused on plasmas in flames with only minimal work that accounted for soot, smoke, and other particulates. Specific studies are needed to answer: how do soot, smoke, and other particulates affect electromagnetic waves when combined with fire-induced plasmas in a house fire? Is this behavior changed if the particulates become negatively charged by mobile electrons attaching to the particulates?
- Air flow and turbulence can affect electromagnetic waves. How does air flow around a fire-induced plasma affect signal propagation?
- How do fire-induced plasmas vary between different fuels?
- At what size does a fire-induced plasma become significant enough to affect propagation?
- How do non-ionizing thermal effects contribute to alter signal propagation?
- For the measurement techniques used, what are the required minimum system specifications and sensitivities?
- To what extent is actual message content from commonly used transmission modes, e. g. P25, conventional trunked radio systems, or Bluetooth, actually affected by fire-induced plasmas?

13.3 Future Directions

This work and other future work may lead to applications beyond locating people trapped in a house. Potential applications include using electromagnetic waves for detecting or extinguish-

ing fires, and evaluating structural stability and fire impingement. For radar units to become standard on the fire ground, prototypes will need to demonstrate a reliable effectiveness. Next, usability studies of units are needed and standards should be developed. Safety of the units for firefighters and for victims that may be scanned by the unit is critical; absorption rates (SAR) and intrinsic safety should be considered. Thermal imaging cameras will not be replaced by radar units in the foreseeable future; therefore, integration of these two units is important so that they may be used effectively together.

Chapter 14

Conclusion

Finding people trapped inside of a burning house is extremely difficult, dangerous, and time consuming. Smoke, heat, unfamiliar floor plans, and possible structural collapse all combine to challenge a firefighter's ability to find a person. Through-wall radar and vital-sign detection radar offer an imaging modality that may be able to help firefighters find victims from outside of a room or even a house; however, electromagnetic (radar) waves can be affected by the weakly-ionized plasma created by a flame. Fundamental understanding of the interactions between electromagnetic waves and fire-induced plasmas is foundational to developing these life saving firefighting technologies. This dissertation describes the investigation of these interactions through basic theory, small- and large-scale fire experiments, and material measurement setups. Results from this research identified fire-induced plasmas from flames using interferometric measurements.

14.1 Fire Experiments

Experiments performed at the Lansing (MI) Fire Department training center measured transmissions through burning cushions. Results showed a significant difference in transmission as

the cushion burned compared to an unlit state. The transmissions had a large difference initially and gradually returned to the unlit state as the cushion was burned. These results are likely due to a combination of fire-induced plasmas and material measurements of the solid mass of the cushion.

Experiments were carried out using propane burners to reduce the possible interaction between electromagnetic waves and the fuel. Plasma-like behavior was not observed in these measurements most likely due to the experimental setup. Refinement of calibration methods should improve future results.

Results from interferometric measurements of flames find plasma electron densities one to two orders of magnitude larger than those found in wildland fire. Measured flames from methanol, sodium chloride solution, or Plexiglass are more representative of house fires than wildland fires. These results therefore represent fire-induced plasmas which could affect fire-fighting search-and-rescue radars.

An additional live-fire experiment was performed to evaluate the effects of fire on transmissions from inside of a burning house. A series of fires were ignited inside of a house and then extinguished. Transmitters at multiple frequencies were placed inside of the house and transmitted through the fire. No significant effects on the transmission strength were observed for the tested fire conditions which were slight to moderate. This means that the transmissions from a firefighter inside of a house with such conditions may not be affected. Because the fire conditions were moderate, it is unknown if severe conditions, such as a flashover, would affect transmissions.

14.2 Two-Wire Transmission Line

A two-wire transmission line and balun were investigated for material measurement purposes. The initial motivation for this design was to measure and characterize flames in the laboratory.

A model of the two-wire transmission line was presented as well as a calibration procedure and an experimental design. A calibration method was developed which showed moderate success in experiments. Calibration standards and the models for these standards can be refined and improved using the measured results.

14.3 Summary

This work presented live-fire experiments which investigated the interaction between electromagnetic waves and fire-induced plasmas. Plasmas were observed in interferometric measurements of live-fire experiments. Continued refinement of experimental designs could provide additional data in this area. A proof-of-concept, two-wire transmission line used for material measurements showed promising results that could be improved with a refined calibration technique. This work has explored an open problem in electromagnetics with live-saving applications to the fire service. Results from this work warrant additional study in this area to improve techniques, with the goal of putting search-and-rescue radars into the hands of firefighters.

APPENDICES

Appendix A

Network Parameters

A metric is needed to evaluate the performance of a device or to compare it to similar devices. A simple, linear circuit may have a voltage-current curve for this purpose. It is difficult to define these values for the fields encountered in microwave devices. Different types of parameters are defined for microwave devices to solve this problem. These include scattering (S), transmission (T or scattering-transfer), ABCD, impedance (Z), and admittance (Y) parameters.

For a more in-depth discussion than what is presented below, the reader is directed to Ramo, Whinnery, and Van Duzer [3, chap. 11]; Pozar [4, chap. 4]; Hewlett-Packard Application Note AN-154 [122] and Wikipedia [123].

A.1 Basic Definitions

A collection of inter-connected devices or components is commonly called a network. To characterize the performance of the network, we may describe the input-output relationship in terms of waves (incident and reflected) or in terms of voltages and currents for a lumped, equivalent circuit [3].

Regardless of which description method we choose, we wish to represent the relationship between inputs and outputs, which is defined at or between ports. A port is a place through which electrical energy enters or leaves a circuit or network. Examples include a waveguide aperture, battery terminals, leads of a resistor, and an SMA connector.

To analyze a network, we start by defining the network according to the rules below [3, p. 532]:

1. voltage, V , and current, I , are proportionally defined to the transverse electric and magnetic fields of the mode, respectively;
2. the average power is $\text{Re}\{VI^*/2\}$;
3. A characteristic impedance for the mode of the incident wave is defined as $Z_0 = V/I$.

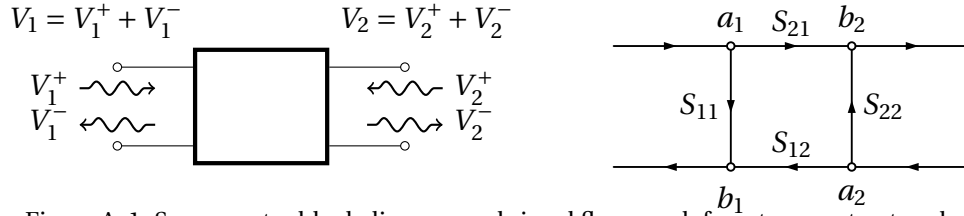


Figure A.1: S-parameter block diagram and signal flow graph for a two-port network.

Note

Remember that voltage, V , and current, I , are complex values and hence quantities derived from these are also complex.

With this understanding, we can define the various parameters used to describe and characterize a network.

A.2 S-Parameters

Scattering parameters, usually referred to as S-parameters, represent the properties of a microwave network in terms of waves. The voltage at a given port is defined as the sum of an incident and a reflected wave, i. e.

$$V = V_+ + V_- \quad (\text{A.1})$$

as shown in Figure A.1 where the + subscript denotes the incident wave and the – subscript denotes the reflected wave. The incident and reflected waves are normalized by the characteristic impedance Z_0 , which is the same for all ports, to

$$a = \frac{V_+}{\sqrt{Z_0}}, \quad \text{and} \quad (\text{A.2})$$

$$b = \frac{V_-}{\sqrt{Z_0}}, \quad (\text{A.3})$$

respectively [3, pp. 539–541]. We define an S-parameter as

$$S_{ij} = \frac{b_j}{a_i} \quad (\text{A.4})$$

where i is the input port and j is the output port when all ports are terminated by a load equal to the characteristic impedance. The indices i and j may be for the same port, and are less than or equal to the number of ports, n , of the network. We may write this relation for the n -port network as a system of n equations,

$$[\mathbf{b}] = [\mathbf{S}] [\mathbf{a}]. \quad (\text{A.5})$$

The common two-port network is therefore described by the system [3, pp. 539–541]

$$\begin{bmatrix} b_1 \\ b_2 \end{bmatrix} = \begin{bmatrix} S_{11} & S_{12} \\ S_{21} & S_{22} \end{bmatrix} \begin{bmatrix} a_1 \\ a_2 \end{bmatrix}. \quad (\text{A.6})$$

Caution

S-parameters depend upon the characteristic impedance, Z_0 , used for normalization. It is important to know what this value is since the incorrect value can drastically change interpretation of what the S-parameter represents.

A.3 T-Parameters

Transmission parameters, also known as scattering-transfer parameters or T-parameters, express the wave quantities at one port as a linear relationship to the wave quantities at the other port. Ramo, Whinnery, Van Duzer define the system as [3, p. 541]

$$\begin{bmatrix} b_2 \\ a_2 \end{bmatrix} = \begin{bmatrix} T_{11} & T_{12} \\ T_{21} & T_{22} \end{bmatrix} \begin{bmatrix} a_1 \\ b_1 \end{bmatrix}. \quad (\text{A.7})$$

If the port numbers are switched, this system becomes

$$\begin{bmatrix} a_1 \\ b_1 \end{bmatrix} = \begin{bmatrix} T_{11} & T_{12} \\ T_{21} & T_{22} \end{bmatrix} \begin{bmatrix} b_2 \\ a_2 \end{bmatrix}. \quad (\text{A.8})$$

as done for the RF Toolbox in MATAB [124, see `s2t()`]. We may also define it as

$$\begin{bmatrix} b_1 \\ a_1 \end{bmatrix} = \begin{bmatrix} T_{11} & T_{12} \\ T_{21} & T_{22} \end{bmatrix} \begin{bmatrix} a_2 \\ b_2 \end{bmatrix}. \quad (\text{A.9})$$

This system is used in the Hewlett-Packard (Agilent/Keysight) Application note number AN-154 [122], Wikipedia [123], and Scikit-RF [125].

Caution

Be aware of the different definitions of T-parameters and understand which one you are (or your software is) using. It is probably better to share network information as S-parameters and convert to/from T-parameters for intermediary calculations.

Relations for converting between S-parameters and T-parameters are given in Table A.1.

A.4 Other Parameters

Besides S- and T-parameters, one may encounter Z-, Y-, and ABCD parameters. Z-parameters or impedance parameters are defined as

$$[\mathbf{V}] = [\mathbf{Z}] [\mathbf{I}]. \quad (\text{A.16})$$

Using Eqn. (A .7) definition

$$[\mathbf{T}] = \begin{bmatrix} \frac{S_{12}S_{21}-S_{11}S_{22}}{S_{12}} & \frac{S_{22}}{S_{12}} \\ \frac{-S_{11}}{S_{12}} & \frac{1}{S_{12}} \end{bmatrix} \quad [\mathbf{S}] = \begin{bmatrix} \frac{-T_{21}}{T_{22}} & \frac{1}{T_{22}} \\ \frac{T_{11}T_{22}-T_{12}T_{21}}{T_{22}} & \frac{T_{22}}{T_{22}} \end{bmatrix} \quad (\text{A .10}) \quad (\text{A .11})$$

Using Eqn. (A .8) definition

$$[\mathbf{T}] = \begin{bmatrix} \frac{1}{S_{21}} & \frac{-S_{22}}{S_{21}} \\ \frac{S_{11}}{S_{21}} & \frac{S_{12}S_{21}-S_{11}S_{22}}{S_{21}} \end{bmatrix} \quad [\mathbf{S}] = \begin{bmatrix} \frac{T_{21}}{T_{11}} & \frac{T_{11}T_{22}-T_{12}T_{21}}{T_{11}} \\ \frac{1}{T_{11}} & \frac{-T_{12}}{T_{11}} \end{bmatrix} \quad (\text{A .12}) \quad (\text{A .13})$$

Using Eqn. (A .9) definition

$$[\mathbf{T}] = \begin{bmatrix} \frac{S_{12}S_{21}-S_{11}S_{22}}{S_{21}} & \frac{S_{11}}{S_{21}} \\ \frac{-S_{22}}{S_{21}} & \frac{1}{S_{21}} \end{bmatrix} \quad [\mathbf{S}] = \begin{bmatrix} \frac{T_{12}}{T_{22}} & \frac{T_{11}T_{22}-T_{12}T_{21}}{T_{22}} \\ \frac{1}{T_{22}} & \frac{-T_{21}}{T_{22}} \end{bmatrix} \quad (\text{A .14}) \quad (\text{A .15})$$

Table A .1: Relations between S-parameters and T-parameters [3, p. 541] and [123].

These coefficients represent the impedance relationship at and between ports. Similarly, Y-parameters or admittance parameters represent the admittance relationship at and between ports. These are defined by the system

$$[\mathbf{I}] = [\mathbf{Y}] [\mathbf{V}]. \quad (\text{A.17})$$

Finally, ABCD parameters provide a relationship between the inputs and outputs of a two-port network,

$$\begin{bmatrix} V_1 \\ I_1 \end{bmatrix} = \begin{bmatrix} A & B \\ C & D \end{bmatrix} \begin{bmatrix} V_2 \\ -I_2 \end{bmatrix} \quad (\text{A.18})$$

Relatively simple expressions exist to transform data from one type of parameters to the other. A table is given on page 192 of Pozar [4] while expressions are scattered throughout Chapter 11 of Ramo, Winnery, and Van Duzer [3].

Appendix B

Cable and Connector Information

Table B .1: Cable numbering scheme, lengths, connector type, gender, and label.

| Serial | Date | End 1 | | | End 2 | | | Label | |
|--------|------------|-------|-----|--------|-------|-----|--------|----------------|------------------|
| | Labeled | Type | Sex | Length | Type | Sex | Line 1 | Line 2 | |
| 001 | 2013-05-17 | SMA | mr | 37 | in | SMA | mr | 2013-05-17-001 | SMA-mr-37-SMA-mr |
| 002 | 2013-05-17 | SMA | m | 120 | in | SMA | m | 2013-05-17-002 | SMA-m-120-SMA-m |
| 003 | 2013-05-17 | SMA | m | 120 | in | SMA | m | 2013-05-17-003 | SMA-m-120-SMA-m |
| 004 | 2013-05-17 | SMA | m | 120 | in | SMA | m | 2013-05-17-004 | SMA-m-120-SMA-m |
| 005 | 2013-05-17 | SMA | m | 48 | in | SMA | m | 2013-05-17-005 | SMA-m-48-SMA-m |
| 006 | 2013-05-17 | SMA | m | 48 | in | SMA | m | 2013-05-17-006 | SMA-m-48-SMA-m |
| 007 | 2013-05-17 | SMA | m | 48 | in | SMA | m | 2013-05-17-007 | SMA-m-48-SMA-m |
| 008 | 2013-05-17 | SMA | m | 48 | in | SMA | m | 2013-05-17-008 | SMA-m-48-SMA-m |
| 009 | 2013-05-17 | SMA | m | 48 | in | SMA | m | 2013-05-17-009 | SMA-m-48-SMA-m |
| 010 | 2013-05-17 | SMA | m | 48 | in | SMA | m | 2013-05-17-010 | SMA-m-48-SMA-m |
| 011 | 2013-05-17 | SMA | m | 48 | in | SMA | m | 2013-05-17-011 | SMA-m-48-SMA-m |
| 012 | 2013-05-17 | SMA | m | 48 | in | SMA | m | 2013-05-17-012 | SMA-m-48-SMA-m |
| 013 | 2013-05-17 | SMA | m | 12 | ft | SMA | m | 2013-05-17-013 | SMA-m-12-SMA-m |
| 014 | 2013-05-17 | SMA | m | 36 | in | SMA | m | 2013-05-17-014 | SMA-m-36-SMA-m |
| 015 | 2013-05-18 | N | m | 96 | in | N | m | 2013-05-18-015 | N-m-96-N-m |
| 016 | 2013-05-18 | N | m | 12 | ft | N | m | 2013-05-18-016 | N-m-12-N-m |
| 017 | 2013-05-18 | N | m | 30 | ft | N | m | 2013-05-18-017 | N-m-30-N-m |
| 018 | 2013-05-18 | N | m | 12 | ft | N | m | 2013-05-18-018 | N-m-12-N-m |
| 019 | 2013-05-18 | N | m | 15 | ft | N | m | 2013-05-18-019 | N-m-15-N-m |
| 020 | 2013-05-18 | N | m | 60 | ft | N | m | 2013-05-18-020 | N-m-60-N-m |
| 021 | 2013-05-18 | N | m | 14 | in | N | m | 2013-05-18-021 | N-m-14-N-m |
| 022 | 2013-05-18 | N | m | 24 | in | N | m | 2013-05-18-022 | N-m-24-N-m |
| 023 | 2013-05-18 | N | m | 27 | in | N | m | 2013-05-18-023 | N-m-27-N-m |
| 024 | 2013-05-18 | N | m | 26 | in | N | m | 2013-05-18-024 | N-m-26-N-m |
| 025 | 2013-05-18 | N | m | 40 | in | N | m | 2013-05-18-025 | N-m-40-N-m |
| 026 | 2013-05-18 | N | m | 27 | in | N | m | 2013-05-18-026 | N-m-27-N-m |
| 027 | 2013-05-18 | N | m | 39 | ft | N | m | 2013-05-18-027 | N-m-39-N-m |
| 028 | 2013-05-18 | N | m | 60 | in | N | m | 2013-05-18-028 | N-m-60-N-m |
| 029 | 2013-05-18 | N | m | 72 | in | N | m | 2013-05-18-029 | N-m-72-N-m |
| 030 | 2013-05-18 | N | m | 72 | in | N | m | 2013-05-18-030 | N-m-72-N-m |
| 031 | 2013-05-18 | N | m | 72 | in | N | m | 2013-05-18-031 | N-m-72-N-m |
| 032 | 2013-05-18 | N | m | 72 | in | N | m | 2013-05-18-032 | N-m-72-N-m |
| 033 | 2013-05-18 | N | m | 72 | in | N | m | 2013-05-18-033 | N-m-72-N-m |
| 034 | 2013-05-18 | N | m | 72 | in | N | m | 2013-05-18-034 | N-m-72-N-m |
| 035 | 2013-05-18 | N | m | 72 | in | N | m | 2013-05-18-035 | N-m-72-N-m |
| 036 | 2013-05-18 | N | m | 12 | ft | N | m | 2013-05-18-036 | N-m-12-N-m |
| 037 | 2013-05-18 | SMA | m | 120 | in | SMA | m | 2013-05-18-037 | SMA-m-120-SMA-m |
| 038 | 2013-05-18 | SMA | m | 120 | in | SMA | m | 2013-05-18-038 | SMA-m-120-SMA-m |
| 039 | 2013-05-18 | SMA | m | 120 | in | SMA | m | 2013-05-18-039 | SMA-m-120-SMA-m |
| 040 | 2013-05-18 | SMA | m | 72 | in | SMA | m | 2013-05-18-040 | SMA-m-72-SMA-m |
| 041 | 2013-05-18 | SMA | m | 60 | in | SMA | f | 2013-05-18-041 | SMA-m-60-SMA-f |
| 042 | 2013-05-18 | | 7 . | 48 | in | | 7 . | 2013-05-18-042 | 7.-48-7.- |
| 043 | 2013-05-18 | | 7 . | 48 | in | | 7 . | 2013-05-18-043 | 7.-48-7.- |
| 044 | 2013-05-18 | | 7 . | 24 | in | | 7 . | 2013-05-18-044 | 7.-24-7.- |
| 045 | 2013-05-18 | | 7 . | 24 | in | | 7 . | 2013-05-18-045 | 7.-24-7.- |
| 046 | 2013-05-27 | SMA | m | 120 | in | SMA | m | 2013-05-27-046 | SMA-m-120-SMA-m |

Table B .2: Results from gaging the assorted connectors in the lab.

| Number | Type | 1 | 2 | 3 | Average x0.0001" | Male Color ^{1,2} | Female Inspection | Female Color ^{3,4} |
|--------|----------|-------|-------|-------|---------------------|------------------------------|----------------------|--------------------------------|
| 1 | SMA | -8 | -8 | -8 | -8.00 | GREEN | GOOD | GREEN |
| 2 | SMA | -15 | -15 | -15 | -15.00 | GREEN | TALL | RED |
| 3 | SMA | -26.5 | -26.5 | -26.5 | -26.50 | GREEN | GOOD | GREEN |
| 4 | SMA | -36 | -36 | -36.5 | -36.17 | RED | SPACE | RED |
| 5 | 3.5 | -11 | -11 | -11 | -11.00 | GREEN | GOOD | GREEN |
| 6 | 3.5 | -18 | -17 | -20 | | | | |
| | | -18 | -18 | -19 | -18.33 | GREEN | GOOD | GREEN |
| 7 | SMA | -26.5 | -27 | -27 | | | | |
| | | -27 | | | -26.88 | GREEN | GOOD | GREEN |
| 8 | SMA | -40 | -40 | -39.5 | -39.83 | RED | GOOD | GREEN |
| 9 | SMA | -49 | -48.5 | -48 | -48.50 | RED | SPACE | RED |
| 10 | SMA | -29 | -30 | -30 | -29.67 | GREEN | GOOD | GREEN |
| 11 | SMA | -32 | -32 | -32 | -32.00 | RED | BAD | RED |
| 12 | SMA | -30 | -30 | -30 | -30.00 | GREEN | GOOD | GREEN |
| 13 | SMA | -50 | -50 | < | -50.00 | RED | GOOD | GREEN |
| 14 | SMA | -14 | -14 | -14 | -14.00 | GREEN | GOOD | GREEN |
| 15 | SMA | -34.5 | -35 | -34 | -34.50 | RED | GOOD | GREEN |
| 16 | SMA | -5 | -7 | -4 | -5.33 | GREEN | n/a | |
| | SMA | 8 | 9 | 10 | 9.00 | RED | n/a | |
| 17 | SMA | > | | > | | RED | n/a | |
| | SMA | 32 | -32 | -32 | -10.67 | GREEN | n/a | |
| 18 | 3.5 | 42 | -43 | -43 | -14.67 | GREEN | n/a | |
| 19 | 3.5 to 7 | 14 | -15 | -15 | -5.33 | GREEN | n/a | |
| HP | 3.5 | 11 | -10 | -10 | -3.00 | GREEN | n/a | |
| | 3.5 | 4 | -4 | -4 | -1.33 | GREEN | n/a | |

Notes

1. Green is assigned if the connector has a recession between 0.0" and 0.0030"
2. Red is assigned if the connector protrudes at all or has a recession greater than 0.0030"
3. Green is assigned if the female connector appears to be in good condition with no defects
4. Red is assigned if there are any defects in the female connector
5. If a connector takes more than one line but only has one average, more than 3 measurements were made

6. If a connector takes up more than one line but has multiple averages, has multiple male ends

#4 Already Marked

#1-#4 were from the red gage box

#5, #6 were new from the bag

#1 is a 10dB attenuator

#10 is a 20dB attenuator

#14 is an right angle connector

Table B .3: Results of gaging the cables provided with the Satimo system.

| Number | Type | 1 | 2 | 3 | Average x0.0001" | Male Color ^{1,2} | Marked |
|--------|------|------|------|------|---------------------|------------------------------|--------|
| 50 ohm | SMA | -100 | -100 | -100 | -100.00 | RED | |
| 3L | SMA | -100 | -100 | -100 | -100.00 | RED | |
| 3R | SMA | -48 | -48 | -48 | -48.00 | RED | |
| 4L | SMA | -100 | -100 | -100 | -100.00 | RED | |
| 4R | SMA | -49 | -49 | -49 | -49.00 | RED | |
| 5L | SMA | -47 | -46 | -46 | -46.33 | RED | |
| 5R | SMA | -100 | -100 | -100 | -100.00 | RED | |
| 6L | SMA | 15 | 15 | 15 | 15.00 | RED | x |
| 6R | SMA | -37 | -35 | -35 | -35.67 | RED | |
| 7L | SMA | -46 | -47 | -47 | -46.67 | RED | |
| 7R | SMA | -25 | -26 | -26 | -25.67 | GREEN | x |
| 8L | SMA | -5 | -6 | -6 | -5.67 | GREEN | x |
| 8R | SMA | 41 | 42 | 42 | 41.67 | RED | x |

Notes

1. Green is assigned if the connector has a recession between 0.0" and 0.0030"

2. Red is assigned if the connector protudes at all or has a recession greater than 0.0030"

3. A measurement of -100 signifies that the length is less than -50, the lowest value on the gage

4. L and R indicate the left or right end of the cable when holding the cable so that the label is properly oriented

Measured by: Andrew Temme
Date: 6/25/2012

Table B .4: Results of gaging the 85052D calibration kit.

| Standard | Sex | Serial Num. | 1 | 2 | 3 | Average x0.0001" |
|--------------------------------|-----|-------------|------|----|------|---------------------|
| Open | M | 14872 | -1.5 | -2 | -1 | -1.50 |
| Short | M | 13864 | -1.5 | -2 | -2 | -1.83 |
| Broadband Load | M | 11011 | -1.5 | -2 | -2 | -1.83 |
| Male to Male, top ¹ | M | 79839 | -4 | -4 | -4.5 | -4.17 |
| Male to Male, bottom | M | 79839 | -4 | -3 | -4 | -3.67 |
| Male to Female | M | 80251 | -7 | -6 | -6.5 | -6.50 |

Notes

1. Top refers to the side on top when properly reading the serial number.

Appendix C

Further details on Sample Trough

The 57 in long metal trough (see Figure C .1) was fabricated from two pieces of aluminum that were joined together as shown in Figure C .2. These two pieces were used because they were obtained for little cost from the MSU Surplus store. The bolt head in the center of the picture holds the two pieces together. The bottom of the bolt and the nut (both unshown) cause the trough to tilt when placed on a flat surface. This was not a problem during the experiment because the trough was always longer than any shelf on which it was set. The gap between each vertical fin on the individual parts is 1 inch on center; however, the width and fillet of the fin mean that the actual width is smaller. The two pieces needed to be joined in order to create a gap larger than 1 inch, hence the initial need for shims. The other bolts visible in Figure C .2 were originally used for aligning samples using strings until a laser level was purchased for the lab. A close-up view of the front-center of the trough is shown in Figure C .3 including the center-line and value of $28\frac{1}{2}$ in. Marks were placed 12 in off center to use in aligning the commonly-sized, 24 in by 24 in samples. The right mark is visible in the top-down view of Figure C .4.

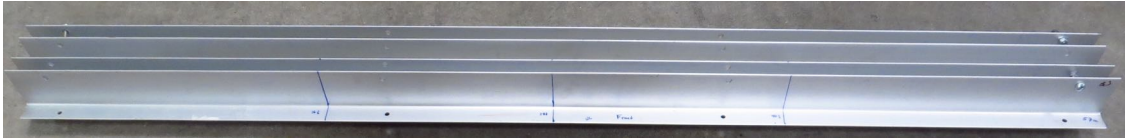


Figure C .1: Metal trough used to hold samples.

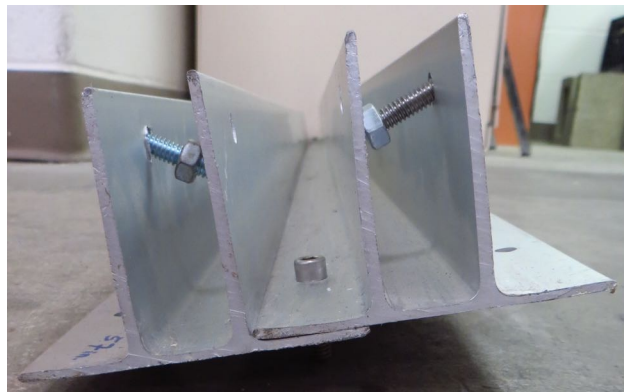


Figure C .2: Side view of the metal trough.



Figure C .3: Center view of the trough showing alignment cue.



Figure C .4: Top-down view of the trough showing alignment marks.

Appendix D

Weather Records

This appendix contains weather records from various experiments.

D .1 May 30, 2013—Experiment at LFD Training Facility

These data correspond to the experiment described in Chapter 4 that occurred on May 30, 2013 at the Lansing Fire Department's Training Facility. Table D .1 shows the observed temperature and humidity as was recorded at the experiment site. Table D .2 shows the weather reported by NOAA/NWS at the Capitol City Airport on the north side of Lansing. No precipitation was recorded in the reported period; therefore, this column has been removed from the table. The wind chill and heat index were report as NA and have been removed from the table.

Table D .1: Observed temperature and humidity at the site of the experiment.

| Time | Temp/°F | Humidity/% | Notes |
|-------|---------|------------|--------------------------------------|
| 9:45 | 77.0 | 64 | |
| 9:53 | 77.8 | 61 | |
| 10:03 | 78.5 | 61 | cal |
| 10:25 | 80.1 | 59 | |
| 10:35 | 80.5 | 59 | |
| 10:46 | 81.5 | 57 | |
| 10:54 | 81.9 | 58 | thermometer moved to top of analyzer |
| 10:57 | 81.7 | 56 | |
| 11:00 | 81.7 | 57 | |
| 11:05 | 81.4 | 57 | plate, empty |
| 11:13 | 82.3 | 58 | plexi |
| 11:23 | 83.0 | 56 | beginning of burn 1 |
| 11:36 | 85.0 | 53 | end of burn 1 |
| 11:50 | 84.4 | 54 | empty |
| 11:58 | 85.3 | 52 | plate |
| 12:03 | 85.5 | 52 | beginning of burn 2 |
| 12:21 | 86.8 | 50 | end of burn 2 |
| 12:51 | 87.7 | 49 | cal near |
| 12:58 | 87.7 | 48 | plate |
| 13:02 | 87.8 | 48 | plexi |
| 13:07 | 87.7 | 48 | beginning of burn 3 |
| 13:20 | 88.6 | 47 | |
| 13:25 | 88.0 | 46 | end of burn 3 |
| 13:33 | 87.8 | 48 | 3 with carboard |
| 13:49 | 87.3 | 49 | |
| 13:51 | 87.5 | 49 | end of 3 with cardboard |
| 13:53 | 87.5 | 49 | burn 3 with small cardboard |
| 14:00 | 88.4 | 48 | |
| 14:07 | 88.7 | 47 | |
| 14:15 | 88.9 | 45 | last plate |
| 14:22 | 89.5 | 45 | |
| 14:34 | 90.0 | 44 | end |
| 14:41 | 89.1 | 44 | |

Table D .2: Weather observations from NOAA/NWS at Capitol City Airport in Lansing for May 30, 2013.

| Time (edt) | Wind (mph) | Vis. (mi.) | Weather | Sky Cond. | Temperature (°F) | | | | Relative Humidity | Pressure | |
|---------------|---------------|---------------|---------------|---------------|------------------|------|------|------|----------------------|-------------------|-------------------|
| | | | | | Air | Dwpt | Max. | Min. | | altimeter (in) | sea level (mb) |
| 6:53 | S 7 | 10 | Fair | CLR | 69 | 60 | | | 73% | 30.03 | 1016.4 |
| 7:53 | S 9 | 10 | Fair | CLR | 71 | 62 | 71 | 66 | 73% | 30.04 | 1016.7 |
| 8:53 | S 13 | 10 | Partly Cloudy | FEW070 SCT090 | 74 | 64 | | | 71% | 30.04 | 1016.8 |
| 9:53 | S 9 G 18 | 10 | Fair | CLR | 78 | 64 | | | 62% | 30.03 | 1016.4 |
| 10:53 | S 12 | 10 | Fair | CLR | 80 | 66 | | | 62% | 30.03 | 1016.3 |
| 11:53 | S 17 | 10 | Partly Cloudy | SCT039 | 82 | 66 | | | 58% | 30.02 | 1015.9 |
| 12:53 | SW 16 G 24 | 10 | Partly Cloudy | SCT041 SCT110 | 84 | 67 | | | 57% | 30.01 | 1015.7 |
| 13:53 | SW 16 G 25 | 10 | Partly Cloudy | SCT043 | 84 | 67 | 85 | 71 | 57% | 30 | 1015.3 |
| 14:53 | SW 15 G 25 | 10 | A Few Clouds | FEW047 | 85 | 65 | | | 51% | 29.98 | 1014.7 |
| 15:53 | S 15 G 26 | 10 | Partly Cloudy | SCT049 | 85 | 64 | | | 50% | 29.97 | 1014.4 |

Appendix E

Site Safety Plan

E.1 LFD Training Facility

SITE SAFETY PLAN
LFD Training Academy 3015 Alpha St Lansing MI
Lansing Fire Department
Michigan State University—Electrical Engineering

MSU Radar Experiment
May 30, 2013

Recognized Safety & Health Hazards

Live Fire Exercise

Trip Hazards

Remediation Method

Standard Fire Operations

Protocols/Firefighter PPE

Hazard marking

Emergency Action Plan

In the event an employee or researcher becomes injured or incapacitated the highest ranking LFD officer will immediately take control of the operation and summon the appropriate assistance from public safety agencies number 911 or Radio Channel LFD MAIN.

Injuries

Employees will follow organizational “workplace injuries” procedures for reporting and documentation. All incidents of injuries on LFD property will be reported to the LFD Chief of Training 517-230-3451 as soon as practical and to MSU if appropriate.

Authority

It is the responsibility of the lead researcher and highest ranking LFD officer to brief and enforce this plan during the duration of the experiment.

Prepared by: Andrew Temme, MSU— Electrical Engineering, May 15, 2013

Approved by: _____

Appendix F

Selected Pages from Laboratory Notebook 00010

00010 - 7
 BOOK PAGE

TITLE ORCBS Burn

Continued from page 8/8/13

PROJECT

| Time | Temp °F | Hum % |
|------|---------|-------|
| 1133 | 80.6 | 49 |
| 1152 | 82.1 | 45 |
| 1158 | 82.1 | 42 |

burn 2 - level 4
- bad timing

burn 3 - after driver temp

| | Temp °F | Hum % |
|---------|---------|-------|
| 1228 B1 | 80.3 | 44 |
| 1242 B2 | 80.8 | 44 |
| 1257 B3 | 83.3 | 40% |

P1 003 - 039
P2 040 - 037

P2 13' 1" P1
 44"
 50 1/2"
 60 1/2"
 89"
 Looking South
 89
 - 60.5
 28.5 width

think 013 may have problems

SIGNATURE *Andrew...*

DISCLOSED TO AND UNDERSTOOD BY

DATE 8/8/13

PROPRIETARY INFORMATION

Continued to page /

Figure F.1: Laboratory Notebook 00011:7

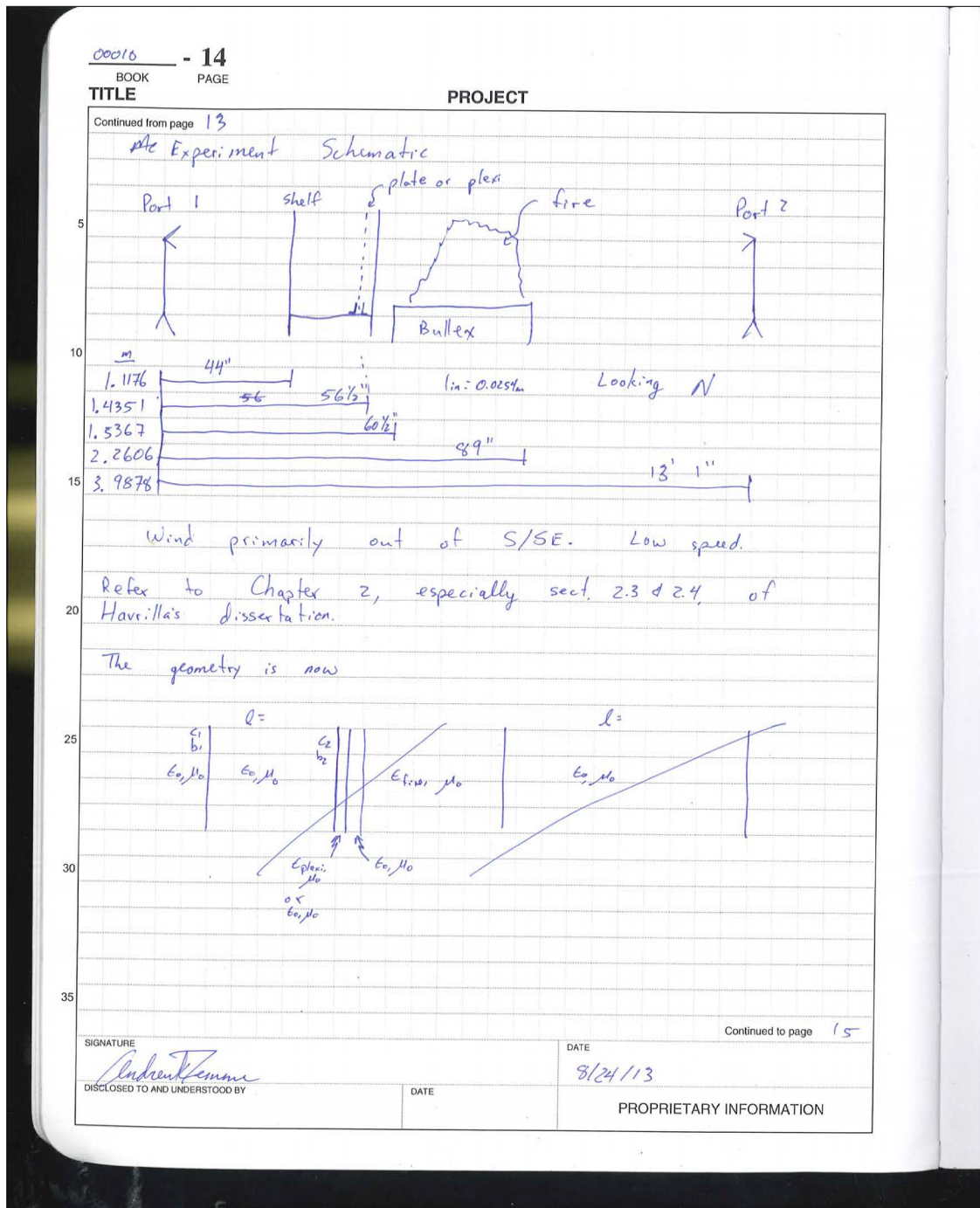


Figure F.2: Laboratory Notebook 00011:14

PROJECT

Continued from page 1

5

Diagram illustrating the flow of air and flame through a plate, showing the relationship between air flow rate (l) and flame length (l).

The diagram is divided into three sections by vertical lines:

- Left Section:** Labeled "air". It shows a vertical line with an arrow pointing left. The air flow rate is given as $l = 1.4351$.
- Middle Section:** Labeled "plate" and "flame". It shows a vertical line with an arrow pointing up. The flame length is given as $l = 0.7239$. Below the plate, the air flow rate is given as $l = 0.072$.
- Right Section:** Labeled "air". It shows a vertical line with an arrow pointing right. The air flow rate is given as $l = 1.7272$.

Calibration/Correction of measured data

$$F_x = \frac{\text{Meas} - \text{Plate}}{\text{Empty} - \text{Plate}}$$

This moves the p first data to the front of the plate.
So our data now has $k=0$ for first part.

Now have

| | | | | |
|----------------|----------------|--------------------|--------------------|-----------------|
| plexi air | air | flame or air | air bo shift | air bo bo |
| c_2 b_2 | c_3 b_3 | c_4 b_4 | c_5 b_5 | c_6 b_6 |
| 1 | 2 | 3 | | |

Total length: 2.8702m
2.5527

$$N=3$$

4 interfaces

$$N = 9$$

5 interfaces

(kinda actually 4
but to make matching
Havrilla w/ $\Delta=0$ are larger
at end easier)

Continued to page 16

SIGNATURE

DISCLOSED TO AND UNDERSTOOD BY

DATE _____

8/24/13

DATE _____

PROPRIETARY INFORMATION

Figure F.3: Laboratory Notebook 00011:15

Continued from page 15

Actually have two systems

$$\begin{array}{|c|c|} \hline \text{plexi} & \text{air} \\ \hline l=0.0254 & l=\pm 2.5273 \\ \hline \end{array} \rightarrow \begin{array}{|c|c|c|} \hline \text{air} & \text{plexi} & \text{air} \\ \hline l=0 & l=0.0254 & l=2.5273 \\ \hline \end{array}$$

$$\begin{array}{|c|c|c|} \hline \text{air} & \text{flame} & \text{air} \\ \hline 0.1016 & 0.7239 & 1.7272 \\ \hline \end{array}$$

Use For plexi, use the 2nd option so that system is 3 layers.

A. parameters calculated using

$$\begin{bmatrix} A_{11}^{sys} & A_{12}^{sys} \\ A_{21}^{sys} & A_{22}^{sys} \end{bmatrix} = \frac{N+1}{i!} \frac{1}{T_i} \begin{bmatrix} e^{\gamma_i l_i} & R_{ie}^{-\gamma_i l_i} \\ R_{ie}^{\gamma_i l_i} & e^{-\gamma_i l_i} \end{bmatrix}$$

$$R_i = \frac{Z_i - Z_{i-1}}{Z_i + Z_{i-1}}$$

$$T_i = 1 + R_i$$

$$\gamma_i = j\beta = j\omega \sqrt{\epsilon \mu_r} / c$$

is this acceptable since $k = \alpha + j\beta$?

$$Z_i = \sqrt{\frac{\mu_i}{\epsilon_i}} = Z_0 \sqrt{\frac{\mu_{ri}}{\epsilon_{ri}}}$$

Assume $\mu_r = 1$ & layers

SIGNATURE

Andrew Jensen

DATE

8/24/13

DISCLOSED TO AND UNDERSTOOD BY

DATE

PROPRIETARY INFORMATION

Continued to page

Figure F.4: Laboratory Notebook 00011:16



| TITLE | | PROJECT | BOOK | PAGE |
|---|--|-------------------------|-------|------|
| Weekly Meeting | | | 00010 | -111 |
| Continued from page 10/2/13 | | | | |
| NDA/CDA | | | | |
| update on phone call | | | | |
| fuel updates & experiment ideas - benchtop & free space | | | | |
| w/ controlled wildland burns - Rothwell's wife may know | | | | |
| what about power receiver for attenuation measurements | | | | |
| drift | | | | |
| two wire balun design | | | | |
| scaling position/time domain | | | | |
| <div style="border: 1px solid black; padding: 5px;"> 8510C Fan Problems 10/7/13 </div> | | | | |
| The fan on the rack is making noise. Has been for awhile. Believe it is the right one when looking at the front | | | | |
| Rack: 85043C Serial: 3312A00542 | | | | |
| fan: 5.7 m ³ /min or 200 ft ³ /min (don't know if for one or both) | | | | |
| Continued to page 112 | | | | |
| SIGNATURE | | DATE | | |
|  | | 10/7/13 | | |
| DISCLOSED TO AND UNDERSTOOD BY | | PROPRIETARY INFORMATION | | |

Figure F .5: Laboratory Notebook 00011:111

TITLE PROJECT

Continued from page 111

| Replacement Fans | | | |
|---|--|-------------------------|--------------|
| | Description | Qty | # |
| 5 | Extractor Fan Assembly - 100-120 V | 1 | C 2786-60024 |
| | OR | | |
| | Extractor Fan Assembly - 200-240 V | 1 | C 2786-60005 |
| | Mounting Screw (Fan Assembly) | 1 | 2680-0278 |
| | Fan Tube - Axial Extractor - 100-120 V | 2 | 3160-0378 |
| | OR | | |
| 10 | Fan Tube - Axial Extractor - 200-240 V | 2 | 3160-0228 |
| Information in the Test Sets & Accessories binder | | | |
| 15 | On Agilent's site, extractor fan for racks | | |
| | E447042 Extractor Fan, 100-120 V (200 cfm) | #288 | 7 wk lead |
| | Fan itself | | |
| 20 | Fan Tube AXIAL 115-VAC 120-CFM AI | | |
| | 3160-0378 #137 | | 11 in stock |
| | Jamco | | |
| 25 | Fan, 115 VAC, 112 CFM, 120x120x38, Ball bearings bearings, Terminals, UI/Csa/Tw/Ce | | |
| | Part # 2725931 | | |
| 30 | mfg: common wealth | | |
| | # FP-108-1 | | |
| | # 10.95 | | |
| 35 | Agilent case # 5466547670 | | |
| SIGNATURE | | DATE | |
|  | | 10/7/13 | |
| DISCLOSED TO AND UNDERSTOOD BY | | DATE | |
| | | PROPRIETARY INFORMATION | |

Continued to page 114

Figure F.6: Laboratory Notebook 00011:112

00010

- 114

BOOK

PAGE

TITLE

8510C Fan problems (cont.)

PROJECT

Continued from page 112 10/8/13

One screw to remove fan assembly

T25

Two screws per fan smaller than T-20

Fans cleaned fans. no improvement

ch fan:

Papst

Type 4600N

115V ~ 50/60Hz 20W

2P

US-PAT-4221546

Assy by Papst in Germany 5.97

Papst-motoren

D-78106 St. Georgen

Papst 4600N

available listed on their website

available at Newark, Mouser, Digkey for ~\$35.

in stock

SIGNATURE

Antony Zema

DATE

10/8/13

DISCLOSED TO AND UNDERSTOOD BY

DATE

PROPRIETARY INFORMATION

Continued to page

Figure F.7: Laboratory Notebook 00011:114

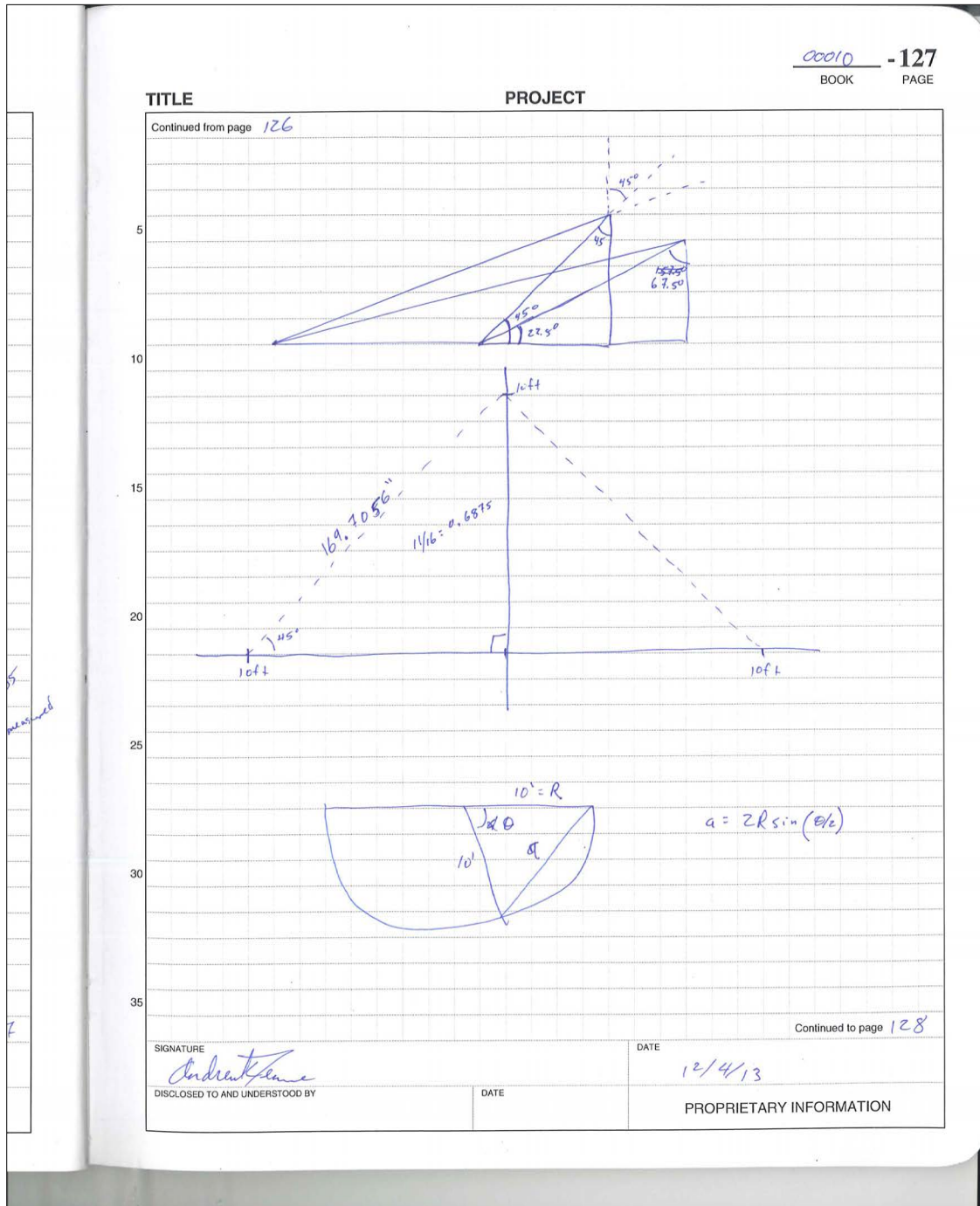


Figure F .9: Laboratory Notebook 00011:127

TITLE

PROJECT

Continued from page 127

R 10

Theta

a 0 0

Theta

60 a 10

Theta

120 17.32051

1 0.174531

61 10.15077

121 17.40711

2 0.349048

62 10.30076

122 17.49239

3 0.523559

63 10.44997

123 17.57634

4 0.69759

64 10.59839

124 17.65895

5 0.872388

65 10.74599

125 17.74022

6 1.046719

66 10.89374

126 17.82010

7 1.220971

67 11.03974

127 17.89859

8 1.395129

68 11.18386

128 17.97598

9 1.569162

69 11.32612

129 18.05171

10 1.743115

70 11.46753

130 18.12616

11 1.916915

71 11.60809

131 18.19933

12 2.090559

72 11.75571

132 18.27091

13 2.264054

73 11.89666

133 18.3412

14 2.437387

74 12.03363

134 18.4101

15 2.610524

75 12.17523

135 18.47759

16 2.783462

76 12.31533

136 18.54388

17 2.956188

77 12.45393

137 18.60895

18 3.128669

78 12.59139

138 18.67285

19 3.300952

79 12.72556

139 18.73563

20 3.472964

80 12.85757

140 18.79734

21 3.644711

81 12.98859

141 18.85795

22 3.81618

82 13.11818

142 18.91747

23 3.987359

83 13.2524

143 18.97591

24 4.158224

84 13.38261

144 19.03328

25 4.328792

85 13.51118

145 19.08959

26 4.499021

86 13.63997

146 19.14485

27 4.668997

87 13.76709

147 19.19907

28 4.838438

88 13.89317

148 19.25223

29 5.0074

89 14.01819

149 19.30435

30 5.176381

90 14.14214

150 19.35544

31 5.344768

91 14.26501

151 19.40551

32 5.512747

92 14.38688

152 19.45457

33 5.680307

93 14.50749

153 19.50263

34 5.847743

94 14.62707

154 19.5497

35 6.014816

95 14.74555

155 19.59579

36 6.18054

96 14.8629

156 19.64089

37 6.344993

97 14.97911

157 19.68501

38 6.508193

98 15.09419

158 19.72815

39 6.671637

99 15.20812

159 19.77031

40 6.834903

100 15.32089

160 19.81148

41 7.000448

101 15.43249

161 19.85166

42 7.167359

102 15.54282

162 19.89085

43 7.333025

103 15.65166

163 19.92905

44 7.499132

104 15.76022

164 19.96626

45 7.665393

105 15.86797

165 20.00247

46 7.831863

106 15.97371

166 20.03768

47 7.997491

107 16.07714

167 20.07189

48 8.162323

108 16.18024

168 20.10510

49 8.326355

109 16.28199

169 20.13731

50 8.489587

110 16.38243

170 20.16852

51 8.651922

111 16.48152

171 20.19873

52 8.813423

112 16.58005

172 20.22794

53 8.974056

113 16.67772

173 20.25615

54 9.133819

114 16.77341

174 20.28336

55 9.292472

115 16.86783

175 20.30957

56 9.450015

116 16.96096

176 20.33478

57 9.606457

117 17.05288

177 20.35899

58 9.761891

118 17.14335

178 20.38220

59 9.916417

119 17.23258

179 20.40441

continued
12/11/13

12/11/13

Continued to page 129

SIGNATURE

DISCLOSED TO AND UNDERSTOOD BY

DATE

12/11/13

DATE

PROPRIETARY INFORMATION

Figure F.10: Laboratory Notebook 00011:128

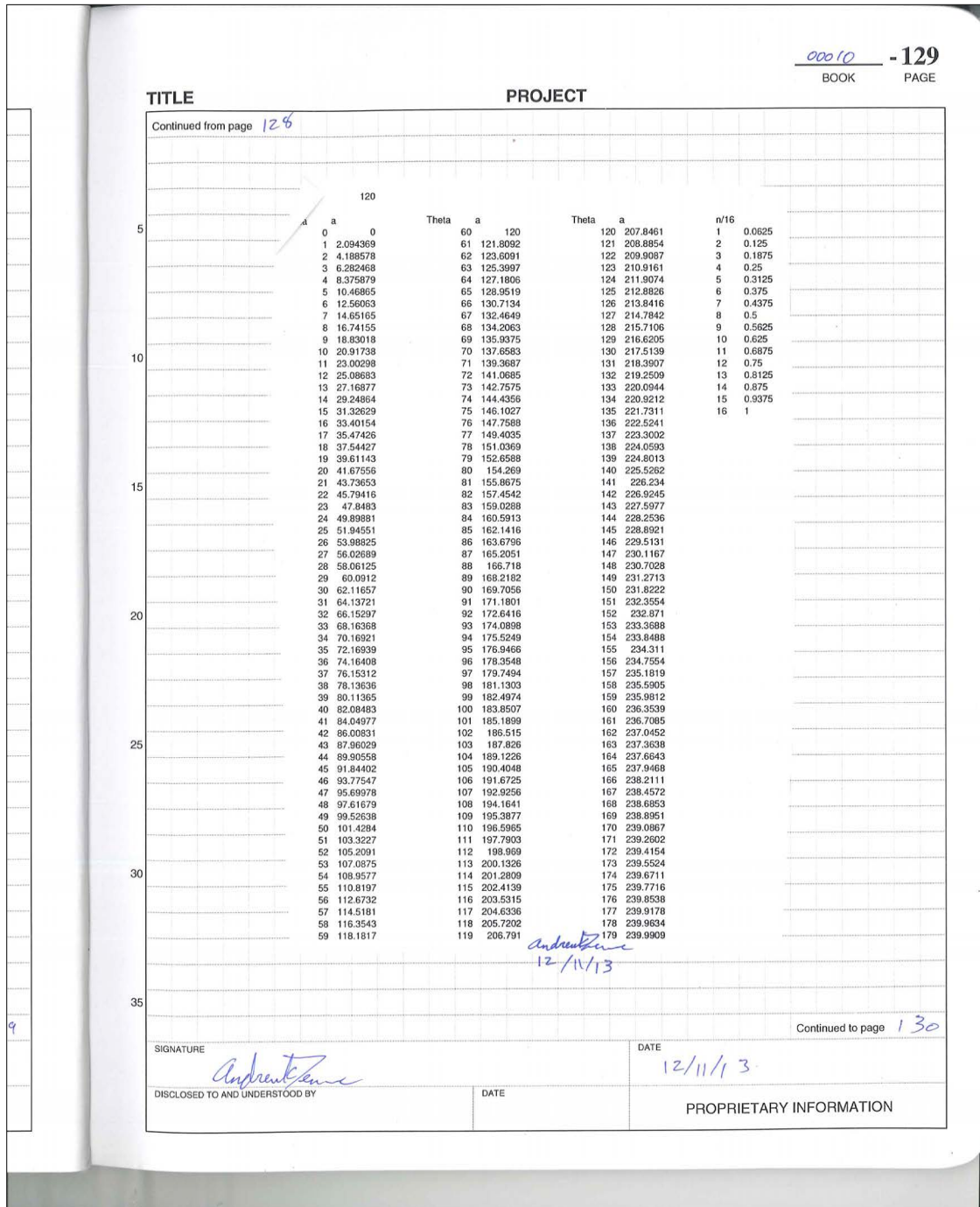


Figure F .11: Laboratory Notebook 00011:129

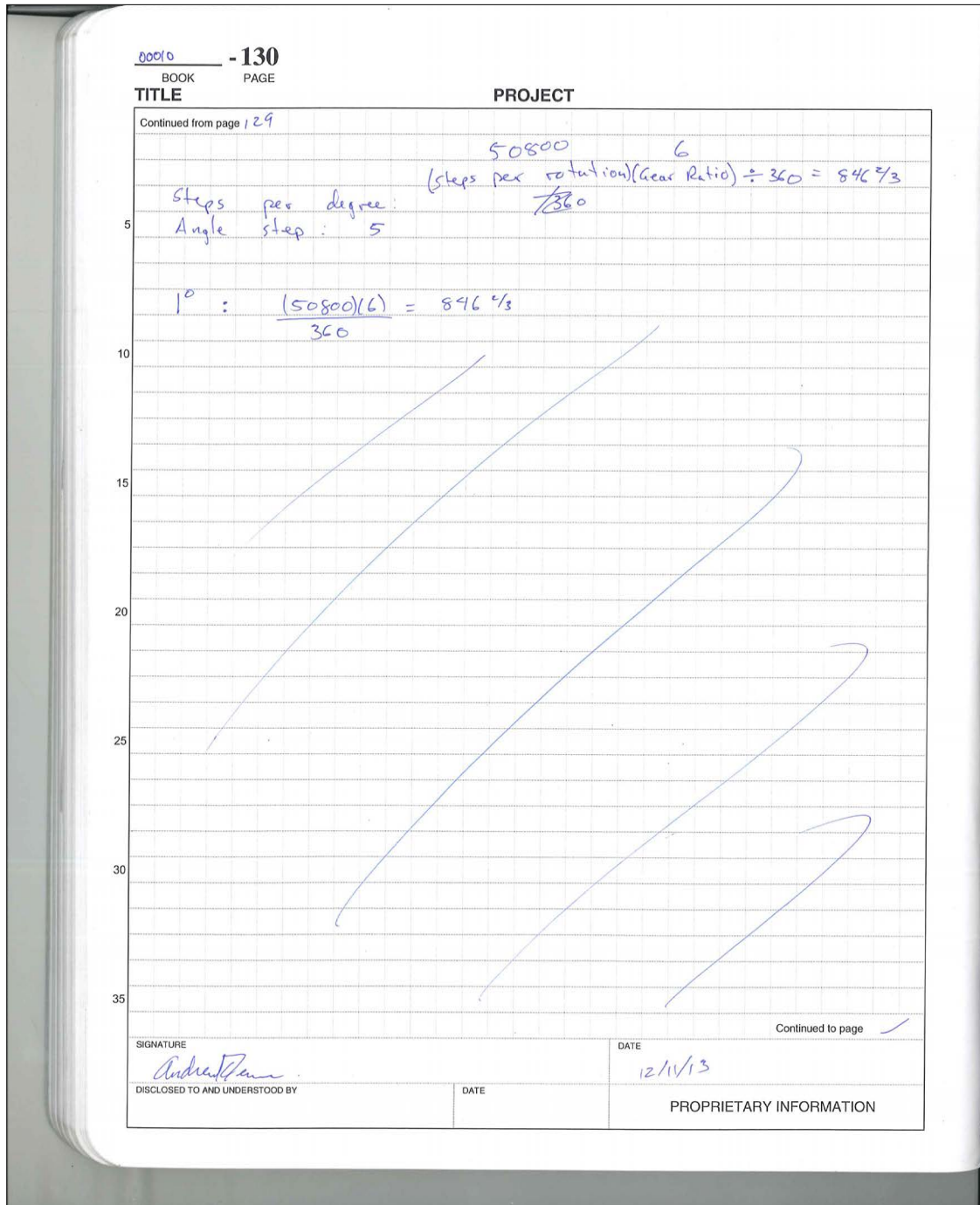


Figure F.12: Laboratory Notebook 00011:130

Appendix G

Selected Pages from Laboratory Notebook 00011

00011 - 3
BOOK PAGE

TITLE Baluns

PROJECT

Continued from page 1/28/14

Marchand Balun

Book on design techniques (chapter 6):
"Multifunctional Adaptive Microwave Circuits & Systems,"
ed. Steer & Palmer, SciTech Publishing, ©2009.
UMN: SCI Tk 7876.5735 2009

Look at minicircuits app note about baluns, esp. the end
sections about Characterization & terms

I think I want to use a slot ~~line~~ line of
some sort

Is there an easy way to connect a coax cable to slotline?
Slotline to twin lead also. Need design equations

What about a power divider?

"Microstrip Circuits," Fred Gardiol, Wiley, 1994.

What about coplanar strips?

SIGNATURE
Andrew Zenne
DISCLOSED TO AND UNDERSTOOD BY

DATE
1/28/2014
PROPRIETARY INFORMATION

Continued to page 4

Figure G.1: Laboratory Notebook 00011:3

TITLE

PROJECT

Continued from page 3

"Microstrip Lines and Slotlines," Gupta, Garg, Bahl, Artech, 1979.

pg 3, §1.1.2 Microstrip Field Configuration

"Microstrip is a two-conductor transmission line which can be considered to have evolved conceptually from a two-wire line as shown in Figure 1.4. Transformation from (a) to (b) is essentially a change in the shape of the conductors, whereas that from (b) to (c) involves placing a conducting sheet at the plane of symmetry. The final configuration (d) is obtained by inserting a thin dielectric slab between the two conductors. As a consequence of the last step, the dielectric medium of the transmission line becomes inhomogeneous."

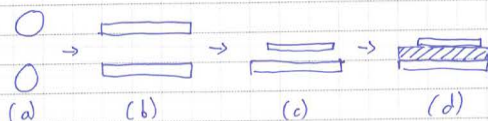
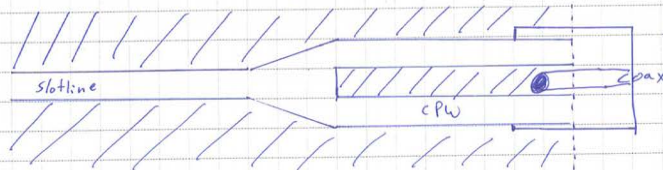


Fig. 1.4 Conceptual Evolution of a Microstrip from a Two-wire Line.

- How do I keep my TEM mode?



Gupta, et al.
Fig. 7.28 (b)

Continued to page 5

SIGNATURE

Andrew Zimm

DATE _____

1/28/14

DATE _____

PROPRIETARY INFORMATION

Figure G .2: Laboratory Notebook 00011:4

00011 - 5
BOOK PAGE

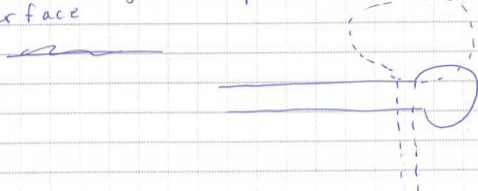

| TITLE | PROJECT |
|--|--|
| Continued from page 4 | |
| | <p>★ Look at Gupta et al more.</p> <p>5 "Microwave & Engineering using Microstrip Circuits," Fooks & Zakarevicius, Prentice Hall, 1990.</p> <p>10 Fig 10.4 (c) pg 234 Microstrip to slotline. Dashed is slot in ground plane. Solid is microstrip on surface</p>  <p>15</p> <p>20 What about microstrip to coplanar waveguide? Fig 10.5 pg 234</p> <p>25 What about "wide band balanced feed"</p> <p>30 In Gupta 2nd ed, pg 440, Fig 7.35 CPW-to-CPS transition. Originally from</p> <p>35 Ho, C. H., et al., "Broadband Uniplanar Hybrid-Ring and Branch-line Couplers," IEEE Trans., vol MTT-41, 1993, pp. 2116-2125. → this paper has a few errors. Carefully review before using a direct quote. At 1/28/13</p> <p>Use this as the first design to try.</p> |
| Continued to page / | |
| SIGNATURE  DISCLOSED TO AND UNDERSTOOD BY | DATE 1/28/14 PROPRIETARY INFORMATION |

Figure G.3: Laboratory Notebook 00011:5

00011 - 7
BOOK PAGE

TITLE Baluns

Continued from page 1/30/14

Possible designs

- From "Microstrip Lines & Slotlines," 2nd ed, Gupta et al
pg 440.
cited from Ho, C. H., et al. at pg 5 bottom

PROJECT

- From "Four Decade Bandwidth Uniplanar Balun," V. Trifunovic and B. Jokanovic, Elec. Letters, Vol 28, No. 6, 1992, pp 534-535. original. Also Jokanovic 1998 & Venkatesan 2003. See Zo text.

CPW-to-Slotline CPS, i.e. coplanar waveguide to coplanar strips
FAP ← finite (width) ground plane

essentially you have a transmission structure that ends in a Y w/ a short & load

SIGNATURE

DISCLOSED TO AND UNDERSTOOD BY

DATE
1/30/14
PROPRIETARY INFORMATION

Continued to page 8

Figure G.4: Laboratory Notebook 00011:7

TITLE

PROJECT

Continued from page 8

"Investigation of the Double-Y Balun for Feeding Pulsed Antennas," J. Venkatesan and W. Scott, Proc. of SPIE, Vol 5089, 2003; has

Venk Venkatesan has a very good, modern discussion of this balun.

A balun needs to suppress the common-mode current. For a coax, this is on the outside surface of the outside conductor.

"Baluns are also designed to provide equal and opposite voltages at the balanced terminals (w/ respect to ground) irrespective of the load."

A taper is need to transform impedances. This balun design ~~does not only~~ does no transformation.

Air bridges are important. (why are these left out of other papers and books?)

Z matrix for 2 ports 1, 4:

$$\begin{aligned} (1) \quad z_{11} &= \frac{(z_6 + z_5)(z_2 + z_3)}{z_2 + z_3 + z_5 + z_6} & z_2 &= jZ_{cps} \tan(\beta_{cps} l_{cps}) \quad (5) \\ (2) \quad z_{14} &= \frac{z_2(z_3 + z_5) - z_3(z_6 + z_2)}{z_2 + z_3 + z_5 + z_6} & z_3 &= -jZ_{cpw} \cot(\beta_{cpw} l_{cpw}) \quad (6) \\ (3) \quad z_{41} &= \frac{z_5(z_2 + z_3) - z_3(z_5 + z_6)}{z_2 + z_3 + z_5 + z_6} & z_5 &= jZ_{cpw} \tan(\beta_{cpw} l_{cpw}) \quad (7) \\ (4) \quad z_{44} &= \frac{(z_6 + z_2)(z_5 + z_3)}{z_2 + z_3 + z_5 + z_6} & z_6 &= -jZ_{cps} \cot(\beta_{cps} l_{cps}) \quad (8) \end{aligned}$$

Z_{cpw} , Z_{cps} are the characteristic impedances of the cpw & cps sections.

Continued to page 10

SIGNATURE

Andrew Amme

DISCLOSED TO AND UNDERSTOOD BY

DATE

DATE

1/30/14

PROPRIETARY INFORMATION

Figure G.6: Laboratory Notebook 00011:9

Continued from page 9

"The input impedance looking into the unbalanced section of the balun is then given by

$$Z_{in} = Z_0 - \frac{5.4841}{(3.441 Z_0)} \quad (9)$$

where Z_0 is the characteristic impedance at port 4"

→ what are β and l ?

If $Z_{cpw} = Z_{cps} = Z_0$ then a balun matched at all freq.

If $Z_{cpw} \neq Z_{cps}$ length of stubs must $\leq \lambda/8$ for highest freq.

cf Fig 5 for a plot of $|Z_{in}|$ vs. stub electrical length

This balun: 50 Ω coax \rightarrow 188.5 Ω V-antenna

Constraints for various reasons:

- widths of gap between conductors: 8 mil } manufacturing tolerances
- center conductor thickness: 8 mil }
- substrate thickness: 39 mil - rigidity
- CPS gap @ antenna feed: ~40 mil because of antenna desig.

→ stubs cho

- coax 50 Ω

- antenna 188.5 Ω

selected → FR4 substrate

→ stubs chosen to be 100 mil → up to 8 GHz

→ CPW Z_0 : 94 Ω } max/min given above tolerances

→ CPS Z_0 : 107 Ω }

used exponential impedance tapers

Continued to page 11

SIGNATURE

Andrew...

DISCLOSED TO AND UNDERSTOOD BY

DATE

1/30/14

DATE

PROPRIETARY INFORMATION

Figure G.7: Laboratory Notebook 00011:10

00011 - 11
BOOK PAGE

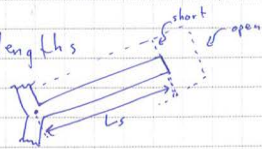
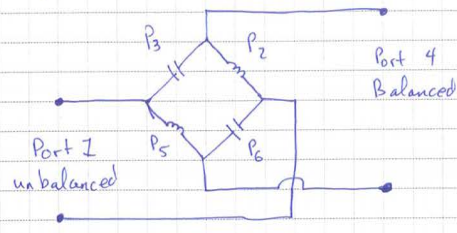
| TITLE | PROJECT |
|---|---|
| Continued from page 10 | |
| | - entire taper limited to 3200mil by project specs. |
| 5 | - Achieved: VSWR ≈ 1.5 , 0.8 - 8 GHz Insertion loss < 2.8 dB |
| 10 | - Balun gives symmetric time domain response for a Gaussian derivative pulse centered @ 3GHz. |
| | - Reference list includes more of Trifunovic & Jovanovic |
| 15 | Need to find design equations for CPW, CPS |
| <div style="border: 1px solid black; padding: 5px; display: inline-block;"> Venkatesan Dissertation Notes 1/31/14 </div> | |
| 20 | <div style="display: flex; align-items: center;"> <div style="flex: 1;"> - Stub lengths </div> <div style="flex: 1;">  </div> <div style="flex: 0.5; text-align: center;"> <p>References to</p> <p>check</p> <p>15</p> <p>16</p> <p>↓</p> <p>22</p> <p>23 } eqns</p> <p>24 }</p> </div> </div> |
| 25 | - Circuit model (noted as being for odd multiples of $\lambda/8$). I say make it general |
| 30 |  |
| 35 | Continued to page 12 |
| <div style="display: flex; justify-content: space-between;"> <div style="width: 45%;"> <p>SIGNATURE</p> <p><i>Andrew Zimme</i></p> <p>DISCLOSED TO AND UNDERSTOOD BY</p> </div> <div style="width: 45%;"> <p>DATE</p> <p>1/31/14</p> <p>PROPRIETARY INFORMATION</p> </div> </div> | |

Figure G.8: Laboratory Notebook 00011:11

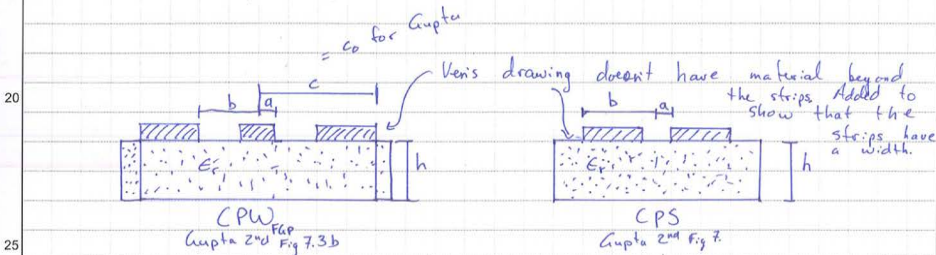
Continued from page 11

- Assumes reflection coefficients at P 2,3,5,6 (uses same Port definitions as paper on pg. 8)
- Assumes electrical length of CPW, CPS open & short stubs are equal

For the discussion of Double-Y balun on her pg 11

- High level reasoning gives reflection coefficients of
 - $e^{j\theta}$ @ P_2, P_3
 - $e^{j\theta+180^\circ}$ @ P_5, P_6
- If all ports have equal Z_0 , then balun matched

Chapter 2 Units?
- FR4: $\epsilon_r = 4.4$, $\delta_{tan} = 0.012$



- CPW Characteristic Impedance

$$Z_{0,cpw} = \frac{30\pi}{\sqrt{\epsilon_{cpw}}} \frac{k'(k_1)}{k(k_1)} \quad (5) \quad G(7.29)$$

$$\epsilon_{cpw} = 1 + \frac{\epsilon_r - 1}{2} \frac{k(k_2)}{k'(k_2)} \frac{k'(k_1)}{k(k_1)} \quad (6) \quad G(7.28)$$

$$k_1 = \frac{a}{b} \sqrt{\frac{1 - 1/2\epsilon_r}{1 - a^2/c^2}} = k_2 \text{ for Gupta} \quad (7) \quad G(7.23)$$

Continued to page 13

SIGNATURE

Andrew Kemme

DATE

1/31/14

DISCLOSED TO AND UNDERSTOOD BY

DATE

PROPRIETARY INFORMATION

Figure G.9: Laboratory Notebook 00011:12

TITLE

PROJECT

Continued from page 12

$$k_e = \frac{\sinh(\pi a/2h)}{\sinh(\pi b/2h)} \sqrt{\frac{1 - \sinh^2(\pi b/2h)/\sinh^2(\pi c/2h)}{1 - \sinh^2(\pi a/2h)/\sinh^2(\pi c/2h)}} = k_y \quad (8)$$

Gupta G(7.27)

k, k' - complete elliptic integrals of the first kind and its complement

$$k'(k) = k(\sqrt{1-k^2}) = k(k')$$

- CPS Characteristic Impedance pg. 403 Gupta 2nd

$$Z_{0,CPS} = \frac{120}{\sqrt{\epsilon_{eff}}} \frac{k(k_3)}{k'(k_3)} \quad (9)$$

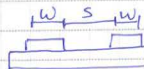
G(7.75)

$$\epsilon_{eff}^{CPS} = 1 + \frac{\epsilon_r - 1}{2} \frac{k(k_4)}{k'(k_4)} \frac{k'(k_3)}{k(k_3)}, \quad \frac{h}{b} > 1 \quad (10)$$

G(7.17)

$$k_3 = \frac{a}{b} = \frac{s}{s+2w} \cdot k_1 \quad \text{Gupta} \quad (11)$$

G(7.76)



$$k_4 = \frac{\sinh(\pi a/2h)}{\sinh(\pi b/2h)} = k_y \quad \text{Gupta} \quad (12)$$

G(7.16)

- Gupta notes:

- line impedance {for CPW} increases ... & effective permittivity decreases ... due to truncation of lateral ground planes. pg 389

- "This configuration can also support a quasi-TEM slotline mode whose characteristic impedance could be comparable to the desired mode. To suppress this mode lateral ground planes are kept at the same potential by means of proper properly spaced conductive air bridges." pg 389

- Consider asymmetric CPW or CPS to adjust impedance more
↳ probably not. asym can lead to radiation of unwanted modes

Continued to page 14

SIGNATURE

DISCLOSED TO AND UNDERSTOOD BY

DATE

1/31/14

DATE

PROPRIETARY INFORMATION

Figure G.10: Laboratory Notebook 00011:13

00011

- 14

BOOK

PAGE

TITLE

PROJECT

Continued from page 13

- pg 463 "conformal mapping does not agree w/ numerical analysis in references."

6(7.17) is good agreement for ϵ_{re} if $\boxed{h/b > 1}$

" $Z_{cps} + Z_{cpw} \approx \text{constant}$ w/ the aspect ratio; that is, CPS and CPW are complementary in behavior."

- Gupta does not have a synthesis equation for use in designing of lines

Ven's Fig 19: $b \text{ const}$

| | | |
|---------------------|-----------------------|--|
| $\frac{h}{b} = 0.1$ | $h < h_0$ | $Z_{0, cpw}$ ↓ decreases as h increases \therefore decrease substrate $\Rightarrow Z_0$ increases |
| 0.4 | $\Rightarrow h = h_0$ | |
| 0.9 | $h > h_0$ | |

CPW:

$h \uparrow$

$\epsilon_r \uparrow$

gap \uparrow

cond. width \downarrow

metal thickness \uparrow

$Z_{0, cpw} \downarrow$

$Z_{0, cpw} \uparrow$

$Z_{0, cpw} \downarrow$

$Z_{0, cpw} \uparrow$

$Z_{0, cpw} \downarrow$

$\epsilon_{re} \downarrow$

$\epsilon_{re} \downarrow$

CPS:

$h \uparrow$

$\epsilon_r \uparrow$

gap \uparrow

cond. width \downarrow

metal thickness \uparrow

$Z_{0, cps} \downarrow$

$Z_{0, cps} \downarrow$

$Z_{0, cps} \uparrow$

$Z_{0, cps} \uparrow$

$Z_{0, cps} \downarrow$

$\epsilon_{re} \downarrow$

$\epsilon_{re} \downarrow$

Continued to page 15

SIGNATURE

DATE

DISCLOSED TO AND UNDERSTOOD BY

DATE

PROPRIETARY INFORMATION

Figure G .11: Laboratory Notebook 00011:14

Continued from page 29

Avoid radiation losses

$$h\sqrt{\epsilon_c} < 0.12\lambda_0$$

↳ wavelength at highest freq.

↑
in free or in dielectric?

$$h = 58 \text{ mils}, \quad Z_0 = 104 \Omega, \quad FR4$$

$$S_{cpw} + 2W_{cpw} R_{gcpw} = S_{cps} + 2W_{cps} R_{gcps}$$

$$\min(S_{cpw}) = 10 \text{ mils}$$

$$\min(S_{cps}) = 6$$

From Trifunovic, 1994

"maximum upper edge of the bandwidth depends on transverse dimensions of the lines forming the double Y junction. The distance from the short and open circuits to the centre of the junction should be a few times greater than the radius of the junction to minimise junction parasitic effects."

want length $\alpha \approx 45^\circ$ @ upper freq.

increase freq band 2-3 times, then reduce gap width 3-5 times

Uen

resonances: $\lambda/8$, dipole, CPW

freq →

$\lambda/8$:

keep stubs less than $\sim 43^\circ$ @ f_{max} to shift this resonance out of band.

Continued to page 31

SIGNATURE

Andrew Fennell

DATE

2/15/14

DISCLOSED TO AND UNDERSTOOD BY

DATE

PROPRIETARY INFORMATION

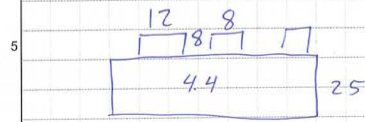
Figure G.12: Laboratory Notebook 00011:30

00011 - 31
BOOK PAGE

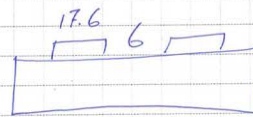
| TITLE | PROJECT | | |
|---|--|---|--|
| Continued from page 30 | | | |
| 5 | <p>CPW: additional bridges along CPW keep currents equal on outside guid's and more help suppress resonance</p> | | |
| 10 | <p>Dipole: overall length equal to ^{odd} multiples of half-wavelength. basically just hope this res. is not a problem.</p> | | |
| 15 | <p>Bridges: - larger vias \downarrow via/bridge impedance. Want - want $Z_{\text{bridge}} = 0$ for a short</p> | | |
| 20 | <p>Minimize overall width @ each freq. </p> | | |
| 25 | <p>Stubs different lengths. Open & short, different. Check Gupta actually seems to have little effect on balun performance</p> | | |
| 30 | <p>Taper: $Z(z) = Z_0 e^{\alpha z}$, $0 < z < L$ $\alpha = \frac{1}{L} \ln \left(\frac{Z_L}{Z_0} \right)$</p> | | |
| 35 | <p>Final design next page</p> | | |
| Continued to page 32 | | | |
| <table border="1" style="width: 100%; border-collapse: collapse;"> <tr> <td style="width: 50%; vertical-align: top;"> SIGNATURE DISCLOSED TO AND UNDERSTOOD BY </td> <td style="width: 50%; vertical-align: top;"> DATE 2/15/14 PROPRIETARY INFORMATION </td> </tr> </table> | | SIGNATURE DISCLOSED TO AND UNDERSTOOD BY | DATE 2/15/14 PROPRIETARY INFORMATION |
| SIGNATURE DISCLOSED TO AND UNDERSTOOD BY | DATE 2/15/14 PROPRIETARY INFORMATION | | |

Figure G.13: Laboratory Notebook 00011:31

Continued from page 31



$$8 + 2(8) + 2(12) = 48$$



$$2 + 2(6) + 2(17.6) = 41.2$$

$$L_s = \{80, 110\}$$

$$L_{\text{feed}} = L_{\text{tap}} = 16 \text{ in}$$

$$L_{\text{tot}} = 9.3 \text{ cm}$$

$$d_{\text{via}} = 6 \text{ mil}$$

$$b_{\text{Wbridge}} = 10 \text{ mil}$$

$$Z_y = 111 \Omega$$

$$Z_{\text{cpw}} = 50 \text{ } \cancel{\text{to } 50} \Omega$$

$$Z_{\text{cps}} = 200 \Omega$$

From Trifunovic 1992

radiation losses start when subs electrical length
exceeds 22° , cannot be neglected above 45°

 \Rightarrow electrical length

Continued to page 33

SIGNATURE

Andrew Kanne

DATE

2/15/14

DISCLOSED TO AND UNDERSTOOD BY

DATE

PROPRIETARY INFORMATION

Figure G.14: Laboratory Notebook 00011:32

00011 - 78

BOOK

PAGE

TITLE

PROJECT

Continued from page 77

metal plate 0.100 x 4 x 4.35

welding 308H 0.93 OD

steel unpolished: 0.119

Wire bonding 4/16/14

Ralmey
Dr. Nelson S. 's group

Ball bonding

| | |
|--------|------|
| Search | 2.27 |
| Power | 2.38 |
| Time | 3.0 |
| Force | 2.5 |

| | |
|------|-----|
| Tail | 4.6 |
| ball | 4.0 |

| | |
|------|-----|
| 3.05 | |
| 3 | 6.6 |
| 2.8 | 5.0 |

1250°C plate - changed to 100°C
 25 µm wire gold
 Kulicke & Soffa & Industries Inc.
 4524 Digital Wire Bonder
 Manual

spark to form ball

pressure & ultra sound to bond

position

pressure & ultra sound to bond, bend to "break"

rip wire from ball

repeat steps

Continued to page 79

SIGNATURE

Andrew Kenna

DATE

4/16/14

DISCLOSED TO AND UNDERSTOOD BY

DATE

PROPRIETARY INFORMATION

Figure G.15: Laboratory Notebook 00011:78

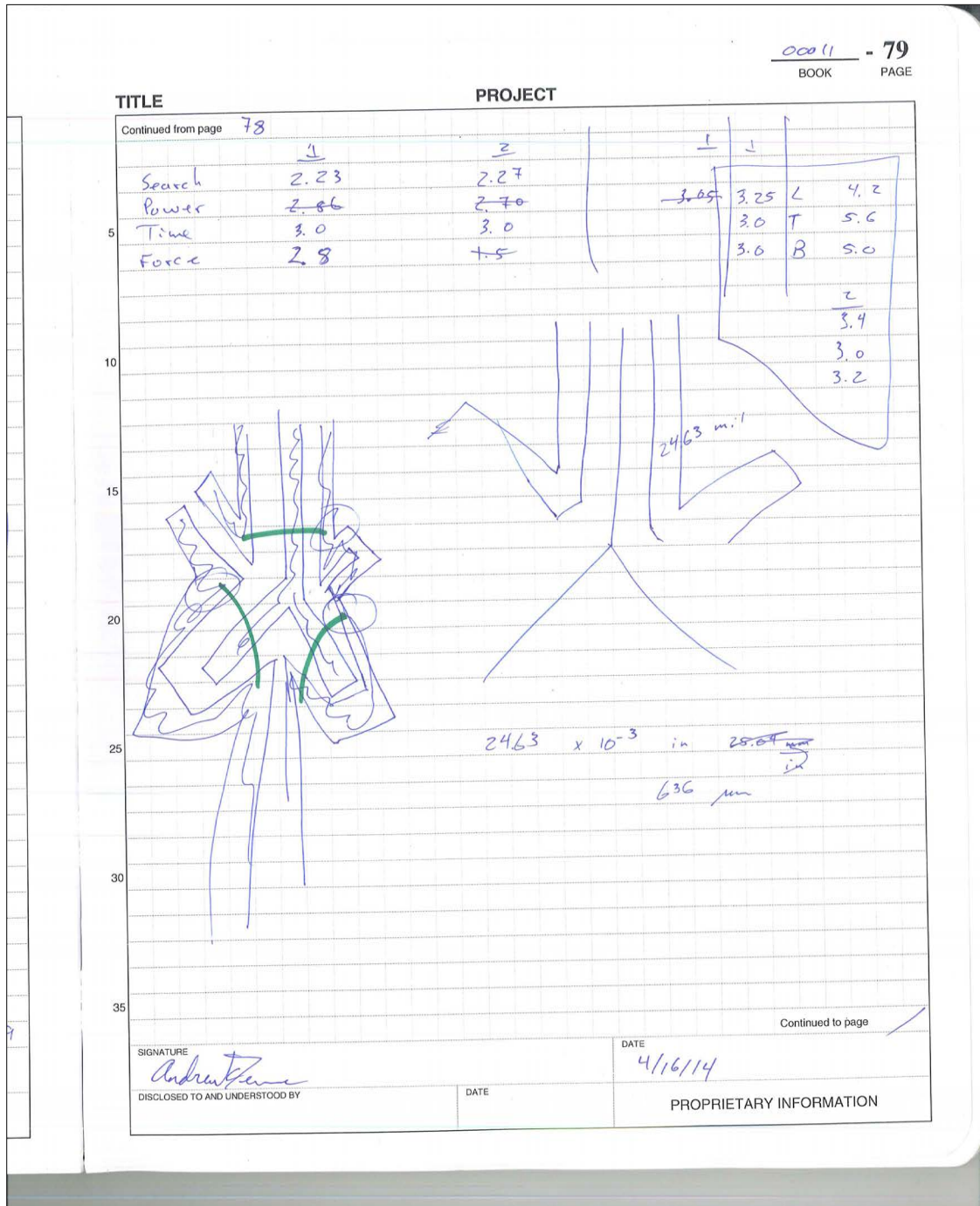


Figure G .16: Laboratory Notebook 00011:79

Appendix H

VNA Data Collection Code

8753,

Listing H .1: Collect full

```
1 #Download a reading from the network analyzer
2
3 from __future__ import division
4
5 import visa
6 import numpy as np
7 from datetime import datetime
8 from os import path, makedirs
9 import skrf
10
11 print "start"
12 #-----
13 fileName = 'btfd-kevin-sep25-calOFF'
14 #-----
15 numGrps = 4
16
17 ena = visa.instrument('GPIB::16', timeout = 120)
18 idn = ena.ask('*IDN?')
19 print idn
20
21 optLine = "# Hz S RI R 50"
22
23 cmd8753D = {\
24 'basicInit': 'HOLD;DUACOFF;CHAN1;S11;LOGM;CONT;AUTO',\
25 'corrQ': 'CORR?',\
26 'freqSpanQ': 'SPAN?',\
27 'freqStartQ': 'STAR?',\
28 'freqStopQ': 'STOP?',\
29 'getImag': 'IMAG;OUTPFORM',\
30 'getLinMag': 'LINM;OUTPFORM',\
31 'getLogMag': 'LOGM;OUTPFORM',\
32 'getPhase': 'PHAS;OUTPFORM',\
33 'getReal': 'REAL;OUTPFORM',\
```

```

34 'hold': 'HOLD',\
35 'IDStr': 'HEWLETT PACKARD,8753D,0,6.14',\
36 'ifbwQ': 'IFBW?',\
37 'numPtsQ': 'POIN?',\
38 'powerQ': 'POWE?',\
39 'preset': 'PRES',\
40 'numGroups': 'NUMG',\
41 'polar': 'POLA',\
42 's11': 'S11',\
43 's21': 'S21',\
44 's12': 'S12',\
45 's22': 'S22'\
46 }
47
48 cmdDict = cmd8753D
49
50
51 #-----
52 ena.write('form4')
53 numPts = ena.ask_for_values(cmdDict['numPtsQ'])[0]
54 freqStart = ena.ask_for_values(cmdDict['freqStartQ'])[0]
55 freqStop = ena.ask_for_values(cmdDict['freqStopQ'])[0]
56 freq = np.linspace(freqStart, freqStop, num=numPts, endpoint=True)
57 ifbw = ena.ask_for_values(cmdDict['ifbwQ'])[0]
58 pwr = ena.ask_for_values(cmdDict['powerQ'])[0]
59 corr = ena.ask(cmdDict['corrQ'])
60
61 dateString = datetime.now().strftime("%Y-%m-%d")
62 timeString = datetime.now().strftime("%H:%M:%S")
63
64 dataDir = 'Data/' + dateString
65 if not path.exists(dataDir):
66     makedirs(dataDir)
67
68 print "here"
69 s11polar = np.array(ena.ask_for_values(cmdDict['s11']+cmdDict['polar']+';'+cmdDict['
    numGroups'] + str(numGrps)+';outpform'))
70 print "there"
71 s11polReal = s11polar[:,2] # real values from the polar data
72 s11polImag = s11polar[:,1] # imaginary values from the polar data
73
74 print "s21"
75 s21polar = np.array(ena.ask_for_values(cmdDict['s21']+cmdDict['polar']+';'+cmdDict['
    numGroups'] + str(numGrps)+';outpform'))
76 s21polReal = s21polar[:,2] # real values from the polar data
77 s21polImag = s21polar[:,1] # imaginary values from the polar data
78
79 print "s12"
80 s12polar = np.array(ena.ask_for_values(cmdDict['s12']+cmdDict['polar']+';'+cmdDict['
    numGroups'] + str(numGrps)+';outpform'))
81 s12polReal = s12polar[:,2] # real values from the polar data

```

```

82 s12polImag = s12polar[1::2]          # imaginary values from the polar data
83
84 print "s22"
85 s22polar = np.array(ena.ask_for_values(cmdDict['s22']+cmdDict['polar']+';'+cmdDict['
    numGroups'] + str(numGrps)+';outpform'))
86 s22polReal = s22polar[:,2]           # real values from the polar data
87 s22polImag = s22polar[1::2]         # imaginary values from the polar data
88
89 visa.vpp43.gpib_control_ren(ena.vi,2)
90 #saveData = s22polar
91 saveData = np.concatenate(([freq],
92                             [s11polReal],[s11polImag],
93                             [s21polReal],[s21polImag],
94                             [s12polReal],[s12polImag],
95                             [s22polReal],[s22polImag])).T
96
97
98 touchFileName = dataDir + "/" + fileName + ".s2p"
99 print touchFileName
100 saveFile = open(touchFileName, "w")
101 saveFile.write("!" + idn + "\n")
102 saveFile.write("!Date: " + dateString + " " + timeString + "\n")
103 saveFile.write("!Data & Calibration Information:\n")
104 if corr == '0':
105     saveFile.write("!Freq S11 S21 S12 S22\n")
106 elif corr == '1':
107     saveFile.write("!Freq S11:Cal(ON) S21:Cal(ON) S12:Cal(ON) S22:Cal(ON)\n")
108
109 saveFile.write("!PortZ Port1:50+j0 Port2:50+j0\n")
110 saveFile.write(("!Above PortZ is port z conversion or system Z0 "
111               "setting when saving the data.\n"))
112 saveFile.write(("!When reading, reference impedance value at option "
113               "line is always used.\n"))
114 saveFile.write("!\n")
115 saveFile.write("!--Config file parameters\n")
116 saveFile.write("!start = " + str(freqStart) + "\n")
117 saveFile.write("!stop = " + str(freqStop) + "\n")
118 saveFile.write("!numPts = " + str(numPts) + "\n")
119 saveFile.write("!avgFact = " + str(numGrps) + "\n")
120 saveFile.write("!power = " + str(pwr) + "\n")
121 saveFile.write("!ifbw = " + str(ifbw) + "\n")
122 saveFile.write("!\n")
123 saveFile.write(optLine + "\n")
124 np.savetxt(saveFile, saveData, delimiter=" ")
125 saveFile.close()
126
127 balun = skrf.Network(touchFileName)
128 balun.plot_s_db()
129 legend(loc=0)

```

Listing H.2: Collect S_{21} continuously from an HP 8753

```

1 #Download a reading from the network analyzer
2
3 from __future__ import division
4
5 import visa
6 import numpy as np
7 from datetime import datetime
8 from os import path, makedirs
9 #import skrf
10
11 print "start"
12 #-----
13 dataPrefix = 'carpet-foam'
14 #-----
15 numGrps = 2
16 ena = visa.instrument('GPIB::16', timeout = 120)
17 idn = ena.ask('*IDN?')
18 print idn
19
20 optLine = "# Hz S RI R 50"
21
22 cmd8753D = {\
23 'basicInit': 'HOLD;DUACOFF;CHAN1;S21;LOGM;CONT;AUTO',\
24 'corrQ': 'CORR?',\
25 'freqSpanQ': 'SPAN?',\
26 'freqStartQ': 'STAR?',\
27 'freqStopQ': 'STOP?',\
28 'getImag': 'IMAG;OUTPFORM',\
29 'getLinMag': 'LINM;OUTPFORM',\
30 'getLogMag': 'LOGM;OUTPFORM',\
31 'getPhase': 'PHAS;OUTPFORM',\
32 'getReal': 'REAL;OUTPFORM',\
33 'hold': 'HOLD',\
34 'IDStr': 'HEWLETT PACKARD,8753D,0,6.14',\
35 'ifbwQ': 'IFBW?',\
36 'numPtsQ': 'POIN?',\
37 'powerQ': 'POWE?',\
38 'preset': 'PRES',\
39 'numGroups': 'NUMG',\
40 'polar': 'POLA',\
41 's11': 'S11',\
42 's21': 'S21',\
43 's12': 'S12',\
44 's22': 'S22'\
45 }
46
47 cmdDict = cmd8753D
48
49
50 #-----
51 ena.write('form4')

```

```

52 ena.write('POIN1601')
53 numPts = ena.ask_for_values(cmdDict['numPtsQ'])[0]
54 freqStart = ena.ask_for_values(cmdDict['freqStartQ'])[0]
55 freqStop = ena.ask_for_values(cmdDict['freqStopQ'])[0]
56 freq = np.linspace(freqStart, freqStop, num=numPts, endpoint=True)
57 ifbw = ena.ask_for_values(cmdDict['ifbwQ'])[0]
58 pwr = ena.ask_for_values(cmdDict['powerQ'])[0]
59 corr = ena.ask(cmdDict['corrQ'])
60
61 dateString = datetime.now().strftime("%Y-%m-%d")
62 timeString = datetime.now().strftime("%H:%M:%S")
63
64 dataDir = 'Data/' + dateString
65 if not path.exists(dataDir):
66     makedirs(dataDir)
67
68 i = 0
69 #saveMeas = True
70 #for i in range(numMeasurements):
71 try:
72     ena.write('pola;numg' + str(numGrps))
73     # while saveMeas:
74     while True:
75         print('Starting Measurement Number: %d' % i)
76         s21polar = np.array(ena.ask_for_values(cmdDict['s21']+cmdDict['polar']+';'+
77             cmdDict['numGroups'] + str(numGrps)+';outpform'))
78         s21polReal = s21polar[:,2] # real values from the polar data
79         s21polImag = s21polar[1::2] # imaginary values from the polar data
80
81         saveData = np.concatenate(([freq],
82             [s21polReal],[s21polImag])).T
83
84
85         timeAppend = datetime.now().strftime("-%Y-%m-%d-%H%M%S")
86         dataName = dataDir + '/' + dataPrefix + timeAppend
87
88         touchFileName = dataName + ".slp"
89         print touchFileName
90         saveFile = open(touchFileName, "w")
91         saveFile.write("!"+idn+"\n")
92         saveFile.write("!Date: " + dateString + " " + timeString + "\n")
93         saveFile.write("!Data & Calibration Information:\n")
94         if corr == '0':
95             saveFile.write("!Freq S21\n")
96         elif corr == '1':
97             saveFile.write("!Freq S21:Cal saved on analyzer\n")
98
99         saveFile.write("!PortZ Port1:50+j0\n")
100         saveFile.write(("!Above PortZ is port z conversion or system Z0 "
101             "setting when saving the data.\n"))

```

```

102     saveFile.write(("!When reading, reference impedance value at option "
103                    "line is always used.\n"))
104     saveFile.write("\n")
105     saveFile.write("--Config file parameters\n")
106     saveFile.write("!start = " + str(freqStart) + "\n")
107     saveFile.write("!stop = " + str(freqStop) + "\n")
108     saveFile.write("!numPts = " + str(numPts) + "\n")
109     saveFile.write("!avgFact = " + str(numGrps) + "\n")
110     saveFile.write("!power = " + str(pwr) + "\n")
111     saveFile.write("!ifbw = " + str(ifbw) + "\n")
112     saveFile.write("\n")
113     saveFile.write(optLine + "\n")
114     np.savetxt(saveFile, saveData, delimiter=" ")
115     saveFile.close()
116
117     i += 1
118 #balun = skrf.Network(touchFileName)
119 #balun.plot_s_db()
120 #legend(loc=0)
121 except KeyboardInterrupt:
122     print('Ctrl-C Interrupt ')
123
124 finally:
125     print('Finally ')
126
127
128
129 visa.vpp43.gpib_control_ren(ena.vi,2)
130 print("Done")

```

8510,

Listing H .3: Collect full

```

1 #Download a reading from the network analyzer
2
3 from __future__ import division
4
5 import visa
6 import numpy as np
7 from datetime import datetime
8 from os import path, makedirs
9 import skrf
10
11 print "start"
12 #-----
13 fileName = 'empty'
14 #-----
15 optLine = "# Hz S RI R 50"
16
17 cmd8510C = {\
18 'basicInit': 'HOLD;CHAN1;S11;LOGM;CONT;AUTO;',\
19 'corrQ': 'CORR?;',\

```



```

20 'freqSpanQ': 'SPAN;OUTPACTI;',\
21 'freqStartQ': 'STAR;OUTPACTI;',\
22 'freqStopQ': 'STOP;OUTPACTI;',\
23 'getImag': 'IMAG;OUTPFORM;',\
24 'getLinMag': 'LINM;OUTPFORM;',\
25 'getLogMag': 'LOGM;OUTPFORM;',\
26 'getPhase': 'PHAS;OUTPFORM;',\
27 'getReal': 'REAL;OUTPFORM;',\
28 'hold': 'HOLD;',\
29 'IdQ': 'OUTPIDEN;',\
30 'IDStr': 'HP8510C.07.10: Mar 30 1995 ',\
31 'ifbwQ': 'DETE?;',\
32 'numPtsQ': 'POIN;OUTPACTI;',\
33 'powerQ': 'POWE;OUTPACTI;',\
34 'preset': 'PRES;',\
35 'numGroups': 'NUMG',\
36 'polar': 'REIP;',\
37 's11': 'S11;',\
38 's21': 'S21;',\
39 's12': 'S12;',\
40 's22': 'S22;',\
41 }
42
43 cmdDict = cmd8510C
44
45 ena = visa.instrument('GPIB::16', timeout = 120)
46 idn = ena.ask(cmdDict['IdQ'])
47 print idn
48
49 numGrps = 16
50 #-----
51 ena.write('form4')
52 numPts = ena.ask_for_values(cmdDict['numPtsQ'])[0]
53 freqStart = ena.ask_for_values(cmdDict['freqStartQ'])[0]
54 freqStop = ena.ask_for_values(cmdDict['freqStopQ'])[0]
55 freq = np.linspace(freqStart, freqStop, num=numPts, endpoint=True)
56
57 # IFBW is different for the 8510
58 ifbw = ena.ask(cmdDict['ifbwQ'])
59 #
60
61 pwr = ena.ask_for_values(cmdDict['powerQ'])[0]
62 corr = ena.ask(cmdDict['corrQ'])
63
64 dateString = datetime.now().strftime("%Y-%m-%d")
65 timeString = datetime.now().strftime("%H:%M:%S")
66
67 dataDir = 'Data/' + dateString
68 if not path.exists(dataDir):
69     makedirs(dataDir)
70

```

```

71 s11polar = np.array(ena.ask_for_values(cmdDict['s11']+cmdDict['polar']+cmdDict['
    numGroups'] + str(numGrps)+';outpform'))
72 s11polReal = s11polar[:,2]          # real values from the polar data
73 s11polImag = s11polar[1:,2]         # imaginary values from the polar data
74
75 s22polar = np.array(ena.ask_for_values(cmdDict['s22']+cmdDict['polar']+cmdDict['
    numGroups'] + str(numGrps)+';outpform'))
76 s22polReal = s22polar[:,2]          # real values from the polar data
77 s22polImag = s22polar[1:,2]         # imaginary values from the polar data
78
79 s12polar = np.array(ena.ask_for_values(cmdDict['s12']+cmdDict['polar']+cmdDict['
    numGroups'] + str(numGrps)+';outpform'))
80 s12polReal = s12polar[:,2]          # real values from the polar data
81 s12polImag = s12polar[1:,2]         # imaginary values from the polar data
82
83 s21polar = np.array(ena.ask_for_values(cmdDict['s21']+cmdDict['polar']+cmdDict['
    numGroups'] + str(numGrps)+';outpform'))
84 s21polReal = s21polar[:,2]          # real values from the polar data
85 s21polImag = s21polar[1:,2]         # imaginary values from the polar data
86
87
88 visa.vpp43.gpib_control_ren(ena.vi,2)
89 saveData = np.concatenate(([freq],
90                             [s11polReal],[s11polImag],
91                             [s21polReal],[s21polImag],
92                             [s12polReal],[s12polImag],
93                             [s22polReal],[s22polImag])).T
94
95
96 touchFileName = dataDir + "/" + fileName + ".s2p"
97 print touchFileName
98 saveFile = open(touchFileName, "w")
99 saveFile.write("!" + idn + "\n")
100 saveFile.write("!Date: " + dateString + " " + timeString + "\n")
101 saveFile.write("!Data & Calibration Information:\n")
102 if corr == '0':
103     saveFile.write("!Freq S11 S21 S12 S22\n")
104 elif corr == '1':
105     saveFile.write("!Freq S11:Cal(ON) S21:Cal(ON) S12:Cal(ON) S22:Cal(ON)\n")
106
107 saveFile.write("!PortZ Port1:50+j0\n")
108 saveFile.write(("!Above PortZ is port z conversion or system Z0 "
109               "setting when saving the data.\n"))
110 saveFile.write(("!When reading, reference impedance value at option "
111               "line is always used.\n"))
112 saveFile.write("!\n")
113 saveFile.write("--Config file parameters\n")
114 saveFile.write("!start = " + str(freqStart) + "\n")
115 saveFile.write("!stop = " + str(freqStop) + "\n")
116 saveFile.write("!numPts = " + str(numPts) + "\n")
117 saveFile.write("!avgFact = " + str(numGrps) + "\n")

```

```
118 saveFile.write("!power = " + str(pwr) + "\n")
119 saveFile.write("!ifbw = " + str(ifbw) + "\n")
120 saveFile.write("! \n")
121 saveFile.write(optLine + "\n")
122 np.savetxt(saveFile, saveData, delimiter=" ")
123 saveFile.close()
124
125 balun = skrf.Network(touchFileName)
126 balun.plot_s_db()
127 legend(loc=0)
```

Appendix I

Wavecalc Macros

Listing I .1: EHS Plexiglass macro

```
1 "Open"
2 2
3 "\\tsclient\Z\Documents\code\Data\2013-08-08\c1x.odf"
4 "1"
5 "CT"
6 2
7 "2"
8 "10"
9 "FFT"
10 6
11 "800"
12 "4096"
13 "8192"
14 "8192"
15 "4.883409E-02"
16 "0"
17 "ZF"
18 2
19 "2"
20 "390"
21 "FFT"
22 6
23 "0"
24 "8192"
25 "4096"
26 "8192"
27 "0.0025"
28 "0"
29 "Trc"
30 2
31 "2.5"
32 "5.5"
33 "Save"
34 1
```

```
35 "\\tsclient\Z\Documents\code\Data\2013-08-08\gated2-390-clx.ODF"
```

Listing I .2: EHS burn macro

```
1 "Open"
2 2
3 "\\tsclient\Z\Documents\code\Data\2013-08-08\c11.odf"
4 "1"
5 "CT"
6 2
7 "2"
8 "10"
9 "FFT"
10 6
11 "800"
12 "4096"
13 "8192"
14 "8192"
15 "4.883409E-02"
16 "0"
17 "ZF"
18 2
19 "5"
20 "390"
21 "FFT"
22 6
23 "0"
24 "8192"
25 "4096"
26 "8192"
27 "0.0025"
28 "0"
29 "Trc"
30 2
31 "2.5"
32 "5.5"
33 "Save"
34 1
35 "\\tsclient\Z\Documents\code\Data\2013-08-08\gated5-390-cl1.ODF"
```

Listing I .3: BTFD Bullex macro

```
1 "Open"
2 2
3 "\\tsclient\Z\Documents\code\Data\2013-12-06\c1a.odf"
4 "1"
5 "CT"
6 2
7 "2"
8 "10"
9 "FFT"
10 6
```

11 "800"
12 "4096"
13 "8192"
14 "8192"
15 "4.883409E-02"
16 "0"
17 "ZF"
18 2
19 "3"
20 "380"
21 "FFT"
22 6
23 "0"
24 "8192"
25 "4096"
26 "8192"
27 "0.0025"
28 "0"
29 "Trc"
30 2
31 "2.5"
32 "5.5"
33 "Save"
34 1
35 "\\tsclient\Z\Documents\code\Data\2013-12-06\gated3-380-c1a.ODF"

Appendix J

Arch Range

When making measurements using the arch range in the Electromagnetic Research Group laboratory, it is important to know the angular position of the horn antennas when they are on the rail. The angular distance from one end was marked using the following procedure (see Fig. J .1):

1. Painter's tape was applied to the rail
2. A laser level was placed near the outside of the rotator with the laser going through the center of the rotator and the angle 180° away from where the laser was placed.
3. The laser was aligned to the edge of the rail.
4. The rotator was repeatedly stepped by 3° and the laser line marked on the tape
5. The ruler in Figure J .3 was used to mark every quarter of a degree by aligning to each mark from the laser.

A few remarks:

- The rotator was stepped by 3° because this is the smallest integer degree that corresponds to a integer step value for the motor of the rotator. Numerically, the motor has 50800 steps and a gear ratio of 1:6 which gives $846\frac{2}{3}$ steps per degree or 2540 steps per 3° (see Notebook 00010:130 in Fig. F .12).
- Painter's tape was used because it was unknown how the markings would turn out. At some point in the future, the rail should be marked in a more permanent manner.
- The ruler was drawn using SolidWorks. The original source file is available in the data archive provided to Dr. Rothwell as well as in my git repository. Refer to the Errata section for more information.



Figure J .1: Arch range rail showing the degree markings.

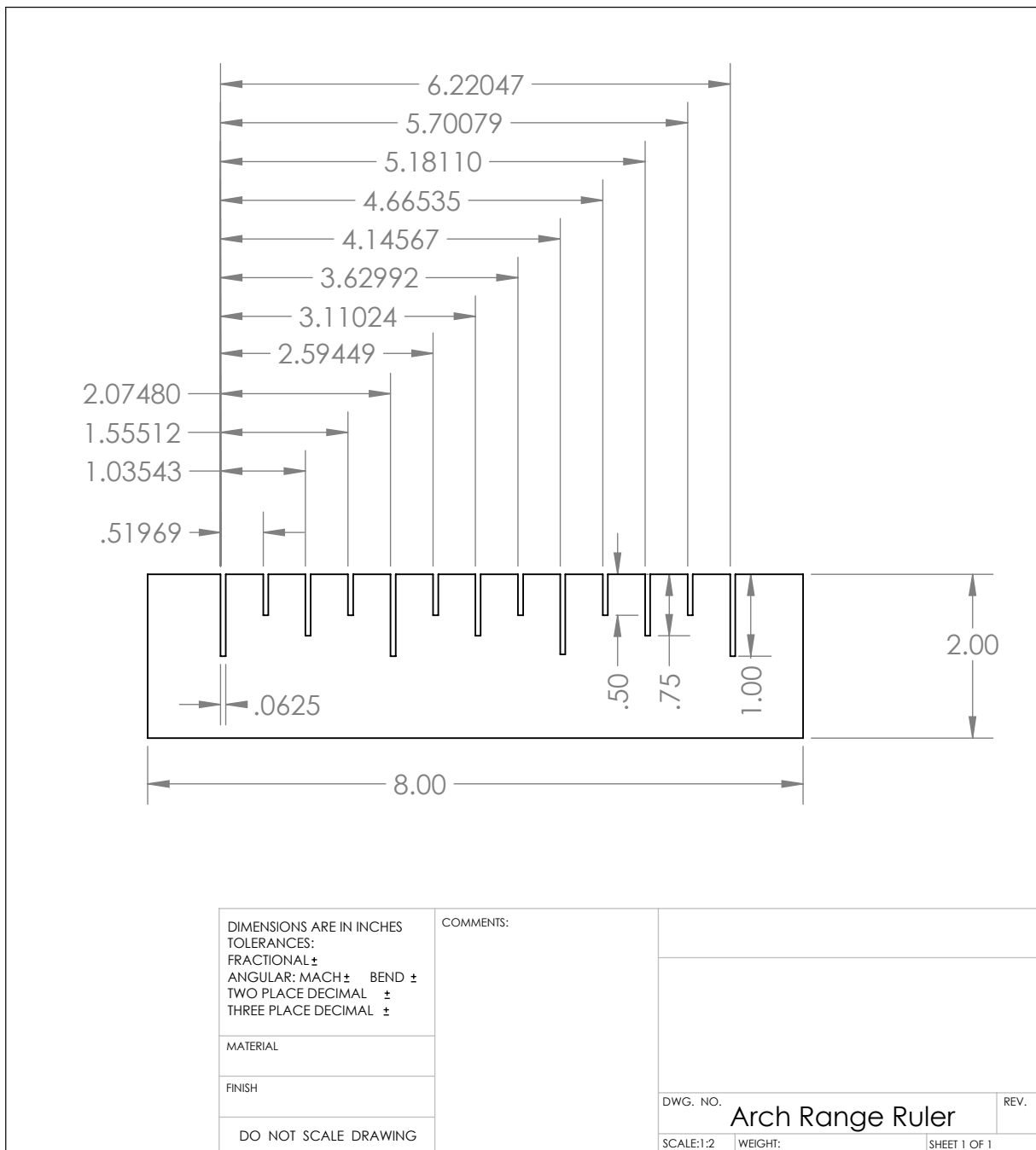


Figure J .2: Dimensional drawing of the ruler used to mark angular distance along the rail of the arch range.

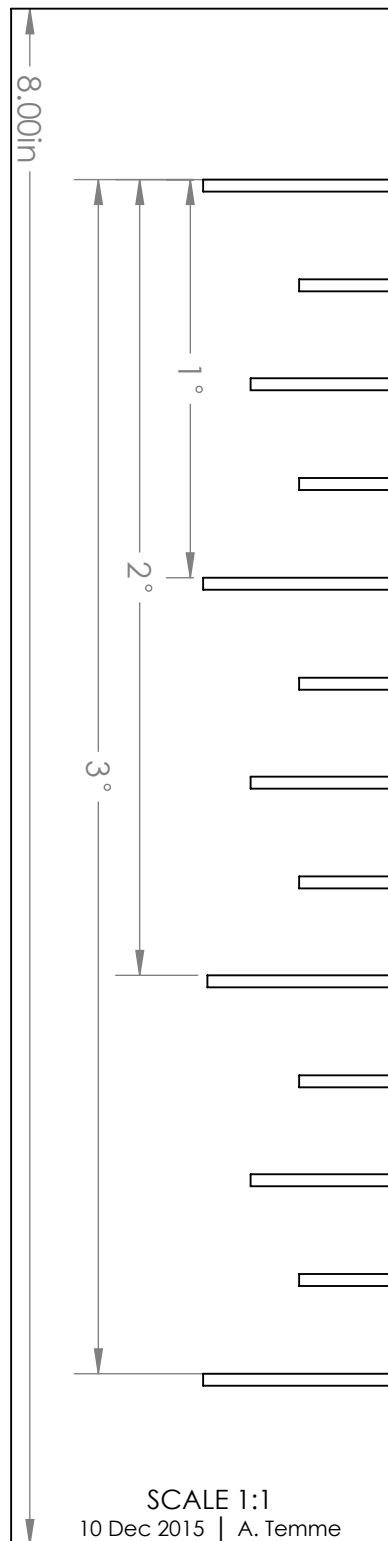


Figure J .3: Ruler used to mark angular distance the rail of the arch range.

Appendix K

IPython notebook: Single-Layer

```
In [ ]: from scipy import constants as const
import numpy as np

# adjust font size for plots
matplotlib.rcParams.update({'font.size': 16})

eta_free = np.sqrt(const.mu_0/const.epsilon_0)

eps_theory = 2.7
eta_plexi = 1/np.sqrt(eps_theory)*eta_free

R = (eta_plexi - eta_free)/(eta_plexi + eta_free)
T = R+1

In [ ]: A11 = (1-R**2*T**2)/((1-R**2)*T)
A12 = -R*(1-T**2)/((1-R**2)*T)
A21 = -A12
A22 = (T**2-R**2)/((1-R**2)*T)

In [ ]: S11 = A21/A11
S12 = (A11*A22 - A21*A12)/A11
S21 = 1/A11
S22 = -A12/A11

print(S21)
print(20*log10(S21))

In [ ]: eps_r = linspace(1,10,200)
eta_free = np.sqrt(const.mu_0/const.epsilon_0)
eta_r = 1/np.sqrt(eps_r)*eta_free
R = (eta_r - eta_free)/(eta_r + eta_free)
T = R+1
A11 = (1-R**2*T**2)/((1-R**2)*T)
A12 = -R*(1-T**2)/((1-R**2)*T)
A21 = -A12
A22 = (T**2-R**2)/((1-R**2)*T)
S11 = A21/A11
```

```

S12 = (A11*A22 - A21*A12)/A11
S21 = 1/A11
S22 = -A12/A11

```

```

In [ ]: fig, ax = subplots()

ax.plot(eps_r,abs(S21))
right = ax.twinx()
right.set_ylim(20*log10(ax.get_ylim()))

ax.set_xlabel(r"$\epsilon_r$")
ax.set_ylabel(r"$|S_{21}|$")
right.set_ylabel(r"$|S_{21}|$ (dB)")

```

Compute the S parameters of a single layer of a material. Plot S_{21}

```

In [ ]: freq = linspace(1e9,20e9,500)
eps_rel = [1, 2.7, 2.7-.05J]
mu_r = 1
L_in = 1 # length of sample in inches
L = L_in*0.0254
Z_0 = np.sqrt(const.mu_0/const.epsilon_0)

fig, axes = subplots(ncols = 2, nrows = 1, figsize=(13,4))

for eps_r in eps_rel:
    Z_1 = Z_0 * np.sqrt(mu_r/eps_r)
    gamma = 1j*2*pi*freq/const.c*np.sqrt(mu_r*eps_r)

    R = (Z_1 - Z_0)/(Z_1 + Z_0)
    P = exp(-gamma*L)

    S11 = R*(1-P**2)/(1-R**2*P**2)
    S22 = S11

    S21 = P*(1-R**2)/(1-R**2*P**2)
    S12 = S21

    axes[0].plot(freq/1e9,20*log10(abs(S21)),
                  label=r'$\epsilon_r = $' + str(eps_r))
    axes[0].set_xlabel('Frequency (GHz)')
    axes[0].set_ylabel(r'$|S_{21}|$ (dB)')

    axes[1].plot(freq/1e9,angle(P,deg=1))
    axes[1].set_xlabel('Frequency (GHz)')
    axes[1].set_ylabel(r'$\angle S_{21}$ (deg)')

    #axes[0].set_title(r'$\epsilon_r = $' + str(eps_r))
fig.subplots_adjust(left=-.05)

#axes[0].legend(loc=0)

```

```

axes[0].legend(bbox_to_anchor=(0., 1.02, 1., .102), loc=3,
               ncol=2, mode="expand", borderaxespad=0.)

In [ ]: cd 'E://control experiments//burn3'

In [ ]: empty1 = np.loadtxt('empty1-t40.odf',delimiter=",")
        empty2 = np.loadtxt('empty2-t40.odf',delimiter=",")
        plate1 = np.loadtxt('plate1-t40.odf',delimiter=",")
        plate2 = np.loadtxt('plate2-t40.odf',delimiter=",")
        plexi1 = np.loadtxt('plexi1-t40.odf',delimiter=',')
        plexi2 = np.loadtxt('plexi2-t40.odf',delimiter=',')
        shelf1 = np.loadtxt('shelf1-t40.odf',delimiter=',')
        shelf2 = np.loadtxt('shelf2-t40.odf',delimiter=',')

In [ ]: freqExp = empty1[:,0]
        cempty1 = empty1[:,1]+1j*empty1[:,2]
        cempty2 = empty2[:,1]+1j*empty2[:,2]
        cplate1 = plate1[:,1]+1j*plate1[:,2]
        cplate2 = plate2[:,1]+1j*plate2[:,2]
        cplexi1 = plexi1[:,1]+1j*plexi1[:,2]
        cplexi2 = plexi2[:,1]+1j*plexi2[:,2]
        cshelf1 = shelf1[:,1]+1j*shelf1[:,2]
        cshelf2 = shelf2[:,1]+1j*shelf2[:,2]

In [ ]: burn = 'Burn 3: '

In [ ]: from scipy import constants
        constants.mu_0
        constants.epsilon_0

In [ ]: eps_r = 2.5
        print eps_r
        fig, axes = subplots(ncols = 2, nrows = 1, figsize=(13,4))
        Z_1 = Z_0 * np.sqrt(mu_r/eps_r)
        gamma = 1j*2*pi*freq/const.c*np.sqrt(mu_r*eps_r)

        R = (Z_1 - Z_0)/(Z_1 + Z_0)
        P = exp(-gamma*L)

        S11 = R*(1-P**2)/(1-R**2*P**2)
        S22 = S11

        S21 = P*(1-R**2)/(1-R**2*P**2)
        S12 = S21

def plotit(plotData, titleString, saveName):
    print titleString
    f = pylab.gcf()
    f.clear()
    figsize(2,2)

    subplot(2,1,1)
    plot(freqExp,20*log10(abs(plotData)))

```

```

plot(freq/1e9,20*log10(abs(S21)), label=r'$\epsilon_r = $' + str(eps_r))
title(titleString)
ylabel('|S21| (dB)')
xlim(2,6)
subplot(2,1,2)
#plot(freqExp,rad2deg(angle(plotData)))
plot(freqExp,rad2deg(angle(plotData*np.exp(-1j*k_0*L))))
plot(freq/1e9,angle(P,deg=1))
ylabel(r'$\angle S21$ (deg)')
xlabel("Frequency (GHz)")
xlim(2,6)
#savefig(saveName + '.pdf')

L_in = 1
L = L_in * 0.0254
k_0 = 2*np.pi*freqExp*1e9*np.sqrt(constants.mu_0*constants.epsilon_0)
plotit((cplexi1-cplate1)/(cempty1-cplate1),
        burn + '(Plexi1-Plate1)/(Empty1-Plate1)', 'plexi1_cald')
# plotit((cplexi2-cplate1)/(cempty1-cplate1),
#         burn + '(Plexi2-Plate1)/(Empty1-Plate1)', 'plexi2_cald')
# plotit((cshelf1-cplate1)/(cempty1-cplate1),
#         burn + '(Shelf1-Plate1)/(Empty1-Plate1)', 'shelf1_cald')
# plotit((cshelf2-cplate1)/(cempty1-cplate1),
#         burn + '(Shelf2-Plate1)/(Empty1-Plate1)', 'shelf2_cald')

In [ ]: empty1 = np.loadtxt('empty1-t17.odf',delimiter=",")
empty2 = np.loadtxt('empty2-t17.odf',delimiter=",")
plate1 = np.loadtxt('plate1-t17.odf',delimiter=",")
plate2 = np.loadtxt('plate2-t17.odf',delimiter=",")
plexi1 = np.loadtxt('plexi1-t17.odf',delimiter=',')
plexi2 = np.loadtxt('plexi2-t17.odf',delimiter=',')
shelf1 = np.loadtxt('shelf1-t17.odf',delimiter=',')
shelf2 = np.loadtxt('shelf2-t17.odf',delimiter=',')

freqExp = empty1[:,0]
cempty1 = empty1[:,1]+1j*empty1[:,2]
cempty2 = empty2[:,1]+1j*empty2[:,2]
cplate1 = plate1[:,1]+1j*plate1[:,2]
cplate2 = plate2[:,1]+1j*plate2[:,2]
cplexi1 = plexi1[:,1]+1j*plexi1[:,2]
cplexi2 = plexi2[:,1]+1j*plexi2[:,2]
cshelf1 = shelf1[:,1]+1j*shelf1[:,2]
cshelf2 = shelf2[:,1]+1j*shelf2[:,2]

eps_r = 2.5-0.05j
print eps_r
fig, axes = subplots(ncols = 2, nrows = 1, figsize=(13,4))
Z_1 = Z_0 * np.sqrt(mu_r/eps_r)
gamma = 1j*2*pi*freq/const.c*np.sqrt(mu_r*eps_r)

R = (Z_1 - Z_0)/(Z_1 + Z_0)
P = exp(-gamma*L)

```

```

S11 = R*(1-P**2)/(1-R**2*P**2)
S22 = S11

S21 = P*(1-R**2)/(1-R**2*P**2)
S12 = S21

def plotit(plotData, titleString, saveName):
    print titleString
    f = pylab.gcf()
    f.clear()
    figsize(2,2)

    subplot(2,1,1)
    plot(freqExp,20*log10(abs(plotData)))
    plot(freq/1e9,20*log10(abs(S21)), label=r'$\epsilon_r = $' + str(eps_r))
    title(titleString)
    ylabel('|S21| (dB)')
    xlim(2,6)
    subplot(2,1,2)
    #plot(freqExp,rad2deg(angle(plotData)))
    plot(freqExp,rad2deg(angle(plotData*np.exp(-1j*k_0*L))))
    plot(freq/1e9,angle(P,deg=1))
    ylabel(r'$\angle S21$ (deg)')
    xlabel("Frequency (GHz)")
    xlim(2,6)
    #savefig(saveName + '.pdf')

L_in = 1
L = L_in * 0.0254
k_0 = 2*np.pi*freqExp*1e9*np.sqrt(constants.mu_0*constants.epsilon_0)
plotit((cplexi1-cplate1)/(cempty1-cplate1),
        burn + '(Plexi1-Plate1)/(Empty1-Plate1)', 'plexi1_cald')
# plotit((cplexi2-cplate1)/(cempty1-cplate1),
#         burn + '(Plexi2-Plate1)/(Empty1-Plate1)', 'plexi2_cald')
# plotit((cshelf1-cplate1)/(cempty1-cplate1),
#         burn + '(Shelf1-Plate1)/(Empty1-Plate1)', 'shelf1_cald')
# plotit((cshelf2-cplate1)/(cempty1-cplate1),
#         burn + '(Shelf2-Plate1)/(Empty1-Plate1)', 'shelf2_cald')

In [ ]: cd '../burn2'

In [ ]: burn = 'Burn 1: '
empty1 = np.loadtxt('empty-2013-05-30-110926-t40.odf',delimiter=",")
empty2 = np.loadtxt('empty-2013-05-30-110945-t40.odf',delimiter=",")
plate1 = np.loadtxt('plate-2013-05-30-110727-t40.odf',delimiter=",")
plate2 = np.loadtxt('plate-2013-05-30-110745-t40.odf',delimiter=",")
plexi1 = np.loadtxt('plexiglass-2013-05-30-111303-t40.odf',delimiter=',')
plexi2 = np.loadtxt('plexiglass-2013-05-30-111321-t40.odf',delimiter=',')
shelf1 = np.loadtxt('shelf-2013-05-30-111532-t40.odf',delimiter=',')
shelf2 = np.loadtxt('shelf-2013-05-30-111551-t40.odf',delimiter=',')

```

```

freqExp = empty1[:,0]
cempty1 = empty1[:,1]+1j*empty1[:,2]
cempty2 = empty2[:,1]+1j*empty2[:,2]
cplate1 = plate1[:,1]+1j*plate1[:,2]
cplate2 = plate2[:,1]+1j*plate2[:,2]
cplexi1 = plexi1[:,1]+1j*plexi1[:,2]
cplexi2 = plexi2[:,1]+1j*plexi2[:,2]
cshelf1 = shelf1[:,1]+1j*shelf1[:,2]
cshelf2 = shelf2[:,1]+1j*shelf2[:,2]

eps_r = 2.5-0.05j
print eps_r
fig, axes = subplots(ncols = 2, nrows = 1, figsize=(13,4))
Z_1 = Z_0 * np.sqrt(mu_r/eps_r)
gamma = 1j*2*pi*freq/const.c*np.sqrt(mu_r*eps_r)

R = (Z_1 - Z_0)/(Z_1 + Z_0)
P = exp(-gamma*L)

S11 = R*(1-P**2)/(1-R**2*P**2)
S22 = S11

S21 = P*(1-R**2)/(1-R**2*P**2)
S12 = S21

def plotit(plotData, titleString, saveName):
    print titleString
    f = pylab.gcf()
    f.clear()
    figsize(2,2)

    subplot(2,1,1)
    plot(freqExp,20*log10(abs(plotData)))
    plot(freq/1e9,20*log10(abs(S21)), label=r'$\epsilon_r = $' + str(eps_r))
    title(titleString)
    ylabel('|S21| (dB)')
    xlim(2,6)
    subplot(2,1,2)
    #plot(freqExp,rad2deg(angle(plotData)))
    plot(freqExp,rad2deg(angle(plotData*np.exp(-1j*k_0*L))))
    plot(freq/1e9,angle(P,deg=1))
    ylabel(r'$\angle S21$ (deg)')
    xlabel("Frequency (GHz)")
    xlim(2,6)
    #savefig(saveName + '.pdf')

L_in = 1
L = L_in * 0.0254
k_0 = 2*np.pi*freqExp*1e9*np.sqrt(constants.mu_0*constants.epsilon_0)
plotit((cplexi1-cplate1)/(cempty1-cplate1),
        burn + '(Plexi1-Plate1)/(Empty1-Plate1)', 'plexi1_cald')

```



```

# plotit((cplexi2-cplate1)/(empty1-cplate1),
#         burn + '(Plexi2-Plate1)/(Empty1-Plate1)', 'plexi2_cald')
# plotit((cshelf1-cplate1)/(empty1-cplate1),
#         burn + '(Shelf1-Plate1)/(Empty1-Plate1)', 'shelf1_cald')
# plotit((cshelf2-cplate1)/(empty1-cplate1),
#         burn + '(Shelf2-Plate1)/(Empty1-Plate1)', 'shelf2_cald')

In [ ]: cd '../burn1'

In [ ]: cd '../burn3'

In [ ]: burn = 'Burn 3: '
empty1 = np.loadtxt('empty1-t17.odf', delimiter=",")
empty2 = np.loadtxt('empty2-t17.odf', delimiter=",")
plate1 = np.loadtxt('plate1-t17.odf', delimiter=",")
plate2 = np.loadtxt('plate2-t17.odf', delimiter=",")
#plexi1 = np.loadtxt('plexi1-t17.odf', delimiter=',')
plexi1 = np.loadtxt('burn3-t17.odf', delimiter=',')
plexi2 = np.loadtxt('plexi2-t17.odf', delimiter=',')
shelf1 = np.loadtxt('shelf1-t17.odf', delimiter=',')
shelf2 = np.loadtxt('shelf2-t17.odf', delimiter=',')

freqExp = empty1[:,0]
cempty1 = empty1[:,1]+1j*empty1[:,2]
cempty2 = empty2[:,1]+1j*empty2[:,2]
cplate1 = plate1[:,1]+1j*plate1[:,2]
cplate2 = plate2[:,1]+1j*plate2[:,2]
cplexi1 = plexi1[:,1]+1j*plexi1[:,2]
cplexi2 = plexi2[:,1]+1j*plexi2[:,2]
cshelf1 = shelf1[:,1]+1j*shelf1[:,2]
cshelf2 = shelf2[:,1]+1j*shelf2[:,2]

eps_r = 1.1-0.05j
print eps_r
fig, axes = subplots(ncols = 2, nrows = 1, figsize=(13,4))
Z_1 = Z_0 * np.sqrt(mu_r/eps_r)
gamma = 1j*2*pi*freq/const.c*np.sqrt(mu_r*eps_r)

R = (Z_1 - Z_0)/(Z_1 + Z_0)
P = exp(-gamma*L)

S11 = R*(1-P**2)/(1-R**2*P**2)
S22 = S11

S21 = P*(1-R**2)/(1-R**2*P**2)
S12 = S21

def plotit(plotData, titleString, saveName):
    print titleString
    f = pylab.gcf()
    f.clear()
    figsize(2,2)

```

```

subplot(2,1,1)
plot(freqExp,20*log10(abs(plotData)))
plot(freq/1e9,20*log10(abs(S21)), label=r'$\epsilon_r = $' + str(eps_r))
title(titleString)
ylabel('|S21| (dB)')
xlim(2,6)
subplot(2,1,2)
#plot(freqExp,rad2deg(angle(plotData)))
plot(freqExp,rad2deg(angle(plotData*np.exp(-1j*k_0*L))))
plot(freq/1e9,angle(P,deg=1))
ylabel(r'$\angle S21$ (deg)')
xlabel("Frequency (GHz)")
xlim(2,6)
#savefig(saveName + '.pdf')

L_in = 1
L = L_in * 0.0254
k_0 = 2*np.pi*freqExp*1e9*np.sqrt(constants.mu_0*constants.epsilon_0)
plotit((cplexi1-cplate1)/(cempty1-cplate1),
       burn + '(Plexi1-Plate1)/(Empty1-Plate1)', 'plexi1_cald')
# plotit((cplexi2-cplate1)/(cempty1-cplate1),
#       burn + '(Plexi2-Plate1)/(Empty1-Plate1)', 'plexi2_cald')
# plotit((cshelf1-cplate1)/(cempty1-cplate1),
#       burn + '(Shelf1-Plate1)/(Empty1-Plate1)', 'shelf1_cald')
# plotit((cshelf2-cplate1)/(cempty1-cplate1),
#       burn + '(Shelf2-Plate1)/(Empty1-Plate1)', 'shelf2_cald')

```

K.1 Control Data for the LFD Report

```

In [ ]: !pwd

In [ ]: !cd ~/Documents/code/Data/2013-05-30/odf/control/burn3/

In [ ]: from scipy import constants as const
import numpy as np

# adjust font size for plots
matplotlib.rcParams.update({'font.size': 16})

burn = 'Burn 3: '
#load data
empty1 = np.loadtxt('empty1-t17.ODF',delimiter=",")
empty2 = np.loadtxt('empty2-t17.ODF',delimiter=",")
plate1 = np.loadtxt('plate1-t17.ODF',delimiter=",")
plate2 = np.loadtxt('plate2-t17.ODF',delimiter=",")
plexi1 = np.loadtxt('plexi1-t17.ODF',delimiter=',')
plexi2 = np.loadtxt('plexi2-t17.ODF',delimiter=',')
shelf1 = np.loadtxt('shelf1-t17.ODF',delimiter=',')
shelf2 = np.loadtxt('shelf2-t17.ODF',delimiter=',')

#parse data into complex values

```

```

freqExp = empty1[:,0]
cempty1 = empty1[:,1]+1j*empty1[:,2]
cempty2 = empty2[:,1]+1j*empty2[:,2]
cplate1 = plate1[:,1]+1j*plate1[:,2]
cplate2 = plate2[:,1]+1j*plate2[:,2]
cplexi1 = plexi1[:,1]+1j*plexi1[:,2]
cplexi2 = plexi2[:,1]+1j*plexi2[:,2]
cshelf1 = shelf1[:,1]+1j*shelf1[:,2]
cshelf2 = shelf2[:,1]+1j*shelf2[:,2]

#theoretical calculations
eps_r = 2.5
print eps_r

eta_free = np.sqrt(const.mu_0/const.epsilon_0)
mu_r = 1
freq = linspace(1e9,20e9,500)
L_in = 1 # length of sample in inches
L = L_in*0.0254
Z_0 = np.sqrt(const.mu_0/const.epsilon_0)
Z_1 = Z_0 * np.sqrt(mu_r/eps_r)
gamma = 1j*2*pi*freq/const.c*np.sqrt(mu_r*eps_r)

R = (Z_1 - Z_0)/(Z_1 + Z_0)
P = exp(-gamma*L)

S11 = R*(1-P**2)/(1-R**2*P**2)
S22 = S11

S21 = P*(1-R**2)/(1-R**2*P**2)
S12 = S21

#calculate how much to shift the data
L_in = 1
L = L_in * 0.0254
k_0 = 2*np.pi*freqExp*1e9*np.sqrt(const.mu_0*const.epsilon_0)

#function to plot results
fig, axes = subplots(ncols = 2, nrows = 1, figsize=(13,8))
def plotit(plotData, titleString, saveName):
    print titleString
    f = pylab.gcf()
    f.clear()
    #figsize(2,2)

    subplot(2,1,1)
    plot(freqExp,20*log10(abs(plotData)),'b-', lw=2, label='Plexiglass Control')
    plot(freq/1e9,20*log10(abs(S21)),'g-.', lw=2,
        label=r'$\epsilon_r = $' + str(eps_r))
    title(titleString)
    ylabel('Magnitude (dB)')

```

```

xlim(2,6)
#legend(loc=4, borderaxespad=0.)
subplot(2,1,2)
#plot unshifted data
#plot(freqExp,rad2deg(angle(plotData)))
#plot shifted data
plot(freq/1e9,angle(S21,deg=1),'g-.', lw=2,
      label=r'$\epsilon_r = $' + str(eps_r))
plot(freqExp,rad2deg(angle(plotData*np.exp(-1j*k_0*L))),'b-', lw=2,
      label='Plexiglass Control')
ylabel('Phase (deg)')
xlabel("Frequency (GHz)")
xlim(2,6)
legend(loc=4, borderaxespad=0.)
# axes[0].legend(bbox_to_anchor=(0., 1.02, 1., .102), loc=3,ncol=2,
#               mode="expand", borderaxespad=0.)
# axes[0].legend(loc=2)
savefig(saveName + '.png')

plotit((cplexi1-cplate1)/(cempty1-cplate1),
      'Results for Plexiglass Control Sample, Burn 3 data',
      'b3-plexi-ctrl-dissertation')

```

Appendix L

IPython notebook: Bullex-at-ORCBS-2013-08-08

L.1 Experiments at MSU EHS using the Bullex Fire Extinguisher Trainer

- Conducted at MSU EHS office at the Engineering Research Complex
- Assisted by Elvet A. Potter from EHS and Tang
- 2013-08-08

L.1.1 Files

```
In [ ]: !ls -l ~/Documents/code/Data/2013-08-08/b[1,2,3]*.odf
```

```
In [ ]: !ls ~/Documents/code/Data/2013-08-08/gated[2,5]*.ODF
```

L.2 Pre-flight

L.2.1 Imports

```
In [ ]: # Import basic modules
        # make sure that division is done as expected
        from __future__ import division

        # plotting setup
        %matplotlib inline
        import matplotlib.pyplot as plt
        plt.style.use('gray_back')

        # get the viridis colormap
        # https://bids.github.io/colormap
        # it will be available as cmaps.viridis
```

```

import colormaps as cmaps

# for 3d graphs
# from mpl_toolkits.mplot3d import axes3d
# for legends of combined fig types
# import matplotlib.lines as mlines

# numerical functions
import numpy as np

# need some constants
from scipy import constants
from numpy import pi

# RF tools!
import skrf as rf

# version information
# %install_ext http://raw.github.com/jrjohansson/version_information/
# master/version_information.py
# %load_ext version_information
# %reload_ext version_information

# %version_information numpy, scipy, matplotlib

```

```

In [ ]: from scipy import stats
        from scipy.constants import inch

```

L.2.2 Parameters, Config, and Constants

```

In [ ]: dataDir = '/mnt/home/temmeand/Documents/code/Data/2013-08-08/'

```

```

doPlot = True
doSave = True
# doSave = False

if doSave: doPlot = True

plt.rcParams['axes.ymargin'] = 0

```

```

In [ ]: fmin = 2.5e9
        fmax = 5.5e9
        fpts = 201

# Plexiglas parameters
plexi = { 'epsr': 2.5
          , 'mur' : 1
          , 'd'  : 1*constants.inch
          }

# Free space parameters
freeSpace = { 'epsr': 1

```

```

        , 'mur' : 1
    }

    # Free space in Plexiglas case
    freePlexi = freeSpace.copy()
    freePlexi['d'] = plexi['d']

    # Free space in Bullex case
    freeFire = freeSpace.copy()
    freeFire['d'] = 27.94*constants.inch

```

L.2.3 Error Checking

```
In [ ]: # none at this time
```

L.2.4 Prelim Calculations

```
In [ ]: freq = np.linspace(fmin, fmax, fpts)
```

L.2.5 Function Definitions

```
In [ ]: def ntwk2odf(ntwk, m=1, n=0, fileName=None, EOL='\\r\\n'):
    '''
    Saves an skrf network in ODF format

    Save one s-parameter from a network as an odf formatted file. In
    the frequency domain, each line contains the frequency, real
    values, and imaginary values seperated by commas.

    'm' and 'n' allow you to pick which S parameter to save

    If no file name is given, the name of the network is used

    Default end of line character is Windows compatible (\\r\\n)

    Parameters
    -----
    ntwk : skrf Network object
           Data to be saved

    m,n : int
           Specifies the S parameter to be saved as S_m,n

    fileName : string
               Name of the saved file. If no string is provided, the
               name of the network is used

    EOL : string
           String to be used at the end of the line
           \\r\\n - Dos
    '''

```

```

        ||n - Unix

Returns
-----
Nothing

'''
fileName = ntwk.name if fileName is None else fileName
with open(fileName+'.odf','w') as fo:
    data = np.vstack((ntwk.f/1e9, ntwk.s_re[:,m,n],ntwk.s_im[:,m,n])).T
    np.savetxt(fo, data, delimiter=',',newline=EOL)

def odf2ntwk(fileName, name=""):
    '''
    Load ODF file as ntwk

    Create a one port s-parameter network from an odf formatted file. In
    the frequency domain, each line contains the frequency, real
    value, and imaginary value seperated by commas.

    Parameters
    -----
    fileName : string
        File to be loaded

    Returns
    -----
    ntwk : skrf Network object
    '''
    # from numpy import loadtxt
    import skrf as rf
    f = open(fileName,'r')
    raw = np.loadtxt(f, delimiter=',')
    f.close()

    if name is "": name = fileName

    freq = raw[:,0]
    data = raw[:,1]+1j*raw[:,2]
    # ntwk = rf.Network(name=fileName,f=axis,f_unit='GHz',z0=50,s=data)
    ntwk = rf.Network(name=name,f=freq,f_unit='GHz',z0=50,s=data)

    return ntwk

def calibrate(raw, empty, plate, thick):
    """
    Calibrate raw data using empty and plate measurement

    For S21 data:

    
$$Cald = (raw-plate) / (empty-plate)*exp(-j*k_0*thick)$$


```



```

Parameters
-----
raw : skrf network
    raw data to be calibrated
empty : skrf network
    empty range measurement
plate : skrf network
    measurement of plate at the position of the sample
thick : number
    thickness of material sample in meters

Returns
-----
cald : skrf network
    Calibrate data
"""

k = wavenumber(raw.f, 1, 1)

cald = (raw-plate) / (empty-plate) * np.exp(-1j*k*thick)
cald.name = cald.name + ", cald"

return cald

def analyze(raw, empty, plate, thick, name="", _doPlot=False, _doSave=False):
    """
    Process the data

    Calibrate the data and plot

    Parameters
    -----
    raw : skrf network
        raw data to be calibrated
    empty : skrf network
        empty range measurement
    plate : skrf network
        measurement of plate at the position of the sample
    thick : number
        sample thickness in meters
    name : string
        label or name to use on graphs
    _doPlot : boolean
        make plots
    _doSave : boolean
        save plots

    Returns
    -----
    cald : skrf network

```

```

        calibrated network
    """
    cald = calibrate(raw, empty, plate, thick)

    if name is not "":
        cald.name = name

    if _doPlot:
        fig, ax = plt.subplots(2,1)
        fig.set_figheight(7)

        ax[0].set_title('Dataset: ' + name)
        raw.plot_s_db(ax=ax[0], label='Raw ')
        cald.plot_s_db(ax=ax[0], label='Cald ')

        raw.plot_s_deg(ax=ax[1], show_legend=False)
        cald.plot_s_deg(ax=ax[1], show_legend=False)

        if _doSave:
            fig.savefig(name+'.pdf')

    return cald

def wavenumber(f, epsr, mur):
    return 2*pi*f*np.sqrt(constants.epsilon_0*epsr
                           *constants.mu_0*mur)

def propFactor(k, d):
    return np.exp(-1j*k*d)

def impedance(epsr=1, mur=1):
    return np.sqrt(constants.mu_0*mur/(constants.epsilon_0*epsr))

def reflectionCoeff(eta, etaf):
    return (eta-etaf)/(eta+etaf)

def transmission(p, g):
    return (1-g**2)*p/(1-p**2*g**2)

def slabTheory(f, d, epsr=1, mur=1):
    """
    Theoretical slab transmission

    
$$S_{21} = (1-\Gamma^2)P / (1-P^2\Gamma^2)$$


    
$$P = \exp(-j k d)$$


    
$$k = \omega \sqrt{\mu \epsilon}$$


    
$$d = \text{thickness}$$


```

```

Gamma = (Z-Z0) / (Z+Z0)

Z = sqrt(mu/eps)
Z0 = sqrt(mu0/eps0)
"""
k = wavenumber(f, epsr, mur)
eta = impedance(epsr, mur)
etaFree = impedance(1, 1)

p = propFactor(k, d)
g = reflectionCoeff(eta, etaFree)
s21 = transmission(p, g)

name = "Theory"

f = f/1e9
ntwk = rf.Network(name=name, f=f, f_unit='ghz', z0=50, s=s21)

return ntwk

```

L.3 Theory

Transmission through a dielectric slab. Normal incidence.

$$S_{21} = (1 - \Gamma^2)P / (1 - P^2\Gamma^2)$$

- $P = e^{-jkd}$
- $k = \omega\sqrt{\mu\epsilon}$
- d is slab thickness
- $\Gamma = (Z - Z_0) / (Z + Z_0)$
- $Z = \sqrt{\mu/\epsilon}$
- $Z_0 = \sqrt{\mu_0/\epsilon_0}$

L.3.1 Plexiglas

```

In [ ]: # calculate plexiglass theory
plexiThy = slabTheory(freq, plexi['d'], plexi['epsr'], plexi['mur'])
plexiThy.name = 'Plexiglas theory'
freeThy = slabTheory(freq, freePlexi['d'], freePlexi['epsr'], freePlexi['mur'])
freeThy.name = 'Free space theory'

# if doPlot:
#     fig, ax = plt.subplots()
#     plexiThy.plot_s_db()
#     freeThy.plot_s_db(label='Free space theory, d=1in')

```

```
# fig, ax = plt.subplots()
# plexiThy.plot_s_deg()
# freeThy.plot_s_deg(label='Free space theory, d=1in')
```

L.3.2 Free Space Across Bullex

```
In [ ]: # calculate Bullex theory
bullexThy = slabTheory(freq, freeFire['d'], freeFire['epsr'], freeFire['mur'])
bullexThy.name = "Theory"

# if doPlot:
# fig, ax = plt.subplots()
# bullexThy.plot_s_db(label="Free space above Bullex, theory, d=28in")
# _ = ax.set_ylim([-0.8, 0.1])

# fig, ax = plt.subplots()
# bullexThy.plot_s_deg(label="Free space above Bullex, theory, d=28in")
```

L.4 Calibrate Data and Export for Time Gating

Originally we imported the data, calibrated it using

$$S_{21}^c = \frac{S_{21}^m - S_{21}^p}{S_{21}^e - S_{21}^p} e^{-jk_0 d}$$

- c cald
- m measured
- p plate
- e empty
- k_0 free space wavenumber
- d sample thickness

Then it was saved so that Wavecalc could be used to time gate it. Time gating consisted of applying a cosine taper in the freq domain, applying an inverse FFT, zero filling between two time points, forward FFT, and then truncating to original frequency range.

Since this is done, we skip this code now and just import the gated data.

```
In [ ]: # original data manip

# # load in ODF files and make them ntws
# b11 = odf2ntwk(dataDir+'b1-b1-2013-08-08-122942.odf', name='sample 1-1')
# b12 = odf2ntwk(dataDir+'b1-b2-2013-08-08-123035.odf', name='sample 1-2')
# b13 = odf2ntwk(dataDir+'b1-b3-2013-08-08-123123.odf', name='sample 1-3')
# b1e = odf2ntwk(dataDir+'b1-empty-2013-08-08-122411.odf', name='empty 1')
# b1p = odf2ntwk(dataDir+'b1-plate-2013-08-08-122638.odf', name='plate 1')
# b1x = odf2ntwk(dataDir+'b1-plexi-2013-08-08-122819.odf', name='Plexiglas 1')
# b21 = odf2ntwk(dataDir+'b2-b1-2013-08-08-124510.odf', name='sample 2-1')
```

```

# b22 = odf2ntwk(dataDir+'b2-b2-2013-08-08-124557.odf', name='sample 2-2')
# b23 = odf2ntwk(dataDir+'b2-b3-2013-08-08-124654.odf', name='sample 2-3')
# b2e = odf2ntwk(dataDir+'b2-empty-2013-08-08-124058.odf', name='empty 2')
# b2p = odf2ntwk(dataDir+'b2-plate-2013-08-08-124332.odf', name='plate 2')
# b2x = odf2ntwk(dataDir+'b2-plexi-2013-08-08-124156.odf', name='Plexiglas 2')
# b31 = odf2ntwk(dataDir+'b3-b1-2013-08-08-130015.odf', name='sample 3-1')
# b32 = odf2ntwk(dataDir+'b3-b2-2013-08-08-130109.odf', name='sample 3-2')
# b33 = odf2ntwk(dataDir+'b3-b3-2013-08-08-130243.odf', name='sample 3-3')
# b34 = odf2ntwk(dataDir+'b3-b4-2013-08-08-130338.odf', name='sample 3-4')
# b3e = odf2ntwk(dataDir+'b3-empty-2013-08-08-125919.odf', name='empty 3')
# b3p = odf2ntwk(dataDir+'b3-plate-2013-08-08-125650.odf', name='plate 3')
# b3x = odf2ntwk(dataDir+'b3-plexi-2013-08-08-125827.odf', name='Plexiglas 3')

# # calibrate all data
# c11 = calibrate(b11, b1e, b1p, 28.5*inch)
# c12 = calibrate(b12, b1e, b1p, 28.5*inch)
# c13 = calibrate(b13, b1e, b1p, 28.5*inch)

# c21 = calibrate(b21, b2e, b2p, 28.5*inch)
# c22 = calibrate(b22, b2e, b2p, 28.5*inch)
# c23 = calibrate(b23, b2e, b2p, 28.5*inch)

# c31 = calibrate(b31, b3e, b3p, 28.5*inch)
# c32 = calibrate(b32, b3e, b3p, 28.5*inch)
# c33 = calibrate(b33, b3e, b3p, 28.5*inch)
# c34 = calibrate(b34, b3e, b3p, 28.5*inch)

# c1x = calibrate(b1x, b1e, b1p, 1*inch)
# c2x = calibrate(b2x, b2e, b2p, 1*inch)
# c3x = calibrate(b3x, b3e, b3p, 1*inch)

# # save data to be time gated
# ntwk2odf(c11, 0,0, fileName=dataDir+'c11')
# ntwk2odf(c12, 0,0, fileName=dataDir+'c12')
# ntwk2odf(c13, 0,0, fileName=dataDir+'c13')
# ntwk2odf(c21, 0,0, fileName=dataDir+'c21')
# ntwk2odf(c22, 0,0, fileName=dataDir+'c22')
# ntwk2odf(c23, 0,0, fileName=dataDir+'c23')
# ntwk2odf(c31, 0,0, fileName=dataDir+'c31')
# ntwk2odf(c32, 0,0, fileName=dataDir+'c32')
# ntwk2odf(c33, 0,0, fileName=dataDir+'c33')
# ntwk2odf(c34, 0,0, fileName=dataDir+'c34')
# ntwk2odf(c1x, 0,0, fileName=dataDir+'c1x')
# ntwk2odf(c2x, 0,0, fileName=dataDir+'c2x')
# ntwk2odf(c3x, 0,0, fileName=dataDir+'c3x')

```

L.5 Import Time Gated Data and Make Useable

```

In [ ]: # load in ODF files and make them ntws
c11 = odf2ntwk(dataDir+'gated5-390-c11.ODF', name='cald 1-1')

```

```

c12 = odf2ntwk(dataDir+'gated5-390-c12.ODF', name='cald 1-2')
c13 = odf2ntwk(dataDir+'gated5-390-c13.ODF', name='cald 1-3')
c21 = odf2ntwk(dataDir+'gated5-390-c21.ODF', name='cald 2-1')
c22 = odf2ntwk(dataDir+'gated5-390-c22.ODF', name='cald 2-2')
c23 = odf2ntwk(dataDir+'gated5-390-c23.ODF', name='cald 2-3')
c31 = odf2ntwk(dataDir+'gated5-390-c31.ODF', name='cald 3-1')
c32 = odf2ntwk(dataDir+'gated5-390-c32.ODF', name='cald 3-2')
c33 = odf2ntwk(dataDir+'gated5-390-c33.ODF', name='cald 3-3')
c34 = odf2ntwk(dataDir+'gated5-390-c34.ODF', name='cald 3-4')

c1x = odf2ntwk(dataDir+'gated2-390-c1x.ODF', name='cald Plexiglas 1')
c2x = odf2ntwk(dataDir+'gated2-390-c2x.ODF', name='cald Plexiglas 2')
c3x = odf2ntwk(dataDir+'gated2-390-c3x.ODF', name='cald Plexiglas 3')

```

Make Network Sets

```

In [ ]: # make a dataset for each burn, uncald and cald
c1 = rf.NetworkSet((c11,c12,c13), name='Burn 1')
c2 = rf.NetworkSet((c21,c22,c23), name='Burn 2')
c3 = rf.NetworkSet((c31,c32,c33), name='Burn 3')
cx = rf.NetworkSet((c1x,c2x,c3x), name='Plexiglas')

```

Linear Regression of Plexiglas Phase

```

In [ ]: m, b, r, p, sterr = stats.linregress(c1x.f/1e9,
                                             np.real(cx.mean_s_deg_unwrap.s[:,0,0]))

xFit_unwrap = m*c1x.f/1e9+b
xFit = ( xFit_unwrap + 180 ) % (360 ) - 180
print r

```

L.6 Burn Results

```

In [ ]: # if doPlot:
#       fig, ax = plt.subplots(2,1)
#       fig.set_figheight(7)

#       c1.mean_s.plot_s_db(ax=ax[0], label='Burn 1 mean')
#       c2.mean_s.plot_s_db(ax=ax[0], label='Burn 2 mean')
#       c3.mean_s.plot_s_db(ax=ax[0], label='Burn 3 mean')
#       bullexThy.plot_s_db(ax=ax[0], c='dimgray', ls='--', lw=0.5)

#       c1.mean_s.plot_s_deg(ax=ax[1], label='Burn 1 mean')
#       c2.mean_s.plot_s_deg(ax=ax[1], label='Burn 1 mean')
#       c3.mean_s.plot_s_deg(ax=ax[1], label='Burn 1 mean')
#       bullexThy.plot_s_deg(ax=ax[1], c='dimgray', ls='--', lw=0.5)
#       _ = ax[1].legend(loc='lower right')

#       fig, ax = plt.subplots(2,1)
#       fig.set_figheight(7)

#       c1x.plot_s_db(ax=ax[0], label='Plexi 1')

```

```

# c2x.plot_s_db(ax=ax[0], label='Plexi 2')
# c3x.plot_s_db(ax=ax[0], label='Plexi 3')
# plexiThy.plot_s_db(ax=ax[0], label='Theory', c='dimgray', ls='--', lw=0.5)
# freeThy.plot_s_db(ax=ax[0], label='Free Space', c='dimgray', ls=':', lw=0.5)
# _ = ax[0].legend(loc='lower left')

# c1x.plot_s_deg(ax=ax[1], y_label='Transmission (dB)', label='Plex 1')
# c2x.plot_s_deg(ax=ax[1], y_label='Transmission (dB)', label='Plex 2')
# c3x.plot_s_deg(ax=ax[1], y_label='Transmission (dB)', label='Plex 3')
# # c1x.plot_s_deg(ax=ax[1], c='k', ls='-')
# # c2x.plot_s_deg(ax=ax[1], c='k', ls='--')
# # c3x.plot_s_deg(ax=ax[1], c='k', ls=':')
# _ = ax[1].plot(c1x.f/1e9, xFit,
#               label="Linear fit")
# _ = ax[1].annotate("r=%.3f\ny=(%.2f)x + (%.2f)"
#                   %(np.real(r), np.real(m), np.real(b)), (2.6, -40))
# plexiThy.plot_s_deg(ax=ax[1], label='Theory', c='dimgray', ls='--', lw=0.5)
# freeThy.plot_s_deg(ax=ax[1], label='Free space', c='dimgray', ls=':', lw=0.5)
# # _ = ax[1].legend()
# _ = ax[1].legend(loc='lower right')
# # _ = ax[1].set_ylim([-180, 0])

```

In []: if doPlot:

```

fig, ax = plt.subplots(2,1)
fig.set_figheight(7)

c1.mean_s.plot_s_db(ax=ax[0], label='Burn 1 mean')
c2.mean_s.plot_s_db(ax=ax[0], ls='-.', label='Burn 2 mean')
c3.mean_s.plot_s_db(ax=ax[0], ls='--', label='Burn 3 mean')
bullexThy.plot_s_db(ax=ax[0], ls=':', c='k', label='Free space')

c1.mean_s.plot_s_deg(ax=ax[1], label='Burn 1 mean', show_legend=False)
c2.mean_s.plot_s_deg(ax=ax[1], ls='-.', label='Burn 2 mean', show_legend=False)
c3.mean_s.plot_s_deg(ax=ax[1], ls='--', label='Burn 3 mean', show_legend=False)
bullexThy.plot_s_deg(ax=ax[1], ls=':', c='k',
                    label='Free space', show_legend=False)

if doSave:
    fig.savefig(dataDir+'2013-08-08-burn.pdf')

# -----
# unwrapped burn
fig, ax = plt.subplots()
c1.mean_s.plot_s_deg_unwrap(ax=ax, label='Burn 1 mean')
c2.mean_s.plot_s_deg_unwrap(ax=ax, ls='-.', label='Burn 2 mean')
c3.mean_s.plot_s_deg_unwrap(ax=ax, ls='--', label='Burn 3 mean')
bullexThy.plot_s_deg_unwrap(ax=ax, ls=':', c='k',
                          label='Free space')

if doSave:
    fig.savefig(dataDir+'2013-08-08-burn-unwrap.pdf')

```

```

# -----
# Plexiglas measurements
fig, ax = plt.subplots(2,1)
fig.set_figheight(7)

cx.mean_s.plot_s_db(ax=ax[0], label='Plexiglas, mean')
plexiThy.plot_s_db(ax=ax[0], ls='--', label=r'Theory, $\epsilon_r=0.1f$',
    % plexi['epsr'])
freeThy.plot_s_db(ax=ax[0], ls='-.', c='k', label='Free Space')
#     _ = ax[0].legend(loc='lower left')

cx.mean_s.plot_s_deg(ax=ax[1], label='Plexiglas, mean', show_legend=False)
plexiThy.plot_s_deg(ax=ax[1], ls='--', label='Theory', show_legend=False)
freeThy.plot_s_deg(ax=ax[1], ls='-.', c='k',
    label='Free space', show_legend=False)

if doSave:
    fig.savefig(dataDir+'2013-08-08-plexi.pdf')

# -----
# unwrapped plexiglass
fig, ax = plt.subplots()
cx.mean_s.plot_s_deg_unwrap(ax=ax, label='Plexiglas, mean')
plexiThy.plot_s_deg_unwrap(ax=ax, ls='--', label=r'Theory, $\epsilon_r=0.1f$',
    % plexi['epsr'])
_ = ax.plot(c1x.f/1e9, xFit_unwrap, label='Best fit of mean')
freeThy.plot_s_deg_unwrap(ax=ax, ls='-.', c='k',
    label='Free space')

if doSave:
    fig.savefig(dataDir+'2013-08-08-plexi-unwrap.pdf')

```


Appendix M

IPython notebook: Bullex-at-BTFD-2013-12-06

M.1 Experiments at BTFD using the Bullex Fire Extinguisher Trainer

- Conducted at BTFD
- 2013-12-06

M.1.1 Files

```
In [ ]: !ls -l ~/Documents/code/Data/2013-12-06/
```

M.2 Pre-flight

M.2.1 Imports

```
In [ ]: # Import basic modules
        # make sure that division is done as expected
        from __future__ import division

        # plotting setup
        %matplotlib inline
        import matplotlib.pyplot as plt
        plt.style.use('gray_back')

        # get the viridis colormap
        # https://bids.github.io/colormap
        # it will be available as cmaps.viridis
        import colormaps as cmaps

        # for 3d graphs
```

```

# from mpl_toolkits.mplot3d import axes3d
# for legends of combined fig types
# import matplotlib.lines as mlines

# numerical functions
import numpy as np

# need some constants
from scipy import constants
from numpy import pi

# RF tools!
import skrf as rf

# version information
# %install_ext http://raw.githubusercontent.com/jrjohansson/version_information/
# master/version_information.py
# %load_ext version_information
# %reload_ext version_information

# %version_information numpy, scipy, matplotlib

```

```
In [ ]: from scipy import stats
```

M.2.2 Parameters, Config, and Constants

```
In [ ]: dataDir = '/mnt/home/temmeand/Documents/code/Data/2013-12-06/'
```

```

doPlot = True
# doSave = True
doSave = False

if doSave: doPlot = True

plt.rcParams['axes.ymargin'] = 0

In [ ]: fmin = 2.5e9
        fmax = 5.5e9
        fpts = 201

        freeFire = { 'epsr': 1
                      , 'mur' : 1
                      , 'd' : 11.25*constants.inch
                      #   , 'd' : 12*constants.inch
                    }

```

M.2.3 Error Checking

```
In [ ]: # none at this time
```

M.2.4 Prelim Calculations

```
In [ ]: freq = np.linspace(fmin, fmax, fpts)
```

M.2.5 Function Definitions

```
In [ ]: def ntwk2odf(ntwk, m=1, n=0, fileName=None, EOL='\r\n'):
    '''
    Saves an skrf network in ODF format

    Save one s-parameter from a network as an odf formatted file. In
    the frequency domain, each line contains the frequency, real
    values, and imaginary values seperated by commas.

    'm' and 'n' allow you to pick which S parameter to save

    If no file name is given, the name of the network is used

    Default end of line character is Windows compatible (\\r\\n)

    Parameters
    -----
    ntwk : skrf Network object
        Data to be saved

    m,n : int
        Specifies the S parameter to be saved as S_m,n

    fileName : string
        Name of the saved file. If no string is provided, the
        name of the network is used

    EOL : string
        String to be used at the end of the line
        \\r\\n - Dos
        \\n - Unix

    Returns
    -----
    Nothing

    '''
    fileName = ntwk.name if fileName is None else fileName
    with open(fileName+'.odf','w') as fo:
        data = np.vstack((ntwk.f/1e9, ntwk.s_re[:,m,n],ntwk.s_im[:,m,n])).T
        np.savetxt(fo, data, delimiter=',',newline=EOL)

def odf2ntwk(fileName, name=""):
    '''
    Load ODF file as ntwk
```

```

Create a one port s-parameter network from an odf formatted file. In
the frequency domain, each line contains the frequency, real
value, and imaginary value seperated by commas.

Parameters
-----
fileName : string
    File to be loaded

Returns
-----
ntwk : skrf Network object
'''
# from numpy import loadtxt
import skrf as rf
f = open(fileName, 'r')
raw = np.loadtxt(f, delimiter=',')
f.close()

if name is "": name = fileName

freq = raw[:,0]
data = raw[:,1]+1j*raw[:,2]
# ntwk = rf.Network(name=fileName, f=freq, f_unit='GHz', z0=50, s=data)
ntwk = rf.Network(name=name, f=freq, f_unit='GHz', z0=50, s=data)

return ntwk

def calibrate(raw, empty, plate, thick):
    """
    Calibrate raw data using empty and plate measurement

    For S21 data:

        
$$Cald = (raw - plate) / (empty - plate) * \exp(-j * k_0 * thick)$$


    Parameters
    -----
    raw : skrf network
        raw data to be calibrated
    empty : skrf network
        empty range measurement
    plate : skrf network
        measurement of plate at the position of the sample
    thick : number
        thickness of material sample in meters

    Returns
    -----
    cald : skrf network
        Calibrate data

```

```

"""

k = wavenumber(raw.f, 1, 1)
cald = (raw-plate) / (empty-plate) * np.exp(-1j*k*thick)
cald.name = cald.name + ", cald"

return cald

def analyze(raw, empty, plate, thick, name="", _doPlot=False, _doSave=False):
    """
    Process the data

    Calibrate the data and plot

    Parameters
    -----
    raw : skrf network
        raw data to be calibrated
    empty : skrf network
        empty range measurement
    plate : skrf network
        measurement of plate at the position of the sample
    thick : number
        sample thickness in meters
    name : string
        label or name to use on graphs
    _doPlot : boolean
        make plots
    _doSave : boolean
        save plots

    Returns
    -----
    cald : skrf network
        calibrated network
    """
    cald = calibrate(raw, empty, plate, thick)

    if name is not "":
        cald.name = name

    if _doPlot:
        fig, ax = plt.subplots(2,1)
        fig.set_figheight(7)

        ax[0].set_title('Dataset: ' + name)
        raw.plot_s_db(ax=ax[0], label='Raw ')
        cald.plot_s_db(ax=ax[0], label='Cald ')

        raw.plot_s_deg(ax=ax[1], show_legend=False)
        cald.plot_s_deg(ax=ax[1], show_legend=False)

```

```

        if _doSave:
            fig.savefig(name+'.pdf')

    return cald

def wavenumber(f, epsr, mur):
    return 2*pi*f*np.sqrt(constants.epsilon_0*epsr
                           *constants.mu_0*mur)

def propFactor(k, d):
    return np.exp(-1j*k*d)

def impedance(epsr=1, mur=1):
    return np.sqrt(constants.mu_0*mur/(constants.epsilon_0*epsr))

def reflectionCoeff(eta, etaf):
    return (eta-etaf)/(eta+etaf)

def transmission(p, g):
    return (1-g**2)*p/(1-p**2*g**2)

def slabTheory(f, d, epsr=1, mur=1):
    """
    Theoretical slab transmission

    
$$S_{21} = \frac{(1-\Gamma^2)P}{(1-P^2\Gamma^2)}$$


    
$$P = \exp(-j k d)$$


    
$$k = \omega \sqrt{\mu \epsilon}$$


    
$$d = \text{thickness}$$


    
$$\Gamma = \frac{Z-Z_0}{Z+Z_0}$$


    
$$Z = \sqrt{\mu/\epsilon}$$

    
$$Z_0 = \sqrt{\mu_0/\epsilon_0}$$

    """
    k = wavenumber(f, epsr, mur)
    eta = impedance(epsr, mur)
    etaFree = impedance(1, 1)

    p = propFactor(k, d)
    g = reflectionCoeff(eta, etaFree)
    s21 = transmission(p, g)

    name = "Theory"

    f = f/1e9
    ntwk = rf.Network(name=name, f=f, f_unit='ghz', z0=50, s=s21)

```

```
return ntwk
```

M.3 Theory

Transmission through a dielectric slab. Normal incidence.

$$S_{21} = (1 - \Gamma^2)P / (1 - P^2\Gamma^2)$$

- $P = e^{-jkd}$
- $k = \omega\sqrt{\mu\epsilon}$
- d is slab thickness
- $\Gamma = (Z - Z_0)/(Z + Z_0)$
- $Z = \sqrt{\mu/\epsilon}$
- $Z_0 = \sqrt{\mu_0/\epsilon_0}$

M.3.1 Free Space Across Bullex

```
In [ ]: # calculate Bullex theory
        bullexThy = slabTheory(freq, freeFire['d'], freeFire['epsr'], freeFire['mur'])
        bullexThy.name = "Theory"

        # if doPlot:
        #     fig, ax = plt.subplots()
        #     bullexThy.plot_s_db(label="Free space above Bullex, theory, d=%.2f in"
        #                        % (freeFire['d']/constants.inch))
        #     _ = ax.set_ylim([-0.8, 0.1])

        #     fig, ax = plt.subplots()
        #     bullexThy.plot_s_deg(label="Free space above Bullex, theory, d=%.2f in"
        #                          % (freeFire['d']/constants.inch))
```

M.4 Calibrate Data and Export for Time Gating

Originally we imported the data, calibrated it using

$$S_{21}^c = \frac{S_{21}^m - S_{21}^p}{S_{21}^e - S_{21}^p} e^{-jk_0 d}$$

- c cald
- m measured
- p plate
- e empty
- k_0 free space wavenumber

- d sample thickness

Then it was saved so that Wavecalc could be used to time gate it. Time gating consisted of applying a cosine taper in the freq domain, applying an inverse FFT, zero filling between two time points, forward FFT, and then truncating to original frequency range.

Since this is done, we skip this code now and just import the gated data.

```
In [ ]: ## original data manip

## load in ODF files and make them ntws
# b1a = odf2ntwk(dataDir+'burn1-2013-12-06-165943.odf', name='burn 1a')
# b2a = odf2ntwk(dataDir+'burn2-2013-12-06-170045.odf', name='burn 2a')
# b3a = odf2ntwk(dataDir+'burn3-2013-12-06-170139.odf', name='burn 3a')
# b3b = odf2ntwk(dataDir+'burn3-2013-12-06-170155.odf', name='burn 3b')
# b4a = odf2ntwk(dataDir+'burn4-2013-12-06-170414.odf', name='burn 4a')
# b4b = odf2ntwk(dataDir+'burn4-2013-12-06-170426.odf', name='burn 4b')
# b5a = odf2ntwk(dataDir+'burn5-2013-12-06-170546.odf', name='burn 5a')
# b5b = odf2ntwk(dataDir+'burn5-2013-12-06-170558.odf', name='burn 5b')
# plate = odf2ntwk(dataDir+'plate-2013-12-06-165331.odf', name='plate')
# thrua = odf2ntwk(dataDir+'through-2013-12-06-164957.odf', name='thru a')
# thrub = odf2ntwk(dataDir+'through-2013-12-06-165012.odf', name='thru b')

## plot plate measurement
# plate.plot_s_db(show_legend=False)
# plt.figure()
# plate.plot_s_deg(show_legend=False)

## plot thru measurements
# if doPlot:
#     fig, ax = plt.subplots()

#     thrua.plot_s_db(ax=ax, label='Thru A')
#     thrub.plot_s_db(ax=ax, label='Thru B')

#     fig, ax = plt.subplots()

#     thrua.plot_s_deg(ax=ax, label='Thru A')
#     thrub.plot_s_deg(ax=ax, label='Thru B')

## diff = np.abs(thrua.s[:,0,0]-thrub.s[:,0,0])
# magDiff = np.abs(thrua.s_db[:,0,0]-thrub.s_db[:,0,0])
# degDiff = np.abs(thrua.s_deg_unwrap[:,0,0]-thrub.s_deg_unwrap[:,0,0])
# if doPlot:
#     fig, ax = plt.subplots()
#     # _ = ax.plot(thrua.f,diff, label="diff")
#     _ = ax.plot(thrua.f,magDiff, label="mag")
#     fig, ax = plt.subplots()
#     _ = ax.plot(thrua.f,degDiff, label="deg")
#     # _ = ax.legend()
```



```

# # calibrate all data
# c1a = calibrate(b1a, thrua, plate, freeFire['d'])
# c2a = calibrate(b2a, thrua, plate, freeFire['d'])
# c3a = calibrate(b3a, thrua, plate, freeFire['d'])
# c3b = calibrate(b3b, thrua, plate, freeFire['d'])
# c4a = calibrate(b4a, thrua, plate, freeFire['d'])
# c4b = calibrate(b4b, thrua, plate, freeFire['d'])
# c5a = calibrate(b5a, thrua, plate, freeFire['d'])
# c5b = calibrate(b5b, thrua, plate, freeFire['d'])

# if doPlot:
#     fig, ax = plt.subplots()
#     c1a.plot_s_db()
#     c2a.plot_s_db()
#     c3a.plot_s_db()
#     c3b.plot_s_db()
#     c4a.plot_s_db()
#     c4b.plot_s_db()
#     c5a.plot_s_db()
#     c5b.plot_s_db()

# if doPlot:
#     fig, ax = plt.subplots()
#     b1a.plot_s_deg()
#     b2a.plot_s_deg()
#     b3a.plot_s_deg()
#     b3b.plot_s_deg()
#     b4a.plot_s_deg()
#     b4b.plot_s_deg()
#     b5a.plot_s_deg()
#     b5b.plot_s_deg()

# if doPlot:
#     fig, ax = plt.subplots()
#     c1a.plot_s_deg()
#     c2a.plot_s_deg()
#     c3a.plot_s_deg()
#     c3b.plot_s_deg()
#     c4a.plot_s_deg()
#     c4b.plot_s_deg()
#     c5a.plot_s_deg()
#     c5b.plot_s_deg()

# # save data to be time gated
# ntwk2odf(c1a, 0,0, fileName=dataDir+'c1a')
# ntwk2odf(c2a, 0,0, fileName=dataDir+'c2a')
# ntwk2odf(c3a, 0,0, fileName=dataDir+'c3a')
# ntwk2odf(c3b, 0,0, fileName=dataDir+'c3b')
# ntwk2odf(c4a, 0,0, fileName=dataDir+'c4a')
# ntwk2odf(c4b, 0,0, fileName=dataDir+'c4b')

```

```
# ntwk2odf(c5a, 0,0, fileName=dataDir+'c5a')
# ntwk2odf(c5b, 0,0, fileName=dataDir+'c5b')
```

M.5 Import Time Gated Data and Make Useable

```
In [ ]: # load in ODF files and make them ntwks
c1a = odf2ntwk(dataDir+'gated3-380-c1a.ODF', name='cald 1a')
c2a = odf2ntwk(dataDir+'gated3-380-c2a.ODF', name='cald 2a')
c3a = odf2ntwk(dataDir+'gated3-380-c3a.ODF', name='cald 3a')
c3b = odf2ntwk(dataDir+'gated3-380-c3b.ODF', name='cald 3b')
c4a = odf2ntwk(dataDir+'gated3-380-c4a.ODF', name='cald 4a')
c4b = odf2ntwk(dataDir+'gated3-380-c4b.ODF', name='cald 4b')
c5a = odf2ntwk(dataDir+'gated3-380-c5a.ODF', name='cald 5a')
c5b = odf2ntwk(dataDir+'gated3-380-c5b.ODF', name='cald 5b')
```

Make Network Sets

```
In [ ]: # make a dataset for each burn, uncald and cald
c = rf.NetworkSet((c1a, c2a, c3a, c3b, c4a, c4b, c5a, c5b),
                  name='Cald/Gated burns')
```

Linear Regression of Plexiglass Phase

```
In [ ]: m, b, r, p, sterr = stats.linregress(c1a.f/1e9,
                                              np.real(c.mean_s_deg_unwrap.s[:,0,0]))

xFit = m*c1a.f/1e9+b
xFit = ( xFit + 180) % (360 ) - 180
print r
```

M.6 Burn Results

```
In [ ]: # if doPlot:
#       fig, ax = plt.subplots(2,1)
#       fig.set_figheight(7)

#       c1a.plot_s_db(ax=ax[0], label='Cald 1a')
#       c2a.plot_s_db(ax=ax[0], label='Cald 2a')
#       c3a.plot_s_db(ax=ax[0], label='Cald 3a')
#       c3b.plot_s_db(ax=ax[0], label='Cald 3b')
#       c4a.plot_s_db(ax=ax[0], label='Cald 4a')
#       c4b.plot_s_db(ax=ax[0], label='Cald 4b')
#       c5a.plot_s_db(ax=ax[0], label='Cald 5a')
#       c5b.plot_s_db(ax=ax[0], label='Cald 5b')
#       bullexThy.plot_s_db(ax=ax[0], c='dimgray', ls='--', lw=0.5)

#       c1a.plot_s_deg(ax=ax[1], label='Cald 1a', c='k', lw='0.5')
#       c2a.plot_s_deg(ax=ax[1], label='Cald 2a', c='k', lw='0.5')
#       c3a.plot_s_deg(ax=ax[1], label='Cald 3a', c='k', lw='0.5')
#       c3b.plot_s_deg(ax=ax[1], label='Cald 3b', c='k', lw='0.5')
```

```

# c4a.plot_s_deg(ax=ax[1], label='Cald 4a', c='k', lw='0.5')
# c4b.plot_s_deg(ax=ax[1], label='Cald 4b', c='k', lw='0.5')
# c5a.plot_s_deg(ax=ax[1], label='Cald 5a', c='k', lw='0.5')
# c5b.plot_s_deg(ax=ax[1], label='Cald 5b', c='k', lw='0.5')
# bullexThy.plot_s_deg(ax=ax[1], c='dimgray', ls='--', lw=0.5)

# _ = ax[1].plot(c1a.f/1e9, xFit, c=plt.rcParams['axes.color_cycle'][0],
#               label="Linear fit")
# _ = ax[1].legend()
# _ = ax[1].annotate("r=%.3f\nny=(%.2f)x + (%.2f)"
#                   %(np.real(r), np.real(m), np.real(b)), (2.6, -40))
# _ = ax[1].legend(loc='upper right')
# _ = ax[1].set_ylim([-180, 0])

```

```

In [ ]: if doPlot:
        fig, ax = plt.subplots(2,1)
        fig.set_figheight(7)

        c.mean_s.plot_s_db(ax=ax[0], label='Mean of all burns')
        bullexThy.plot_s_db(ax=ax[0], label='Free space', ls='--')

        c.mean_s.plot_s_deg(ax=ax[1], show_legend=False)
        bullexThy.plot_s_deg(ax=ax[1], ls='--', show_legend=False)

        if doSave:
            fig.savefig(dataDir+'2013-12-06-burn.pdf')

        # -----
        # unwrapped phase
        fig, ax = plt.subplots()
        c.mean_s.plot_s_deg_unwrap(ax=ax, label='Mean of all burns')
        bullexThy.plot_s_deg_unwrap(ax=ax, ls='--', label='Free space')

        if doSave:
            fig.savefig(dataDir+'2013-12-06-burn-unwrap.pdf')

```

Appendix N

IPython notebook: analysis-of-2015-02-15

N.1 Analysis of Interferometric Measurements from 2015-02-15

Description

Available datasets are:

| Data Set Name | Cat | No Files | Description |
|---------------|-------|----------|-------------|
| ----- | ----- | ----- | ----- |

N.2 Pre-flight

This section sets up the notebook.

N.2.1 Imports

```
In [ ]: # Import basic modules
        # make sure that division is done as expected
        from __future__ import division

        # plotting setup
        %matplotlib inline
        import matplotlib.pyplot as plt
        plt.style.use('gray_back')
        plt.rcParams['axes.ymargin'] = 0

        # get the viridis colormap
        # https://bids.github.io/colormap
        # it will be available as cmaps.viridis
        import colormaps as cmaps

        # for 3d graphs
        from mpl_toolkits.mplot3d import axes3d
```

```

# for legends of combined fig types
# import matplotlib.lines as mlines

# numerical functions
import numpy as np

# need some constants
from scipy import constants
from numpy import pi

# RF tools!
import skrf as rf

# version information
# %install_ext http://raw.githubusercontent.com/jrjohansson/
# version_information/master/version_information.py
# %load_ext version_information
# %reload_ext version_information

# %version_information numpy, scipy, matplotlib

In [ ]: from matplotlib import colors, colorbar
import os
import glob

```

N.2.2 Parameters, Config, and Constants

```

In [ ]: dataDir = './wichman/Data/2015-02-15/'
        cmapUse = cmaps.viridis
        cmapRel = plt.get_cmap(name='PRGn')
        normAll = 78

In [ ]: doPrint = True
        doPlot = True
        doLongPlot = True
        # doLongPlot = False
        doSave = True
        # doSave = False

        if doSave: doPlot = True

```

N.2.3 Error Checking

```

In [ ]: # none at this time

```

N.2.4 Prelim Calculations

```

In [ ]: # none at this time

```

N.2.5 Function Definitions

```
In [ ]: def ntwk2odf(ntwk, m=1, n=0, fileName=None, EOL='\r\n'):
    '''
    Saves an skrf network in ODF format

    Save one s-parameter from a network as an odf formatted file. In
    the frequency domain, each line contains the frequency, real
    values, and imaginary values seperated by commas.

    'm' and 'n' allow you to pick which S parameter to save

    If no file name is given, the name of the network is used

    Default end of line character is Windows compatible (\\r\\n)

    Parameters
    -----
    ntwk : skrf Network object
        Data to be saved

    m,n : int
        Specifies the S parameter to be saved as S_m,n

    fileName : string
        Name of the saved file. If no string is provided, the
        name of the network is used

    EOL : string
        String to be used at the end of the line
        \\r\\n - Dos
        \\n - Unix

    Returns
    -----
    Nothing

    '''
    fileName = ntwk.name if fileName is None else fileName
    with open(fileName+'.odf', 'w') as fo:
        data = np.vstack((ntwk.f/1e9, ntwk.s_re[:,m,n], ntwk.s_im[:,m,n])).T
        np.savetxt(fo, data, delimiter=',', newline=EOL)

def odf2ntwk(fileName, name=""):
    '''
    Load ODF file as ntwk

    Create a one port s-parameter network from an odf formatted file. In
    the frequency domain, each line contains the frequency, real
    value, and imaginary value seperated by commas.

    Parameters
```

```

-----
fileName : string
    File to be loaded

Returns
-----
ntwk : skrf Network object
'''
# from numpy import loadtxt
import skrf as rf
f = open(fileName, 'r')
raw = np.loadtxt(f, delimiter=',')
f.close()

if name is "": name = fileName

freq = raw[:,0]
data = raw[:,1]+1j*raw[:,2]
# ntwk = rf.Network(name=fileName, f=axis, f_unit='GHz', z0=50, s=data)
ntwk = rf.Network(name=name, f=freq, f_unit='GHz', z0=50, s=data)

return ntwk

def processWichBurnODF(dataDir, emptyName, sampleName, D, fRange="",
                        figTitle="", skip=[], ntwkODF="odf"):
    """
    D in inches
    """

    from scipy.constants import c, inch

    if ntwkODF is "odf":
        eList = []
        sList = []

        skip = [dataDir + s for s in skip]

        for o in glob.glob(dataDir+emptyName+"*.ODF"):
            if o not in skip:
                n = odf2ntwk(o)
                if fRange is not "":
                    n = n[fRange]
                # print n
                eList.append(n)
            else:
                print "removed %s" % o

        for o in glob.glob(dataDir+sampleName+"*.ODF"):
            if o not in skip:
                n = odf2ntwk(o)
                if fRange is not "":

```

```

        n = n[fRange]
        #         print n
        sList.append(n)
    else:
        print "removed %s" % o

#     print len(eList)
#     print len(sList)

    empty = rf.NetworkSet(eList)
    salt = rf.NetworkSet(sList)
elif ntwkODF is "ntwk":
    empty = rf.NetworkSet(rf.read_all(dataDir,contains=emptyName))
    salt = rf.NetworkSet(rf.read_all(dataDir,contains=sampleName))

empty.sort()
salt.sort()

freq = salt[0].f/1e9
phase = salt[0].s_deg_unwrap[:,0,0]
for n in salt[1:]:
    phase = np.vstack([phase, n.s_deg_unwrap[:,0,0]])

empty = empty.mean_s
emptyPhase = empty.s_deg_unwrap[:,0,0]
diff = phase-emptyPhase
N = lambda p,f: np.deg2rad(p)/(2.82e-15*(c/f)*D*inch)

Ne = N(diff,freq*1e9)

diffMask = diff < 0
diffMasked = np.ma.array(diff,mask=diffMask)
neMask = Ne < 0
NeMasked = np.ma.array(Ne,mask=neMask)

diffSurf = diff.copy()
diffLessZero = diffSurf < 0
diffSurf[diffLessZero] = 0

NeSurf = Ne.copy()
NeLessZero = NeSurf < 0
NeSurf[NeLessZero] = 0

absMaxDiff = np.max([np.max(diff), abs(np.min(diff))])
absMaxNe = np.max([np.max(Ne), abs(np.min(Ne))])
print absMaxDiff
print absMaxNe

#     from mpl_toolkits.mplot3d import Axes3D
#     import matplotlib.pyplot as plt

```



```

# -----
# -----
#     fig = plt.figure()
#     ax = fig.gca(projection='3d')
#
#     for i, n in enumerate(diff):
#         ax.plot(freq, n, i, zdir='y')
#
#     # ax.legend()
#     ax.set_xlim3d(min(freq),max(freq))
#     ax.set_ylim3d(-1,diff.shape[0])
#     ax.set_zlim3d(diff.min(),diff.max())
#
#     ax.set_xlabel('Frequency (GHz)')
#     ax.set_ylabel('Sample No. ')
#     ax.set_zlabel('Phase Difference (deg)')
#
#     if figTitle is not "":
#         ax.set_title(figTitle)
#
# plt.show()
#
# *****
#
# plt.figure()
# empty.plot_s_db(show_legend=False)
# if figTitle is not "":
#     plt.title(figTitle)
# plt.legend(['Empty'])
#
# *****
#
# plt.figure()
# salt.plot_s_db(show_legend=False)
# if figTitle is not "":
#     plt.title(figTitle)
# plt.legend(['Salt'])
#
# *****
#
# plt.figure()
# empty.plot_s_deg(show_legend=False)
# if figTitle is not "":
#     plt.title(figTitle)
# plt.legend(['Empty'])
#
# *****
#
# plt.figure()
# salt.plot_s_deg(show_legend=False)

```

```

# if figTitle is not "":
#     plt.title(figTitle)
# plt.legend(['Salt'])
#
# *****
#
# plt.figure()
# for x in diff:
#     plt.plot(freq,x)
# plt.xlabel('Frequency (GHz)')
# plt.ylabel('Phase Difference (deg)')
# if figTitle is not "":
#     plt.title(figTitle)
#
# from scipy.constants import c, inch
#
# *****
#
# plt.figure()
# for x in Ne:
#     plt.plot(freq,x)
#
# plt.xlabel('Frequency (GHz)')
# plt.ylabel(r'Electron Density,  $N$  ( $m^{-3}$ )')
# if figTitle is not "":
#     plt.title(figTitle)
#
# ax2 = twinx()
# ax2.set_xscale('log')
# grid(False, 'both', 'both')
# ax2.xlabel('Plasma Thickness (mm)')
# ax2.set_xlim([min(D), max(D)])
# t = [30, 50, 100, 200, 300, 500]
# ax2.set_xticks(t)
# ax2.set_xticklabels(t)
# ax2.invert_xaxis()
# plot(freq,empty.s_deg[:,0,0])
#
# *****
#
# fig = plt.figure()
# ax = fig.gca(projection='3d')
#
# for i, n in enumerate(Ne):
#     ax.plot(freq, n, i, zdir='y')
#
# ax.legend()
#
# ax.set_xlim3d(min(freq),max(freq))
# ax.set_ylim3d(-1,Ne.shape[0])
# ax.set_zlim3d(Ne.min(),Ne.max())

```

```

#
#     ax.set_xlabel('Frequency (GHz)')
#     ax.set_ylabel('Sample No.')
#     ax.set_zlabel(r'Electron Density, N (m-3)')
#
#     if figTitle is not "":
#         ax.set_title(figTitle)
#
#     plt.show()
#
# # -----
# # -----
# # -----
# # -----
#
#     # 3D graphs of Phase Difference
#     # -----
#     fig = plt.figure()
#     ax = fig.gca(projection='3d')
#
#     X = freq
#     Y = np.arange(1,diff.shape[0]+1)
#     X, Y = np.meshgrid(X, Y)
#     Z=diffSurf
#     surf = ax.plot_surface(X,Y,Z, rstride=1, cstride=1, linewidth=0,
#                             cmap=cmapUse)#, vmin=0, vmax=absMaxDiff)
#
#     # ax.legend()
#     ax.set_xlim3d(min(freq),max(freq))
#     ax.set_ylim3d(-1,Z.shape[0])
#     ax.set_zlim3d(Z.min(),Z.max())
#
#     ax.set_xlabel('Frequency (GHz)')
#     ax.set_ylabel('Sample No.')
#     ax.set_zlabel(r'Phase Difference,  $\angle_1 - \angle_0$  (deg)')
#     if figTitle is not "":
#         ax.set_title(figTitle)
#
#     plt.show()
#
#     # *****
#
#     plt.figure()
#     plt.imshow(diffMasked,interpolation='none',origin='lower',
#                 cmap=cmapUse,# vmin=0, vmax=absMaxDiff,
#                 extent=[freq.min(),freq.max(),1,diff.shape[0]+1],aspect='auto')
#     plt.grid('off')
#     cb=plt.colorbar()
#     cb.set_label(r'Phase Difference,  $\angle_1 - \angle_0$  (deg)')
#     plt.xlabel('Frequency (GHz)')
#     plt.ylabel('Sample Number')

```

```

#         if figTitle is not "":
#             plt.title(figTitle)
#
# # -----
#
#         # 3D graphs of Electron Density
#         # -----
#         fig = plt.figure()
#         ax = fig.gca(projection='3d')
#
#         X = freq
#         Y = np.arange(1,Ne.shape[0]+1)
#         X, Y = np.meshgrid(X, Y)
#         Z=NeSurf
#         surf = ax.plot_surface(X,Y,Z, rstride=1, cstride=1, linewidth=0,
#                                cmap=cmapUse)#, vmin=0, vmax=absMaxNe)
#
#
#         # ax.legend()
#         ax.set_xlim3d(min(freq),max(freq))
#         ax.set_ylim3d(-1,Z.shape[0])
#         ax.set_zlim3d(Z.min(),Z.max())
#
#         ax.set_xlabel('Frequency (GHz)')
#         ax.set_ylabel('Sample No.')
#         ax.set_zlabel(r'Electron Density, N (m-3)')
#         if figTitle is not "":
#             ax.set_title(figTitle)
#
#         plt.show()
#
#         # *****
#
#         plt.figure()
#         plt.imshow(NeMasked, interpolation='none', origin='lower',
#                    cmap=cmapUse, # vmin=0, vmax=absMaxNe,
#                    extent=[freq.min(),freq.max(),1,Ne.shape[0]+1], aspect='auto')
#         plt.grid('off')
#         cb=plt.colorbar()
#         cb.set_label(r'Electron Density, N (m-3)')
#         plt.xlabel('Frequency (GHz)')
#         plt.ylabel('Sample Number')
#         if figTitle is not "":
#             plt.title(figTitle)
#
# # -----
# # -----
# # -----
# # -----
# # Relative Colors
# # -----
#

```

```

# 3D graphs of Phase Difference
# -----
fig = plt.figure()
ax = fig.gca(projection='3d')
ax.set_axis_bgcolor('white')

X = freq
Y = np.arange(1,diff.shape[0]+1)
X, Y = np.meshgrid(X, Y)
Z=diff
surf = ax.plot_surface(X,Y,Z, rstride=1, cstride=1, linewidth=0,
                        cmap=cmapRel, vmin=-absMaxDiff, vmax=absMaxDiff)

# ax.legend()
ax.set_xlim3d(min(freq),max(freq))
ax.set_ylim3d(-1,Z.shape[0])
ax.set_zlim3d(Z.min(),Z.max())

ax.set_xlabel('Frequency (GHz)')
ax.set_ylabel('Sample No.')
ax.set_zlabel(r'Phase Difference, $\angle_1-\angle_0$ (deg)')
# if figTitle is not "":
#     ax.set_title(figTitle)

plt.show()

if doSave:
    fig.savefig(dataDir+figTitle+"-3d.pdf")
    fig.savefig(dataDir+figTitle+"-3d.jpg")
# *****

# plt.figure()
# plt.imshow(diff,interpolation='none',origin='lower',
#             cmap=cmapRel, vmin=-absMaxDiff, vmax=absMaxDiff,
#             extent=[freq.min(),freq.max(),1,diff.shape[0]+1],aspect='auto')
# plt.grid('off')
# cb=plt.colorbar()
# cb.set_label(r'Phase Difference, $\angle_1-\angle_0$ (deg)')
# plt.xlabel('Frequency (GHz)')
# plt.ylabel('Sample Number')
# if figTitle is not "":
#     plt.title(figTitle)

# if doSave:
#     plt.savefig(dataDir+figTitle+"-2d.pdf")
#     plt.savefig(dataDir+figTitle+"-2d.jpg")
#
#
# # -----
#
# # 3D graphs of Electron Density

```

```

# -----
# fig = plt.figure()
# ax = fig.gca(projection='3d')
#
# X = freq
# Y = np.arange(1,Ne.shape[0]+1)
# X, Y = np.meshgrid(X, Y)
# Z=Ne
# surf = ax.plot_surface(X,Y,Z, rstride=1, cstride=1, linewidth=0,
#                        cmap=cmapRel, vmin=-absMaxNe, vmax=absMaxNe)
#
#
# ax.legend()
# ax.set_xlim3d(min(freq),max(freq))
# ax.set_ylim3d(-1,Z.shape[0])
# ax.set_zlim3d(Z.min(),Z.max())
#
# ax.set_xlabel('Frequency (GHz)')
# ax.set_ylabel('Sample No.')
# ax.set_zlabel(r'Electron Density, N (m$^{-3}$)')
# if figTitle is not "":
#     ax.set_title(figTitle)
#
# plt.show()
#
# *****
#
# plt.figure()
# plt.imshow(Ne, interpolation='none', origin='lower',
#            cmap=cmapRel, vmin=-absMaxNe, vmax=absMaxNe,
#            extent=[freq.min(),freq.max(),1,Ne.shape[0]+1], aspect='auto')
# plt.grid('off')
# cb=plt.colorbar()
# cb.set_label(r'Electron Density, N (m$^{-3}$)')
# plt.xlabel('Frequency (GHz)')
# plt.ylabel('Sample Number')
# if figTitle is not "":
#     plt.title(figTitle)
# -----
# 2d figure with 2 colorbars

fig = plt.figure(figsize=(6,4))
ax = fig.add_axes([0.05,0.05,0.7,0.7])
p = ax.imshow(diff, interpolation='none', origin='lower',
              cmap=cmapRel, vmin=-absMaxDiff, vmax=absMaxDiff,
              extent=[freq.min(),freq.max(),1,diff.shape[0]+1], aspect='auto')
ax.grid('off')
plt.xlabel('Frequency (GHz)')
plt.ylabel('Sample Number')

cb=plt.colorbar(p)

```

```

cb.set_label(r'Phase Difference, $\angle_1-\angle_0$ (deg)')
axC = fig.add_axes([0.8,0.05,.02,.7])
norm = colors.Normalize(vmin=-absMaxNe, vmax=absMaxNe)
cb2 = colorbar.ColorbarBase(axC, cmap=cmapRel, norm=norm)
cb2.set_label('Electron Density, $m^{-3}$')

# if figTitle is not "":
#     plt.title(figTitle)

if doSave:
    plt.savefig(dataDir+figTitle+"-2d.pdf")
    plt.savefig(dataDir+figTitle+"-2d.jpg")

# -----
# Normalized 2d figure

plt.figure()
plt.imshow(diff,interpolation='none',origin='lower',
            cmap=cmapRel, vmin=-normAll, vmax=normAll,
            extent=[freq.min(),freq.max(),1,diff.shape[0]+1],aspect='auto')
plt.grid('off')
#     cb=plt.colorbar()
#     cb.set_label(r'Phase Difference, $\angle_1-\angle_0$ (deg)')
#     plt.xlabel('Frequency (GHz)')
#     plt.ylabel('Sample Number')
plt.axis('off')

if doSave:
    plt.savefig(dataDir+figTitle+"-norm.pdf")
    plt.savefig(dataDir+figTitle+"-norm.jpg")

# ~~~~~
# ~~~~~
# ~~~~~
# ~~~~~
# ~~~~~
# ~~~~~

def wavenumber(f, epsr, mur):
    return 2*pi*f*np.sqrt(constants.epsilon_0*epsr
                          *constants.mu_0*mur)

def calibrate(raw, empty, plate, thick):
    """
    Calibrate raw data using empty and plate measurement

    For S21 data:

    Cald = (raw-plate) / (empty-plate)*exp(-j*k_0*thick)

```

```

Parameters
-----
raw : skrf network
    raw data to be calibrated
empty : skrf network
    empty range measurement
plate : skrf network
    measurement of plate at the position of the sample
thick : number
    thickness of material sample in meters

Returns
-----
cald : skrf network
    Calibrate data
"""

k = wavenumber(raw.f, 1, 1)
cald = (raw-plate) / (empty-plate) * np.exp(-1j*k*thick)
cald.name = cald.name + ", cald"

return cald

def writeZFmacro(macroName, folder, zfStart, zfStop, trMin, trMax, prefix):
    with open(macroName+'.MAC','w') as fo:
        for f in os.listdir(folder):
            if f[-3:] == ".s1p":
                fName=f[:-4]
                fo.write("\"Open\"\\r\\n")
                fo.write("2\\r\\n")
                fo.write(("\"\\\\\\\\\\\\\\\\tsclient\\\\Z\\\\Documents\\\\plasmaInterferometer"
                    + "\"\\\\wichman\\\\Data\\\\2015-02-15\\\\"+fName+".odf\"\\r\\n"))
                fo.write("\"1\"\\r\\n")
                fo.write("\"CT\"\\r\\n")
                fo.write("2\\r\\n")
                fo.write("\"2\"\\r\\n")
                fo.write("\"10\"\\r\\n")
                fo.write("\"FFT\"\\r\\n")
                fo.write("6\\r\\n")
                fo.write("\"200\"\\r\\n")
                fo.write("\"1024\"\\r\\n")
                fo.write("\"2048\"\\r\\n")
                fo.write("\"2048\"\\r\\n")
                fo.write("\"4.885198E-02\"\\r\\n")
                fo.write("\"0\"\\r\\n")
                fo.write("\"ZF\"\\r\\n")
                fo.write("2\\r\\n")
                fo.write("\""+str(zfStart)+"\"\\r\\n")
                fo.write("\""+str(zfStop)+"\"\\r\\n")
                fo.write("\"FFT\"\\r\\n")
                fo.write("6\\r\\n")

```



```

fo.write("\0\r\n")
fo.write("\2048\r\n")
fo.write("\1024\r\n")
fo.write("\2048\r\n")
fo.write("\0.01\r\n")
fo.write("\0\r\n")
fo.write("\Trc\r\n")
fo.write("2\r\n")
fo.write("\"+str(trMin)+"\r\n")
fo.write("\"+str(trMax)+"\r\n")
fo.write("\Save\r\n")
fo.write("1\r\n")
fo.write(("\\\\\\\\tsclient\\\\Z\\\\Documents\\\\plasmaInterferometer"
        +\\"\\wichman\\\\Data\\\\2015-02-15\\"+prefix+fName
        +".ODF\r\n"))

def loadAll(ntwks):
    loaded = {}
    for key, val in ntwks.items():
        loaded[key] = rf.NetworkSet(rf.read_all(dataDir,contains=val))
    #     ntwk2odf(loaded[key].mean_s, m=0, n=0, fileName=dataDir+val+'-mean')
    #     if doPlot:
    #         fig, ax = plt.subplots()
    #         loaded[key].plot_uncertainty_bounds_s_deg(show_legend=False)
    #         _ = ax.set_title(val)
    #         #         ax2 = ax.twinx()
    #         #         loaded[key].plot_uncertainty_bounds_s_deg(show_legend=False,
    #         #         #         c=plt.rcParams['axes.color_cycle'][1])
    #         _ = ax.set_ylim([-180, 180])
    return loaded

def plotAll(cnt, ntwkNames, frange=""):
    for key, val in sorted(ntwkNames.items()):
        if frange is not "":
            val.mean_s[frange].plot_s_db(ax=ax[cnt-1], c='k', lw=0.5,
                                         show_legend=False)
        else:
            val.mean_s.plot_s_db(ax=ax[cnt-1], c='k', lw=0.5, show_legend=False)

```

N.3 Gate Data

```
In [ ]: # writeZFmacro('zfMe', dataDir, 3.9, 120, 2, 6, 'gated-3-9--')
```

```
In [ ]: # for f in os.listdir(dataDir):
#     if f[-3:] == "s1p":
#         ntwk2odf(rf.Network(dataDir+f), m=0, n=0, fileName=f[:-4])

```

N.4 Compare Empty Data

```
In [ ]: # freqRange = '2-6ghz'
#
# names = {'1foilDish' : 'empty-foil-lined-dish-2015',
#          '2dishPlexi' : 'dish-with-plexi-meth-2015',
#          '3preMethanol' : 'empty-methanol-pre-2015',
#          '4between' : 'empty-between-meth-salt-2015',
#          '5saltPost' : 'empty-salt-post-2015',
#          '6plexiPost' : 'empty-plexi-2-post-2015',
#          }
#
# emptys = loadAll(names)
#
# num = len(names)
# firstColor = plt.rcParams['axes.color_cycle'][0]
#
# if doLongPlot:
#     fig, ax = plt.subplots(num,1)
#     fig.set_figheight(num*3)
#
#     for key, val in sorted(emptys.items()):
#         i = int(key[0])
#         plotAll(i, emptys)
#         # val.mean_s[freqRange].plot_s_db(ax=ax[i-1], show_legend=False,
#         #                                c=firstColor)
#         # val.mean_s.plot_s_db(ax=ax[i-1], show_legend=False,
#         #                      c=firstColor)
#         _ = ax[i-1].legend([names[key]])
```

N.5 Plot Burns

```
In [ ]: processWichBurnODF(dataDir, 'gated-3-9--empty-methanol-pre-2015',
                              'gated-3-9--methanol-pure-2015', D=6*constants.inch,
                              fRange='2.5-5.5ghz',
                              figTitle='2015-02-15-meth',
                              ntwkODF='odf')
```

```
In [ ]: processWichBurnODF(dataDir, 'gated-3-9--empty-methanol-pre-2015',
                              'gated-3-9--salt-250ml-2015', D=6*constants.inch,
                              fRange='2.5-5.5ghz',
                              figTitle='2015-02-15-salt',
                              ntwkODF='odf')
```

```
In [ ]: processWichBurnODF(dataDir, 'gated-3-9--empty-methanol-pre-2015',
                              'gated-3-9--plexi-2-flame-2015', D=6*constants.inch,
                              fRange='2.5-5.5ghz',
                              figTitle='2015-02-15-plexi',
                              ntwkODF='odf')
```

Appendix O

IPython notebook: AR8200-data-fit

O.1 Fit LM Values to dBm Values

S-meter readings are acquired over a serial connection using the LM command on the AR8200 scanner. One piece of documentation has a table relating the S-meter readings to dBm. This fits a curve to that data.

O.2 Pre-flight

This section sets up the notebook.

O.2.1 Imports

```
In [ ]: # Import basic modules
        # make sure that division is done as expected
        from __future__ import division

        # plotting setup
        %matplotlib inline
        import matplotlib.pyplot as plt
        plt.style.use('gray_back')
        plt.rcParams['axes.ymargin'] = 0

        # get the viridis colormap
        # https://bids.github.io/colormap
        # it will be available as cmaps.viridis
        # import colormaps as cmaps

        # for 3d graphs
        # from mpl_toolkits.mplot3d import axes3d
        # for legends of combined fig types
        # import matplotlib.lines as mlines

        # numerical functions
```

```

import numpy as np

# need some constants
from scipy import constants
from numpy import pi

# RF tools!
# import skrf as rf

# version information
# %install_ext http://raw.githubusercontent.com/jrjohansson/version_information/
# master/version_information.py
# %load_ext version_information
# %reload_ext version_information

# %version_information numpy, scipy, matplotlib

```

O.2.2 Parameters, Config, and Constants

```

In [ ]: doPrint = True
        doPlot = True
        doSave = True
        # doSave = False

        if doSave: doPlot = True

        plt.rcParams['lines.linewidth'] = 2

```

O.3 Fit Curve

```

In [ ]: lm = np.array([0, 10, 27, 42, 55, 68, 86, 97, 103, 106, 109, 112])
        dbm = np.array([-115, -110, -105, -100, -95, -90, -80, -70, -60, -50, -40, -30])

        x = np.linspace(0,120)

        z = np.polyfit(lm, dbm, 6, full=True)
        print z
        p = np.poly1d(z[0])

        if doPlot:
            fig, ax = plt.subplots()
            _ = ax.plot(x, p(x), label='Best fit')
            _ = ax.scatter(lm, dbm, s=35, marker='s',
                           c=plt.rcParams['axes.color_cycle'][1],
                           label='Tabular value')
            _ = ax.set_xlabel('LM value')
            _ = ax.set_ylabel('dBm value')
            _ = ax.legend()

```

```
if doSave:  
    fig.savefig('ar8200-curve.pdf')
```

Appendix P

IPython notebook: CPW-CPS-Impedance

P.1 Coplanar Line Impedance Calculations

Most of this work comes from Gupta, K C. *Microstrip Lines and Slotlines*, 2nd ed. Boston: Artech House, 1996, Venkatesan, Jaikrishna, 2004. "Investigation of the Double-Y Balun for Feeding Pulsed Antennas," Dissertation. <http://hdl.handle.net/1853/5036>, or Simons, Rainee. 2001. *Coplanar Waveguide Circuits, Components, and Systems*. New York: John Wiley. <http://ieeexplore.ieee.org/xpl/bkabstractplus.jsp?bkn=5201692>. Also check out the CPS calculator at http://www1.sphere.ne.jp/i-lab/ilab/tool/cps_e.htm

```
In [1]: from __future__ import division

import scipy.constants as const
from scipy.special import ellipk
from scipy.optimize import fsolve, minimize, fminbound
from numpy import abs, log, sqrt
from IPython.core.display import Image
import git
repo = git.Repo("./")
# a 79-char ruler:
#234567891123456789212345678931234567894123456789512345678961234567897123456789
# a 72-char ruler:
#23456789112345678921234567893123456789412345678951234567896123456789712
```

```
In [2]: print repo.head.commit.hexsha

dd2179db63cbbf351e47a02e76ea2404ee8b40b5
```

<http://docs.python.org/2/tutorial/inputoutput.html>

This program runs with SciPy 0.11.0 and NumPy 1.6.1. The minimization routine is not available in 0.9.0 and I was having problems getting everything to work in 0.13.0.

P.1.1 MSU Substrate Properties and Manufacturing

The MSU EM group typically uses 1.575mm thick Rogers RT/duroid 5870 as a substrate. The ECE Shop usually mills circuit boards out of 0.06 in thick FR4 with 1 oz/sq. ft copper on both sides.

Properties of Rogers RT/duroid 5870 include:

```
<li>1.575mm=62mils thickness</li>
<li>Relative permittivity  $\epsilon_r=2.33$ </li>
<li>Relative permeability  $\mu_r=1$ </li>
<li>Loss tangent  $\tan\delta=0.0012$ </li>
<li>Smallest gap possible 0.2mm=7.87mils</li>
```

Properties of the FR4 include:

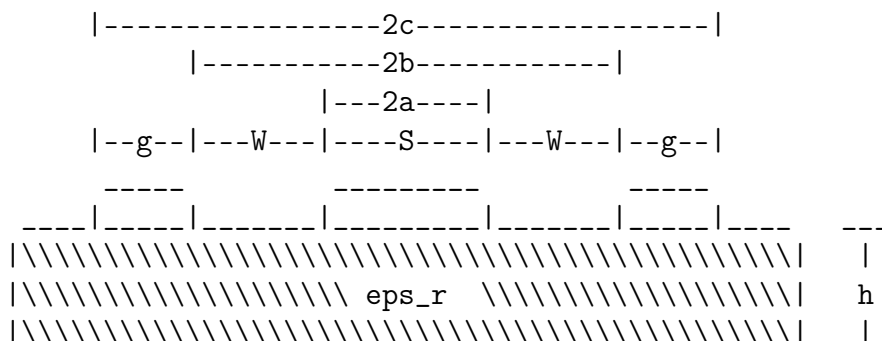
```
<li>0.06in=60mils thickness</li>
<li>Copper thickness 1 oz/sq.ft =  $34.1 \mu\text{m} = 1.34 \text{ mil}$ </li>
<li>Relative permittivity  $\epsilon_r=4.4$ </li>
<li>Relative permeability  $\mu_r=1$ </li>
<li>Loss tangent  $\tan\delta=0.02$ </li>
<li>smallest gap possible 12mils=0.3mm</li>
```

The EM group uses photolithography to create circuit boards. Past students' experience suggest that the minimum trace width is 1 mm (~39 mils), maybe even 0.75 mm (~29.5 mils), and that the minimum gap is 0.2 mm (7.87 mils).

The ECE Shop manufacturing tolerances are reportedly 0.20 – 0.25 mm (8-10 mils) for the minimum width of a trace and 0.3 mm (12 mils) for the minimum width of a gap for their machining process. The shop notes that traces near this minimum width are easily lifted off the substrate by the application of heat. The engineer should be careful when soldering such traces. [From emails with the ECE Shop]

P.1.2 Geometry

Reference Geometry



P.1.4 Computations

Functions

Note that the electircal length and permittivity functions have not been tested rigorously by themselves.

In [3]: #23456789112345678921234567893123456789412345678951234567896123456789712

```
def KKPrime(k):
    """
    An approximate calculation of  $K(k)/K'(k)$ 

    Using an approximation, calculates a complete elliptic integral of the
    first kind over its complement. The approximation is given in Gupta, 1st
    ed.

    Parameters
    -----
    k : scalar
        argument of the elliptic integral

    Returns
    -----
    result : scalar
        An approximate value for  $K(k)/K'(k)$ 
    """
    if 0 <= k and k < 0.707:
        kp = sqrt(1-k**2)
        result = const.pi/log(2* (1+sqrt(kp))/(1-sqrt(kp)))
    elif 0.707 <= k and k <=1:
        result = log(2* (1+sqrt(k))/(1-sqrt(k)))/const.pi
    else:
        print k
        raise NameError('Elliptic Argument out of range, k=', k)
    return result

def KPrimeK(k):
    """
    An approximate calculation of  $K'(k)K(k)$ 

    Using an approximation, calculates a complementary complete elliptic
    integral of the first kind over the original integral. The
    approximation is given in Gupta, 1st ed.

    Parameters
    -----
    k : scalar
        argument of the elliptic integral

    Returns
    -----
```

```

    result : scalar
        An approximate value for  $K'(k)K(k)$ 
    """
    return 1/KKPrime(k)

def lenElectric(physicalL, freq, eps_eff):
    """
    Calculates the electrical length of a transmission line

    Parameters
    -----
    physicalL : scalar
        The physical length of the line in meters
    freq : scalar
        Frequency (Hz)
    eps_eff : scalar
        Effective permittivity of the transmission line

    Returns
    -----
    d : scalar
        Electrical length in degrees
    """
    omega=2*pi*freq
    r = physicalL*omega*sqrt(eps_eff*const.mu_0*const.epsilon_0)
    d = r*180/pi
    return d

def lenPhysical(elecL, freq, eps_eff):
    """
    Converts electric length (deg) to physical length

    Parameters
    -----
    elecL : scalar, degrees
        The physical length of the line in meters
    freq : scalar
        Frequency (Hz)
    eps_eff : scalar
        Effective permittivity of the transmission line

    Returns
    -----
    p : scalar
        Physical length in meters
    """
    omega=2*pi*freq
    r = elecL*pi/180
    p = r/(omega*sqrt(eps_eff*const.mu_0*const.epsilon_0))
    return p

```

```

def unitmmtomil(x):
    """
    Convert 'mm' to 'mil'
    """
    return x/0.0254

def unitmiltomm(x):
    """
    Convert 'mil' to 'mm'
    """
    return x*0.0254

def zCPS(gap, trace, h, eps_r, approx=True):
    """
    Calc the impedance of a symmetric coplanar stripline. Default approx

    Calculate the impedance of a symmetric coplanar stripline (CPS) with
    a gap of width 'gap' and traces 'trace', on a substrate of height
    'h', and relative permittivity 'eps_r'. By default, it uses an
    approximate value for  $K/K'$  or  $K'/K$ .

    Parameters
    -----
    gap : scalar
        Gap width
    trace : scalar
        Trace width (assumes symmetric CPS)
    h : scalar
        Substrate height
    eps_r : scalar
        Relative permittivity of the substrate
    approx : bool, optional
        If true, use an approximation for  $K/K'$  and  $K'/K$ , the elliptic
        integrals

    Returns
    -----
    z : scalar
        Calculated impedance of the CPS
    """
    a = gap/2
    b = gap/2+trace

    k1 = a/b
    #not sure which version of k2 to use. Some books have
    #the sinh squared and some don't
    #k2 = sinh(const.pi*a/(2*h))**2/sinh(const.pi*b/(2*h))**2
    k2 = sinh(const.pi*a/(2*h))/sinh(const.pi*b/(2*h))
    if approx:
        vecKKP = numpy.vectorize(KKPrime)

```

```

        vecKPK = numpy.vectorize(KPrimeK)
        eps_eff = 1+(eps_r-1)/2*vecKKP(k2)*vecKPK(k1)
        z = 120*const.pi/sqrt(eps_eff)*vecKKP(k1)
    else:
        k1Prime = sqrt(1-k1**2)
        k2Prime = sqrt(1-k2**2)
        eps_eff = (1
            +(eps_r-1)/2*ellipk(k2)/ellipk(k2Prime)*ellipk(k1Prime)/ellipk(k1))
        z = 120*const.pi/sqrt(eps_eff)*ellipk(k1)/ellipk(k1Prime)
    return z

def epsCPS(gap, trace, h, eps_r, approx=True):
    """
    Calc eps_eff of a symmetric coplanar stripline. Default approx

    Calculate the effictive permittivity of a symmetric coplanar
    stripline (CPS) with a gap of width 'gap' and traces 'trace', on a
    substrate of heigth 'h', and relative permittivity 'eps_r'. By
    default, it uses an approximate value for K/K' or K'/K.

    Parameters
    -----
    gap : scalar
        Gap width
    trace : scalar
        Trace width (assumes symmetric CPS)
    h : scalar
        Substrate heigth
    eps_r : scalar
        Relative permittivity of the substrate
    approx : bool, optional
        If true, use an approximation for K/K' and K'/K, the elliptic
        integrals

    Returns
    -----
    eps_eff : scalar
        Calculated effictive permittivity of the CPS
    """
    a = gap/2
    b = gap/2+trace

    k1 = a/b
    #not sure which version of k2 to use. Some books have
    #the sinh squared and some don't
    #k2 = sinh(const.pi*a/(2*h))**2/sinh(const.pi*b/(2*h))**2
    k2 = sinh(const.pi*a/(2*h))/sinh(const.pi*b/(2*h))
    if approx:
        vecKKP = numpy.vectorize(KKPrime)
        vecKPK = numpy.vectorize(KPrimeK)
        eps_eff = 1+(eps_r-1)/2*vecKKP(k2)*vecKPK(k1)

```

```

else:
    k1Prime = sqrt(1-k1**2)
    k2Prime = sqrt(1-k2**2)
    eps_eff = (1
                +(eps_r-1)/2*ellipk(k2)/ellipk(k2Prime)*ellipk(k1Prime)/ellipk(k1))
return eps_eff

def epsCPW(cntr, gap, gnd, h, eps_r, approx=True):
    """
    Calc eps_eff of a symmetric coplanar waveguide. Default approx

    Calculate the effective permittivity of a symmetric coplanar
    waveguide (CPW) with a center trace of width 'cntr', gaps of width
    'gap', and ground traces of width 'g', on a substrate of height 'h',
    and relative permittivity 'eps_r'. By default, it uses an
    approximate value for K/K' or K'/K.

    Parameters
    -----
    cntr : scalar
        Center trace width
    gap : scalar
        Gap width (assumes symmetric CPW)
    gnd : scalar
        Ground trace width (assumes symmetric CPW)
    h : scalar
        Substrate height
    eps_r : scalar
        Relative permittivity of the substrate
    approx : bool, optional
        If true, use an approximation for K/K' and K'/K, the elliptic
        integrals

    Returns
    -----
    eps_eff : scalar
        Calculated effective permittivity of the CPW
    """
    a = cntr/2
    b = (cntr+2*gap)/2
    c = (cntr+2*gap+2*gnd)/2

    k3 = a/b*sqrt((1-b**2/c**2)/(1-a**2/c**2))
    k4 = (sinh(const.pi*a/(2*h))/sinh(const.pi*b/(2*h))
          *sqrt((1-sinh(const.pi*b/(2*h))**2/sinh(const.pi*c/(2*h))**2)
                /(1-sinh(const.pi*a/(2*h))**2/sinh(const.pi*c/(2*h))**2)))
    if approx:
        vecKKP = numpy.vectorize(KKPrime)
        vecKPK = numpy.vectorize(KPrimeK)
        eps_eff = 1+(eps_r-1)/2*vecKKP(k4)*vecKPK(k3)

```

```

else:
    k3Prime = sqrt(1-k3**2)
    k4Prime = sqrt(1-k4**2)
    eps_eff = (1
                +(eps_r-1)/2*ellipk(k4)/ellipk(k4Prime)*ellipk(k3Prime)/ellipk(k3) )
return eps_eff

def zCPW(cntr, gap, gnd, h, eps_r, approx=True):
    """
    Calc the impedance of a symmetric coplanar waveguide. Default approx

    Calculate the impedance of a symmetric coplanar waveguide (CPW) with
    a center trace of width 'cntr', gaps of width 'gap', and ground
    traces of width 'g', on a substrate of height 'h', and relative
    permittivity 'eps_r'. By default, it uses an approximate value for
    K/K' or K'/K.

    Parameters
    -----
    cntr : scalar
        Center trace width
    gap : scalar
        Gap width (assumes symmetric CPW)
    gnd : scalar
        Ground trace width (assumes symmetric CPW)
    h : scalar
        Substrate height
    eps_r : scalar
        Relative permittivity of the substrate
    approx : bool, optional
        If true, use an approximation for K/K' and K'/K, the elliptic
        integrals

    Returns
    -----
    z : scalar
        Calculated impedance of the CPW
    """
    a = cntr/2
    b = (cntr+2*gap)/2
    c = (cntr+2*gap+2*gnd)/2

    k3 = a/b*sqrt((1-b**2/c**2)/(1-a**2/c**2))
    k4 = (sinh(const.pi*a/(2*h))/sinh(const.pi*b/(2*h))
          *sqrt((1-sinh(const.pi*b/(2*h))**2/sinh(const.pi*c/(2*h))**2)
                /(1-sinh(const.pi*a/(2*h))**2/sinh(const.pi*c/(2*h))**2)))
    if approx:
        vecKKP = numpy.vectorize(KKPrime)
        vecKPK = numpy.vectorize(KPrimeK)
        eps_eff = 1+(eps_r-1)/2*vecKKP(k4)*vecKPK(k3)
        z = 30*pi/sqrt(eps_eff)*vecKPK(k3)

```

```

else:
    k3Prime = sqrt(1-k3**2)
    k4Prime = sqrt(1-k4**2)
    eps_eff = ( 1
        +(eps_r-1)/2*ellipk(k4)/ellipk(k4Prime)*ellipk(k3Prime)/ellipk(k3) )
    z = 30*pi/sqrt(eps_eff)*ellipk(k3Prime)/ellipk(k3)
return z

def zEqual(dims, gnd, h, eps_r, approx=True):
    """
    Calculates the impedance differences between CPS and CPW

    Calculates the impedance difference between a coplanar strip and a
    coplanar waveguide.

    Parameters
    -----
    dims : array
        An array of the CPS and CPW parameters.
        cpwCntr = dims[0]
        cpwGap = dims[1]
        cpsGap = dims[2]
        cpsTrace = dims[3]
    gnd : scalar
        Ground trace width (assumes symmetric CPW)
    h : scalar
        Substrate height
    eps_r : scalar
        Relative permittivity of the substrate
    approx : bool, optional
        If true, use an approximation for  $K/K'$  and  $K'/K$ , the elliptic
        integrals

    Returns
    -----
    zDiff : scalar
        The absolute difference between the impedance of a CPS
        and a CPW
    """
    cpwCntr = dims[0]
    cpwGap = dims[1]
    cpsGap = dims[2]
    cpsTrace = dims[3]
    cpw = zCPW(cpwCntr, cpwGap, gnd, h, eps_r, approx)
    cps = zCPS(cpsGap, cpsTrace, h, eps_r, approx)
    zDiff = abs(cpw-cps)
    return zDiff

def zEqualOutsideWidths(dims, cpwCntr, cpwGap, cpsGap, h, eps_r, approx=True):
    """
    Wrapper for zEqual with a different order of args

```

```

Parameters
-----
dims : array
    An array of the outside widths of a CPW and CPS
    cpsTrace = dims[0]
    cpwGnd = dims[1]
cpwCntr : scalar
    Width of the CPW center strip
cpwGap : scalar
    Width of the CPW gap
cpsGap : scalar
    Width of the CPS gap
h : scalar
    Substrate height
eps_r : scalar
    Relative permittivity of the substrate
approx : bool, optional
    If true, use an approximation for  $K/K'$  and  $K'/K$ , the elliptic
    integrals

Returns
-----
zDiff : scalar
    The absolute difference between the impedance of a CPS
    and a CPW
"""
cpsTrace = dims[0]
cpwGnd = dims[1]
cpw = zCPW(cpwCntr, cpwGap, cpwGnd, h, eps_r, approx)
cps = zCPS(cpsGap, cpsTrace, h, eps_r, approx)
zDiff = abs(cpw-cps)
return zDiff

# Wrapper functions
def cpsS(S, W, h, eps_r, approx): return zCPS(S, W, h, eps_r, approx)
def cpsW(W, S, h, eps_r, approx): return zCPS(S, W, h, eps_r, approx)
def cpsh(h, S, W, eps_r, approx): return zCPS(S, W, h, eps_r, approx)
def cpsEps_r(eps_r, S, W, h, approx): return zCPS(S, W, h, eps_r, approx)

def cpwS(S, W, g, h, eps_r, approx): return zCPW(S, W, g, h, eps_r, approx)
def cpwW(W, S, g, h, eps_r, approx): return zCPW(S, W, g, h, eps_r, approx)
def cpwh(h, S, W, g, eps_r, approx): return zCPW(S, W, g, h, eps_r, approx)
def cpwg(g, S, W, h, eps_r, approx): return zCPW(S, W, g, h, eps_r, approx)
def cpwEps_r(eps_r, S, W, g, h, approx): return zCPW(S, W, g, h, eps_r, approx)

def minimizeGivenGnd(minGap, minTrace, cpwGnd, eps_r, h, approxK,
                      printResults = True):
    """
    Find CPS/CPW dimensions given minimums and a cpw ground width

```


This function finds the dimensions for a coplanar stripline (CPS) and a coplanar waveguide (CPW), given a minimum gap width, minimum trace width, and a width for the CPW ground (outside) traces. The returned solution should have lines that are equal in total width and have equal impedances.

The initial guess is simply the minimum values

Parameters

minGap : scalar

Minimum width of a gap

minTrace : scalar

Minimum width of a trace

cpwGnd : scalar

Width of the ground traces for the coplanar waveguide (CPW)

eps_r : scalar

The relative permittivity of the substrate

h : scalar

Height of the substrate

approxK : bool

If true, use an approximation for K/K' and K'/K , the elliptic integrals

printResults : bool, optional

Print results and other information about the input values and the solution

Returns

res : Result

The result returned by `scipy.optimize.minimize`. `res.x` has the solution values.

Notes

See documentation for ‘`scipy.optimize.minimize`’ for more info.

The variables for solving are defined in the following order:

x[-]

** S_{cpw}*

** W_{cpw}*

** S_{cps}*

** W_{cps}*

Constraints are either ‘eq’ for equality or ‘ineq’ for ‘>0’

The following constraint is used so that the lines are of equal width:

$$x[0] + 2*x[1] + 2*p['cpwGnd'] - x[2] - 2*x[3]$$

That is

```

$$S_{cpw} + 2W_{cpw} + 2g_{cpw} - (S_{cps} + 2W_{cps}) = 0$$

"""
p = {'minGap' : minGap,
     'minTrace' : minTrace,
     'cpwGnd' : cpwGnd,
     'eps_r' : eps_r,
     'h' : h,
     'approxK' : approxK}
#argument order:
resOrder = ('cpwCntr (S)', 'cpwGap (W)', 'cpsGap (S)', 'cpsTrace (W)')
args = p['cpwGnd'], p['h'], p['eps_r'], p['approxK']
initGuess = (p['minTrace'], p['minGap'], p['minGap'], p['minTrace'])
            #cpwCntr, cpwGap, cpsGap, cpsTrace
bnds = ((p['minTrace'], 200), (p['minGap'], 200), (p['minGap'], 200),
        (p['minTrace'], 200))
cons = ({'type':'eq',
         'fun': lambda x: x[0] + 2*x[1]+2*p['cpwGnd']-x[2]-2*x[3]})
res = minimize(zEqual, initGuess, args, method='SLSQP', bounds=bnds,
               constraints=cons)

if printResults:
    aCpwCntr, aCpwGap, aCpsGap, aCpsTrace = res.x
    aCpwGnd = cpwGnd
    cpwWidth = aCpwCntr + 2*aCpwGap + 2*aCpwGnd
    cpsWidth = aCpsGap + 2*aCpsTrace
    cpsZ = zCPS(aCpsGap,aCpsTrace,h,eps_r,approxK)
    cpwZ = zCPW(aCpwCntr,aCpwGap,cpwGnd,h,eps_r,approxK)
    cpsEpsEff = epsCPS(aCpsGap, aCpsTrace, h, eps_r, approxK)
    cpwEpsEff = epsCPW(aCpwCntr, aCpwGap, cpwGnd, h, eps_r, approxK)

    FREQ = 8e9
    cpsStub45 = lenPhysical(45, FREQ, cpsEpsEff)
    cpwStub45 = lenPhysical(45, FREQ, cpwEpsEff)

    checks = {'Width, CPW' : cpwWidth,
              'Width, CPS' : cpsWidth,
              'Width, |Diff|' : abs(cpwWidth-cpsWidth),
              'Z, CPS' : cpsZ,
              'Z, CPW' : cpwZ,
              'Z, |Diff|' : abs(cpsZ-cpwZ)}

    print "Command\n-----"
    print ("minimizeGivenGnd(minGap = {}, minTrace = {}, cpwGnd = {}, "
           "eps_r = {}, "
           .format(minGap, minTrace, cpwGnd,eps_r))
    print ("\t\tth = {}, approxK = {}, printResults = {})"
           .format(h, approxK, printResults))
    print "\nResults\n-----\n", res
```

```

for a in range(4):
    print '{0:15} = {1:15f}'.format(resOrder[a],res.x[a])
print "\nParameters\n-----"
print "{0:15} = {1:15}".format('Initial guess', initGuess)
for it, val in sorted(p.items()):
    print '{0:15} = {1:15f}'.format(it, val)
print "\nChecks\n-----"
for it, val in sorted(checks.items()):
    print "{0:15} = {1:15f}".format(it, val)
print "\nEffective Permittivity\n-----"
print "CPS = {}".format(cpsEpsEff)
print "CPW = {}".format(cpwEpsEff)
print ( "\n45 deg Length in mil (mm) at {}GHz\n"
        "-----".format(FREQ/1e9) )
print "CPS = {} ({} )".format(unitsmmtomil(cpsStub45/1e-3),
                                cpsStub45/1e-3)
print "CPW = {} ({} )".format(unitsmmtomil(cpwStub45/1e-3),
                                cpwStub45/1e-3)

print "\nCommit\n-----"
print repo.head.commit.hexsha

return res

```

Verification

Here some basic tests are done to try the functions defined above. First we will test that zEqual computes the difference correctly.

```

In [4]: #Make sure that Zequal computes the difference correctly
S_cps=15 #mils
W_cps=23.21 #mils
S_cpw=10 #mils
W_cpw=11.54 #mils
gtry = 8 #mils
htry = 62 #mils
eps_rtry = 2.33

print zEqual([S_cpw, W_cpw, S_cps, W_cps], gtry, htry, eps_rtry, approx = False)

a = zCPW(S_cpw, W_cpw, gtry, htry, eps_rtry, approx = False)
b = zCPS(S_cps, W_cps, htry, eps_rtry, False)

print abs(a-b)
#should be 16.635...

16.6354052377
16.6354052377

```

Now check the computation of the impedance for specific lines. From Figure 29 of Venkatesan's PhD dissertation, we expect that the impedance should be around 104Ω when an approximate expression for the Elliptical Integrals is used. The dimensions from the figure are:

- CPS
 - Gap (S) = 6
 - Trace (W) = 21.51
 - Height (h) = 58
 - Rel. Perm. (eps_r) = 4.4
- CPW
 - Center Trace (S) = 10
 - Gap (W) = 11.54
 - Ground Trace (g) = 8
 - Height (h) = 58
 - Rel. Perm. (eps_r) = 4.4

At this time, I do not know have a source to which to compare the impedance when approximations are not used.

```
In [5]: print zCPS(6, 21.51, 58, 4.4, False)
        print zCPS(6, 21.51, 58, 4.4, True) #~104
        print zCPW(10, 11.54, 8, 58, 4.4, False)
        print zCPW(10, 11.54, 8, 58, 4.4, True) #~104
```

```
97.6507742856
104.134634884
110.319293355
104.131367052
```

Let's try to match Figure 7.9 in Gupta. This figure is a plot of the “(a) Variation of the characteristic impedance for a CPW with finite width ground planes on GaAs substrate ($\epsilon_r = 13$, $h = 300 \mu\text{m}$, and $2b = 200 \mu\text{m}$) and (b) variation of the effective dielectric constant for a CPW with finite width ground planes on GaAs substrate... (from [26]).”

```
In [6]: b = 200/2 #micrometers

        abFrac = linspace(.01,.8,99)
        cbFrac = 1.5
        a = b*abFrac
        c = b*cbFrac

        S=2*a
        W=b-a
        g=c-b
        h = 300 #micrometers
        eps_r = 13

        plot(abFrac,zCPW(S,W,g,h,eps_r,False))
```

```
Out[6]: [<matplotlib.lines.Line2D at 0x3474390>]
```

Trying to match Figure 7.15 in Gupta 2nd ed.

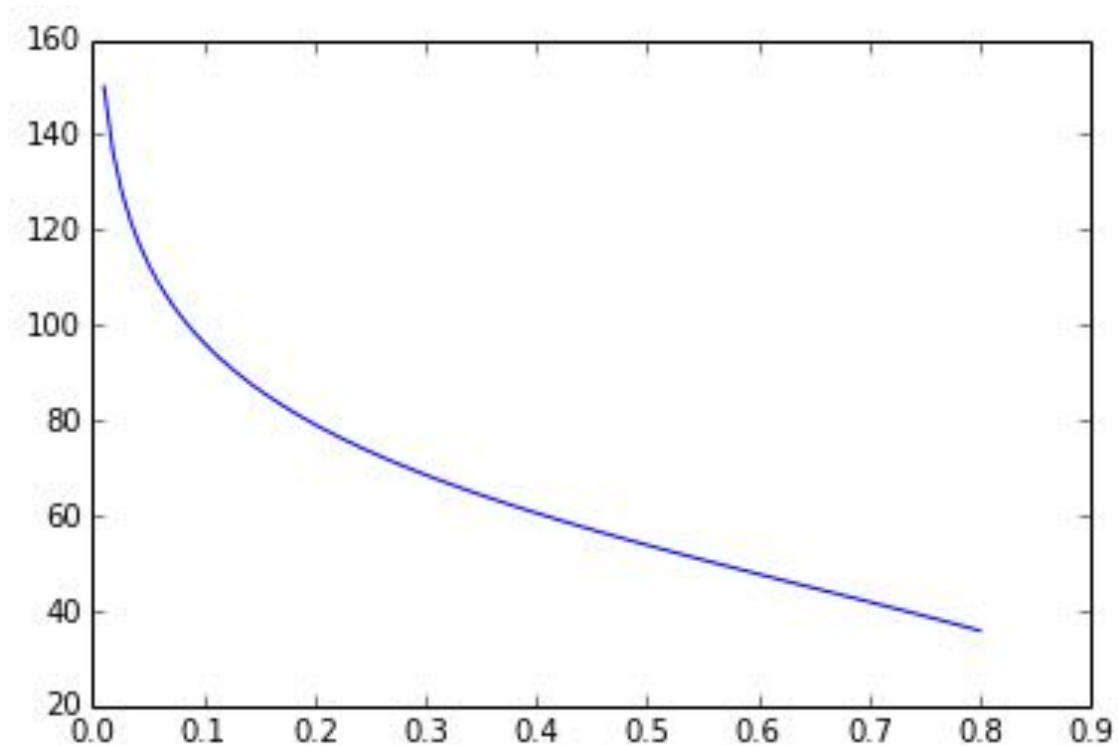


Figure P.1: notebook figure

```
In [7]: eps_r=13
        b=100
        h=2*b

        abFrac = linspace(.01,.9,99)
        a = b*abFrac
        S=2*a
        W=b-a

        vfunc = numpy.vectorize(zCPS)
        z = vfunc(S,W,h,eps_r,True)

        semilogx(abFrac,z,abFrac,zCPS(S,W,h,eps_r,False))
        #semilogx(abFrac,z)
        #semilogx(abFrac,Z_0cps(S,W,h,eps_r,0))

Out[7]: [<matplotlib.lines.Line2D at 0x3490fd0>,
        <matplotlib.lines.Line2D at 0x34a7550>]
```

P.1.5 Testing Solving

Let's try finding the slot width of the traces for a CPS given an impedance and trace width. These values are based on Figure 29 of Venkatesan's dissertation.

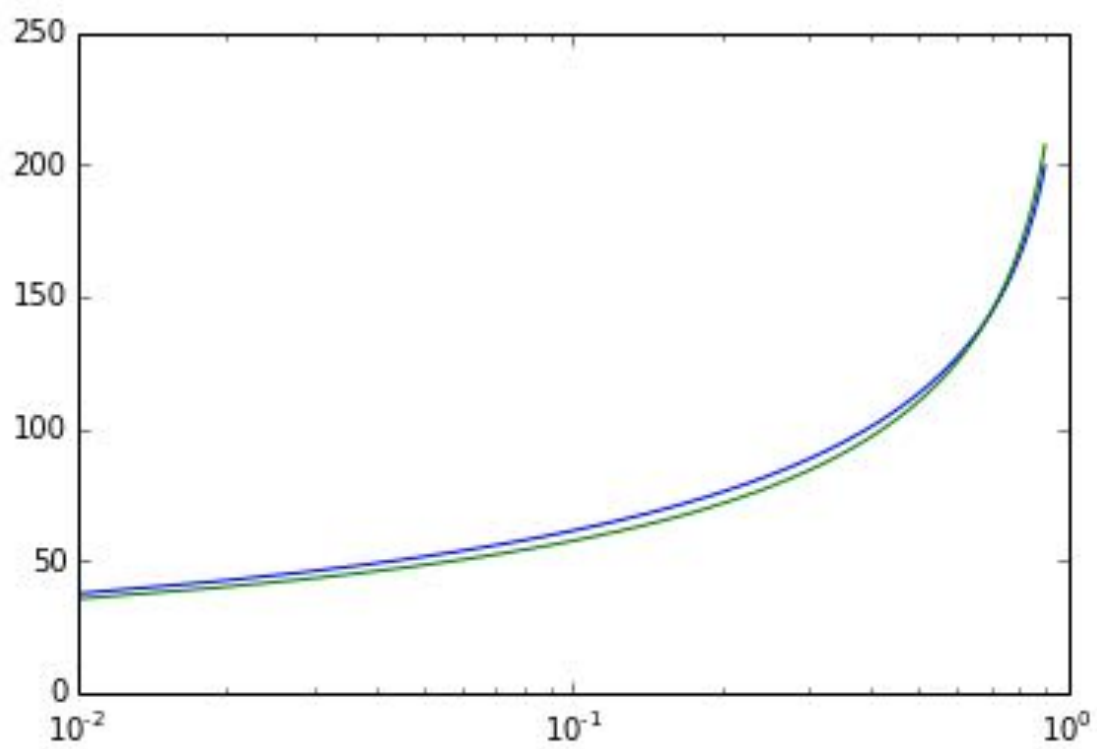


Figure P .2: notebook figure

- CPS
 - Gap (S) = 6
 - Trace (W) = 21.51
 - Height (h) = 58
 - Rel. Perm. (eps_r) = 4.4

- CPW
 - Center Trace (S) = 10
 - Gap (W) = 11.54
 - Ground Trace (g) = 8
 - Height (h) = 58
 - Rel. Perm. (eps_r) = 4.4

```
In [8]: cpsGap = 6
        h = 58
        eps_r = 4.4
        approx = True
        ztarget = 104
        fargs = cpsGap, h, eps_r, approx
        def sol(W, S, h, eps_r, approx): return abs(cpsW(W, S, h, eps_r, approx)-ztarget)
        cpsTrace = fsolve(sol,15,fargs)
        print "CPS Trace Width (W) found to be: {}".format(cpsTrace)
        print "Expected: 21.51"
```

```
        cpwCntr = 10
        cpwGap = 11.54
        h = 28
        eps_r = 4.4
        approx = True
        ztarget = 104
        initGuess = 10
        fargs = cpwCntr, cpwGap, h, eps_r, approx
        def sol(g, S, W, h, eps_r, approx):
            return abs(cpwg(g, S, W, h, eps_r, approx)-ztarget)
        gcpw = fsolve(sol,initGuess,fargs)
        print "CPW ground trace width (g) found to be: {}".format(gcpw)
        print "Expected: 8"
```

```
CPS Trace Width (W) found to be: [ 21.62419289]
Expected: 21.51
CPW ground trace width (g) found to be: [ 8.44234866]
Expected: 8
```

P.1.6 Solving for the Balun Design

Minimization

See the documentation for `scipy.optimize.minimize` for an example of solving a problem with bounds and constraints. The problem is Example 16.4 from Nocedal, J, and S J Wright. 2006. Numerical Optimization. Springer New York. Theoretical solution is (1.4, 17.7).

Checking optimization around Venkatesan's design in Figure 29 of his PhD. Again, his design is

- CPS
 - Gap (S) = 6
 - Trace (W) = 21.51
 - Height (h) = 58
 - Rel. Perm. (eps_r) = 4.4
- CPW
 - Center Trace (S) = 10
 - Gap (W) = 11.54
 - Ground Trace (g) = 8
 - Height (h) = 58
 - Rel. Perm. (eps_r) = 4.4

```
In [9]: ans = minimizeGivenGnd(minGap = 5, minTrace = 5, cpwGnd = 8, eps_r = 4.4,  
                               h = 58, approxK = True, printResults = True)
```

Command

```
minimizeGivenGnd(minGap = 5, minTrace = 5, cpwGnd = 8,eps_r = 4.4,  
                  h = 58, approxK = True, printResults = True)
```

Results

```
status: 0  
success: True  
njev: 8  
nfev: 60  
fun: 5.3060588811604248e-08  
x: array([ 5.56456239,  8.18915459,  5.19301774, 16.37492691])  
message: 'Optimization terminated successfully.'  
jac: array([-4.77325726,  4.17049885, -5.38675499,  1.65678978,  0.          ])  
nit: 8  
cpwCntr (S)      =      5.564562  
cpwGap (W)       =      8.189155  
cpsGap (S)       =      5.193018  
cpsTrace (W)     =     16.374927
```


Parameters

```
Initial guess = (5, 5, 5, 5)
approxK       =          1
cpwGnd        =          8
eps_r         =         4.4
h             =         58
minGap        =          5
minTrace      =          5
```

Checks

```
Width, CPS    =      37.942872
Width, CPW    =      37.942872
Width, |Diff| =      0.000000
Z, CPS       =     107.357323
Z, CPW       =     107.357323
Z, |Diff|    =      0.000000
```

Effective Permittivity

```
CPS = 2.67849405337
CPW = 2.699593365
```

45 deg Length in mil (mm) at 8.0GHz

```
CPS = 112.683847983 (2.86216973877)
CPW = 112.242630524 (2.86216973877)
```

Commit

```
dd2179db63cbbf351e47a02e76ea2404ee8b40b5
```

Two different results based upon slightly different initial conditions.

First set has initial paramaters of minGap = 5, minTrace = 5, and cpwGnd = 8.

Results

```
status: 0
success: True
njev: 8
nfev: 60
fun: 5.3060588811604248e-08
x: array([ 5.56456239,  8.18915459,  5.19301774, 16.37492691])
message: 'Optimization terminated successfully.'
jac: array([-4.77325726,  4.17049885, -5.38675499,  1.65678978,  0. ])
nit: 8
cpwCntr      =      5.564562
cpwGap       =      8.189155
```

```

cpsGap      =      5.193018
cpsTrace    =      16.374927

```

Parameters

```

-----
Initial guess = (5, 5, 5, 5)
approxK       =      1
cpwGnd        =      8
eps_r         =      4.4
h             =      58
minGap        =      5
minTrace      =      5

```

Checks

```

-----
Width, CPS    =      37.942872
Width, CPW    =      37.942872
Width, |Diff| =      0.000000
Z, CPS        =      107.357323
Z, CPW        =      107.357323
Z, |Diff|     =      0.000000

```

The second set has initial paramaters of minGap = 5.8, minTrace = 7.5, and cpwGnd = 8.

Results

```

-----
status: 0
success: True
njev: 13
nfev: 99
fun: 2.3782860125720617e-07
x: array([ 8.39335319, 11.27949445,  6.45282611, 20.24975799])
message: 'Optimization terminated successfully.'
jac: array([ 3.04381466, -1.3562355 ,  4.36965179, -1.3295393 ,  0.])
nit: 13
cpwCntr      =      8.393353
cpwGap        =      11.279494
cpsGap        =      6.452826
cpsTrace      =      20.249758

```

Parameters

```

-----

```

```

Initial guess    = (7.5, 5.8, 5.8, 7.5)
approxK          = 1
cpwGnd          = 8
eps_r           = 4.4
h               = 58
minGap          = 5.8
minTrace        = 7.5

```

Checks

```

-----
Width, CPS      = 46.952342
Width, CPW      = 46.952342
Width, |Diff|   = 0.000000
Z, CPS          = 107.714192
Z, CPW          = 107.714192
Z, |Diff|       = 0.000000

```

These results suggest that the solution is very sensitive to the initial guess/input parameters and also that multiple solutions are possible. This is plausible because of the numerous possible combinations of dimensions for the geometry.

Balun Optimization

Etching Rogers Substrate Design We want to find the parameters for the CPW and CPS lines in the balun. We need the impedance to be the same for maximum power transfer and to avoid problems with the length of the stubs.

After determining the balun dimensions, we can find the dimensions for the 50Ω coax feed.

After that we design the dimensions for the two-wire t-line feed.

In the end we want the overall width of the CPW to be the same as the CPS. This means that

$$S_{cpw} + 2W_{cpw} + 2g_{cpw} = S_{cps} + 2W_{cps}.$$

Our bounds are:

- Line impedance the same, i.e. $Z_{0,cpw} = Z_{0,cps} \Rightarrow Z_{0,cpw} - Z_{0,cps} = 0$
- Overall width equal, i.e. $S_{cpw} + 2W_{cpw} + 2g_{cpw} = S_{cps} + 2W_{cps} \Rightarrow S_{cpw} + 2W_{cpw} + 2g_{cpw} - (S_{cps} + 2W_{cps}) = 0$
- Gaps larger than 10 mils, i.e. S_{cps} and $W_{cpw} > 10$ mils (for now using Rogers and photo etch)
- Traces larger than 30 mils, i.e. S_{cpw} , g_{cpw} and $W_{cps} > 30$ mils (for now using Rogers and photo etch)

Known values are:

- $h = 62$ mils

- $\epsilon_r = 2.33$

Gupta suggests keeping g_{cpw} as small as possible so try $g_{cpw} = 40$ mils.

Let's try for a design using Roger's board and MSU's photoetching tolerances.

From above:

Properties of Rogers RT/duroid 5870 include:

- 1.575mm=62mils thickness
- Relative permittivity $\epsilon_r = 2.33$
- Relative permeability $\mu_r = 1$
- Loss tangent $\tan\delta = 0.0012$
- Smallest gap possible 0.2mm=7.87mils

The EM group uses photolithography to create circuit boards. Past students' experience suggest that the minimum trace width is 1 mm (~39 mils), maybe even 0.75 mm (~29.5 mils), and that the minimum gap is 0.2 mm (7.87 mils).

```
In [10]: ans = minimizeGivenGnd(minGap = 10, minTrace = 30, cpwGnd = 30, eps_r = 2.33,
                                h = 62, approxK = True, printResults = True)
```

Command

```
-----
minimizeGivenGnd(minGap = 10, minTrace = 30, cpwGnd = 30,eps_r = 2.33,
                  h = 62, approxK = True, printResults = True)
```

Results

```
-----
status: 0
success: True
njev: 13
nfev: 102
fun: 4.2085090967702854e-08
x: array([ 30.25031242,  26.83738566,  11.48377189,  66.22065592])
message: 'Optimization terminated successfully.'
jac: array([-0.95010185,  1.48096275, -2.54771805,  0.37209129,  0.          ])
nit: 13
cpwCntr (S)    =      30.250312
cpwGap (W)     =      26.837386
cpsGap (S)     =      11.483772
cpsTrace (W)   =      66.220656
```

Parameters

```
-----
Initial guess  = (30, 10, 10, 30)
approxK        =          1
cpwGnd         =          30
eps_r          =          2.33
h              =          62
minGap         =          10
```

```

minTrace      =          30

Checks
-----
Width, CPS    =      143.925084
Width, CPW    =      143.925084
Width, |Diff| =         0.000000
Z, CPS        =      120.030812
Z, CPW        =      120.030812
Z, |Diff|     =         0.000000

Effective Permittivity
-----
CPS = 1.58958675438
CPW = 1.64859004902

45 deg Length in mil (mm) at 8.0GHz
-----
CPS = 146.273244525 (3.71534041093)
CPW = 143.631823869 (3.71534041093)

Commit
-----
dd2179db63cbbf351e47a02e76ea2404ee8b40b5

```

Milling FR4 Design Properties of the FR4 inclde:

```

<li>0.06~in=60mils thickness</li>
<li>Copper thickness 1 oz/sq.ft =  $34.1\ \mu$m = 1.34 mill</li>
<li>Relative permittivity $\epsilon_r=4.4$</li>
<li>Relative permeability $\mu_r=1$</li>
<li>Loss tangetn $\tan\delta=0.02$</li>
<li>smallest gap possible 12mils=0.3mm</li>

```

The ECE Shop manufacturing tolerances are reportedly 0.20 – 0.25 mm (8-10 mils) for the minimum width of a trace and 0.3 mm (12 mils) for the minimum width of a gap for their machining process. The shop notes that traces near this minimum width are easily lifted off the substrate by the application of heat. The engineer should be careful when soldering such traces. [From emails with the ECE Shop]

```

In [11]: ans = minimizeGivenGnd(minGap = 15, minTrace = 10, cpwGnd = 10, eps_r = 4.4,
                                h = 60, approxK = False, printResults = True)

```

```

Command
-----
minimizeGivenGnd(minGap = 15, minTrace = 10, cpwGnd = 10,eps_r = 4.4,
                  h = 60, approxK = False, printResults = True)

```

Results

```

-----
status: 0
success: True
njev: 10
nfev: 72
fun: 6.2007970313970873e-08
x: array([ 10.31348856, 17.08618148, 15.23289466, 24.62647843])
message: 'Optimization terminated successfully.'
jac: array([ 2.85736275, -2.39193249, 2.44193268, -1.38985634, 0.      ])
nit: 10
cpwCntr (S)      =      10.313489
cpwGap (W)       =      17.086181
cpsGap (S)       =      15.232895
cpsTrace (W)     =      24.626478

Parameters
-----
Initial guess    = (10, 15, 15, 10)
approxK          =      0
cpwGnd          =      10
eps_r           =      4.4
h               =      60
minGap          =      15
minTrace        =      10

Checks
-----
Width, CPS      =      64.485852
Width, CPW      =      64.485852
Width, |Diff|   =      0.000000
Z, CPS         =      122.488955
Z, CPW         =      122.488955
Z, |Diff|      =      0.000000

Effective Permittivity
-----
CPS = 2.63153917822
CPW = 2.69632614237

45 deg Length in mil (mm) at 8.0GHz
-----
CPS = 113.684718893 (2.88759185988)
CPW = 112.310613887 (2.88759185988)

Commit
-----
dd2179db63cbbf351e47a02e76ea2404ee8b40b5

```

No idea if this is actually the *BEST* design, but it works. Checks are good.

P.1.7 Taper Design

The above solution needs to be matched to either the 50 ohm coax or the two-wire transmission line.

Let's begin with matching the CPW to a 50 ohm coax cable. Since the CPW impedance is greater than 50 ohms, we can decrease the gap or increase the width of the traces.

A possible CPW geometry was found in the datasheet for the Pasternack PE4542 SMA Female Connector Solder Attachment 0.062 inch End Launch PCB, .030 inch Diameter after looking at various possible connectors. This datasheet happened to have a drawing and table for a connector to CPW over ground plane to microstrip transition. For a board thickness of 62 mils, the center conductor is 90 mils wide, a gap width of 80 mils, and a ground trace of 95 mils in width. For a CPW with finite width ground plane, these dimensions on 60 mils thick FR4 ($\epsilon_r = 4.4$) give an impedance of

```
In [12]: zCPW(90, 80, 95, 60, 4.4)
```

```
Out[12]: 103.11657421385755
```

This impedance is too high. Past experience

Past experience suggests that 50 ohms cannot be reached by simply extending the ground plane. This is supported by the following graph.

```
In [13]: gnd = linspace(50,500, 201)
         vfunc = numpy.vectorize(zCPW)
         z = vfunc(90, 80, gnd, 60, 4.4)
         plot(gnd, z)
```

```
Out[13]: [<matplotlib.lines.Line2D at 0x3c17ed0>]
```

The impedance does not reach 98 ohms even when the CPW is over one inch in total width. Trail and error for reducing the gap and increasing the trace widths gives the following close solution for 50 ohms:

```
In [14]: zCPW(190, 15, 200, 60, 4.4)
```

```
Out[14]: 50.083760262937176
```

Using this information, a solution for the center width is sought.

```
In [15]: cpwGap = 15
         cpwGnd = 200
         h = 60
         eps_r = 4.4
         ztarget = 50
         initGuess = 200
         approx = (True, False)
         for a in approx:
             fargs = cpwGap, cpwGnd, h, eps_r, a
             def sol(S, W, g, h, eps_r, a): return abs(cpwS(S, W, g, h, eps_r, a) - ztarget)
             scpw = fsolve(sol, initGuess, fargs)
             print ("Approx: {} \n CPW center trace width (S) found to be: {}".format(a, scpw))
```

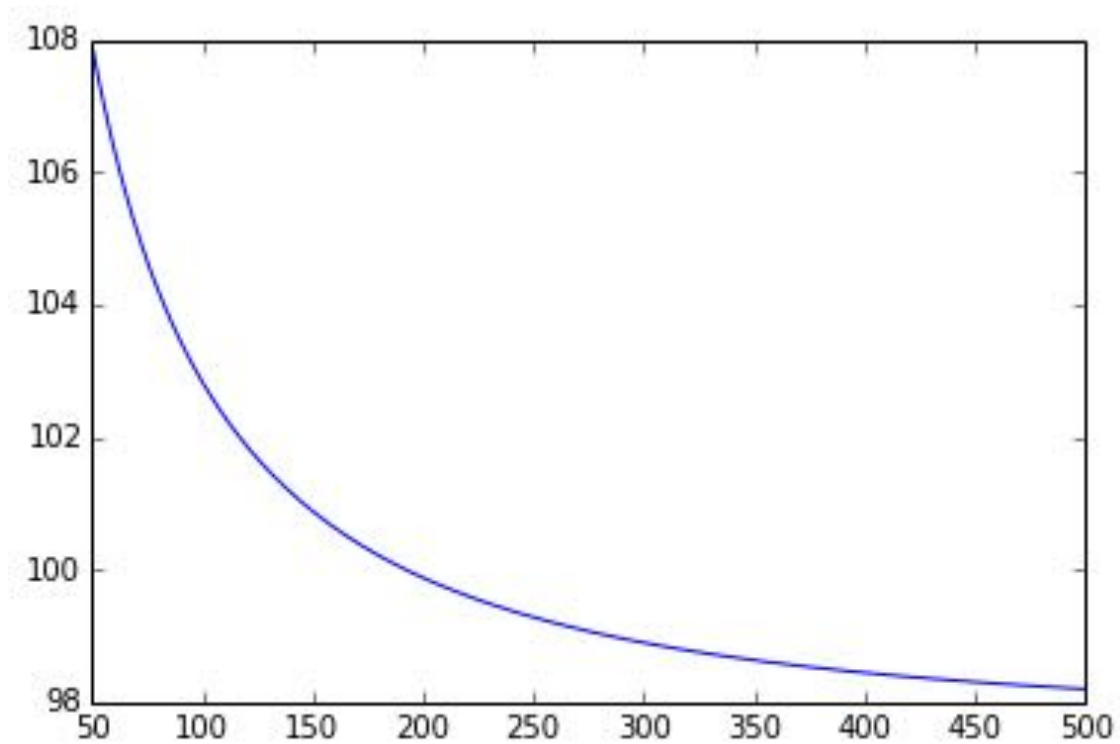


Figure P.3: notebook figure

Approx: True

CPW center trace width (S) found to be: [192.17178487]

Approx: False

CPW center trace width (S) found to be: [173.91823265]

HFSS results suggest that the 173.91 mils wide center trace is a better match to 50 ohms because S11 is lower.

Ven uses an exponential taper from Pozar, (pg 262, 4th ed). The impedance at any point along the taper is given by

$$Z(z) = Z_0 e^{\alpha z}, \quad 0 \leq z \leq L,$$

where

$$\alpha = \frac{1}{L} \ln \left(\frac{Z_L}{Z_0} \right),$$

L is the length of the taper, Z_0 is the source impedance, and Z_L is the load impedance. This can also be expressed as

$$Z(z) = Z_0 \left(\frac{Z_L}{Z_0} \right)^{z/L}.$$

Pozar notes that the length should be greater than $\lambda/2$ ($\beta L > \pi$) to minimize the mismatch at low frequencies. (pg263) A longer line, however, has more loss; therefore, a balance must be selected.

In HFSS, this is entered as $(S/2+W+g)*((bS/2+bW+bg)/(S/2+W+g))^{(t/L)}$ for a equation based curve. Here a prefix of b corresponds to dimensions on the balun side of the taper while no prefix corresponds to dimensions on the coax side of the taper.

```
In [16]: L = 1
         Z_src = 50
         Z_L = 122.49
         z = linspace(0,L,200)
         alpha = 1/L*log(Z_L/Z_src)
         Zofz = Z_src*(Z_L/Z_src)**(z/L)
         plot(z, Zofz)

Out[16]: [<matplotlib.lines.Line2D at 0x3a862d0>]
```

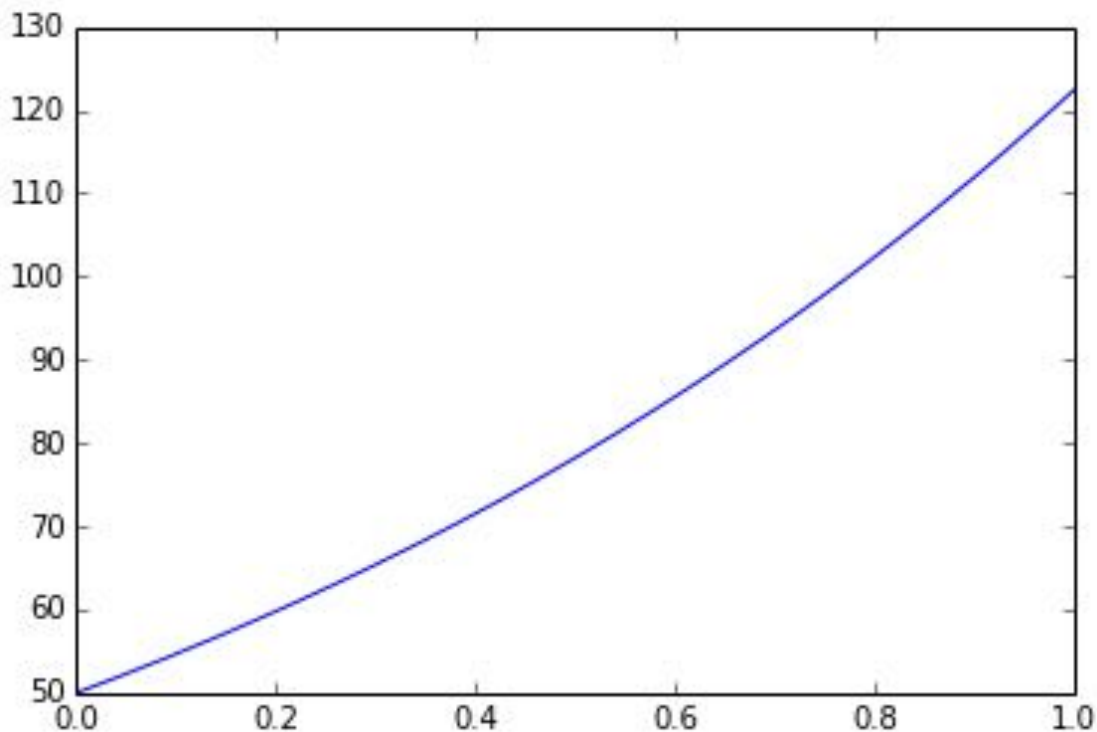


Figure P.4: notebook figure

We are simply going to apply this same curve to the dimensions of the transmission lines. In the end, we get a gradual transistion, so hopefully it works well.

To determine length, let us use the 1GHz as our frequency and an effective permittivity from the balun design above. $\lambda/2$ is then

```
In [17]: lenPhysical(180, 1e9, 2.69)
```

```
Out[17]: 0.091393343832089732
```

meters. This is pretty big. Probably not going to satisfy this criteria.

The above design works; however, the width of the center strip is probably too wide. I had Brian in the shop measure the dielectric of a connector and he said 4.3mm in diameter. This is 169.29 mils. We will try a design with a center strip width of 150 and 125 mils to see what the ground plane sizes end up being.

```
In [18]: cpwCntr = 150
         cpwGap = 15
         h = 60
         eps_r = 4.4
         ztarget = 50
         initGuess = 300
         approx = (True, False)
         for a in approx:
             fargs = cpwCntr, cpwGap, h, eps_r, a
             def sol(g, S, W, h, eps_r, a): return abs(cpwg(g, S, W, h, eps_r, a) - ztarget)
             gcpw = fsolve(sol, initGuess, fargs)
             print ("Approx: {} \n CPW ground trace width (g) found to be: {}".format(a, gcpw))
```

```
-c:291: RuntimeWarning: overflow encountered in square
-c:292: RuntimeWarning: overflow encountered in square
-c:291: RuntimeWarning: overflow encountered in sinh
-c:292: RuntimeWarning: overflow encountered in sinh
/opt/software/SciPy/0.11.0--GCC-4.4.5/lib/python2.7/site-packages/scipy/
optimize/minpack.py:221: RuntimeWarning: The iteration is not making good
progress, as measured by the
improvement from the last ten iterations.
warnings.warn(msg, RuntimeWarning)
```

```
Approx: True
```

```
CPW ground trace width (g) found to be: [ 10983888.26897169]
```

```
Approx: False
```

```
CPW ground trace width (g) found to be: [ 17610084.44435658]
```

That's not really working. If we vary g, what is the asymptotic impedance?

```
In [19]: gnd = linspace(50,500, 201)
         vfunc = numpy.vectorize(zCPW)
         z = vfunc(150, 15, gnd, 60, 4.4, False)
         plot(gnd, z)
         z = vfunc(125, 15, gnd, 60, 4.4, False)
         plot(gnd, z)
         z = vfunc(125, 12, gnd, 60, 4.4, False)
         plot(gnd, z)
```

```
Out[19]: [<matplotlib.lines.Line2D at 0x3e12c10>]
```

Oh. That's why it is not working. Can't really get down low enough. Let us try to vary the gap size with a 200 mil wide ground trace. First though, what is the impedance if we just shrink the center trace?

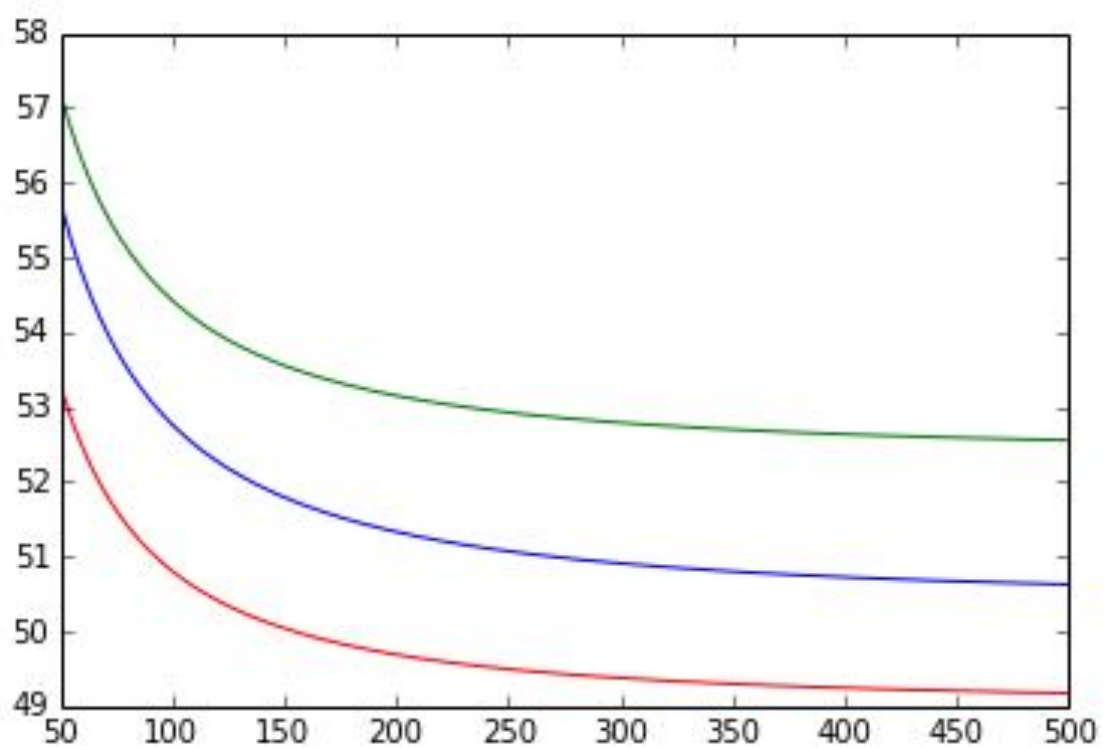


Figure P .5: notebook figure

```
In [20]: print zCPW(173.92, 15, 200, 60, 4.4, False)
         print zCPW(150, 15, 200, 60, 4.4, False)
         print zCPW(125, 15, 200, 60, 4.4, False)
```

```
49.9999128626
51.3290784764
53.1489813028
```

Not bad. Certainly useable. Let's try varying the gap now.

```
In [21]: gap = linspace(8,15, 201)
         vfunc = numpy.vectorize(zCPW)
         z = vfunc(125, gap, 200, 60, 4.4)
         plot(gap, z)
```

```
Out[21]: [<matplotlib.lines.Line2D at 0x41afd10>]
```

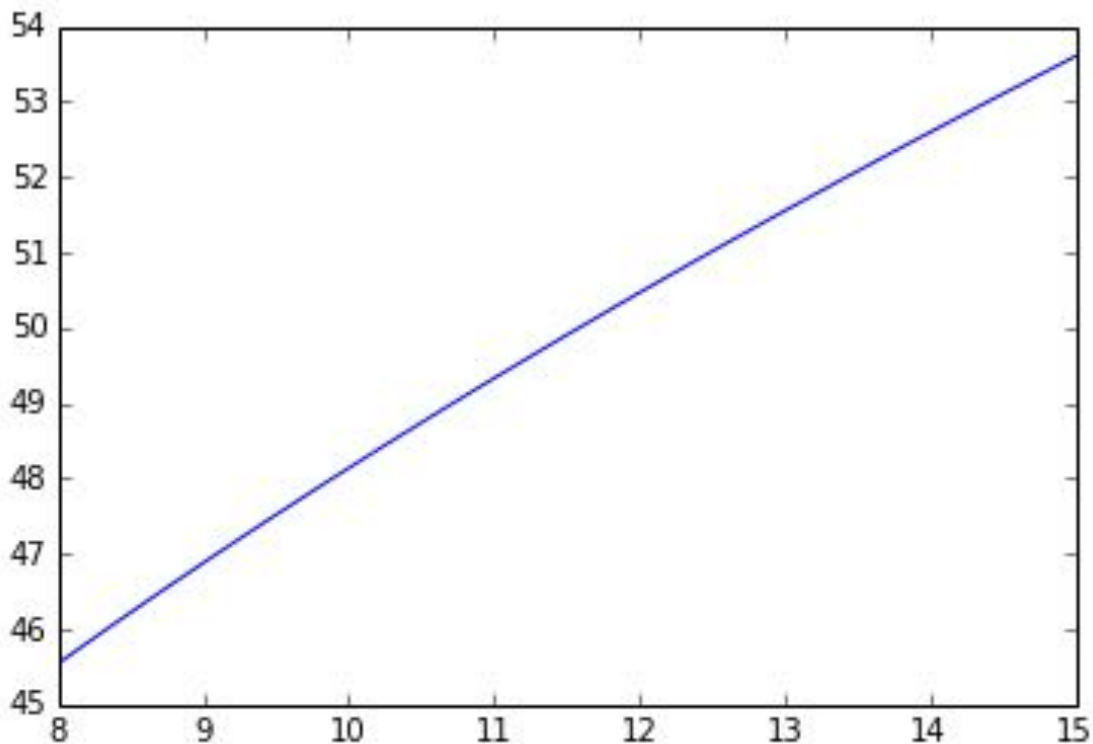


Figure P .6: notebook figure

The shop says that the minimum gap size is 12 mils. This gives

```
In [22]: print zCPW(125, 12, 200, 60, 4.4, False)
```

```
49.687145128
```

Let's optimize for 12 then.

```

In [23]: cpwCntr = 125
         cpwGap = 12
         h = 60
         eps_r = 4.4
         ztarget = 50
         initGuess = 200
         approx = (True, False)
         for a in approx:
             fargs = cpwCntr, cpwGap, h, eps_r, a
             def sol(g, S, W, h, eps_r, a): return abs(cpwg(g, S, W, h, eps_r, a) - ztarget)
             gcpw = fsolve(sol, initGuess, fargs)
             print ("Approx: {} \n CPW GROUND trace width (g) found to be: {}".format(a, gcpw))

```

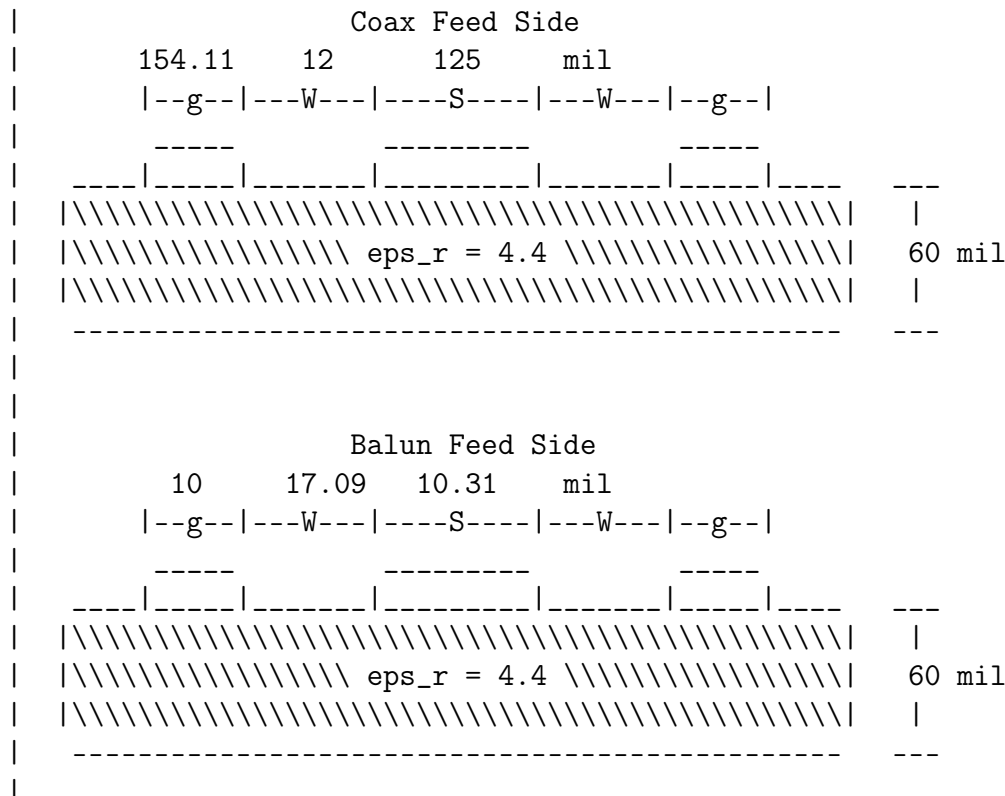
```

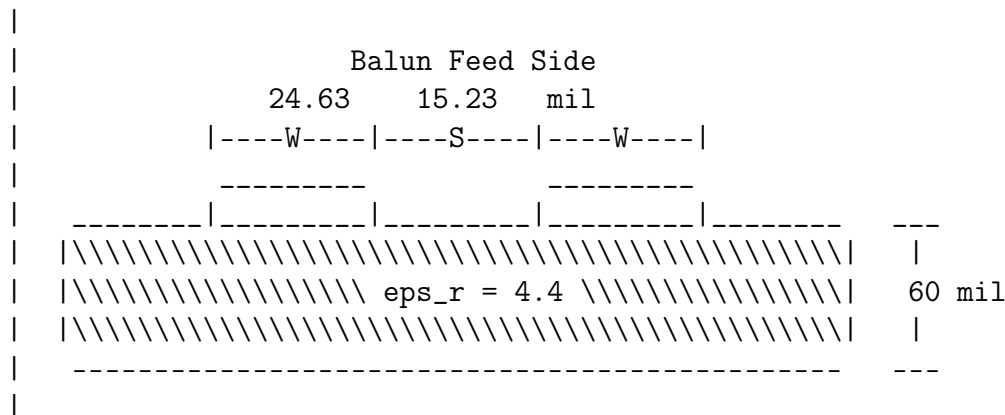
Approx: True
CPW GROUND trace width (g) found to be: [ 494.24149395]
Approx: False
CPW GROUND trace width (g) found to be: [ 154.11046673]

```

Here is a good time to point out the difference between using a true approximation versus the functions for K/K' . One sees that when using the approximation, the trace width is 494 mils instead of 154. This is a significant difference. We should try simulating this and see what the actual difference is. To note, though, is that we may be operating in the normal bounds of the CPW equations.

In summary, we have the following dimensions::





P.2 Two-Wire Transmission Line

From the comprehensive exam, the transmission line parameters for a two-wire transmission line are

$$R = \sqrt{\frac{\omega \mu_c}{2\pi^2 a^2 \sigma_c [1 - (2a/D)^2]}}$$

$$L = \frac{\mu}{\pi} \cosh^{-1} \left(\frac{D}{2a} \right)$$

$$G = \frac{\omega \pi \epsilon''}{\cosh^{-1}(D/2a)}$$

$$C = \frac{\pi \epsilon'}{\cosh^{-1}(D/2a)}$$

where D is the center-to-center distance, a is the radius of the wire, σ_c is the conductivity of the wire, μ_c is the permeability of the wire (usually $\mu_c = \mu_0$), and finally μ and $\epsilon^c = \epsilon' - j\epsilon''$ are the permeability and permittivity, respectively, of the material surrounding the wires.

```
In [2]: #234567891123456789212345678931234567894123456789512345678961234567897123456789
# a 72-char ruler:
#23456789112345678921234567893123456789412345678951234567896123456789712
def twoWireParameters(freq, a, D, sigma_c=inf, mu_c=1,
    eps_r = 1, tanDelta = 0, mu_r=1,
    unitsScale=1):
    """
    Return R, L, G, C, Z_0 for a two-wire line

    Calculates and returns the resistance, impedance, conductance,
    and capacitance for a two-wire transmission line. Geometric and
    electrical properties are given for the wire and the media in
    which the wires are located.
```

```

Parameters
-----
freq : scalar
    Frequency at which the parameters should be calculated
a : scalar
    Wire radius
D : scalar
    center-to-center distance of the wires
sigma_c : scalar
    Conductivity of the wires
mu_c : scalar, optional
    Relative permeability of the wires. Default is 1.
eps_r : scalar, optional
    Relative permittivity of the environment. Used as
    epsilon = eps_r*eps_0*(1-j*tanDelta). Default is 1.
tanDelta : scalar, optional
    Loss tangent of the environment. Used as
    epsilon = eps_r*eps_0*(1-j*tanDelta). Default is 0.
mu_r : scalar, optional
    Relative permeability of the environment. Default is 1
unitsScale : scalar, optional if using meters
    Scaling factor for units. For mm, use 1e-3, for in use
    0.0254.

Returns
-----
R : scalar
    Resistance of the two-wire transmission line
L : scalar
    Impedance of the two-wire transmission line
G : scalar
    Conductance of the two-wire transmission line
C : scalar
    Capacitance of the two-wire transmission line
Z_0 : scalar
    Complex impedance of the two-wire transmission line
"""
#from __future__ import division
import scipy.constants as const

# Scale dimensions
a = a*unitsScale
D = D*unitsScale
eps_sgl = const.epsilon_0*eps_r
eps_dbl = const.epsilon_0*eps_r*tanDelta

omega=2*pi*freq
#delta_cond = 1/np.sqrt(const.pi*freq*sigma_c)

invCosh = np.arccosh(D/(2*a))

```

```

    #R = 1/(const.pi*a*sigma_c*delta_cond)
    R = np.sqrt(omega*mu_c/
                (2*(const.pi*a)**2*sigma_c
                 *(1-(2*a/D)**2)))
    G = (const.pi*omega*eps_dbl)/invCosh
    L = const.mu_0/pi*invCosh
    C = pi*eps_sgl/invCosh

    Z_0 = np.sqrt((R+1j*omega*L)/(G+1j*omega*C))

    return R, L, G, C, Z_0

In [3]: foo = twoWireParameters(1e9, .125/2, 0.25, unitsScale=0.0254)
        twoWireParameters(
        print foo

(0.0, 5.2678315876992667e-07, 0.0, 2.1121595053488982e-11, (157.92561800064058+0j))

impedance 350
    $begin 'Properties'
        VariableProp('radius', 'UD', '', '(.812/2) mm')
        VariableProp('length', 'UD', '', '(12*25.4) mm')
        VariableProp('spacing', 'UD', '', '7.5mm')
        VariableProp('portSize', 'UD', '', 'spacing*66') #.812
        VariableProp('layerThickness', 'UD', '', '5mm')
        VariableProp('layerWidth', 'UD', '', '25mm')
        VariableProp('layerL', 'UD', '', '25mm')
    $end 'Properties'

radius .812/2mm .406
length 12*25.4mm 304.8
spacing 7.5mm
portSize spacing*66 495mm
port 1mm
top rect 3.5mm
bottom rect 3
20mm absolute offset

In [25]: a = 1.0237e-3/2
        D = 6.35e-3

        sigma_cond = 5.96*10**7

        eps_r = np.linspace(0.9,1.1,200)
        tanD = 0.00015
        freq = 1e9

#234567891123456789212345678931234567894123456789512345678961234567897123456789

```



```

R, G, L, C, Z_0 = twoWireParameters(freq, a, D, sigma_cond, eps_r = eps_r,
                                     tanDelta=tanD)

fig, axes = subplots(ncols = 2, nrows = 1, figsize=(13,4))
axes[0].plot(eps_r,Z_0.real)
axes[0].set_xlabel(r'Relative Permittivity  $\epsilon_r$ ')
axes[0].set_ylabel(r'Re $\{Z_0\}$ ')
axes[0].set_title(r'Twin-lead Theoretical Impedance')

axes[1].plot(eps_r,Z_0.imag)
axes[1].set_xlabel(r'Relative Permittivity  $\epsilon_r$ ')
axes[1].set_ylabel(r'Im $\{Z_0\}$ ')

fig.subplots_adjust(left=-.05)

```

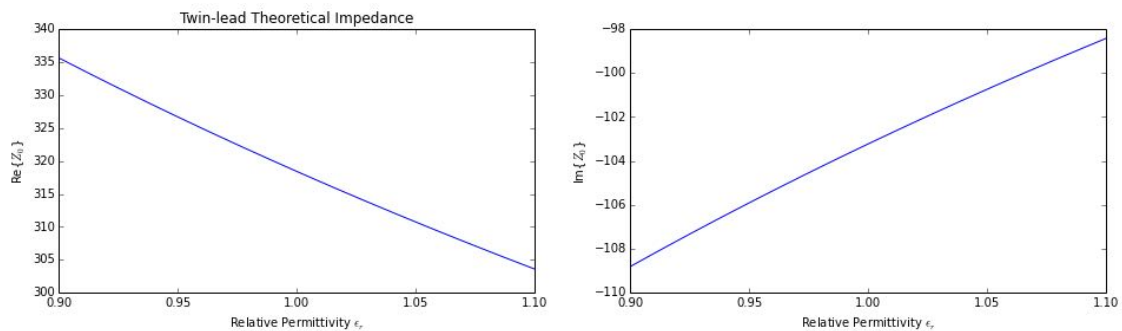


Figure P.7: notebook figure

Try testing the function for a 300 ohm cable.

```

In [26]: a = 0.0625/2
         D = .375
         sigma_cond = 5.96*10**7
         sigma_cond = inf

         eps_r = 1
         tanD = 0
         freq = 1e9

         R, G, L, C, Z_0 = twoWireParameters(freq, a, D, eps_r = eps_r,
                                             tanDelta=tanD, unitsScale = 0.0254)

         print R
         print G
         print L
         print C
         print sqrt(L/C)
         zcalc = np.sqrt((R+1j*2*pi*freq*L)/(G+1j*2*pi*freq*C))
         print zcalc
         print sqrt(L/C)
         print "Returned impedance: {}".format(Z_0)

```

```

print "Magnitude of returned impedance: {}".format(abs(Z_0))
print "Impedance calculated from parameters: {}".format(zcalc)
print type(L)
print type(C)
omega = 2*pi*freq
print np.sqrt((R+1j*omega*L)/(G+1j*omega*C))

0.0
9.91155492115e-07
0.0
1.12257871233e-11
0.0
0j
0.0
Returned impedance: (297.140941241+0j)
Magnitude of returned impedance: 297.140941241
Impedance calculated from parameters: 0j
<type 'numpy.float64'>
<type 'numpy.float64'>
0j

```

P.2.1 Problem above

Why does $\sqrt{L/C}$ give 0 here but not below?

$$Z_0 = \sqrt{\frac{R + j\omega L}{G + j\omega C}}$$

```

In [27]: D = .375 * 0.0254
a = 0.0625/2 * 0.0254
L = const.mu_0/pi*arccosh(D/(2*a))
C = pi * const.epsilon_0/arccosh(D/(2*a))
R = 0
G = 0
Z = sqrt(L/C)
print L
print C
print sqrt(L/C)
print Z
print type(L)
print type(C)

9.91155492115e-07
1.12257871233e-11
297.140941241
297.140941241
<type 'numpy.float64'>
<type 'numpy.float64'>

```

P.2.2 Two Wire Geometry Design

Impedances for varying separation distances and wire diameters. This is meant to replicate the table at <http://www.qsl.net/co8tw/openline.htm>

```
In [28]: spacing = np.linspace(0.5, 6, 12)
        a = array([.128, .102, .081, .064, .051])/2
        units = 0.0254
        print "D    | Impedances for varying radii"
        print "      | " + str(a)
        print "---- | -----"
        for el in spacing:
            _, _, _, Z0 = twoWireParameters(1e9, a, el, eps_r= 1, unitsScale=units)
            pStr = str(el) + ' | '
            for val in abs(Z0):
                pStr = pStr+'{: .1f}\t'.format(val)
            print pStr
```

| D | Impedances for varying radii | | | | |
|------|------------------------------|-------|--------|-------|---------|
| | [0.064 | 0.051 | 0.0405 | 0.032 | 0.0255] |
| ---- | ----- | | | | |
| 0.5 | 244.5 | 272.5 | 300.6 | 329.1 | 356.6 |
| 1.0 | 329.1 | 356.6 | 384.3 | 412.6 | 439.9 |
| 1.5 | 378.0 | 405.3 | 433.0 | 461.3 | 488.6 |
| 2.0 | 412.6 | 439.9 | 467.6 | 495.8 | 523.1 |
| 2.5 | 439.4 | 466.7 | 494.4 | 522.6 | 549.9 |
| 3.0 | 461.3 | 488.6 | 516.2 | 544.5 | 571.7 |
| 3.5 | 479.8 | 507.1 | 534.7 | 563.0 | 590.2 |
| 4.0 | 495.8 | 523.1 | 550.7 | 579.0 | 606.2 |
| 4.5 | 510.0 | 537.2 | 564.9 | 593.1 | 620.3 |
| 5.0 | 522.6 | 549.9 | 577.5 | 605.8 | 633.0 |
| 5.5 | 534.0 | 561.3 | 588.9 | 617.2 | 644.4 |
| 6.0 | 544.5 | 571.7 | 599.4 | 627.6 | 654.8 |

These impedances match for some combinations but not others. Need to continue to try to verify my calculations.

What impedances are possible for a CPS given a certain spacing to match that of the two wire t-line?

```
In [29]: gnd = linspace(25,500, 201)
        vfunc = numpy.vectorize(zCPS)
        spacing = np.linspace(50, 150, 5)
        for D in spacing:
            z = vfunc(D, gnd, 60, 4.4, False)
            plot(gnd,z, label=D)
        legend()
```

```
Out[29]: <matplotlib.legend.Legend at 0x3c35310>
```

A CPS geometry needs to be found that matches or is compatible with a two-wire transmission line geometry. First,

$$2a + D \leq gap + 2trace$$

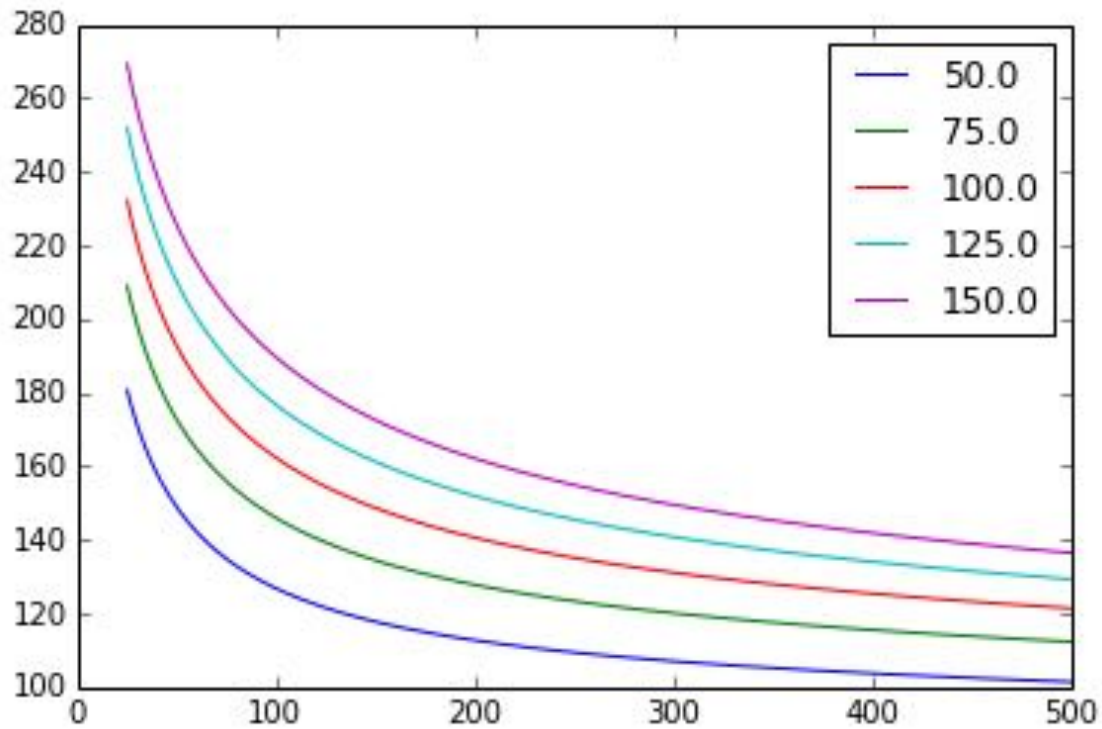


Figure P.8: notebook figure

```
In [30]: freq = 2e9
        diam = 0.122
        a = diam/2
        D = 0.25
        units = 0.0254
        _, _, _, _, Z2wire = twoWireParameters(freq, a, D, unitsScale=units)
        print "Diameter: {} in".format(diam)
        print "Center-Center Dist: {} in".format(D)
        print "Gap between: {}".format(D-diam)
        print "Total Width: {}".format(D+diam)
        print "Two-wire impedance: {}".format(Z2wire)
        cpsGap = (50, 75, 100, 125, 150)
        h = 60
        eps_r = 4.4
        ztarget = abs(Z2wire)
        initGuess = 25
        approx = False

        print ""
        print "Gap\t|\tTrace\tImpedance\tSol.\tTot\tAccpets"
        print "\t|\tWidth\t\t\t\tAcc.\tWidth\t2 Wire"
        print "----\t|\t-----\t-----\t\t---\t\t-----\t-----"
        for gap in cpsGap:
            fargs = gap, h, eps_r, approx
```

```

def sol(W, S, h, eps_r, aprox): return abs(zCPS(S,W,h,eps_r,aprox)-ztarget)
wCPS = fsolve(sol,initGuess,fargs)
print "{}\t|\t{:.3f}\t{:.3f}\t{:.2}\t{:.3f}\t{}".format(gap, wCPS[0],
                                                         zCPS(gap, wCPS, h, eps_r, aprox)[0],
                                                         sol(wCPS,*fargs)[0], gap+2*wCPS[0],
                                                         gap+2*wCPS > (diam+D)*1000)

# print "Gap: {}".format(gap)
# print "CPS trace width (W) found to be: {}".format(wCPS)
# print "Impedance: {}".format(zCPS(gap, wCPS, h, eps_r, aprox))
# print "Solution Acc.: {}".format(sol(wCPS,*fargs))
# print "Total width: {}".format(gap+2*wCPS)
# print "Accepts 2 wire : {}".format(gap+2*wCPS > (diam+D)*1000)

```

Diameter: 0.122 in
 Center-Center Dist: 0.25 in
 Gap between: 0.128
 Total Width: 0.372
 Two-wire impedance: (161.276087605+0j)

| Gap | Trace | Impedance | Sol. | Tot | Accpets | |
|------|---------|-----------|------|---------|---------|---------|
| | Width | | Acc. | Width | 2 Wire | |
| ---- | ----- | ----- | ---- | ----- | ----- | |
| 50 | 37.143 | 161.276 | | 5.7e-14 | 124.286 | [False] |
| 75 | 65.188 | 161.276 | | 8.5e-14 | 205.376 | [False] |
| 100 | 102.736 | 161.276 | | 1.1e-13 | 305.472 | [False] |
| 125 | 149.724 | 161.276 | | 7.7e-13 | 424.447 | [True] |
| 150 | 205.014 | 161.276 | | 3e-12 | 560.028 | [True] |

Using the smallest gap that accepts the 2 wire geometry gives

| Gap | Trace | Impedance | Sol. | Tot | Accpets | |
|------|---------|-----------|---------|---------|---------|--|
| | Width | | Acc. | Width | 2 Wire | |
| ---- | ----- | ----- | ---- | ----- | ----- | |
| 125 | 149.724 | 161.276 | 7.7e-13 | 424.447 | [True] | |

When I go to manufacture this, the wires may be aligned anywhere on the ~150 mil trace. What range of impedances should I expect from this possible misalignment?

Consider the wires being closest together. This means that the gap between the wires is the same as the gap between the traces, i.e. 125 mils. This gives

$$\begin{aligned}
 125 &= D - 2a \\
 \Rightarrow D &= 125 + 2a \\
 \Rightarrow D &= 125 + 122
 \end{aligned}$$

```

In [31]: DSmall = 125+122
print "{} mils".format(DSmall)

```

247 mils

The impedance is then

```
In [32]: _, _, _, _, zSmall = twoWireParameters(freq, a, DSmall/1000, unitsScale=units)
          print zSmall
          print "Difference: {}".format(zSmall - Z2wire)

(159.614310234+0j)
Difference: (-1.66177737126+0j)
```

This difference should be acceptable.

Going now to the maximum separation, we would have the outside dimensions of the two-wire transmission line equal to 424.447 (reading from table above). This means that the center-to-center spacing is

$$\begin{aligned} 424.447 &= D + 2a \\ \Rightarrow D &= 424.447 - 2a \\ \Rightarrow D &= 424.447 - 122 \end{aligned}$$

```
In [33]: DLarge = 424.447-122
          print "{} mils".format(DLarge)

302.447 mils
```

The impedance is then

```
In [34]: _, _, _, _, zLarge = twoWireParameters(freq, a, DLarge/1000, unitsScale=units)
          print zLarge
          print "Difference: {}".format(zLarge - Z2wire)

(186.785145094+0j)
Difference: (25.5090574891+0j)
```

This is larger than when the wires are pushed towards the center.

From this we can conclude that it is best to keep the wires more towards the center than towards the outside.

P.2.3 Summary

Copying from above we get the following geometries

```
|
|               Balun Side
|           24.63    15.23   mil
|         |----W----|----S----|----W----|
|
|             -----
|      _____|_____||_____|_____||_____
|  ||||||||||||||||||| eps_r = 4.4 ||||||||||||||||||| 60 mil
|  |||||||||||||||||||                |||||||||||||||||||
|  |||||||||||||||||||                |||||||||||||||||||
```



```
In [36]: resist = 720 #nano ohms per meter
sigma = 1/(resist*1e-9)
print "Conductivity: {} S/m".format(sigma)
_,_,_,_, zLossy = twoWireParameters(1e9, a, spacing, sigma_c = sigma,
                                     unitsScale = units)

print "Impedance: {}".format(zLossy)
print "Impedance Magnitude: {}".format(abs(zLossy))
print "Lossless impedance mag: {}".format(abs(z2Wire))
```

```
Conductivity: 1388888.88889 S/m
Impedance: (161.41842333-6.77723816809j)
Impedance Magnitude: 161.560633657
Lossless impedance mag: 161.276087605
```

The impedance doesn't really change much when we use a lossy case. The spacing effects the impedance more so. Now let's build it and get the spacing correct.

P.2.4 Manufacturing Notes

Manufactured gap for two-wires is 138 mils. This gives an impedance of

```
In [37]: manufacturedGap = 138
DSmall = 122+manufacturedGap
print "{} mils".format(DSmall)
_, _, _, _, zSmall = twoWireParameters(freq, a, DSmall/1000, unitsScale=units)
print zSmall
print "Difference: {}".format(zSmall - Z2wire)
```

```
260 mils
(nan+nan*j)
Difference: (nan+nan*j)

-c:64: RuntimeWarning: invalid value encountered in arccosh
```

```
In [37]:
```


Appendix Q

IPython notebook: WireTemperature

Q.1 Introduction

We wish to measure properties of a flame using a two wire transmission line. The flame will be at the center of the transmission line. Over time the temperature of the wires will increase. At the center of the line, we shall assume that the wire is the same temperature as the flame. The entire transmission line would reach this temperature if there were no losses. Losses at this time will only be air at room temperature. It is assumed that the air temperature does not increase where in reality it would near the wire. We believe that this is negligible. We would like to determine the temperature at the ends of the wire so that we know the maximum temperature that the wire junctions must be able to withstand.

Tungsten has the highest melting point. It also has a relatively higher electrical resistivity. Nickel should be avoided because of its magnetic properties.

Labnotebook 00009:150–159.

Q.2 Tungsten Resources

- <http://hypertextbook.com/facts/2004/DeannaStewart.shtml>
- <http://www.matweb.com/search/datasheettext.aspx?matguid=4ec9eefceac0484c832b4fc6ee608345>
- <http://www.a-msystems.com/v-27-tungsten.aspx>
- <http://www.mcmaster.com/#metal-wire/=nuhl1t>
- google search tungsten copper alloy melting point
- <http://neon.mems.cmu.edu/laughlin/pdf/130.pdf>
- <http://puhep1.princeton.edu/~mcdonald/e166/Walz/sign%20Manual%20WHA%20.doc> De-
- <http://www.eaglealloys.com/c-16-tungstentungsten-alloys.html>
- <http://eaglealloys.com/t-tungsalloyscopper.html>
- <http://www.specialmetals.com/documents/Incoloy%20alloy%20825.pdf>

Q.3 Heat Transfer Books

- <http://site.ebrary.com.proxy1.cl.msu.edu/lib/michstate/tail.action?docID=10540860> docDe-
- <http://site.ebrary.com.proxy1.cl.msu.edu/lib/michstate/tail.action?docID=10503000> docDe-
- <http://site.ebrary.com.proxy1.cl.msu.edu/lib/michstate/tail.action?docID=10506157> docDe-
- <http://link.springer.com.proxy1.cl.msu.edu/book/10.1007/978-3-642-03932-4/page/1>
- <http://link.springer.com.proxy1.cl.msu.edu/book/10.1007/978-3-642-19183-1/page/1>

Q.4 Other Resources

- <http://tutorial.math.lamar.edu/Classes/DE/HeatEqnNonZero.aspx>
- http://en.wikipedia.org/wiki/Heat_equation
- <http://www.physics.miami.edu/~nearing/mathmethods/pde.pdf>
- <http://ocw.mit.edu/courses/mechanical-engineering/2-51-intermediate-heat-and-mass-transfer-fall-2008/index.htm>

Q.5 Fin Temperature at Tip

A fin is a projection from a wall or other body into an environment with the purpose of transferring heat. Fins are commonly seen on CPU heatsinks and other heatsinks in electronics. Fins are discussed in many heat transfer textbooks. The mathematics presented below were derived by following the discussion on fins in section 4.5 of A Heat Transfer Textbook, 4th ed. by Lienhard and Lienhard. This is the textbook for MIT Open Course Ware's Intermediate Heat and Mass Transfer class.

A fin has a characteristic dimension given by the ratio of the area to the perimeter of the fin and a longitudinal dimension, the length.

For a small segment of a fin the energy balance is given as

$$-kA \frac{dT}{dx} \Big|_{x+\delta x} + kA \frac{dT}{dx} \Big|_x + \bar{h}(P\delta x)(T - T_\infty) \Big|_x = 0$$

where k is the thermal conductivity (W/m·K), T is the temperature in Kelvin as a function of position, T_∞ is the ambient temperature, x is a linear distance, A is the cross-sectional area, P is the perimeter distance of the fin, k is the thermal conductivity of the fin, and \bar{h} is the heat transfer coefficient. It is assumed that \bar{h} is constant along the fin. The temperature at the base of the fin is denoted by T_0 .

At the tip of the fin, heat may or may not be exchanged. This is governed by the heat transfer coefficient \bar{h}_L . This value is usually different than the heat transfer coefficient for the rest of the bar. In many cases \bar{h}_L is small enough to be neglected. It is also difficult to determine this

value. As this value reduces the overall heat exchange, when \bar{h}_L is neglected the fin tip will have a slightly higher temperature (assuming $T_\infty < T_0$) than if \bar{h}_L is not neglected. This is acceptable for our purposes as we wish to estimate the maximum temperature a junction could reach.

The above equation may be simplified because

$$\frac{dT/dx|_{x+\delta x} - dT/dx|_x}{\delta x} \rightarrow \frac{d^2T}{dx^2} = \frac{d^2(T - T_\infty)}{dx^2}.$$

The above energy balance equation now becomes

$$\frac{d^2(T - T_\infty)}{dx^2} = \frac{\bar{h}P}{kA}(T - T_\infty)$$

This is the equation for a simple harmonic oscillator. As shown in the book and with simple manipulation including specifying that the fin has circular cross-section of diameter d in meters, the following solution is given for the insulated tip case:

$$T = T_\infty + \frac{(T_0 - T_\infty) \cosh\left(2L\sqrt{\frac{\bar{h}}{kd}}(1 - x/L)\right)}{\cosh\left(2L\sqrt{\frac{\bar{h}}{kd}}\right)}.$$

The temperature at the tip is given by

$$T = T_\infty + \frac{(T_0 - T_\infty)}{\cosh\left(2L\sqrt{\frac{\bar{h}}{kd}}\right)}$$

because $\cosh(0) = 1$.

According to Linehard in the fin literature it is common to define the quantity

$$mL = \sqrt{\frac{\bar{h}P}{kA}}L$$

If $mL \geq 5$ (was originally typed as \leq but it makes more sense to be \geq), then

$$\frac{T - T_\infty}{T_0 - T_\infty} \approx e^{-mL(x/L)}$$

and

$$\frac{T_{\text{tip}} - T_\infty}{T_0 - T_\infty} \approx 0.0067$$

For this problem it is ideal to operate under the condition $mL \gg 5$.

Q.6 Wire Diameter

Wire diameter may be determined from the following wire gauge chart from McMaster-Carr.

```
In [1]: from IPython.core.display import Image
        Image('http://images2.mcmaster.com/Contents/gfx/small/'
              + 'about-wire-size-chart(d01b)-2s.png')
```

Out[1]:

| Wire Size (AWG) | Wire Dia. Inches mm | | Wire Size (AWG) | Wire Dia. Inches mm | |
|--------------------|--------------------------|------|--------------------|--------------------------|-------|
| 40 | 0.003" | 0.08 | 10 | 0.102" | 2.59 |
| 38 | 0.004" | 0.10 | 8 | 0.129" | 3.26 |
| 36 | 0.005" | 0.13 | 6 | 0.162" | 4.12 |
| 34 | 0.006" | 0.16 | 4 | 0.204" | 5.19 |
| 32 | 0.008" | 0.20 | 2 | 0.258" | 6.54 |
| 30 | 0.010" | 0.26 | 1 | 0.289" | 7.35 |
| 28 | 0.013" | 0.32 | 1/0 | 0.324" | 8.25 |
| 26 | 0.016" | 0.41 | 2/0 | 0.365" | 9.27 |
| 24 | 0.020" | 0.51 | 3/0 | 0.410" | 10.40 |
| 22 | 0.025" | 0.64 | 4/0 | 0.460" | 11.68 |
| 20 | 0.032" | 0.81 | 250 MCM | 0.500" | 12.70 |
| 18 | 0.040" | 1.02 | 300 MCM | 0.540" | 13.72 |
| 16 | 0.051" | 1.29 | 350 MCM | 0.590" | 14.99 |
| 14 | 0.064" | 1.63 | 400 MCM | 0.630" | 16.00 |
| 12 | 0.080" | 2.05 | 500 MCM | 0.700" | 17.78 |

Figure Q.1: notebook figure

Q.7 Calculations for 20 AWG

Eagle Alloys supplies a tungsten copper alloy. It is nominally 45% copper and 55% tungsten by weight, has an electrical conductivity of 55 %ACS, thermal conductivity of 2.40 W/(CM degC) over the temperature of 20-400degC.

According to Wikipedia the heat transfer coefficient for air is between 10 and 100 W/(m² K). According to Engineering Toolbox it is between 5 and 25 W/(m² K) for free convection.

Let us do the math with the following parameters:

```
<li>$L_{\text{wire}}=1\text{m}</li>
<li>$\bar{h}=20\text{ W}/(\text{m}^2\text{K})</li>
<li>$k=2.40\text{ W}/(\text{cm degC})=240\text{ W}/(\text{m degC})</li>
<li>$T_0=2000^\circ\text{C}</li>
<li>$T_\infty=25^\circ\text{C}</li>
<li>$d=0.81\text{mm}</li>
```

```
In [10]: # Import basic modules
         # make sure that division is done as expected
         from __future__ import division

         # plotting setup
         %matplotlib inline
         import matplotlib.pyplot as plt
         plt.style.use('white_back')

         # for 3d graphs
         # from mpl_toolkits.mplot3d import axes3d
         # for legends of combined fig types
         # import matplotlib.lines as mlines

         # numerical functions
         import numpy as np

         # need some constants
         from scipy import constants
         from numpy import pi

In [15]: Lwire = 1
         L = Lwire/2
         h=20
         k=2.40*100
         T_0 = 2000+273
         T_inf = 25+273
         d = 0.81*10**-3

         P = pi*d
         A = pi*(d/2)**2

         T = T_inf + (T_0-T_inf)/(np.cosh(2*L*np.sqrt(h/(k*d))))
         print "Temperaute at tip: " + str(T-273)

         m = np.sqrt(h*P/(k*A))
         print "mL=" + str(m*L)

         #Let's plot this as temp vs length

         Lwire = np.linspace(0.05,1,200)
         L=Lwire/2 #since flame is at the center
```

```

P = pi*d
A = pi*(d/2)**2

T = T_inf + (T_0-T_inf)/(np.cosh(2*L*np.sqrt(h/(k*d))))
#semilogy(Lwire,T-273)
fig, ax = plt.subplots()
lin = ax.plot(L,T-273)
_ = ax.set_ylim([min(T)-273, max(T)-273])
_ = ax.set_xlabel('Wire half-length (m)')
_ = ax.set_ylabel(r'Temperature ($^\circ$C)')
_ = ax.set_title('Temperature at the Tip of a Wire vs Wire Half-Length')

up = fig.add_axes([.4, .4, .45, .45])
lin = up.plot(L,T-273)
_ = up.axis([0.15, .5, 0, 200])
# fig.savefig('tipTemp-20awg.pdf',transparent=True)

```

Tempertaute at tip: 25.1554331617
 mL=10.1430103242

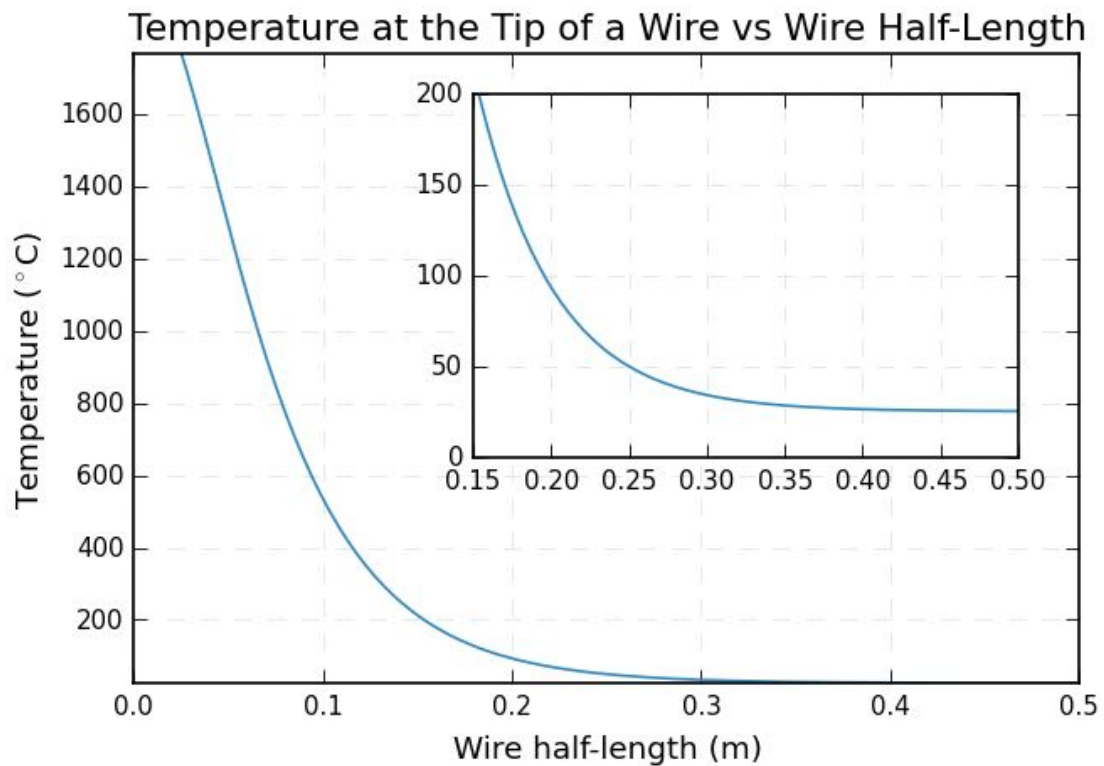


Figure Q .2: notebook figure

Q.8 Calculations for Tungsten Welding Rod

A pure tungsten welding rod, 1/8in by 12in was purchased from Diamond Ground Products. Tungsten has a thermal conductivity of 174 W/(m K) and an electrical resistivity of $5.3 \times 10^{-8} \Omega m$

According to Wikipedia the heat transfer coefficient for air is between 10 and 100 W/(m² K). According to Engineering Toolbox it is between 5 and 25 W/(m² K) for free convection. We will use 20 W/(m² K).

Let us do the math with the following parameters:

```
<li>$L_{\text{wire}}=12\text{in}</li>
<li> $\bar{h}=20\text{ W/(m}^2\text{K)}</li>
<li> $k=174\text{W/(m degK)}</li>
<li> $T_0=2000^\circ\text{C}</li>
<li> $T_\infty=25^\circ\text{C}</li>
<li> $d=0.125\text{in}</li>
```

Q.8.1 CAUTION

The calculations rely on the assumption that $mL \geq 5$ which is not the case for this rod. This really should be re-done with the exact solution and not the approximations/simplifications.

```
In [5]: Lwire = 12*constants.inch
        h=20
        k=174
        T_0 = 2000+273
        T_inf = 25+273
        d = 0.125*constants.inch

        # Define length as half the actual length since
        # the flame will be in the middle and we want the
        # temp at the end
        L = Lwire/2

        # perimeter
        P = pi*d
        # area
        A = pi*(d/2)**2

        # temperature at tip
        T = T_inf + (T_0-T_inf)/(np.cosh(2*L*np.sqrt(h/(k*d))))
        print "Temperature at tip: " + str(T-273) + "C"

        # mL ratio
        m = np.sqrt(h*P/(k*A))
        print "mL=" + str(m*L)

        #Let's plot this as temp vs length
        L = np.linspace(0.01,1,201)
```

```

P = pi*d
A = pi*(d/2)**2

T = T_inf + (T_0-T_inf)/(np.cosh(2*L*np.sqrt(h/(k*d))))

fig, ax = plt.subplots()
lin = ax.plot(L,T-273)
_= ax.set_ylim([min(T)-273, max(T)-273])
_= ax.set_xlabel('Fin length (m)')
_= ax.set_ylabel(r'Temperature ($^\circ$C)')
_= ax.set_title('Temperature at the Tip of a Wire vs Fin (Wire) Length')

up = fig.add_axes([.4, .4, .45, .45])
lin = up.plot(L,T-273)
_= up.axis([0.3, .5, 0, 200])

Temperaute at tip: 640.433814338C
mL=1.83393302627

```

Temperature at the Tip of a Wire vs Fin (Wire) Length

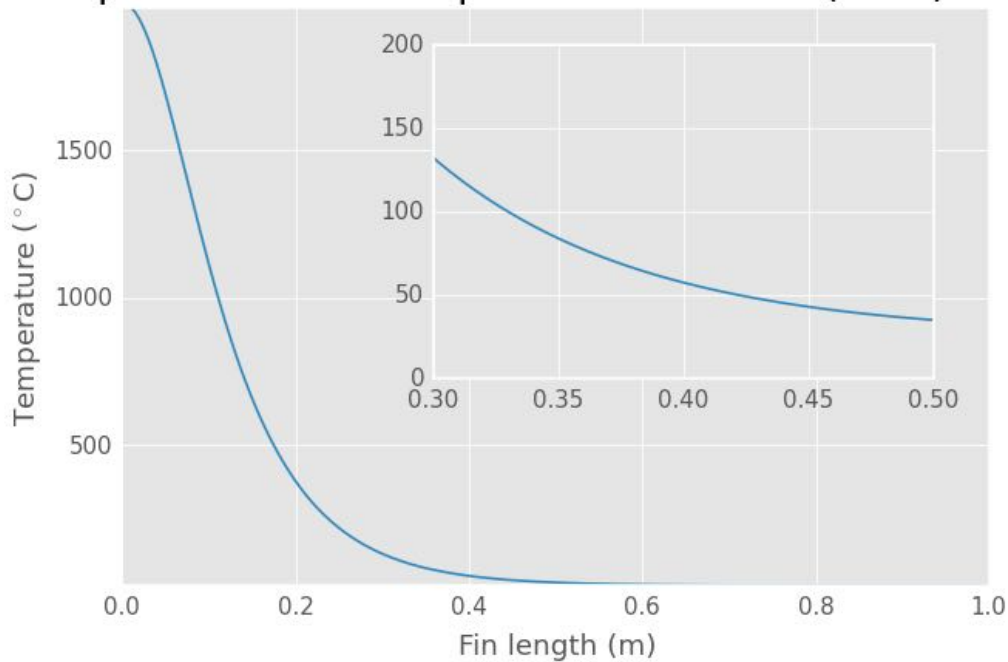


Figure Q .3: notebook figure

Appendix R

IPython notebook: T-lineCalibration-diss

R.1 Calibration of a Transmission Line

The purpose of this notebook is to examine the one- and two-port calibration of a transmission line. This will use a two-wire transmission line and the measurement a shorting plate located at three different locations along the line.

R.1.1 Derivation

Dr. Rothwell did the derivation. Add it in here at some point.

Below relates to the one-port calibration of a 2-port network. This would be used to calibrate out a single cable so that measurements could be made at the end of the cable.

We can find the S-parameters of a 2-port network by measuring S_{11} with three known loads connected individually to port 2 of the network. This provides three different measured S_{11} values, S_{11}^i (0 indexing will be used since that is what Python uses). The loads used for this calibration are shorts located at different distances along the transmission line. The measured response a shorted transmission line is theoretically just

$$\Gamma_i = -e^{-j2\beta d_i}.$$

Placing a short in three different locations gives three different values of Γ which are known (in theory).

Begin by defining

$$K = \frac{\frac{1}{\Gamma_2} - \frac{1}{\Gamma_0} S_{11}^0 - S_{11}^1}{\frac{1}{\Gamma_1} - \frac{1}{\Gamma_0} S_{11}^0 - S_{11}^2}$$

then the S-parameters can be calculated in the following order:

$$S_{22} = \frac{\frac{1}{\Gamma_2} - \frac{1}{\Gamma_1} K}{1 - K}$$

$$S = S_{12}S_{21} = \frac{S_{11}^0 - S_{11}^1}{\frac{1}{\Gamma_1} - \frac{1}{\Gamma_0}} \left(\frac{1}{\Gamma_0} - S_{22} \right) \left(\frac{1}{\Gamma_1} - S_{22} \right)$$

$$S_{11} = S_{11}^0 - \frac{S}{\frac{1}{\Gamma_0} - S_{22}}$$

R.2 Preflight

Begin with the necessary imports

```
In [3]: # Import basic modules
        # make sure that division is done as expected
        from __future__ import division

        # plotting setup
        %matplotlib inline
        import matplotlib.pyplot as plt
        plt.style.use('gray_back')
        plt.rcParams['axes.ymargin'] = 0

        # get the viridis colormap
        # https://bids.github.io/colormap
        # it will be available as cmaps.viridis
        # import colormaps as cmaps

        # for 3d graphs
        # from mpl_toolkits.mplot3d import axes3d
        # for legends of combined fig types
        # import matplotlib.lines as mlines

        # numerical functions
        import numpy as np

        # need some constants
        from scipy import constants
        from numpy import pi

        # RF tools!
        import skrf as rf

        # version information
        # %install_ext http://raw.githubusercontent.com/jrjohansson/
        #   version_information/master/version_information.py
        # %load_ext version_information
        # %reload_ext version_information

        # %version_information numpy, scipy, matplotlib

In [4]: import os
```

```
In [14]: doSave = True
        # doSave = False
```

Definition of functions that will be needed.

```
In [6]: def twoWireParameters(freq, a, D, sigma_c=np.inf, mu_c=1,
                             eps_r = 1, tanDelta = 0, mu_r=1,
                             unitsScale=1):
    """
    Return R, L, G, C for a two-wire line

    Calculates and returns the resistance, impedance, conductance,
    and capacitance for a two-wire transmission line. Geometric and
    electrical properties are given for the wire and the media in
    which the wires are located.

    Parameters
    -----
    freq : scalar
        Frequency at which the parameters should be calculated
    a : scalar
        Wire radius
    D : scalar
        center-to-center distance of the wires
    sigma_c : scalar
        Conductivity of the wires
    mu_c : scalar, optional
        Relative permeability of the wires. Default is 1.
    eps_r : scalar, optional
        Relative permittivity of the environment. Used as
        epsilon = eps_r*eps_0*(1-j*tanDelta). Default is 1.
    tanDelta : scalar, optional
        Loss tangent of the environment. Used as
        epsilon = eps_r*eps_0*(1-j*tanDelta). Default is 0.
    mu_r : scalar, optional
        Relative permeability of the environment. Default is 1
    unitsScale : scalar, optional if using meters
        Scaling factor for units. For mm, use 1e-3, for in use
        0.0254.

    Returns
    -----
    R : scalar
        Resistance of the two-wire transmission line
    L : scalar
        Impedance of the two-wire transmission line
    G : scalar
        Conductance of the two-wire transmission line
    C : scalar
        Capacitance of the two-wire transmission line
    """
    #from __future__ import division
```

```

import scipy.constants as const

# Scale dimensions
a = a*unitsScale
D = D*unitsScale
eps_sgl = const.epsilon_0*eps_r
eps_dbl = const.epsilon_0*eps_r*tanDelta

omega=2*pi*freq
#delta_cond = 1/np.sqrt(const.pi*freq*sigma_c)

invCosh = np.arccosh(D/(2*a))

#R = 1/(const.pi*a*sigma_c*delta_cond)
R = np.sqrt(omega*mu_c/
            (2*(const.pi*a)**2*sigma_c
             *(1-(2*a/D)**2)))
G = (const.pi*omega*eps_dbl)/invCosh
L = const.mu_0/pi*invCosh
C = pi*eps_sgl/invCosh
return R, L, G, C

def reflectionCoeff(dist, beta):
    """
    Calculate the reflection coefficient of a short.

    Calculate the reflection coefficient of a short in a given media at
    a given distance in meters.

    gamma = -exp(2j*beta*dist)

    Parameters
    -----
    dist : array_like
        Distance to the short from some reference plane
    beta : array_like
        Propagation constant, beta, for the media containing the short

    Returns
    -----
    coeff : array_like
        The reflection coefficient calculated as
        gamma = exp(-j*beta*dist)
    """
    coeff = -np.exp(2j*beta*dist)
    return coeff

def find1PortTransition(beta, dist, shorts):
    #23456789112345678921234567893123456789412345678951234567896123456789712
    """
    Calculated *SOME* of the S-parameters for a transition. READ DETAILS
    """

```

Calculate S_{11} , S_{22} , and $S_{12}S_{21}$ for a transition. This is used when you want to de-embed a sample from the transition and the sample.

This requires scikit-rf version with source after April 4, 2014. Probably will be version 0.15. You might need to get this from github (<https://github.com/scikit-rf/scikit-rf>).

Parameters

beta : array_like

The propagation constant, beta, used to calculate the reflection coefficient of each short. This should be the same for all three shorts.

dist : ndarray

A NumPy array containing the distance from the refence plane to each of the three shorts in meters.

Ex: array([1.3e-3, 4e-3, 7.87e-3])

shorts : list

*A list of the file names for the Touchstone files, i.e. *.s*p, for each short. The order of files should match the distances in 'dist'. Only the S11 data will be used so these may be multi-port Touchstone files and all do not have to be the same number of ports.*

Returns

ntwkS11, ntwkS22, ntwkS12S21 : skrf.network.Network

1-port networks for the calculated S-parameters to be used for de-embedding a sample.

To-Do

Should throw in some error checking to make sure that the three shorts have the same network properties

"""

#g is 1/Gamma

g = [1/reflectionCoeff(beta, d) for d in dist]

sc = [rf.Network(a).s[:,0,0] for a in shorts]

tempNtwk = rf.Network(shorts[0]).s11

freq = tempNtwk.f

z0 = tempNtwk.z0

K = (g[2]-g[0])/(g[1]-g[0])(sc[0]-sc[1])/(sc[0]-sc[2])*

*s22 = (g[2]-g[1]*K)/(1-K)*

s12s21 = (sc[0]-sc[1])/(g[1]-g[0])(g[0]-s22)*(g[1]-s22)*

s11 = sc[0]-s12s21/(g[0]-s22)

ntwkS11 = rf.Network(name="Transition S11", f = freq, z0 = z0, s=s11)

ntwkS22 = rf.Network(name="Transition S22", f = freq, z0 = z0, s=s22)

```

ntwkS12S21 = rf.Network(name="Transition S12S21",f=freq, z0 = z0,s=s12s21)
return ntwkS11, ntwkS22, ntwkS12S21

def deembed(trans, raw):
#23456789112345678921234567893123456789412345678951234567896123456789712
    """
    De-embed a 1-port sample.

    De-embed a 1-port sample from a transition that has been
    characterized using a three short method.

    Parameters
    -----
    trans : tuple of skrf.network.Network
        A tuple of scikit-rf 1-Port Networks that correspond to the
        characterized S-parameters of the transition. Order should be
        S_11, S_22, S_12*S_21.
    raw : skrf.network.Network
        The raw data measurement that includes the sample and the
        transition. The sample will be de-embedded from this data

    Returns
    -----
    sample : skrf.network.Network
        The de-embedded sample
    """
    b = [x.s[:,0,0] for x in trans]
    #print b[0]
    inv = b[1]+b[2]/(raw.s[:,0,0]-b[0])
    sample = trans[0]
    sample.s = 1/inv
    return sample

```

R.3 2014-08-05

R.4 Complex Propagation Constant

This data set is when I realized that the reflection coefficient was not taking into account losses on the line.

```

In [8]: #13-6mm-foam-I-short.s1p
        #17-2mm-foam-H-short.s1p
        #5-9mm-foam-F-short.s1p
        #9-7mm-foam-G-short.s1p
        #line.s1p
        #scratch.s1p
        #short-against-plexi.s1p

        #F, 5.9, mm, white

```

```

#G, 9.7, mm, white
#H, 17.2, mm, white
#I, 13.6, mm, white
dataDir = os.path.join(os.path.expanduser("~"), "Documents",
                        "plexiglass-holder-data", "Data", "2014-08-05")
rawSample = rf.Network(os.path.join(dataDir, "13-6mm-foam-I-short.s1p"))
sampleDist = 13.6*1e-3

short1 = os.path.join(dataDir, "5-9mm-foam-F-short.s1p")
short2 = os.path.join(dataDir, "9-7mm-foam-G-short.s1p")
short3 = os.path.join(dataDir, "17-2mm-foam-H-short.s1p")
shortDistances = np.array([5.9, 9.7, 17.2])*1e-3

ntwkF = rf.Network(short1)
ntwkG = rf.Network(short2)
ntwkH = rf.Network(short3)
ntwkI = rawSample

freq = rawSample.f
diam = 0.122
radius = diam/2
cntr2cntr = 0.25
sigma = 1/(7.2e-7)
R, L, G, C = twoWireParameters(freq = freq, a=radius, D=cntr2cntr,
                                sigma_c=sigma, unitsScale=0.0254)
rRad = 30*(2*pi*freq**2*constants.epsilon_0*constants.mu_0)*cntr2cntr**2
R=R+rRad

gamma = np.sqrt((R+1j*2*pi*freq * L)*(G+1j*2*pi*freq*C))
rfFreq = rf.Frequency(freq[0], freq[-1], freq.shape[0], 'Hz')
theory = rf.media.DistributedCircuit(rfFreq, C, L, R, G).delay_short(sampleDist)

shorts = [short1, short2, short3]
balun = find1PortTransition(1j*gamma, shortDistances, shorts)
sample = deembed(balun, rawSample)

fig, ax = plt.subplots(2,1)
fig.set_figheight(7)

_ = rawSample.plot_s_db(ax=ax[0], ls=":", label='Original - I')
_ = sample.plot_s_db(ax=ax[0], label='Calibrated using F, G, H')
_ = theory.plot_s_db(ax=ax[0], ls="--", label='Theory')

_ = rawSample.plot_s_deg(ax=ax[1], ls=":", label='Original', show_legend=False)
_ = sample.plot_s_deg(ax=ax[1], label='Calibrated', show_legend=False)
_ = theory.plot_s_deg(ax=ax[1], ls="--", label='Theory', show_legend=False)

if doSave:
    fig.savefig('deembed-I.pdf')

```

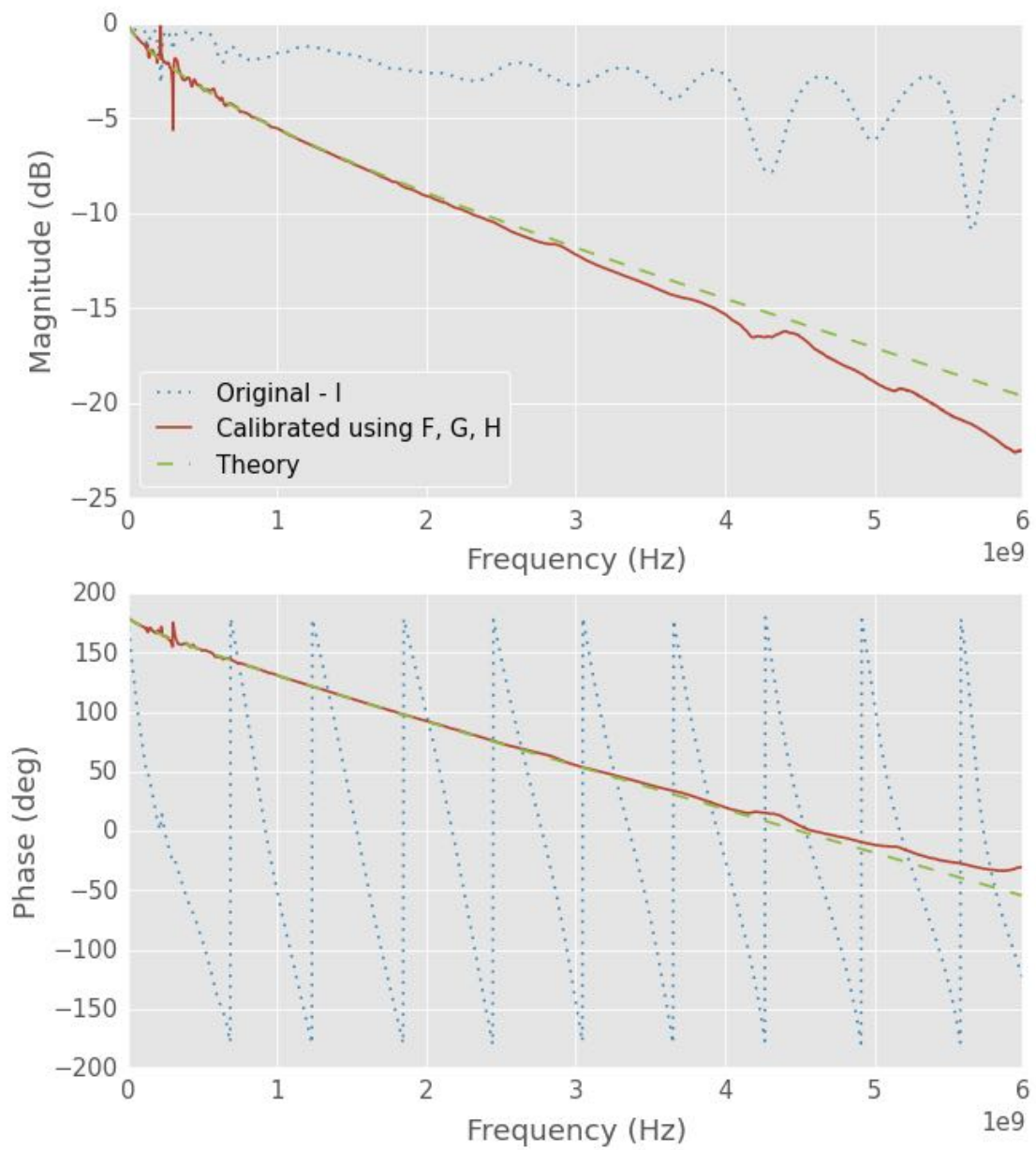


Figure R .1: notebook figure


```

In [9]: # plt.rcParams['axes.ymargin'] = 0
fig, ax = plt.subplots(2,1)
fig.set_figheight(7)

_ = ntwkF.plot_s_db(ax=ax[0], label="F 5.9mm")
_ = ntwkG.plot_s_db(ax=ax[0], label="G 9.7mm")
_ = ntwkI.plot_s_db(ax=ax[0], label="I 13.6mm")
_ = ntwkH.plot_s_db(ax=ax[0], label="H 17.2mm")

_ = ntwkF.plot_s_deg(ax=ax[1], label="F 5.9mm", show_legend=False)
_ = ntwkG.plot_s_deg(ax=ax[1], label="G 9.7mm", show_legend=False)
_ = ntwkI.plot_s_deg(ax=ax[1], label="I 13.6mm", show_legend=False)
_ = ntwkH.plot_s_deg(ax=ax[1], label="H 17.2mm", show_legend=False)

if doSave:
    fig.savefig('short-s-param.pdf')

```

R.5 2014-08-07 vs -05 vs -11

```

In [11]: # compare shorts from different days
dataDir = os.path.join(os.path.expanduser("~"), "Documents",
                        "plexiglass-holder-data", "Data", "2014-08-05")
I5 = rf.Network(os.path.join(dataDir, "13-6mm-foam-I-short.s1p"), name='5th')
dataDir = os.path.join(os.path.expanduser("~"), "Documents",
                        "plexiglass-holder-data", "Data", "2014-08-07")
I7 = rf.Network(os.path.join(dataDir, "13-6mm-foam-I-short.s1p"), name='7th')
dataDir = os.path.join(os.path.expanduser("~"), "Documents",
                        "plexiglass-holder-data", "Data", "2014-08-11")
I11 = rf.Network(os.path.join(dataDir, "13-6mm-foam-I-short.s1p"), name='11th')

# diff = np.abs(I5.s[:,0,0]-I7.s[:,0,0])
# magDiff = np.abs(I5.s_db[:,0,0]-I7.s_db[:,0,0])
# degDiff = np.abs(I5.s_deg_unwrap[:,0,0]-I7.s_deg_unwrap[:,0,0])
# fig, ax = plt.subplots()
# _ = ax.plot(I5.f,diff, label="diff")
# _ = ax.plot(I5.f,magDiff, label="mag")
# _ = ax.plot(I5.f,degDiff, label="deg")
# _ = ax.legend()

fig, ax = plt.subplots()
_ = I5.plot_s_db(ax=ax)
_ = I7.plot_s_db(ax=ax)
_ = I11.plot_s_db(ax=ax)

fig, ax = plt.subplots()
_ = I5.plot_s_deg(ax=ax)
_ = I7.plot_s_deg(ax=ax)
_ = I11.plot_s_deg(ax=ax)

```

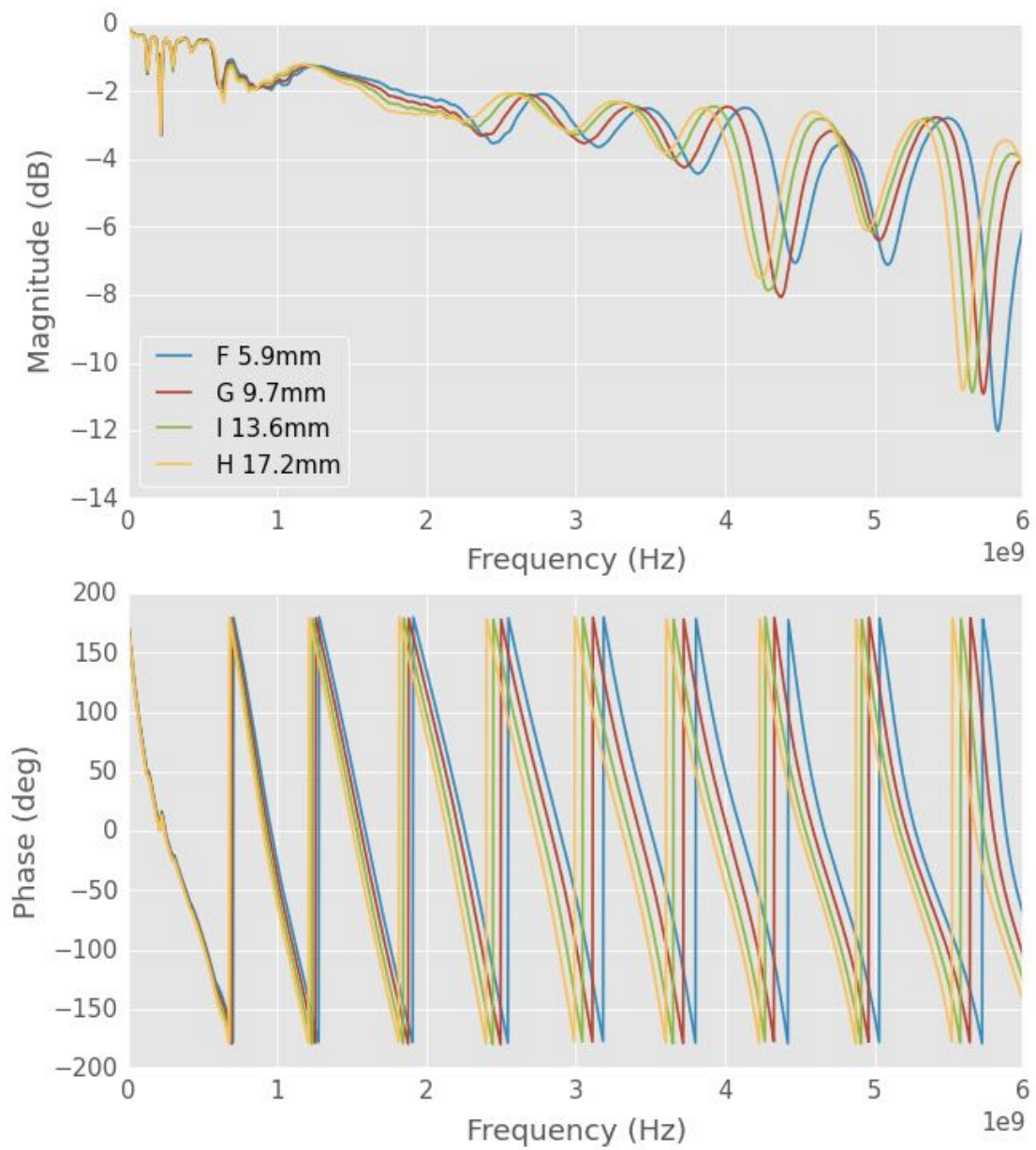


Figure R .2: notebook figure

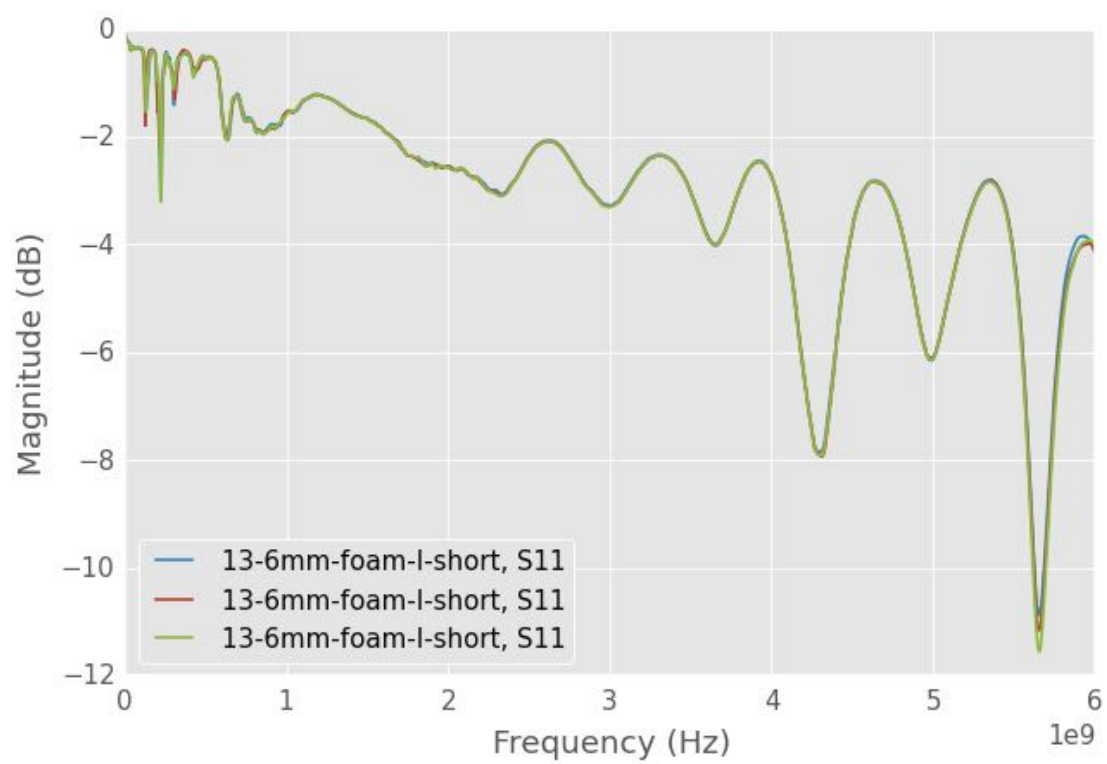


Figure R .3: notebook figure

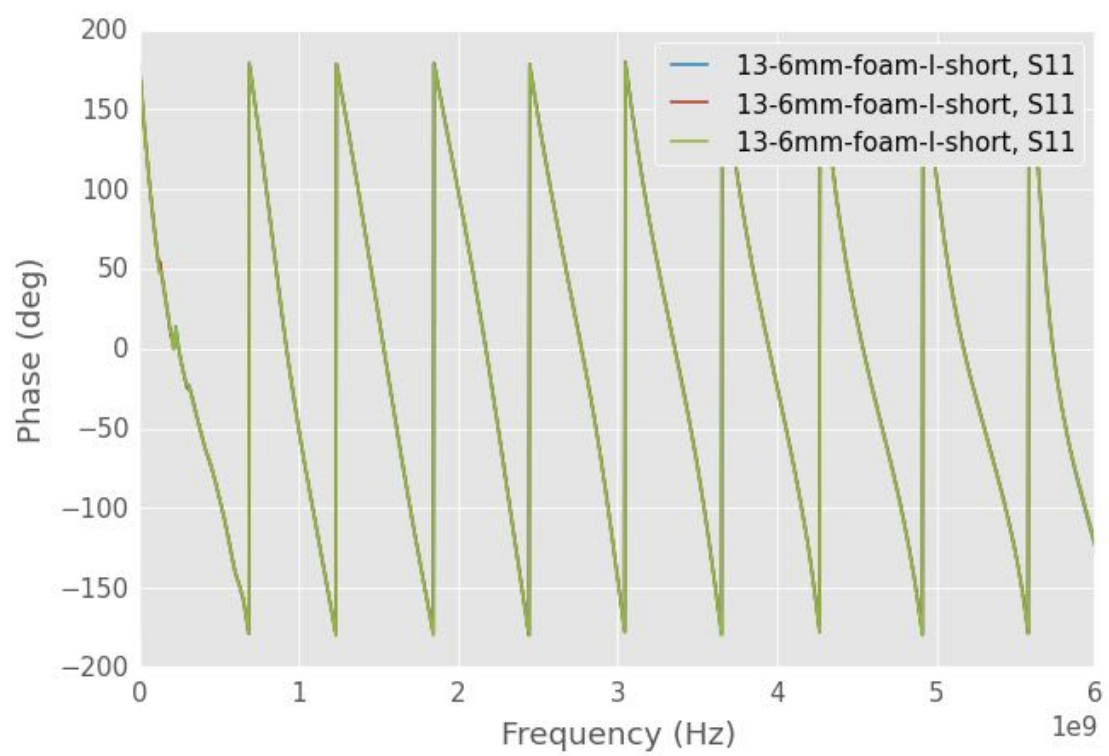


Figure R .4: notebook figure

R.6 2014-08-11

```
In [12]: #Cal data from 2014-08-05
#13-6mm-foam-I-short.slp
#17-2mm-foam-H-short.slp
#5-9mm-foam-F-short.slp
#9-7mm-foam-G-short.slp
#line.slp
#scratch.slp
#short-against-plexi.slp

#11-7mm-air-short.slp
#13-6mm-foam-I-short.slp
#5-9mm-foam-F-6-6mm-teflon-22-4mm-foamG-short.slp
#6-0mm-foam-F-12-9mm-delrin-28-7mm-foamG-short.slp

#F, 5.9, mm, white
#G, 9.7, mm, white
#H, 17.2, mm, white
#I, 13.6, mm, white
dataDir = os.path.join(os.path.expanduser("~"), "Documents",
                        "plexiglass-holder-data", "Data", "2014-08-05")
rawDir = os.path.join(os.path.expanduser("~"), "Documents",
                        "plexiglass-holder-data", "Data", "2014-08-11")
rawSample = rf.Network(os.path.join(rawDir,
                                     "6-0mm-foam-F-12-9mm-delrin-28-7mm-foamG-short.slp"))
sampleDist = 28.7*1e-3

short1 = os.path.join(dataDir, "5-9mm-foam-F-short.slp")
short2 = os.path.join(dataDir, "9-7mm-foam-G-short.slp")
short3 = os.path.join(dataDir, "17-2mm-foam-H-short.slp")
shortDistances = np.array([5.9, 9.7, 17.2])*1e-3

freq = rawSample.f
diam = 0.122
radius = diam/2
cntr2cntr = 0.25
sigma = 1/(7.2e-7)
R, L, G, C = twoWireParameters(freq = freq, a=radius, D=cntr2cntr,
                                sigma_c=sigma, unitsScale=0.0254)
rRad = 30*(2*pi*freq**2*constants.epsilon_0*constants.mu_0)*cntr2cntr**2
R=R+rRad

gamma = np.sqrt((R+1j*2*pi*freq * L)*(G+1j*2*pi*freq*C))
rfFreq = rf.Frequency(freq[0], freq[-1], freq.shape[0], 'Hz')
theory = rf.media.DistributedCircuit(rfFreq, C, L, R, G).delay_short(sampleDist)

shorts = [short1, short2, short3]
balun = find1PortTransition(1j*gamma, shortDistances, shorts)
sample = deembed(balun, rawSample)
```

```

fig, ax = plt.subplots(2,1)
fig.set_figheight(7)

_ = rawSample.plot_s_db(ax=ax[0], ls=":", label='Original')
_ = sample.plot_s_db(ax=ax[0], label='Calibrated Delrin using F, G, H')
_ = theory.plot_s_db(ax=ax[0], ls="--", label='Air Line')

_ = rawSample.plot_s_deg(ax=ax[1], ls=":", label='Original', show_legend=False)
_ = sample.plot_s_deg(ax=ax[1], label='Calibrated Delrin', show_legend=False)
_ = theory.plot_s_deg(ax=ax[1], ls="--", label='Air Line', show_legend=False)

if doSave:
    fig.savefig('delrin-layered.pdf')

```

In [15]:

```

fig, ax = plt.subplots(2,1)
fig.set_figheight(7)

_ = rawSample.plot_s_db(ax=ax[0], ls=":", label='Original', lw=3)
_ = sample.plot_s_db(ax=ax[0], label='Calibrated', lw=3)
_ = theory.plot_s_db(ax=ax[0], ls="--", label='Air Line', lw=3)

_ = rawSample.plot_s_deg(ax=ax[1],ls=":",label='Original',show_legend=False,lw=3)
_ = sample.plot_s_deg(ax=ax[1], label='Calibrated', show_legend=False, lw=3)
_ = theory.plot_s_deg(ax=ax[1],ls="--",label='Air Line', show_legend=False, lw=3)

_ = ax[0].legend(fontsize=16)
_ = ax[0].set_xlabel('Frequency (Hz)', fontsize=16)
_ = ax[0].set_ylabel('Magnitude', fontsize=16)
_ = ax[1].set_xlabel('Frequency (Hz)', fontsize=16)
_ = ax[1].set_ylabel('Phase (deg)', fontsize=16)

if doSave:
    fig.savefig('delrin-layered-defense.pdf')

```

R.7 Layered De-embed Measurement

```

In [9]: #Cal data from 2014-08-05
        #13-6mm-foam-I-short.s1p
        #17-2mm-foam-H-short.s1p
        #5-9mm-foam-F-short.s1p
        #9-7mm-foam-G-short.s1p
        #line.s1p
        #scratch.s1p
        #short-against-plexi.s1p

        #11-7mm-air-short.s1p
        #13-6mm-foam-I-short.s1p
        #5-9mm-foam-F-6-6mm-teflon-22-4mm-foamG-short.s1p
        #6-0mm-foam-F-12-9mm-delrin-28-7mm-foamG-short.s1p

```

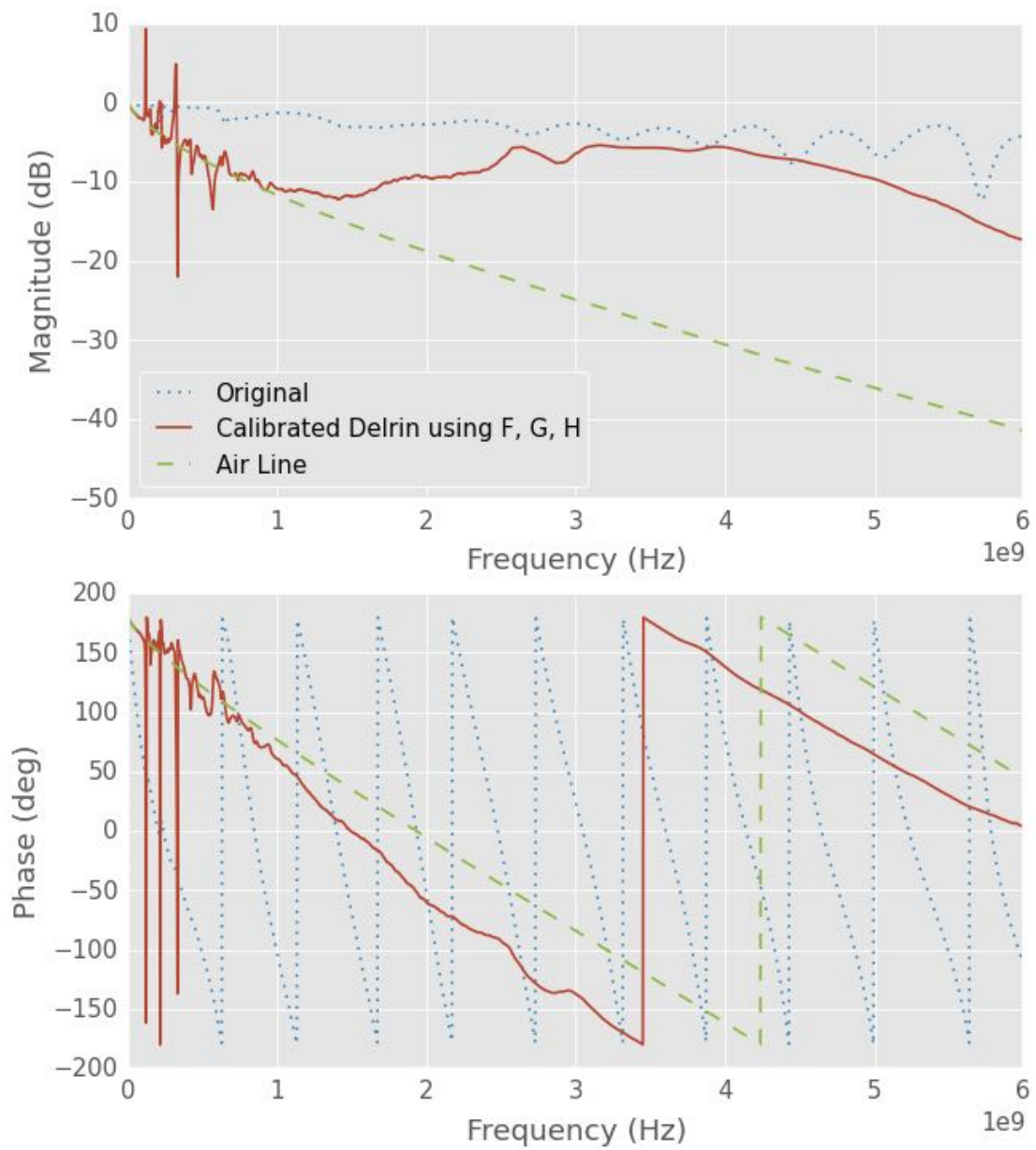


Figure R .5: notebook figure

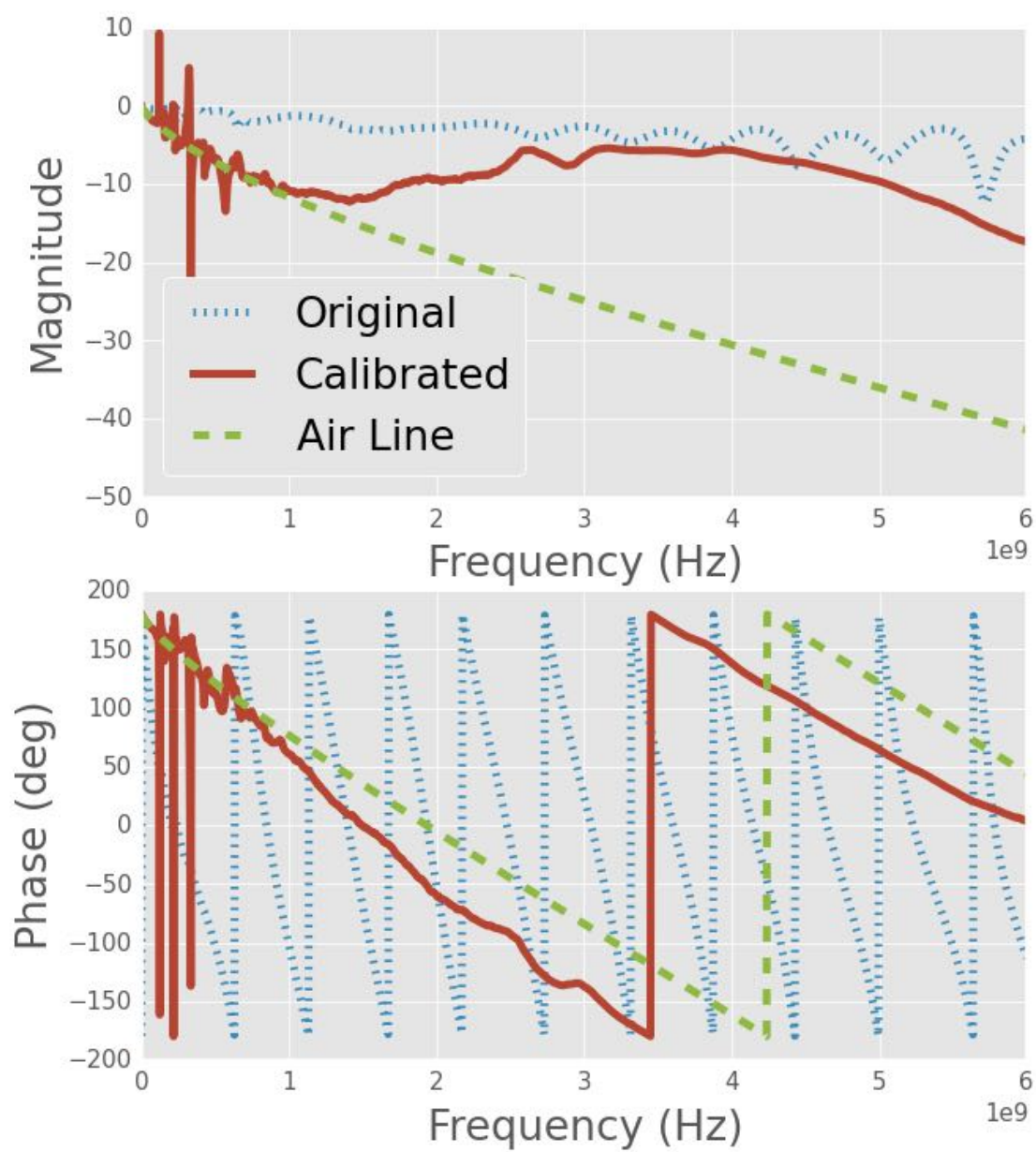


Figure R .6: notebook figure


```

dataDir = os.path.join(os.path.expanduser("~"), "hpc",
                       "plexiglass-holder-data", "Data", "2014-08-05")
rawDir = os.path.join(os.path.expanduser("~"), "hpc",
                       "plexiglass-holder-data", "Data", "2014-08-11")

rawSample = rf.Network(os.path.join(rawDir,
                                     "6-0mm-foam-F-12-9mm-delrin-28-7mm-foamG-short.s1p"))
sampleDist = 28.7*1e-3

short1 = os.path.join(dataDir, "5-9mm-foam-F-short.s1p")
short2 = os.path.join(dataDir, "9-7mm-foam-G-short.s1p")
short3 = os.path.join(dataDir, "17-2mm-foam-H-short.s1p")
shortDistances = np.array([5.9, 9.7, 17.2])*1e-3

freq = rawSample.f
diam = 0.122
radius = diam/2
cntr2cntr = 0.25
sigma = 1/(7.2e-7)
R, L, G, C = twoWireParameters(freq = freq, a=radius, D=cntr2cntr,
                                sigma_c=sigma, unitsScale=0.0254)
rRad = 30*(2*pi*freq**2*constants.epsilon_0*constants.mu_0)*cntr2cntr**2
R=R+rRad

gamma = np.sqrt((R+1j*2*pi*freq * L)*(G+1j*2*pi*freq*C))
rfFreq = rf.Frequency(freq[0], freq[-1], freq.shape[0], 'Hz')
airLine = rf.media.DistributedCircuit(rfFreq, C, L, R, G).delay_short(sampleDist)

#####
#Cascade
#####
layerEps_r = np.array([1, 3.7, 1])
tanDelta = 1.5e-4
lengths = np.array([6, 12.9, 28.7-6-12.9])*1e-3

R, L, G, C = twoWireParameters(freq, radius, cntr2cntr, sigma, eps_r=1,
                                tanDelta=0, unitsScale=0.0254)

R += rRad
Z = np.sqrt((R+1j*2*pi*freq * L)/(G+1j*2*pi*freq*C))
Z_norm = Z
sect1 = rf.media.DistributedCircuit(rfFreq, C, L, R, G).line(lengths[0])
sect1.renormalize(Z_norm) # added 10/31/2015

#foam and short section
sect3 = rf.media.DistributedCircuit(rfFreq, C, L, R, G).delay_short(lengths[-1])
sect3.renormalize(Z_norm)

#sample section
R, L, G, C = twoWireParameters(freq, radius, cntr2cntr, sigma,
                                eps_r=layerEps_r[1], tanDelta=tanDelta,

```

```

unitsScale=0.0254)

R += rRad
sect2 = rf.media.DistributedCircuit(rfFreq, C, L, R, G).line(lengths[1])
sect2.renormalize(Z_norm)

totalLine = sect1**sect2**sect3

#
# De-embed
#
shorts = [short1, short2, short3]
balun = find1PortTransition(1j*gamma, shortDistances, shorts)
sample = deembed(balun, rawSample)

#airLine.renormalize(50)
#totalLine.renormalize(50)
print sample
print airLine
print totalLine

#
# Plotting
#
# sample.plot_s_db(show_legend=False)
# airLine.plot_s_db(show_legend=False)
# totalLine.plot_s_db(show_legend=False)
# #rawSample.plot_s_db(show_legend=False)
# plt.figure()
# sample.plot_s_deg(show_legend=False)
# airLine.plot_s_deg(show_legend=False)
# totalLine.plot_s_deg(show_legend=False)

fig, ax = plt.subplots()
_ = sample.plot_s_db(ax=ax, label='De-embedded')
_ = airLine.plot_s_db(ax=ax, label='Air line')
_ = totalLine.plot_s_db(ax=ax, label='Theory')

fig, ax = plt.subplots()
_ = sample.plot_s_deg(ax=ax, label='De-embedded')
_ = airLine.plot_s_deg(ax=ax, label='Air line')
_ = totalLine.plot_s_deg(ax=ax, label='Theory')

1-Port Network: 'Transition S11', 30000-60000000000 GHz, 1601 pts, z0=[ 50.+0.j]
1-Port Network: '', 30000-60000000000 Hz, 1601 pts, z0=[ 2806.49894742-2801.86123236j]
1-Port Network: '', 30000-60000000000 Hz, 1601 pts, z0=[ 2806.49894742-2801.86123236j]

```

R.8 Theory Done Manually

```

In [10]: def ABCD(gamma, length, Z):
        """

```

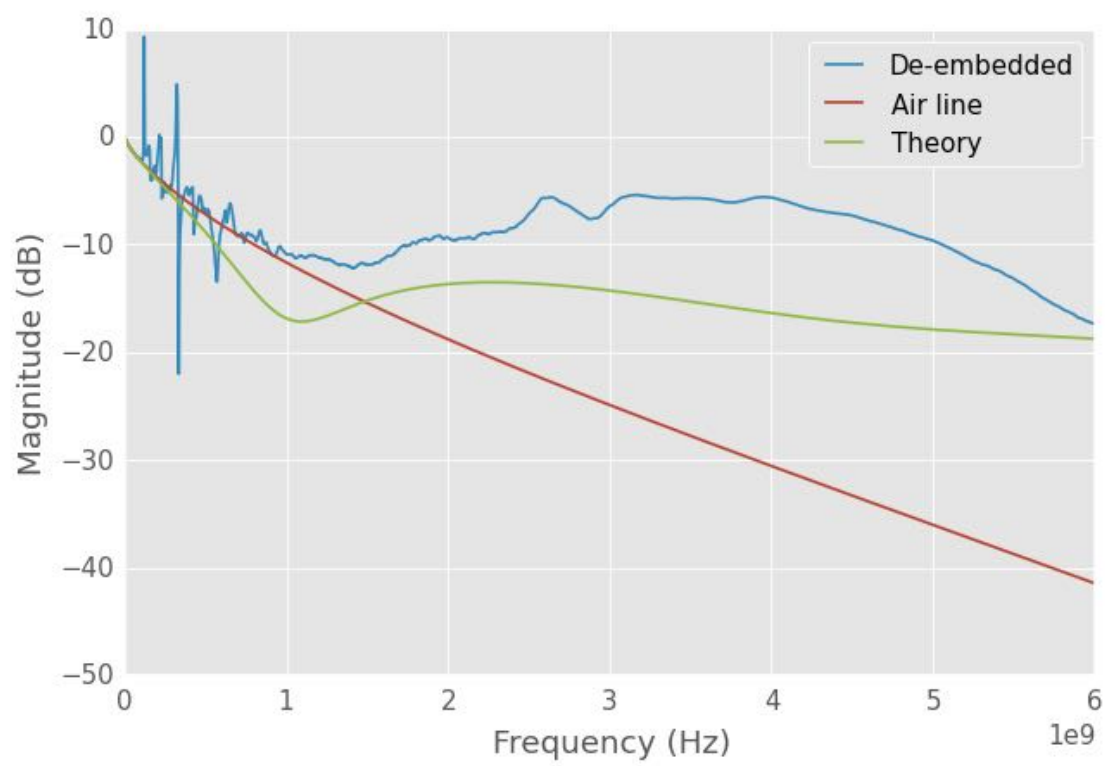


Figure R.7: notebook figure

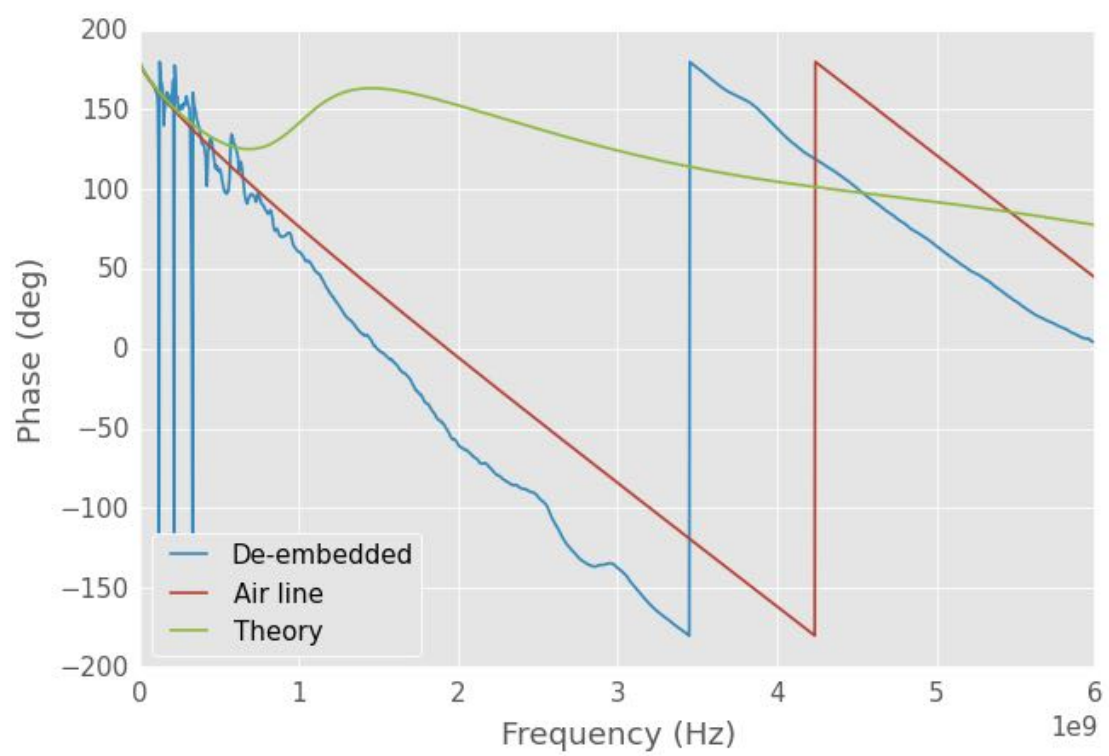


Figure R .8: notebook figure

```

Calculate the ABCD parameters for a t-line

A = cosh(gamma*length)
B = Z*sinh(gamma*length)
C = (1/Z)*sinh(gamma*length)
D = cosh(gamma*length)

Parameters
-----
gamma : numpy array-like
    Gamma for the transmission line, freq. dep.
length : value
    length of transmission line segment
Z : numpy array-like
    Characteristic impedance of transmission line, freq. dep.

Returns
-----
A : numpy array
    A parameter
B : numpy array
    B parameter
C : numpy array
    C parameter
D : numpy array
    D parameter
"""
A = np.cosh(gamma*length)
B = Z*np.sinh(gamma*length)
C = (1/Z)*np.sinh(gamma*length)
D = np.cosh(gamma*length)
return A, B, C, D

def a2s(A,B,C,D,Z):
    """
    Convert ABCD params to S params

    
$$S_{11} = \frac{A + B/Z - C*Z - D}{A + B/Z + C*Z + D}$$


    
$$S_{12} = \frac{2(A*D - B*C)}{A + B/Z + C*Z + D}$$


    
$$S_{21} = \frac{2}{A + B/Z + C*Z + D}$$


    
$$S_{22} = \frac{-A + B/Z - C*Z + D}{A + B/Z + C*Z + D}$$


```

```

        
$$A + B/Z + C*Z + D$$


Parameters
-----
A, B, C, D : numpy array
    A, B, C, D parameters

Returns
-----
s11, s12, s21, s22 : numpy array
    S-parameters
"""

denom = A + B/Z + C*Z + D

s11 = (A+B/Z-C*Z-D)/denom
s12 = 2*(A*D-B*C)/denom
s21 = 2/denom
s22 = (-A+B/Z-C*Z+D)/denom

return s11, s12, s21, s22

In [11]: dataDir = os.path.join(os.path.expanduser("~"), "hpcc",
                                "plexiglass-holder-data", "Data", "2014-08-05")
rawDir = os.path.join(os.path.expanduser("~"), "hpcc",
                      "plexiglass-holder-data", "Data", "2014-08-11")

rawSample = rf.Network(os.path.join(rawDir,
                                     "6-0mm-foam-F-12-9mm-delrin-28-7mm-foamG-short.s1p"))

short1 = os.path.join(dataDir, "5-9mm-foam-F-short.s1p")
short2 = os.path.join(dataDir, "9-7mm-foam-G-short.s1p")
short3 = os.path.join(dataDir, "17-2mm-foam-H-short.s1p")
shortDistances = np.array([5.9, 9.7, 17.2])*1e-3

layerEps_r = np.array([1, 3.7, 1])
tanDelta = 1.5e-4

lengths = np.array([6, 12.9, 28.7-6-12.9])*1e-3
totalLen = 28.7*1e-3

freq = rawSample.f
diam = 0.122
radius = diam/2
cntr2cntr = 0.25
sigma = 1/(7.2e-7)

```

R.8.1 Air Line

Scikit-RF

```
In [12]: R, L, G, C = twoWireParameters(freq = freq, a=radius, D=cntr2cntr,
                                         sigma_c=sigma, unitsScale=0.0254)
rRad = 30*(2*pi*freq**2*constants.epsilon_0*constants.mu_0)*cntr2cntr**2
R=R+rRad

gamma = np.sqrt((R+1j*2*pi*freq * L)*(G+1j*2*pi*freq*C))
rfFreq = rf.Frequency(freq[0], freq[-1], freq.shape[0], 'Hz')
# airLine = rf.media.DistributedCircuit(rfFreq,C,L,R, G).delay_short(sampleDist)
airLine = rf.media.DistributedCircuit(rfFreq, C, L, R, G).line(totalLen,'m')
airLine.renormalize(50)
```

Manually

```
In [13]: R, L, G, C = twoWireParameters(freq = freq, a=radius, D=cntr2cntr,
                                         sigma_c=sigma, unitsScale=0.0254)
rRad = 30*(2*pi*freq**2*constants.epsilon_0*constants.mu_0)*cntr2cntr**2
R=R+rRad

gamma = np.sqrt((R+1j*2*pi*freq * L)*(G+1j*2*pi*freq*C))
Z = np.sqrt((R+1j*2*pi*freq * L)/(G+1j*2*pi*freq*C))
rfFreq = rf.Frequency(freq[0], freq[-1], freq.shape[0], 'Hz')
a,b,c,d = ABCD(gamma, totalLen,Z)
s11, s12, s21, s22 = a2s(a,b,c,d,50)

In [14]: # plt.rcParams['axes.ymargin'] = 0
fig, ax = plt.subplots(2,2)
fig.set_figheight(7)
fig.set_figwidth(10)

_ = airLine.plot_s_db(ax=ax[0,0])

_ = ax[0,1].plot(airLine.f, 20*np.log10(s11), label="thy 11")
_ = ax[0,1].plot(airLine.f, 20*np.log10(s12), label="thy 12")
_ = ax[0,1].plot(airLine.f, 20*np.log10(s21), label="thy 21")
_ = ax[0,1].plot(airLine.f, 20*np.log10(s22), label="thy 22")
_ = ax[0,1].legend()

_ = airLine.plot_s_deg(ax=ax[1,0])

_ = ax[1,1].plot(airLine.f, np.rad2deg(np.angle(s11)), label="thy 11")
_ = ax[1,1].plot(airLine.f, np.rad2deg(np.angle(s12)), label="thy 12")
_ = ax[1,1].plot(airLine.f, np.rad2deg(np.angle(s21)), label="thy 21")
_ = ax[1,1].plot(airLine.f, np.rad2deg(np.angle(s22)), label="thy 22")
_ = ax[1,1].legend()
# if doSave:
#     fig.savefig('short-s-param.pdf')
```

```
//anaconda/lib/python2.7/site-packages/numpy/core/numeric.py:462:
ComplexWarning: Casting complex values to real discards the imaginary part
return array(a, dtype, copy=False, order=order)
```

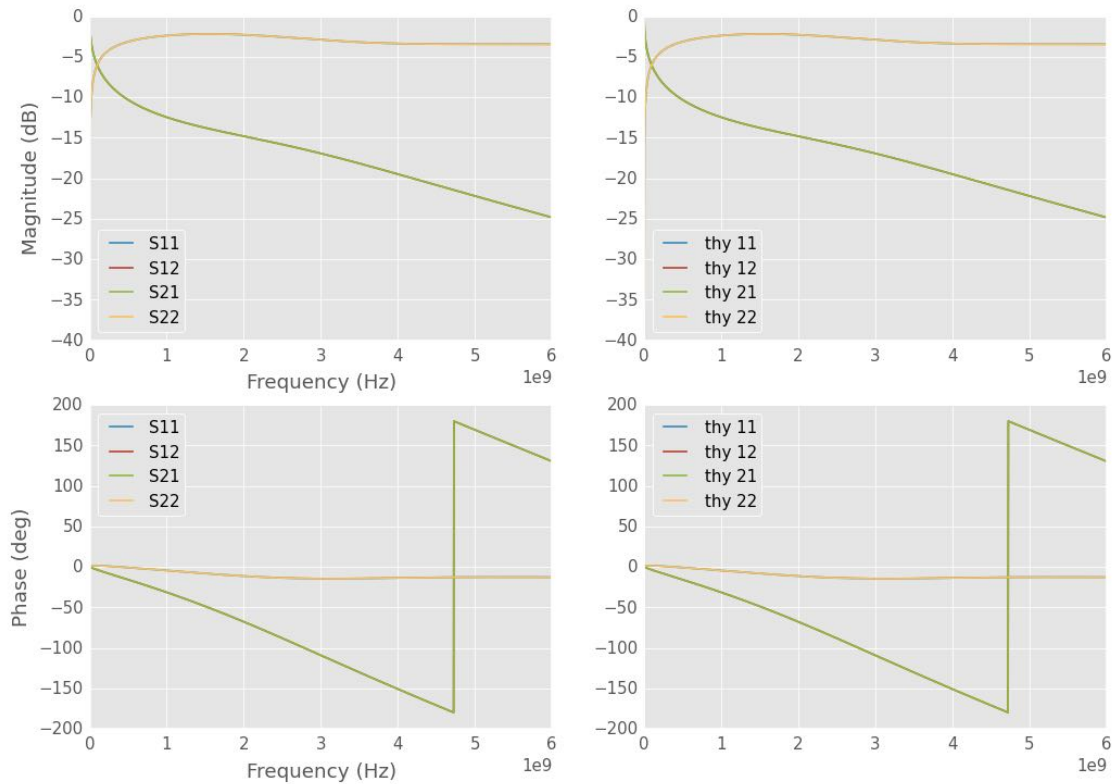


Figure R.9: notebook figure

R.8.2 Cascaded Line

Scikit-RF

```
In [15]: freq = rawSample.f
diam = 0.122
radius = diam/2
cntr2cntr = 0.25
sigma = 1/(7.2e-7)
R, L, G, C = twoWireParameters(freq = freq, a=radius, D=cntr2cntr,
                                sigma_c=sigma, unitsScale=0.0254)

rRad = 30*(2*pi*freq**2*constants.epsilon_0*constants.mu_0)*cntr2cntr**2
R=R+rRad

gamma = np.sqrt((R+1j*2*pi*freq * L)*(G+1j*2*pi*freq*C))
rfFreq = rf.Frequency(freq[0], freq[-1], freq.shape[0], 'Hz')
airLine = rf.media.DistributedCircuit(rfFreq,C, L, R, G).delay_short(sampleDist)
```



```

#####
#Cascade
#####

R, L, G, C = twoWireParameters(freq, radius, cntr2cntr, sigma, eps_r=1,
                                tanDelta=0, unitsScale=0.0254)

R += rRad
Z = np.sqrt((R+1j*2*pi*freq * L)/(G+1j*2*pi*freq*C))
Z_norm = Z
sect1 = rf.media.DistributedCircuit(rfFreq, C, L, R, G).line(lengths[0])
sect1.renormalize(Z_norm) # added 10/31/2015

#foam and short section
sect3 = rf.media.DistributedCircuit(rfFreq, C, L, R, G).delay_short(lengths[-1])
sect3.renormalize(Z_norm)

#sample section
R, L, G, C = twoWireParameters(freq, radius, cntr2cntr, sigma,
                                eps_r=layerEps_r[1], tanDelta=tanDelta,
                                unitsScale=0.0254)

R += rRad
sect2 = rf.media.DistributedCircuit(rfFreq, C, L, R, G).line(lengths[1])
sect2.renormalize(Z_norm)

totalLine = sect1**sect2**sect3

#
# De-embed
#
shorts = [short1, short2, short3]
balun = find1PortTransition(1j*gamma, shortDistances, shorts)
sample = deembed(balun, rawSample)

#airLine.renormalize(50)
#totalLine.renormalize(50)
print sample
print airLine
print totalLine

#
# Plotting
#
# sample.plot_s_db(show_legend=False)
# airLine.plot_s_db(show_legend=False)
# totalLine.plot_s_db(show_legend=False)
# #rawSample.plot_s_db(show_legend=False)
# plt.figure()
# sample.plot_s_deg(show_legend=False)
# airLine.plot_s_deg(show_legend=False)
# totalLine.plot_s_deg(show_legend=False)

```

```

fig, ax = plt.subplots()
_ = sample.plot_s_db(ax=ax, label='De-embedded')
_ = airLine.plot_s_db(ax=ax, label='Air line')
_ = totalLine.plot_s_db(ax=ax, label='Theory')

fig, ax = plt.subplots()
_ = sample.plot_s_deg(ax=ax, label='De-embedded')
_ = airLine.plot_s_deg(ax=ax, label='Air line')
_ = totalLine.plot_s_deg(ax=ax, label='Theory')

1-Port Network: 'Transition S11', 30000-60000000000 GHz, 1601 pts, z0=[ 50.+0.j]
1-Port Network: '', 30000-60000000000 Hz, 1601 pts, z0=[ 2806.49894742-2801.86123236j]
1-Port Network: '', 30000-60000000000 Hz, 1601 pts, z0=[ 2806.49894742-2801.86123236j]

```

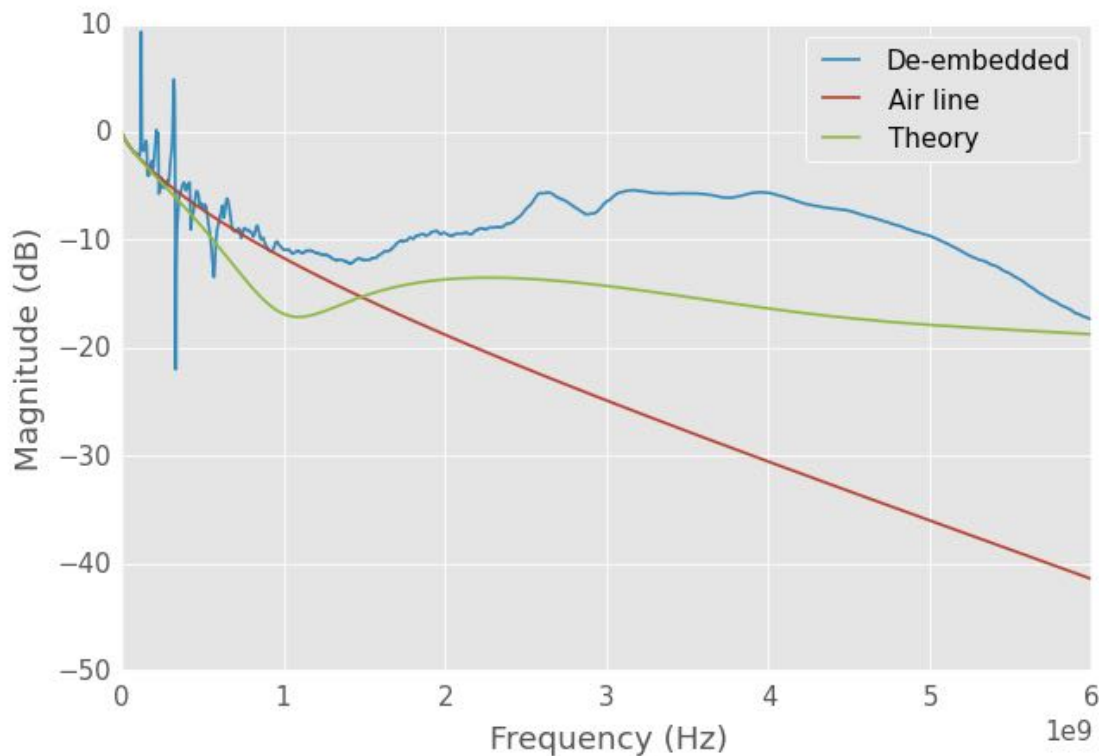


Figure R.10: notebook figure

Manual

```

In [16]: R, L, G, C = twoWireParameters(freq, radius, cntr2cntr, sigma, eps_r=1,
                                         tanDelta=0, unitsScale=0.0254)

R += rRad
gamma = np.sqrt((R+1j*2*pi*freq * L)*(G+1j*2*pi*freq*C))
Z = np.sqrt((R+1j*2*pi*freq * L)/(G+1j*2*pi*freq*C))

```

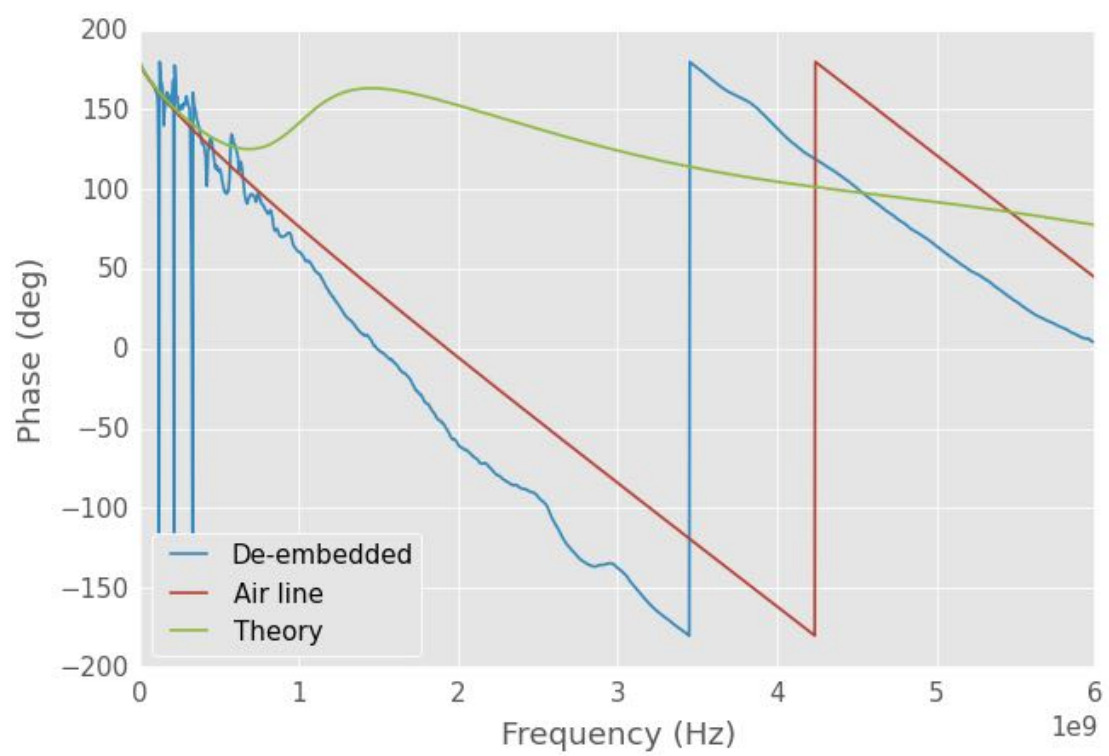


Figure R.11: notebook figure

```

t1a, t1b, t1c, t1d = ABCD(gamma, lengths[0], Z)
t1 = np.array([[t1a, t1b], [t1c, t1d]])

#foam no. 2
t3a, t3b, t3c, t3d = ABCD(gamma, lengths[2], Z)
t3 = np.array([[t3a, t3b], [t3c, t3d]])

#sample section
R, L, G, C = twoWireParameters(freq, radius, cntr2cntr, sigma,
                                eps_r=layerEps_r[1], tanDelta=tanDelta,
                                unitsScale=0.0254)

R += rRad
gamma = np.sqrt((R+1j*2*pi*freq * L)*(G+1j*2*pi*freq*C))
Z = np.sqrt((R+1j*2*pi*freq * L)/(G+1j*2*pi*freq*C))
t2a, t2b, t2c, t2d = ABCD(gamma, lengths[2], Z)
t2 = np.array([[t2a, t2b], [t2c, t2d]])

t = t1*t2*t3
s11, s12, s21, s22 = a2s(t[0,0], t[0,1], t[1,0], t[1,1], 50)

In [17]: for i in [t1, t2, t3]:
        s11, s12, s21, s22 = a2s(i[0,0], i[0,1], i[1,0], i[1,1], 50)

        fig, ax = plt.subplots()
        _ = ax.plot(airLine.f, 20*np.log10(s11), label="thy 11")
        _ = ax.plot(airLine.f, 20*np.log10(s12), label="thy 12")
        _ = ax.plot(airLine.f, 20*np.log10(s21), label="thy 21")
        _ = ax.plot(airLine.f, 20*np.log10(s22), label="thy 22")
        _ = ax.legend()

        fig, ax = plt.subplots()
        _ = ax.plot(airLine.f, np.rad2deg(np.angle(s11)), label="thy 11")
        _ = ax.plot(airLine.f, np.rad2deg(np.angle(s12)), label="thy 12")
        _ = ax.plot(airLine.f, np.rad2deg(np.angle(s21)), label="thy 21")
        _ = ax.plot(airLine.f, np.rad2deg(np.angle(s22)), label="thy 22")
        _ = ax.legend()

In [18]: # plt.rcParams['axes.ymargin'] = 0
fig, ax = plt.subplots(2,2)
fig.set_figheight(7)
fig.set_figwidth(10)

# _ = airLine.plot_s_db(ax=ax[0,0])

_ = ax[0,1].plot(airLine.f, 20*np.log10(s11), label="thy 11")
_ = ax[0,1].plot(airLine.f, 20*np.log10(s12), label="thy 12")
_ = ax[0,1].plot(airLine.f, 20*np.log10(s21), label="thy 21")
_ = ax[0,1].plot(airLine.f, 20*np.log10(s22), label="thy 22")
_ = ax[0,1].legend()

```

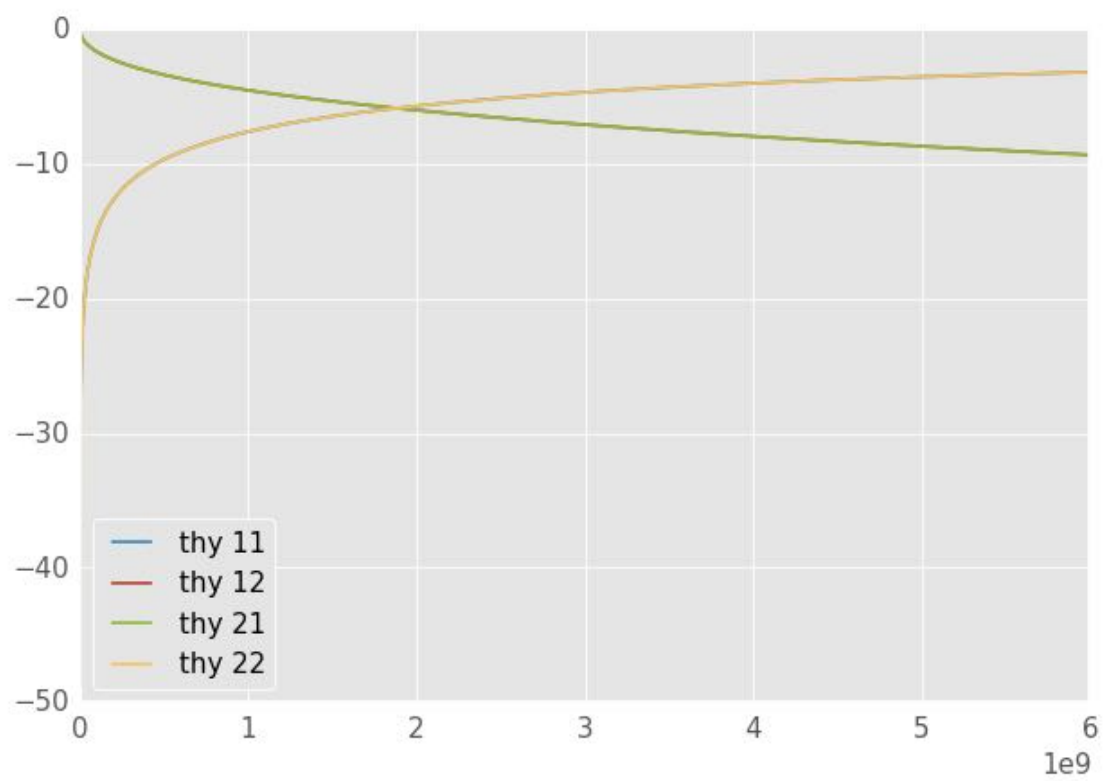


Figure R .12: notebook figure

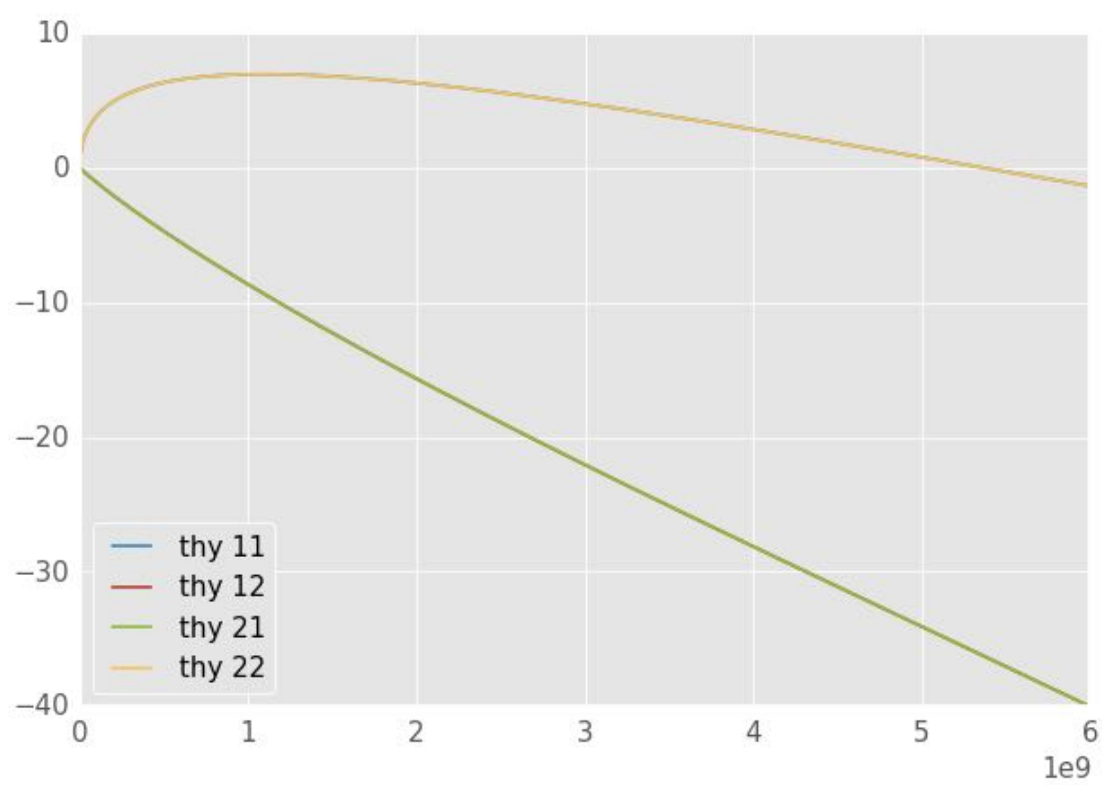


Figure R .13: notebook figure

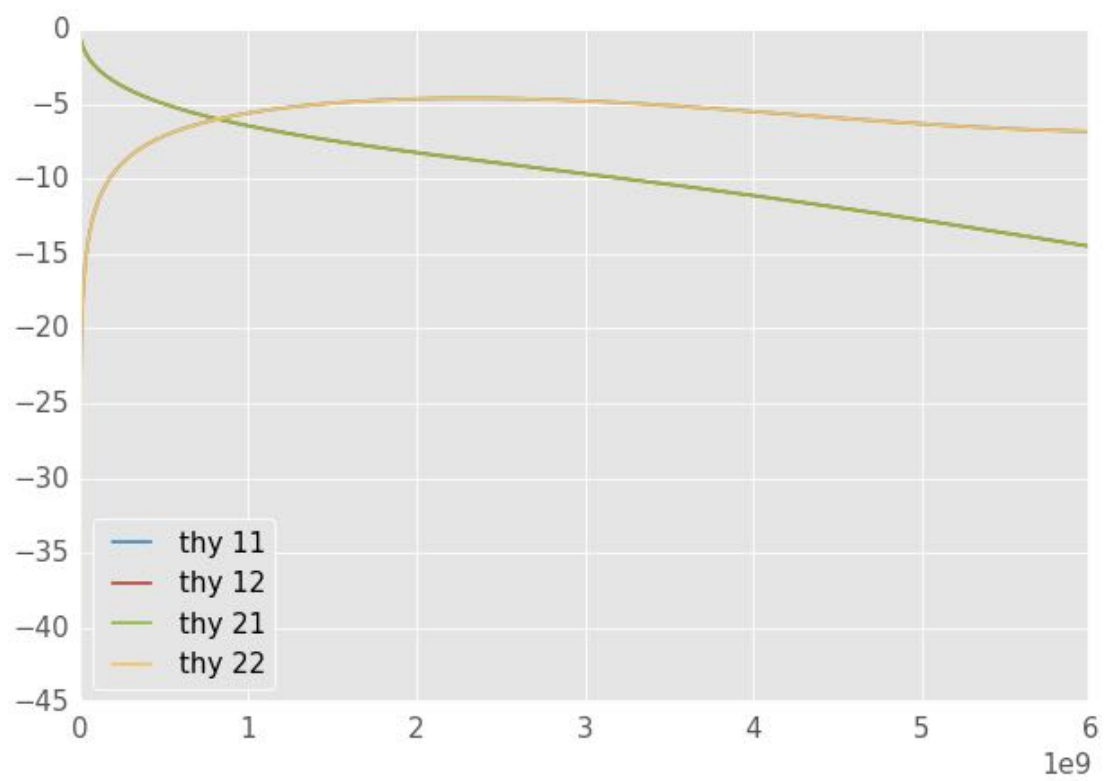


Figure R .14: notebook figure

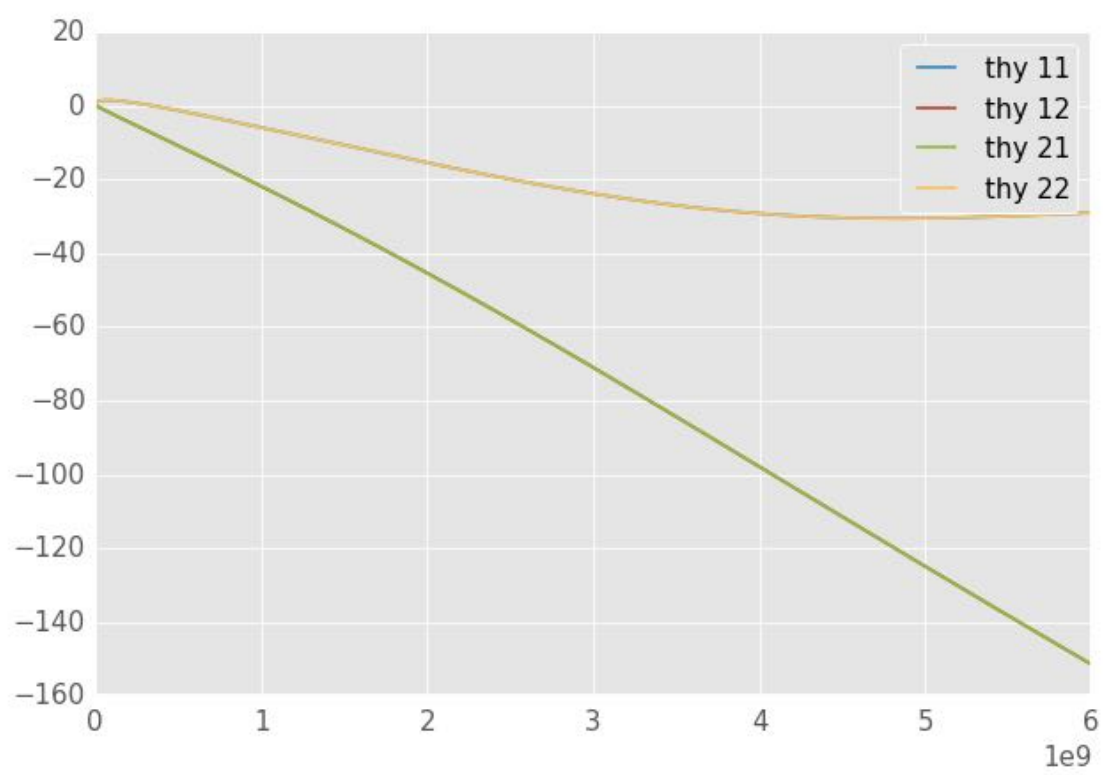


Figure R .15: notebook figure

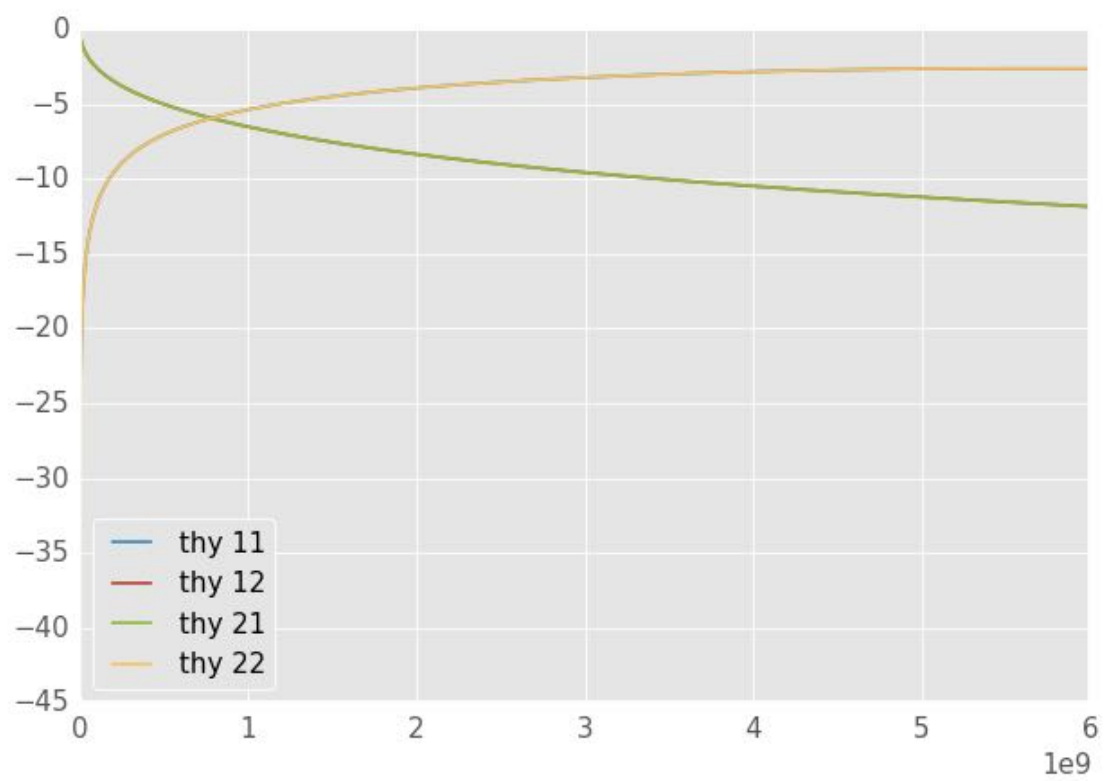


Figure R .16: notebook figure

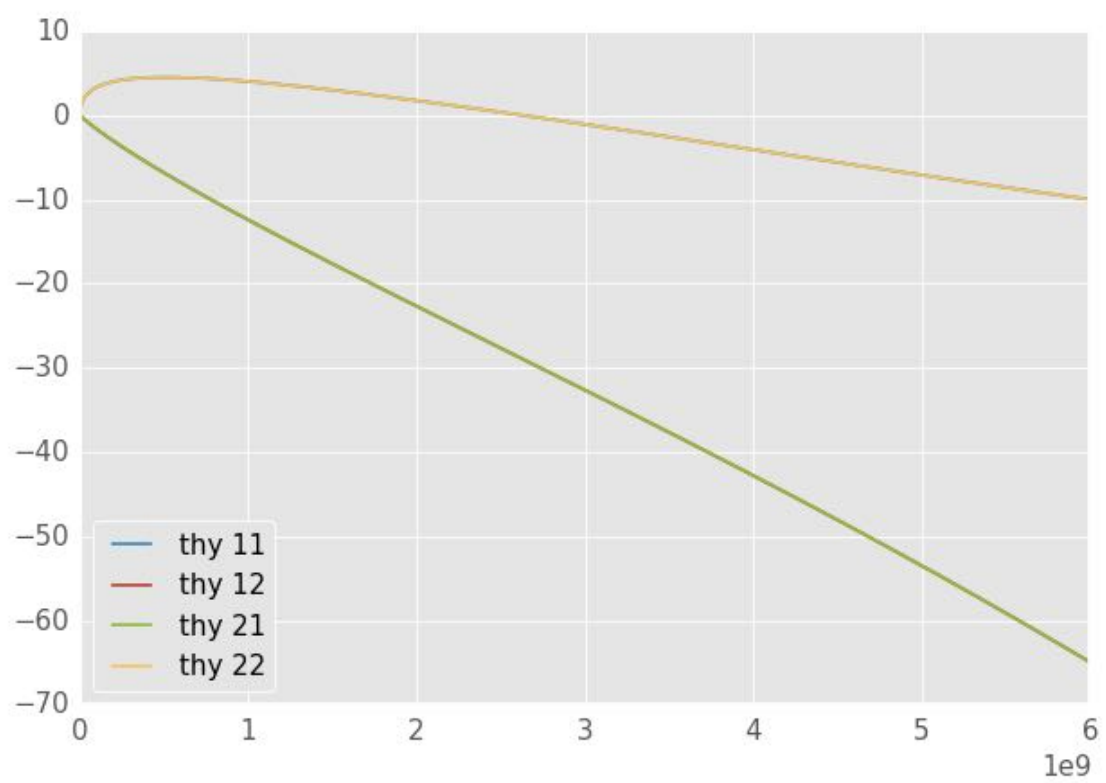


Figure R .17: notebook figure

```

# _= airLine.plot_s_deg(ax=ax[1,0])

_= ax[1,1].plot(airLine.f, np.rad2deg(np.angle(s11)), label="thy 11")
_= ax[1,1].plot(airLine.f, np.rad2deg(np.angle(s12)), label="thy 12")
_= ax[1,1].plot(airLine.f, np.rad2deg(np.angle(s21)), label="thy 21")
_= ax[1,1].plot(airLine.f, np.rad2deg(np.angle(s22)), label="thy 22")
_= ax[1,1].legend()

# if doSave:
#     fig.savefig('short-s-param.pdf')

```

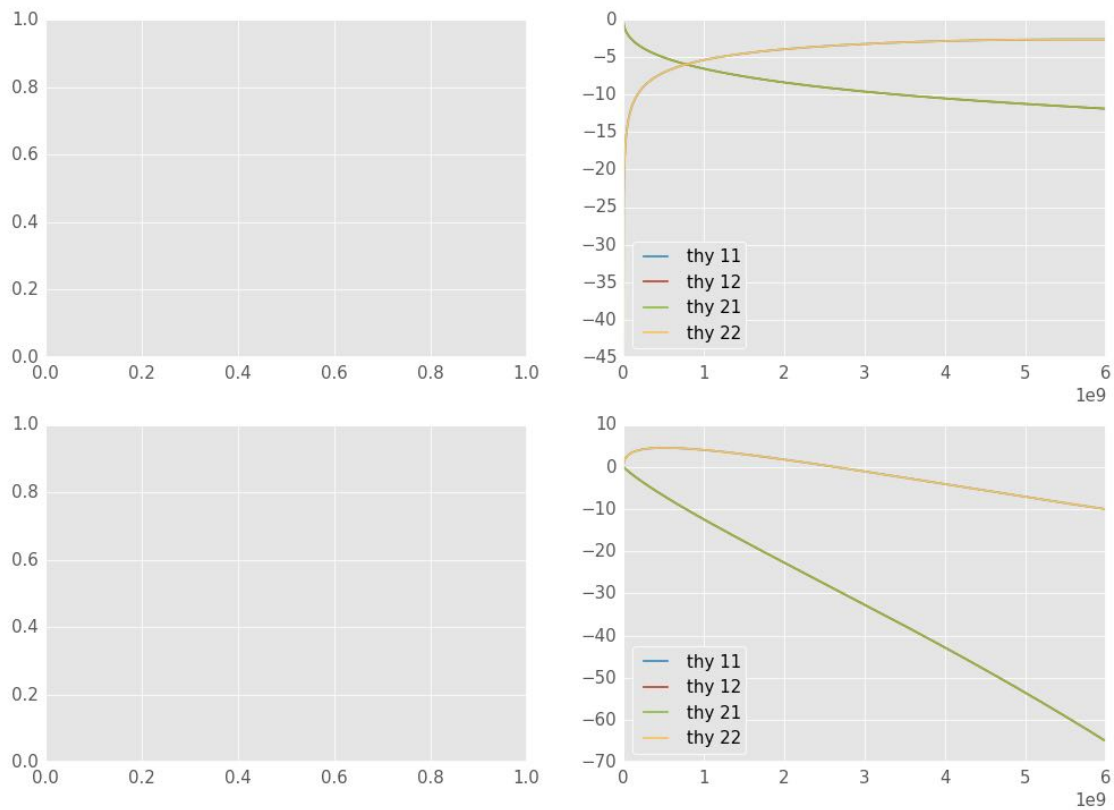


Figure R.18: notebook figure

In []:

Appendix S

IPython notebook: T-lineCalibration-With-Water-diss

S.1 Water Calibration and De-Embedding

This notebook is a first attempt at calibrating using deionized water. It started as a copy of T-lineCalibration. Original and first commit are in commit 83bb869eac88fde4aa8976c2033b607d76d598fe.

The new notebook was created so that I wouldn't mess up functions that were used for the solids.

S.2 Basic Imports

```
In [1]: # Import basic modules
        # make sure that division is done as expected
        from __future__ import division

        # plotting setup
        %matplotlib inline
        import matplotlib.pyplot as plt
        plt.style.use('gray_back')

        # get the viridis colormap
        # https://bids.github.io/colormap
        # it will be available as cmaps.viridis
        # import colormaps as cmaps

        # for 3d graphs
        # from mpl_toolkits.mplot3d import axes3d
        # for legends of combined fig types
        # import matplotlib.lines as mlines

        # numerical functions
```

```

import numpy as np

# need some constants
from scipy import constants
from numpy import pi

# RF tools!
import skrf as rf

# version information
# %install_ext http://raw.github.com/jrjohansson/
# version_information/master/version_information.py
# %load_ext version_information
# %reload_ext version_information

# %version_information numpy, scipy, matplotlib

```

S.3 Pre-flight

```

In [20]: import os
         plt.rcParams['axes.ymargin'] = 0

         doSave = True
         # doSave = False

In [3]: # a 79-char ruler:
         #234567891123456789212345678931234567894123456789512345678961234567897123456789
         # a 72-char ruler:
         #23456789112345678921234567893123456789412345678951234567896123456789712

def twoWireParameters(freq, a, D, sigma_c=np.inf, mu_c=1,
                      eps_r = 1, tanDelta = 0, mu_r=1,
                      unitsScale=1):
    """
    Return R, L, G, C for a two-wire line

    Calculates and returns the resistance, impedance, conductance,
    and capacitance for a two-wire transmission line. Geometric and
    electrical properties are given for the wire and the media in
    which the wires are located.

    Parameters
    -----
    freq : scalar
        Frequency at which the parameters should be calculated
    a : scalar
        Wire radius
    D : scalar
        center-to-center distance of the wires
    sigma_c : scalar

```

```

        Conductivity of the wires
    mu_c : scalar, optional
        Relative permeability of the wires. Default is 1.
    eps_r : scalar, optional
        Relative permittivity of the environment. Used as
        epsilon = eps_r*eps_0*(1-j*tanDelta). Default is 1.
    tanDelta : scalar, optional
        Loss tangent of the environment. Used as
        epsilon = eps_r*eps_0*(1-j*tanDelta). Default is 0.
    mu_r : scalar, optional
        Relative permeability of the environment. Default is 1
    unitsScale : scalar, optional if using meters
        Scaling factor for units. For mm, use 1e-3, for in use
        0.0254.

    Returns
    -----
    R : scalar
        Resistance of the two-wire transmission line
    L : scalar
        Impedance of the two-wire transmission line
    G : scalar
        Conductance of the two-wire transmission line
    C : scalar
        Capacitance of the two-wire transmission line
    """
    #from __future__ import division
    import scipy.constants as const

    # Scale dimensions
    a = a*unitsScale
    D = D*unitsScale
    eps_sgl = constants.epsilon_0*eps_r
    eps_dbl = constants.epsilon_0*eps_r*tanDelta

    omega=2*pi*freq
    #delta_cond = 1/np.sqrt(constants.pi*freq*sigma_c)

    invCosh = np.arccosh(D/(2*a))

    #R = 1/(constants.pi*a*sigma_c*delta_cond)
    R = np.sqrt(omega*mu_c/
        (2*(constants.pi*a)**2*sigma_c
        *(1-(2*a/D)**2)))
    G = (constants.pi*omega*eps_dbl)/invCosh
    L = constants.mu_0/pi*invCosh
    C = pi*eps_sgl/invCosh
    return R, L, G, C

def find1PortTransitionWater(measured, theory):
#23456789112345678921234567893123456789412345678951234567896123456789712

```

```

"""
Calculated *SOME* of the S-parameters for a transition. READ DETAILS

Calculate S11, S22, and S12*S21 for a transition. This is used
when you want to de-embed a sample from the transition and the
sample.

This requires scikit-rf version with source after April 4, 2014.
Probably will be version 0.15. You might need to get this from
github (https://github.com/scikit-rf/scikit-rf).

Parameters
-----
measured : list of 1-port skrf Network objects
    A list of skrf.networks for the three measured standards used
    to de-embed the sample
theory : list of 1-port skrf Network objects
    A list of skrf.networks for the theoretical three standards
    used to de-embed the sample. S11 is used as the reflection
    coefficient.

Returns
-----
ntwkS11, ntwkS22, ntwkS12S21 : skrf Network object
    1-port networks for the calculated S-parameters to be used for
    de-embedding a sample.

To-Do
-----
Should throw in some error checking to make sure that the three
shorts have the same network properties
"""

#g is 1/Gamma
g = [1/t.s[:,0,0] for t in theory]
sc = [m.s[:,0,0] for m in measured]
tempNtwk = measured[0].s11
freq = tempNtwk.f
z0 = tempNtwk.z0

K = (g[2]-g[0])/(g[1]-g[0])*(sc[0]-sc[1])/(sc[0]-sc[2])
s22 = (g[2]-g[1]*K)/(1-K)
s12s21 = (sc[0]-sc[1])/(g[1]-g[0])*(g[0]-s22)*(g[1]-s22)
s11 = sc[0]-s12s21/(g[0]-s22)

ntwkS11 = rf.Network(name="Transition S11", f = freq, z0 = z0, s=s11)
ntwkS22 = rf.Network(name="Transition S22", f = freq, z0 = z0, s=s22)
ntwkS12S21 = rf.Network(name="Transition S12S21", f = freq, z0=z0, s=s12s21)
return ntwkS11, ntwkS22, ntwkS12S21

def deembed(trans, raw):
#23456789112345678921234567893123456789412345678951234567896123456789712

```

```

"""
De-embed a 1-port sample.

De-embed a 1-port sample from a transition that has been
characterized using a three short method.

Parameters
-----
trans : tuple of skrf.network.Network
    A tuple of scikit-rf 1-Port Networks that correspond to the
    characterized S-parameters of the transition. Order should be
    S_11, S_22, S_12*S_21.
raw : skrf.network.Network
    The raw data measurement that includes the sample and the
    transition. The sample will be de-embedded from this data

Returns
-----
sample : skrf Network object
    The de-embedded sample
"""
b = [x.s[:,0,0] for x in trans]
#print b[0]
inv = b[1]+b[2]/(raw.s[:,0,0]-b[0])
sample = trans[0]
sample.s = 1/inv
return sample

def debye(f):
    """
    Calculate the complex permittivity of pure water using Debye equation

    Calculate the complex permittivity of pure water using the Debye equation

    .. math::
        \begin{aligned}
        |\epsilon| &= |\epsilon'| + j|\epsilon''| \\
        \epsilon' &= \epsilon_{\infty} + \frac{\epsilon_s - \epsilon_{\infty}}{1 + \omega^2 \tau^2} \\
        \epsilon'' &= \frac{(\epsilon_s - \epsilon_{\infty}) \omega \tau}{1 + \omega^2 \tau^2}
        \end{aligned}

    At 25degC  $\epsilon_s=78.408$ ,  $\epsilon_{\infty}=5.2$  and  $\tau=8.27$  ps.

    Reference: CRC Handbook of Chemistry and Physics, 95th Ed., 2014-2015.

    Parameters
    -----
    f : array-like
        Frequency array

    Returns
    """

```



```

-----
eps : array-like
    Complex relative permittivity, epsilon
    """
omega = 2*pi*f

es = 78.408
einf = 5.2
tau = 8.27e-12

ep = einf + (es - einf)/(1+omega**2*tau**2)
edp = ((es-einf)*omega*tau)/(1+omega**2*tau**2)
eps = ep+1j*edp

return eps

def airWaterShort(water, short, paramAir, paramWater, rfFreq):
    """
    Returns 1-port of a air, water, short 2 wire t-line

    A 1-port network is created to simulate a short circuited two-wire
    transmission line submerged in water with an air gap between the
    balun and the water level.

    This actually ignores a small portion of the line (total-short). I
    did this becuae one can add this offset manually if needed. This
    keeps things simpler (from programming and uniformity perspective).

    If I want to de-embed and use the largest amount of water as my
    reference plane, I set water=0 and short=short_0-water_0 where
    _0 means the original values.

    The air section is created using the RLGC parameters supplied in
    paramAir. A line from skrf's distributed circuit media is created.
    The length of this line is

    .. math::
        length = water

    A delayed short is created using the RLGC parameters supplied in
    paramWater. The short is located at a distance of

    .. math::
        length = short-water

    The line and delayed short are then cascaded to create a single
    one-port network which is returned.

    Here's a cool picture because I figured out how to use VIM to make
    ASCII art (its in the amazing VIM manual: usr_25.txt Editing
    formatted text).

```

```

-----/
/
/
/-----+-----/ s /
/
/
/ air + liquid / h /
/ balun /
/ <-- total-short+water -->+<-- short-water --> / r /
/-----+-----/ t /
/
/
/-----/
/==== water ===/
/==== short =====/
/==== total =====/

Parameters
-----
water : number
    Distance measured to the surface of the water in meters (m)
short : number
    Distance measured to the short in meters (m)
paramAir : tuple
    A tuple as returned by twoWireParameters for the air line
paramWater : tuple
    A tuple as returned by twoWireParameters for the water
freq : skrf Frequency object

Returns
-----
ntwk : skrf Network object
"""
C, L, R, G = paramAir[3], paramAir[1], paramAir[0], paramAir[2]
line = rf.media.DistributedCircuit(rfFreq, C, L, R, G).line(water)
C, L, R, G = paramWater[3], paramWater[1], paramWater[0], paramWater[2]
short = rf.media.DistributedCircuit(rfFreq,C,L,R,G).delay_short(short-water)
ntwk = line**short
return ntwk

```

S.3.1 Debye Equation

$$\epsilon = \epsilon' + j\epsilon'' \epsilon' = \epsilon_{\infty} + \frac{\epsilon_s - \epsilon_{\infty}}{1 + \omega^2 \tau^2} \epsilon'' = \frac{(\epsilon_s - \epsilon_{\infty})\omega\tau}{1 + \omega^2 \tau^2}$$

At 25degC $\epsilon_s = 78.408$, $\epsilon_{\infty} = 5.2$ and $\tau = 8.27$ ps.

```

In [4]: freq = np.array([0,1e3,1e6,10e6,100e6,200e6,500e6,1e9,2e9,
                          3e9,4e9,5e9,10e9,20e9,30e9,40e9,50e9])
foo = debye(freq)
for x in foo:
    print x

```

```

(78.408+0j)
(78.408+3.80402988584e-06j)
(78.4079998023+0.00380402987556j)
(78.4079802335+0.0380402885873j)
(78.4060234055+0.380392717815j)
(78.4000942625+0.760723817672j)
(78.3586171384+1.90073192821j)
(78.2108674842+3.79378649739j)
(77.6257888874+7.52676935397j)
(76.6712213609+11.1413504822j)
(75.3763335831+14.5859944393j)
(73.7788529053+17.8174520536j)
(62.8438971946+29.9528887095j)
(40.3958596401+36.5769046903j)
(26.5431968048+33.271018948j)
(18.9607223632+28.6013545624j)
(14.6460610982+24.5417841774j)

```

This is close to matching 6-14 of CRC Handbook of Chemistry and Physics, 95th Ed., 2014-2015 but off after about the first decimal place.

S.4 Balun Testing

I connected the balun to the 8510 test cable with an apadter. I shorted the balun with a piece of wire across the two wire terminals. This gives me a short of just the balun. I also captured data in the same position/setup with the transmission lines shorted using the copper plate. Results are below

```

In [5]: dataDir = '../plexiglass-holder-data/Data/2014-08-15/'
        fig, ax = plt.subplots()
        rf.Network(dataDir+'balun-wire-short.s1p').plot_s_db(ax=ax, lw=2, label='Balun')
        rf.Network(dataDir+'balun-tline-short.s1p').plot_s_db(ax=ax, lw=2,
                                                                linestyle='-.', label='2WTL')

        ax.legend(loc='lower left')

        fig, ax = plt.subplots()
        rf.Network(dataDir+'balun-wire-short.s1p').plot_s_deg(ax=ax, lw=2, label='Balun')
        rf.Network(dataDir+'balun-tline-short.s1p').plot_s_deg(ax=ax, lw=2,
                                                                linestyle='-.', label='2WTL')

        ax.legend(loc='lower left')

```

```

Out[5]: <matplotlib.legend.Legend at 0x2b6ac317bb50>

```

S.5 Testing of airWaterShort Function

```

In [6]: generic = rf.Network('../plexiglass-holder-data/Data/2014-08-15/'
                             'beaker-mm-51-39.s1p')

```

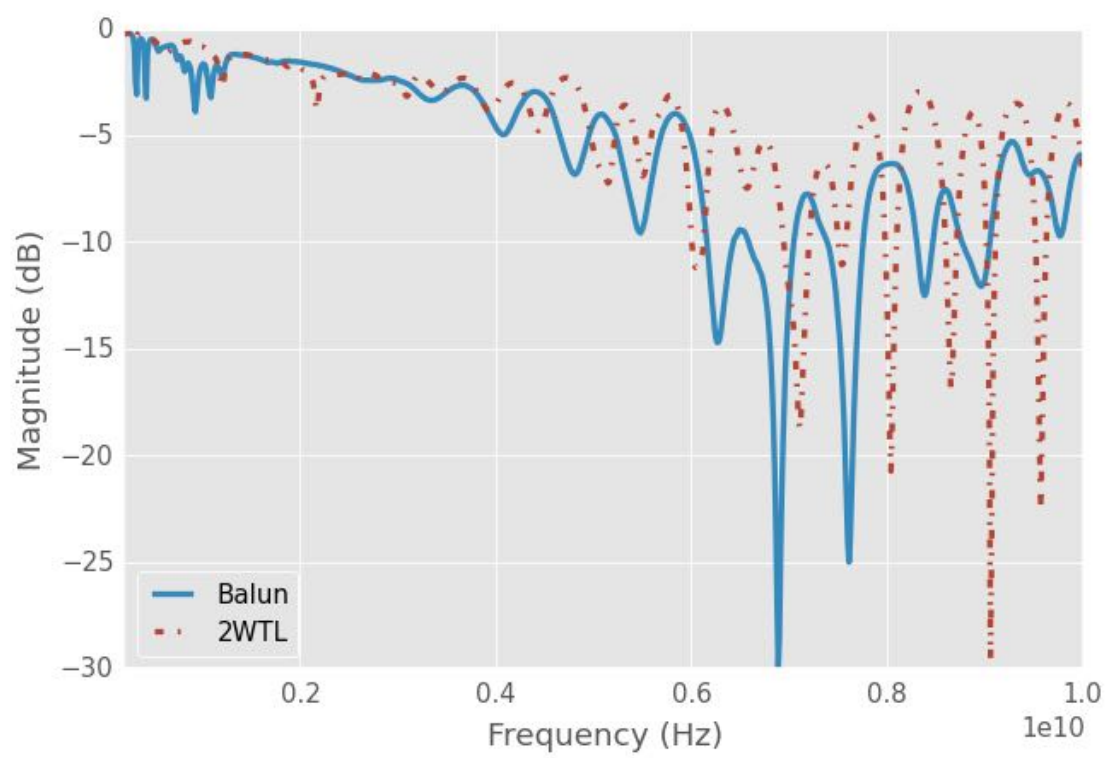


Figure S.1: notebook figure

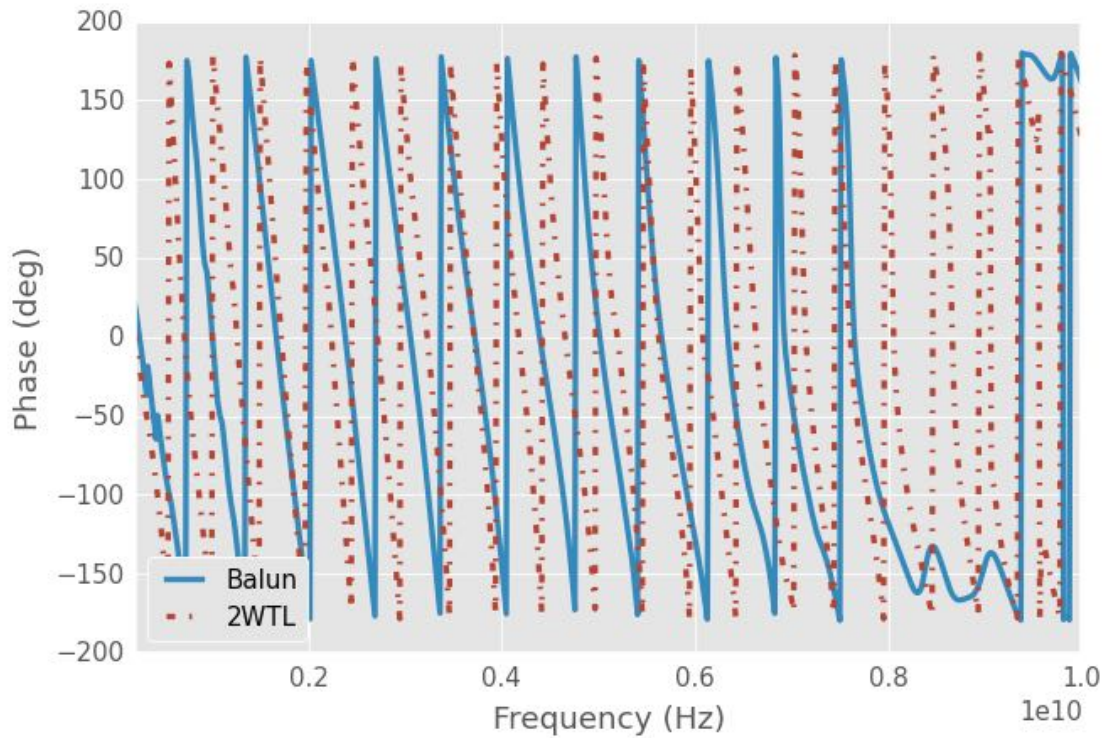


Figure S.2: notebook figure

```

shortDist = 72.38e-3

diam = 0.126
radius = diam/2
cntr2cntr = 0.25
sigma = 5.96e7
R, L, G, C = twoWireParameters(freq = generic.f, a=radius, D=cntr2cntr,
                                sigma_c=sigma, unitsScale=0.0254)
rRad = 30*(2*pi*generic.f**2*constants.epsilon_0*constants.mu_0)*cntr2cntr**2
R += rRad
paramAir = tuple([R, L, G, C])

waterEps = debye(generic.f)
tanD = waterEps.imag/waterEps.real
R, L, G, C = twoWireParameters(freq = generic.f, a=radius, D=cntr2cntr,
                                sigma_c=sigma, eps_r=waterEps.real,
                                tanDelta=tanD, unitsScale=0.0254)
rRad = 30*(2*pi*generic.f**2*waterEps.real*constants.mu_0)*cntr2cntr**2
R += rRad
paramWater = tuple([R, L, G, C])

theory = airWaterShort(21.40e-3,shortDist,paramAir,paramWater,generic.frequency)
theory.plot_s_db()

```

```
plt.figure()
theory.plot_s_deg()
```

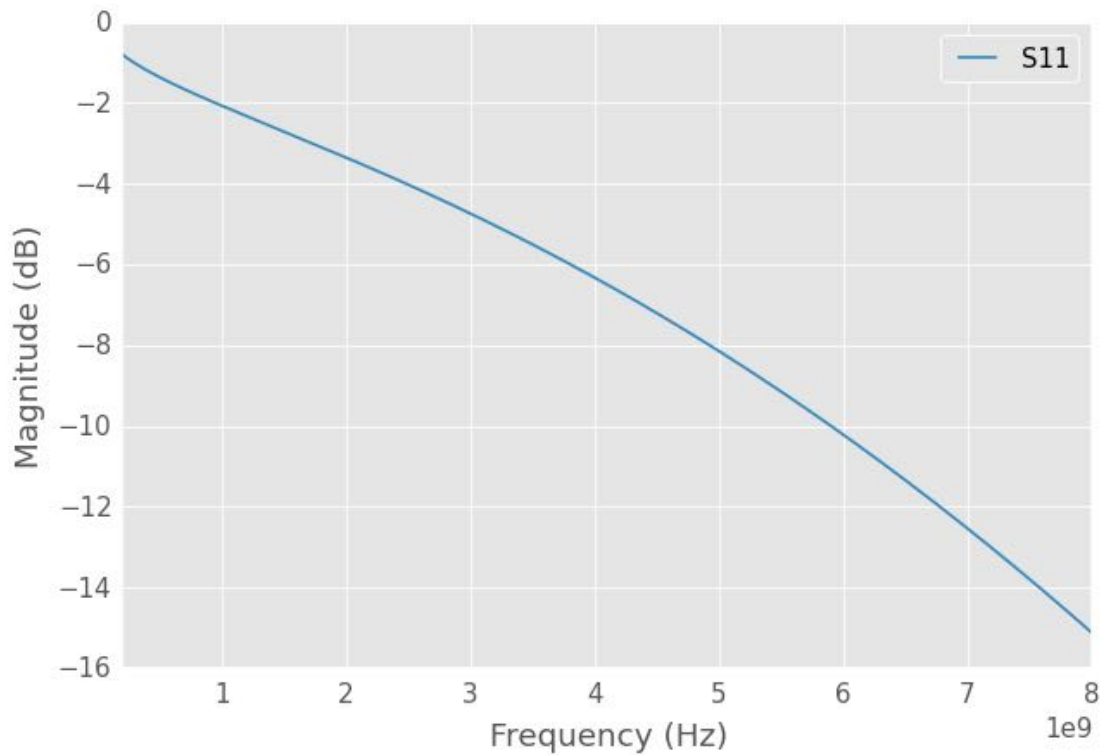


Figure S .3: notebook figure

Seems reasonable. Let's try some more testing

```
In [7]: generic = rf.Network('../plexiglass-holder-data/Data/2014-08-15/'
                             'beaker-mm-51-39.s1p')

shortDist = 21.4e-3

diam = 0.126
radius = diam/2
cntr2cntr = 0.25
sigma = 5.96e7
R, L, G, C = twoWireParameters(freq = generic.f, a=radius, D=cntr2cntr,
                               sigma_c=sigma, unitsScale=0.0254)
rRad = 30*(2*pi*generic.f**2*constants.epsilon_0*constants.mu_0)*cntr2cntr**2
R += rRad
paramAir = tuple([R, L, G, C])

airCompare=rf.media.DistributedCircuit(generic.frequency,C,L,R,G).line(21.4e-3)

waterEps = debye(generic.f)
```

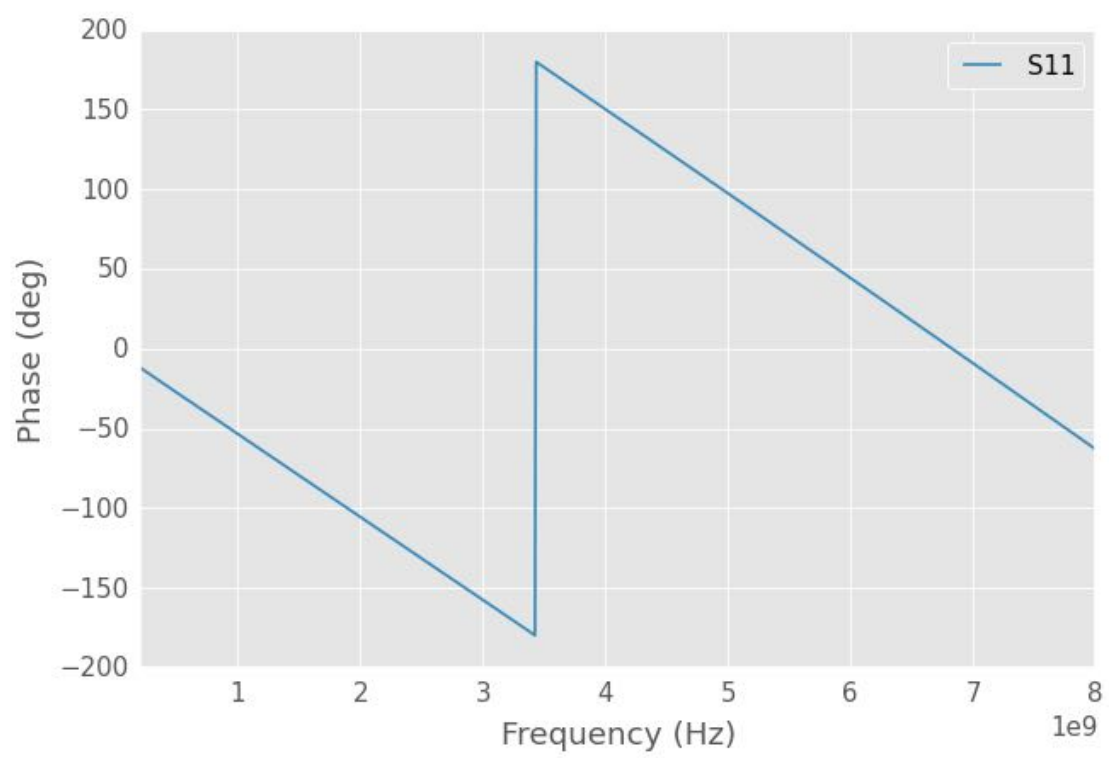


Figure S .4: notebook figure

```

tanD = waterEps.imag/waterEps.real
R, L, G, C = twoWireParameters(freq = generic.f, a=radius, D=cntr2cntr,
                                sigma_c=sigma,eps_r=waterEps.real,
                                tanDelta=tanD, unitsScale=0.0254)

rRad = 30*(2*pi*generic.f**2*waterEps.real*constants.mu_0)*cntr2cntr**2
R += rRad
paramWater = tuple([R, L, G, C])

theory = airWaterShort(21.40e-3,shortDist,paramAir,paramWater,generic.frequency)
theory.plot_s_db()
#airCompare.plot_s_db(0)
plt.figure()
theory.plot_s_deg()
#airCompare.plot_s_deg(0)

```

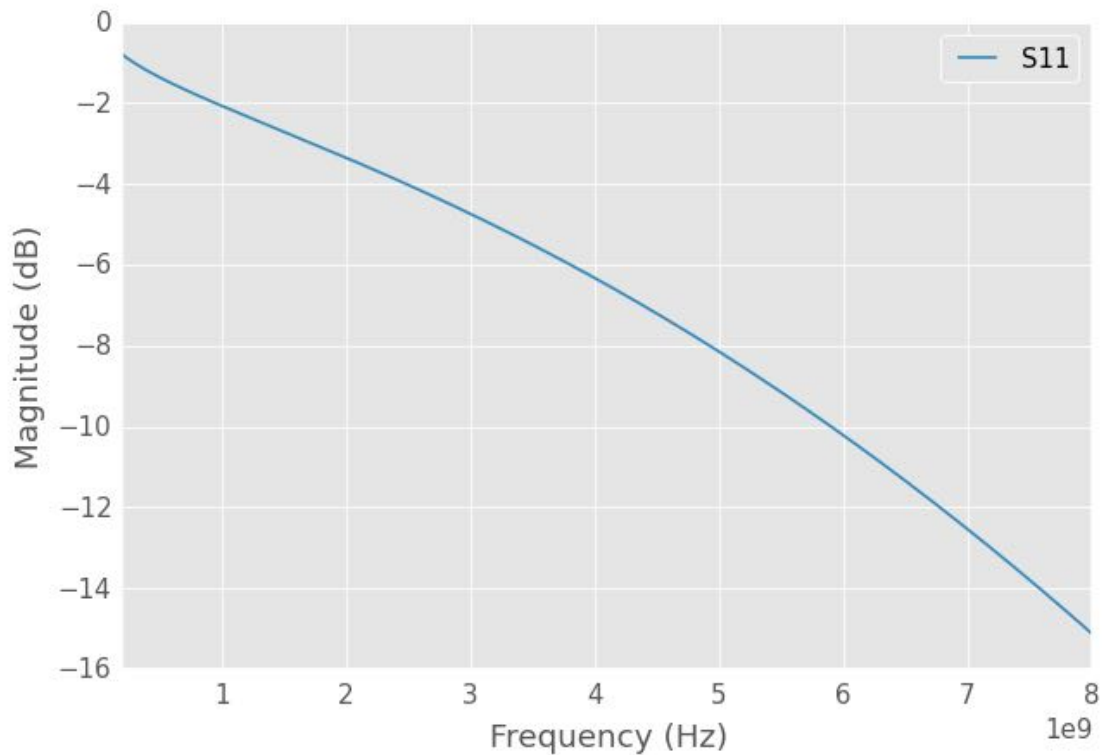


Figure S .5: notebook figure

S.6 Water Calibration

Steps:

- Calc water permittivity

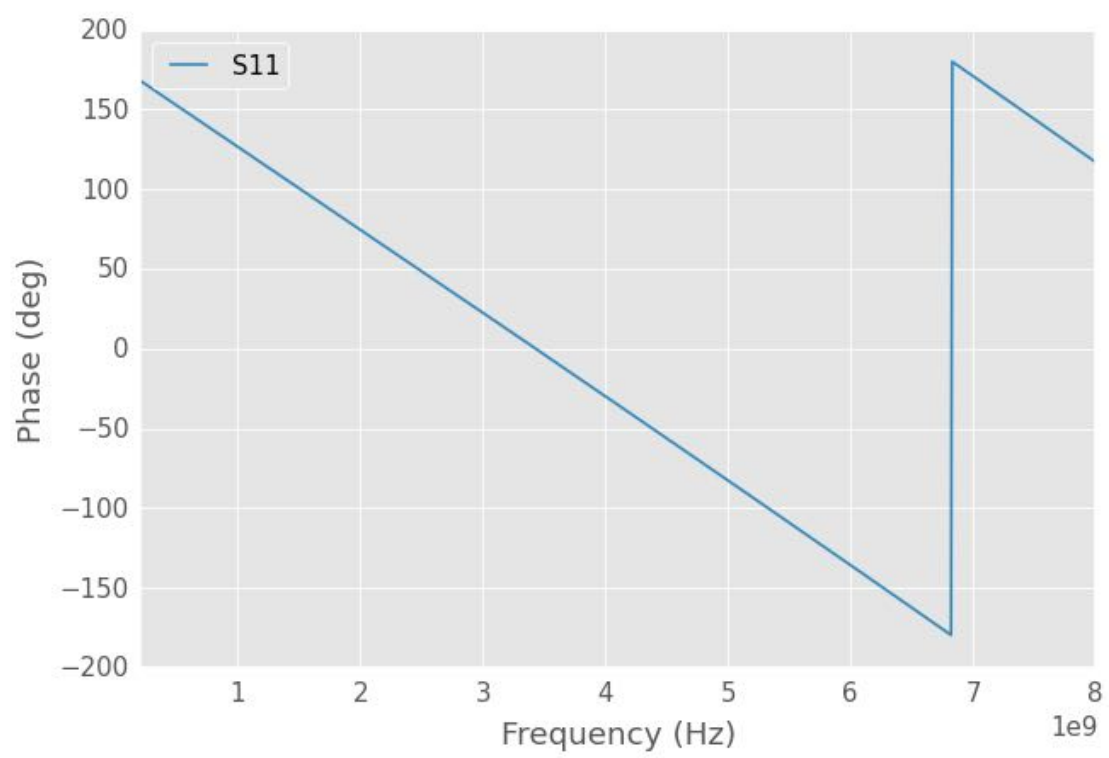


Figure S .6: notebook figure

- Create media of different sections
 - air
 - water
 - short
- Calc s11=reflection coefficient
- De-embed like normal

```
In [8]: rawSample = rf.Network('../plexiglass-holder-data/Data/2014-08-15/'
                                'beaker-mm-54-31.sip')

standards = [rf.Network('../plexiglass-holder-data/Data/2014-08-15/'
                          'beaker-mm-51-39.sip'),
              rf.Network('../plexiglass-holder-data/Data/2014-08-15/'
                          'beaker-mm-57-43.sip'),
              rf.Network('../plexiglass-holder-data/Data/2014-08-15/'
                          'beaker-mm-60-02.sip')]

offset = -1*50e-3

sampleDist = offset+54.31e-3
stdDist = offset+np.array([51.39,57.43,60.02])*1e-3

shortDist = offset+72.38e-3

freq = rawSample.f
rfFreq = rawSample.frequency
diam = 0.126
radius = diam/2
cntr2cntr = 0.25
sigma = 5.96e7
R, L, G, C = twoWireParameters(freq = freq, a=radius, D=cntr2cntr,
                                sigma_c=sigma, unitsScale=0.0254)
rRad = 30*(2*pi*freq**2*constants.epsilon_0*constants.mu_0)*cntr2cntr**2
R += rRad
paramAir = tuple([R, L, G, C])

waterEps = debye(freq)
tanD = waterEps.imag/waterEps.real
R, L, G, C = twoWireParameters(freq = freq, a=radius, D=cntr2cntr,sigma_c=sigma,
                                eps_r=waterEps.real, tanDelta=tanD,
                                unitsScale=0.0254)
rRad = 30*(2*pi*freq**2*waterEps.real*constants.mu_0)*cntr2cntr**2
R += rRad
paramWater = tuple([R, L, G, C])

theory1 = airWaterShort(stdDist[0], shortDist, paramAir, paramWater,rfFreq)
theory2 = airWaterShort(stdDist[1], shortDist, paramAir, paramWater,rfFreq)
theory3 = airWaterShort(stdDist[2], shortDist, paramAir, paramWater,rfFreq)
```

```

theory = airWaterShort(sampleDist, shortDist, paramAir, paramWater,rfFreq)

balun = find1PortTransitionWater(standards, [theory1, theory2, theory3])
sample = deembed(balun, rawSample)

fig, ax = plt.subplots()
sample.plot_s_db(label="Cald",show_legend=False)
theory.plot_s_db(label="Theory",show_legend=False)
rawSample.plot_s_db(label="Raw",show_legend=True)
ax.set_title("Deionized: 54.31c51.39-57.43-60.02")
# if doSave:
#     fig.savefig("deionized-54.31c51.39-57.43-60.02-mag.png")
fig, ax = plt.subplots()
sample.plot_s_deg(label="Cald",show_legend=False)
theory.plot_s_deg(label="Theory",show_legend=True)
ax.set_title("Deionized: 54.31c51.39-57.43-60.02")
# if doSave:
#     fig.savefig("deionized-54.31c51.39-57.43-60.02-phase.png")

```

Out[8]: <matplotlib.text.Text at 0x2b6ac3162790>

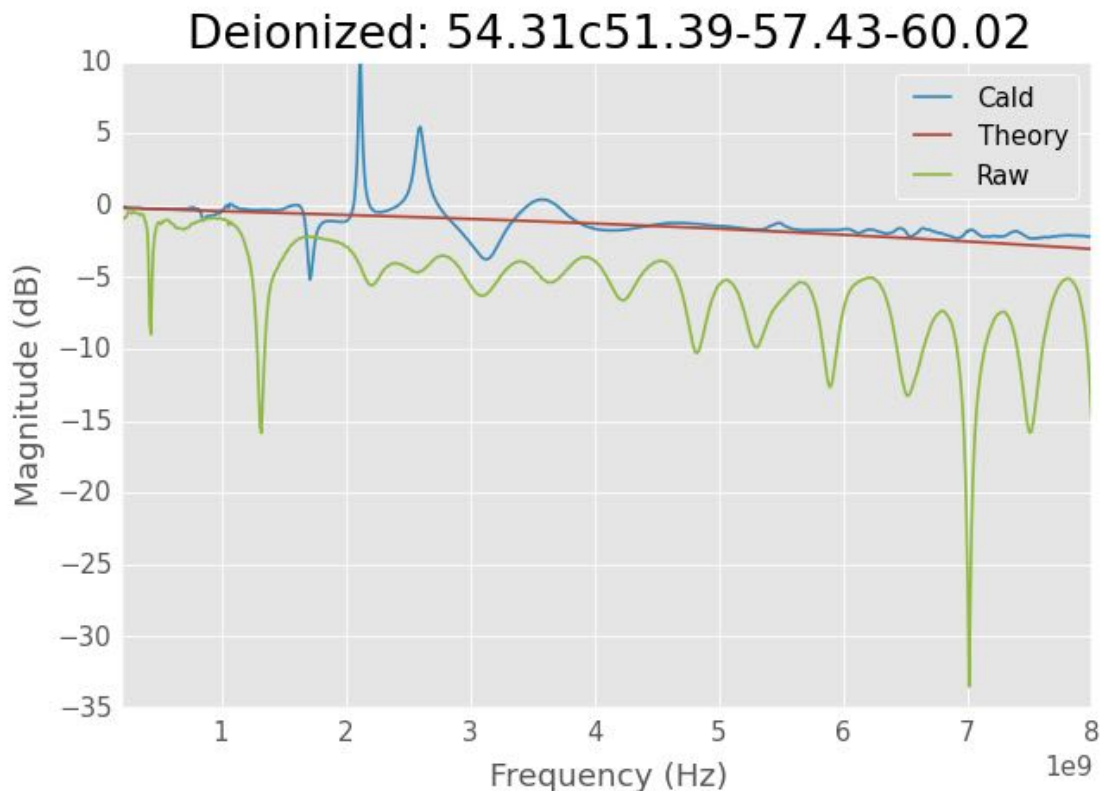


Figure S.7: notebook figure

```

In [9]: # composite figure
fig, ax = plt.subplots(2,1)

```

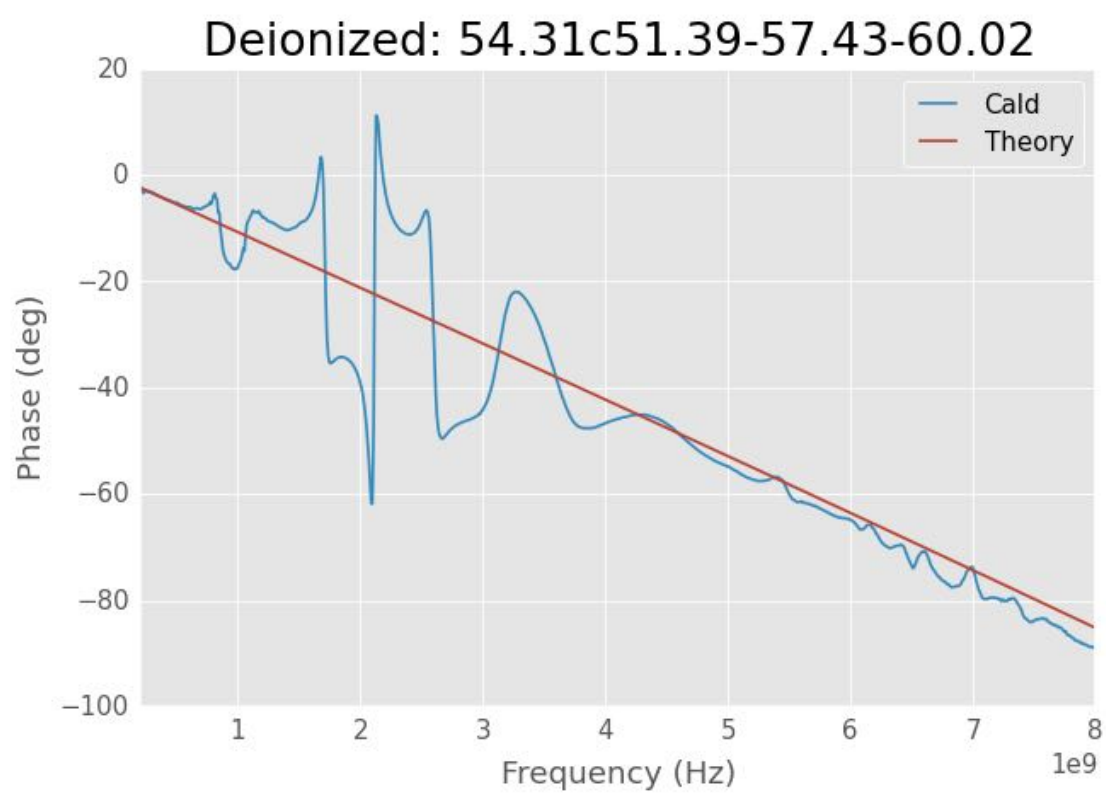


Figure S.8: notebook figure

```

fig.set_figheight(7)

rawSample.plot_s_db(ax=ax[0], label="Original", ls=":", show_legend=True)
sample.plot_s_db(ax=ax[0], label="Calibrated", show_legend=True)
theory.plot_s_db(ax=ax[0], label="Theory", ls="--", show_legend=True)
# ax.set_title("Deionized: 54.31c51.39-57.43-60.02")
ax[0].annotate('Cal dist:\n51.39mm\n57.34mm\n60.02mm',
               xy=(2.5e9,-33))
ax[0].annotate('Sample\n54.31mm\n\n', xy=(4e9,-33))

rawSample.plot_s_deg(ax=ax[1], label="Original", ls=":", show_legend=False)
sample.plot_s_deg(ax=ax[1], label="Cald", show_legend=False)
theory.plot_s_deg(ax=ax[1], label="Theory", ls="--", show_legend=False)

if doSave:
    fig.savefig("deionized-cal.pdf")

In [22]: # composite figure
fig, ax = plt.subplots(2,1)
fig.set_figheight(7)

rawSample.plot_s_db(ax=ax[0], label="Original", ls=":", show_legend=True, lw=3)
sample.plot_s_db(ax=ax[0], label="Calibrated", show_legend=True, lw=3)
theory.plot_s_db(ax=ax[0], label="Theory", ls="--", show_legend=True, lw=3)
_= ax[0].legend(fontsize=16)
_= ax[0].set_xlabel('Frequency (Hz)', fontsize=16)
_= ax[0].set_ylabel('Magnitude', fontsize=16)
# ax.set_title("Deionized: 54.31c51.39-57.43-60.02")

rawSample.plot_s_deg(ax=ax[1], label="Original", ls=":", show_legend=False, lw=3)
sample.plot_s_deg(ax=ax[1], label="Cald", show_legend=False, lw=3)
theory.plot_s_deg(ax=ax[1], label="Theory", ls="--", show_legend=False, lw=3)
_= ax[1].set_xlabel('Frequency (Hz)', fontsize=16)
_= ax[1].set_ylabel('Phase (deg)', fontsize=16)

if doSave:
    fig.savefig("deionized-cal-defense.pdf")

In [ ]: rawSample = rf.Network('../plexiglass-holder-data/Data/2014-08-15/'
                              'beaker-mm-60-02.sip')

standards = [rf.Network('../plexiglass-holder-data/Data/2014-08-15/'
                        'beaker-mm-51-39.sip'),
             rf.Network('../plexiglass-holder-data/Data/2014-08-15/'
                        'beaker-mm-54-31.sip'),
             rf.Network('../plexiglass-holder-data/Data/2014-08-15/'
                        'beaker-mm-57-43.sip')]

offset = -1*50e-3

sampleDist = offset+60.02e-3

```

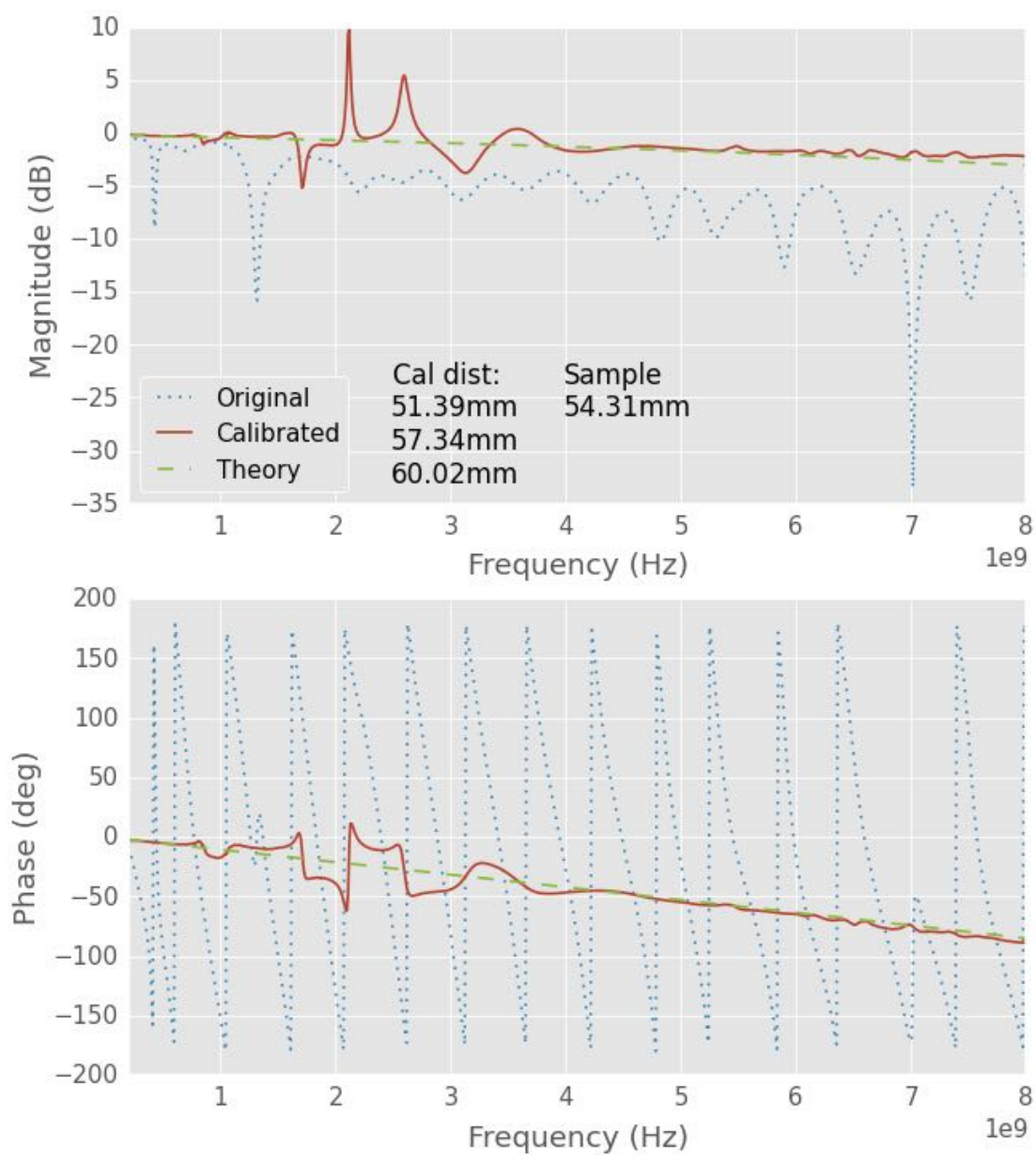


Figure S.9: notebook figure

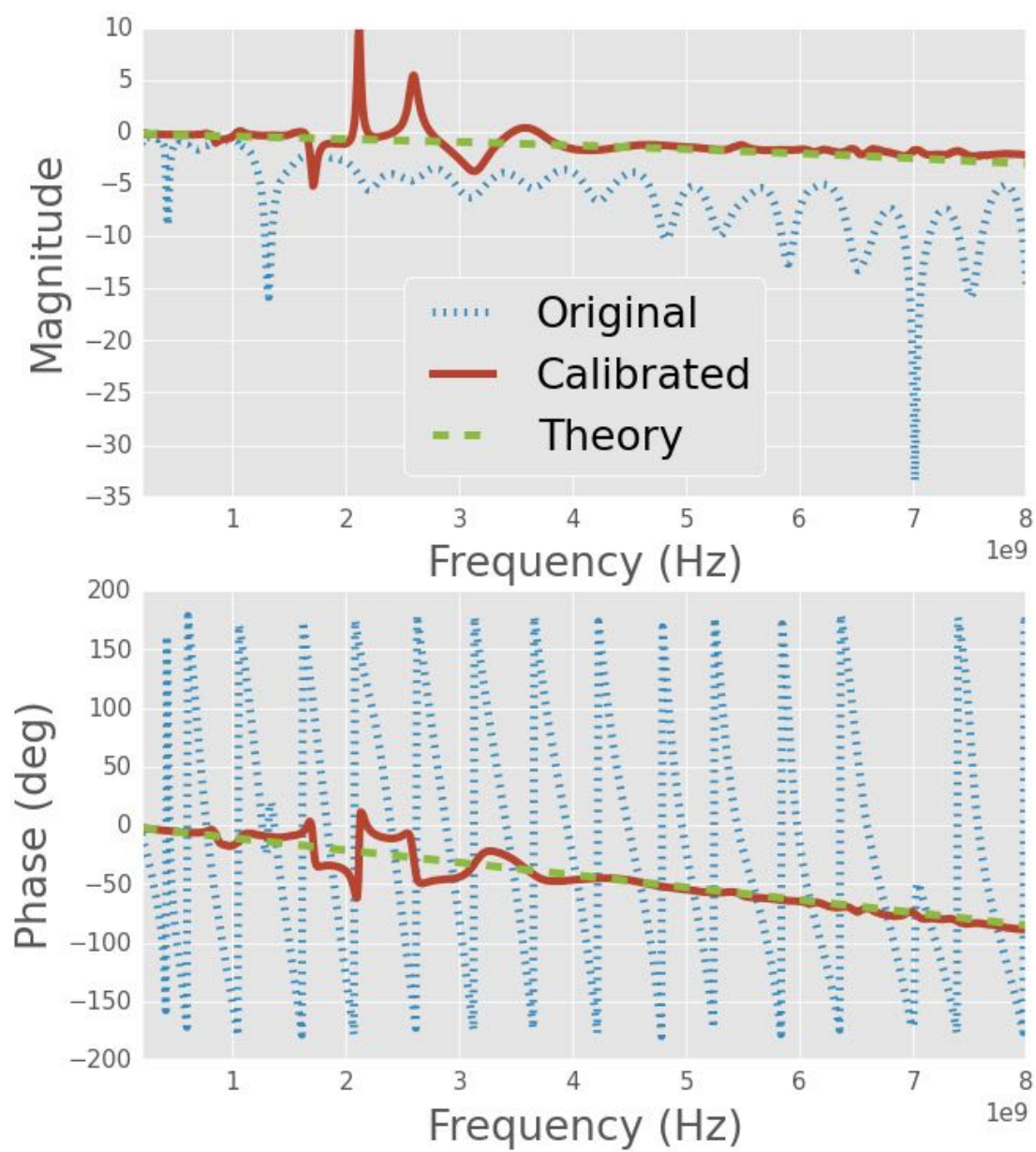


Figure S .10: notebook figure

```

stdDist = offset+np.array([51.39,54.31,57.43])*1e-3

shortDist = offset+72.38e-3

freq = rawSample.f
rfFreq = rawSample.frequency
diam = 0.126
radius = diam/2
cntr2cntr = 0.25
sigma = 5.96e7
R, L, G, C = twoWireParameters(freq = freq, a=radius, D=cntr2cntr,
                                sigma_c=sigma, unitsScale=0.0254)
rRad = 30*(2*pi*freq**2*constants.epsilon_0*constants.mu_0)*cntr2cntr**2
R += rRad
paramAir = tuple([R, L, G, C])

waterEps = debye(freq)
tanD = waterEps.imag/waterEps.real
R, L, G, C = twoWireParameters(freq = freq, a=radius, D=cntr2cntr,sigma_c=sigma,
                                eps_r=waterEps.real, tanDelta=tanD,
                                unitsScale=0.0254)
rRad = 30*(2*pi*freq**2*waterEps.real*constants.mu_0)*cntr2cntr**2
R += rRad
paramWater = tuple([R, L, G, C])

theory1 = airWaterShort(stdDist[0], shortDist, paramAir, paramWater,rfFreq)
theory2 = airWaterShort(stdDist[1], shortDist, paramAir, paramWater,rfFreq)
theory3 = airWaterShort(stdDist[2], shortDist, paramAir, paramWater,rfFreq)
theory = airWaterShort(sampleDist, shortDist, paramAir, paramWater,rfFreq)

balun = find1PortTransitionWater(standards, [theory1, theory2, theory3])
sample = deembed(balun, rawSample)

fig, ax = plt.subplots()
sample.plot_s_db(show_legend=False)
theory.plot_s_db(show_legend=False)
rawSample.plot_s_db(show_legend=False)

fig, ax = plt.subplots()
sample.plot_s_deg(show_legend=False)
theory.plot_s_deg(show_legend=False)

In [ ]: rawSample = rf.Network('../plexiglass-holder-data/Data/2014-08-15/'
                                'beaker-mm-06-02.sip')

standards = [rf.Network('../plexiglass-holder-data/Data/2014-08-15/'
                          'beaker-mm-11-67.sip'),
              rf.Network('../plexiglass-holder-data/Data/2014-08-15/'
                          'beaker-mm-24-41.sip'),
              rf.Network('../plexiglass-holder-data/Data/2014-08-15/'
                          'beaker-mm-40-27.sip')]

```



```

offset = -1*3e-3

sampleDist = offset+6.02e-3
stdDist = offset+np.array([11.67,24.41,40.27])*1e-3

shortDist = offset+72.38e-3

freq = rawSample.f
rfFreq = rawSample.frequency
diam = 0.126
radius = diam/2
cntr2cntr = 0.25
sigma = 5.96e7
R, L, G, C = twoWireParameters(freq = freq, a=radius, D=cntr2cntr,
                                sigma_c=sigma, unitsScale=0.0254)
rRad = 30*(2*pi*freq**2*constants.epsilon_0*constants.mu_0)*cntr2cntr**2
R += rRad
rAir = rRad
paramAir = tuple([R, L, G, C])

waterEps = debye(freq)
tanD = waterEps.imag/waterEps.real
R, L, G, C = twoWireParameters(freq = freq, a=radius, D=cntr2cntr,sigma_c=sigma,
                                eps_r=waterEps.real, tanDelta=tanD,
                                unitsScale=0.0254)
rRad = 30*(2*pi*freq**2*waterEps.real*constants.mu_0)*cntr2cntr**2
R += rRad
paramWater = tuple([R, L, G, C])
rWater = rRad

theory1 = airWaterShort(stdDist[0], shortDist, paramAir, paramWater,rfFreq)
theory2 = airWaterShort(stdDist[1], shortDist, paramAir, paramWater,rfFreq)
theory3 = airWaterShort(stdDist[2], shortDist, paramAir, paramWater,rfFreq)
theory = airWaterShort(sampleDist, shortDist, paramAir, paramWater,rfFreq)

balun = find1PortTransitionWater(standards, [theory1, theory2, theory3])
sample = deembed(balun, rawSample)
sample.plot_s_db(show_legend=False)
theory.plot_s_db(show_legend=False)
rawSample.plot_s_db(show_legend=False)
plt.figure()
sample.plot_s_deg(show_legend=False)
theory.plot_s_deg(show_legend=False)

```

BIBLIOGRAPHY

BIBLIOGRAPHY

- [1] S. Ramo, J. R. Whinnery, and T. Van Duzer, *Fields and Waves in Communication Electronics*, 3rd ed. New York: Wiley, 1994.
- [2] "Scattering parameters," Nov. 2014, page Version ID: 632781014. [URL] http://en.wikipedia.org/w/index.php?title=Scattering_parameters&oldid=632781014
- [3] IFSTA, *Essentials of Fire Fighting and Fire Department Operations*, 5th ed. Prentice Hall, Jan. 2008.
- [4] J. A. Bittencourt, *Fundamentals of plasma physics*, 3rd ed. Springer, 2004.
- [5] D. M. Pozar, *Microwave Engineering*, 4th ed. Hoboken, NJ: Wiley, 2012.
- [6] J. A. Stratton, *Electromagnetic theory*, 1st ed., ser. International series in physics. New York, London: McGraw-Hill book company, inc, 1941.
- [7] L. Brillouin, *Wave Propagation and Group Velocity*, ser. Pure and Applied Physics. New York: Academic Press, 1960.
- [8] E. J. Rothwell and M. J. Cloud, *Electromagnetics*, 2nd ed. Boca Raton, Fla: CRC Press, 2009. [URL] <https://catalog.loc.gov/vwebv/holdingsInfo?searchId=7961&recCount=25&recPointer=1&bibId=12227004>
- [9] E. R. Andrew, D. W. E. Axford, and T. M. Sugden, "The measurement of ionisation in a transient flame," *Transactions of the Faraday Society*, vol. 44, p. 427, 1948. [URL] <http://pubs.rsc.org.proxy2.cl.msu.edu/en/Content/ArticleLanding/1948/TF/tf9484400427>
- [10] H. Belcher and T. M. Sugden, "Studies on the Ionization Produced by Metallic Salts in Flames. I. The Determination of the Collision Frequency of Electrons in Coal-Gas/Air Flames," *Proceedings of the Royal Society of London. Series A, Mathematical and Physical Sciences*, vol. 201, no. 1067, pp. 480–488, May 1950. [URL] <http://www.jstor.org/stable/98501>
- [11] H. Belcher and T. M. Sugden, "Studies on the Ionization Produced by Metallic Salts in Flames II. Reactions Governed by Ionic Equilibria in Coal-Gas/Air Flames Containing Alkali Metal Salts," *Proceedings of the Royal Society of London. Series A, Mathematical and Physical Sciences*, vol. 202, no. 1068, pp. 17–39, Jun. 1950. [URL] <http://www.jstor.org/stable/98512>
- [12] H. Smith and T. M. Sugden, "Studies on the Ionization Produced by Metallic Salts in Flames. III. Ionic Equilibria in Hydrogen/Air Flames Containing Alkali Metal Salts," *Proceedings of the Royal Society of London. Series A, Mathematical and Physical Sciences*, vol. 211, no. 1104, pp. 31–58, Feb. 1952. [URL] <http://www.jstor.org/stable/98839>

- [13] H. Smith and T. M. Sugden, "Studies on the Ionization Produced by Metallic Salts in Flames. IV. The Stability of Gaseous Alkali Hydroxides in Flames," *Proceedings of the Royal Society of London. Series A, Mathematical and Physical Sciences*, vol. 211, no. 1104, pp. 58–74, Feb. 1952. [URL] <http://www.jstor.org/stable/98840>
- [14] F. P. Adler, "Measurement of the Conductivity of a Jet Flame," *Journal of Applied Physics*, vol. 25, no. 7, pp. 903–906, Jul. 1954. [URL] http://jap.aip.org.proxy2.cl.msu.edu/resource/1/japiau/v25/i7/p903_s1
- [15] K. E. Shuler and J. Weber, "A Microwave Investigation of the Ionization of Hydrogen-Oxygen and Acetylene-Oxygen Flames," *The Journal of Chemical Physics*, vol. 22, no. 3, pp. 491–502, Mar. 1954. [URL] <http://link.aip.org/link/JCPSA6/v22/i3/p491/s1&Agg=doi>
- [16] J. Boan, "FDTD for tropospheric propagation with strong cold plasma effects," in *IEEE Antennas and Propagation Society International Symposium 2006*, Jul. 2006, pp. 3905 – 3908, <http://digital.library.adelaide.edu.au/dspace/displaystats?handle=2440/35259>.
- [17] J. A. Boan, "Radio Propagation in Fire Environments," in *Workshop on the Applications of Radio Science 2006*, Luera, Australia, Feb. 2006, <http://www.ips.gov.au/IPSHosted/NCRS/wars/wars2006-meeting/index.html>. [URL] <http://www.ips.gov.au/IPSHosted/NCRS/wars/wars2006/proceedings/index.htm>
- [18] J. J. Boan, "Radio Experiments With Fire," *IEEE Antennas and Wireless Propagation Letters*, vol. 6, pp. 411–414, 2007.
- [19] C. Coleman and J. Boan, "A Kirchhoff Integral approach to radio wave propagation in fire," in *2007 IEEE Antennas and Propagation Society International Symposium*. IEEE, 9-15 June 2007, pp. 3752–3755.
- [20] J. A. Boan, "Radio propagation in fire environments," Thesis, University of Adelaide, Adelaide, Australia, 2009. [URL] <http://digital.library.adelaide.edu.au/dspace/handle/2440/58684>
- [21] M. L. Heron and K. M. Mphale, "Radio wave attenuation in bushfires, tropical cyclones and other severe atmospheric conditions," Australian Emergency Management, Final Report EMA Project 60/2001, Apr. 2004. [URL] <http://www.em.gov.au/Documents/EMA%20Project%2010-2001.PDF>
- [22] K. M. Mphale, D. Letsholathebe, and M. L. Heron, "Effective complex permittivity of a weakly ionized vegetation litter fire at microwave frequencies," *Journal of Physics D: Applied Physics*, vol. 40, no. 21, pp. 6651–6656, Nov. 2007. [URL] <http://iopscience.iop.org/0022-3727/40/21/026>
- [23] K. Mphale and M. Heron, "Absorption and Transmission Power Coefficients for Millimeter Waves in a Weakly Ionised Vegetation Fire," *International Journal of Infrared and Millimeter Waves*, vol. 28, no. 10, pp. 865–879, 2007. [URL] <http://www.springerlink.com/content/n48v060420267w32/abstract/>

- [24] K. Mphale, M. Heron, and T. Verma, "Effect of Wildfire-Induced Thermal Bubble on Radio Communication," *Progress In Electromagnetics Research*, vol. 68, pp. 197–228, 2007. [URL] <http://www.jpier.org/PIER/pier.php?paper=06072202>
- [25] K. Mphale and M. Heron, "Microwave measurement of electron density and collision frequency of a pine fire," *Journal of Physics D: Applied Physics*, vol. 40, no. 9, pp. 2818–2825, May 2007. [URL] <http://eprints.jcu.edu.au/2587/>
- [26] K. Mphale, M. Jacob, and M. Heron, "Prediction and Measurement of Electron Density and Collision Frequency in a Weakly Ionised Pine Fire," *International Journal of Infrared and Millimeter Waves*, vol. 28, no. 3, pp. 251–262, Mar. 2007. [URL] <http://eprints.jcu.edu.au/2655/>
- [27] K. Mphale and M. Heron, "Ray Tracing Radio Waves in Wildfire Environments," *Progress In Electromagnetics Research*, vol. 67, pp. 153–172, 2007. [URL] <http://www.jpier.org/PIER/pier.php?paper=06082302>
- [28] K. Mphale and M. Heron, "Wildfire plume electrical conductivity," *Tellus B*, vol. 59, no. 4, pp. 766–772, Sep. 2007. [URL] <http://www.tellusb.net/index.php/tellusb/article/view/17055>
- [29] K. M. Mphale and M. L. Heron, "Plant alkali content and radio wave communication efficiency in high intensity savanna wildfires," *Journal of Atmospheric and Solar-Terrestrial Physics*, vol. 69, no. 4–5, pp. 471–484, Apr. 2007. [URL] <http://www.sciencedirect.com/science/article/pii/S1364682606003063>
- [30] K. M. Mphale and M. Heron, "Nonintrusive measurement of ionisation in vegetation fire plasma," *The European Physical Journal Applied Physics*, vol. 41, no. 2, pp. 157–164, Feb. 2008. [URL] <http://www.epjap.org.proxy2.cl.msu.edu/action/displayAbstract?fromPage=online&aid=8015723>
- [31] K. Mphale, P. Luhanga, and M. Heron, "Microwave attenuation in forest fuel flames," *Combustion and Flame*, vol. 154, no. 4, pp. 728–739, Sep. 2008. [URL] <http://www.sciencedirect.com/science/article/pii/S0010218008002101>
- [32] K. Mphale and M. Heron, "Measurement of Electrical Conductivity for a Biomass Fire," *International Journal of Molecular Sciences*, vol. 9, no. 8, pp. 1416–1423, Aug. 2008. [URL] <http://www.mdpi.com/1422-0067/9/8/1416>
- [33] K. M. Mphale, "Radiowave propagation measurements and prediction in bushfires," PhD, James Cook University, Australia, 2008. [URL] <http://eprints.jcu.edu.au/2028/>
- [34] K. Mphale, M. Heron, R. Ketlhwaaftse, D. Letsholathebe, and R. Casey, "Interferometric measurement of ionization in a grassfire," *Meteorology and Atmospheric Physics*, vol. 106, no. 3, pp. 191–203, 2010. [URL] <http://www.springerlink.com/content/n4621420l5466177/abstract/>

- [35] M. Born and E. Wolf, *Principles of optics : electromagnetic theory of propagation, interference and diffraction of light*, 6th ed. Cambridge, UK ; New York ; Cambridge University Press, 1997.
- [36] M. Skolnik, *Introduction to Radar Systems*, 3rd ed. McGraw-Hill Science/Engineering/Math, Dec. 2002.
- [37] A. C. Bemis, "Weather radar research at MIT," *Bulletin of the American Meteorological Society*, vol. 28, no. 3, pp. 115–117, 1947.
- [38] L. F. Radke, D. A. Hegg, P. V. Hobbs, J. D. Nance, J. H. Lyons, K. K. Laursen, R. E. Weiss, P. J. Riggan, and D. E. Ward, "Particulate and trace gas emissions from large biomass fires in North America," *Global biomass burning: Atmospheric, climatic, and biospheric implications*, pp. 209–224, 1991. [URL] [http://www.fs.fed.us/psw/publications/riggan/psw_1991_riggan001\(radke\).pdf?](http://www.fs.fed.us/psw/publications/riggan/psw_1991_riggan001(radke).pdf?)
- [39] R. M. Banta, L. D. Olivier, E. T. Holloway, R. A. Kropfli, B. W. Bartram, R. E. Cupp, and M. J. Post, "Smoke-Column Observations from Two Forest Fires Using Doppler Lidar and Doppler Radar," *Journal of Applied Meteorology*, vol. 31, no. 11, pp. 1328–1349, Nov. 1992. [URL] [http://journals.ametsoc.org/doi/abs/10.1175/1520-0450\(1992\)031%3C1328:SCOFTF%3E2.0.CO;2](http://journals.ametsoc.org/doi/abs/10.1175/1520-0450(1992)031%3C1328:SCOFTF%3E2.0.CO;2)
- [40] R. R. Rogers and W. O. J. Brown, "Radar Observations of a Major Industrial Fire," *Bulletin of the American Meteorological Society*, vol. 78, no. 5, pp. 803–814, May 1997. [URL] [http://journals.ametsoc.org/doi/abs/10.1175/1520-0477\(1997\)078<0803:ROOAMI>2.0.CO;2](http://journals.ametsoc.org/doi/abs/10.1175/1520-0477(1997)078<0803:ROOAMI>2.0.CO;2)
- [41] V. M. Melnikov, D. S. Zrnica, and R. M. Rabin, "Polarimetric radar properties of smoke plumes: A model," *Journal of Geophysical Research: Atmospheres*, vol. 114, no. D21, p. D21204, Nov. 2009. [URL] <http://onlinelibrary.wiley.com/doi/10.1029/2009JD012647/abstract>
- [42] T. A. Jones, S. A. Christopher, and W. Petersen, "Dual-Polarization Radar Characteristics of an Apartment Fire," *Journal of Atmospheric and Oceanic Technology*, vol. 26, no. 10, pp. 2257–2269, Oct. 2009. [URL] <http://journals.ametsoc.org/doi/abs/10.1175/2009JTECHA1290.1>
- [43] T. A. Jones and S. A. Christopher, "Satellite and Radar Remote Sensing of Southern Plains Grass Fires: A Case Study," *Journal of Applied Meteorology and Climatology*, vol. 49, no. 10, pp. 2133–2146, May 2010. [URL] <http://journals.ametsoc.org/doi/abs/10.1175/2010JAMC2472.1>
- [44] T. Baum, L. Thompson, and K. Ghorbani, "A Complex Dielectric Mixing Law Model for Forest Fire Ash Particulates," *Geoscience and Remote Sensing Letters, IEEE*, vol. 9, no. 5, pp. 832–835, Sep. 2012.
- [45] C. K. Law, *Combustion Physics*, 1st ed. Cambridge University Press, Aug. 2010.

- [46] W. M. Haynes, Ed., *CRC Handbook of Chemistry and Physics, 92nd Edition (Internet Version 2012)*. CRC Press/Taylor and Francis, Boca Raton, FL., 2012. [URL] <http://www.hbcpnetbase.com/>
- [47] K. Yee, "Numerical solution of initial boundary value problems involving maxwell's equations in isotropic media," *IEEE Transactions on Antennas and Propagation*, vol. 14, no. 3, pp. 302–307, May 1966.
- [48] F. Akleman and L. Sevgi, "A novel finite-difference time-domain wave propagator," *IEEE Transactions on Antennas and Propagation*, vol. 48, no. 5, pp. 839–841, May 2000.
- [49] L. Nickisch and P. Franke, "Finite-difference time-domain solution of Maxwell's equations for the dispersive ionosphere," *IEEE Antennas and Propagation Magazine*, vol. 34, no. 5, pp. 33–39, Oct. 1992.
- [50] J. Young, "Propagation in linear dispersive media: finite difference time-domain methodologies," *IEEE Transactions on Antennas and Propagation*, vol. 43, no. 4, pp. 422–426, Apr. 1995.
- [51] K. Lan, Y. Liu, and W. Lin, "A higher order (2,4) scheme for reducing dispersion in FDTD algorithm," *IEEE Transactions on Electromagnetic Compatibility*, vol. 41, no. 2, pp. 160–165, May 1999.
- [52] T. T. Zygiridis and T. D. Tsiboukis, "Higher-order finite-difference schemes with reduced dispersion errors for accurate time-domain electromagnetic simulations," *International Journal of Numerical Modelling: Electronic Networks, Devices and Fields*, vol. 17, no. 5, pp. 461–486, 2004. [URL] <http://onlinelibrary.wiley.com/doi/10.1002/jnm.551/abstract>
- [53] Y. Itikawa, "Effective collision frequency of electrons in gases," *Physics of Fluids*, vol. 16, no. 6, pp. 831–835, Jun. 1973. [URL] http://pof.aip.org/resource/1/pfldas/v16/i6/p831_s1
- [54] P. E. Ciddor, "Refractive index of air: new equations for the visible and near infrared," *Applied Optics*, vol. 35, no. 9, pp. 1566–1573, Mar. 1996. [URL] <http://ao.osa.org/abstract.cfm?URI=ao-35-9-1566>
- [55] C. D. Grant, W. A. Loneragan, J. M. Koch, and D. T. Bell, "Fuel characteristics, vegetation structure and fire behaviour of 11-15 year-old rehabilitated bauxite mines in western australia," *Australian Forestry*, vol. 60, no. 3, pp. 147–157, 1997.
- [56] National Institute of Standards and Technology (NIST), "Fire Dynamics Simulator." [URL] <http://code.google.com/p/fds-smv/>
- [57] E. Koretzky and S. P. Kuo, "Characterization of an atmospheric pressure plasma generated by a plasma torch array," *Physics of Plasmas*, vol. 5, no. 10, pp. 3774–3780, Oct. 1998. [URL] http://pop.aip.org.proxy1.cl.msu.edu/resource/1/phpaen/v5/i10/p3774_s1

- [58] A. Krutz, "Electromagnetic Material Characterization Using Free-Field Transmission Measurements," Ph.D. dissertation, 1997.
- [59] T. A. Zwietasch, "Transient Reflection of Plane Waves from a Plasma Half-Space," Diplom Wirtschaftsingenieur, University of Kaiserslautern, Kaiserslautern, Germany, 2006.
- [60] B. T. Perry, "Natural resonance representation of the transient field reflected from a multi-layered material," Ph.D. dissertation, Michigan State University, East Lansing, Michigan, United States of America, 2005.
- [61] S. Kerber, "Analysis of Changing Residential Fire Dynamics and Its Implications on Firefighter Operational Timeframes," UL, Tech. Rep., 2011. [URL] http://newscience.ul.com/wp-content/uploads/2014/04/Analysis_of_Changing_Residential_Fire_Dynamics_and_Its_Implications_on_Firefighter_Operational_Timeframes.pdf
- [62] S. Kerber, "Analysis of Changing Residential Fire Dynamics and Its Implications on Firefighter Operational Timeframes," *Fire Technology*, vol. 48, no. 4, pp. 865–891, Dec. 2011. [URL] <http://link.springer.com/article/10.1007/s10694-011-0249-2>
- [63] J. Ross, "Wavecalc," Moab, UT. [URL] <http://www.johnross.com/wavecalc.html>
- [64] W. Gunn, Jr., "Application of the Three Short Calibration Technique in a Low Frequency Focus Beam System," M.S., Air Force Institute of Technology, Wright-Patterson Air Force Base, Ohio, Mar. 2010. [URL] <http://www.dtic.mil/dtic/tr/fulltext/u2/a518512.pdf>
- [65] O. Tudisco, A. Lucca Fabris, C. Falcetta, L. Accatino, R. De Angelis, M. Manente, F. Ferri, M. Florean, C. Neri, C. Mazzotta, D. Pavarin, F. Pollastrone, G. Rocchi, A. Selmo, L. Tasinato, F. Trezzolani, and A. A. Tuccillo, "A microwave interferometer for small and tenuous plasma density measurements," *Review of Scientific Instruments*, vol. 84, no. 3, pp. 033 505–033 505–7, Mar. 2013. [URL] http://rsi.aip.org/resource/1/rsinak/v84/i3/p033505_s1
- [66] M. A. Heald and C. B. Wharton, *Plasma Diagnostics with Microwaves*. Huntington, N.Y: R. E. Krieger Pub. Co, 1978.
- [67] D. W. Williams, J. S. Adams, J. J. Betten, G. F. Whitty, and G. T. Richardson, "Operation Euroka: An Australian Mass Fire Experiment," Australia Defense Standards Laboratory, Maribyrnorr, Victoria, Tech. Rep. 386, 1970.
- [68] J. E. Foster, *Bushfire : history, prevention and control*. Sydney: Reed, 1976.
- [69] "Byonics - MicroTrak." [URL] <http://www.byonics.com/mf>
- [70] "Internet Datalogging With Arduino and XBee WiFi." [URL] <https://learn.sparkfun.com/tutorials/internet-datalogging-with-arduino-and-xbee-wifi>

- [71] “AR8200 Bulletin Page.” [URL] <http://www.thiecom.de/ftp/aor/ar8200/information/ar8200bul.pdf>
- [72] “NetSurveyor 802.11 Network Discovery Tool.” [URL] <http://nutsaboutnets.com/netsurveyor-wifi-scanner/>
- [73] D. K. Cheng, *Field and Wave Electromagnetics*, 2nd ed. Reading, MA: Addison-Wesley, 1989.
- [74] R. Plonsey and R. E. Collin, *Principles and applications of electromagnetic fields*, ser. McGraw-Hill series in electrical engineering. Electromagnetics. New York: McGraw-Hill, 1961.
- [75] L. V. Bewley, *Two-Dimensional Fields in Electrical Engineering*. Dover Publication, 1963.
- [76] R. W. P. King, *Transmission-Line Theory*. New York: McGraw-Hill, 1955.
- [77] A. Temme and E. Rothwell, “Material characterization using a two-wire transmission line,” in *Radio Science Meeting (Joint with AP-S Symposium), 2014 USNC-URSI*, Jul. 2014, pp. 11–11.
- [78] A. Temme and E. Rothwell, “Evaluation of Material Characterization Systems that Utilize a Two-Wire Transmission Line,” Vancouver, BC, Canada, Jul. 2015. [URL] <https://github.com/temmeand/Temme-and-Rothwell-URSI-2015>
- [79] IEEE, “IEEE Standard Definitions of Terms for Radio Wave Propagation,” *IEEE Std 211-1997*, 1998.
- [80] J. R. Carson, “Wave propagation over parallel wires: The proximity effect,” *Philosophical Magazine Series 6*, vol. 41, no. 244, pp. 607–633, 1921. [URL] <http://www.tandfonline.com/doi/abs/10.1080/14786442108636251>
- [81] D. J. Infante, “Full-wave integral-operator description of propagation modes excited on stripline structures,” Ph.D., Michigan State University, East Lansing, Michigan, United States of America, 1999.
- [82] J. Venkatesan, “Investigation of the Double-Y Balun for Feeding Pulsed Antennas,” Dissertation, Georgia Institute of Technology, Jul. 2004. [URL] <https://smartech.gatech.edu/handle/1853/5036>
- [83] C. R. Paul, *Introduction to Electromagnetic Compatibility*, 2nd ed. Hoboken, New Jersey: Wiley-Interscience, 2006.
- [84] “Title 47: Telecommunication PART 15—RADIO FREQUENCY DEVICES Subpart F—Ultra-Wideband Operation.” [URL] <http://www.ecfr.gov/cgi-bin/text-idx?SID=6717b8161d802bc6e2caf2d6bc1e8fb7&mc=true&node=sp47.1.15.f&rgn=div6>

- [85] "First Report and Order. Revision of Part 15 of the Commission's Rules Regarding Ultra WideBand Transmission Systems. FFC 02-48," Feb. 2002. [URL] https://transition.fcc.gov/Bureaus/Engineering_Technology/Orders/2002/fcc02048.pdf
- [86] S. Kim, S. Jeong, Y.-T. Lee, D. Kim, J.-S. Lim, K.-S. Seo, and S. Nam, "Ultra-wideband (from DC to 110 GHz) CPW to CPS transition," *Electronics Letters*, vol. 38, no. 13, pp. 622–623, Jun. 2002.
- [87] B. Jokanović, V. Trifunović, and B. Reljic, "Balance measurements in double-Y baluns," *Microwaves, Antennas and Propagation, IEE Proceedings*, vol. 149, no. 56, pp. 257–260, Oct. 2002.
- [88] K. Chang, Ed., *Encyclopedia of RF and Microwave Engineering*. Hoboken, N.J: John Wiley, 2005. [URL] <http://onlinelibrary.wiley.com/book/10.1002/0471654507>
- [89] V. Trifunović and B. Jokanović, "New uniplanar balun," *Electronics Letters*, vol. 27, no. 10, pp. 813–815, May 1991.
- [90] V. Trifunović and B. Jokanović, "Four decade bandwidth uniplanar balun," *Electronics Letters*, vol. 28, no. 6, pp. 534–535, Mar. 1992.
- [91] V. Trifunović and B. Jokanović, "Review of printed Marchand and double Y baluns: characteristics and application," *IEEE Transactions on Microwave Theory and Techniques*, vol. 42, no. 8, pp. 1454–1462, Aug. 1994.
- [92] B. Jokanović and V. Trifunović, "Double-Y baluns for MMICs and wireless applications," *Microwave Journal, International ed.*, vol. 41, no. 1, pp. 70–92, Jan. 1998. [URL] <http://search.proquest.com/docview/204946934/F7D291AB0403486EPQ/18?accountid=12598>
- [93] B. Jokanović, A. Marincić, and B. Kolundzija, "Analysis of the parasitic effects in double-Y baluns," *Microwaves, Antennas and Propagation, IEE Proceedings*, vol. 148, no. 4, pp. 239–245, Aug. 2001.
- [94] J. B. Venkatesan and J. Scott, Waymond R., "Investigation of the double-y balun for feeding pulsed antennas," in *Proceedings of the SPIE*, vol. 5089, 2003, pp. 830–840. [URL] <http://dx.doi.org/10.1117/12.487372>
- [95] J. Venkatesan, "Novel Version of the Double-Y Balun: Microstrip to Coplanar Strip Transition," *IEEE Antennas and Wireless Propagation Letters*, vol. 5, no. 1, pp. 172–174, Dec. 2006.
- [96] Y.-G. Kim, D.-S. Woo, K. W. Kim, and Y.-K. Cho, "A New Ultra-wideband Microstrip-to-CPS Transition," in *Microwave Symposium, 2007. IEEE/MTT-S International*, Jun. 2007, pp. 1563–1566.

- [97] D. S. Woo, Y. G. Kim, I. B. Kim, Y. K. Cho, and K. W. Kim, "Broadband antennas using a planar ultra-wideband balun," in *11th IEEE International Conference on Communication Technology, 2008. ICCT 2008*, Nov. 2008, pp. 305–308.
- [98] Y.-G. Kim, I.-B. Kim, D.-S. Woo, M.-G. Choi, Y.-K. Cho, and K. W. Kim, "Ultra-wideband components using a microstrip-to-CPS balun," in *34th International Conference on Infrared, Millimeter, and Terahertz Waves, 2009. IRMMW-THz 2009*, Sep. 2009, pp. 1–2.
- [99] K. C. Gupta, R. Garg, I. J. Bahl, and P. Bhartia, *Microstrip lines and slotlines*. Dedham, Mass: Artech House, 1979.
- [100] K. C. Gupta, R. Garg, and I. Bahl, *Microstrip lines and slotlines*, 2nd ed., ser. The Artech House microwave library. Boston: Artech House, 1996. [URL] <http://www.scribd.com/doc/112426565/Gupta-Et-Al-1996-Microstrip-Lines-and-Slotlines-2nd-Ed#scribd>
- [101] R. Garg, I. J. Bahl, and M. Bozzi, *Microstrip lines and slotlines*, 3rd ed., ser. Artech House microwave library. Boston: Artech House, 2013.
- [102] R. N. Simons, *Coplanar Waveguide Circuits, Components, and Systems*. New York, USA: John Wiley & Sons, Inc., Mar. 2001. [URL] <http://ieeexplore.ieee.org.proxy2.cl.msu.edu/xpl/bkabstractplus.jsp?bkn=5201692>
- [103] Y. Ichikawa, "I-Laboratory[TOOL]," Feb. 2014. [URL] http://www1.sphere.ne.jp/i-lab/ilab/tool/tool_e.htm
- [104] J. W. Duncan and V. P. Minerva, "100:1 Bandwidth Balun Transformer," *Proceedings of the IRE*, vol. 48, no. 2, pp. 156–164, Feb. 1960.
- [105] K. Hettak, N. Dib, A. Sheta, A. Omar, G.-Y. Delisle, M. Stubbs, and S. Toutain, "New miniature broadband CPW-to-slotline transitions," *IEEE Transactions on Microwave Theory and Techniques*, vol. 48, no. 1, pp. 138–146, Jan. 2000.
- [106] T. Hirota, Y. Tarusawa, and H. Ogawa, "Uniplanar MMIC Hybrids—A Proposed New MMIC Structure," *IEEE Transactions on Microwave Theory and Techniques*, vol. 35, no. 6, pp. 576–581, Jun. 1987.
- [107] C.-H. Ho, L. Fan, and K. Chang, "Broad-band uniplanar hybrid-ring and branch-line couplers," *IEEE Transactions on Microwave Theory and Techniques*, vol. 41, no. 12, pp. 2116–2125, Dec. 1993.
- [108] P. A. R. Holder, "X-band microwave integrated circuits using slotline and coplanar waveguide," *Radio and Electronic Engineer*, vol. 48, no. 1.2, pp. 38–42, Jan. 1978.
- [109] Y.-G. Kim, S.-Y. Song, and K. W. Kim, "A Pair of Ultra-Wideband Planar Transitions for Phase Inversion Applications," *IEEE Microwave and Wireless Components Letters*, vol. 20, no. 9, pp. 492–494, Sep. 2010.

- [110] G. A. Kouzaev, M. J. Deen, and N. K. Nikolova, "Chapter Two - Transmission Lines and Passive Components," in *Advances in Imaging and Electron Physics*, ser. Silicon-Based Millimeter-wave Technology Measurement, Modeling and Applications, M. Jamal Deen, Ed. Elsevier, 2012, vol. Volume 174, pp. 119–222. [URL] <http://www.sciencedirect.com/science/article/pii/B9780123942982000028>
- [111] H.-Y. Lee and T. Itoh, "Wideband and low return loss coplanar strip feed using intermediate microstrip," *Electronics Letters*, vol. 24, no. 19, pp. 1207–1208, Sep. 1988.
- [112] M. Manohar, R. Kshetrimayum, and A. Gogoi, "Printed monopole antenna with tapered feed line, feed region and patch for super wideband applications," *IET Microwaves, Antennas Propagation*, vol. 8, no. 1, pp. 39–45, Jan. 2014.
- [113] S.-G. Mao, C.-T. Hwang, R.-B. Wu, and C. H. Chen, "Analysis of coplanar waveguide-to-coplanar stripline transitions," *IEEE Transactions on Microwave Theory and Techniques*, vol. 48, no. 1, pp. 23–29, Jan. 2000.
- [114] H. Nakajima, T. Kosugi, and T. Enoki, "Hyperbolic tangent tapered slot antenna," *Electronics Letters*, vol. 46, no. 21, pp. 1422–1424, Oct. 2010.
- [115] V. K. Tripp, "Tapered double balun," U.S. Patent US7 994 874 B2, Aug., 2011, u.S. Classification 333/26, 343/821, 333/34, 343/859; International Classification H01Q1/50, H03H7/42, H01Q9/16, H03H7/38; Cooperative Classification H01P5/10, H01Q9/27; European Classification H01P5/10, H01Q9/27.
- [116] M. J. White, "Broadband balun," U.S. Patent US20 120 019 333 A1, Jan., 2012, u.S. Classification 333/26; International Classification H01P5/10; Cooperative Classification H01P5/10, H01P5/12; European Classification H01P5/10, H01P5/12.
- [117] S. J. Zegelin, I. White, and D. R. Jenkins, "Improved field probes for soil water content and electrical conductivity measurement using time domain reflectometry," *Water Resources Research*, vol. 25, no. 11, pp. 2367–2376, 1989. [URL] <http://onlinelibrary.wiley.com/doi/10.1029/WR025i011p02367/abstract>
- [118] K. F. Chackett, P. Reasbeck, and D. G. Tuck, "A note on joining tungsten wire to other metals," *Journal of Scientific Instruments*, vol. 33, no. 12, p. 505, Dec. 1956. [URL] <http://iopscience.iop.org/0950-7671/33/12/417>
- [119] J. G. Dodd, G. Schwarz, and A. J. Bearden, "Soft Soldering to Tungsten Wire," *American Journal of Physics*, vol. 34, no. 10, pp. xvi–xvi, Oct. 1966. [URL] <http://scitation.aip.org/content/aapt/journal/ajp/34/10/10.1119/1.1972398>
- [120] I. E. Petrunin and L. L. Grzhimal'skii, "Interaction of tungsten with copper, manganese, silver, and tin," *Metal Science and Heat Treatment*, vol. 11, no. 1, pp. 24–26, Jan. 1969. [URL] <http://link.springer.com/article/10.1007/BF00655167>

- [121] J. H. Lienhard, IV and J. H. Lienhard, V, *A Heat Transfer Textbook*, 4th ed. Cambridge, MA, USA: Phlogiston Press, 2012. [URL] <http://web.mit.edu/lienhard/www/ahtt.html>
- [122] “Intermediate Heat and Mass Transfer.” [URL] <http://ocw.mit.edu/courses/mechanical-engineering/2-51-intermediate-heat-and-mass-transfer-fall-2008/>
- [123] Hewlett-Packard, “S-Parameter Design,” Hewlett-Packard, Application Note AN 154, 1990. [URL] <http://cp.literature.agilent.com/litweb/pdf/5952-1087.pdf>
- [124] “MATLAB,” The MathWorks, Inc., Natick, Massachusetts, United States.
- [125] “Scikit-rl.” [URL] <http://www.scikit-rl.org>